NUREG/CP-0058
Vol. 1

Proceedings of the U.S. Nuclear Regulatory Commission

# Twelfth Water Reactor Safety Research Information Meeting

Volume 1
- Plenary Session - I
- Integral System Tests
- Separate Effects
- International Programs in Thermal Hydraulics
- Calculation of Appendix K Conservatisms

Held at
National Bureau of Standards
Gaithersburg, Maryland
October 22-26, 1984

**U.S. Nuclear Regulatory Commission**

**Office of Nuclear Regulatory Research**

Available from

GPO Sales Program
Division of Technical Information and Document Control
U.S. Nuclear Regulatory Commission
Washington, D.C. 20555

Printed copy price: $8.50

and

National Technical Information Service
Springfield, VA 22161

NUREG/CP-0058
Vol. 1
R1 and R2

Proceedings of the U.S. Nuclear Regulatory Commission

# Twelfth Water Reactor Safety Research Information Meeting

Volume 1
- Plenary Session - I
- Integral System Tests
- Separate Effects
- International Programs in Thermal Hydraulics
- Calculation of Appendix K Conservatisms

Held at
National Bureau of Standards
Gaithersburg, Maryland
October 22-26, 1984

Date Published: January 1985

Compiled by: Stanley A. Szawlewicz, Consultant

**Office of Nuclear Regulatory Research**
**U.S. Nuclear Regulatory Commission**
**Washington, D.C. 20555**

ABSTRACT

The papers published in this six volume report were presented at the Twelfth Water Reactor Safety Research Information Meeting held at the National Bureau of Standards, Gaithersburg, Maryland during the week of October 22-26, 1984. The papers describe progress and results of programs in nuclear safety research conducted in this country and abroad. Foreign participation in the meeting included twenty-six different papers presented by researchers from seven European countries, Japan, and Canada.

PROCEEDINGS OF THE
TWELFTH WATER REACTOR SAFETY RESEARCH
INFORMATION MEETING

October 22-26, 1984

Published in Six Volumes

GENERAL INDEX

PROCEEDINGS OF THE
TWELFTH WATER REACTOR SAFETY RESEARCH
INFORMATION MEETING

held at the

NATIONAL BUREAU OF STANDARDS
Gaithersburg, Maryland
October 22-26, 1984

TABLE OF CONTENTS - VOLUME 1

INTEGRAL SYSTEM TESTS (Cont'd)



SEPARATE EFFECTS
Chairman: W. D. Beckner, NRC



INTERNATIONAL PROGRAMS IN THERMAL HYDRAULICS
Chairman: Fuat Odar, NRC

CALCULATIONS OF APPENDIX K CONSERVATISMS
Chairman: W. D. Beckner, NRC

## PREFACE

This report, published in six volumes, contains 176 papers out of the 205 that were presented at the Twelfth Water Reactor Safety Research Information Meeting. The papers are printed in the order of their presentation in each session. The titles of the papers and the names of the authors have been updated and may differ from those which appear in the final agenda for the meeting. The papers listed under the session on Human Factors and Safeguards Research did not appear in the agenda but were prepared for the panel discussions that made up that session.

"Highlights of Reactor Safety Research"

Remarks by Robert B. Minogue, Director
Office of Nuclear Regulatory Research
U. S. Nuclear Regulatory Commission

Before The
Twelfth Water Reactor Safety Research Information Meeting
October 22, 1984

Thank you very much. Before I welcome you, I want to pass on some bad news. Saul Levine who I am sure was known to most of you died suddenly last Thursday. All his life he was a very energetic person who worked hard for nuclear safety and he died on the job, so to speak, of a heart attack. I am sure that all of us will remember him for his many contributions. I knew him myself since 1954, and I was just telling Commissioner Asselstine that, probably more than any person I know in this business, he was a man who had dedicated his entire career to nuclear safety and to advancing the cause of nuclear safety. He was known for his energy and his innovative ideas. I think he will be a great loss to all of us. I am sorry to start on such a note of bad news.

I would like to welcome all of you to this conference. We have a very good panel of speakers this morning so I intend to be very brief in my own remarks. The title of my talk is "Highlights of Reactor Safety Research." What I would like to do in just a few minutes is to identify five principal areas that I think require a continuing research capability and briefly identify what I think some of the major problems are and some of the major research that is needed in each of those areas.

The first area relates to the mechanisms and significance of aging and degradation in service. As plants mature, several phenomena--corrosion, radiation embrittlement, fatigue, and other effects--have raised serious questions about the continued safety and viability of the plants and in particular about the integrity of the primary coolant pressure boundaries. These questions led to the perception of a need to improve techniques of nondestructive examination in terms of both detecting flaws and properly characterizing them. An important development of some time ago that illustrates my point was the role of the PISC program in flagging the deficiencies in ultrasonic examination techniques. Fortunately, because these deficiencies were identified early, there was time for a major effort to resolve some of the questions by improvements in nondestructive examination techniques. That has been very helpful in recent years as flaws have been

detected and judgments have had to be made as to what kind of inspection is required, when to require it, and whether plants could be allowed to operate prior to those inspections and also in making assessments of the significance of flaws and possible mechanisms of flaw propagation. Steam generator problems are so widespread and so serious that they hardly need to be discussed. I think there has been one major success in this area. The pressurized thermal shock issue, I believe, is largely resolved for the present plants. However, we face the fact that there may be degradation of other components or currently unrecognized effects of degradation as plants age. The NRC has recently made arrangements with the cooperation of the Naval Reactor staff of the Department of Energy to examine components from the Shippingport reactor to determine whether insights can be obtained from that plant regarding degradation mechanisms not previously recognized. We have also given a great deal of attention to environmental qualification programs for both electrical and mechanical equipment to develop testing techniques by which one can better predict performance throughout life.

The second major area is that of system response to complex operational and thermal hydraulic transients. In the first years of commercial nuclear power, work in this area was largely oriented toward large-break loss-of-coolant accident (LOCA) issues and reflected an underlying perception that the whole range of transients could be adequately characterized by analysis of an extreme limiting case. The TMI accident showed all of us that this is a questionable assumption. In recent years, the emphasis has shifted much more to small-break LOCAs and other transients and toward best-estimate calculations. As the range of transients considered has been broadened, it has also become clear that there are several implications from this research. As you move toward best-estimate codes and wider treatment of transients, there are implications that affect system reliability and on-line availability and thus can offer a significant potential savings to the industry beyond that of simply resolving safety questions. Certainly the utility industry and the manufacturers have participated heavily in these programs in the last few years. The proper approach to this type of program as I see it is, first, to understand the basic phenomena, which means that the smaller scale and separate effects programs are extremely important, second, to demonstrate and validate the codes with large-scale integral tests, and third, to have the ability to assess the

applicability of those codes to new problems as they may arise. Particular applications of the results are in the evaluation of plant transients, the training of operators, the simplification of operating procedures, and the use of these sophisticated codes in the development of a basis for plant analyzers that can be used widely in assessing operations and in developing operating procedures. A particular end use in this area that I think is most important relates to the wide variation in designs. Unexpected transients that may occur on a plant must be evaluated as they may apply to many other reactors of different configurations. It is because of the likely continuing need to assess code applicability in such analyses that we are seriously considering the desirability of a long-term highly flexible integral facility that could be used to continue to do testing of the type now done on the semiscale facility. And I might add on the FIST and MIST facilities as well.

The third area is that of severe accident research in which I would include the source term question. I will begin by saying that the proper first objective of severe accident research is always to prevent the accident. The work that one does looking at thermal hydraulic transients in that sense is part of severe accident research. With that qualification I see the rest of the severe accident work as being in two categories. The first category concerns accidents that involve degradation of the core in an arrested sequence where the problems are really those of fission product release, plateout, and things of that type. The phenomenology of this category is near resolution, at least in a regulatory sense, that is, in the sense that enough is known to begin to deal with questions of siting and emergency planning. There is of course a longer term problem in such accidents relating to the activity distribution within the plant and its systems in such arrested sequences. That is a longer term problem requiring much more work. The second category under severe accident research concerns severe core degradation. Here I think the issues are coolability of degraded cores, loads on containment that occur with core meltdown, for example, from gas production or effects of core/concrete interactions, and containment failure modes. The last of these is particularly critical. Too often containments are thought of as simple pressure vessels, and containment failure modes and margins are thought of in that context. In reality, containments are full of penetrations and irregularities, and it is

there that the failure mechanisms can be important. Early containment failure is clearly an element in risk dominant sequences. The whole area of severe accident research is one in which we see a need to improve the quantification of residual risks and foresee potential problems of public acceptance. I think it is important that in-pile capability for fuel damage work be retained.

The fourth major area is research related to reactor operations and probabilistic risk assessment. Here the main issues relate to the application of the insights obtained from the two areas I have just discussed to plant operation, to assessments of operational capabilities, instrumentation, monitoring, control room design, operating procedures, and operator training, technical specifications and generally to incorporating these insights into the human factors areas. As to the probabilistic risk assessments themselves, there clearly is a need for significant improvement in PRAs if they are to be fully useful. I see these improvements in two categories. The first is improvement in the data base. This means better data on component reliability, better data on maintenance experience, and better data feedback from operating plants. I also believe that an important source of information for an improved data base is the incorporation into PRAs of the insights and understandings that have developed from the experimental and thermal hydraulic programs. The second category is improvement in the methodology itself by incorporating human factors and common cause failure modes such as might arise from earthquakes, internal and external flooding, or sabotage.

Let me go on to the fifth and last area, which is seismic safety margins research. With the continuing improvement and understanding of geology and seismology in recent years, we have come to realize that a number of the older plants may have been designed for seismic hazard levels that are not high enough. Thus, although we believe that there is a considerable seismic safety margin in present designs, we see a need for improved, well-validated seismic analysis methods that could be used to reassess these currently operating plants to ensure that margins do exist and, ideally, to quantify those margins to some degree. Also, the PRAs that have been done have shown that seismic risk is a significant contributor. Last, we have the perception that the design approach that has been used in the past is not a good approach. It is not cost

effective and, in some respects, may even be counterproductive. This is what is often referred to as the stiff versus flexible piping issue.

The following research is needed to deal with these points. The first is a better approach to defining seismic hazard on a regional basis. The technique used in NRC's regulations is unduly conservative when applied in areas where the seismicity cannot be related to specific geological structures. The second is hard experimental data that can be used to validate the nonlinear seismic response models that have been developed. This sort of research requires extensive and expensive shake testing. The last seismic research need is a simplified design approach that can be compared against or benchmarked against these validated nonlinear methods I have just mentioned. I think such simplified techniques are necessary in order to take advantage of possible simplifications as modifications may be made in present plants. For future plants, they should lead to a much simpler and more straightforward design approach.

Well, I have gone very quickly through these five major areas. Because there is a very significant international participation in this meeting, I want to close by making the comment that I have the impression that there is a broad international consensus on the importance of these areas. Just within the last few weeks, I was privileged to participate in a meeting of the European Community somewhat similar to this one, and I found in talking to my opposite numbers in other countries that we have much the same perception as to the areas that need research. Certainly there is a current trend toward joint programs and greater cooperation in planning of programs. Although this is largely driven by budget constraints, I believe it is improving the quality of the research. Nuclear safety issues are complex and require multidisciplinary, highly interactive efforts in order to resolve them. They need the cross fertilization that comes from having a number of participants. Further, every country has a parallel interest in resolution of the nuclear safety research problems. A problem for one is a problem for all. Thank you again for coming to this meeting and I hope it is a very successful one. Thank you.

Regulating in an Environment of Uncertainty

Remarks By

Commissioner James K. Asselstine

U.S. Nuclear Regulatory Commission

Before The

Twelfth Water Reactor Safety Research

Information Meeting

October 22, 1984

Good morning, ladies and gentlemen. It is a real pleasure to be with you today to participate in this twelfth water reactor safety research information meeting. At the outset, let me add my welcome to those you have already received to this conference. I would especially like to welcome our guests from other countries. The international exchange of ideas and information on the many significant safety topics to be discussed during these meetings is an important element of these sessions. We place great value on these exchanges, as well as on our ongoing international cooperative safety research efforts, and we hope that these sessions will be of benefit to you as well.

I have chosen as the topic for my remarks regulating in an environment of uncertainty. I want to focus my comments on one aspect of regulatory decisionmaking: The problem of new and rapidly changing regulatory requirements. I can think of no greater challenge facing us than the need to develop an approach to this aspect of nuclear regulation that fairly balances the need for greater stability with the recognition of

the many technical uncertainties that still exist concerning plant and human performance. This morning, I want to discuss two possible approaches to providing greater stability in nuclear regulation. I will characterize the first approach as the deregulation or regulatory reform approach. As I see it, this approach has two basic elements: significant reform of our licensing process; and a safety goal that relies heavily on probabilistic risk assessment techniques. The second approach would consider a new regulatory philosophy aimed at the root causes of the proliferation of new safety requirements that have been imposed in recent years.

For the past few years, the concepts of deregulation and regulatory reform have been in fashion in Washington, and the commercial nuclear power program has not remained unaffected. Many look to these concepts to provide greater stability in our regulatory program. The NRC, the nuclear industry and the Administration have all been avidly pursuing regulatory reform initiatives, which take the form of both legislative and administrative proposals. Many of these proposals really look to the future, and, if adopted, would have little impact on currently operating nuclear power plants or plants now under construction. However, a few would apply to the present generation of plants.

In their less controversial aspects, these proposals seek to establish a framework for future plant applications that would encourage the expanded use of more complete standardized plant designs in this country. Typically, these proposals would provide for the issuance of

standardized plant design approvals, early site permits that can be issued separate from a specific plant design, and combined construction permits and operating licenses that would resolve most, if not all, design questions prior to the start of plant construction. Although many of these provisions are useful and I have supported them , I have to say that given the absence of interest in new plant orders, they are less relevant today and probably for some years to come than are matters affecting the plants now in operation and under construction.

In their more controversial aspects, the various licensing reform proposals would have a direct and significant impact on the Commission's ability to impose new safety requirements and the extent of public involvement in our licensing process. Certainly the nuclear industry's first priority has been backfitting -- the process for imposing new safety requirements on existing plants. Backfitting proposals sponsored by the nuclear industry and the Administration seek to set a high safety threshold, to impose requirements for detailed written analyses, to establish requirements that imply the need for a quantifiable comparison of economic costs and safety benefits, and to set internal NRC review procedures that would apply to the Agency's consideration of any new generic or plant-specific requirement. In my judgment, these proposals would severely restrict the Commission's discretion to require new safety measures for existing plants, particularly in those cases in which the safety benefit of the measure is more judgmental in nature and cannot be precisely quantified.

A second category of more controversial licensing reform proposals involves changes to the NRC's hearing process for licensing nuclear power plants. These proposals attempt to eliminate altogether some opportunities for obtaining a hearing on significant safety and environmental issues. This would be the case, for example, for plant construction quality assurance issues, for emergency planning, and for issues regarding the qualifications of the plant operating staff under some of the proposals for the use of combined construction permits and operating licenses. The hearing proposals also attempt to change the type of hearing required from the present trial-type hearing to a more informal approach involving a combination of legislative-style and trial-type hearing procedures. In addition, some of the hearing proposals attempt to curtail the rights of public participants in the hearing by restricting their access to information, by imposing a higher threshold for the admission of contentions, by requiring the early filing of contentions before all relevant information is available and by restricting opportunities for cross-examination.

Still a third category of these licensing reform proposals involves changes to the internal management of the NRC licensing process. These include changes to the role of the NRC staff in licensing hearings, changes to the ex parte restrictions that prevent Agency decisionmakers from communicating privately with NRC staff members on issues that are in controversy in the hearings, changes to the internal appeal process for reviewing initial licensing board decisions, and changes to the

process by which the Commissioners personally review and approve the issuance of each full-power operating license for a nuclear power plant.

These licensing reform proposals have been accompanied by another recent reform initiative: A proposed safety Goal. The proposed safety goal would seek to establish numerical goals for reactor safety which focus mainly on near-term offsite health effects. The numerical nature of these goals necessitates reliance on probabilistic risk assessment techniques which our staff and the Advisory Committee on Reactor Safeguards contend may not be reliable for this purpose. Moreover, the narrow focus of the safety goals on near-term offsite health effects excludes other key bases for regulatory action such as onsite property losses and the broader public benefits in avoiding serious nuclear accidents.

Taken together, these more controversial "reform" proposals would result in a significant measure of deregulation. The Commission would be hampered to a considerable degree in its ability to impose new safety requirements for existing plants, and opportunities for public participation in the NRC licensing process would be much more limited. In those areas in which members of the public could still participate, their hearing rights would be much more narrowly defined. All of this would bring some measure of short-term stability to nuclear regulation by decreasing both the number of new NRC safety requirements and the uncertainty associated with licensing hearings. But those gains are likely to be transitory at best given the failure of these reform

measures to address the root causes that have led to the proliferation of new and changing regulatory requirements in recent years. Moreover, any short-term gains in regulatory stability will likely be accompanied by a substantial loss in public confidence in the Commission's ability to assure safety, in the basic fairness of our regulatory program, and ultimately, in the safety of the plants that we regulate. For these reasons, I conclude that the more controversial regulatory reform proposals do not provide a prudent or effective approach to nuclear regulations.

This does not mean that all efforts to improve the licensing process should be abandoned. Some regulatory reform measures can and should be adopted. These include a more modest legislative proposal that focuses on the less controversial elements of a licensing framework for future standardized designs. In addition, some measures to address backfitting are appropriate. These measures could establish a more formal and disciplined review process for new requirements that does not turn our staff into cost-benefit analysis writers and that avoids establishing artificial barriers to the adoption of justified safety improvements. Some improvements in the internal NRC management of the licensing process and in our hearing procedures could also be made. The focus of all of these changes should be on improving the quality of our safety and licensing decisions. However, by assuring sound decisions as early as possible in the licensing process, these measures will provide at least some additional measure of regulatory stability. But these gains

are likely to be gradual, and most evident in the case of any future plants.

Similarly, it may be useful to develop a workable answer to the question of how safe is safe enough. But any safety goal must include the full range of justifications for new regulatory requirements. In addition, my numerical safety goal must not depend upon bottom line PRA estimates of risk -- estimates which are still beyond the reliable capabilities of existing PRA techniques.

If sweeping changes to our licensing process are not the answer, I nevertheless see an alternative path to greater regulatory stability. That path would more directly address the problems that have led to the proliferation of new safety requirements and the manner in which those requirements have been imposed. At the same time, this approach would recognize the technical uncertainties that still exist in this area. But to better understand this approach, it is perhaps useful to spend a few minutes on the origins of the nuclear regulatory philosophy in this country and the positive and negative sides of the current nuclear safety ledger.

The first regulatory philosophy was formulated, in concert with congressional direction, in the mid-1950's. According to that philosophy, the AEC should impose the minimum amount of regulation while fulfilling its obligations to protect the public health and safety. To nurture further development of the technology in the private sector, the Federal

Government offered free R&D in government laboratories and waived certain loan charges to those utilities willing to undertake a demonstration project. These incentives and the regulatory philosophy behind them were justified on the ground that the private industry had assumed the economic risk of the proposed project. The initial regulatory philosophy of the 1950's and early 1960's was also premised on the AEC's excellent reactor safety record which, in turn, was based on careful, conscientious, and skillful operation; and adequate maintenance. In short the minimum regulatory philosophy was based on the assumption that each project would be done correctly, and would be done correctly the first time. As we began to learn more about the plants in the 1970's, it became apparent that some of the assumptions underlying the minimum regulation philosophy were incorrect. This led to an ever-increasing number of new and progressively more prescriptive requirements, regulations and reinterpretations. By far the greatest number of these occurred after the Three Mile Island accident.

In terms of the present safety ledger, I see several elements on the positive side. First, there has been a significant change in safety attitudes among our licensees since the TMI accident. Most, if not all, understand the enormity and complexity of the challenge they face in assuring the safe operation of the plants. Second, many of the post-TMI safety improvements are now in effect. More personnel are involved in plant operations, and they are better trained and qualified to deal with emergency situations. Emergency procedures, which are oriented toward understanding and responding to the symptoms of accident situations,

have been developed. Better accident diagnostic tools and instrumentation are now available. Emergency planning has been substantially improved. And some hardware changes have been developed to address specific accident problems. The success of many of these post-TMI efforts has been evident in utility responses to serious operating events such as those at Crystal River and Ginna.

Third, the nuclear industry has initiated a coordinated effort to improve operational performance. The centerpiece of this effort is INPO the Institute for Nuclear Power Operations. Finally, there has been generally good start-up experience for the new plants licensed since the Three Mile Island Accident. For operating reactors, plant operations have been generally successful, with some notable improvements in plants that had been consistently weak performers.

However, I also see several elements on the negative side of the safety ledger. Just as there have been some notable successes in the post-TMI period, there have been some notable failures. Examples are the Salem ATWS event, the Grand Gulf start-up program and the Zimmer construction quality assurance breakdown. Second, a number of post-TMI changes are taking much longer than anticipated. These include the Safety Parameter Display Systems, the Technical Support Centers, the Post Accident Sampling Systems and the Reactor Coolant Inventory instrumentation. The last item, in particular, probably will not be installed and operational in some plants until 10 years after the TMI accident.

Third, we are having great difficulty in resolving some lingering problems. Two examples are fire protection and the environmental qualification of electrical equipment. With regard to fire protection, we are now approaching four years after the adoption of the Commission's rule. Yet a substantial number of plants still do not comply and some utilities are still arguing over the requirements. Similarly, for environmental qualification, it is now nearly two years after the Commission issued its rule, and much of the equipment in operating plants has not been demonstrated to have the ability to withstand the effects of an accident environment and still perform its intended function.

Fourth, we are continuing to experience problems with plant equipment and components that significantly affect reliability and that are of potential safety significance. Two examples are pipe cracks for boiling water reactors and steam generator tube ruptures for pressurized water reactors. Fifth, the role of plant personnel continues to be a key factor in safety significant operating events. Personnel errors in maintenance and surveillance testing have become the principal contributor in about one-half of all abnormal occurrences reported to Congress by the NRC in the past few years.

A sixth problem area relates to acquiring and retaining qualified plant personnel, particularly licensed reactor operators. A number of utilities, including some with substantial nuclear operating experience, are having difficulty in putting together qualified operating crews for the

new plants. These utilities are experiencing particular difficulty in obtaining operators with previous licensed operating experience at a similar type of plant. As a result, some plants will begin operating without having any member of the licensed operating crew with any previous experience as a licensed reactor operator. In such cases, the industry has proposed, and the Commission has accepted, an approach that would rely on either the experience gained at a six-month visit to an operating plant or the use of non-licensed shift advisors with previous operating experience.

Finally, the Commission and the industry have not yet fully faced up to the severe accident question. The Three Mile Island accident demonstrated that a severe accident leading to large-scale degradation of the reactor core can occur. Despite this fact, NRC's principal severe accident efforts thus far have focused on future plant designs rather than on the roughly 120 plants now in operation or under construction. In addition, there is a disturbing tendency to emphasize procedural changes -- changes that would inevitably place a greater burden on plant operating personnel -- rather than to consider possible hardware modifications to prevent or mitigate the consequences of severe accidents.

What this all means to me is that we are not yet to the point that would justify a return to the minimum regulation approach of the 1950's and 1960's. We have much to do in addressing the safety problems we are now aware of, and I expect that we will continue to identify new ones. If

we continue with our current regulatory approach, we will be involved in a continual exercise to address the latest safety problem. This reactive approach to safety is likely to lead to further new requirements, prescriptive regulations and reinterpretations. The more extreme regulatory reform measures that I have described would only serve to postpone this result, perhaps with disastrous consequences.

Given this state of affairs, it seems prudent to consider alternative regulatory approaches that would put the Commission in a more active regulatory mode. Such a new regulatory philosophy might well include one or more of the following elements: a shift in regulatory focus to industry management; the establishment of reliability standards or performance objectives, particularly in areas of general weakness throughout the industry; increased emphasis on inherent safety, and the use of more creative NRC-industry relationships.

A key element in the success or failure of nuclear plant operation is the licensee's staff, management and organization. We ought to recognize this fact and target our regulatory efforts toward assuring effective, capable plant management with a strong commitment to safety as the first priority. We should give particular attention to the weak performers and we should reward the strong ones. Such an approach could effectively reduce the number of operating problems that have led to the development of new, prescriptive requirements in the past.

The development of more detailed reliability standards and performance objectives could help assure overall improvement in areas of weakness, while minimizing the potential for changing prescriptive requirements. I was particularly pleased to see that you have scheduled a session later this week on reliability assurance programs in non-nuclear areas. That session may provide some useful insights on the potential benefits of a reliability assurance program for nuclear plants.

Greater attention to inherent safety could both improve our overall assurance of the ability to prevent or mitigate severe accidents and minimize the need for subsequent prescriptive responses to individual plant operating events. It is clear that many other countries have given much greater weight to the benefits of inherent safety measures than we have. Finally, new relationships between the NRC and the industry, including the recognition of industry efforts such as INPO that are having demonstrated success and the use of designated Federal representatives within the industry, could help improve industry performance.

I see a significant continuing rule for safety research under such a new regulatory approach. A strong and effective safety research program can identify and address safety weaknesses before they are translated into serious operating events at the plants. Moreover, a strong research capability provides a necessary safety net to respond to unforeseen events when they do occur. Without this capability, significant operating events are much more likely to impact on plant operations. In

recent years, we have seen a substantial erosion in our safety research budget. This erosion has proceeded to the point where it now jeopardizes our capabilities to identify and correct weaknesses before they become serious safety problems, and to respond quickly to significant operating events. We must renew our efforts to preserve our research capability, and we must do a better job in explaining to the congress why a strong and effective research program is so essential.

Taken together, these elements of a new regulatory philosophy, together with a strong continuing safety research program, could perhaps more effectively address the types of problems that have led us to the present reactive and prescriptive approach to regulation. It seems to me that now is the time to think about constructive new approaches -- approaches that will not merely postpone problems but rather will solve them. Thank you.

# LWR Safety Research at JAERI

Ichiro Miyanaga
Japan Atomic Energy Research Institute
Tokyo, Japan

## ABSTRACT

JAERI initiated the LWR safety research in 1972 and later expanded to include a wide range of reactor safety aspects, i.e. fuel behavior, structural integrity, thermohydraulics, code development and environmental safety. However since the TMI-2 accident, reactor safety researches have been re-oriented to better understand a broad range of a rector accident including a severe accident. It is well recognized in the world that another accident like the TMI-2 would generate serious public concern on safety of a nuclear reactor no matter where it should happen. In that resepct, an international research collaboration should play an important role in the safety research field including not only evaluation of accident consequence, but also accident prevention and mitigation.

## INTRODUCTION

The water reactor safety research information meeting known as the WRSR information meeting has received a world recognition as an important meeting within nuclear community, especially among those who are engaged in water reactor safety researches in the world. For this respect, the United States Nuclear Regulatory Commission (USNRC) should be congratulated.

It was exactly ten years ago in 1974 when JAERI was invited for the first time to attend the second WRSR information exchange meeting that was held in Germantown and one of the safety research programs was introduced to USNRC.

At that time, JAERI was on the verge of extensive research activities on a light water reactor safety at the Reactor Safety Research Center which was established in 1973, the same year that the first WRSR information meeting was held.

In the past ten years, the WRSR information meeting evolved through several stages from early years of emphasizing the large break loss-of-coolant accident (LOCA) oriented researches to the recent developments in various safety aspects including severe accidents. During this evolution, the Three Mile Island Unit 2 (TMI-2) accident had a siginificant impact on reactor saferty research as everybody recognizes. To mention a few examples, small break LOCA and operational transient, human factors, man-machine interface, and severe accident evaluation are among the safety issues which have received considerable attentions since the TMI-2

accident. The increase of presentations on those safety issues in the past several years at this meeting show the indication of USNRC's emphasis on those isssues as the first priority. With that resepct, we are in the same track.

Another trend that could be recognized through the evolution of presentations is that contribution from foreign countries on reactor safety research have become a part of the WRSR meeting. JAERI's first contribution was the experimental result of hydrogen uptake due to oxidation at the inner surface of fuel cladding in 1978. Since then JAERI has participated in the meeting by presenting results of the ROSA experiment, the large scale reflooding experiment and other reactor safety researches performed at JAERI. This year should be earmarked by the fact that for the first time at this meeting, the Japanese industry will present results of their safety researches. The results should be another important contribution to the LWR safety.

As described in the above, the history of the WRSR information meeting coincided with the history of the Reactor Safety Research Center of JAERI, and this year is the tenth year since JAERI started to attend the WRSR meeting. It is appropriate at this time to review our research efforts and achievements on a light water reactor safety at JAERI in the past 12 years.

## LWR SAFETY RESEARCH

For the past 12 years since 1972, JAERI successfully conducted the ROSA-I, II and III experiments, all dealing with LOCA/ECCS (Emergency Core Cooling System) study for BWR and PWR, the containment spray experiments for PWR and BWR, the pressure suppression experiment for BWR Mark II containment, and several other small scale separate effect tests. During this period, the LWR safety research has been expanded to include a wide range of reactor safety aspects such as fuel behaviors, structural integrity, thermohydraulics, safety analysis and environmental safety.

The TMI-2 accident had a significant impact on reactor safety research at JAERI and it lead us to initiation of the ROSA-IV program, risk analysis and severe accident analysis program. Those research will not only quantify a potential risk and the safety margin of an LWR, but also provide informations on prevention and mitigation prcoedure of severe accidents. It is expected through the researches related to severe accidents that the anticipated public risk of a nuclear reactor accident will be shown to be much less than the currently estimated level.

Some of major achievements and the current status of JAERI's LWR safety research will be described in the following sections.

### Fuel Behavior

Objectives of safety research on fuel behavior are to confirm the itegrity of a fuel rod and to evaluate fission products (FP) release from

fuel pellet under normal operation, operational transient and accident conditions.

JAERI constructed a large scale fuel examination facility in 1978 to perform a post-irradiation examination (PIE) of fuel assemblies from commercial power reactors. With this faciliyt, a full size fuel assembly can be examined in place for various examinations. Among the findings with the facility was that a slight diameter decrement occurrs due to cladding creep-down during normal operation.

To clarify the dominant mechanism of pellet-cladding interaction (PCI) related to fuel failure, JAERI conducted in-pile experiments at the Japan Material Testing Reactor (JMTR) of JAERI, the Halden Reactor HBWR and the R2 reactor at Studsvik. The PCI failure threshold obtained from the power ramp experiments at Halden is shown in Figure 1. Relation between the fuel burnups and the ramp terminal power level is recognized in this figure. The experimental data were utilized for development and verification of the computer code FEMAXI-III (Fuel Element Modelling by Axisymmetric Finite Element Method). Comparison of the PCI-failure threshold predicted by the FEMAXI-III code and the results of the Halden overpower ramp experiment is shown in Figure 2. The FEMAXI-III code well predicted the PCI-failure bound. Development of the FEMAXI-III was completed and the FEMAXI-IV code is under development to extend calculational capability to include fuel behavior under operational transients.

For an investigation of fuel behavior under accident conditions, JAERI constructed the Nuclear Safety Research Reactor (NSRR) in 1975 and extensive studies more than 600 experiments on fuel behavior during reactivity initiated accident (RIA) have been carried out. Figure 3 shows the four basic failure mechanisms identified in the NSRR experiments. Cladding melt or brittle failure is a typical incipient failure mode in an RIA. This failure mode have been also experienced in PCM and LOCA conditions. Molten UO2 failure would occur if an energy deposition is larger than 380 cal/g.UO2. The third failure mode is high temperature cladding burst due to the difference between the internal and the external pressure. This could occur durint RIA and LOCA conditions. Low temperature cladding burst was experienced in the experiment for a water-logged fuel rod. The results have been incorporated in the new licensing guideline for an RIA analysis in 1984 as shown in Figure 4.

For the analysis of fuel behavior during RIA, the computer code NSR-77 was developed. The first version of the NSR-77 code has been in use for experiment prediction and anlaysis.

Having completed most of the RIA experiments, experiment on severe fuel damage using NSRR was initiated in 1983 and failure mechanism of fuel rod was investigated. During the tests, visual observation of the failure process was made possible with the optical system specially designed for taking high-speed motion pictures. The results provided us valuable informations to understand the failure mechanism of fuel under severe accident conditions.

The NSRR reactor will be modified for future test with an irradiated fuel rod.

Fuel cladding behavior under LOCA conditions has been focused on Zircaloy-steam reaction and ductility of the reacted zircaloy tubing, and the ballooning of the zircaloy cladding by internatl pressure. It was found that a ruputured cladding takes hydrogen as well as oxygen. The acceptable limit of cladding embrittlement including hydrogen uptate was established. This result was already introduced to the WRSR information meeting to support the present safety evalution criteria. Figure 5 shows that if oxidation is calculated with consideration of hydrogen uptake at less than 15 % by using the Baker-Just equation, the fuel rod does not fail during quenching by coolant water.

## Integrity and Safety of Pressure Boundary Components

In the safety researches on structural integrity, pressure boundary components of an LWR primary system were examined. There are four subprograms.

Fracture toughness was investigated for un-irradiated and irradiated steels for LWR pressure vessels as the IAEA coordinated research program. The crack growth rate of reactor structural steel was investigated under the influence of reactor water environment. The work was initiated in 1968 for predicting the life of flaw-containing steel used for pressure vessel lid of the Japan Power Demonstrating Reactor (JPDR) BWR at JAERI. One of the tests was conducted to evaluate the effect of sulfer content in steels. Typical results are shown in Figure 6. It showed that the larger the sulphur content is, the faster is the crack growth acceleration. It should be mentioned that sulphur content in steels used for Japanese reactor vessels are fortunately lower than other older reactors in the world.

Jet and pipe whip tests are still in progress to estimate the jet impingement force and jet thrust force, and to study the pipe whipping behavior under LOCA conditions of PWR and BWR. Growth behavior of fatigue cracks is also being investigated under cyclic bending loads.

As a part of safety research on a reactor component, research on the integrity of polymeric materials for reactor use was initiated in 1979 in order to study methodologies for the qualification testing of electric wires and cable under normal operation and LOCA conditions. The details will be presented in this meeting.

## Thermo-hydraulics in a Primary System

As described in the introduction, the LWR safety research at JAERI started with the ROSA program to investigate thermohydraulic behavior of primary coolant and ECCS behavior during LOCA. The research was later expanded to include reflood research, BWR suppression pool test and containment spray test.

The ROSA program consists of four phases . In the ROSA-I program, a vessel blowdown was investigated. In the ROSA-II program and the ROSA-III program, thermohydraulic behavior of coolant in the primary system during a LOCA were investigated by using the test facilities simulating a typical PWR and BWR, respectively. One of the result is shown in Figure 7 in which the peak cladding temperatures were shown with different break positions and sizes. It became clear that all the peak cladding temperaures are far below the maximum temperature of 1473 K specified for the safety evaluation.

Currently ongoing ROSA-IV program was initiated immediately after the TMI-2 accident. Objective of the program is to investigate a small break LOCA and operational transients including a mitigation procedure. The result would be an extremely important because not only it simulates the TMI-2 accident scenario but also the facility represents most important components of a nuclear reactor with a sizeable scale factor of 1/48. An international collaboration has been reached with USNRC. The similar collaboration with other countries is now under consideration. The details of the program will be presented during this meeting.

The research program on the reflooding during PWR-LOCA started in 1973 with a small scale separate effect test and later it became the large scale reflood test program which consists of the integral tests with the cylindrical core test facility (CCTF) and the separate effect tests with the slab core test facility (SCTF). This program has been conducted as the 2D/3D program based upon the tri-lateral agreement between Japan, Federal Republic of Germany and the United States of America.

The BWR pressure suppression pool test was performed between 1977 and 1983 to investigate the hydrodynamic load induced in the BWR Mark II containment system during a LOCA. The test result shown in Figure 8 demonstrates the conservatism of our licensing model for the pool level swelling velocity and elevation. The results also confirmed the "multi-vent effect", which refers to the decrease in the magnitude of condensation induced loads with the increase of volumetric scaling ratio of the facility.

The containment spray test was completed in 1982. The experiment was performed to obtain confirmatory data of the spray effectiveness under the design basis accident. The experimental result successfully showed that the containment spray currently installed in a typical BWR and PWR effectively reduces containment pressure and removes iodine in a containment under accident conditions.

## Code Development

In addition to the experimental programs, the code development program have been an important part of the LWR reactor safety research at JAERI. Major efforts of the code development till today have been to develop and verify LOCA evaluation codes. The code development program was initiated in 1973 when the deaprtment of nuclear safety evaluation was established in the Reactor Safety Research Center. Since then, the LOCA evaluation code system

was developed and most of the codes were verified. This table shows the summary of the present status of the code development.

It should be pointed out that some of the codes were transmitted to JAERI from USNRC and modifications and improvements have been made. One example is WREM-J2 which is now being used for licensing purposes.

Recently the code devlopment program has been shifted from LOCA/ECCS evaluation to operational transient type of events and severe accident analysis. For the operational transient type of events, the development of the MINCS code was initiated in 1982. For the severe accident analysis, the code development was initiated in 1983 with objectives of better quantifying a potential risk of a nuclear reactor and consequence of severe accidents.

In relation to the risk assessment of a nuclear reactor, the research program on probabilistic risk assessment methodology was initiated in 1980. Here reliability analysis, accident delineation and evaluation, accident and consequence analysis, integration of models, and standardization are the subject of the methodology development.

## Severe Core Damage Accident (SCD) Research

With the recognition of the lessons learned from the TMI-2 accident, severe core damage accident (SCD) has become one of major concerns on an LWR safety. JAERI has then initiated severe core damage research program and it was accelerated by participating in the USNRC's severe fuel damage (SFD) and fission products release and transport (FPRT) program in 1983.

Objectives of the SCD research at JAERI are to identify dominant phenomena which are anticipated to occur during severe accident of an LWR and to quantify a risk of a nuclear reactor Results of the experiments are expected to supplement the data obtained from the SFD and FPRT program.

## Evaluation and Analysis of Environmental Radioactivity

The research program related to an emergency planning for a nuclear reactor accident started in 1980. The program includes; development of aerial radiological survey system, development of models for predicting the concentration and environmental doses, and establishment of the code system, atmoshperic dispersion experiments for verification of the calculation models, and experimental study for preparing technical data for use in planning of emergency countermeasures.

As a part of the program, the computer code system SPEEDI (System for Prediction of Environmental Emergency Dose Information) has been developed. The main feature of the SPEEDI is to predict the dose information using an online computer as time to time basis as an accident proceeds as schematically shown in Figure 9.

Results of sample calculation are shown in Figures 10 through 12

Figure 10 shows the observed wind directions and speed at different locations which were transmitted from monitoring stations. With the statistical adjustment, horizontal wind field is drawn as shown in Figure 11. The atmospheric dispersion of released radioactive materials is simulated by a particle-in-cell model and a random-walk model with the assumption of a unit release. The external gamma dose equivalent is then predicted as shown in Figure 12 within several minutes after the system gets into operation.

The verification of the models in the SPEEDI system is being made with the results of atmospheric diffusion experiments and also with wind tunnel experiments.

## CONCLUSION

JAERI initiated the LWR safety research in 1972 and later expanded to include a wide range of reactor safety aspects which were rather strongly linked to the design basis accident. However since the TMI-2 accident, reactor safety researches have been re-oriented to better understand a wider range of a reactor accident including a severe accident.

In order to assure the safety of a nuclear reactor to public, we must recognize potential risk of a nuclear reactor and we must have enough knowledge of not only the consequence of accident, but also the prevention and mitigation. This is the reason for the need of reactor safety research.

We all aware that another accident like the TMI-2 would generate public concern on safety of a nuclear reactor no matter where it shoud happen. In that respect, an international collaboration should play an important role in the safety research field. For that reason, JAERI has already participated in several major international projects and have had bilateral or trilateral agreements with other countries as listed in Table 2.

# LWR SAFETY RESEARCH AT JAERI

Ichiro Miyanaga
Japan Atomic Energy Research Institute

Presented at the 12-th WRSR Information Meeting
October 22-26, 1984
Gaithersburg, Maryland, U.S.A.

## LWR SAFETY RESEARCH AT JAERI

- Fuel Behavior
  Normal Operation, Operational Transient and Accident Conditions
- Integrity and Safety of Pressure Boundary Components
- Thermohydraulic Behavior in a Primary System During LOCA
- Code Development
- SCD Research
- Evaluation and Analysis of Environmental Radioactivity
- International Collaboration Programs

## Fuel Behavior Research

- Normal Operation
- Operational Transient
- Accident Conditions



Figure 1

## Threshold of Failure by Ramp Experiments of Irradiated Fuels

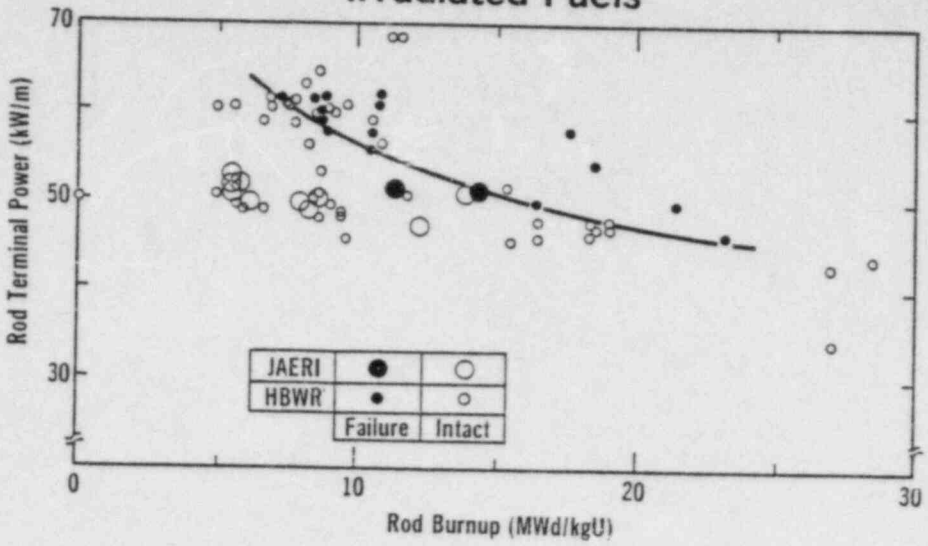


Figure 2

## PCI Failure Threshold Calculated by FEMAXI-III Code and Results from Halden Overpower Ramp Experiments

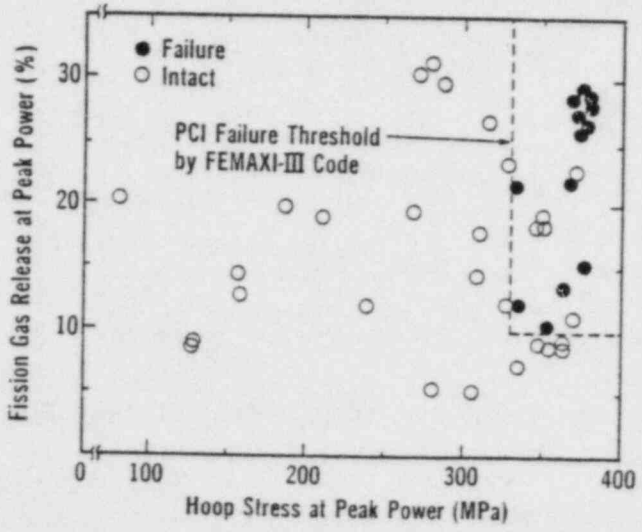

## Fuel Behavior under Accident Conditions

- RIA (Reactivity Initiated Accident)
- LOCA (Loss of Coolant Accident)

Figure 4

**Cladding Failure Limit as a Function of Fuel Rod Internal-External Pressure Difference**

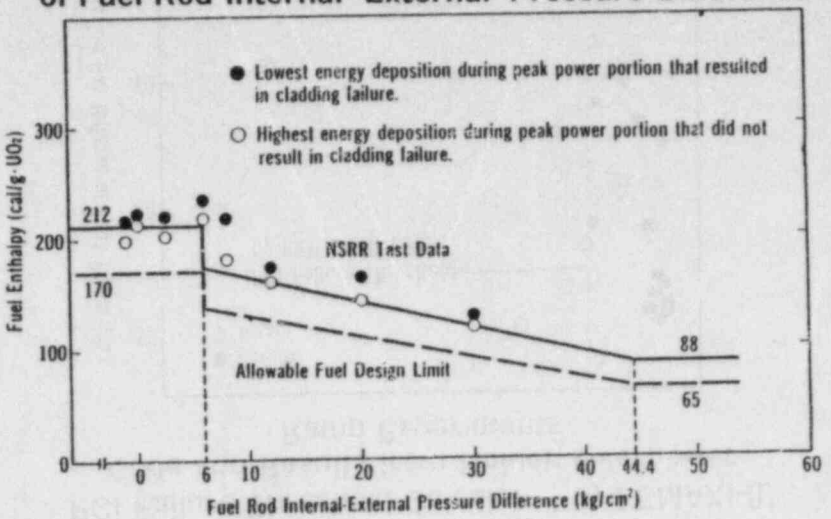




Figure 3

Fuel Failure Modes in Various Postulated Accidents

| Failure Mechanisms | Fuel Rod Appearances | Postulated Accidents | | |
|---|---|---|---|---|
| | | RIA | LOCA | PCM |
| Cladding Embrittlement | 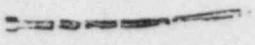 | ○ | ○ | ○ |
| Fuel Pellet Melting |  | ○ | | |
| High Temperature Cladding Burst |  | ○ | ○ | |
| Low Temperature Cladding Burst |  | ○ | | |

Figure 5

**Failure Map for Zircaloy-4 Cladding by Thermal Shock under Restrained Condition**

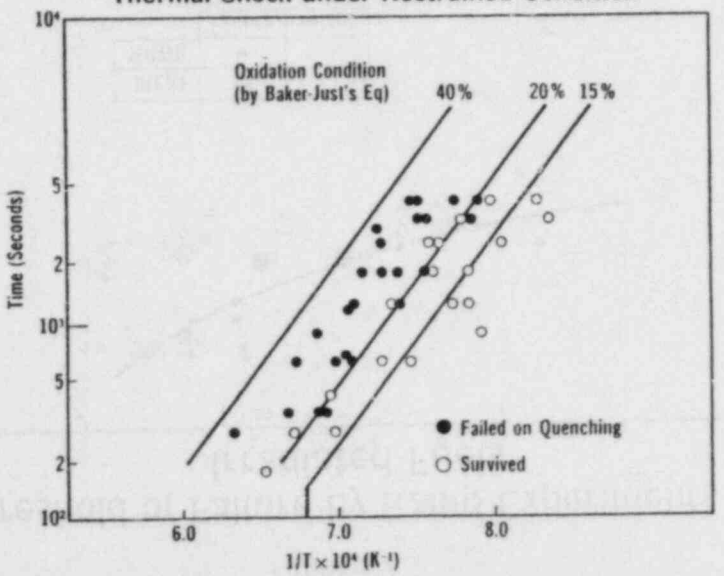

## Integrity and Safety of Pressure Boundary Components

- Fracture Toughness of Steels
- Environment-assisted Cracking of Pressure Boundary Components
- Jet and Pipe Whip Tests
- Growth Behavior of Fatigue Cracks

Figure 6

### Effect of Sulfer Content in Steel on Crack Growth Acceleration

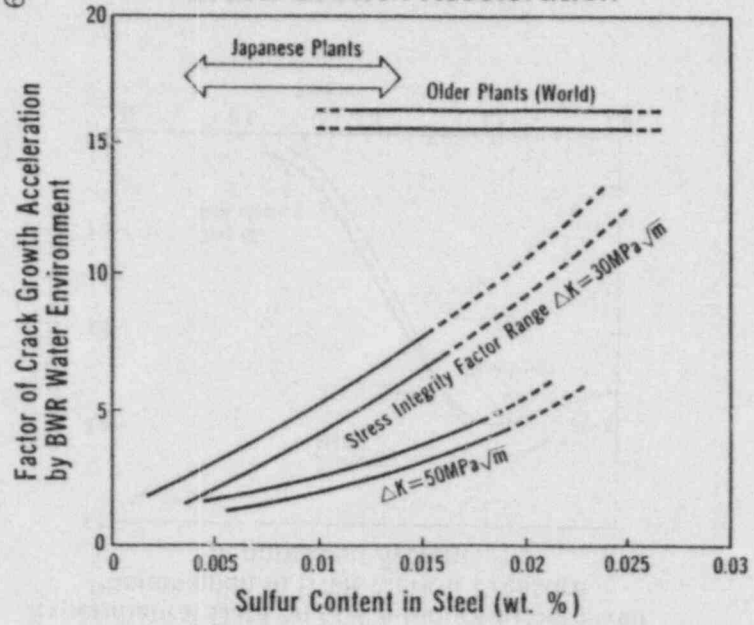




## Thermohydraulic Behavior in a Primary Circuit during LOCA

- ROSA Program
- Reflood Research Program
- BWR Pressure Suppression Pool Test Program
- Containment Spray Experiments

## ROSA Program

- ROSA-I Vessel Blowdown
- ROSA-II PWR LOCA
- ROSA-III BWR LOCA
- ROSA-IV PWR SBLOCA and Transients

Figure 7

### Peak Cladding Temperature of ROSA III Test without HPCS

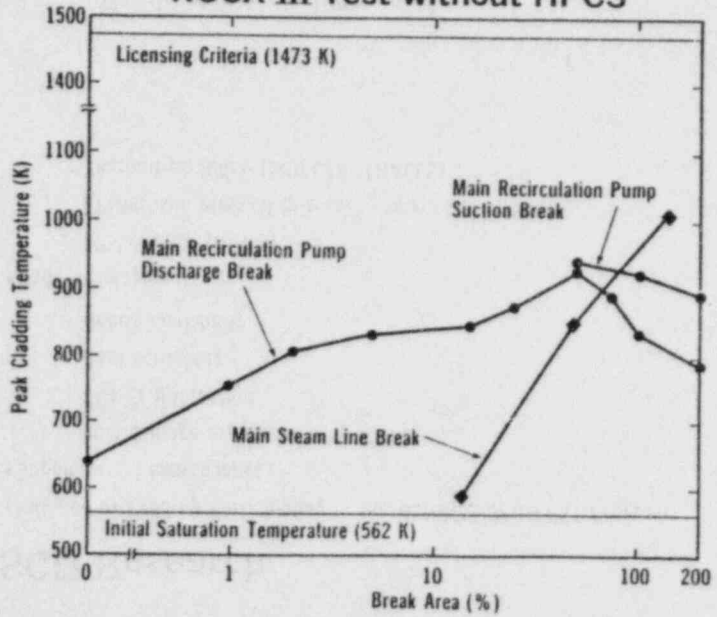

Figure 8

**Comparison between Model Prediction and Experimental Data on LOCA-Induced Pool Swell Phenomenon in BWR Mark-II Pressure Suppression System**

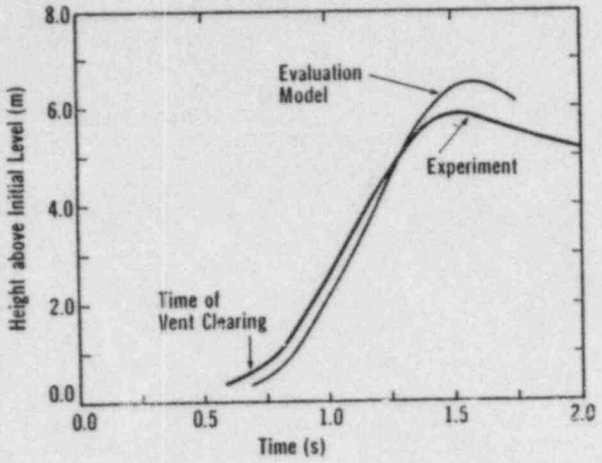




Table 1

## STATUS OF SAFETY EVALUATION CODE DEVELOPMENT AT JAERI

| Type of Event | Code name | Features | Status |
|---|---|---|---|
| LOCA/ECCS | JECCS-B2<br>ALARM-B2<br>THYDE-B1/Mod. 1<br>SCORCH-B2 | Evaluation of BWR ECCS Performance | Completed |
| | ALARM-P1 | PWR Blowdown | Completed |
| | THYDE-P | PWR LOCA | Completed |
| | WREM-J2 | JAERI Improved Version of WREM | Completed |
| | REFLA | PWR LOCA Reflood | Under Development |
| Miscellaneous Use | THYDE-W | Extension of THYDE-P | Under Development |
| | MINCS | Transient Two Phase Flow | Under Development |

## SCD Research

- Initiated in 1983 by Participating in the USNRC'S SFD/FPST Program.
- Supplemental experiments
  - ... Fuel damage experiments by NSRR
  - ... $UO_2$-Zr interaction
  - ... Pool scrubbing
  - ... Debris coolability
- Code development
  - ... FP behavior (HORN)
  - ... FP/Aerosol removal in a containment (REMOVAL)
  - ... Thermohydraulics (MUFLAR, THALES)

## Evaluation and Analysis of Environmental Radioactivity

- Development of aerial radiological survey systems.
- Development of models for predicting the concentration and environmental doses, and establishment of the code system.
- Atmospheric dispersion experiments for the model verification.
- Experimental study for preparing technical data.

## SPEEDI

- System for Prediction of Environmental Emergency Dose Information

Figure 9

## Computation Flowsheet in SPEEDI System

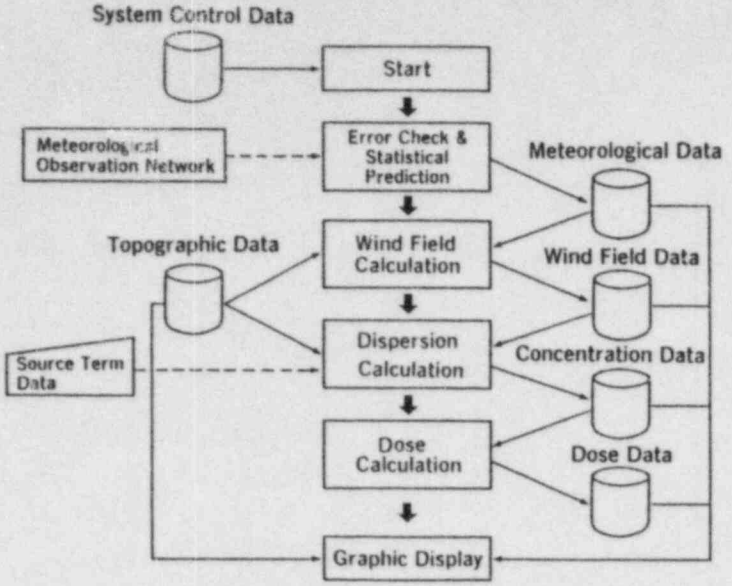


Figure 11

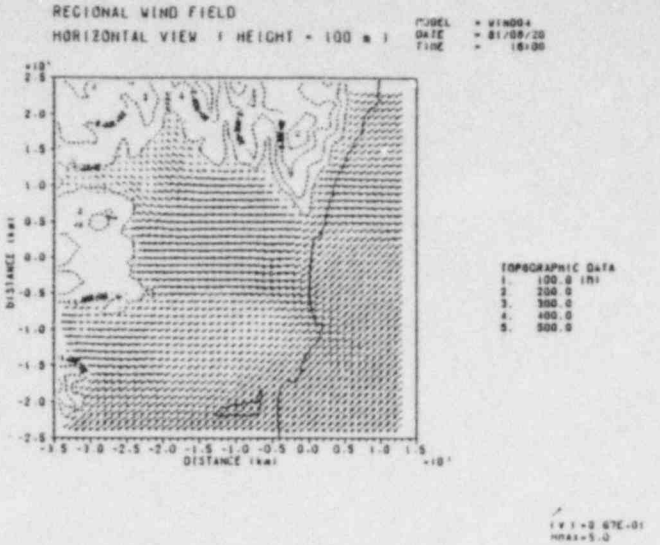


Figure 10

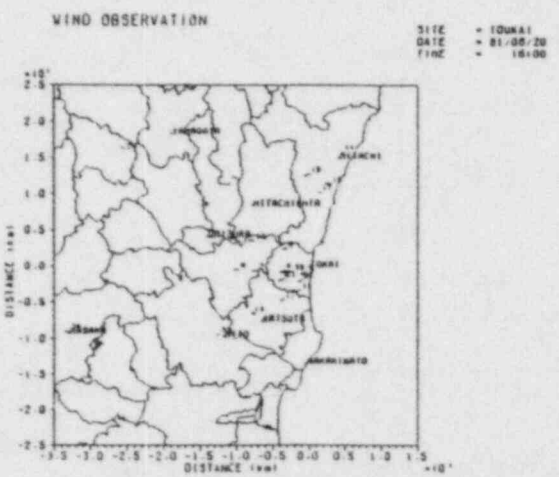


Figure 12

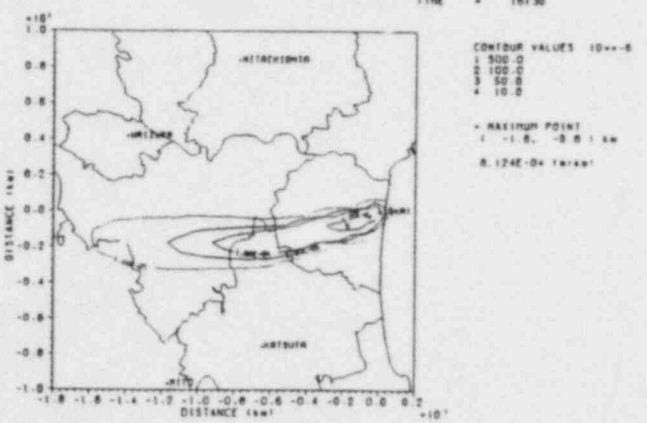

Table 2

## INTERNATIONAL COOPERATIVE PROGRAM FOR LWR SAFETY RESEARCH PARTICIPATED BY JAERI

| Research Area | Project Name | Host Organization | Periods |
|---|---|---|---|
| Fuel Interity Study | Halden | OECD/NEA | 1967 – 1987 |
| | HBEP | USDOE | 1980 – 1987 |
| Fuel Behavior under Accident Conditions | NSRR-Phebus | JAERI, CEA/Cadarache | 1981 – 1985 |
| Severe Fuel Damange | SFD | USNRC | 1983 – 1987 |
| | NSRR-PNS | JAERI, KFK | 1985 – 1988 |
| Integrity of Pressure Boundary Components | Steel Irradiation | IAEA | 1971 – |
| Engineered Safety Features of LOCA | 2D/3D | USNRC, BMFT, JAERI | 1980 – 1985 |
| | LOFT | OECD/NEA | 1983 – 1988 |
| | ROSA-IV | JAERI | 1983 – 1987 |

# INTRODUCTION TO THE SEMISCALE PROGRAM

By: Donald E. Solberg

As is often the case with overview presentations some of this may be repetitious to many of you. This presentation will provide a brief description of the Semiscale system, a referenceable tabulation of past testing, some precautions on the use of Semiscale data, our planned programs for 1985 and 1986, and our plans for developing an advanced thermal hydraulic integral systems facility, as indicated in Mr. Minogue's presentation.

Semiscale is a 1/1700 scale, electrically heated model of a 1100 Mwe 4 loop PWR. It has two loops, is scaled on the basis of power to volume ratio and has full elevation of components. It models all of the essential components in a PWR and is capable of operating at full pressure, temperature, and core power density of the large commercial reactors. It is extensively instrumented to provide data to increase our understanding, as well as to develop and validate analysis models for the wide range of transients that can be conducted in the facility.

The Semiscale testing program was initiated in 1968, and based on current plans, will complete testing in 1986 and be shutdown in 1987. Throughout this history, the design has been changed many times. This includes extensive system design changes in 1984 that were needed to perform the steam line/feedwater line break experiments in 1985, and may also involve additional changes for planned tests in 1986. The first five slides give you an overview of the range of testing and major design modifications associated with each test series since late 1974. As you can see the slides identify and define the test series, the principal experimental variables, the range of dates over which each series was run, identifies the system mod in which the tests were performed and is keyed to the list of Quick-Look Reports that is provided at the end of this paper. One objective of the presentation is to provide attendees and others who receive the tranactions of these meetings with a handy

list of references for the entire series; in 1986, as the program nears completion, it is our intent to have the contractor prepare a summary report which discusses the most important lessons learned from all of these Semiscale tests, and provides a more complete set of references for use by future researchers.

From the NRC perspective, Semiscale has been one of our most valuable experimental systems for developing timely and credible response data for the evaluation of regulatory issues. It is essential to recognize and make allowances for the distortions in the transient responses that result from a system of this small scale and scaling approach. The overall experimental objectives are to provide a transient response in which important phenomena are representative of those occurring in the commerical reactors and that they occur in real time. It is not recommended that a direct correlation between Semiscale and the commerical PWR response be made. Rather Semiscale data should be used to evaluate system code capability and then these codes used to predict LWR responses.

In 1984, the steam generator tube rupture test series was completed. The next paper by Dr. Shaw will discuss this series. In addition, two severe accident sequence boiloff experiments were performed with EPRI funding. The last slide presents planned activities and schedule for 1985. A total of six secondary system steam line/feedwater line breaks are planned. These will be selected shortly from those described in Dr. Wolf's paper that follows. In addition, final reports will be published during the year for the offsite power loss and steam generator tube rupture test series. Finally, the planning for 1986 testing including an evaluation of desgin modifications and improvements, if required, will be initiated.

Three small test series are planned for 1986, each consisting of two tests. The first will provide data on small break LOCAs without high pressure emergency core coolant injection to evaluate effectiveness of operator actions for safe recovery. The second will provide data on large break LOCAs with upper head emergency core coolant injection simulating the Westinghouse design. The final series will provide two tests in Semiscale which will duplicate tests

in the LOBI and ROSA-IV facilities for use in an international evaluation of scaling effects.

As it may become apparent to you from the presentations that follow, NRC's system experimental facilities are scheduled to be shutdown by 1987. Therefore, we are examining systems research data needs beyond 1987 and the associated research facility requirements for providing that data. Need for both operations and thermal/hydraulic research beyond 1987 has been expressed by the NRC licensing staff, as well as by a wide range of industry management. Two studies were performed for RES in 1984 to evaluate future systems research needs and to provide facility cost estimates. These studies are currently being distributed for review and comment. Further studies are planned in 1985 to define and prioritize specific research needs, develop facility criteria, and provide a recommended design basis, as needed to initiate detailed design work in 1986. The program objective is to develop a flexible research facility that will be capable of generating research data needed to resolve a wide range of future generic LWR systems safety and operational issues.

# Semiscale Experiments

| Date | Mod | Series | Principal Variables | QLR Ref |
|---|---|---|---|---|
| Oct-Dec 1974 | 1 | S-01<br>Isothermal Blowdown with Core Simulator 200% Break | Pressure, ECC Injection Location, Loop Resistance PCP Trip, LP Volume | 1-8 |
| Apr-Oct 1975 | 1 | S-02<br>Blowdown Heat Transfer Tests 200% Break | Break Location, Radial Power Shape, Core Power, Core Flow, PCP Trip, ECC | 9-18 |
| Jan-Mar 1976 | 1 | S-03<br>Reflood Heat Transfer Tests | Reflood Rate/ECC Flow Rate Core Power, Radial Power Profile, Pressure, Initial Rod Temp, ECC Subcooling | 19-28 |
| Apr-May 1976 | 1 | S-29<br>Integral Blowdown Reflood Tests | Break Size, Pressure Radial Power Profile | 29-30 |

WRR8488-1

# Semiscale Experiments (cont'd)

| Date | Mod | Series | Principal Variables | QLR Ref |
|---|---|---|---|---|
| May-Sep 1976 | 1 | S-04<br>Baseline ECC Experiments<br>200% Cold Leg Break | Radial Power Profile, Lower Plenum Volume<br>ECC Injection Rates | 31-34 |
| Oct 76 - Mar 77 | 1 | S-05<br>Alternate ECC Injection Tests<br>200% Cold Leg Break | Core Flow, Lower Plenum Volume, ECC Location and Flow Rate | 35-41 |
| Apr-May 1977 | 1 | S-06<br>LOFT LBLOCA Counterpart Tests<br>200% Cold Leg Break | Core Power<br>PCP Trip | 42-46 |
| Jun-Sep 1977 | 1 | S-28<br>LBLOCA with Steam Generator Tube Rupture<br>200% Cold Leg Break | Number of Tubes<br>Time of Tube Rupture | 47-51 |

WRR8466-2

# Semiscale Experiments (cont'd)

| Date | Mod | Series | Principal Variables | QLR Ref |
|---|---|---|---|---|
| Jun 78 - Apr 79 | 3 | S-07<br>Mod-3 Baseline Tests | ECC Location and Subcooling<br>Containment Pressure,<br>Power Profile, PZR Location,<br>PCP Trip, $N_2$ Injection | 52-59 |
| Sep-Oct 79 | 3 | S-UHD<br>Upper Head Drain Tests | UHI Temperature | 60 |
| Nov 79 - Apr 80 | 3 | S-SB<br>Small Break Tests | Break Size, Core Power<br>Heat Losses, PCP Trip,<br>Break Location | 61-67 |
| May 1980 | 3 | S-TR<br>Station Blackout Tests - Planning for Mod-2A Tests | Test Duration | 68 |

WRR8455-3

# Semiscale Experiments (cont'd)

| Date | Mod | Series | Principal Variables | QLR Ref |
|---|---|---|---|---|
| Dec 80 - Apr 81 | 2A | S-UT<br>Small Break LOCA with UHI | Break Size<br>w/wo UHI<br>w/wo Guard Heaters<br>UHI Pressure | 69-74 |
| Jun-Nov 1981 | 2A | S-NC<br>Natural Circulation Tests | System Inventory, No. Loops<br>Secondary Pressure<br>$N_2$ Injection, Recovery Procedures, ECC Injection<br>Guard Heaters | 75-83 |
| Jan-Feb 1982 | 2A | S-IB<br>Intermediate Break Tests | Break Size, Core Power, HPIS | 84-86 |
| Jun 1982 | 2A | S-SR<br>Primary Feed and Bleed during Natural Circulation | SI Pressure | 87 |

WRR8455-4

# Semiscale Experiments (cont'd)

| Date | Mod | Series | Principal Variables | QLR Ref |
|---|---|---|---|---|
| Jul-Sep 1982 | 2A | S-SF<br>Secondary Feed and Steam Line Break Tests | Break Size and Location<br>Core Power, Inventory, Recovery Procedure | 88-89 |
| Jan-Jun 1983 | 2B | S-PL<br>Power Loss Tests | Recovery Procedure<br>w/wo SCRAM<br>w/wo SBLOCA<br>w/wo Aux Feed<br>Time to Restore Emergency Power | 90-94 |
| Aug 83 - Mar 84 | 2B | S-SG<br>Steam Generator Tube Rupture Tests | No. Tubes, RCP Trip, Recovery Procedure, Loss of Power, ECC | 95-103 |
| Apr 1984 | 2B | S-PBO<br>Primary System Boiloff Tests (EPRI) | w/wo SBLOCA | 104 |

WRR8455-5

# FY-85 Semiscale Schedule

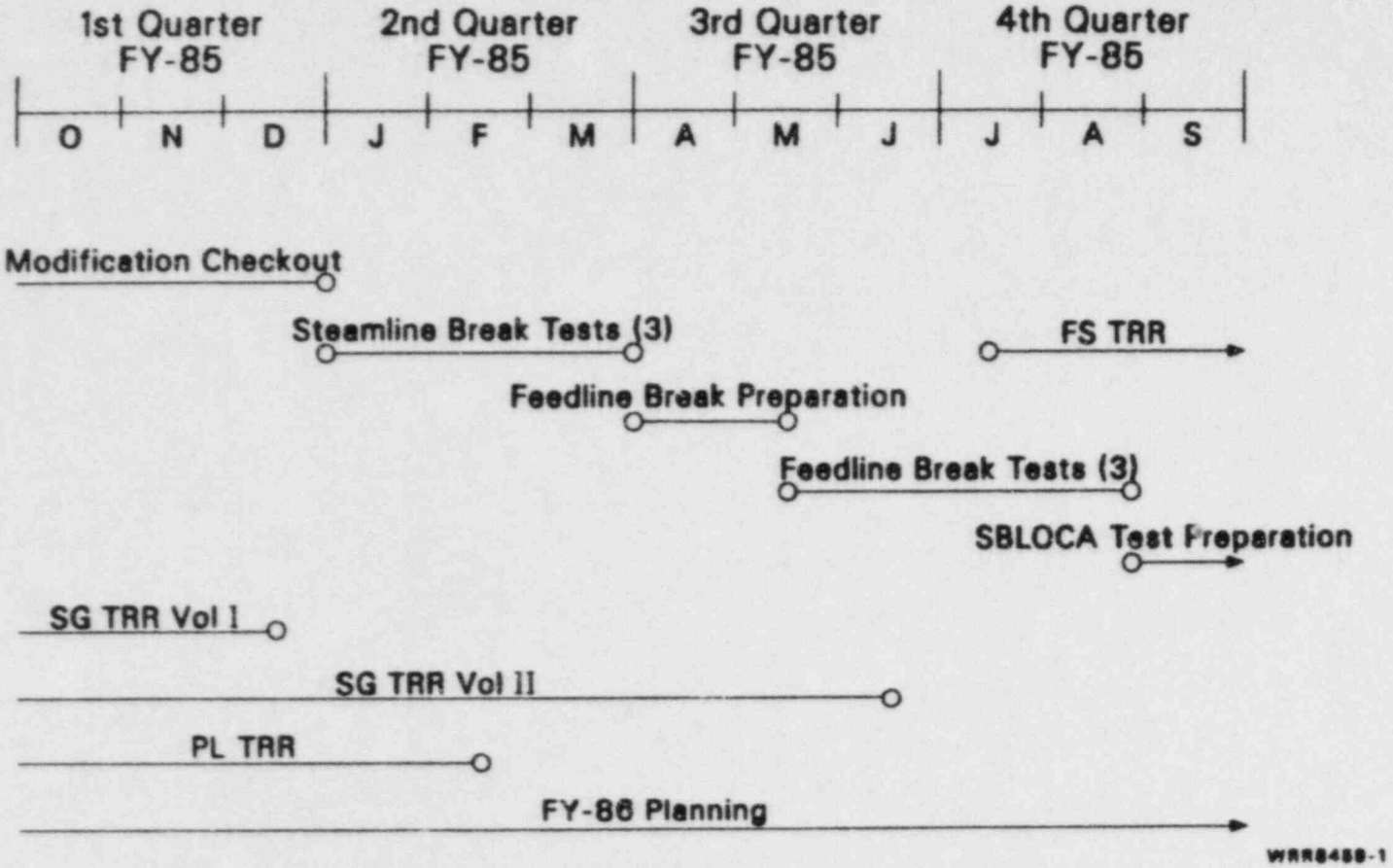

## REFERENCES TO SEMISCALE QUICK LOOK REPORTS

| Ref. No. | Letter or Report No. | Date | Author | Experiments Referenced |
|---|---|---|---|---|
| 1 | Zan-134-74 | 12/4/74 | Cartmill | S-01-1 |
| 2 | Zan-141-74 | 12/16/74 | Cartmill | S-01-1B |
| 3 | Zan-83-74 | 9/3/74 | Cartmill | S-01-2 |
| 4 | Zan-108-74 | 10/29/74 | Cartmill | S-01-3 |
| 5 | Zan-121-74 | 11/12/74 | Cartmill | S-01-4 |
| 6 | Zan-147-74 | 12/20/74 | Cartmill | S-01-4A |
| 7 | Zan-123-74 | 11/14/74 | Cartmill | S-01-5 |
| 8 | Zan-125-75 | 7/16/75 | Cartmill | S-01-6 |
| 9 | Zan-77-75 | 5/7/75 | Larson | S-02-1 |
| 10 | Zan-94-75 | 5/23/75 | Larson | S-02-2 |
| 11 | Zan-111-75 | 6/10/75 | Larson | S-02-3 |
| 12 | Zan-189-75 | 9/19/75 | Larson | S-02-4 |
| 13 | Zan-206-75 | 10/15/75 | Larson | S-02-5 |
| 14 | Zan-273-76 | 11/5/76 | Snider | S-02-6 |
| 15 | Zan-170-75 | 9/2/75 | Larson | S-02-7 |
| 16 | Zan-19-76 | 1/22/76 | Langerman | S-02-8 |
| 17 | Zan-220-75 | 10/30/75 | Larson | S-02-9 |
| 18 | Zan-210-75 | 10/21/75 | Larson | S-02-9A |
| 19 | Zan-10-76 | 1/13/76 | Peterson | S-03-1,2 |
| 20 | Zan-22-76 | 1/28/76 | Peterson | S-03-3 |
| 21 | Zan-28-76 | 1/30/76 | Peterson | S-03-4 |
| 22 | Zan-66-76 | 3/19/76 | Peterson | S-03-5 |
| 23 | Zan-76-76 | 3/30/76 | Peterson | S-03-6,7 |
| 24 | Zan-59-76 | 3/10/76 | Peterson | S-03-8 |
| 25 | Zan-52-76 | 2/27/76 | Peterson | S-03-A |
| 26 | Zan-46-76 | 2/19/76 | Peterson | S-03-B |
| 27 | Zan-41-76 | 2/12/76 | McCreery | S-03-C |
| 28 | Zan-45-76 | 2/19/77 | McCreery | S-03-D |
| 29 | Zan-102-76 | 5/6/76 | Tomasko | S-29-1 |
| 30 | Zan-126-76 | 5/28/76 | Cozzuol | S-29-2,3 |
| 31 | Zan-138-76 | 6/4/76 | Cozzuol | S-04-1 |
| 32 | Zan-152-76 | 6/14/76 | Cozzuol | S-04-2 |
| 33 | Zan-180-76 | 8/23/76 | Cartmill | S-04-3,4 |
| 34 | Zan-250-76 | 10/15/76 | Cozzuol | S-04-5,6 |

References to Semiscale Quick Look Reports (Cont'd.)

| Ref. No. | Letter or Report No. | Date | Author | Experiments Referenced |
|---|---|---|---|---|
| 35 | Zan-278-76 | 11/11/76 | Hanner | S-05-1 |
| 36 | Zan-287-76 | 11/19/76 | Peterson | S-05-2 |
| 37 | Zan-13-77 | 1/14/77 | Harvego | S-05-2A,2B |
| 38 | Zan-309-76 | 12/15/76 | Harvego | S-05-3 |
| 39 | Zan-298-76 | 12/3/76 | Peterson | S-05-4 |
| 40 | DJO-12-77 | 1/28/77 | Harvego | S-05-5 |
| 41 | DJO-73-77 | 3/24/77 | Harvego | S-05-6,7 |
| 42 | DJO-96-77 | 4/29/77 | Cozzuol | S-06-1,2 |
| 43 | DJO-63-78 | 5/23/78 | Langerman | S-06-3 |
| 44 | DJO-195-77 | 9/22/77 | Langerman | S-06-4 |
| 45 | DJO-61-77 | 3/17/77 | Cozzuol | S-06-5 |
| 46 | DJO-124-77 | 6/2/77 | Langerman | S-06-6 |
| 47 | DJO-151-77 | 7/6/77 | Cozzuol | S-28-1,2 |
| 48 | DJO-162-77 | 7/27/77 | Cozzuol | S-28-3,4 |
| 49 | DJO-179-77 | 8/19/77 | Cozzuol | S-28-5 |
| 50 | DJO-192-77 | 9/9/77 | Hanner | S-28-6 |
| 51 | DJO-199-77 | 9/30/77 | Cozzuol | S-28-7-12 |
| 52 | DJO-90-78 | 7/10/78 | Hanson | S-07-1 |
| 53 | DJO-99-78 | 8/1/78 | Hanson | S-07-2 |
| 54 | DJO-107-78 | 8/22/78 | Cozzuol | S-07-3 |
| 55 | DJO-78-78 | 6/19/78 | Harvego | S-07-4 |
| 56 | DJO-116-78 | 9/11/78 | Hanson | S-07-5 |
| 57 | DJO-127-78 | 10/9/78 | Cozzuol | S-07-6 |
| 58 | DJO-63-79 | 5/23/79 | Hanson | S-07-8,9 |
| 59 | EGG-SEMI-5201 | 7/80 | Shimeck | S-07-10 |
| 60 | EGG-SEMI-5018 | 10/79 | Cozzuol | S-UHD-1,2 |
| 61 | EGG-SEMI-5062 | 11/79 | Fauble | S-SB-4,4A |
| 62 | EGG-SEMI-5073 | 12/79 | Cozzuol | S-SB-2 |
| 63 | EGG-SEMI-5113 | 3/80 | Fauble | S-SB-2A |
| 64 | EGG-SEMI-5137 | 4/80 | Dingman | S-SB-P1,P2,P7 |
| 65 | LPL-55-80 | 4/17/80 | Leach | S-SB-P3 |

References to Semiscale Quick Look Reports (Cont'd.)

| Ref. No. | Letter or Report No. | Date | Author | Experiments Referenced |
|---|---|---|---|---|
| 66 | LPL-58-80 | 4/22/80 | Leach | S-SB-P4 |
| 67 | LPL-61-80 | 4/25/80 | Leach | S-SB-P6 |
| 68 | EGG-SEMI-5227 | 8/80 | Hanson | S-TR-1,2 |
| 69 | EGG-SEMI-5331 | 1/81 | Blakeley | S-UT-1 |
| 70 | EGG-SEMI-5333 | 1/81 | Blakeley | S-UT-2 |
| 71 | EGG-SEMI-5429 | 4/81 | Shimeck | S-UT-4 |
| 72 | EGG-SEMI-5431 | 4/81 | Shimeck | S-UT-5 |
| 73 | EGG-SEMI-5446 | 5/81 | Cozzuol | S-UT-6 |
| 74 | EGG-SEMI-5442 | 5/81 | Hanson | S-UT-7 |
| 75 | EGG-SEMI-5492 | 7/81 | Loomis | S-NC-1 |
| 76 | EGG-SEMI-5507 | 7/81 | Loomis | S-NC-2B |
| 77 | EGG-SEMI-5522 | 8/81 | Loomis | S-NC-3 |
| 78 | EGG-SEMI-5549 | 8/81 | Soda | S-NC-4B |
| 79 | EGG-SEMI-5591 | 9/81 | Soda | S-NC-5,6 |
| 80 | EGG-SEMI-5639 | 10/81 | Shimeck | S-NC-7C |
| 81 | EGG-SEMI-5678 | 12/81 | Loomis | S-NC-8A,8B |
| 82 | EGG-SEMI-5679 | 11/81 | Shimeck | S-NC-9 |
| 83 | PN-130-81 | 10/9/81 | North | S-NC-10 |
| 84 | EGG-SEMI-5859 | 4/82 | Stephens | S-IB-1 |
| 85 | EGG-SEMI-6021 | 8/82 | Stephens | S-IB-2 |
| 86 | EGG-SEMI-6013 | 8/82 | Boucher | S-IB-3 |
| 87 | EGG-SEMI-6022 | 9/82 | Shimeck | S-SR-1,2 |
| 88 | EGG-SEMI-5940 | 7/82 | Shimeck | S-SF-1,2,3 |
| 89 | EGG-SEMI-6079 | 11/82 | Berglund | S-SF-4,5 |
| 90 | EGG-SEMI-6227 | 4/83 | Wolf | S-PL-1 |
| 91 | EGG-SEMI-6180 | 4/83 | Chapman | S-PL-2 |
| 92 | EGG-SEMI-6429 | 10/83 | Wolf | S-PL-3 |
| 93 | EGG-SEMI-6314 | 6/83 | Chapman | S-PL-4 |
| 94 | EGG-SEMI-6330 | 7/83 | Chapman | S-PL-7 |
| 95 | EGG-SEMI-6395 | 9/83 | Loomis | S-SG-1 |
| 96 | EGG-SEMI-6405 | 9/83 | Loomis | S-SG-2 |
| 97 | EGG-SEMI-6526 | 2/84 | Loomis | S-SG-3 |
| 98 | EGG-SEMI-6560 | 3/84 | Owca | S-SG-4 |

References to Semiscale Quick Look Reports (Cont'd.)

| Ref. No. | Letter or Report No. | Date | Author | Experiments Referenced |
|---|---|---|---|---|
| 99 | EGG-SEMI-6448 | 11/83 | Owca | S-SG-5 |
| 100 | EGG-SEMI-6571 | 4/84 | Loomis | S-SG-6 |
| 101 | EGG-SEMI-6471 | 12/83 | Loomis | S-SG-7 |
| 102 | EGG-SEMI-6597 | 4/84 | Owca | S-SG-8 |
| 103 | EGG-SEMI-6590 | 4/84 | Loomis | S-SG-9 |
| 104 | EGG-SEMI-6626 | 5/84 | Owca | S-PBO-1,2 |

# Analogy of LOBI-MOD1 and LOFT System Responses to DECL Break LOCEs

C. Addabbo, L. Piplies, W. L. Riebold
Commission of the European Communities
EURATOM - Joint Research Centre - Ispra Establishment
Thermodynamics Division - LOBI Project
I-21010 ISPRA (I)

## INTRODUCTION

The validation of system codes used in the safety analysis of nuclear power plants has to rely on experimental data from scaled, separate effects or integral system test facilities. The acquisition of experimental data from full size plants is, in fact, mainly confined to operational transients whilst it is rather limited or even precluded in accident conditions for obvious economical reasons and practical considerations.

Experimental investigations relevant to water reactor safety research have been either performed or planned for execution in various test facilities. Although detailed information on specific phenomena governing the thermal-hydraulic behaviour of individual plant components may be best acquired in separate effects test facilities, it is maintained that a systematic assessment of large system codes has to be based on experimental data from integral system test facilities to account for the dynamic coupling between major system components especially in transient conditions.

Characteristic features of the most important integral system test facilities operating in the full pressure range for the investigation of loss-of-coolant accident (LOCA) and anticipated transient conditions in pressurised water reactors (PWRs) are summarised in Table 1. To a certain extent, each facility differs in scaling and design criteria to satisfy specific simulation and operational requirements envisaged in the companion experiment programmes. Basically, however, they represent variants of the same reactor system and hence have inherent configurational and operational similarities.

It is generally recognised that direct application or extrapolation of experimental data acquired in scaled test facilities to the safety evaluation of large PWRs is impaired by distortions in the transient behaviour of certain components which may arise from design decisions,

technical feasibility and operational constraints. Problems of scaling and extrapolation of experimental results in the area of fluid flow and heat transfer related to reactor safety analysis have been dealt with in several technical reports and conference papers /1,2,3,4,5/. In order to assess the typicality of experimental data from facilities which are not full size, it is emphasised that it would clearly be beneficial if the phenomena they represent were shown to be not test facility dependent.

Among all test facilities which have provided experimental data relevant to a LOCA and related emergency core cooling system (ECCS) performance in PWRs, the LOFT facility is unique for its nuclear characteristics. All other test facilities, including LOBI, use electrically heated rods and a proper transient power curve has to be established to simulate the nuclear heat source. Evaluation of the relative thermal-hydraulic behaviour of the LOBI-MOD1 and LOFT test facilities in double ended cold leg (DECL) break loss-of-coolant experiments (LOCEs) has shown, however, a rather remarkable phenomenological analogy especially with respect to core thermal response during the early blowdown phase. The aim of the present paper is to highlight relevant similarities as well as differences identified in the thermal-hydraulic response of the two facilities during tests having common specific objectives.

## THE LOBI AND LOFT TEST FACILITIES

The LOBI Test Facility is a high pressure integral system blowdown-refill test facility designed, constructed and operated in the Joint Research Centre of the European Communities, Ispra Establishment, Italy. It was commissioned in December 1979 and was operated until June 1982 in the MOD1 configuration /6/ providing data for the large break LOCA scenario. It was then extensively modified to accommodate new programme requirements leading to the present MOD2 configuration /7/.

The LOBI test facility is an approximately 1:712 scale model of a four-loop 1300 MWe PWR of KWU design and has two active primary loops. The simulated core consists of a full length direct electrically heated 64 rod bundle arranged in a 8 x 8 square matrix inside the pressure vessel model. The heater rods have a cosine-shaped axial power profile with a maximum linear heat generation rate of about 212 W/cm at a nominal heating power of 5.28 MW. Lower plenum, upper plenum and an annular downcomer are additional major components of the reactor model assembly. The LOBI-MOD1 test facility was originally configured with a 50 mm downcomer gap width which was later replaced with one of 12 mm to assess the downcomer scaling problem which is well known for the conflicting requirements needed to preserve the governing physical phenomena during the various phases of a LOCA. The test facility in its MOD1 configuration was operated at normal PWR conditions of 290°/323°C and 155 bar on the primary side and 210°C feedwater temperature and 54 bar on the secondary side.

The LOFT Test Facility design features and operational characteristics have been extensively documented in open literature /8,9/. For completeness, a brief description will be given here.

The LOFT facility is a fully operational PWR designed for experimental

investigations during off-normal conditions caused either by rupture of the pressure boundary or by intact circuit faults. It is approximately a 1:50 scale model of a commercial PWR and is operated by EG&G Idaho, Inc., at the Idaho National Engineering Laboratory for the United States Nuclear Regulatory Commission. At normal power level, the maximum linear heat generation rate is about 400 W/cm.

A comparison of LOBI-MOD1 and LOFT system configuration and major components characteristics is given in Table 2. The two facilities differ substantially in heating method, core length and axial power profile (Fig.1).

DECL BREAK LOCEs IN LOBI-MOD1 AND LOFT

Data from the two facilities, either measured (pressure, temperature, etc) or computed (mass flows) are compared in this section. The reference period is the early blowdown phase of a 2A DECL break LOCE. Due to differences in the configuration of the ECCS in LOBI-MOD1 and LOFT, the comparison is rather restricted following tripping of the accumulator injection system (42 bars in LOFT, 27 bars in LOBI-MOD1). Clearly, this comparative analysis is not exhaustive; it is phenomena oriented and hence emphasis is placed on qualitative rather than quantitative similarities in the relative thermal-hydraulic response of the two facilities. Data from the following tests, which to a certain extent are directly comparable in specific objectives as well as in initial and boundary conditions, are considered:

| | Test | MLHGR* (W/cm) | Break Size | Relevant Description |
|---|---|---|---|---|
| LOBI | A1-06 | 213 | 2A DECL | LOCE with early intact loop pump coastdown (Fig.2). Speed simulation of pump in reference plant |
| | A1-72 | 211 | " | LOCE with delayed intact loop pump coastdown (Fig.2). Head simulation of pump in reference plant |
| LOFT | L2-3 | 390 | " | LOCE with intact loop pump running throughout (Fig.2) |
| | L2-5 | 400 | " | LOCE with atypical intact loop pump coastdown (Fig.2) |

* MLHGR: Maximum Linear Heat Generation Rate

## TABLE 1 : PWR HIGH PRESSURE INTEGRAL SYSTEM TEST FACILITIES

| Facility | Volume scale | Power (MWth) | Configuration | | Remarks | Country |
|---|---|---|---|---|---|---|
| | | | Loops | Downcomer S** (mm) | | |
| **LOFT** | 50 | 50* | 2 | annular 50 | Operational PWR 1 active loop | US |
| **LOBI** | 712 | 5.28 | 2 | annular 50, 12 | Active loops | EUR |
| **Semiscale -MOD 2** | 1600 | 2 | 2 | external 55 ID | Active loops | US |
| **LSTF** (ROSA IV) | 50 | 19 | 2 | annular 60 | Under construction Limited power | J |
| **BETHSY** | 100 | 3 | 3 | external (?) | Being Commissioned Limited Power | F |
| **SPES** | 427 | 6.5 | 3 | external (?) | Under construction | I |

* Nuclear Heating

** Size

## TABLE 2 : LOBI-MOD1 and LOFT CHARACTERISTICS

| Component | Parameter | LOBI-MOD1 | LOFT |
|---|---|---|---|
| **System** | - Loops | 2 (2 active) | 2 (1 active) |
| **Volume** | - Total ($m^3$) | 0.6* | 7.22 |
| | Scale reduction | 712 | 50 |
| **Core** | - Power (MWth) | 5.28 | 50 |
| | Length (m) | 3.9 | 1.68 |
| | No. Rods | 64 | 1300 |
| | Matrix | 1 (8 x 8)□ | 5 (15 x 15)□<br>4 (12 x 12)△ |
| | Heating | Electrical | Nuclear |
| **Downcomer** | - Configuration | Annular | Annular |
| | Gap Width (mm) | 50, 12 | 50 |
| **Operation** | - Pressure (MPa) | 15.5 | 15.0 |
| | Temperature (C) | 290/323 | 283/319 |
| **COUNTRY** | | EUR | US |

* With 12 mm Downcomer Gap Width

In addition data from test A1-04R which was performed in the LOBI-MOD1 test facility with a 50 mm downcomer gap width installed are included to depict the influence of this component on overall system response (A1-06 and A1-72 were performed with a 12 mm downcomer gap width).

A comparison of primary system pressure responses during a typical DEGL break LOCE in LOBI-MOD1 and LOFT is given in Fig.3. The LOFT data /10,11/, are encompassed by the LOBI-MOD1 data /12,13,14/ which clearly show the dependence of depressurisation rate on initial primary system fluid inventory. Qualitatively, the pressure traces are in good agreement indicating the occurrence of similar phenomena during the course of the transient. Quantitative differences could be accounted for by the different volume/power ratios of the two LOBI-MOD1 configurations and LOFT; i.e. 0.15 $m^3$/MW and 0.11 $m^3$/MW respectively in LOBI-MOD1 with the 50 mm and 12 mm downcomer sizes, and 0.14 $m^3$/MW in LOFT.

Core thermal response in both LOBI-MOD1 and LOFT exhibited similar rewet and quench phenomena which were largely influenced by the intact loop pump operation mode; also, the occurrence of such phenomena in the two facilities varied with core elevation. In Figs. 4 to 6 most representative heater rod cladding temperatures in the central fuel assembly of the LOFT facility and in LOBI are compared.

Heater rod cladding temperature responses in the core lower half are shown in Fig.4. The same thermocouple (TH37C404) at 0.7 m elevation of an inner heater rod was used for both LOBI tests. In LOFT, the cladding temperature at 0.20 m elevation of a fuel rod in assembly 5 (TE-5H07-008) was used. The rather substantial difference in linear heat generation rate prior to blowdown at these elevations (about 174 W/cm and 272 W/cm for LOBI and LOFT, respectively) resulted in higher peak cladding temperatures in LOFT following the initial departure from nucleate boiling. However, reiterating the present comparison philosophy which is mainly phenomena oriented, it can be seen that the early rewetting in both facilities occurred in a similar fashion and was strongly coupled to the intact loop pump operation mode (Fig.2).

A comparison of peak cladding temperatures is given in Fig.5. It should be noted that due to difference in core length and power axial profile, peak cladding temperatures were attained in LOFT at 0.4 m elevation in L2-3 (TE-5E08-015) and at 0.6 m elevation in L2-5 (TE-5H06-024) /15/, and at 2.2 m elevation in LOBI (TH33D407). Referring to Fig.5, core thermal response in LOFT test L2-3 and L2-5 differed in that the early core rewet observed in test L2-3 was suppressed in test L2-5. In LOBI the early core rewet in the middle high powered elevations was not observed regardless of intact loop pump operation mode. Heater rod temperature rise was, however, lower in test A1-72 than in test A1-06.

Cladding temperatures in the core upper half are shown in Fig.6. They refer to 1.02 m and 3.2 m elevation in LOFT (TE-5H07-041) and LOBI (TH34F209), respectively. The core early rewet was observed both in LOBI test A1-72 and LOFT test L2-3 which are directly comparable due to similarity in intact loop pump operation mode. In LOBI the early rewet at this elevation is to

be attributed to precursory cooling which, however, was not as effective in test A1-06.

A rather similar phenomenological behaviour was exhibited by core thermal response in the time span 10 to 20 s. LOBI test A1-72 and LOFT test L2-3 showed a top-down quench which was caused by fallback of a relatively high density mixture de-entrained in the upper vessel. This phenomenon was observed also in LOFT test L2-5 (Fig.6). In LOBI test A1-06 it occurred at the uppermost elevations only.

As previously mentioned, core early rewet was seen to be hydraulically controlled being caused by a period of re-established positive core flow which was, on the other hand, strongly coupled to intact loop pump operation mode and to the transition from subcooled to saturated critical flow at the break nozzle on the vessel-side. The combined effect of the reduction of the demand at the break and sustained intact loop cold leg flow resulted in an enhancement of flow into the vessel downcomer. This may be inferred from the net mass flow in intact and broken loop cold legs for LOBI test A1-72 and for LOFT test L2-3 as shown in Fig.7. The LOFT data /16/ have been scaled to LOBI by the volume ratio of the two facilities (i.e. 7.22/0.6). A marked analogy was also seen in the qualitative and even quantitative evolution of the break mass flows in the two facilities (Fig.8). The LOFT break mass flow (scaled to LOBI) was obtained by adding the computed mass flow in the cold leg (FR-BR-116) and in the hot leg (FR-BL-216) of the broken loop /10/. It should be noted that the accuracy of the LOFT data in this paper suffers from the coarse averaging procedure used in hand plotting.

The LOBI-MOD1 test facility with a 50 mm downcomer gap width installed exhibited a core wide bottom-up early rewet as shown by the envelopes of cladding temperature in the IC-zone of the bundle cross section (Fig.9). The influence of downcomer gap width and volume on overall system response has been documented in detail in /17,18/. The larger initial liquid inventory due to a downcomer gap of 50 mm, largely suppressed reverse core flow during blowdown and provided effective core cooling, so limiting peak cladding temperatures and enhancing the likelihood of early core rewet.

## CONCLUDING REMARKS

LOBI-MOD1 and LOFT system responses to DECL break LOCEs have shown a rather remarkable analogy especially in those phenomena affecting core thermal response. Certain qualitative and even quantitative differences were seen to be due mainly to differences in system configuration, core length and axial power profile, which could be properly accounted for in a deeper analysis.

The repeatability of experimental results in different test facilities is certainly desirable in an attempt to prove their typicality. Furthermore, comparison of related experimental results from facilities having different scaling and design rationales, may clearly enhance the assessment of distortions in the thermal-hydraulic behaviour of certain components which may be induced by design decisions, technical feasibility and operational constraints. Further work is proposed in this area.

REFERENCES


1. L.J.Ybarrondo et al.:
"Examination of LOFT Scaling".
ASME Winter Annual meeting, Paper 74-WA/HT 53, 1974.

2. L.S.Tong:
"Water Reactor Safety Research Program; Application of Research Results"
Nuclear Safety (19) 1978.

3. N.Zuber:
"Problems in Modelling of Small Break LOCA"
NUREG-0724, 1980.

4. F.Mayinger:
"Scaling and Modeling Laws in Two-Phase Flow and Boiling Heat Transfer, Two Phase Flow and Heat Transfer in Power and Processing Industries"
Hemisphere, Washington, 1981.

5. H.Karwat:
"Problems of Scaling and Extrapolation of Experimental Results in the Area of Fluiddynamics and Associated Heat Transfer Related to Reactor Safety". (A State of the Art Report);
Study Contract Nr.ECI-930-B7221-82-D(O), CEC, Brussels (DG XII), 1983.

6. W.L.Riebold, H.Staedtke:
"LOBI-Influence of PWR Primary Loops on Blowdown. First Results"
Proceedings of the 9th Water Reactor Safety Research Information Meeting of the USNRC, October 26-30, 1981, Gaithersburg/MD, USA.
NUREG/CP-0024.

7. C.Addabbo, L.Piplies, W.Riebold:
"LOBI-MOD2: Facility Description and Specification for OECD-CSNI International Standard Problem No.18 (ISP 18); Volume I: Geometrical Configuration of the Test Facility".
CEC-JRC, Communication No. 4010, 1983.

8. H.L.Coplen, L.J.Ybarrondo:
"The LOFT Integral Test Facility and Program".
Nuclear Safety, June 1974.

9. D.L.Reeder:
"LOFT System and Test Description (5.5-ft Nuclear Core 1 LOCEs)"
NUREG/CR-0247, TREE-1208, 1978.

10. P.G.Prassinos, B.M.Galusha, D.B.Engleman:
"Experiment Data Report for LOFT Power Ascension Experiment L2-3"
NUREG/CR-0792, TREE-1326, 1979.

11. P.D.Bayless, J.M.Divine:
"Experiment Data Report for LOFT Large Break Loss-of-Coolant Experiment L2-5"
NUREG/CR-2826, EGG-2210, 1982.

12. E.Ohlmer, T.Fortescue, W.Kolar, J.Eder:
"Experimental Data Report on LOBI Test A1-04R"
CEC-JRC, LEC 80-03, 1980.

13. L.Regel, E.Ohlmer:
"Experimental Data Report on LOBI Test A1-06"
CEC-JRC, LEC 82-17, 1982.

14. J.Sanders, E.Ohlmer:
"Experimental Data Report on LOBI Test A1-72"
CEC-JRC, LEC 83-24, 1983.

15. J.P.Adams:
"Quick Look Report on LOFT Nuclear Test L2-5"
EGG-LOFT-5921, 1982.

16. J.C.Lin:
"Post Test Analysis of LOFT Loss-of-Coolant Experiment L2-3"
EGG-LOFT-5075, 1980.

17. H.Staedtke, D.Carey, W.L.Riebold:
"Influence of Downcomer Volume and Gap Width on Blowdown"
Proceedings of the International Meeting on Thermal Nuclear Reactor Safety, August 29-September 2, 1982, Chicago, Illinois, USA.
NUREG/CP-0027

18. W.L.Riebold, L.Piplies, H.Staedtke:
"LOBI Experimental Programme Results and Plans: Status Sept. 1982"
Proceedings of USNRC 10th Water Reactor Safety Information Meeting, October 12 - 15, 1982.
NUREG/CP-0041

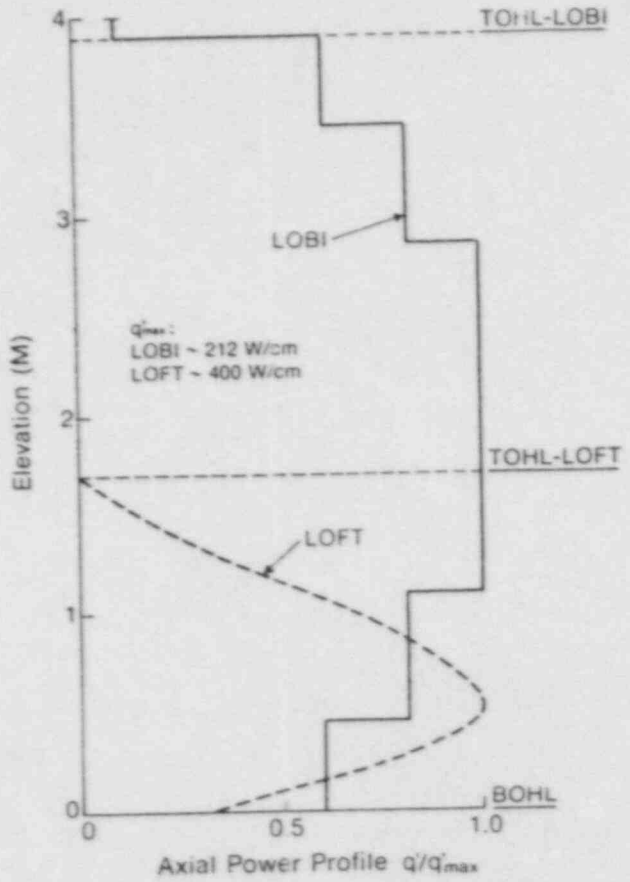


FIG. 1 : Axial Power Profile in LOBI and LOFT

## LOBI Project

**Objectives :**

- To investigate the thermal hydraulic behaviour of a simulated PWR system during LOCA or Special Transients conditions
- To provide experimental data required for the assessment of system codes used in the safety analysis of LPWR

**Founded by :**

- Commission of the European Communities (CEC)
- Bundes Minister für Forschung und Technologie (FRG)

**Place :**

- **Euratom** Joint Research Centre
  Ispra Establishment (I)

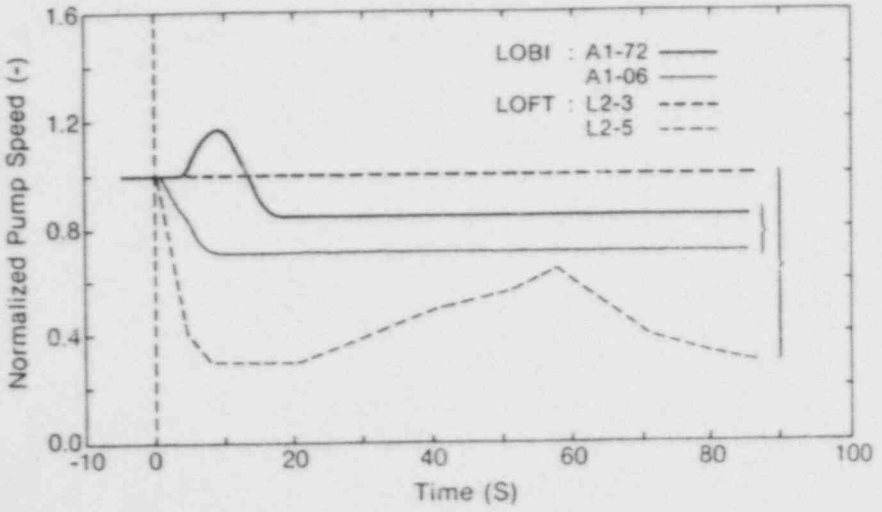


FIG. 2 : Normilized Speed of Intact Loop Primary Pump

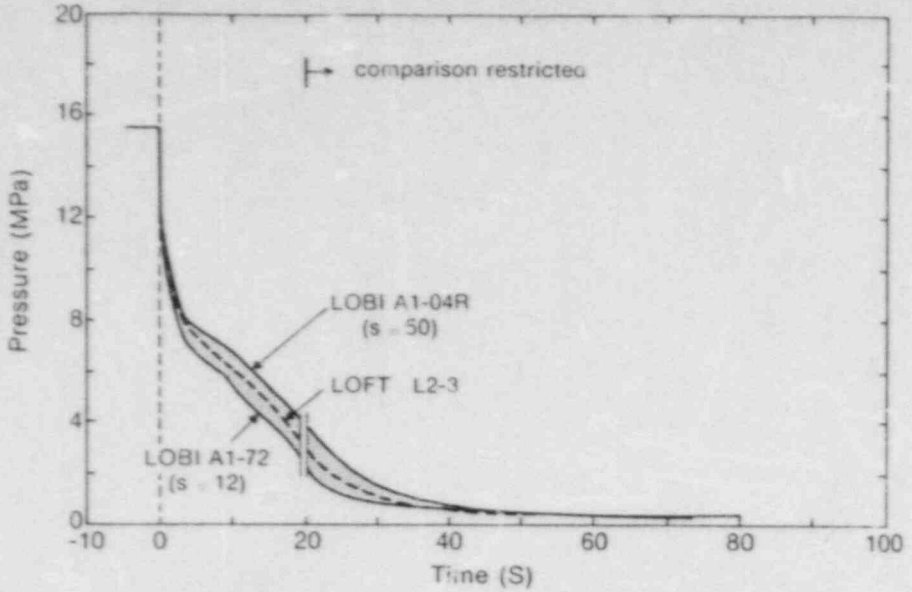


FIG. 3 : PCS Pressure Response to a DECL Break LOCE
(s : Downcomer Gap Width in mm)

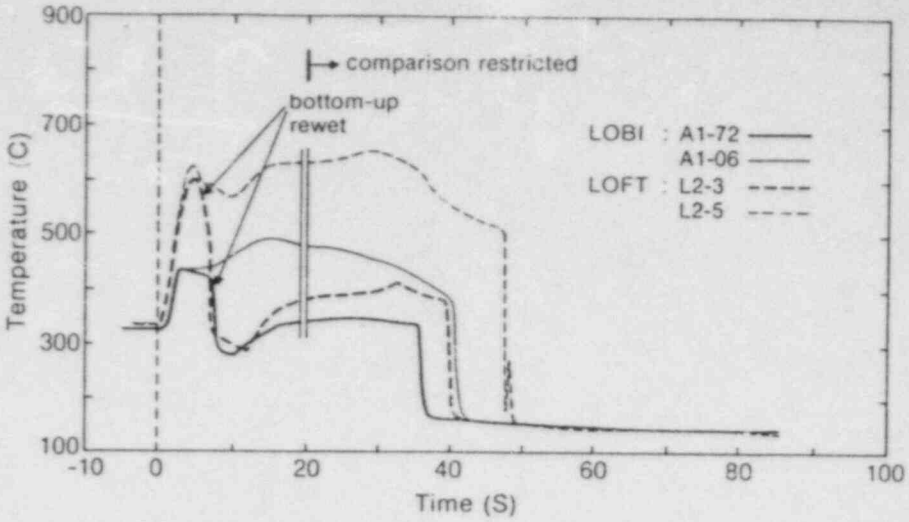


FIG. 4 : Cladding Temperatures in the Core Lower Half

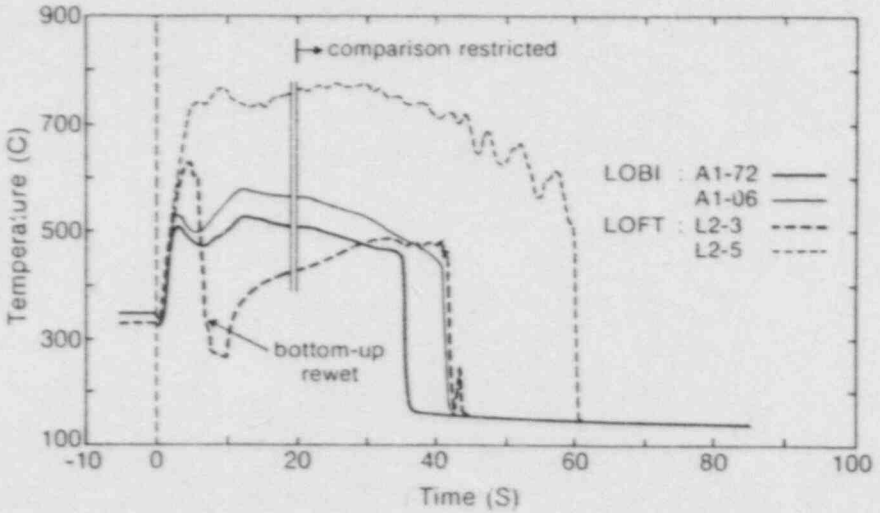


FIG. 5 : Maximum Cladding Temperatures

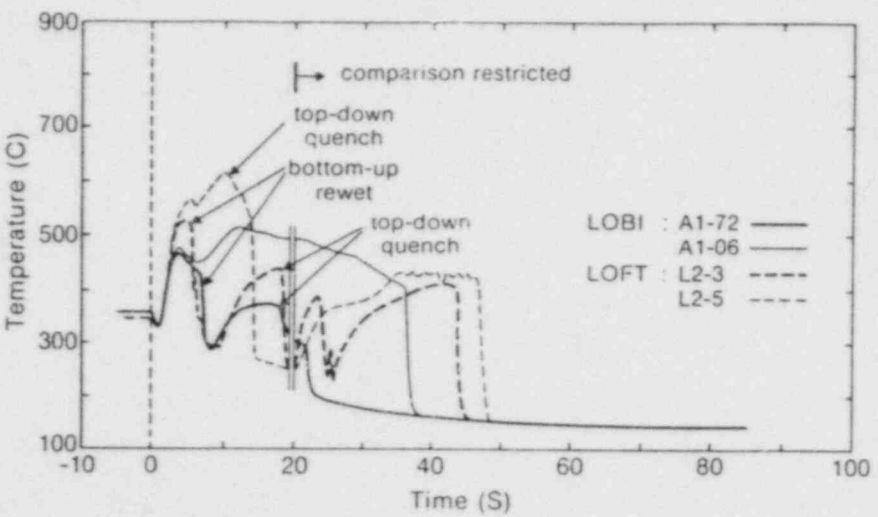


FIG. 6 : Cladding Temperatures in the Core Upper Half

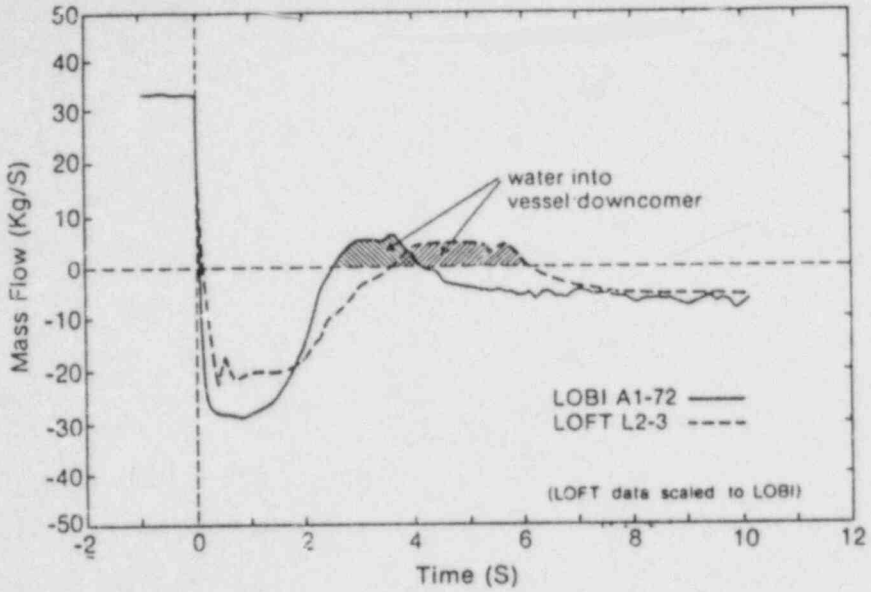


FIG. 7 : Net Mass Flow in Intact and Broken Loop Cold Legs for a DECL break LOCE

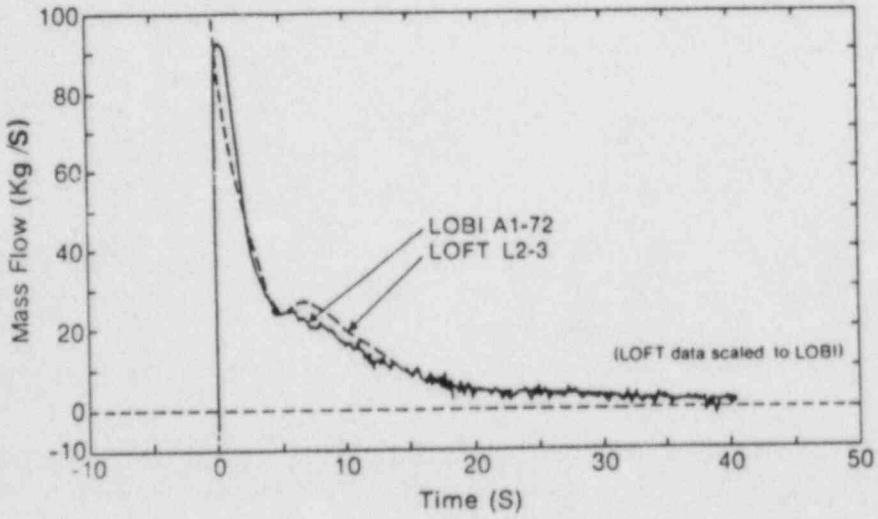


FIG. 8 : Break Mass Flow for a DECL Break LOCE

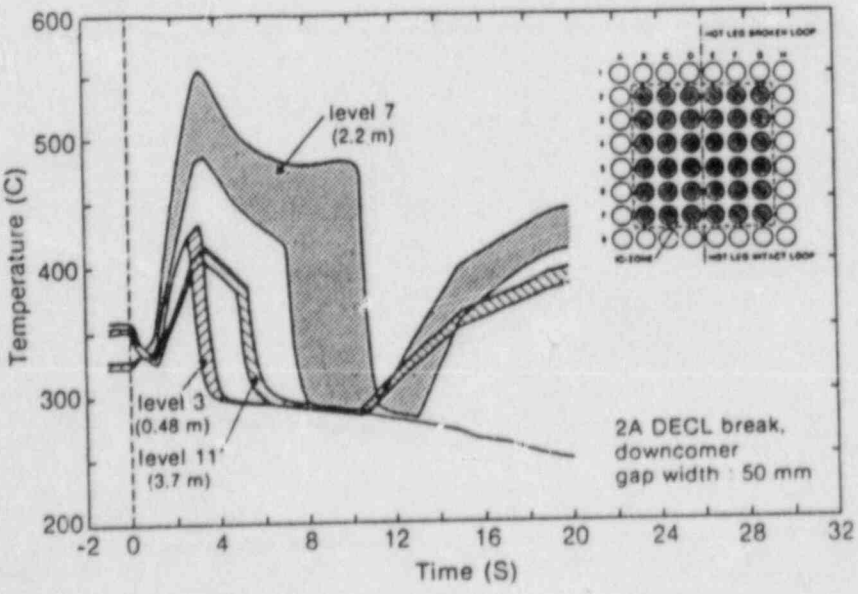


FIG. 9 : LOBI Test A1-04R : Envelopes of Cladding Temperatures in IC-Zone (Short Time Select)

# BWR FIST TEST AND ANALYSIS

W. A. Sutherland
W. S. Hwang

Nuclear Fuel Engineering Department
General Electric Company
San Jose, California

## ABSTRACT

The Full Integral Simulation Test (FIST) program has developed a best-estimate analysis capability for BWR systems. Analytical method development extended the BWR-TRAC computer code for improved application modeling and flexibility. Additional experiments extended the data base with the FIST facility to a wider range of LOCA tests and to operational transients simulation. Evaluation of these results provided an improved understanding of controlling phenomenon and the effects of facility scaling on system response; and analysis of these results demonstrates TRAC as a best-estimate method and a vehicle for applying the integral test experience to reactor systems.

## INTRODUCTION

The full height BWR system simulator FIST has been used to investigate system response to various transients. Tests were conducted to investigate Loss-of-Coolant Accident (LOCA) transients, power transients, degraded ECCS transients, and natural circulation performance characteristics. Analysis of the first test phase results provided insights into the controlling phenomena and system interactions[1]. Two LOCA tests, the large break and small break, were also used for TRAC qualification, comparing test data with predictions from a pretest analysis[2,3]. TRAC was also used in a post test analysis[4] of FIST to quantify the effect of excess stored

heat in the vessel. This paper presents results of LOCA tests with different break sizes and power transient tests that simulate a Main Steamline Isolation Valve (MSIV) closure without control rod insertion.

The FIST facility (Figure 1), scaled to a BWR/6-218 standard plant, is designed to model BWR system thermal-hydraulic response, in real time, over the full range of reactor conditions. The core is simulated with a full size electrically heated bundle capable of full power, as well as decay and/or transient power. Kinetic feedback effects are simulated by programming bundle power to match the core average rod surface heat flux determined from BWR analysis. Scaling the facility to one full size bundle for the core region leads to a scaling ratio of 1/624 for the regional volumes, flows, and internal component performance. The eight major regions, regional interfaces, and internal component characteristics are closely simulated, with few scaling compromises.

As in a BWR, FIST has two external recirculation loops, each with a centrifugal pump driving a jet pump that circulates flow from the downcomer through the core. The drive pump inertia is sized so that the flow coastdown following a trip is simulated. One recirculation loop is used for the pipe break simulation to achieve the correct interaction between the break flow and the recirculation flow. Five valves are installed along the steamline for simulating the safety relief valve (S/RV) group functions. S/RV opening and closing setpoints, operational logic, and the automatic depressurization system function (ADS) are simulated.

A heated feedwater system enables the FIST facility to achieve steady-state operation at full power with correct initial conditions. FIST is also equipped with BWR water level instrumentation to provide level signals for real time simulation of key control events in a transient, such as MSIV closure, ADS activation, HPCS initiation, recirculation pump trip, etc.

TEST RESULTS

## A. LOCA Tests

The LOCA tests series carried out under the FIST program is shown in Table 1. This series covers system response to pipe breaks of various sizes, locations, and with different ECCS combinations, as shown in Figure 2. Four tests representative of the LOCA simulation test series are discussed herein. The test conditions for these tests are listed in Table 2. Three are recirculation line breaks and the fourth is an LPCI line break.

### 1. System Pressure

System pressure response is shown in Figure 3. In large break test 6DBA1B a high inventory loss rate from the downcomer region leads to break uncovery early in the transient, at 8 seconds, followed by rapid system depressurization as steam is then vented through the break. In the three smaller break tests the system pressure is maintained by the pressure control valve until it is fully closed. System pressure increase upon MSIV closure, at about 65 seconds in small break 6SB2C, is because the energy discharge rate through the break test is less than the core power input. Tests with mid-size breaks, 6IB1 and 6LB1, have a slow depressurization because the energy discharge rate through the break is greater than the core power input. Rapid depressurization later in transient is due to ADS activation, tripped by the downcomer water level signal. Timing of ADS activation is therefore affected by the break flow rate (i.e., break size).

The pressure responses in Figure 3 illustrate an important characteristic of BWR system response to a LOCA. That is, for cases where the water level is not maintained by the high pressure inventory makeup systems, there is prompt depressurization by either the break uncovery or the ADS activation and the low pressure ECC Systems (LPCS and LPCI) refill and reflood the system. The major effect is

the timing of the depressurization. System response and governing phenomena during the large break test are similar to those following ADS in smaller break tests. Depressurization leads to bulk flashing in the system, water level swell, and Counter Current Flow Limiting (CCFL) at various locations.

2. System Mass

Total system mass response is shown in Figure 4. Early in the transient the break flow is predominantly liquid. The system mass decreases very rapidly in the large break test and proportionally slower in tests with smaller break sizes. Upon break uncovery, at about 8, 33, and 75 seconds in tests 6DBA1B, 6LB1, and 6IB1 respectively, the break flow becomes predominantly steam and the system mass depletion rate is significantly reduced. An increase of the inventory depletion rate at about 120, 130, and 195 seconds in tests 6LB1, 6IB1, and 6SB2C respectively, is due to ADS steam discharge in addition to the break flow. The system depressurization leads to initiation of the low pressure ECCS, increasing ECCS flow, and decreasing break flow. Figure 4 shows that the system inventory is quickly recovered by the ECCS for all LOCA events.

3. Bundle Hydraulic Response

The bundle average fluid density measurement, Figure 5, shows the bundle inventory during the transient. In the large break (6DBA1B) event, the bundle inventory is quickly depleted and the bundle begins to uncover. The rapid depressurization leads to a lower plenum flashing surge into the core. This is followed by the steam generation in the lower plenum creating Counter Current Flow Limiting (CCFL) at both the Side Entry Orifice (SEO) and the Upper Tie Plate (UTP) that holds water in the bundle until refill at about 125 seconds. The bundle refill/reflood quickly quenches all the rods and keeps the bundle well cooled. In tests with smaller breaks the bundle remains covered with a two-phase mixture prior to ADS. Governing phenomena and system response during the post-ADS period are similar to that observed in the large break

blowdown. CCFL is seen to occur at SEO and UTP, and the bundle uncovery that occurrs after the lower plenum flashing surge subsides depends on break size, location, and available ECC Systems.

4. Bundle Rod Temperature

Rod temperatures measured at the midplane and the upper region of the bundle are shown in Figures 6 and 7. There is no rod heatup in the intermediate break test, 6IB1, because the bundle remains covered with two-phase mixture throughout the transient. Rod heatup occurs in the other three tests shortly after the bundle begins to uncover. Timing of the bundle uncovery, and the extent of the heat-up, is affected by the inventory depletion rate, flashing due to ADS, and the ADS time delay. The peak cladding temperature is also affected by the duration, and bundle power, of the bundle uncovery period. The rod temperature increase is limited by the ECCS injection, and all the rods quench upon bundle reflood, and remain at saturation temperature for the remainder of the transient.

B. Power Transient Tests

Tests performed in FIST to simulate system power transients involving Main Steamline Isolation Valve closure without control rod insertion, with and without HPCS, one with depressurization, and a turbine trip transient are listed in Table 3. The system is shown schematically in Figure 8. Two representative tests, 6PMC1 and 6PMC3, are discussed here. Test 6PMC1 is a power transient with HPCS. This simulates system response from initiation of the transient by MSIV closure, through the pressure/power surge and negative reactivity feedback, trip of the recirculation pumps, and finally the pressure/power cycling in response to S/RV operation while operating in natural circulation. The operator may further reduce the core power by lowering the water level and/or depressurizing the system to increase core void fraction. Test 6PMC3 simulates system response during this depressurization transient.

1. Test 6PMC1

The test simulates a power transient caused by a pressure increase, void collapse, and neutron kinetic feedback in the early transient. The power applied in the test (Figure 9) is programmed to match a BWR power transient analysis. The bundle power surges to 7.3 MW at about 4 seconds, and then quickly decreases to below 2 MW for the remainder of the test. Oscillations in this period are due to void changes in response to the pressure increase and decrease caused by S/RV operation.

Figure 10 is the system pressure response during the transient. Pressure increases rapidly upon system isolation by the MSIV closure. The high pressure trips for the recirculation pumps and all S/RV valves are reached on this initial rise. The large steam discharge through the S/RV valves reduces the system pressure. The system pressure is then maintained within the range of S/RV setpoints by the automatic opening and closing of the S/RV valves. Figures 9 and 10 show the system pressure and power oscillations are generally in phase, and the coupling between the pressure and power appears to be adequately simulated with programmed power.

Following the feedwater system trip, the steam boiloff by the bundle power is discharged through the S/RV valves, decreasing the system inventory in the early transient (Figure 11). The system inventory is then maintained by HPCS injection into the upper plenum. The circulation pump is tripped at about one second into the transient when the pressure reaches 1150 PSIA. The flow coastdown is completed at about 20 seconds and the system operates in natural circulation. Measured jet pump flow is shown in Figure 12. Prior to HPCS injection at 50 seconds, the makeup for the boiloff is primarily supplied by the level change in the downcomer. Later in the transient the HPCS flow into the upper plenum makes up for the boiloff, the system reaches a natural circulation condition within the core shroud (i.e. down the bypass), and there is no significant flow through the jet pumps.

2. Test 6PMC3

Results of the power transient test, 6PMC1, have shown that the system is quickly brought into a stable operating condition following a power transient event. The system pressure is maintained within the S/RV operational range, the water level is maintained by the HPCS, and the bundle power eventually reaches about 8% of full power (371 KW).

Test 6PMC3 simulates the system response as the system is depressurized from the above equilibrium condition, over the period of an hour, by opening one S/RV valve. S/RV activation leads to flashing and void increase in the core, reducing the bundle power to decay power during the depressurization transient (Figure 13). The depressurization is completed by closing the S/RV valve when the system pressure reaches about 200 PSIA, Figure 14. The system flashing then stops, the bundle void decreases, and the bundle power gradually returns to about the 8% level.

During the depressurization the operator maintains the downcomer water level at the top of active fuel elevation by controlling HPCS flow, Figure 15. Figure 16 shows the bundle to bypass flow measured in the test (i.e., a negative flow indicates flow from the bypass into the bundle). The bypass-to-bundle flow, driven by the natural circulation between these two regions, increases with time due to the increased steam void at lower pressure. The flow perturbations, due to variation in level, is caused by the HPCS make-up being controlled manually. The results clearly demonstrate that system depressurization in a power transient is achieved smoothly by opening an S/RV value.

SUMMARY

The FIST testing program has been successfully completed. The tests investigated BWR system responses to various transients, of which four LOCA tests and two power transient tests are discussed herein. System response and governing phenomena in LOCA tests with different breaks are identified in this study. Prior to ADS activation in the

mid-size and small breaks, the system performance is natural circulation and the bundle remains covered. System response to the large break event is similar to automatic depressurization. The depressurization leads to system bulk flashing and CCFL at various locations. For some situations the bundle is uncovered and the effectiveness of ECCS cooling to limit the heatup is clearly demonstrated, and the system inventory is completely recovered by ECCS injection. Power transient tests conducted in FIST show that the coupling between pressure and power is adequately simulated by programmed power in the test. The system quickly reaches a stable condition, then is depressurized using S/RV and HPCS flow controls to a stable low pressure condition.

In summary, various transients in a BWR system have been studied in the FIST test program. Data obtained in the tests have provided valuable information and have extended the data base for further evaluation and assessing of assumptions and models used in analyses.

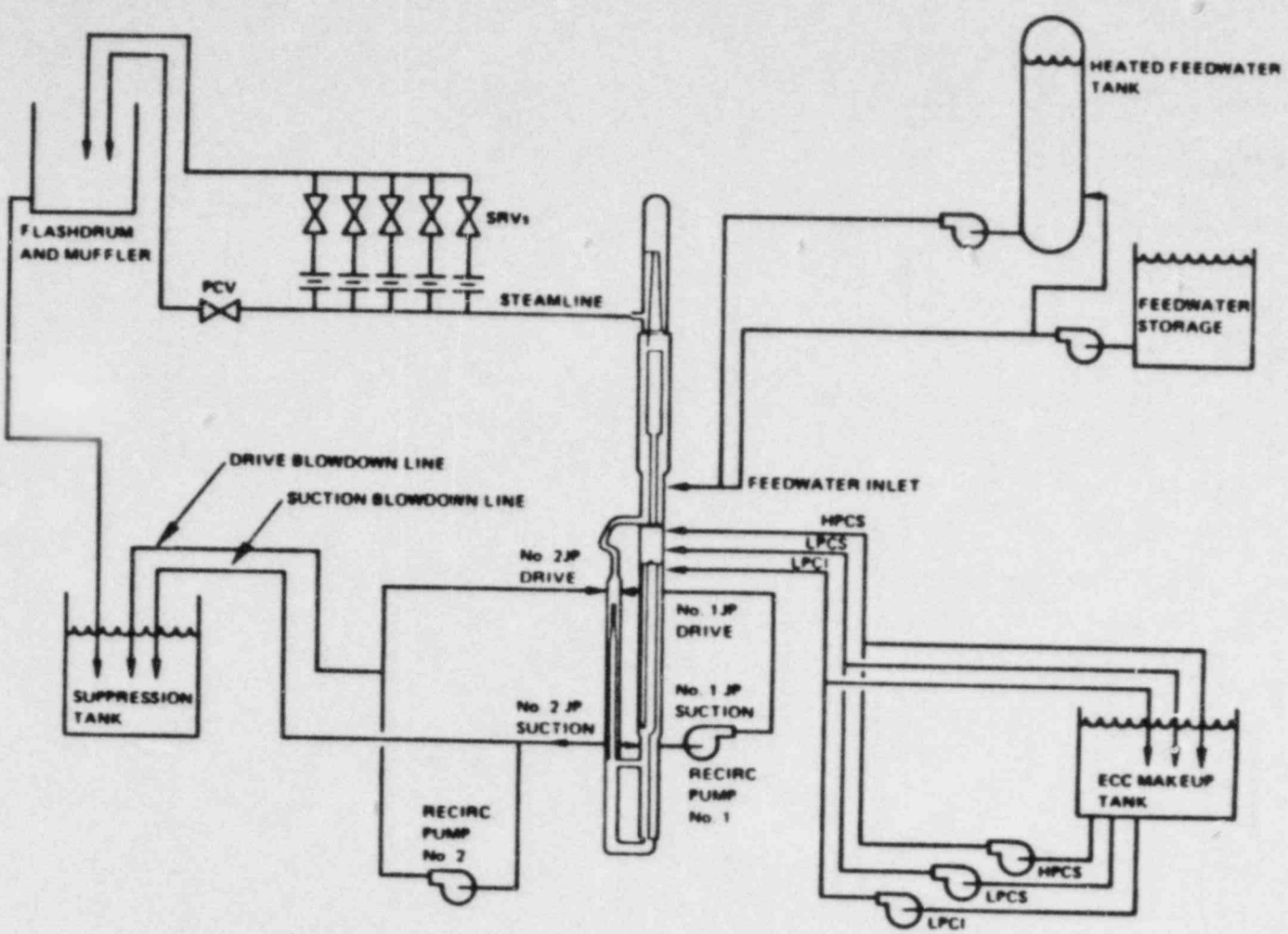


FIGURE 1. BWR FIST TEST FACILITY SCHEMATIC

TABLE 1 FIST LOCA TESTS

| | | | |
|---|---|---|---|
| 4 DBA 1 | LARGE RECIRCULATION BREAK | 6.09 Mw | HPCS<br>LPCS<br>2 LPCI |
| 6 DBA 1B | LARGE RECIRCULATION BREAK | 5.05 Mw | HPCS<br>LPCS<br>1 LPCI |
| 6 LB 1 | LPCI LINE BREAK | 4.64 Mw | LPCS<br>2 LPCI |
| 6 IB 1 | INTERMEDIATE RECIPCULATION BREAK | 4.64 Mw | HPCS<br>2 LPCI |
| 6 SB 2C | SMALL RECIRCULATION BREAK | 5.05 Mw | LPCS<br>3 LPCI |
| 6 SB 1 | SMALL RECIRCULATION BREAK | 4.64 Mw | LPCS<br>3 LPCI<br>SPV |
| 6 MSB 1 | MAIN STEAM LINE BREAK | 4.64 Mw | HPCS<br>LPCS<br>1 LPCI |



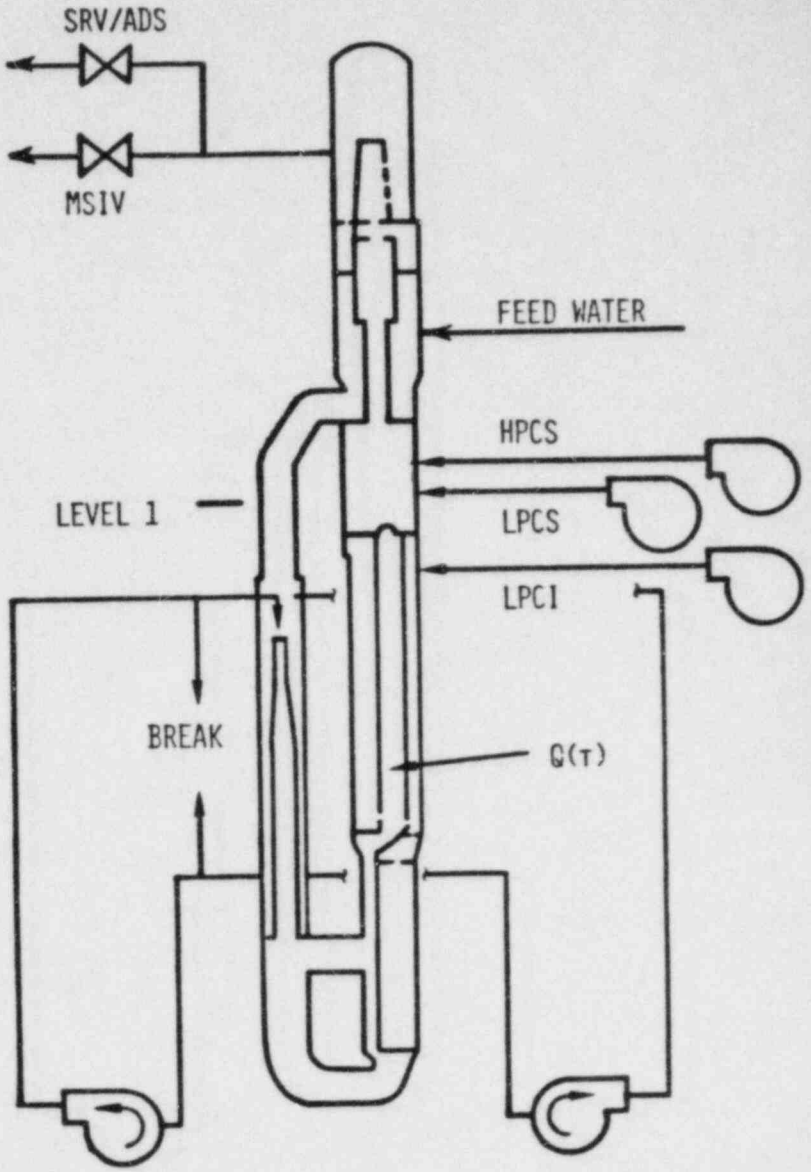


FIGURE 2. FIST LOCA TESTS

Table 2

TEST CONDITIONS OF FIST LOCA TESTS

| | Large Break 6DBA1B | LPCI Break 6LB1 | Intermediate Break, 6IB1 | Small Break 6SB2C |
|---|---|---|---|---|
| Break Location | Recir. | LPCI | Recir. | Recir. |
| Break Simulation | Nozzle and Orifice | Orifice | Orifice | Orifice |
| Break Size, (BWR, $ft^2$) | 1.878 and 0.348 | 0.34 | 0.20 | 0.05 |
| Initial Power | 5.05 | 4.64 | 4.64 | 5.05 |
| MSIV Trip (sec) (Signal/Time) | 0 | 17 | 26 | 27 |
| ECCS Injection (Sec.) | | | | |
| HPCS | 27 | - | 27 | - |
| LPCS | 64 | 204 | - | 310 |
| LPCI | 75 | 217 | 227 | 335 |
| ADS | | | | |
| Trip (Sec.) | 2 | 17 | 26 | 75 |
| Time Delay (sec) | 105 | 105 | 105 | 120 |

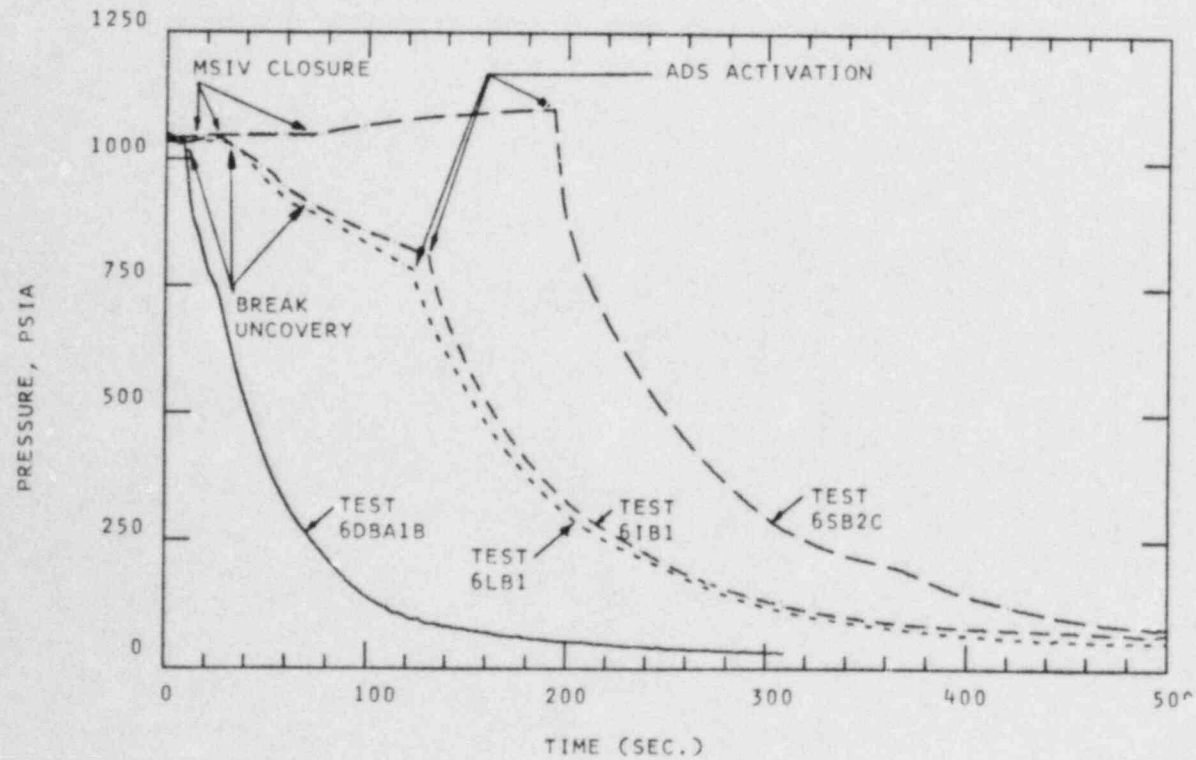


FIGURE 3. SYSTEM PRESSURE

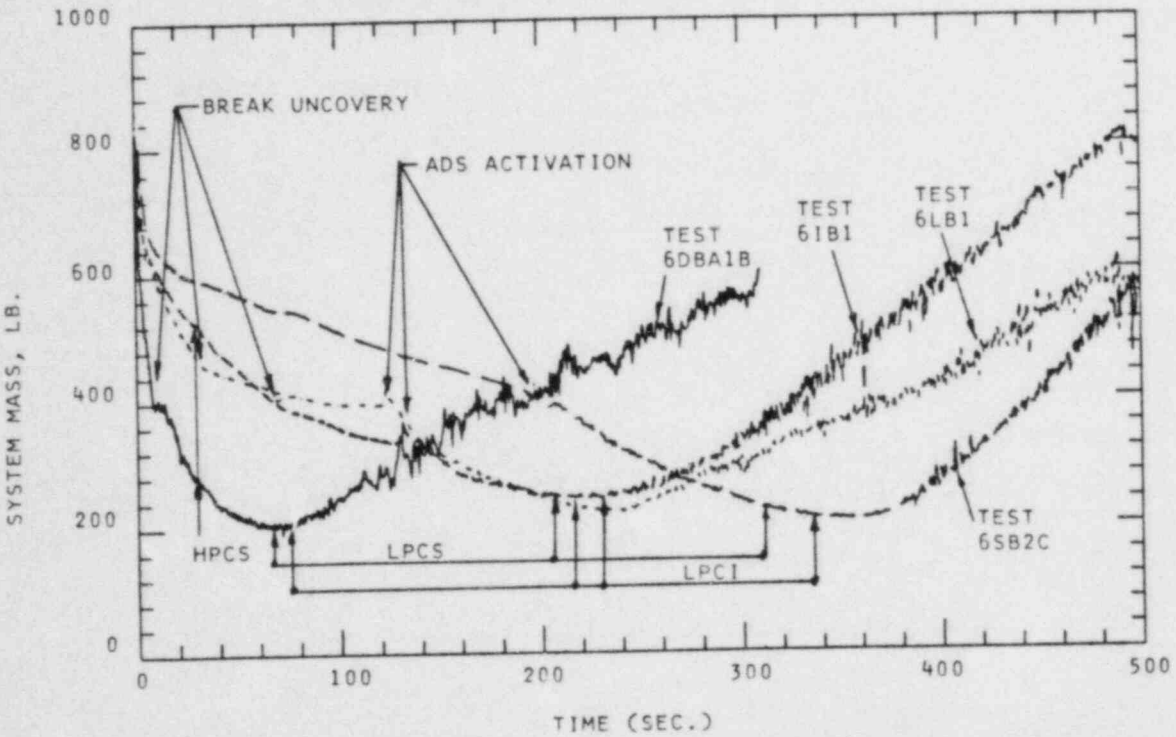


FIGURE 4. SYSTEM MASS

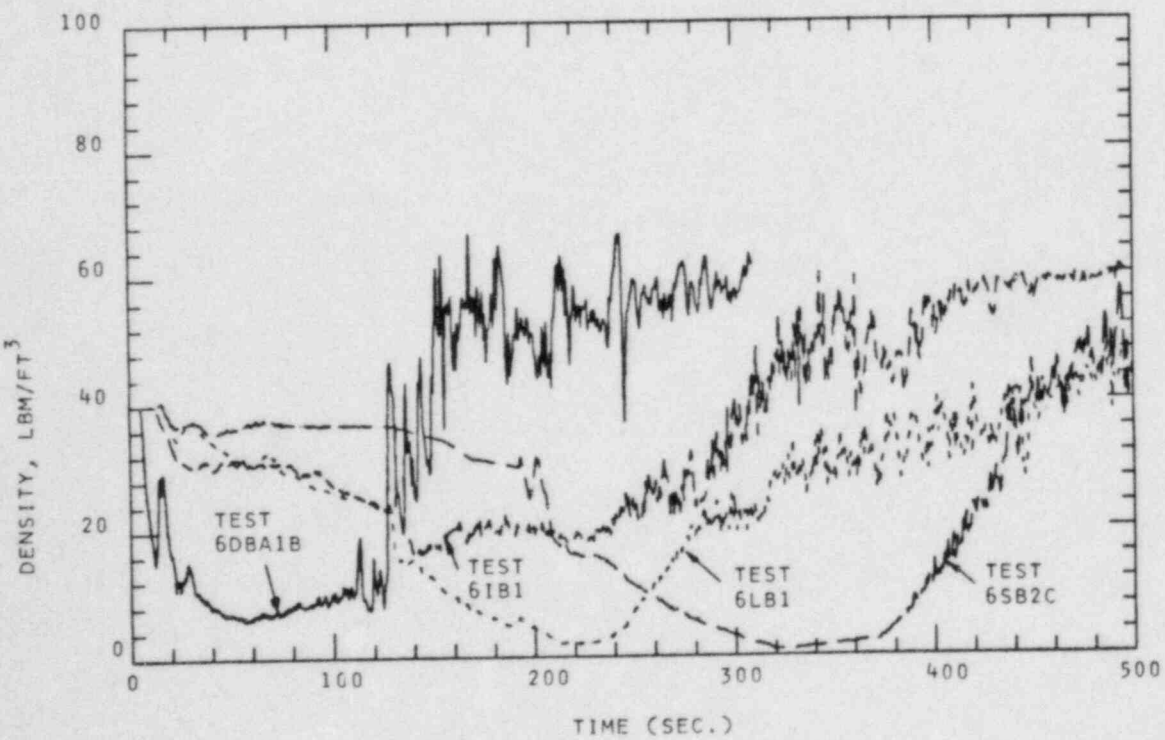


FIGURE 5. BUNDLE AVERAGE DENSITY

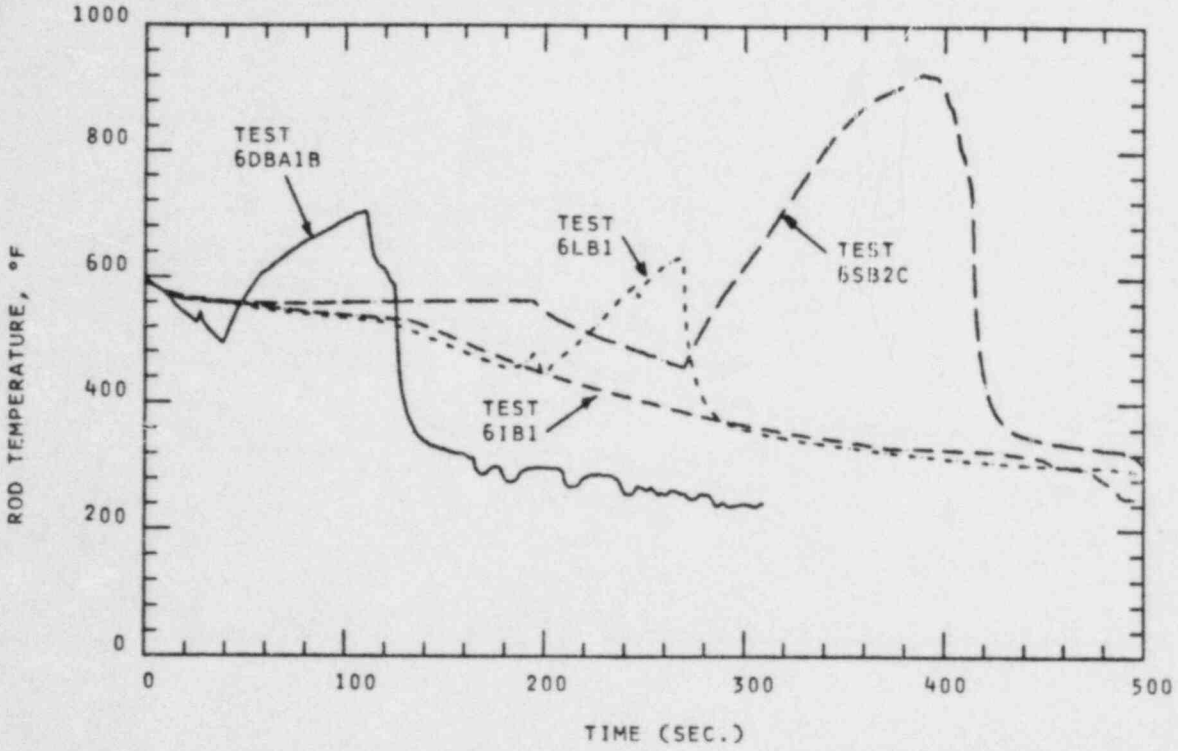


FIGURE 6. ROD TEMPERATURE, ELEVATION 77 INCHES

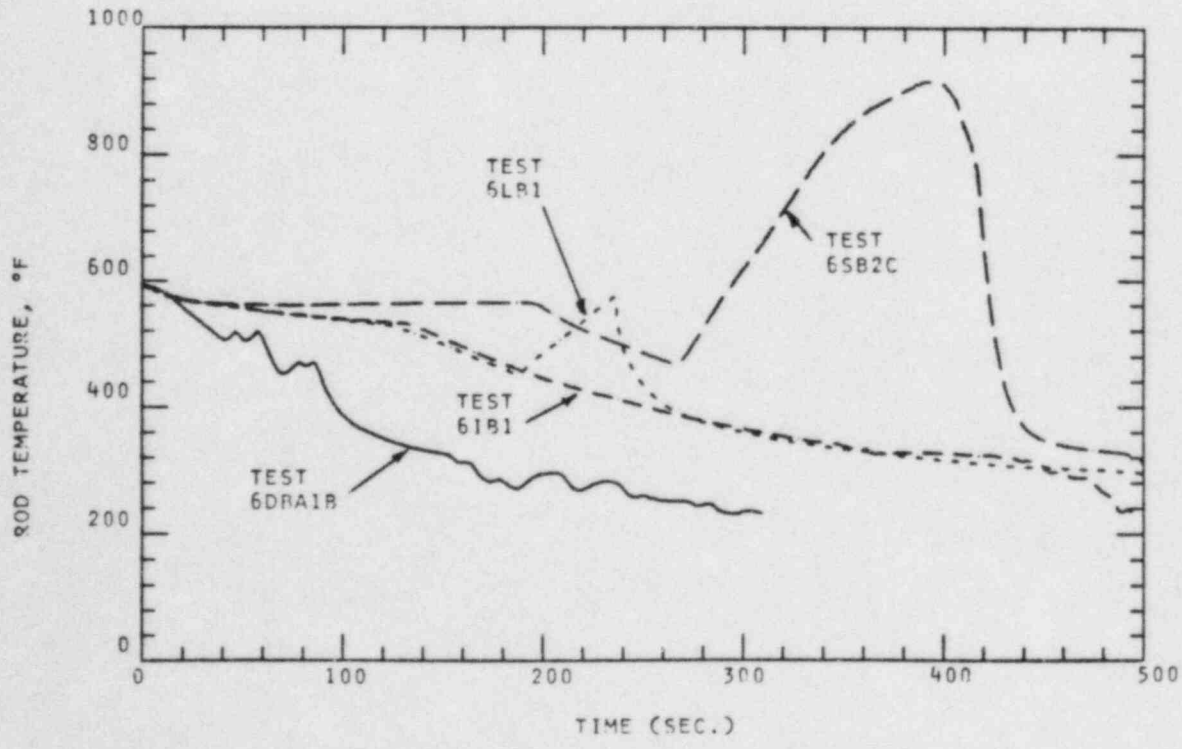


FIGURE 7. ROD TEMPERATURE, ELEVATION 97 INCHES

TABLE 3 FIST POWER TRANSIENT TESTS

| | | | |
|---|---|---|---|
| 6 PMC 1 | MSIV Closure | 4.64 Mw | HPCS RCIC |
| 6 PMC 2A | MSIV Closure | 4.64 Mw | RCIC |
| 6 PMC 3A | Blowdown | 0.371 Mw | HPCS S/RV |
| 4 PMC 1 | MSIV Closure | 4.35 Mw | HPCI |
| 4 PTT 1 | Turbine Trip | 2.98 Mw | FW |
| 6 PNC 1 | Steady State | 0.5 - 3.0 Mw | FW |
| 6 PNC 2 | Steady State | 0.1 - 3.0 Mw | FW |
| 6 PNC 3 | Steady State | 0.6 Mw | HPCS |
| 6 PMC 3B | Steady State P = 200 | 0.371 Mw<br>0.742 Mw | FW |

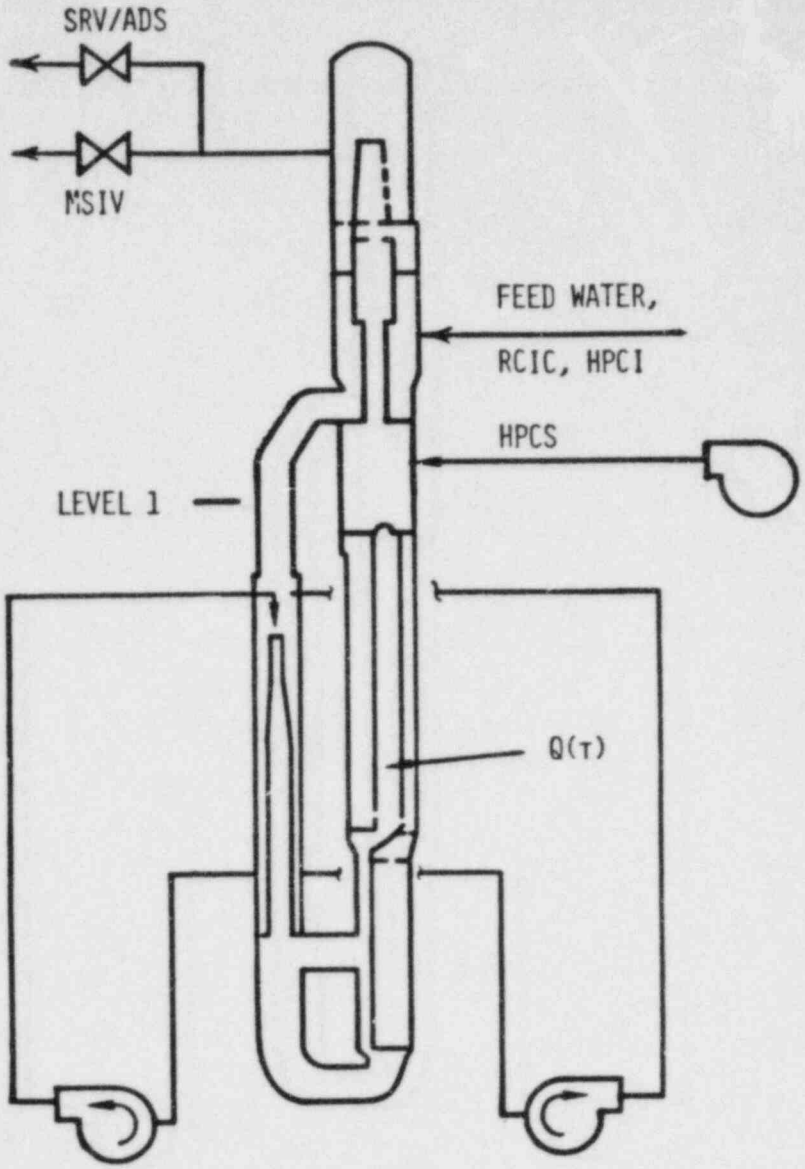


FIGURE 8. FIST POWER TRANSIENT TESTS

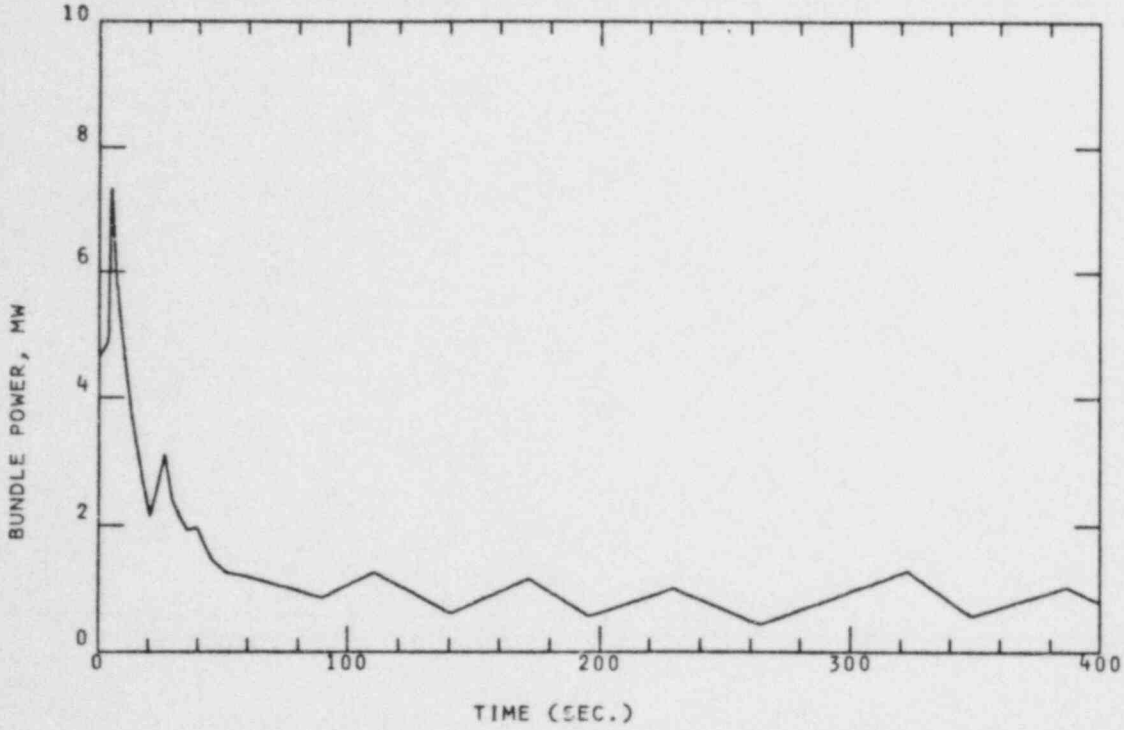


FIGURE 9. BUNDLE POWER, TEST 6PMC1

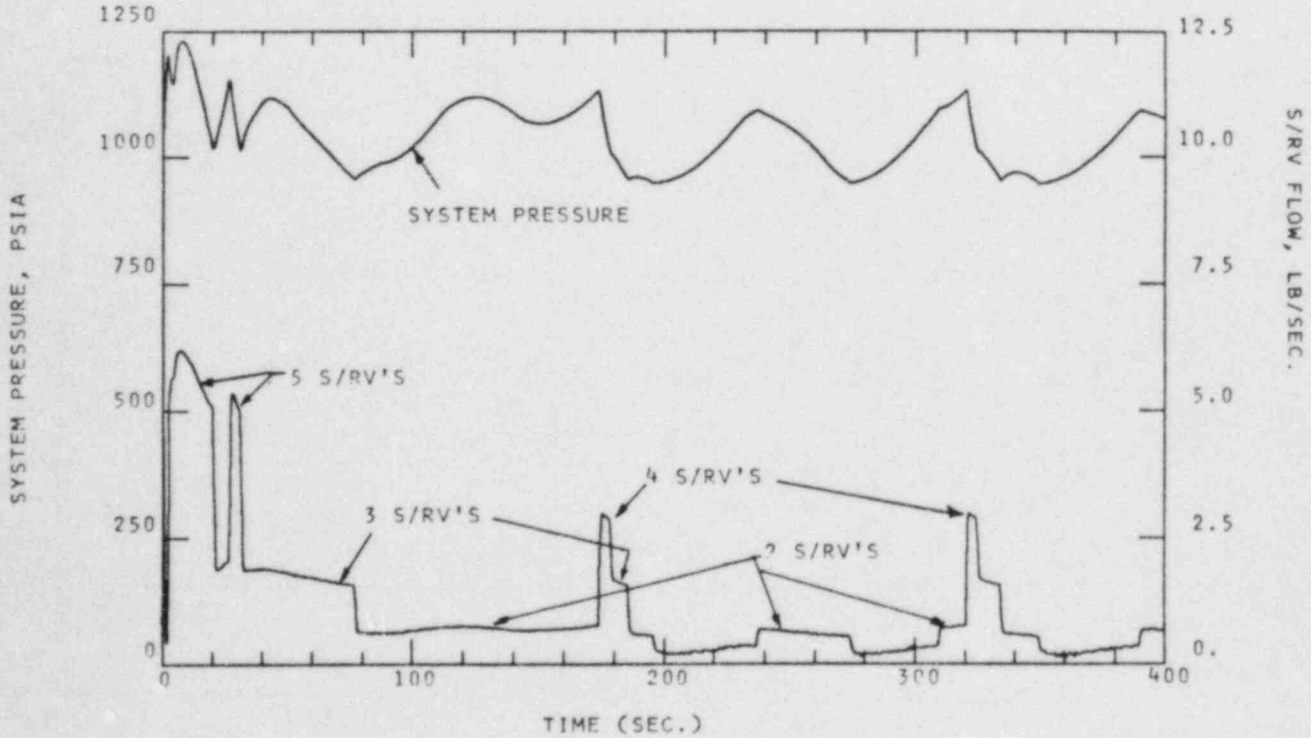


FIGURE 10. SYSTEM PRESSURE AND S/RV FLOW, TEST 6 PMC1

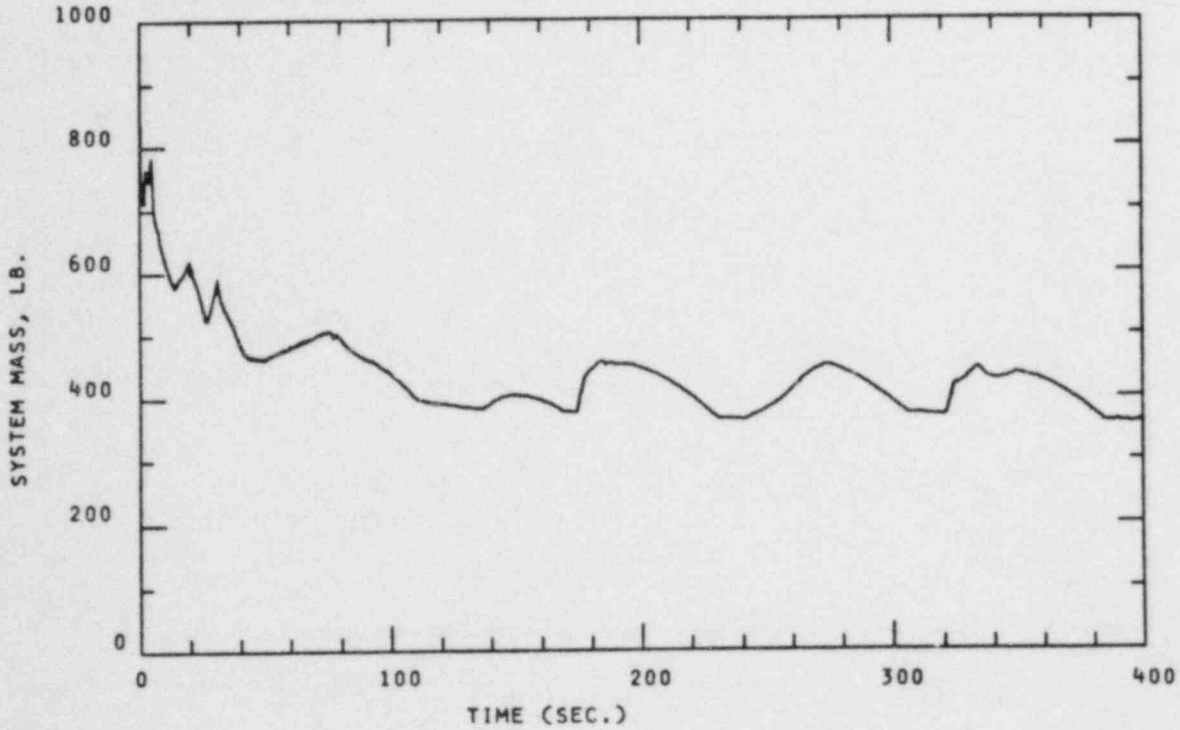


FIGURE 11. SYSTEM MASS, TEST 6PMC1

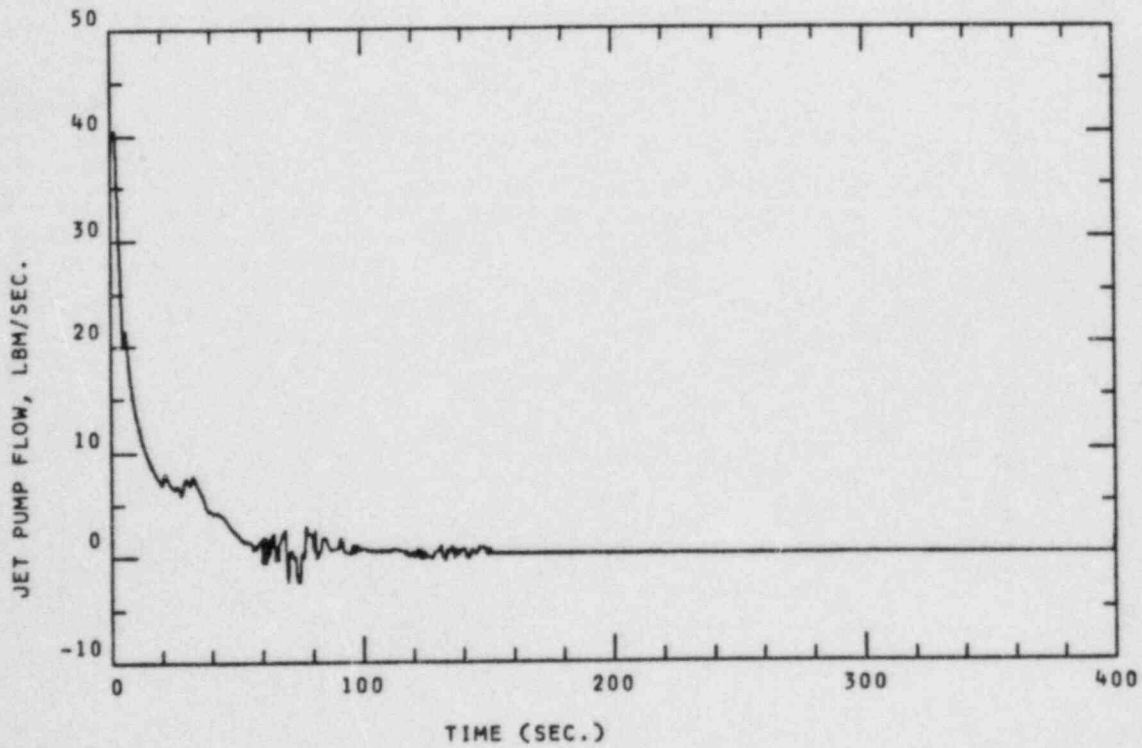


FIGURE 12. JET PUMP FLOW, TEST 6MPC1

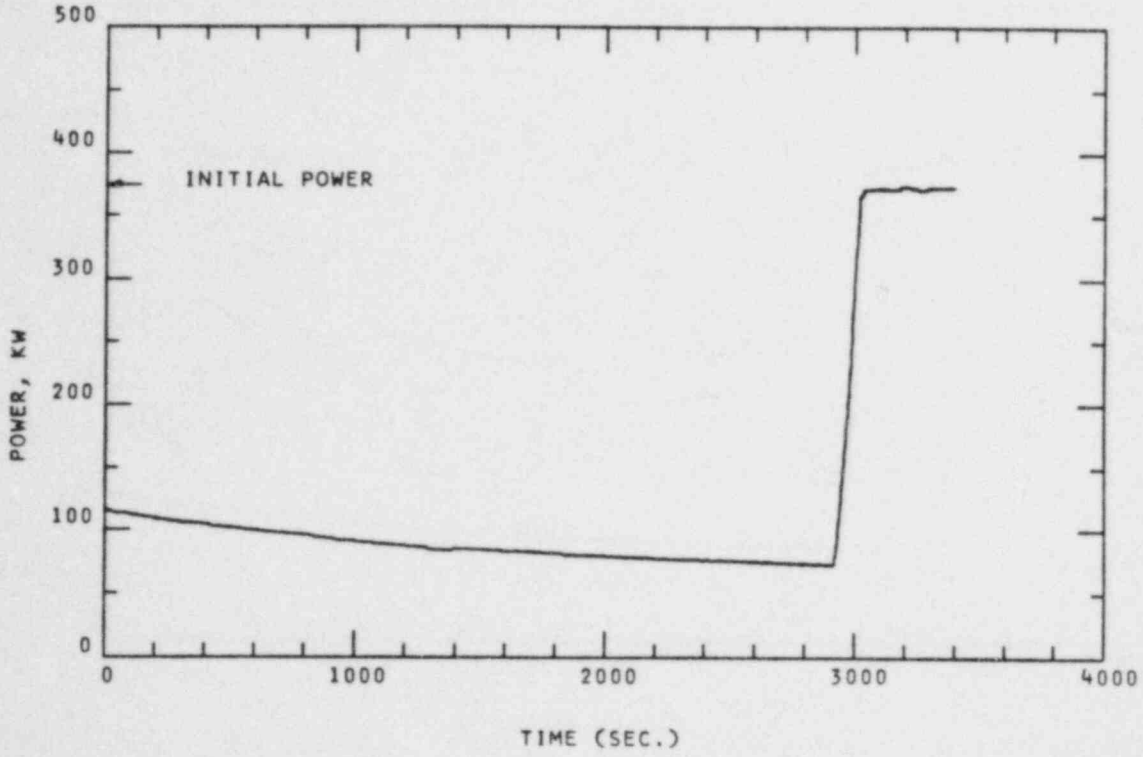


FIGURE 13. BUNDLE POWER, TEST 6PMC3

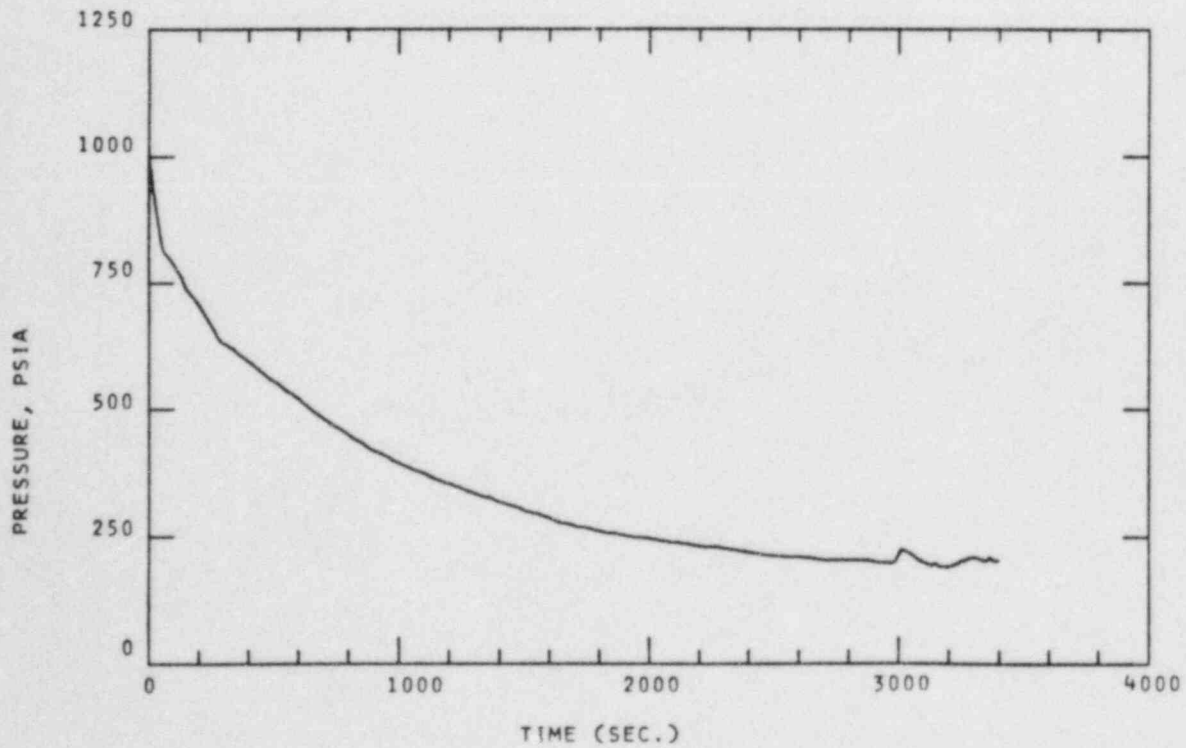


FIGURE 14. SYSTEM PRESSURE, TEST 6PMC3

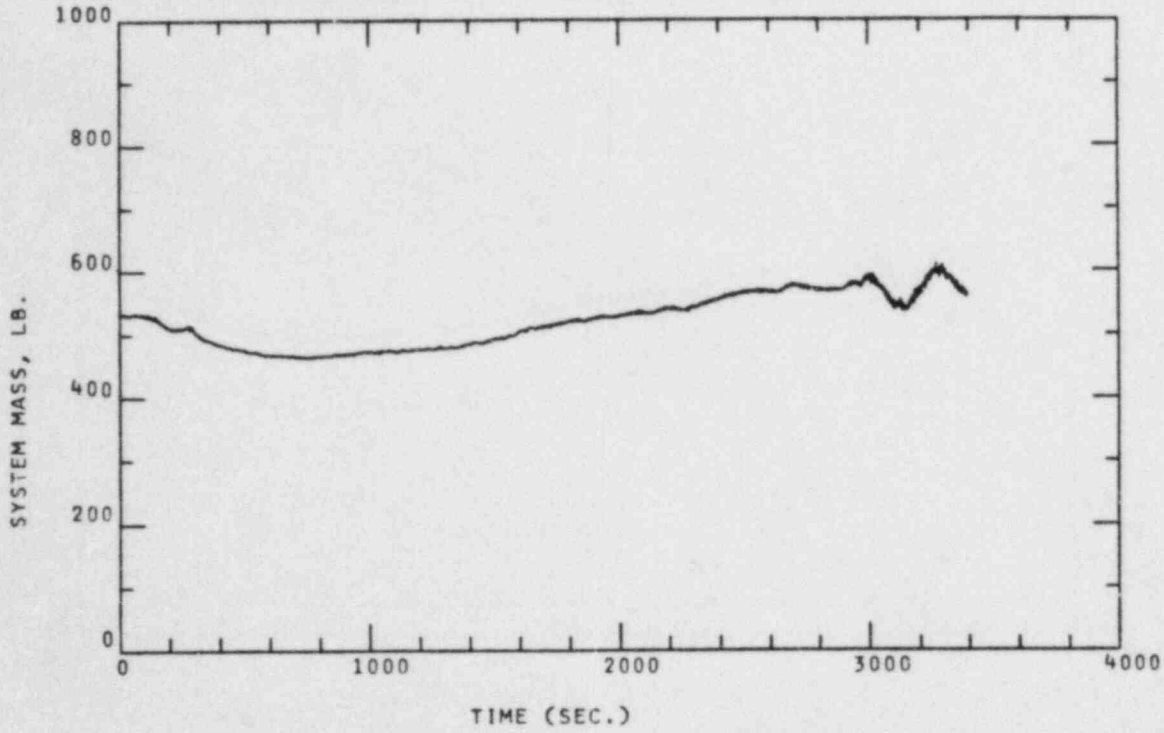


FIGURE 15. SYSTEM MASS, TEST 6PMC3

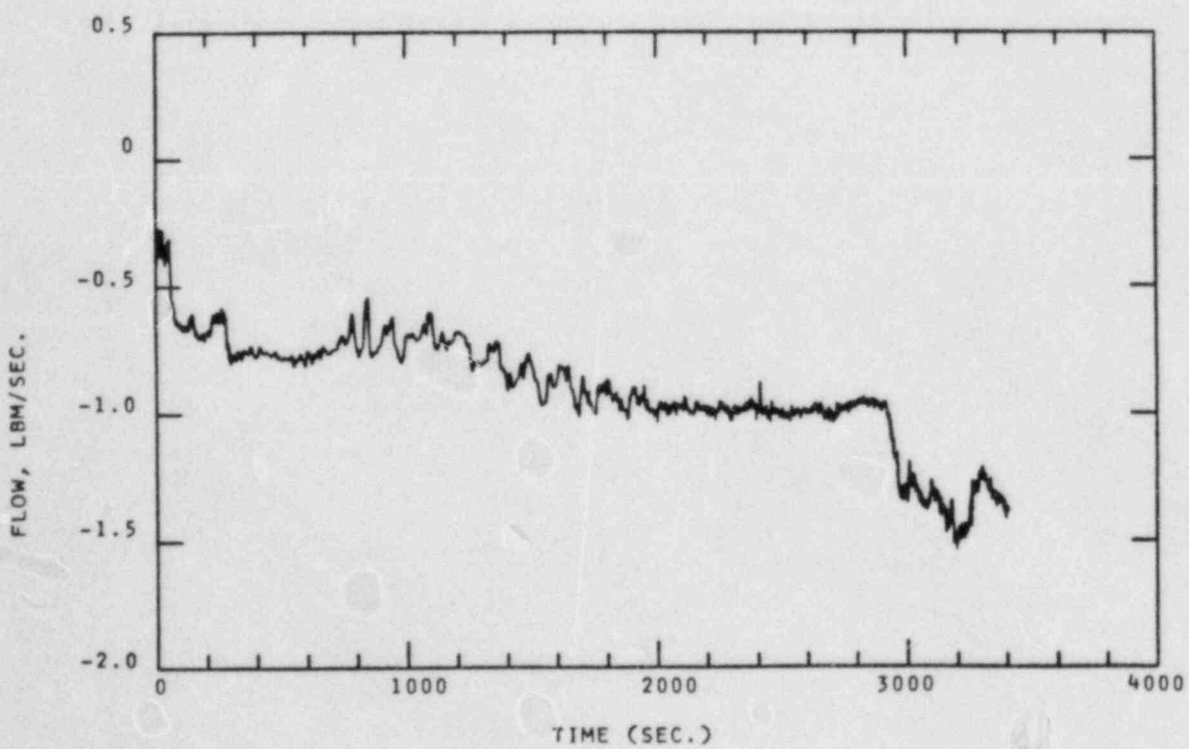


FIGURE 16. BUNDLE/BYPASS LEAKAGE FLOW, TEST 6PMC3

REFERENCES


1. W. S. Hwang, Md. Alamgir, and Wm. A. Sutherland, "BWR Full Integral Simulation Test (FIST) - Phase 1 Test Results", NUREG/CR-3711, EPRI NP-3602, GEAP-30496, November 1983.

2. Md. Alamgir and Wm. A. Sutherland, "FIST Small Break Accidient Analysis with BWR TRAC02 - Pretest Predictions", ANS Topical Meeting - Anticipated and Abnormal Plant Transients in Light Water Reactors, Jackson, Wyoming, September 26-29, 1983.

3. Wm. A. Sutherland and Md. Alamgir, "BWR Full Integral Simulation Test (FIST) Pretest Predictions with TRACB02", Eleventh Water Reactor Safety Research Information Meeting, NUREG/CP-0048 Volume 1, National Bareau of Standards, Gaithersburg, Maryland, October 24-28, 1983.

4. Md. Alamgir and Wm. A. Surtherland, "Using TRAC to Apply Integral Test Experience to Reactor System Analysis", Transactions of ANS, Volume 46, New Orleans. Louisana, June 3-7, 1984.

# POSTTEST DATA ANALYSIS OF FIST EXPERIMENTAL TRAC-BD1/MOD1 POWER TRANSIENT EXPERIMENT

P. D. WHEATLEY
K. C. WAGNER

IDAHO NATIONAL ENGINEERING LABORATORY
EG&G IDAHO, INC.
P.O. BOX 1625
IDAHO FALLS, ID 83415 USA

## ABSTRACT

The FIST power transient test 6PMC2 was analyzed to further the understanding of the FIST facility and provide an assessment of TRAC-BD1/MOD1. FIST power transient 6PMC2 investigated the thermal-hydraulic response following inadvertent closure of the main steam isolation valve and the subsequent failure of the reactor to scram. Failure of the high pressure core spray system was also assumed, resulting in only the reactor core isolation cooling flow for inventory makeup during the transient. The experiment was a sensitivity study with relatively high core power and low makeup rates.

This study provides one of the first opportunities to assess TRAC-BD1/MOD1 under power transient and natural circulation conditions with data from a facility with prototypical BWR geometry. The power transient test was analyzed with emphasis on the following phenomena; (a) the system pressure response, (b) the natural circulation flows and rates, and (c) the heater rod cladding temperature response. Based on the results of this study, TRAC-BD1/MOD1 can be expected to calculate the thermal-hydraulic behavior of a BWR during a power transient.

## INTRODUCTION

Interest in boiling water reactor (BWR) plant behavior during transients, with a failure to scram, has increased in recent years due to several events at commercial sites. This interest has led to the development or enhancement of several computer codes to calculate plant behavior, and an experimental program which in part investigated the BWR response during power transients. The Full Integral Simulation Test (FIST) program, co-sponsored by the United States Nuclear Regulatory Commission (USNRC), Electric Power Research Institute (EPRI) and the General Electric Company (GE), included several experiments during phase I testing to investigate BWR thermal-hydraulic response during a power transient. FIST is well suited to investigate power transients as it is a full height facility with a full sized bundle. Being full height, FIST provides the prototypical water level movement, static head, for fidelity in natural circulation flow. FIST provides some of the first power transient experimental data that can be utilized to assess and benchmark computer codes.

TRAC-BD1/MOD1 (Reference 1), an advanced best estimate thermal-hydraulic computer code, was used to simulate the FIST power transient. The code results were first used to analyze the thermal-hydraulic responses measured in the FIST facility and secondly to assess the capability of TRAC-BD1/MOD1 to simulate the power transient. FIST test 6PMC2 was chosen for analysis as it provides the power transient for the first part of the experiment and a refill/reflood during the later part of the experiment. Thus two very different type transient phenomena were present during one experiment.

## FACILITY DESCRIPTION

The FIST facility was designed and constructed to represent the nuclear steam supply system (NSSS) of a BWR/6 with a vessel diameter of 5.537 m (218 inch). The facility includes two complete, independent recirculation loops. Pump inertia is adjusted for each loop to achieve proper core flow coastdown which is characteristic of a BWR. A heated feedwater system capable of delivering make-up water at BWR rated temperature and scaled flow rates is also featured in the FIST facility to allow steady state operating conditions and provide characteristic downcomer temperature gradients. Other systems included in the facility which were used during power transients are: reactor core isolation cooling (RCIC) system and the safety relief valves (SRV). Five SRVs are used to simulate the five banks of SRVs in the BWR.

The FIST pressure vessel is shown in Figure 1 with the BWR vessel for comparison. The FIST facility is full BWR height with volume scaling (1/624) to a single full sized fuel bundle. All flow areas were scaled based on the single bundle in FIST to the 624 bundles in a BWR. Thus the fluid volumes are also representative of the BWR on a 1 to 624 basis. The simulated downcomer annulus and part of the lower plenum form a separate region connected to the main vessel. The main vessel contains the remainder of the lower plenum and downcomer, along with the other simulated BWR regions. This division of the vessel allows installation of two scaled jet pumps as well as maintaining a scaled cross-sectional area in the downcomer. The jet pumps are designed to provide the appropriate core flow and are the same height as a BWR which provides a prototypical core liquid level and proper natural circulation flow.

The core region contains a single, full size, electrically powered 8 x 8 bundle employing direct heaters. The bundle is surrounded by a typical BWR zircaloy channel which is physically and thermally in contact with the bypass region, thereby allowing bundle to bypass heat transfer typical of a BWR. The FIST bundle inlet and outlet regions are geometrically similar to those in a BWR.

The FIST facility is fully instrumented to measure pressure, temperature, differential pressure, liquid level, and other miscellaneous parameters. Table I summarizes the measurements. A complete description of the facility and the instrumentation can be found in the Facility Description Report (Reference 2).

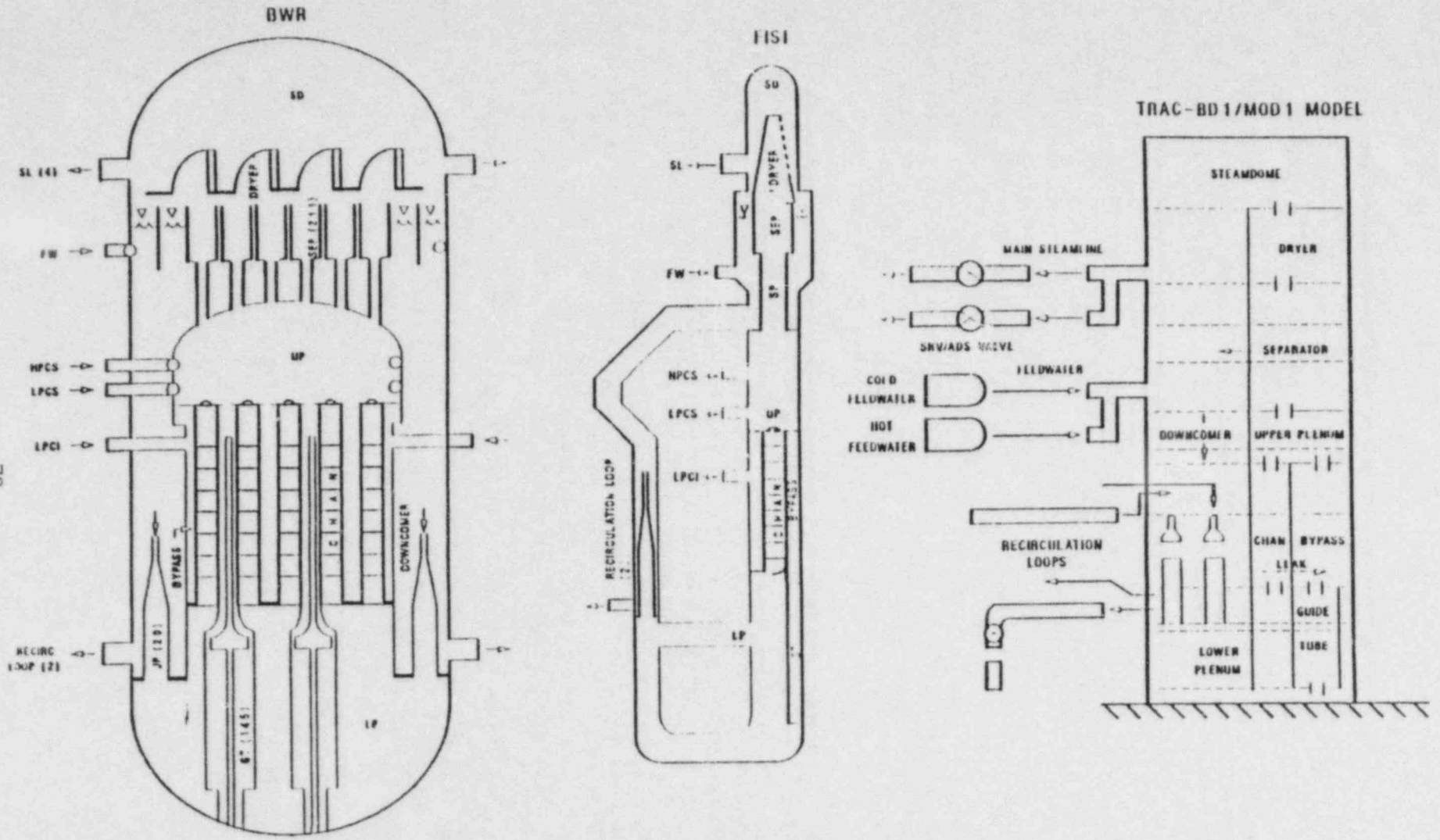


Figure 1. Comparison of FIST facility with a BWR and TRAC analytical model.

TABLE I. FIST EXPERIMENTAL MEASUREMENT SUMMARY

| Parameter | Number of Measurements | Percent of Total |
|---|---|---|
| Pressure | 8 | 1.9 |
| Differential pressure | 126 | 29.9 |
| Conductivity | 45 | 10.1 |
| Metal temperature | 21 | 4.9 |
| Fluid temperature | 82 | 19.3 |
| Heater rod temperature | 112 | 26.4 |
| Miscellaneous | 32 | 7.5 |

## CODE AND MODEL DESCRIPTION

TRAC-BD1/MOD1 provides a best-estimate analysis capability for analyzing the full range of postulated accidents or transients in a BWR system and related experimental facilities. The code allows consistent and unified analysis capability for all areas of a large or small break loss-of-coolant accident, beginning with the blowdown phase, through heatup, reflood with quenching and finally, the refill phase of the accident.

Unique features of the code include: (a) a full nonhomogeneous, nonequilibrium two-fluid thermo-hydraulic model of two-phase flow in all portions of the BWR system, with a three-dimensional thermal-hydraulic treatment of the vessel; (b) detailed modeling of a BWR fuel bundle, including a thermal radiation heat transfer model for radiative heat transfer between multiple fuel rod groups, liquid and vapor phases, and the fuel channel wall with quench front tracking on all fuel rod surfaces and the inside and outside of the fuel channel wall for both bottom flooding and falling film quench fronts; (c) detailed models of BWR hardware such as jet pumps and separator-dryers; and (d) a countercurrent flow limiting model for BWR-like geometries. Other features of the code include a nonhomogeneous, thermal equilibrium critical flow model, and flow regime dependent constitutive relations for the interchange of mass, energy, and momentum between the fluid phases and between the phases and the structure.

The TRAC-BD1 FIST model nodalization is also shown in Figure 1. The model used a vessel component to simulate the lower plenum, bypass, downcomer, upper plenum, separators, dryers, and the steam dome. The FIST vessel had one radial ring and two azimuthal sectors separating the downcomer from the core region. This configuration allowed one-dimensional flow through the vessel and modeling of the vessel walls for both the downcomer and core regions. Double sided heat slabs were used to model the vessel walls and an average heat transfer coefficient was applied to the outside of the heat slab modeling heat losses to the surroundings.

A CHAN component was placed in the core region (Cell 2) at Levels 5 and 6. It simulated an average power bundle with two rod groups, one group representing the water rods and one group for the 62 heated rods. Other systems modeled included (a) the main steamline, main steam isolation valve (MSIV) and the SRVs, (b) the feedwater and the RCIC system, and (c) both recirculation loops with each driving a JET PUMP component.

The FIST TRAC model was run in the steady state mode to establish pretest conditions similar to those in the experiment. A summary of the code calculated initial conditions and those measured prior to the start of the experiment are given in Table II. Several boundary conditions were

TABLE II. FIST INITIAL CONDITIONS FOR TEST 6PMC2

| Parameter | Measured Data | TRAC |
|---|---|---|
| Steamline flow (kg/s) | 2.37 ± 0.12 | 2.49 |
| Feedwater flow (kg/s) | 2.44 ± 0.12 | 2.44 |
| Power (kW) | 4640. ± 30.0 | 4640.0 |
| Jet pump flow (kg/s) | 17.8 ± 0.53 | 17.9 |
| Bypass flow (kg/s) | 1.7 ± 0.34 | 1.67 |
| Steam dome pressure (kPa) | 7173.0 ± 50 | 7199.0 |
| Downcomer level (m) | 10.72 ± 0.13 | 10.77 |
| Downcomer temperature (K) | 552.0 ± 2.0 | 552.0 |

specified as tabular input or a time trip. The following were input in a tabular form; the feedwater flow rate and the RCIC flow rate. The recirculation pumps were tripped on high pressure and the loops were isolated at 73 s by a time trip. The core power was terminated on high heater rod cladding temperature similar to the experiment.

The SRV flow was calculated by the code during the transient after the valve area had been sized during sensitivity runs. The sensitivity runs were necessary as TRAC allows the user to input a single value of the hydraulic diameter and valve area. This method is adequate as long as the valves being modeled are identical (such as in an actual BWR). However, the FIST facility used 5 valves to represent the 16 valves in a BWR. Each FIST valve modeled a valve bank prototypical of a BWR/6 and was therefore of a different size.

The TRAC code assumes the hydraulic diameter varies linearly with valve area. This is a good assumption if multiples of identical valves are being modeled. However the five FIST SRVs were scaled to represent one, three, four, and seven valves. In this case, the hydraulic diameter would vary more like the square root of the flow area. Thus the valves were sized during sensitivity runs to match the flow at the design point of the BWR valves.

## TEST DESCRIPTION

FIST power transient 6PMC2 investigated the thermal-hydraulic response following the inadvertent closure of the main steam isolation valves (MSIV) and the subsequent failure of the reactor to scram. Test 6PMC2 was a sensitivity experiment with relatively high core power and low inventory makeup rates. The core power history was calculated using a BWR/6 plant deck and a one-dimensional neutronic code. Assumptions in the neutronics calculation were boron injection at 120 s and the high pressure core spray (HPCS) system was available. When the 6PMC2 experiment was conducted the HPCS system was inhibited. Therefore, the power curve was higher than the RCIC system would be expected to handle. The effects of this will be discussed shortly.

The experiment was initiated, after a short period at steady state by activating the preprogrammed bundle power controller. The steam valve (MSIV) closed 2 s after test initiation. The programmed bundle power peaked at 7300 kW (157% nominal) at 5.5 s. The bundle power was terminated at 357 s when an administrative limit of 895 K on rod cladding temperatures was reached. The rod cladding heatup was a direct result of using a power curve generated assuming HPCS operation and conducting the experiment with only RCIC operational. A rod heatup is not expected during a power transient in which only RCIC is available, see test 6PMC2A of the FIST test series (Reference 3).

As system pressure increased, after steam valve closure, the SRVs opened to halt the pressure rise. The SRVs opened and closed on pressure setpoints identical to the BWR settings. The high system pressure tripped the recirculation pumps at 4 s and started the timer for loop isolation which occurred at 73 s. The feedwater system was operated as close to a BWR as possible within the FIST feedwater pump shut-off head restrictions. Liquid level in the downcomer decreased as system inventory was lost through the SRVs. Level 2 was reached at 70 s and the RCIC flow was activated at 85 s. RCIC flow was not large enough to restore the downcomer level until core power was terminated and the SRVs closed.

The rod cladding temperatures above the 1.448 m level in the core underwent heatup. The peak cladding temperature of 895 K was reached at the 2.972 m elevation. The cladding temperatures turned around and decreased due to the bundle power trip at 357 s and following reflood by the RCIC system. The core uncovery and rod heatup was a result of the mismatch in the programmed power and the unavailability of the HPCS system in the experiment, as discussed previously.

## RESULTS

The power transient calculation was analyzed and compared with data in what were considered to be the areas of most interest to individuals using the data in the field of severe accident analysis. This section will provide a review of the data and code capabilities in the following areas: (a) system pressure response, (b) natural circulation flow rates, and (c) the heater rod cladding response.

A key parameter during the power transient is the system pressure response, as this parameter has a large influence on the void feedback in a nuclear plant. The FIST system pressurization results were analyzed using both the neutronics code results and the TRAC-BD1/MOD1 code results. The preprogrammed power input was based upon a neutronics code calculation of a BWR/6 facility. Unfortunately, the full output from the neutronics code calculation was not available. Consequently, the characteristics of the BWR/6 pressurization behavior were analyzed using the preprogrammed power input, the measured system pressure response, and the TRAC-BD1 calculated system response.

Some information relative to a BWR/6 response may be deduced by examining the preprogrammed power input (see Figure 2). The spiked behavior of the core power profile was induced by the calculated SRV response. When several SRVs were calculated to open, the system pressure decreased and the core void fraction increased. The increased core void fraction moderated the neutronics reaction and caused a subsequent decrease in the core thermal power. Similarly, when several SRVs were closed, the system pressure was calculated to increase and the voids in the core collapsed. Consequently, the lower core void fraction caused the core thermal power to increase. Thus, the peaks in the programmed power input represent SRV openings and the troughs represent SRV closings. The peaks and troughs were concluded to represent the cyclic pressure response in a BWR/6 between upper and lower SRV pressure setpoints, respectively.

The TRAC-BD1 calculated and the FIST measured results for the steam dome pressure are presented in Figure 3. The system pressure increased in response to the MSIV closure. The code calculated a peak of 8525 kPa versus a measured peak of 8425 kPa at about 6 s. The pressure rise was halted by the opening of all the SRVs in both the calculation and the experiment. The pressure oscillated between 6650 kPa and 7900 kPa, the setpoint for the SRVs. The pressure response of the facility lagged that of the calculation after the SRV closing as the system repressurized. During the fifth pressurization the calculated pressure reached the setpoint of the third and fourth SRVs and they opened unlike the experiment. The experiment was very close to the setpoint (within 300 kPa) but the SRVs in the facility did not open. The programmed power decreased (indicating a SRV opening in the BWR6) shortly thereafter and the measured pressure decreased. It is believed that the large flanges in the FIST facility damped the pressure response slightly and were enough to prevent the system pressure from reaching the SRV setpoint before the programmed power decreased. The large flanges, which are not prototypical, were not modeled in the TRAC calculation. Consequently a higher pressurization rate was calculated.

Next, the FIST natural circulation flow was examined. The FIST facility has an external downcomer to assure proper volumetric and flow area scaling. Although the geometrical dimensions were properly scaled to a BWR/6, the FIST external downcomer presented two problems relative to heat transfer considerations. First, an external downcomer does not have any heat transfer from the core region of the vessel as in a prototypical BWR/6 annular downcomer. Secondly, the FIST facility has a high relative heat loss from the downcomer. The combination of these two deficiencies could cause the FIST

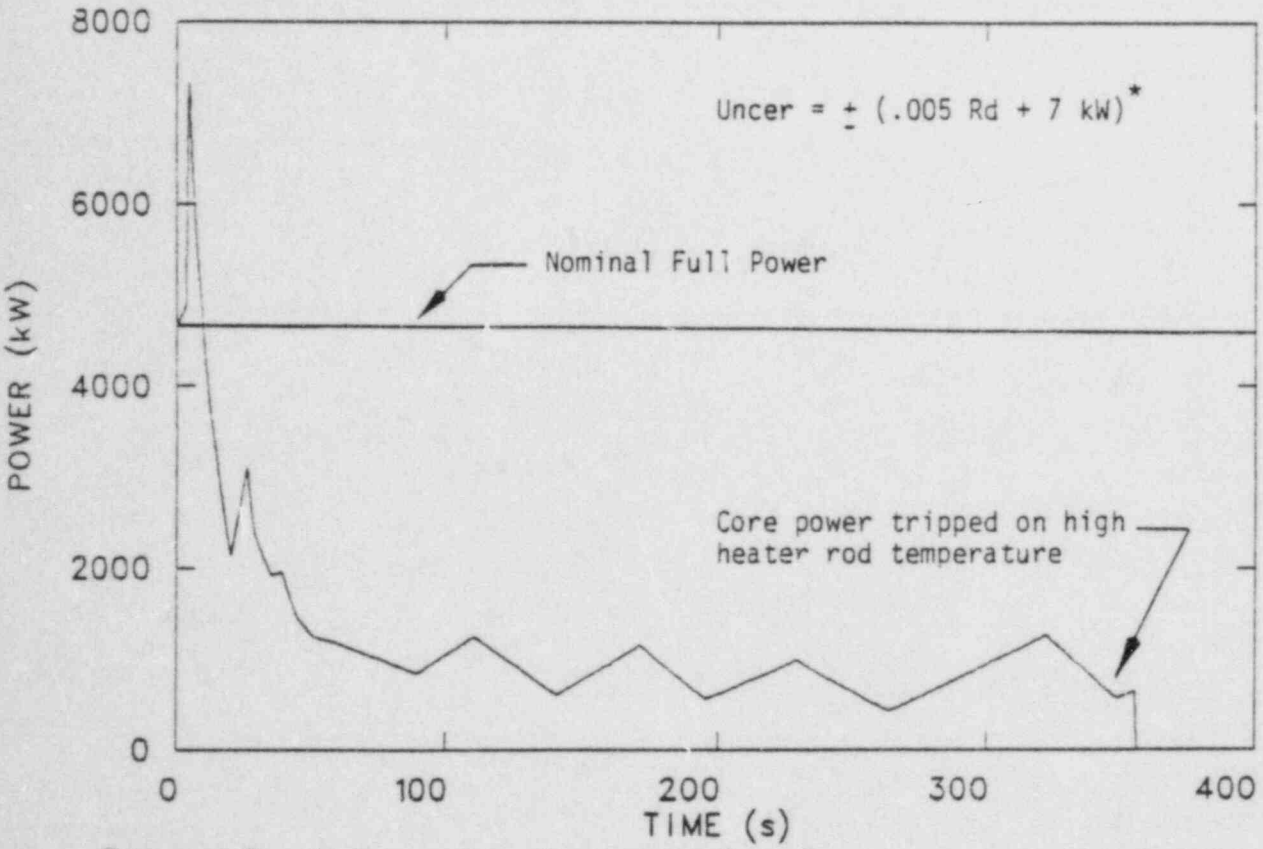


Figure 2. Measured core power input.

* Uncer = Uncertainty
Rd = Reading

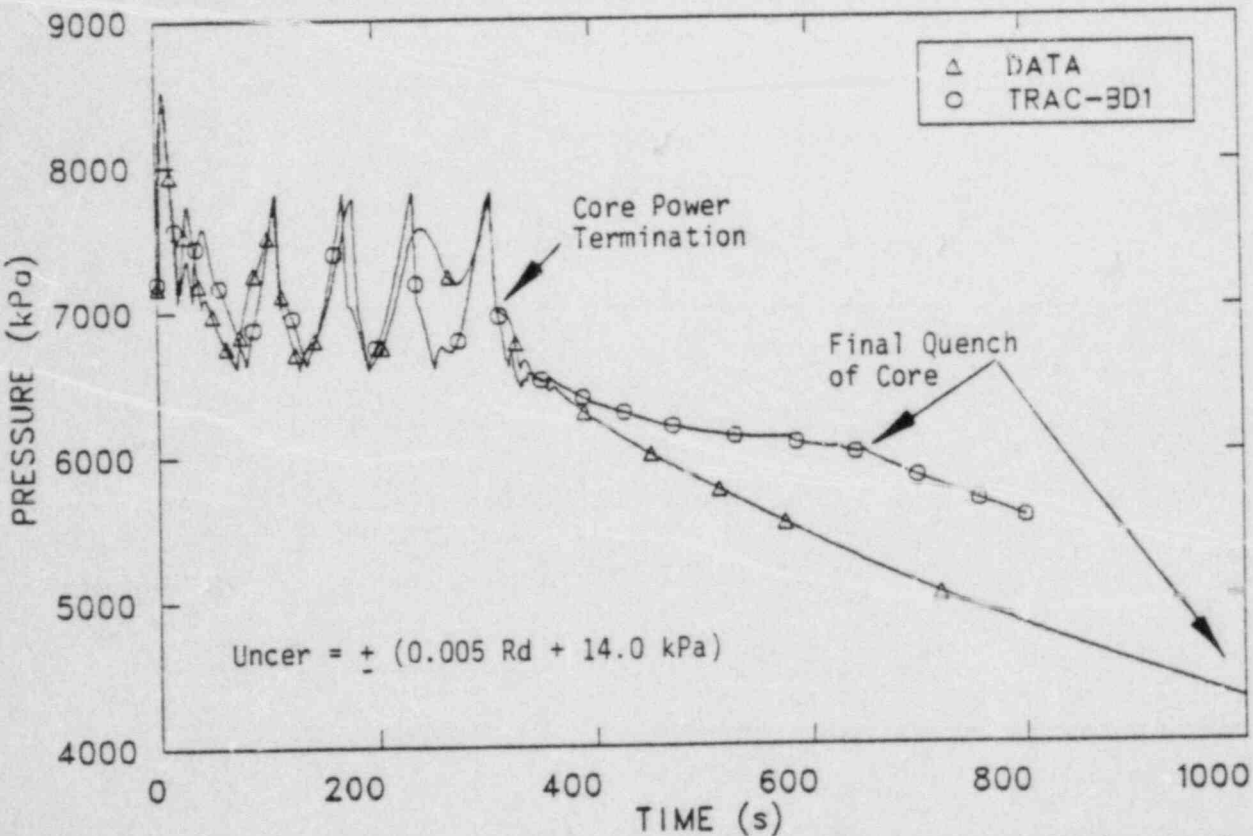


Figure 3. Comparison of calculated and measured steam dome pressure through 1000 s.

facility to have a lower downcomer temperature than would be prototypical. Consequently, the natural circulation in the FIST vessel was investigated for any discrepancies relative to the additional heat loss in the downcomer.

The bundle inlet flow rate was examined as a function of the liquid level in the downcomer. The code calculated values and those measured during the experiment were in good agreement as shown in Figure 4. At the lower elevations, around seven meters, the code calculated flow was slightly less than the measured flow. The ambient heat loss was smeared over the entire vessel, due to the limitation of the code, whereas the downcomer was the highest heat loss region experimentally. The downcomer temperatures were slightly lower in the experiment leading to the higher flow rate. The smaller heat loss from the downcomer during the calculation would probably be more prototypical of BWR/6 for reasons previously discussed. However, the natural circulation flow results were fairly insensitive to the heat loss distribution. Consequently, if the FIST facility downcomer heat loss was not prototypical of a BWR/6, it was concluded to have a small influence upon the natural circulation flow.

The downcomer water level is interrelated with the natural circulation flow rate. The flow may be correct for a given elevation in the downcomer but the level movement with time must also be correct to provide a truly accurate description of the transient phenomena. Figure 5 compares the calculated and measured downcomer liquid levels. Early in the transient there was excellent agreement between the two. At 41 s the measured level decreased as the level passed the bottom of the separator skirt. The calculated level did not show a similar decrease as the separator still had a reasonably low void mixture which drained into the downcomer. The liquid drainage from the separator was due to the nodalization of the facility. Subsequent models have moved the separator liquid discharge to Level 11 eliminating the liquid storage in the separator. Though the measured and calculated levels differ for the remainder of the transient, the level movement does show similar slope and trends.

The discussion will now shift to the refill/reflood of the core after the bundle power termination and the phenomena which is usually associated with loss-of-coolant accidents but may be important during a power transient with several auxiliary system failures.

The heater rod cladding response was examined and a typical TRAC calculated rod temperature and several measured cladding temperatures at the same elevation are shown in Figure 6. The TRAC calculated temperature shows a departure from saturation conditions approximately 35 s earlier than the measured values. The early heatup is due to the higher integrated vessel mass loss when the SRVs opened during the fifth vessel repressurization, as discussed earlier.

Both the calculated and measured temperatures peaked at 895 K when the bundle power was terminated. The measured temperatures rolled over as the bundle power was terminated and decreased as the core was reflooded. The calculated temperatures rapidly decreased 25 K before showing a cooling rate similar to the experiment. The differences were due to the location of the measured versus the calculated temperatures. The measured temperatures were

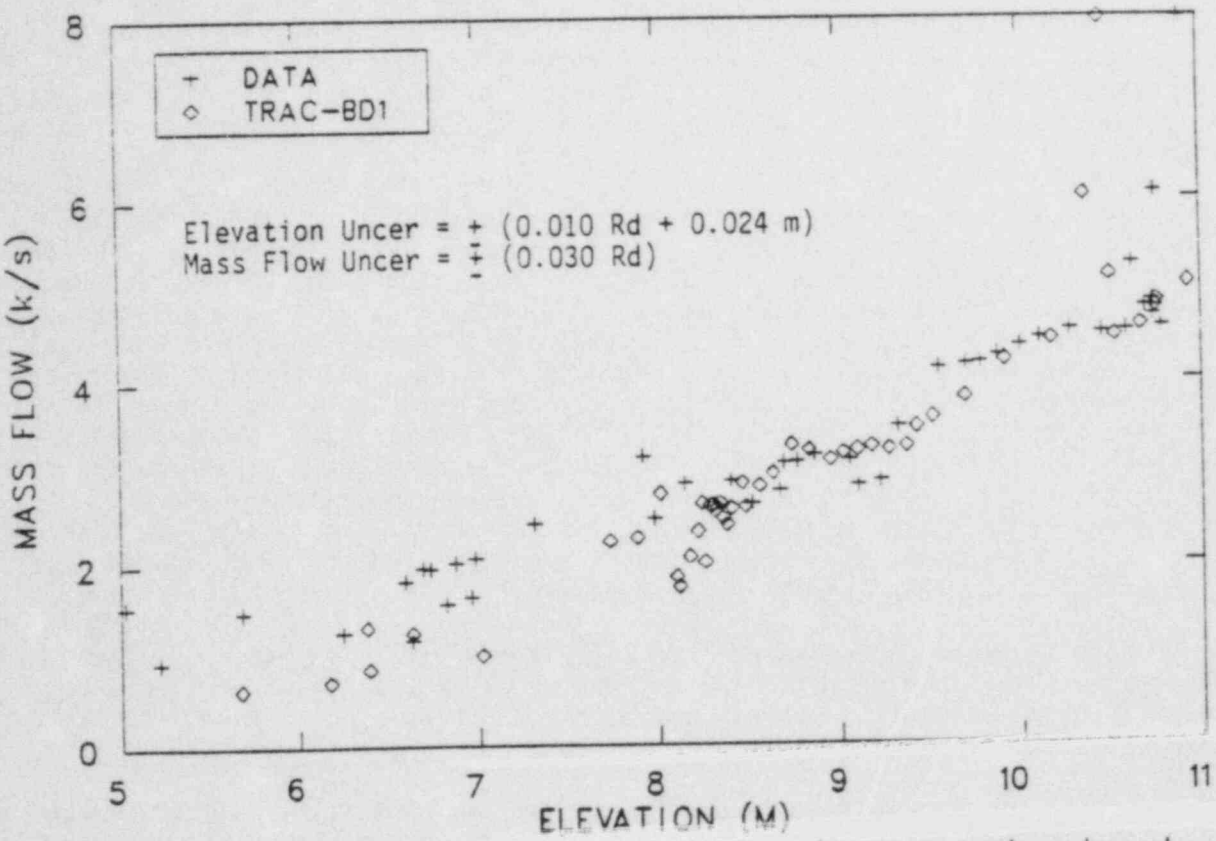


Figure 4. Comparison of calculated and measured natural circulation flow versus downcomer level.

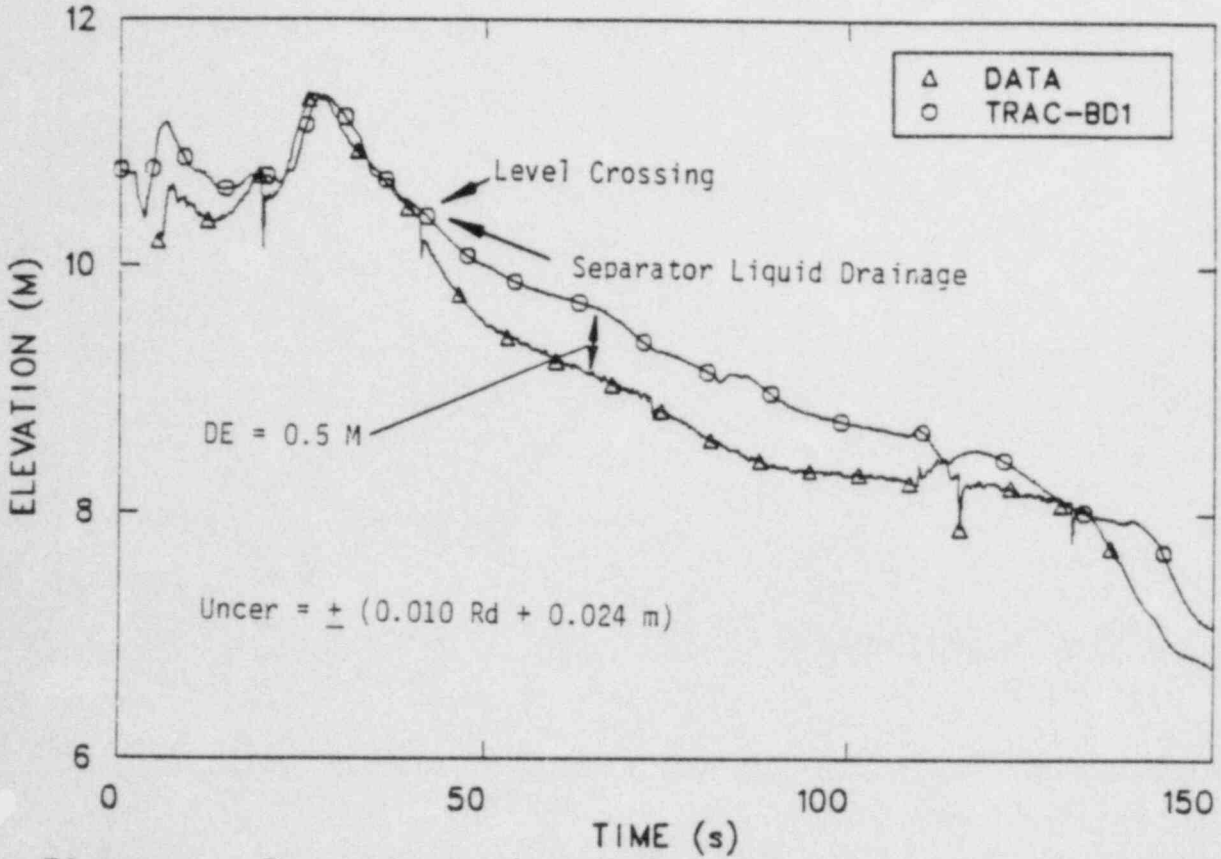


Figure 5. Comparison of calculated and measured downcomer level.

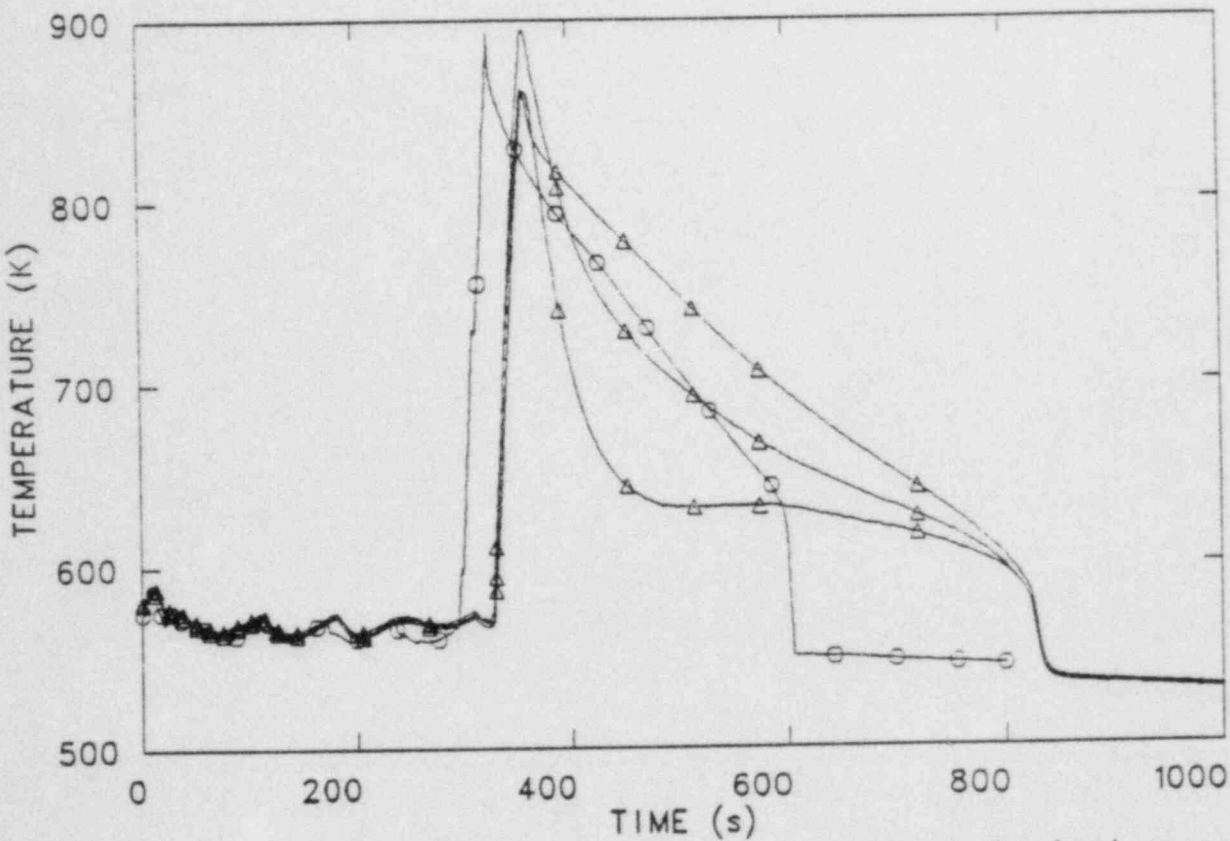


Figure 6. Comparison of calculated and three typical measured heater rod temperatures at 2.972 m (117 inch) level.

on the inside of the cladding and thus exhibited a delay in cooling after bundle power trip, whereas the calculated temperatures were for the outside of the cladding. Due to code limitations on where cladding temperature can be monitored and plotted it was necessary to use the calculated outside temperatures and inside measured temperatures. After the initial turnaround the temperatures are believed to differ very little from inside to outside.

The TRAC calculation showed quenching earlier than the experiment. The core quench front position versus the core liquid level is shown in Figure 7. The liquid level and quench position were the same for the experiment. The TRAC calculation showed a quench front preceding the liquid level. Entrainment of fluid in the bundle caused the quench front to precede the liquid level. The top three nodes in the channel quenched as fluid in the lower downcomer flashed forcing liquid into the bundle. The flashing was apparently caused by too little heat loss in that portion of the downcomer; therefore liquid flashed as the pressure decreased.

## CONCLUSIONS

Both the natural circulation and downcomer liquid level agreed well with the TRAC calculation. The heater rod response and peak cladding temperature were also in good agreement with the code. System pressure matched the calculated pressure well enough that pressure effects should be represented adequately for the neutronics package in TRAC when used for plant calculations. FIST power transient data from both test phases can be used to assess current codes and is considered typical of the phenomena occurring in the BWR. Calculated quench front propagation and time to quench were not in good agreement with the data due to entrainment within the bundle, TRAC-BD1/MOD1 was capable of calculating the thermal-hydraulic phenomena in the FIST facility during a power transient event.

## REFERENCES


1. D. D. Taylor et al., TRAC-BD1/MOD1: An Advanced Best Estimate Computer Code for Boiling Water Reactor Transient Analysis, NUREG-CR-3633, EGG-2294, April 1984.

2. A. G. Stephens et al., Full Integral Simulation Test Facility Description Report, General Electric, to be published July 1984.

3. W. S. Hwang et al., BWR Full Integral Simulation Test (FIST) Phase I Test Results, General Electric, to be published July 1984.

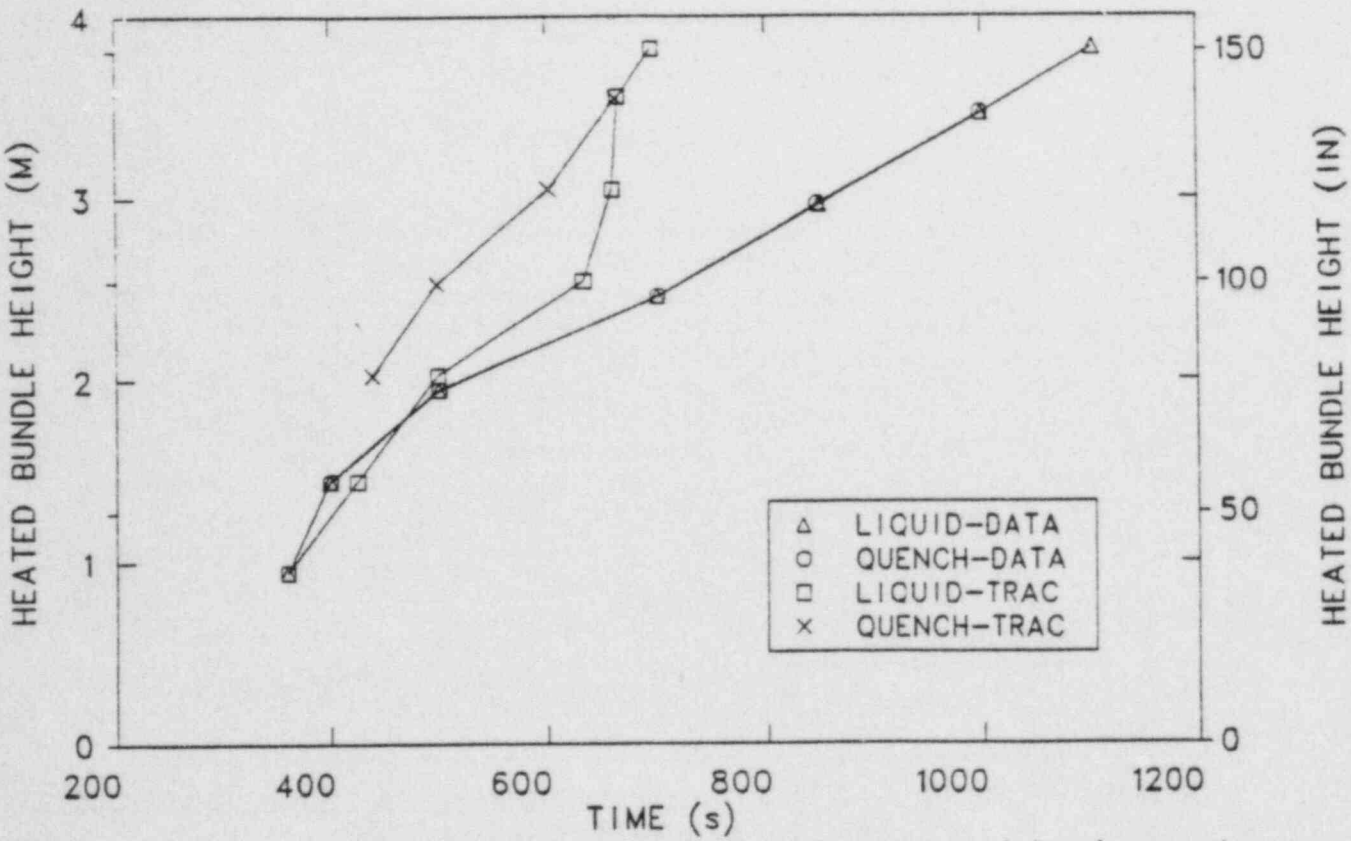


Figure 7. Comparison of calculated and measured heater rod quench front and core liquid level.

# RELAP5/MOD2 BLIND CALCULATION OF GERDA SMALL BREAK TEST AND DATA COMPARISON

Donald M. Ogden
James L. Steiner
Michael E. Waterman
EG&G Idaho, Inc.

## INTRODUCTION

The GERDA (Geradrohr Dampferzeuger Anlange/straight tube steam generator) facility, located in Alliance, Ohio was built by Babcock and Wilcox (B&W) for Brown-Boveri Reaktor of Mannheim, Germany. The Multiloop Integral Systems Test (MIST) program, which is jointly funded by B&W, B&W owners group, Electric Power Research Institute (EPRI) and the United States Nuclear Regulatory Commission (USNRC), purchased the GERDA facility and test data that had previously been produced to address licensing issues for the German Mulheim-Karlich plant. The Idaho National Engineering Laboratory (INEL), in support of the USNRC, has developed a RELAP5/MOD2 model of the GERDA facility to be used for analysis of the GERDA data, particularly relative to the phenomena of natural circulation and the boiler condenser mode of heat transfer. A blind calculation of GERDA Test 1605AA and a preliminary comparison with experimental data has been performed.

## FACILITY DESCRIPTION

The GERDA facility is a single loop integral facility with an electrically heated core. A general arrangement diagram of the facility is shown in Figure 1. The GERDA facility was designed for the performance of both separate effects and overall systems tests with scaled power up to 5% of

3760 Mwt. The primary side of the loop is configured with a 19 tube once through steam generator (OTSG); a simulated vessel with an external downcomer, lower plenum, core region, and upper plenum; a single hot leg and cold leg; and a simulated pressurizer. Also included are simulated high pressure injection, reactor vessel vent valves and high point vent valves. The secondary side components include the OTSG, a water cooled condenser, hot well, circulating pump, feedwater heaters and associated control valves.

Scaling for the GERDA facility was accomplished with the following priority:

1. full elevation simulation
2. maintaining governing phenomena of small break LOCA
3. volumetric simulation
4. conserving loop irrecoverable losses.

As a result of these scaling considerations, the overall secondary heat-transfer length is preserved and the relative relationship of the major components is preserved. The scale factor is 1686 and applies to the secondary heat removal capacity, the system volume, the core power, pressurizer volume, and leak, injection, venting, and relief valve flowrates. Loop piping is not volume scaled but rather is scaled to the Froude number to preserve the ratio of bouyant and inertial forces. Orifice plate resistance was used to scale the irrecoverable loop losses.

## TEST DESCRIPTION

Test 1605AA was a small break natural circulation test with automatic and manual control functions typical of a German PWR. The leak (break) was located in the lower plenum and was scaled to represent a 10 $cm^2$ leak in a full scale plant. The circulation pump was used only to establish the initial conditions and was valved out of the primary system during the transient part of the test. The transient decay power during Test 1605AA was 1.2 times the ANS decay power plus .21% of scaled full power, to account for ambient heat losses. The steam generator secondary pressure

was controlled by a control valve located at the end of the steam discharge line. The control valve set point was varied with time during the test as shown in Figure 2. Auxiliary feedwater was injected into the lower steam generator secondary during the test and was regulated to control the collapsed level in the secondary as shown in Figure 3. From 0-348 s the level set point was 10 ft (above the tubesheet) and after 348 s the level set point was maintained at 26 ft. The high point vent, located at the top of the hot leg U-bend (candy cane), was opened at 1908 s in the test and calculation. Time zero corresponds to the time when the data acquisition system was turned on. At 132 s the circulation pump was valved out and at 156 s the leak was initiated.

## MODEL DESCRIPTION

The RELAP5 model used for the calculation had a total of 91 volumes, 91 junctions, and 89 heat structures. The RELAP5 nodalization is shown in Figure 4 and a physical description of the RELAP5 components is given in Table 1. Heat structures were used in the model to represent the loop piping, vessel and pressurizer walls, steam generator shell and tubes, and heater rods in the core. The outer surfaces of the pressurizer, surge line and hot leg were modeled adiabatically since these components are externally heated in the GERDA facility. Heat losses from the remaining components were modeled using a constant heat transfer coefficient at the component outer surface. The value of the heat transfer coefficient was determined by comparing calculated heat losses to experimentally determined heat losses provided by B&W.

The version of RELAP5/MOD2 used contained updates to partition the heat transfer from heat structures to each phase of the adjacent fluid. With the updates, the heat transfer to each phase was determined by the calculated heat transfer mode and the void fraction. Previously, the total surface heat transfer was not an explicit function of the void fraction. The updates are general in nature and will be made permanent in a future version of RELAP5/MOD2. An update was also used to calculate the primary

to secondary heat transfer rate in the lower region of the steam generator boiler region. The update removed the natural circulation heat transfer coefficient contribution from the total heat transfer term.

## ANALYSIS OF TEST DATA

The results of the RELAP5/MOD2 blind calculation of GERDA Test 1605AA are described in this section. Differences between the calculated results and the test data are addressed. The system responses observed in Test 1605AA are explained using the results of the RELAP5/MOD2 calculation. It is emphasized that this report should not be considered an assessment of RELAP5/MOD2, since the calculation was performed without the benefit of test data for the specification of boundary conditions.

Small break transients are characterized by the primary and secondary system pressures since the physical phenomena occurring during small break transients are reflected in these pressures. The primary system pressure is generally determined by the total mass and energy of the fluid in the primary system. In a very small break transient, such as Test 1605AA, the rate of change of fluid mass in the primary system is low, and heat transfer to the primary system fluid in the steam generator, vessel, and loop piping is the important mechanism controlling the primary system pressure.

The calculated and measured primary and secondary system pressures are shown in Figure 5. Both the calculated and measured primary system pressures decreased rapidly after leak initiation at 156 s due to the flow of subcooled liquid through the leak and expansion of the liquid remaining in the primary system. The subcooled decompression ended at approximately 400 s in both the calculation and in the experiment when the saturation pressure was reached in the hot leg and flashing was initiated. The calculated primary system pressure at this time was lower because the initial hot leg tempature was lower (Figure 6) and flashing was initiated somewhat later. The reduction in primary system pressure resulted in initiation of high pressure injection (HPI) flow.

The hot leg and steam generator tube bundle liquid level responses are shown in Figure 7. The levels began decreasing when the hot leg saturation pressure was reached. The decreasing collapsed liquid level was caused by a combination of (a) flashing of liquid to vapor as the primary system reached saturation pressure, (b) decreasing primary system inventory caused by the leak flow, (c) decreasing primary system average temperature caused by the programmed decrease in core power, and (d) heat transfer to the secondary system which caused a reduction in the primary system average temperature and consequently shrank the primary system coolant.

The cold leg flow rate response is shown in Figure 8. The cold leg flow rate decreased in the calculation and the test as the hot leg and steam generator tube bundle liquid levels decreased. The calculated cold leg flow rate was reduced to nearly stagnant conditions by 530 s, while the flow rate in the test was somewhat greater in magnitude until 1670 s. The higher flow rate in the test was responsible for the essentially constant primary system pressure response shown in Figure 5 from 400-2000 s. The nearly stagnant conditions in the calculation resulted in the primary system average temperature increasing from 400-1600 s because the heat added by the core could not be transferred to the steam generator secondary.

The reduction in the steam generator tube bundle liquid level was responsible for the initiation of an important period in the calculation and the test. The axial temperature distribution of the tube bundle walls is governed by the secondary system conditions. The temperature usually increases with increasing elevation. The vapor region in the tube bundle primary side expanded downward as the steam generator liquid level decreased. When the saturated vapor region reached the level in the tube bundle where the tube wall temperature was less than the saturated vapor temperature, the vapor began condensing on the wall surface. The resulting phase change of the vapor to the liquid phase liberated substantial energy, which was subsequently transferred through the tube walls to the secondary system. This process of vapor condensation with subsequent increased heat transfer is referred to as boiler-condenser mode (BCM) heat transfer. The initiation of BCM occurred at 1744 s in the calculation and 2032 s in the

test, as indicated by the sudden increases in the primary to secondary heat transfer rates shown in Figure 9 and the relatively rapid pressure changes shown in Figure 5. The difference in the timing of the BCM phase was caused by an underprediction of the vapor generation rate in the core, which resulted in the overprediction of steam generator level decrease rate shown in Figure 7.

The BCM caused the primary system pressure to decrease via the cooling of the primary system caused by the increased heat transfer to the secondary. HPI flow increased when the primary system pressure significantly decreased below the HPI set point (1710 psia). The HPI flow exceeded the leak flow around 2190 s in the calculation and 2420 s in the test, as indicated by the primary system mass responses shown in Figure 10. The subsequent refilling of the steam generator tube bundle caused the BCM phase to end at 2565 s in the calculation and 3228 s in the test. While the calculated period of BCM did not agree with the test data, the magnitudes of the pressure responses were reasonably well predicted, as shown in Figure 5. It is important to note that the primary system pressure would not have significantly decreased below the HPI setpoint (1710 psia) if the BCM had not begun. Without the increased HPI flow, the primary system would have refilled much later, and significant core uncovery would have probably occurred.

After the BCM, the primary system was pressurized by vapor generation in the vessel while the vessel was being refilled. Figure 11 shows that the vessel was refilled to the hot leg elevation at 2800 s in the calculation and at 3600 s in the experiment. This difference was due to the timing of the BCM heat transfer periods.

The vessel liquid level responses shown in Figure 11 were different in the calculation and the test. The differences were caused by two RELAP5 modeling factors. First, the core power used in the RELAP5 model was less than the power used in the test (Figure 12). Consequently, the vapor generation rate in the calculation was lower than in the test which resulted in less vapor inventory in the vessel upper head. The second

factor was the omission of the vertical stratification flow regime option in the vessel components (the vertical stratification flow regime option limits the vapor condensation rates when liquid enters a vapor filled volume). These two factors combined to limit the amount of vapor in the vessel upper head. The vessel upper head pressure was the highest primary system pressure in the test because a substantial amount of vapor filled the vessel upper head. This resulted in the vessel acting like a pressurizer, with the hot and cold legs acting as surge lines. In the test, the vessel continued to fill until the vessel level reached the hot leg elevation, then the hot leg began filling because the upper head was at a higher pressure than the top of the hot leg candy cane.

In the calculation, the vessel upper head pressure was lower than the hot leg candy cane pressure; consequently, the vessel level increased up to the reactor vessel vent valve (RVVV) elevation. The pressure above the core region was higher than in the downcomer and the RVVV cycled open and closed. This promoted increased circulation from the vessel downcomer into the core which subsequently reduced the hot leg temperature and caused the primary to slowly depressurize due to coolant shrinkage. The vessel refilled prior to the hot leg and steam generator tube bundle because the upper head pressure was lower than the hot leg candy cane pressure.

While the calculated vessel and hot leg refill responses did not agree with the test data, their contrast with the test data highlighted the importance of the vapor region in the vessel upper head with regard to primary system refill response.

As the steam generator tubes were refilled in the calculation the calculated primary system pressure was increased by vapor generation in the hot leg between the steam generator and the U-bend. This increase in the primary system pressure at 7000 s (Figure 5) occurred in the calculation but not in the experiment. The difference was caused by the modeling of the upper volume in the hot leg U-bend. The high point vent valve (HPVV) was connected to the centerline of the U-bend instead of the top. Hence, when liquid entered this volume it was discharged through the valve instead

o, overflowing into the steam generator side of the hot leg, as it did in the test. If the liquid had overflowed it would have quenched the piping wall and steam generator upper plenum. The resulting vapor would have then been discharged through the HPVV. The location of the HPVV connection resulted in preventing vapor generated by the refilling steam generator from being discharged. The resulting compression of the vapor caused the pressure increase seen at 7000 s.

A final increase in the calculated primary system pressure occurred at 8485 s in the calculation, when the primary system was entirely refilled, except for the pressurizer. In the experiment, the upper vessel refilled more slowly than in the calculation (Figure 5) resulting in a slower increase in the measured primary system pressure after the hot leg was refilled. The increase in the measured system pressure at 7200 s resulted from vapor generation in the pressurizer as the pressurizer began to refill.

## CONCLUSIONS

The general response of GEDA Test 1605AA was well predicted until the vessel refilled to the hot leg elevation. The boiler-condenser mode heat transfer phenomenon was correctly predicted except for the time of initiation. The time of BCM initiation was underpredicted because (a) the calculated vapor generation rate in the vessel was less than in the test due to less core power and in the test, and (b) vapor condensation in the core was overpredicted because the vertical stratification model option was not used in the vessel model. Hence, the vapor generation affect on steam generator tube bundle level that was seen in Test 1605AA was underpredicted in the calculation, which caused the difference in the timing of the major events prior to the refilling of the vessel to the hot leg elevation. The relative timing of major phenomena, however, was correctly predicted.

The underprediction of the vapor generation rate and the overprediction of the condensation rate in the reactor vessel resulted in major differences in the prediction of primary system component refill times. The vessel upper plenum and head were predicted to refill before

the hot leg and steam generator; whereas, in the test, the hot leg and steam generator refilled before the reactor vessel. This difference in predicted system response caused an overprediction in the time natural circulation resumed.

The calculation of GERDA Test 1605AA using RELAP5/MOD2 was influenced by the model of the test facility; and while some differences in system response were calculated, these differences can be explained by modeling considerations. Revisions of the RELAP5/MOD2 model of the GERDA test facility will result in more accurate analyses of GERDA test responses in future calculations.

TABLE 1. RELAP5 MODEL COMPONENTS

| GERDA Facility Component | RELAP5 Components |
|---|---|
| Primary System | |
| Hot leg piping | 100, 105, 110, 120, 121, 124 |
| Pressurizer | 200 |
| Pressurizer surge line | 201, 210, 211 |
| Steam generator | 130, 135, 140, 145, 150 |
| Cold leg piping | 160, 165 |
| Downcomer | 170, 175, 180, 185 |
| Lower plenum | 502, 510 |
| Core | 520 |
| Upper plenum | 530, 540, 550 |
| Steam Generator Secondary | |
| Boiler | 300, 310, 320 |
| Auxiliary feed | 350, 351, 360, 361 |
| Discharge line | 370 |
| Discharge control valve | 372, 374, 376, 378 |
| Boundary Conditions | |
| Leak | 192, 194 |
| High point vent valve | 122, 123 |

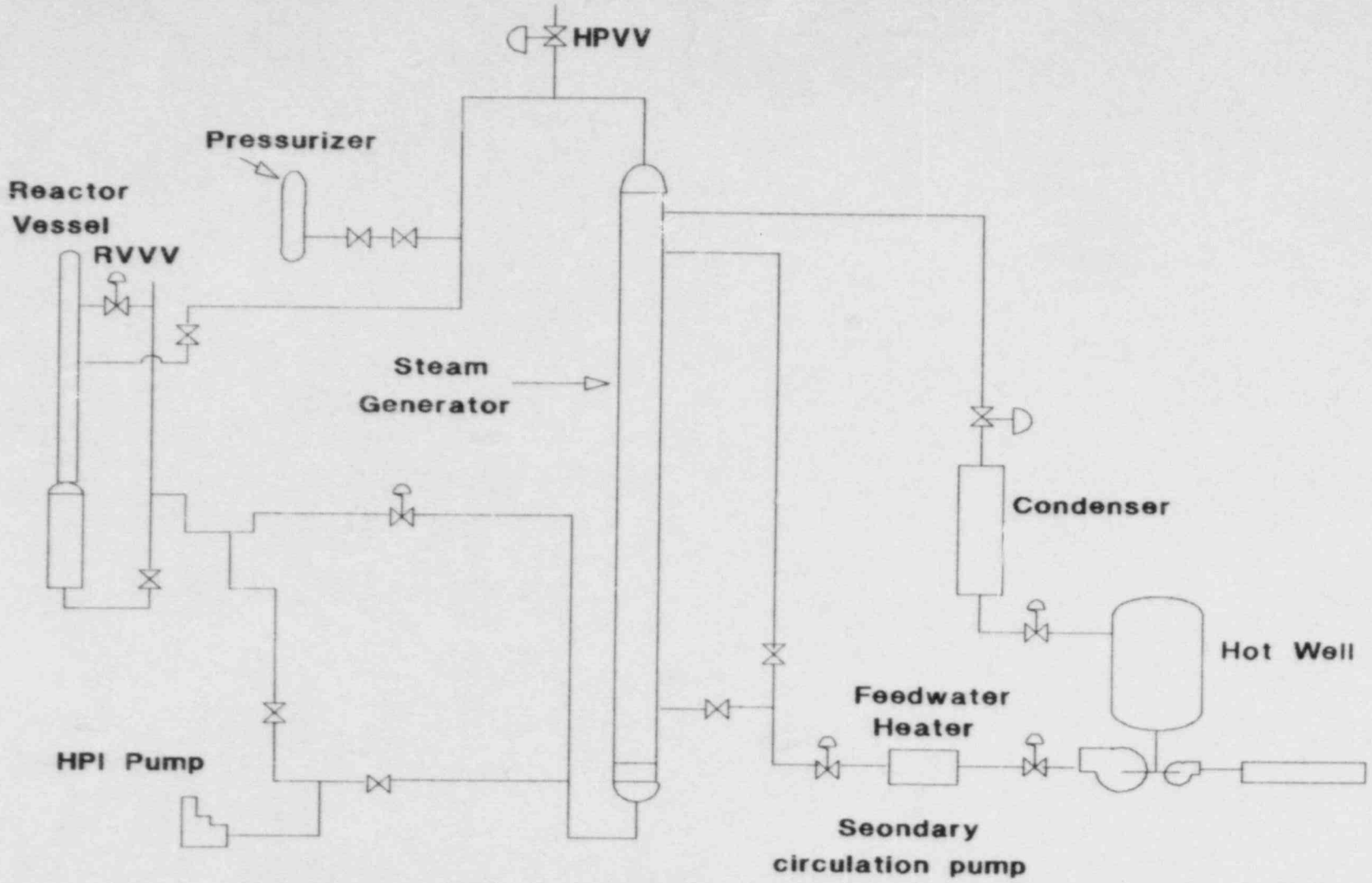


Figure 1. General arrangement of GERDA Facility.

EEJ00014

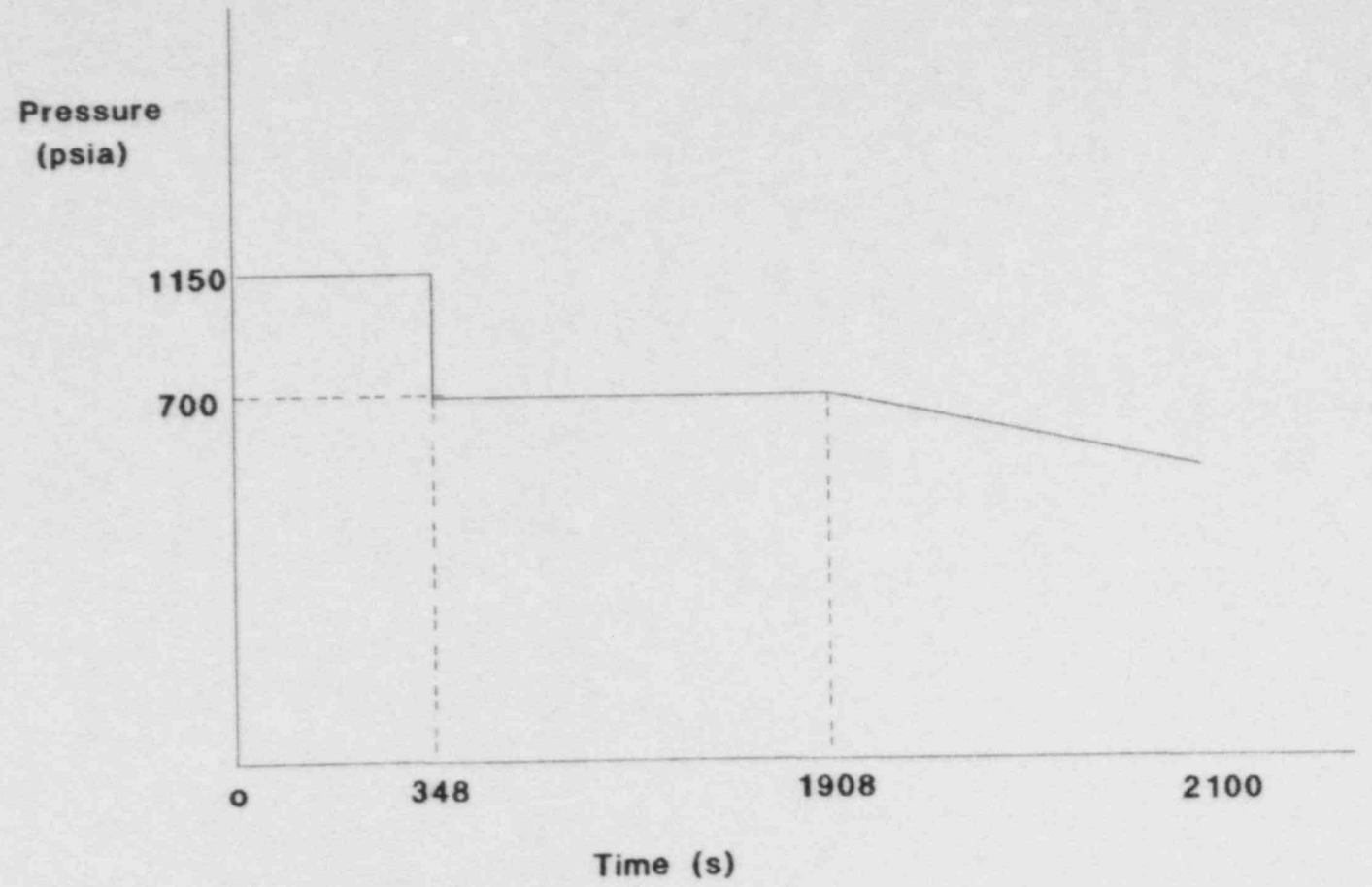


Figure 2. Control valve set point pressure.

EEJ00033

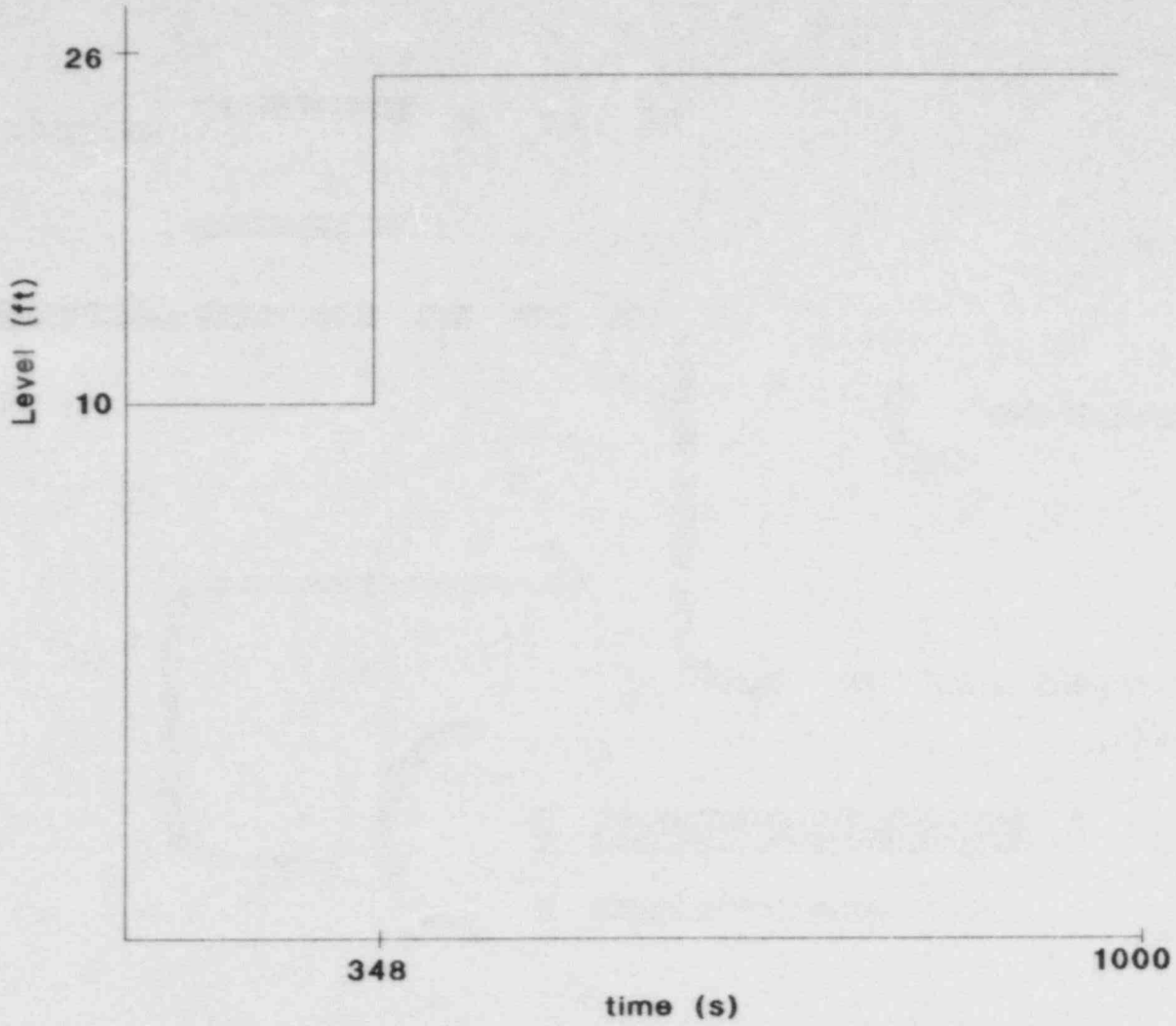


Figure 3. Steam generator programed level.

EEJ00024

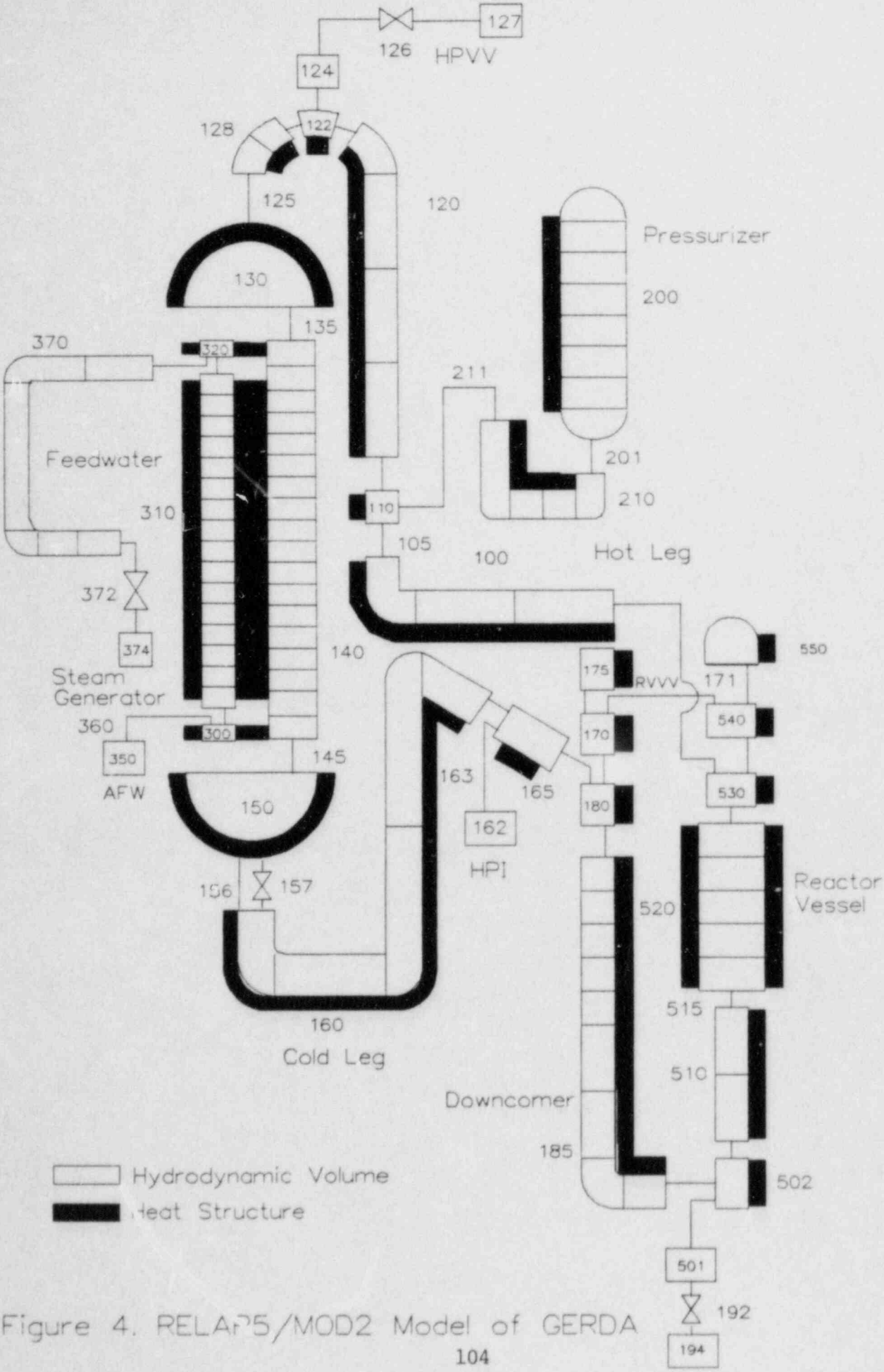


Figure 4. RELAP5/MOD2 Model of GERDA

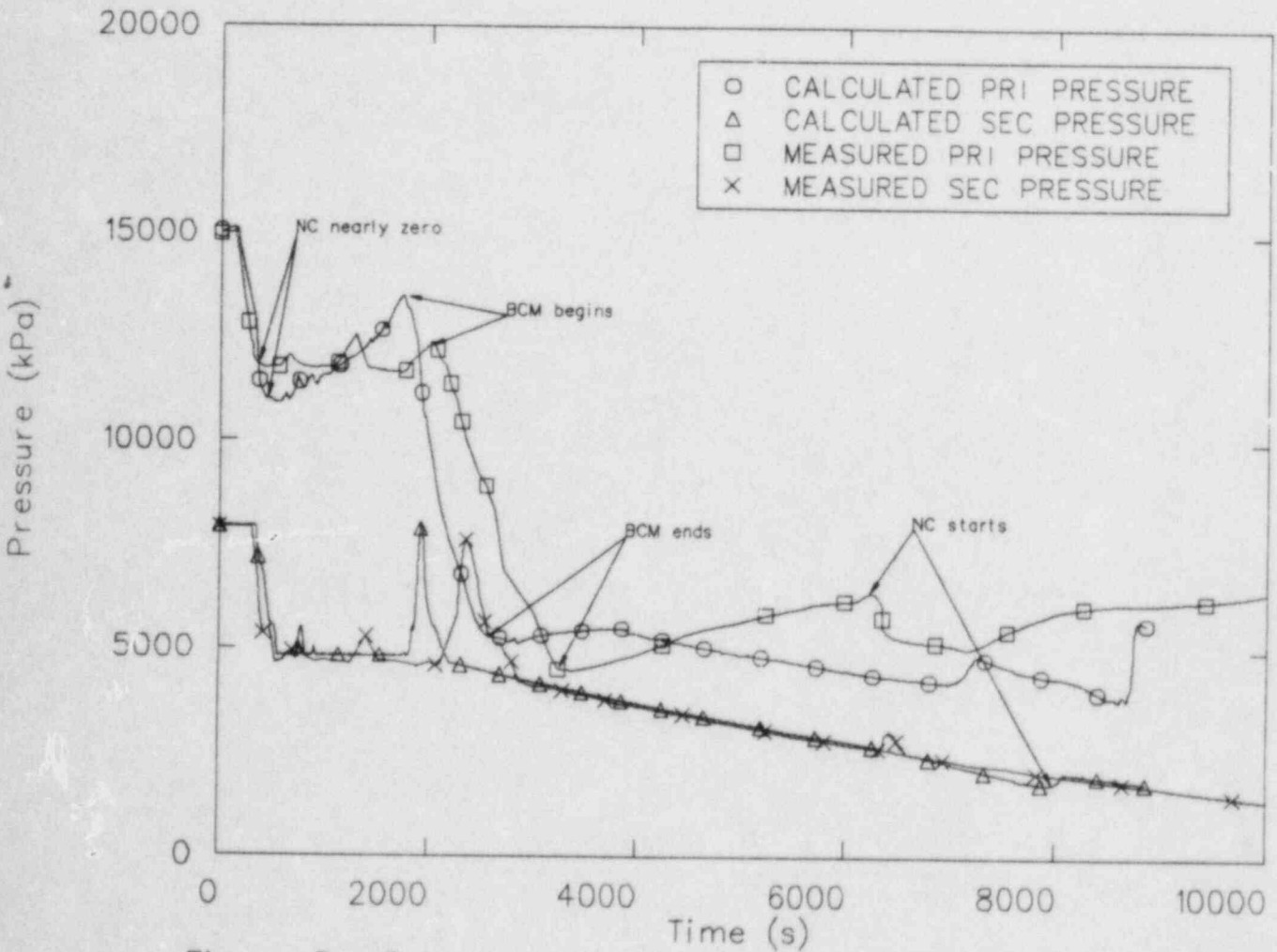


Figure 5. Primary and secondary system pressures.

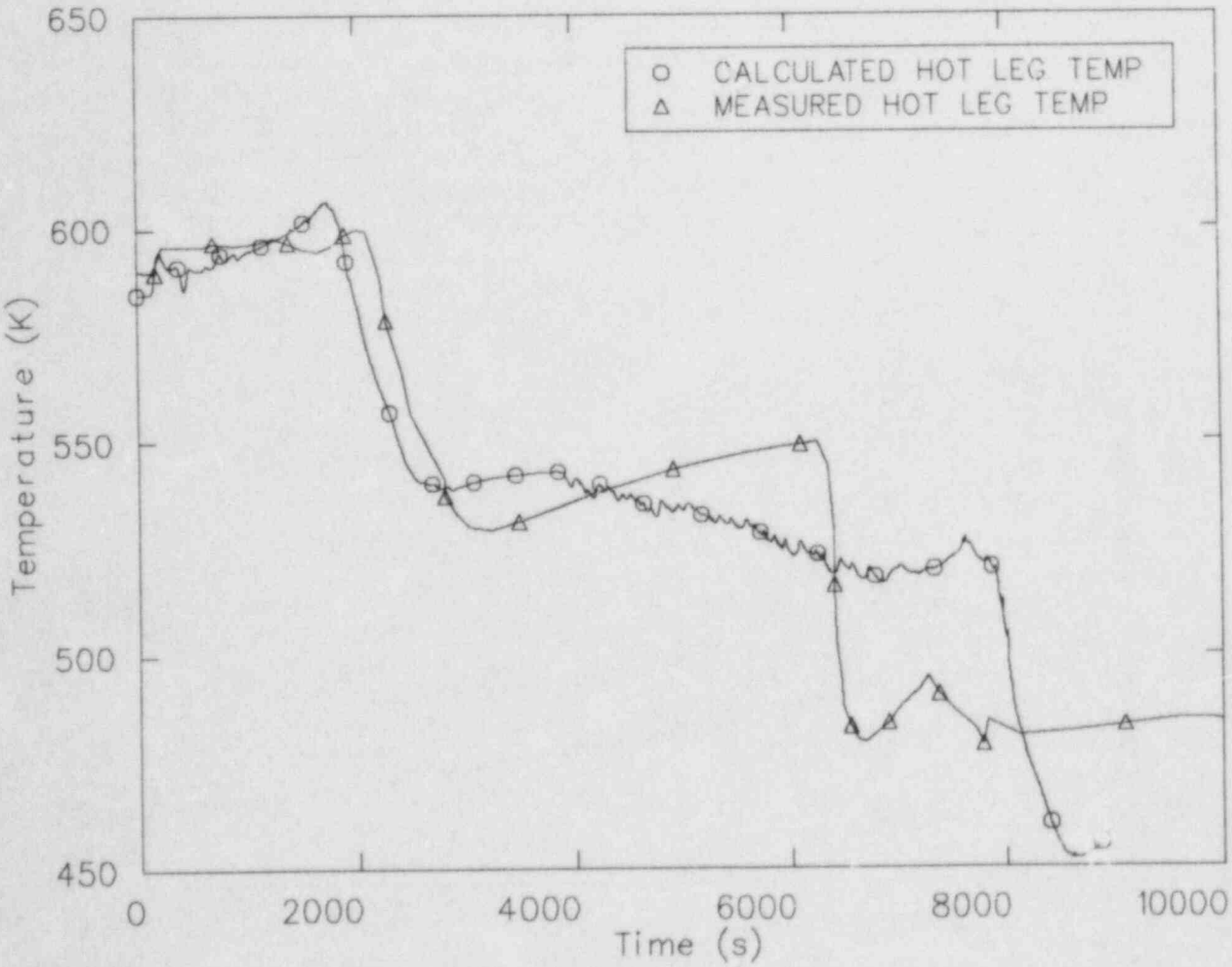


Figure 6. Hot leg fluid temperatures.

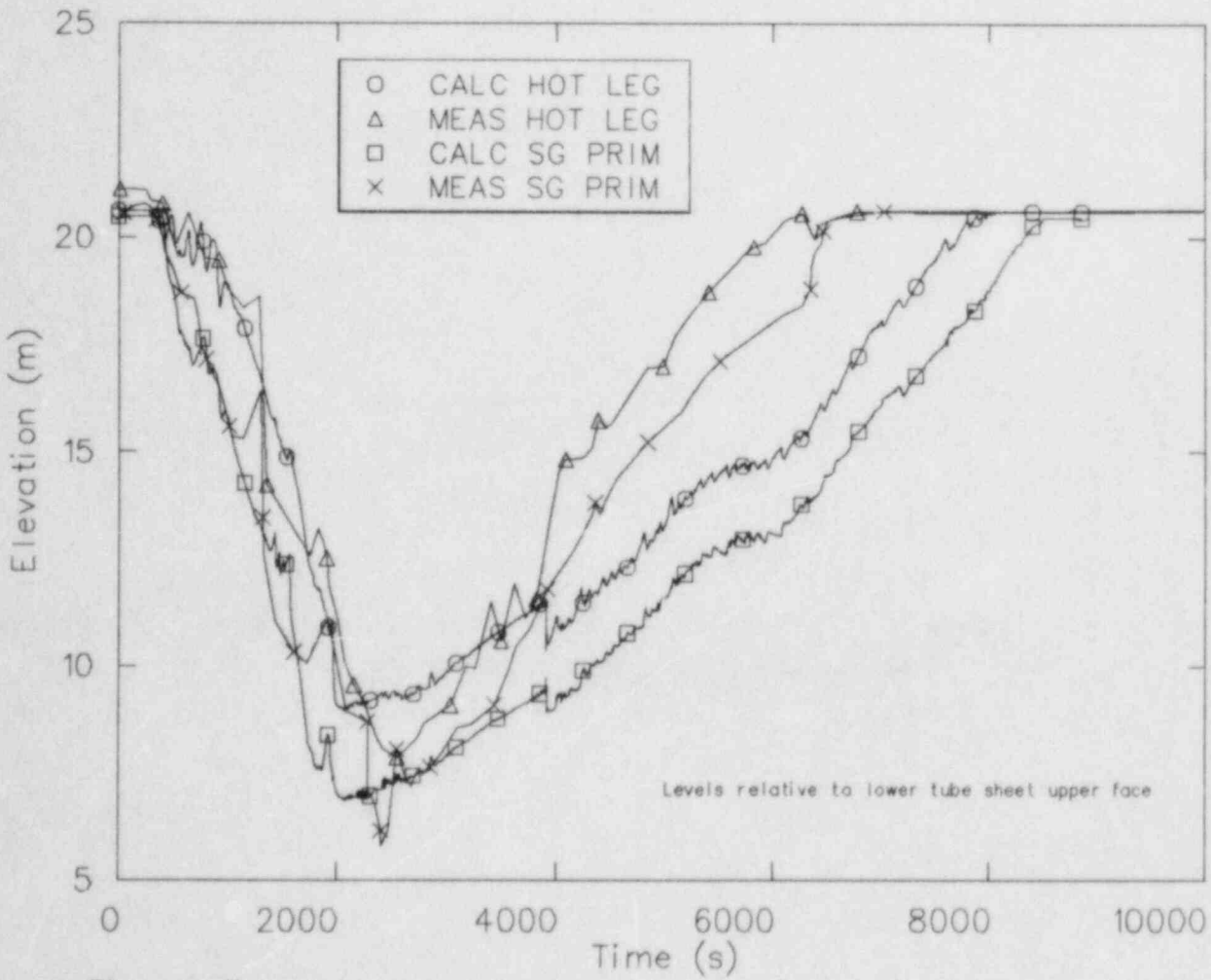


Figure 7. Hot leg and steam generator primary collapsed liquid levels.

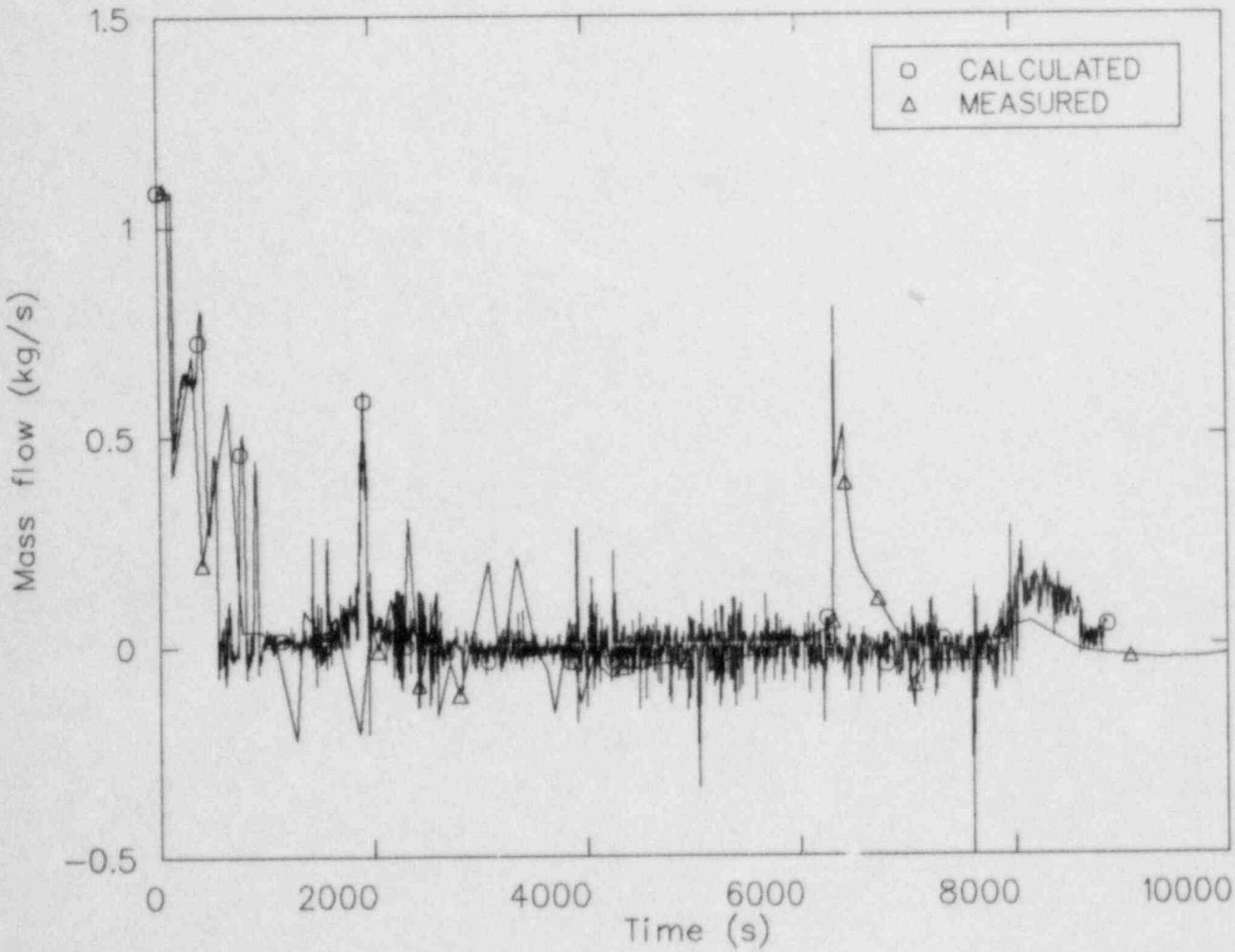


Figure 8. Cold leg flow rate.

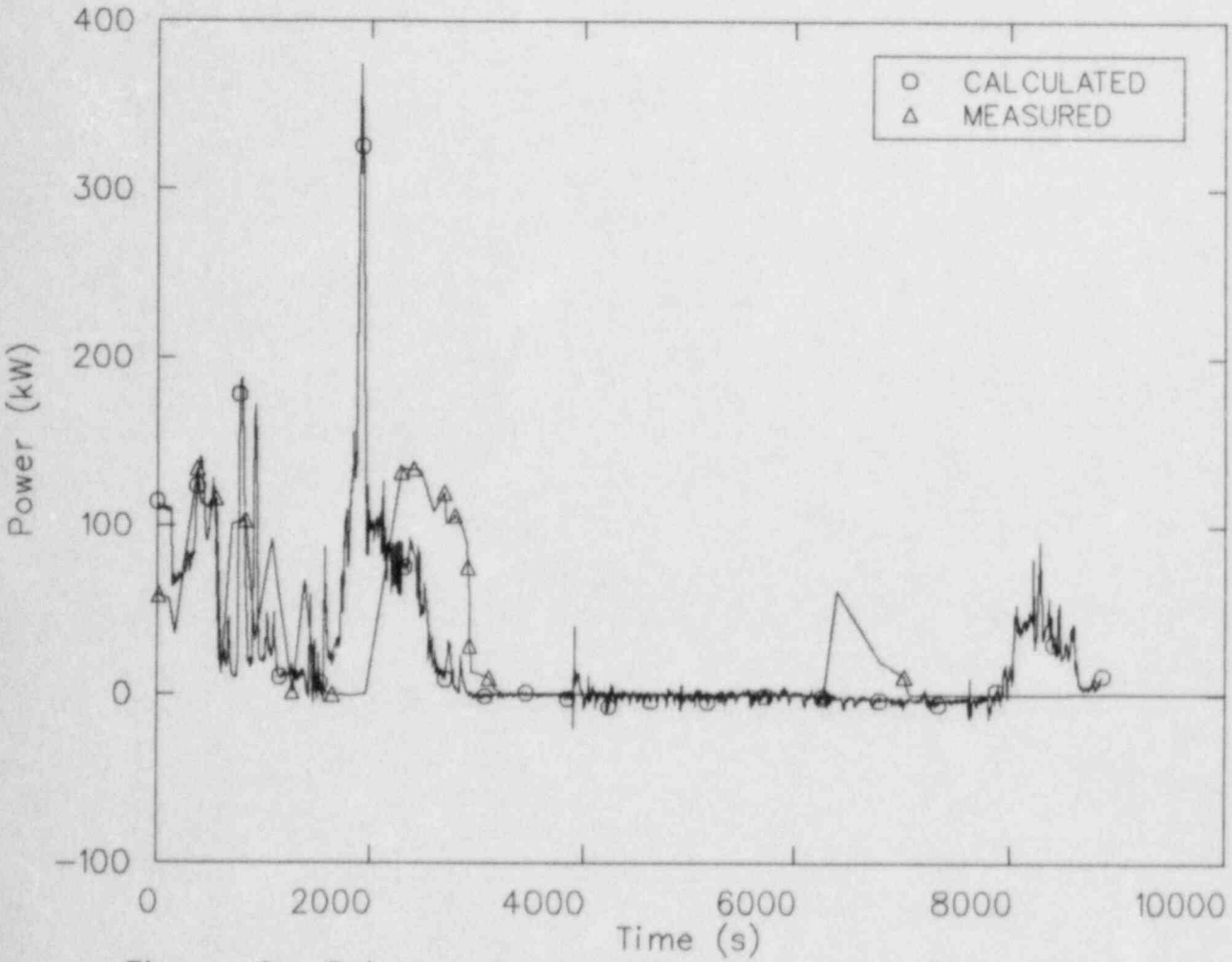


Figure 9. Primary to secondary heat transfer rate.

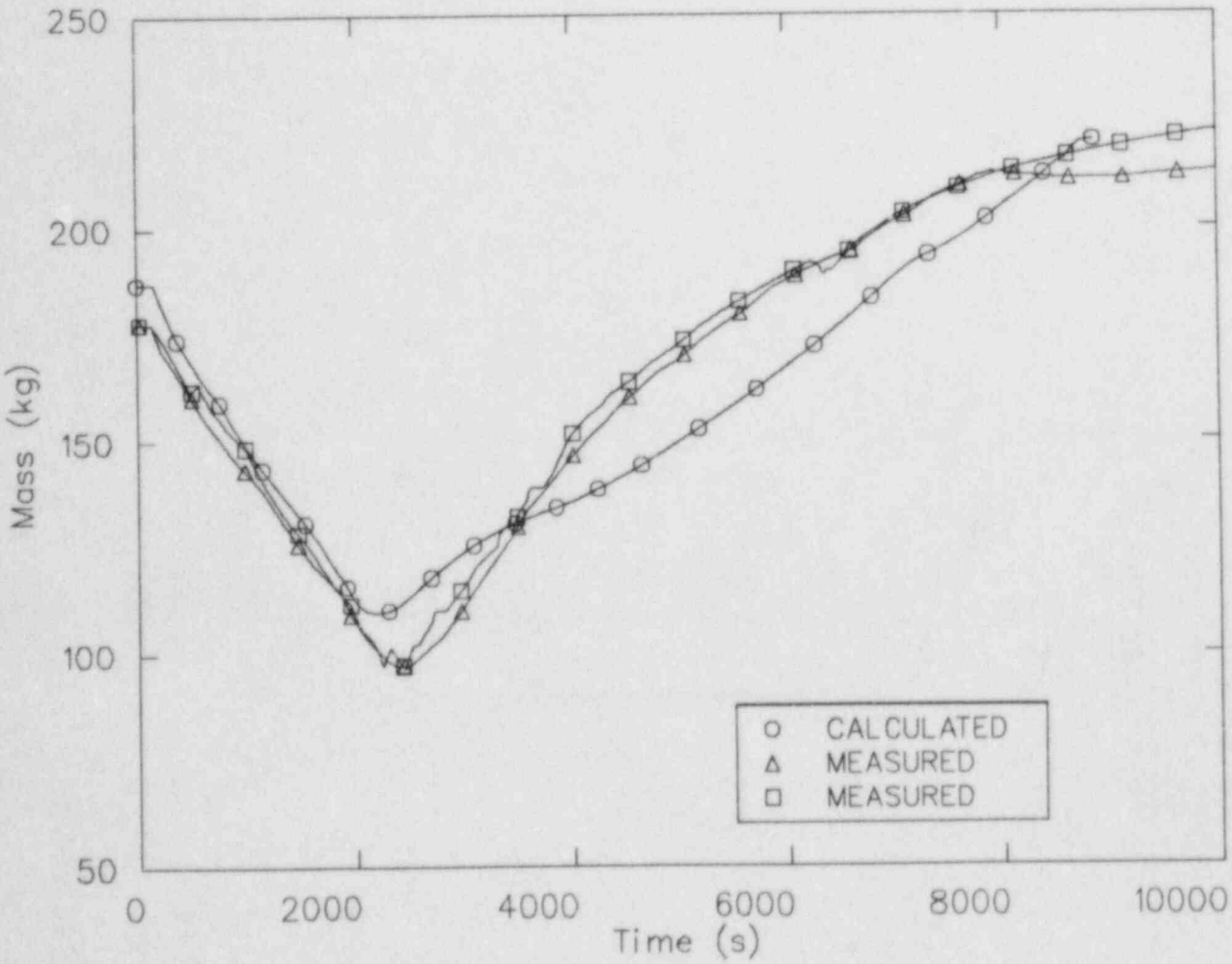


Figure 10. Primary system mass.

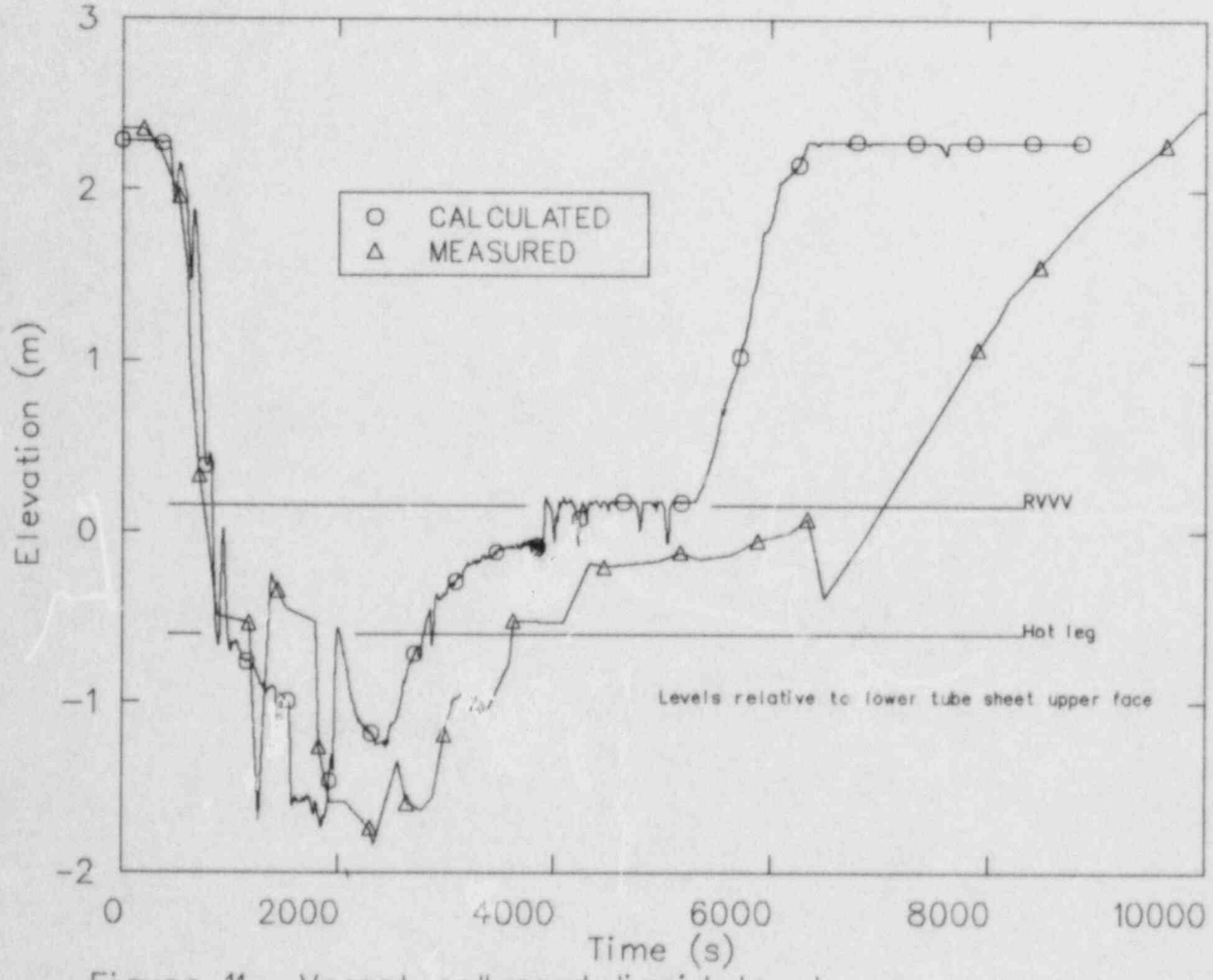


Figure 11. Vessel collapsed liquid level.

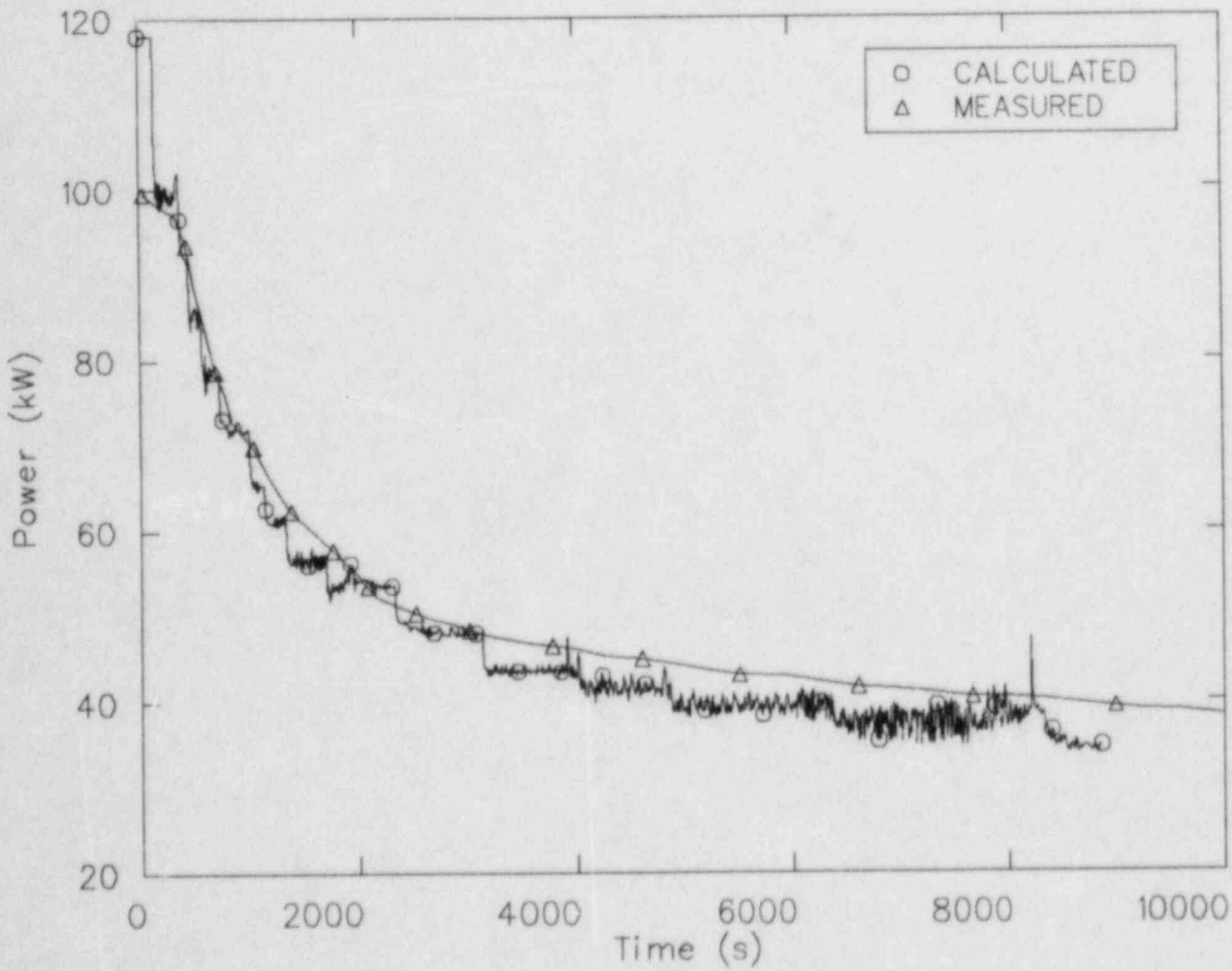


Figure 12. Core power.

# An Experimental Study of the Post-Small Break Loss-of-Coolant Accident Phenomena in a Scaled Babcock & Wilcox System

H. R. Carter and J. R. Gloudemans
The Babcock & Wilcox Company

## ABSTRACT

A scaled, experimental facility, designated the Once-Through Integral System (OTIS), was used to acquire post-small break loss-of-coolant accident (SBLOCA) data for benchmarking system codes. OTIS was also used for confirming the Abnormal Transient Operating Guidelines (ATOG) used in the Babcock & Wilcox (B&W) designed Nuclear Steam Supply System (NSSS) during the course of a SBLOCA. OTIS was a single-loop facility with a plant to model power scale factor of 1686. OTIS maintained the key elevations, component phenomena, approximate component volumes, and loop flow resistances of a B&W raised-loop nuclear plant.

A test matrix consisting of 15 tests divided into four categories was performed. The largest group contained 10 tests and was defined to parametrically obtain an extensive set of plant-typical experimental data for code benchmarking. Parameters such as leak size, leak location, and high-pressure injection (HPI) shut-off head were individually varied. The remaining categories were specified in order to study the impact of ATOG (2 tests), to note the effect of facility operation on observed phenomenon (2 tests), and to provide a data set for comparison with previous test experience (1 test) [1].

A summary of the test results and a detailed discussion of Test 220100 is presented. Test 220100 was the nominal or reference test for the parametric studies. This test was performed with a scaled 10 $cm^2$ leak located in the cold leg suction piping.

The OTIS test results provide a challenging SBLOCA data set, based on plant-typical boundary system variations, for system code benchmarking. The OTIS results also illustrate the effectiveness of ATOG for rapid system recovery from a SBLOCA.

## INTRODUCTION

Experimental integral system data was obtained for benchmarking system codes and for confirmation of the ATOG used in B&W designed NSSS during a SBLOCA. This program was cooperatively performed by the Nuclear Regulatory Commission (NRC), the Electric Power Research Institute (EPRI), B&W, and the B&W Owners Group. The scaling approach, hardware, and instrumentation used in the experimental facility (OTIS) are described. The tests performed and the basis for the test matrix are also discussed.

An overview of the results from selected tests is presented. Detailed discussions of the nominal SBLOCA test are included.

## DESCRIPTION OF TEST FACILITIES

### Hardware

The OTIS facility was designed to provide a test facility for separate effect and integral system studies of the natural circulation phases of a SBLOCA. The facility was a single hot leg and a single cold leg (1 x 1 loop) representation of the B&W raised loop NSSS. The general arrangement of the major OTIS components and systems is shown in Figure 1. The loop consisted of one 19-tube once-through steam generator (OTSG), a simulated reactor, a pressurizer, a single hot leg, and a single cold leg. Reactor decay heat was simulated by electrical heaters in the reactor vessel capable of 180 kW or about 8% scaled power. Other loop components included a reactor vessel vent valve (RVVV), pressurizer power-operated relief valve (PORV), a hot leg high-point vent (HPV), and a reactor vessel upper-head vent (RVUHV). Auxiliary systems were available for scaled HPI, control primary leaks in five loop locations, a secondary forced circulation system for providing auxiliary feedwater (AFW) to the OTSG, and a gas addition system for the primary loop.

The loop configuration was governed by scaling considerations. The major scaling criteria, in order of priority, were loop elevations, post-SBLOCA flow phenomena, component volumes, and irrecoverable pressure losses. Core cooling during much of a SBLOCA transient is provided by natural circulation. In a B&W NSSS, natural circulation flow rate is controlled by the established driving head between the reactor vessel/hot leg and the steam generator/cold leg side of the loop. Full elevation scaling was incorporated in OTIS to maintain representative scaled natural circulation flow rates. Key loop elevations such as the hot leg U-bend spillover (the lower surface of the hot leg U-bend pipe, see Figure 2), the cold leg spillunder (the upper surface of the lowest point in the cold leg pipe), the reactor coolant pump spillover, the hot leg/reactor vessel nozzle, the cold leg/reactor vessel nozzle, the thermal centers of the core and steam generator, and the spillover elevation of the RVVV were selected to match the corresponding plant elevations.

The flow characteristics in the hot leg were of particular interest. During the course of a SBLOCA, the hot leg fluid may be subcooled liquid, saturated liquid, saturated steam, superheated steam, or a two-phase liquid steam mixture. Froude number scaling was used to preserve the characteristic flow conditions in the OTIS hot leg. (Froude number scaling also resulted in approximate irrecoverable losses.) This approach matched the two-phase flow regimes and flooding phenomena expected in the plant according to Taitel et al., [2] and Wallis [3], respectively. Froude number scaling resulted in a 3-inch Schedule 160 hot leg that was twice the diameter obtained by ideal volumetric scaling. This added approximately 20% extra volume to the ideal primary system volume. However, the 3-inch diameter pipe was considered most likely to avoid the whole pump slugging behavior observed in other experimental programs. Froude number scaling was also applied to the OTIS cold leg and resulted in the use of 2-1/2 inch Schedule 160 piping.

The reactor vessel, pressurizer, and steam generator, were predominantly volume scaled. The OTIS power and volume scale factor originated with the size of the model OTSG (shown in Figure 2). The model OTSG contained 19 full-length and plant-typical tubes, which represented the 32,026 tubes in the two steam generators in the raised loop NSSS. Therefore, the power and volume scale factor

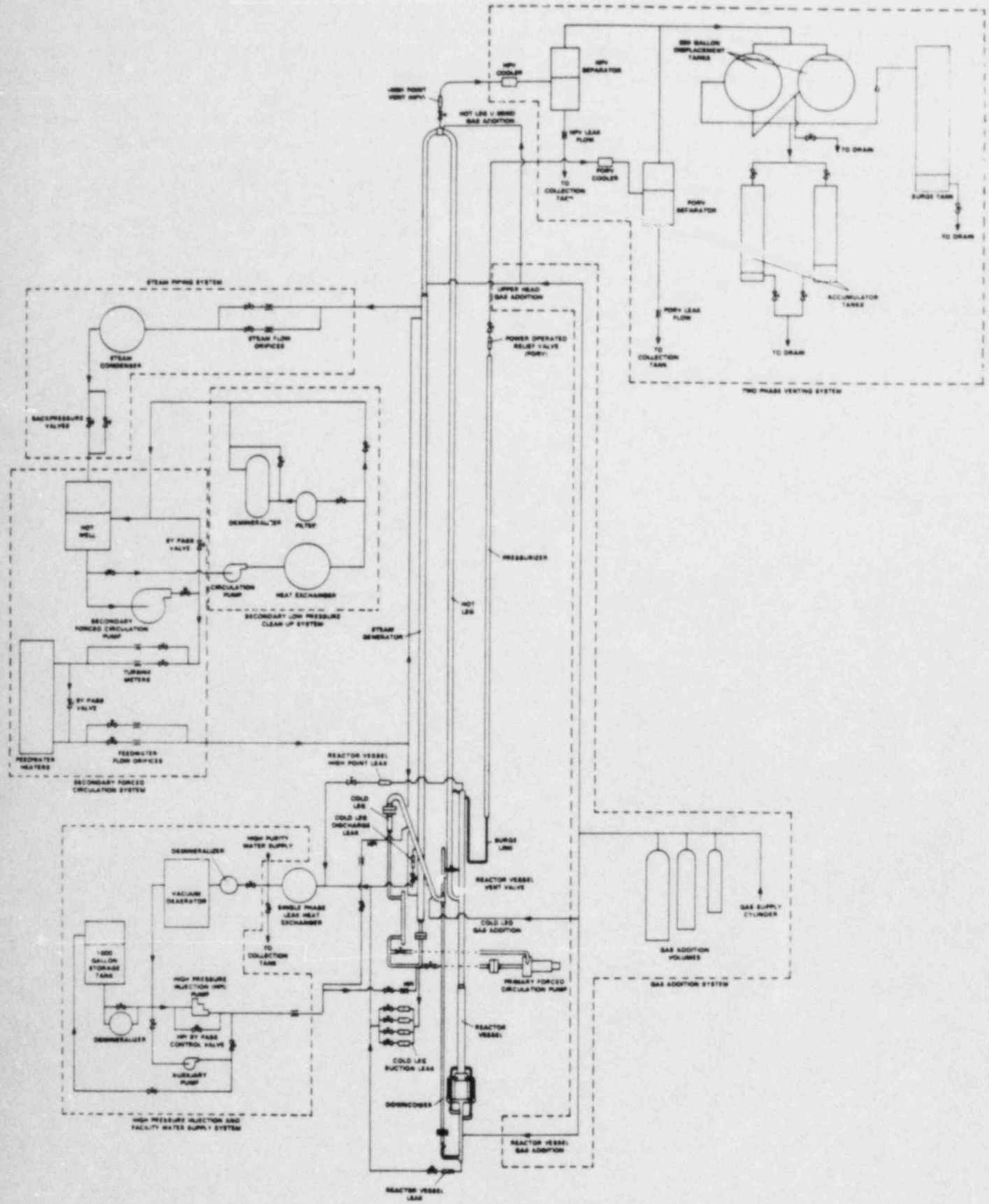


Figure 1. OTIS test facility.

for OTIS was 1/1686. The OTIS primary loop volume was 10.1 cubic feet compared to an ideally scaled volume of 8.5 cubic feet. The excess loop volume over the ideally scaled volume resulted predominantly from the larger hot leg diameter.

Prototypical loop irrecoverable resistance was maintained to preserve the correct scaled, natural circulation flow rates. The primary loop irrecoverable pressure loss was low; therefore, fixed plate orifices were installed at two locations. One in the cold leg pipe at the outlet of the steam generator, and the second near the bottom of the reactor vessel downcomer. These fixed restrictors provided the correct resistance for natural circulation flow rate and the proper split between outer loop and inner loop circulation (circulation from the reactor vessel through the vent valve down the downcomer and back to the reactor vessel).

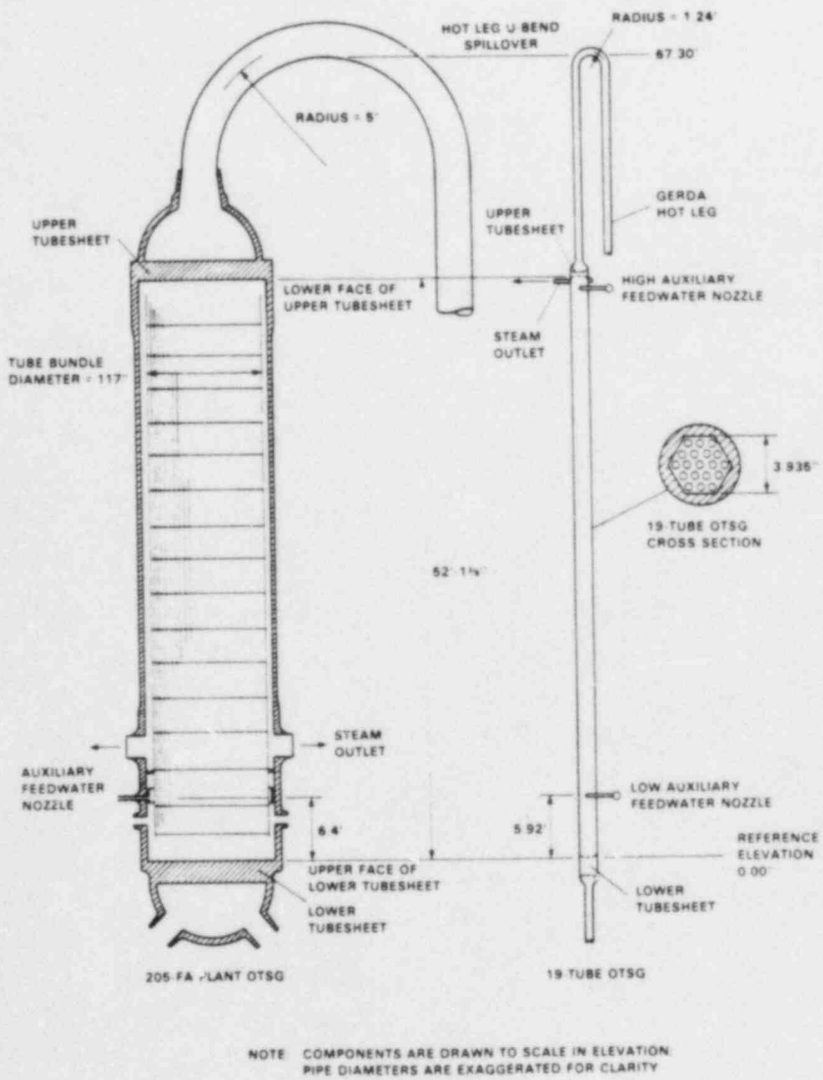


Figure 2. Comparing full-size 205-FA plant OTSG to 19-tube OTSG in OTIS.

System leaks and vents were controlled in OTIS by critical flow orifices. Scaled leaks from 3 $cm^2$ to 15 $cm^2$ were used. The diameter of the scaled leak was obtained from the ideal scaling factor of 1686. For example, a scaled leak of 10 $cm^2$ had a diameter of 0.034 inch. Prior to performance of the OTIS tests, scaled leaks of 3 $cm^2$ to 40 $cm^2$ were characterized in saturated steam and saturated water. The characterization test provided data on the critical flow rate of the orifices at pressures of 1000 and 2000 psi. The characterization test results indicated that the scaling approach for the leaks was acceptable and provided good agreement with analytical results, as shown in Figure 3.

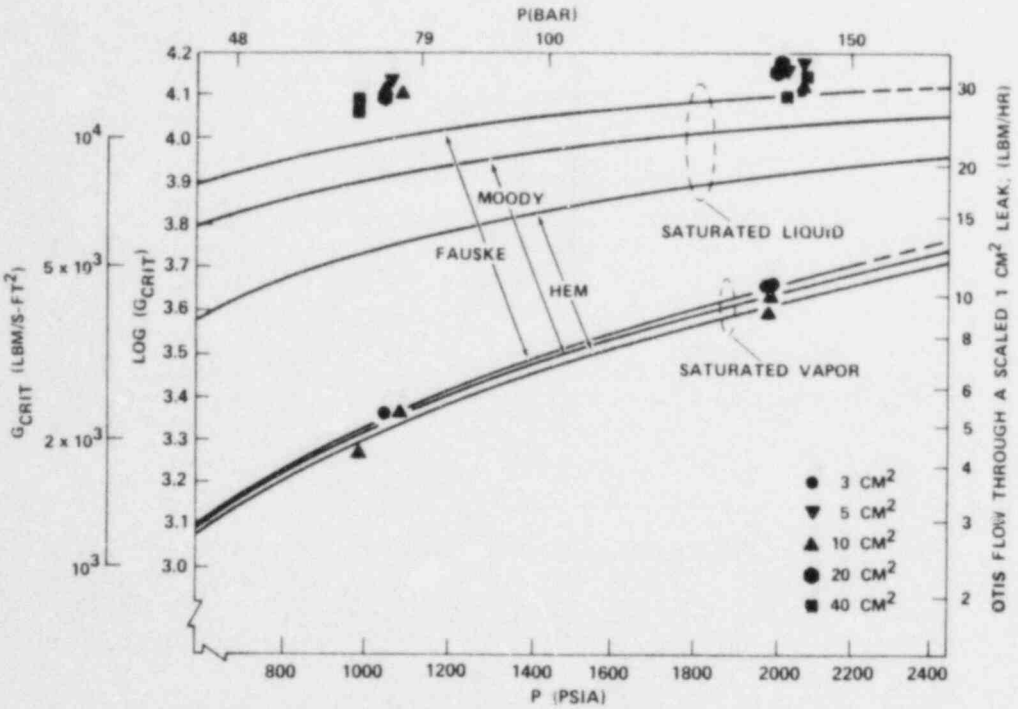


Figure 3. Measured and predicted critical flows.

An inherent atypicality experienced in scaled test facilities is higher piping heat losses than is experienced in the plant. The higher model heat losses result from the larger piping surface area to enclosed fluid volume ratio and instrument penetrations in the model. Active and passive insulation were used on the hot leg, pressurizer, and reactor vessel upper head to minimize the impact of the higher heat losses. The insulation approach used is illustrated in Figure 4. The active portion of the insulation utilized ribbon heaters that were controlled by the temperature difference across the control insulation boundary. The rest of the loop was covered with passive insulation.

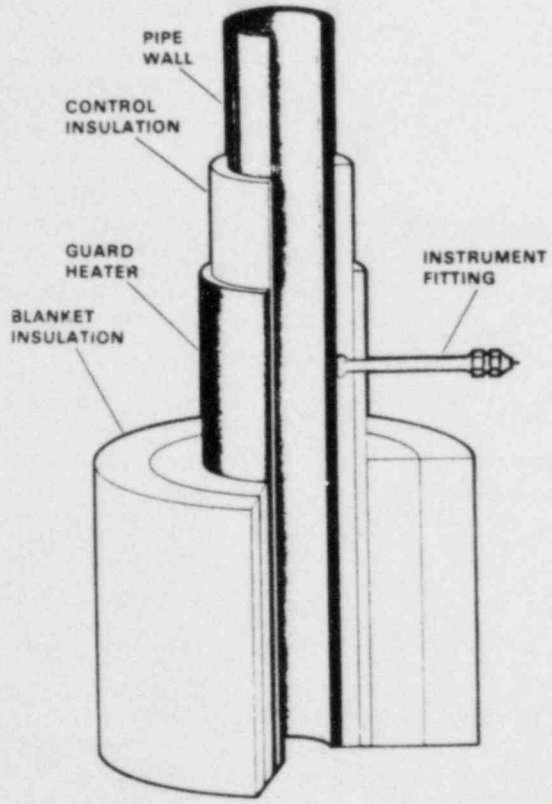


Figure 4. OTIS guard heater arrangement.

### Instrumentation

OTIS had approximately 250 instruments to measure the thermal and hydraulic conditions. These instruments were interfaced to a computer-controlled, high-speed data acquisition system that provided the capability to record all instrument readings in 25 milliseconds. The OTIS instrumentation provided:

- Pressure and differential pressure measurements
- Thermocouple and resistance temperature detector measurements of fluid and metal temperatures
- Fluid level and phase indication by optical viewports, fluid conductivity probes, and differential pressures
- Pitot tube, head-flow meters, and turbine meters for flow rate measurements

Mass fluxes into and out of the facility were controlled and measured at the facility boundaries.

### Test Matrix

Four test categories were defined for the OTIS program. These were OTIS/GERDA benchmark (Category I), single variable tests (Category II), composite

tests (Category III), and system evaluation tests (Category IV). Category I was defined to provide a direct comparison with test results obtained from the previously performed GERDA program. In addition, this test provided steady-state information to evaluate the differences in loop response when high elevation auxiliary feedwater compared to low elevation auxiliary feedwater injection was used with a partially voided reactor coolant system.

Category II was defined to highlight the effects of major system variables on the course of a SBLOCA transient. The initial conditions and operator actions were duplicated in each test; however, one of the major system variables (leak size, leak location, or HPI characteristics) was varied. The initial loop conditions for the single variable test were defined to simulate plant conditions at approximately 1-2/3 minutes after a reactor trip and assumed that the reactor coolant pump had coasted down and the boundary systems (HPI and AFW) were available and activated. The resulting OTIS initial conditions were 5% scaled core power, reactor coolant system in subcooled natural circulation, primary pressure at 2200 psia, and the pressurizer level set at 10 feet. The secondary side of the system was initialized with a 5-foot level in the steam generator, with AFW being injected at the upper elevation at approximately 100°F, and with secondary steam pressure controlled to obtain primary hot leg fluid temperatures of approximately 610°F. During loop initialization, HPI and leaks were not used.

Initiation of the single variable tests was performed in two steps. These steps were defined to obtain plant similar conditions at the time of loop fluid saturation. The first step was performed by opening the designated leak and the second was performed at the point of pressurizer inventory depletion. When the pressurizer liquid height reached approximately 2 feet, HPI was activated to the cold leg discharge piping, a core power ramp simulating post-decay power from 1-2/3 minutes was initiated, and the auxiliary feedwater control characteristics were changed to obtain a 3-foot/minute level increase until a 38-foot control level was reached. One additional operator control action was required after test initiation. When the secondary steam generator level reached the 38-foot control level, the operator started a secondary depressurization from approximately 1000 psi to obtain a 50°F per hour secondary cooldown.

Five hours after opening the leak, the facility operators determined whether the hot leg U-bend had refilled or if refill was eminent. If refill had not occurred and was not expected, the hot leg HPV was opened and testing was continued for two additional hours. At seven hours, if refill had not been achieved, the power-operated relief valve was opened and testing was continued for one additional hour. Eight hours after opening the leak, if the hot leg had not refilled, the core power was gradually reduced to sustain the loop at the current temperature and the test was terminated after an additional hour at sustaining power.

Category III introduced a wide range of operator actions into the loop control. In contrast to the Category II tests, in which operator actions were minimized to highlight the effects of major system variables on test performance, Category III maximized operator actions specifically to examine their effects on the course of the SBLOCA transient. An engineer trained in plant operator guidelines was on-site and provided loop operating instructions based on observed loop conditions. The engineer was furnished with loop conditions consistent with the information that would be available in a plant. The initialization and initiation procedures for the Category III tests paralleled those used for the

single variable tests. After leak opening, the plant-trained operator directed the loop cooldown by following the prescribed pressure temperature envelope. The operator used model systems simulating those of the plant, such as HPI, PORV actuation, hot leg or reactor vessel upper-head vents, pressurizer heaters, etc., to achieve the loop cooldown within the prescribed limits. According to test-defined procedures, the leak was isolated at one-half hour after test initiation, and AFW was unavailable until one hour after test initiation.

Category IV was performed to study the influence of model guard heaters on the course of the SBLOCA transient. Two evaluation tests were performed duplicating the procedures followed for one of the single variable tests. One test was performed with the guard heaters active while the second was performed with the heaters de-energized.

Table 1 presents the OTIS tests that were selected to be presented and discussed in the following sections.

## RESULTS

### Characteristic Phases of a SBLOCA

Five major phases were predicted and observed during OTIS SBLOCA tests. These were (1) pressurizer draining and loop saturation, (2) intermittent reactor coolant system circulation, (3) boiler-condenser mode (BCM), (4) refill, and (5) post-refill cooldown.

Table 1

SELECTED OTIS TESTS

| Category | Test Number | Description | Leak Size $cm^2$ | Leak Location | Leak Isolation | Steam Generator Secondary Level Control, ft. | HPI Capacity/ Shut-Off Head |
|---|---|---|---|---|---|---|---|
| II | 220100 | Nominal Test | 10 | Cold Leg Suction (CLS) | No | Initial 3' Final 38' | Full/>2500 psi |
| II | 220201 | Leak Size | 15 | CLS | No | Initial 3' Final 38' | Full/>2500 psi |
| II | 220304 | HPI Characteristics | 10 | CLS | No | Initial 3' Final 38' | Half/>2500 psi |
| II | 220402 | Steam Generator Characteristics | 10 | CLS | No | 10' | Full/>2500 psi |
| II | 220503 | Leak Location | 10 | Cold Leg Discharge | No | Initial 3' Final 38' | Full/>2500 psi |
| II | 220604 | HPI Characteristics | 10 | CLS | No | Initial 3' Final 38' | Full/1630 psi |
| III | 230199 | Nominal HPI | 10 | CLS | Yes | Initial 3' Final 38' | Full/>2500 psi |
| III | 230299 | Low-Head HPI | 10 | CLS | Yes | Initial 3' Final 38' | Full/1630 psi |

Figure 5 provides an indication of the duration and temporal relation of these phases using the primary and secondary pressure curves for Test 220100. This test was initialized, initiated, and performed as described for the single variable tests. The scaled 10 $cm^2$ cold leg suction leg was opened at t = 46 minutes. The pressurizer draining and loop saturation phase lasted for approximately 4 minutes. Initially, the primary depressurized at approximately 100 psi/minute until the pressurizer drained at t = 49-1/2 minutes and then at 350 psi/minute until t = 50 minutes, as shown in Figure 6. Four minutes after leak opening (t = 50), the fluid in the hot leg U-bend saturated and the primary pressure stabilized at approximately 1700 psia.

The second phase, intermittent circulation, started at t = 50 minutes (4 minutes after leak opening) and continued until t = 90 minutes. Natural circulation flow was first interrupted at t = 50.3 minutes. With interrupted flow, the primary repressurized (as noted in Figure 6) at t = 56 and 63.3 minutes. The magnitude of the repressurizations was controlled by the duration of the flow interruption. Major intermittent spillovers occurred at t = 58.7 and 63.8 minutes (as noted in Figure 6) by a change in secondary pressures at these times. The loop conditions during this phase are illustrated in Figure 7.

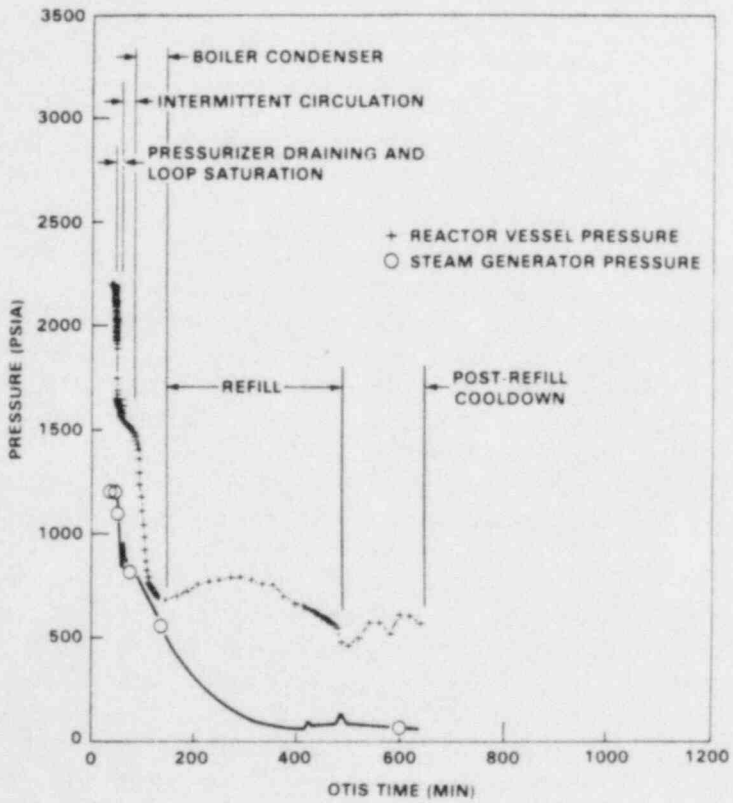


Figure 5. SBLOCA phases for OTIS Test 220100.

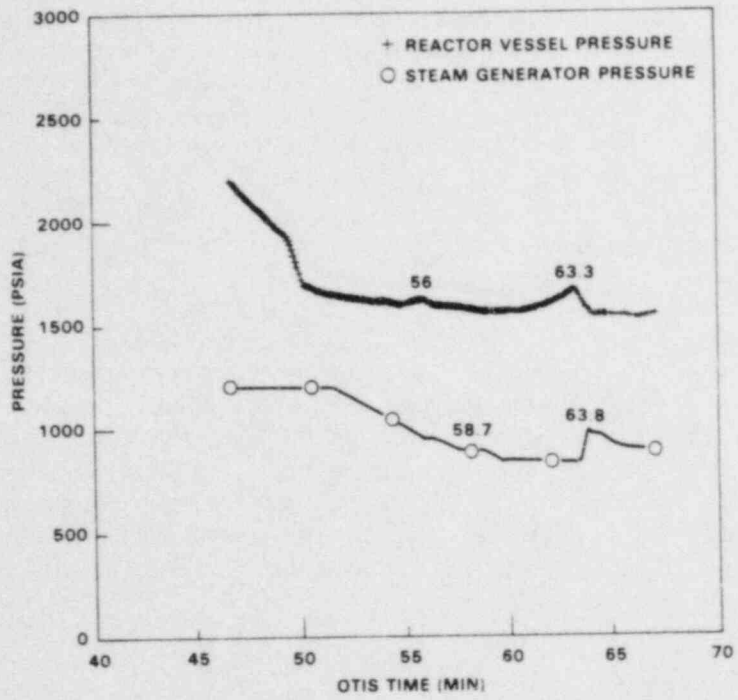


Figure 6. Primary and secondary pressures for OTIS Test 220100 (t = 46 to 68 minutes).

During the intermittent circulation phase, the decreased primary loop flow caused the reactor vessel to downcomer differential pressure to increase, actuating the RVVV. Warmer fluid was admitted to the upper downcomer, cooled by mixing with HPI fluid, then returned to the core inlet completing the inner flow circuit. The void in the reactor vessel upper head continued to grow, displacing fluid into the hot leg, raising its liquid level. This caused the intermittent or spillover circulation that was mentioned previously. The spillover circulation propelled saturated liquid flows over the hot leg U-bend. The liquid fell through the voided downstream piping and into the steam generator transferring heat.

Phase 3, the BCM, was initiated at t = 90 minutes (44 minutes after leak initiation) when the steam generator primary level approached the steam generator secondary level. Condensation of the primary steam caused the primary to depressurize from approximately 1400 psia at t = 90 minutes, to approximately 770 psia at t = 110 minutes. The BCM depressurization continued to 700 psia at t = 150 minutes. In the BCM, steam was produced in the core and condensed in the steam generator. Because this type of BCM required the overlap of levels within the generator, it is called "pool BCM". Primary vapor condensation rapidly decreased primary pressure and primary total energy. The condensation process was sufficiently effective to reduce primary pressure to that of the steam generator secondary.

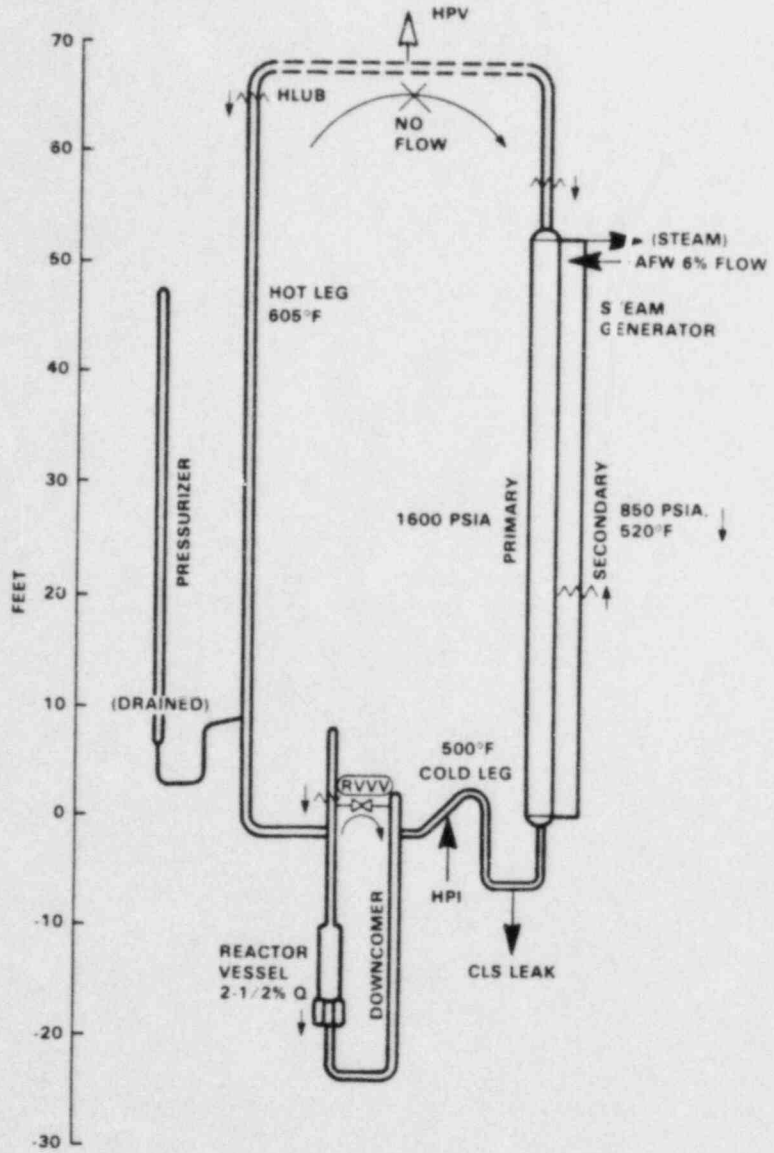


Figure 7. Loop conditions during intermittent circulation (4 to 40 minutes).

The decreasing primary pressure increased HPI flow and decreased leak flow. The HPI and leak flow rate changes were sufficient to start primary system refill. The increasing primary levels weakened heat removal in the BCM phase; however, this heat removal mode persisted until the primary steam generator level passed the elevation of the upper tubesheet at t = approximately 150 minutes. Loop conditions representative of the boiler-condenser phase are illustrated in Figure 8.

System refill started at t = 100 minutes (54 minutes after leak opening); however, for purposes of discussion the refill phase (Phase 4) was considered to start when primary condensation stopped. The refill phase continued until t = 480 minutes.

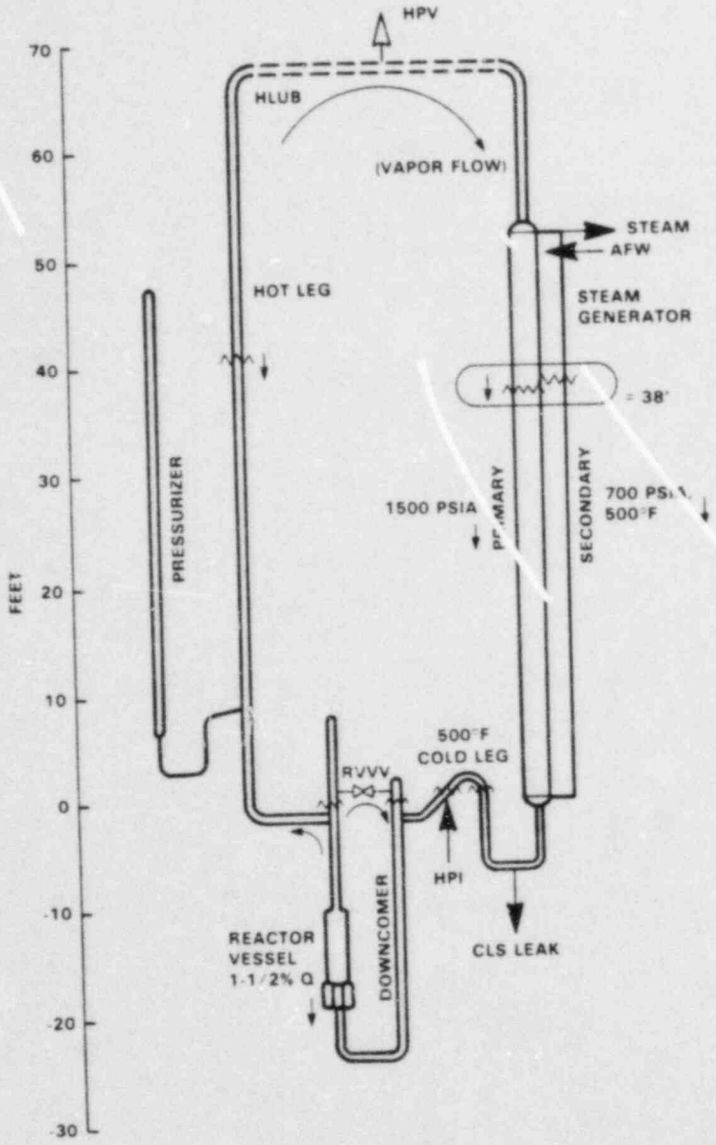


Figure 8. Loop conditions during pool boiler-condenser mode (40 to 100 minutes).

Figure 9 illustrates the primary system conditions after the primary side of the steam generator (SG) has been refilled. The hot leg level upstream of the hot leg U-bend spillover was insufficient to sustain circulation, although sporadic spillovers occurred. The cold HPI fluid lowered leak fluid temperature such that the leak flow rate increased, but the heat transfer by HPI leak cooling decreased (the effect of leak fluid temperature decrease exceeded that of the leak flow rate increase). The primary repressurized from 680 psia to 790 psia, causing the primary system to approach fluid mass and energy equilibrium.

The relatively stable primary conditions indicated that core power was being matched by HPI leak cooling. Loop flow was interrupted and the steam generator was inactive for heat transfer; however, the inner-loop flow was active. Core exit fluid flowed out the RVVV, down the downcomer, and back into the core. HPI condensed vented steam and cold leg discharge region mixing and/or counter-flow process transport heated fluid reaching the leak site. The HPI and leak

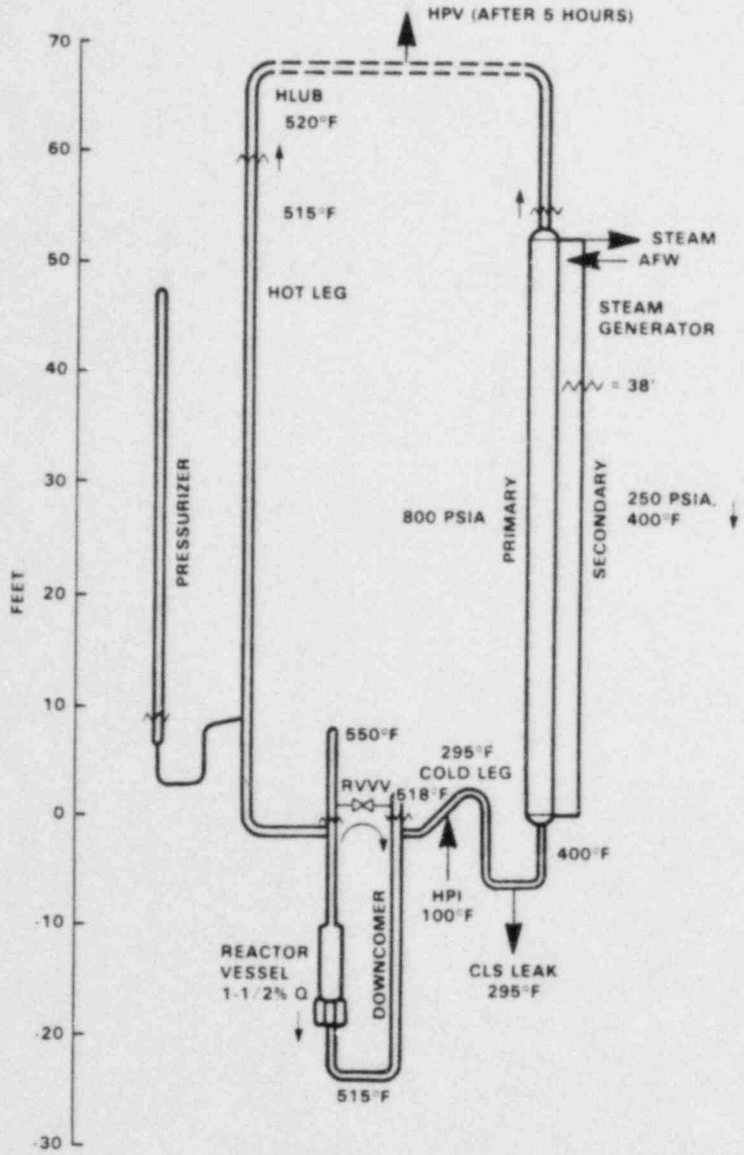


Figure 9. Loop conditions during refill (1 to 7 hours).

flow rates were nearly equal. The heat-up from HPI temperature to leak discharge temperature approximately equaled core power. These conditions were quite stable.

At five hours (t = 352 minutes from test start), the hot leg high-point vent was opened. The vapor that was discharged from the HPV caused a mild primary depressurization; vapor flow to the vent cooled the upper-elevation hot leg metal. The primary system refill rate increased, spillovers occurred more frequently, and the loop filled at seven hours (t = 480 minutes from test start).

Natural circulation started immediately after refill was reached, starting the post-refill cooldown. The primary loop flow rate stabilized at approximately 2% scaled flow and remained constant for approximately two additional hours of controlled cooldown. Figure 10 illustrates the loop conditions during this phase.

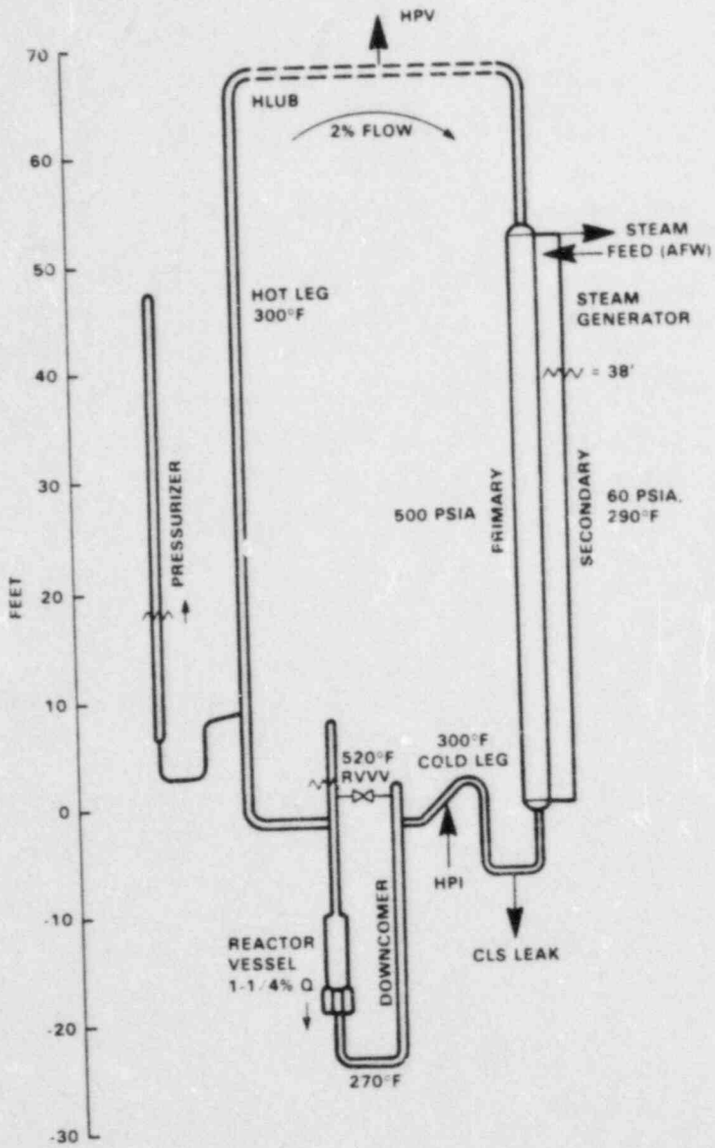


**Figure 10. Loop conditions during post-refill cooldown (7 to 10 hours).**

Table 2 compares the duration of the five characteristic SBLOCA phases for selected OTIS tests. Exact identification of the beginning and end of a phase is not exact. The phase times in Table 2 were based on the following:

- The pressurizer draining and loop saturation phase started with leak opening and ended when voids were first detected at the hot leg U-bend.
- The intermittent circulation phase extended from loop saturation until the steam generator primary level dropped to the AFW elevation, making boiler-condenser operation possible.
- Boiler condenser continued from intermittent circulation and ended with the primary steam generator level passing above the AFW elevation.

- Refill extended from boiler condenser and concluded when the hot leg U-bend was filled.

- The post-refill cooldown started with refill and ended with test termination.

The time to loop saturation was approximately the same (4 minutes) for all tests. Test 220201, which used a 15 $cm^2$ leak compared to the nominal 10 $cm^2$, reached loop saturation sooner because of the larger leak, causing a more rapid depressurization.

The end of the intermittent circulation phase was reached in 12 to 44 minutes after leak opening. Two groupings of tests were noted; those taking less than 20 minutes and those requiring greater than 20 minutes to the phase end. Tests 220201 (leak size), 220304 (half HPI capacity), 220604 (HPI low head), and 230299 (low head HPI, composite) required 20 minutes or less to reach the end of intermittent circulation. The shorter phase duration was caused by the larger-than-nominal leak size or reduced HPI characteristics.

Three main test groupings were apparent for the time to the end of the boiler-condenser and start of the refill phase. Tests 230199 (nominal HPI, composite) and 230299 (low head HPI, composite) reached the end of the boiler-condenser phase in 65 minutes or less. These were the shortest times encountered and resulted from operator guideline actions and leak isolation. A second group of tests, 220201 (leak size) and 220304 (half HPI capacity), required greater than 200 minutes to reach the start of the refill phase. These tests displayed the longest time to reach the start of refill. The extended times were caused by the larger-than-nominal leak size or reduced HPI flow capacity. The remaining tests reached the end of the boiler-condenser phase in 100 to 150 minutes.

The elapsed times to the end of refill ranged from 389 to 459 minutes except for Test 220304 (half HPI capacity), which did not refill at 590 minutes. Test 220304 was terminated at 590 minutes based on pre-defined test procedures.

#### Composite Tests

Two composite tests (230199 and 230299) introduced operator guidelines. An operator trained in plant procedures controlled evolution. The initialization and initiation conditions paralleled those of the single-variable tests except that AFW was not available until one hour after test initiation. Also, the 10 $cm^2$ cold leg suction leak was isolated after 30 minutes of testing. Both tests simulated full HPI capacity. Test 230199 simulated high-head HPI characteristics, while low head HPI was simulated in Test 230299.

The operator controlled system conditions similarly in the two tests. With feed unavailable, the operator used intermittent PORV actuations to control primary pressure. When AFW became available, the operator used throttled feed to depressurize the primary using BCM. Refill, post-refill circulation, and cooldown were rapidly achieved. The operator felt that model interactions were realistic and would provide valuable experience for plant operators.

Table 2

## DURATION OF CHARACTERISTIC SBLOCA PHASES FOR SELECTED OTIS TESTS

| Category | Test Number | Description | Variable | Time (After Leak Opening) for Each Phase of SBLOCA, Minutes | | | | |
|---|---|---|---|---|---|---|---|---|
| | | | | Pressurizer Draining and Loop Saturation | Intermittent Circulation | Boiler Condenser | Refill | Post-Refill Cooldown |
| II | 220100 | Nominal Test<br>- Scaled 10 $cm^2$ Cold Leg Suction Break<br>- Full HPI Capacity<br>- 38' Steam Generator Secondary Control Level | -- | 0-4 | 4-44 | 44-104 | 104-434 | 434-601 |
| II | 220201 | Leak Size | Scaled 15 $cm^2$ Cold Leg Suction Leak | 0-2 | 2-13 | 13-207 | 207-459 | 459-511 |
| II | 220304 | HPI Characteristics | HPI Half Capacity | 0-3 | 3-18 | 18-218 | 218-* | -- |
| II | 220402 | Steam Generator Characteristics | 10' Steam Generator Secondary Control | 0-3 | 3-34 | 34-150 | 150-424 | 424-484 |
| II | 220503 | Leak Location | Scaled 10 $cm^2$ Cold Leg Discharge Leak | 0-3 | 3-23 | 23-120 | 120-425 | 425-485 |
| II | 220604 | HPI Characteristics | Low Head (1630 psia) Shut-Off | 0-4 | 4-12 | 12-100 | 100-389 | 389-495 |
| III | 230199 | Nominal HPI Composite | ATOG Guidelines | 0-4 | 4-44 | 44-60** | 60-75 | 75-100 |
| III | 230299 | Low-Head HPI Composite | HPI Shut-Off Head | 0-4 | 4-20 | 20-65** | 65-78 | 78-240 |



* Refill was not reached after 590 minutes of transient time.

** Boiler condenser possible during this period based on level, but did not occur until approximately 60 minutes after opening leak since AFW was not available until 60 minutes after leak opening.

## HPI Leak Cooling

The role and mechanisms of HPI leak cooling have been described with the nominal transient. HPI leak cooling and refill are addressed from a more rigorous standpoint in the following paragraphs.

Figures 11 through 15 form the basis for this discussion. Figure 11 displays the OTIS nominal HPI characteristics. This simulated two high-head plant HPI pumps with mass flow rate scaled by 1686. The HPI head-flow characteristics were altered at the lower pressures to simulate low-pressure injection (LPI). OTIS had no core flood tank simulation, and the LPI contribution was injected at the HPI site, that is, at the cold leg discharge rather than the upper downcomer.

Figure 12 displays leak mass flow rate versus system pressure for various leak fluid temperatures. This figure represents a scaled 10 $cm^2$ (0.010 $ft^2$) liquid-region break. The modified Burnell prediction of critical flow was used, and the predicted flow was multiplied by 0.85 on the basis of OTIS observations of critical flow.

The leak flow rates of Figure 12 provided a vehicle with which to estimate HPI leak cooling (see Figure 13). The calculations used leak mass flow rate; the effects of HPI flow rate excess or deficit were ignored. Then the HPI leak cooling was simply:

$$q = \dot{m}\, Cp\, DT$$

where the temperature difference was leak fluid temperature minus the temperature of HPI (~90°F). The plot displays "QCOR" -- this is the total core power offset by HPI leak cooling, plus 1/2% losses to ambient (1% = 21.4 kW). The time after reactor trip may be associated with each of these core power levels by entering the decay power schedule. Consider the QCOR = 2% curve at 36 minutes. (The decay portion of this core power is 2 - 1/2 = 1-1/2%, the decay of core power reaches 1-1/2% at 36 minutes after reactor trip). If the primary conditions reside to the right of this curve (toward higher power levels), then HPI leak cooling was sufficient to offset core power. However, if primary conditions at one-half hour lie to the left of this curve, the HPI leak cooling was insufficient to offset core power.

The composite of HPI characteristics, leak flow rates versus temperature, and HPI leak cooling combine to develop a conditions map, (refer to Figure 14). Again, the times on this figure reflect core power decay. If the timing of the primary fluid conditions lag those listed, then HPI leak cooling was sufficient to offset core power.

Figure 15 presents the previously described nominal transient on the conditions map. Only the major transient events are shown. The map was entered from the right as the loop fluid saturates (4 minutes after test initiation). Primary pressure was relatively constant and the leak fluid temperature remained elevated during the half-hour of intermittent circulation. HPI leak cooling became increasingly sufficient to offset core power, and leak flow continued to exceed the HPI rate.

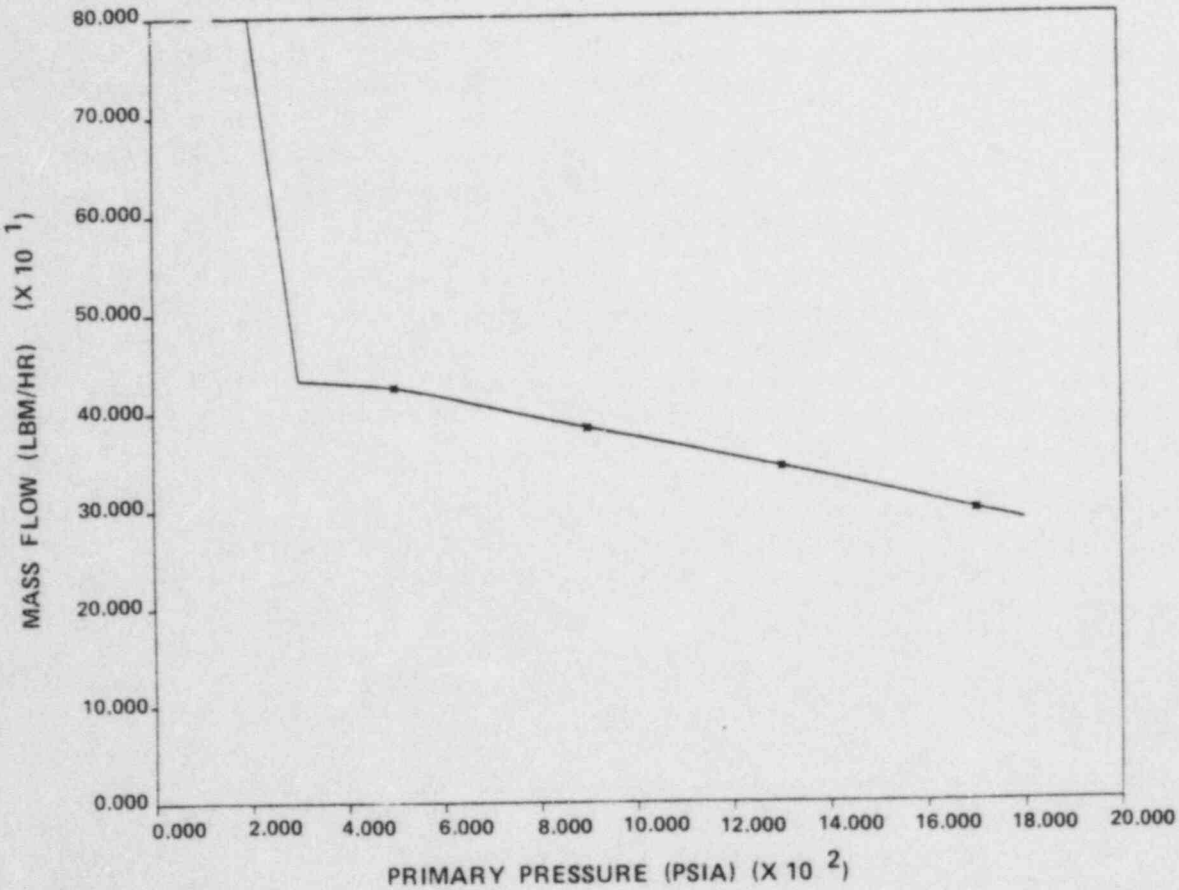


HPI mass flow rate versus system pressure.

HPI flow rate increased at lower pressure to simulate low-pressure injection (LPI).

The model simulates 2 higher head plant pumps with flow rate scaled by S = 1686.

**Figure 11. OTIS high-pressure injection.**

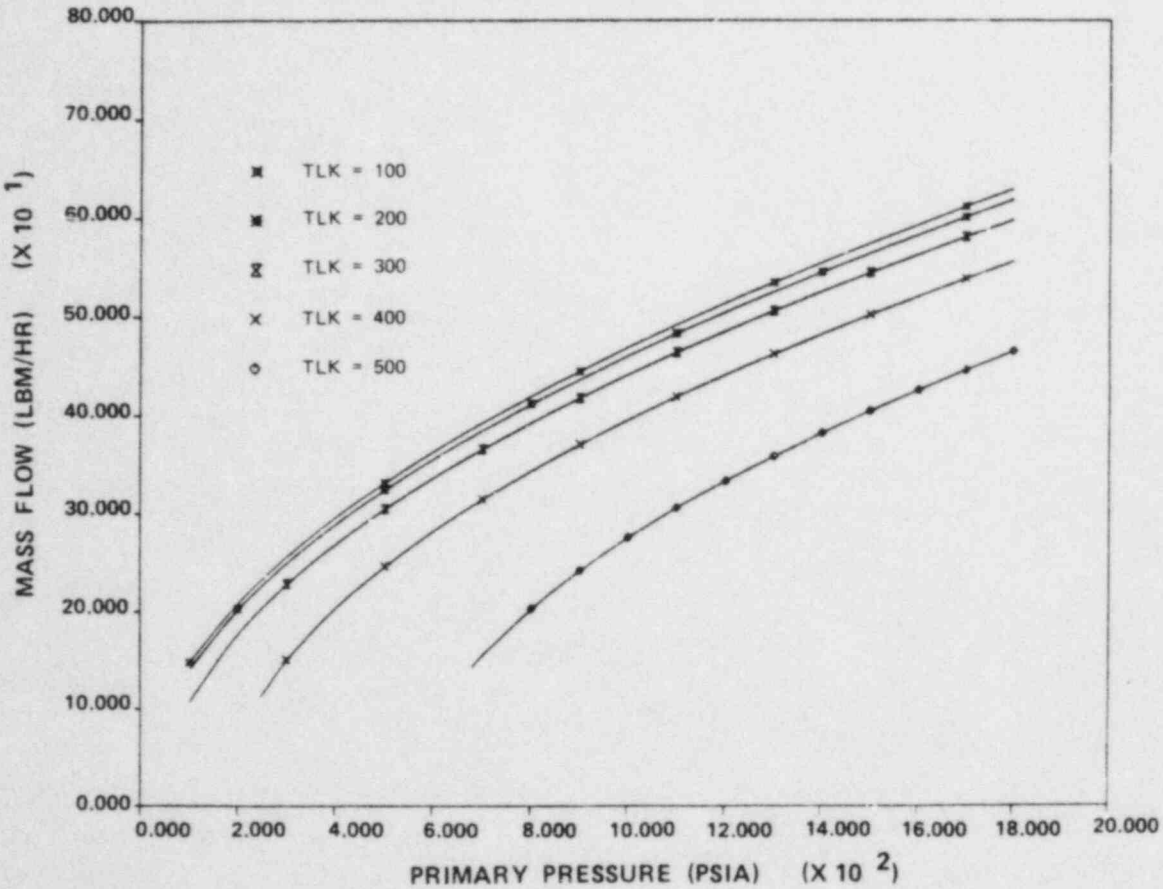


Scaled 10 $cm^2$ liquid-region leak (scale factor = 1686).

Liquid critical flow predicted using 0.87 x modified Burnell ("0.87" was selected based on OTIS data).

Leak mass flow rate versus pressure is shown for leak fluid temperatures (TLK) from 100F to 500F.

**Figure 12. OTIS leak flow rate.**

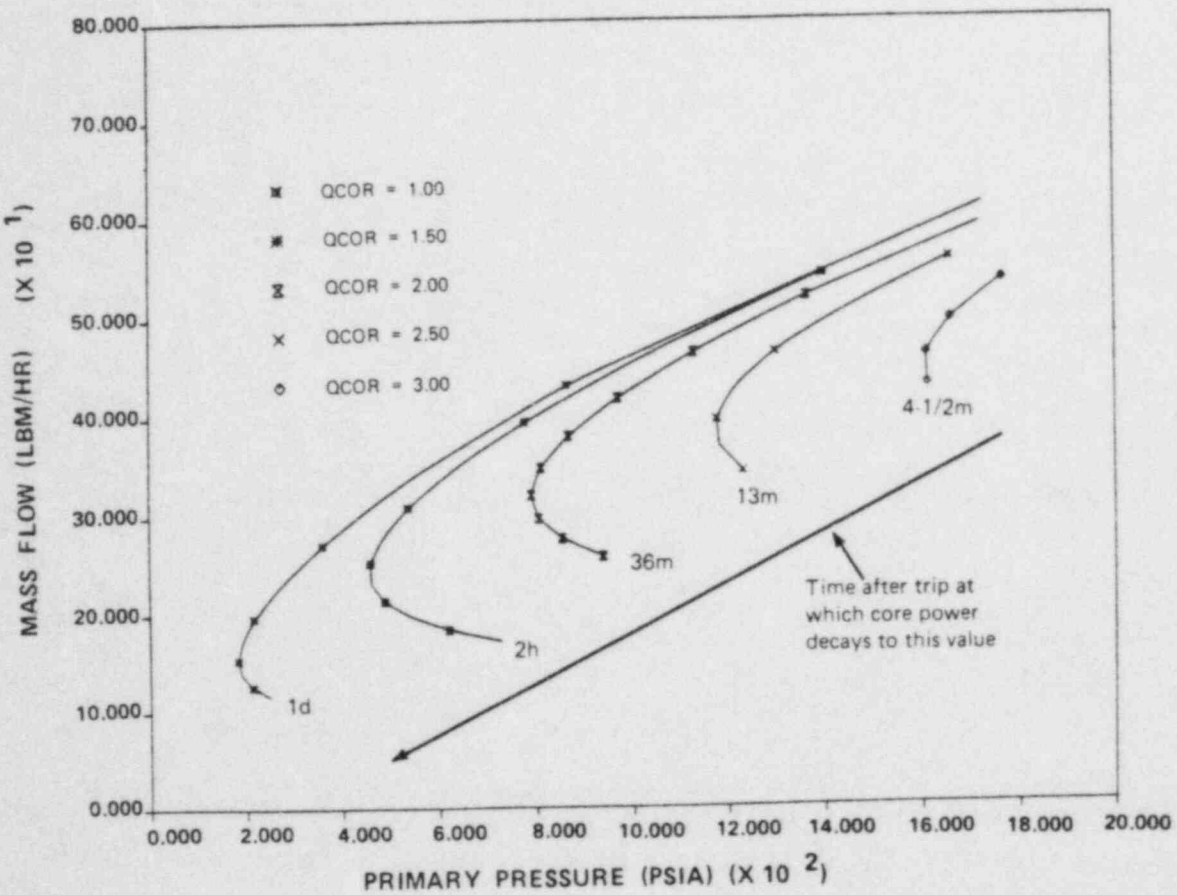


Core power offset (QCOR) by HPI-leak cooling plus 1/2% lost to ambient.

Power is expressed as percent of scaled full power (1% of 21.4 kW, scale factor = 1686).

HPI leak cooling is the heat transfer rate required to heat the HPI fluid (~90F) to the leak fluid temperature, at the leak mass flow rate.

Leak flow rate is calculated for a scaled 10 $cm^2$ liquid-region break using 0.85 x modified Burnell.

**Figure 13. OTIS high-pressure injection leak cooling.**

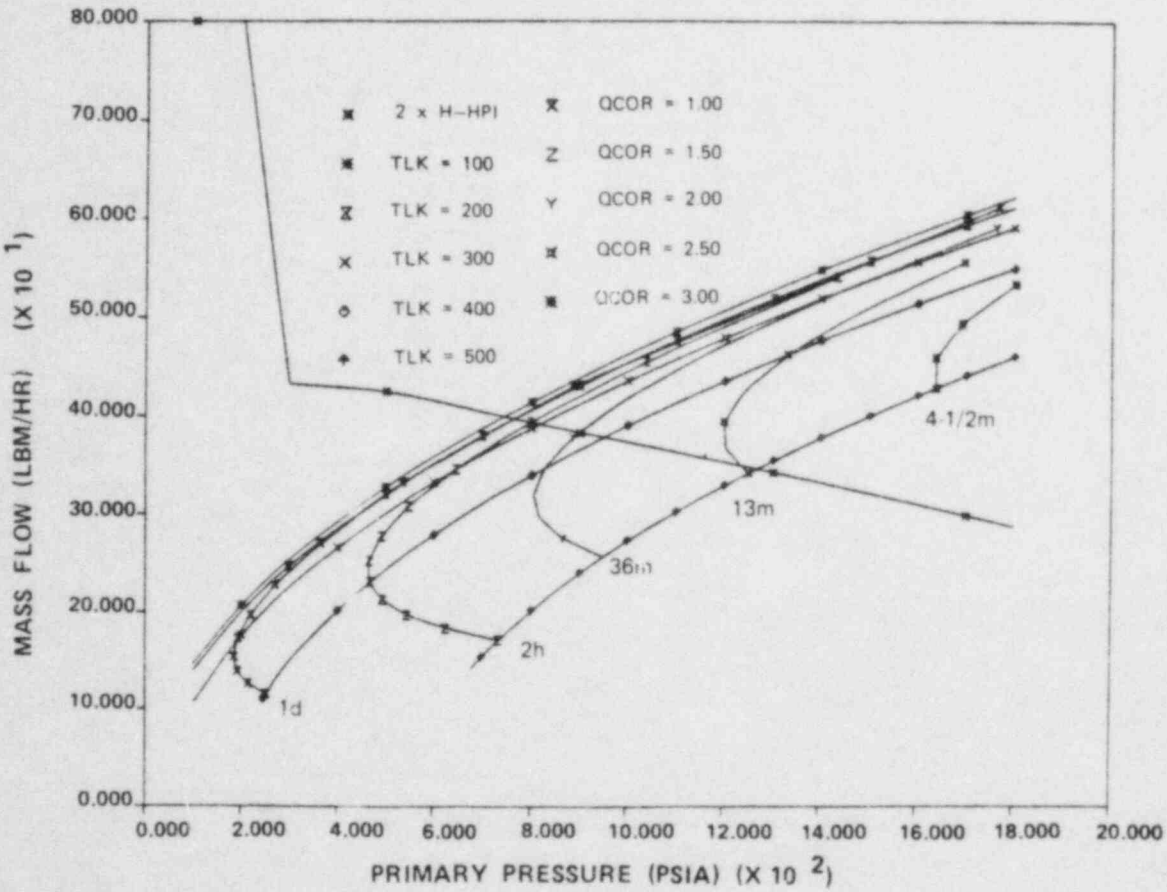


HPI mass flow rate versus pressure. (2 x H-HPI)

Leak mass flow rate versus pressure at various leak fluid temperatures. (TLK)

Core power offset by HPI leak cooling plus ambient losses. (QCOR)

**Figure 14. OTIS conditions -- 10 cm$^2$ liquid-region leak, high-head high-pressure injection.**

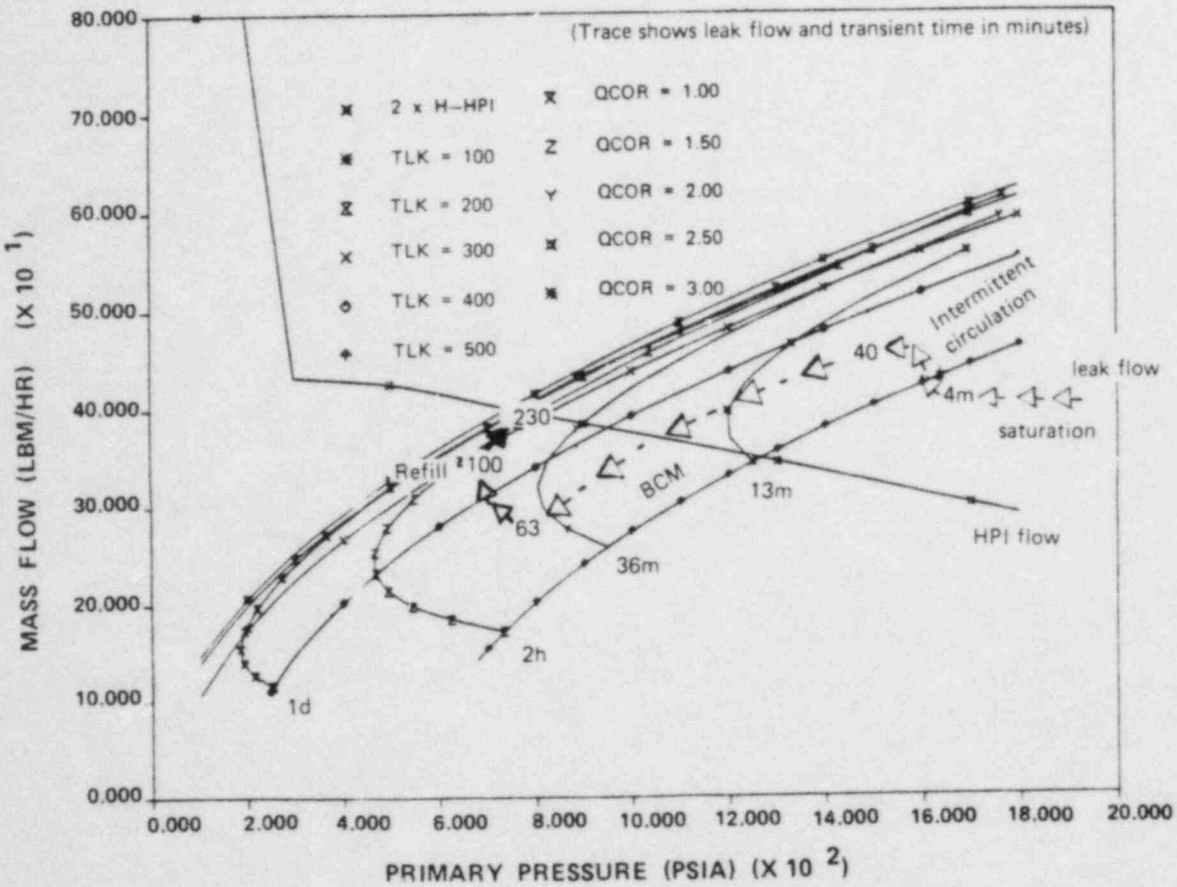


| TIME | EVENT | DISCUSSION |
|---|---|---|
| 0-4m | Depressurization to Saturation | Leak flow exceeds HPI, SG coupled. |
| 4-44m | Intermittent Circulation | Leak fluid cools due to HPI influence |
| 44-63m | BCM | SG heat transfer depressurizes primary causing HPI flow to exceed leak flow. |
| 63-100m | Continuing BCM with Refill | HPI cools leak fluid, SG heat transfer continues. |
| 100m-5hr | Refill | SG decoupled as primary level rises above generator. Leak flow rate increases with continued HPI cooling. HPI leak heat transfer decreases, primary pressurizes. Primary approaches mass and energy equilibrium. |

**Figure 15. Conditions during OTIS nominal transient; 10 $cm^2$ cold leg suction leak, high-head and full capacity high-pressure injection (Test 220100).**

The BCM pool, at 44 minutes, rapidly altered primary conditions toward lower pressure, but at a roughly constant leak fluid temperature. HPI flow began to exceed leak flow, the leak fluid temperature decreased, and the power, offset by HPI leak cooling, diminished. When the primary level exceeded the steam generator elevation, and the steam generator was decoupled after 100 minutes, the primary repressurized slowly. Equilibrium was approached at four hours. HPI and leak flow rates were approximately equal, and HPI leak cooling was approximately equal to core power.

## SUMMARY

OTIS was a 1 x 1 full-elevation model of a domestic, raised-loop B&W plant. Testing was performed to obtain integral system data for code benchmarking.

The expected post-SBLOCA events were encountered in OTIS, these included: depressurization to loop saturation, intermittent circulation with repressurization, the boiler-condenser mode refill with HPI leak cooling, and post-refill circulation, cooldown, and depressurization.

The BCM was an effective means of primary depressurization and heat removal. Two types of BCM were observed:

- AFW BCM, in which primary steam was condensed by the introduction of cold AFW while the primary level in the steam generator was above that of the secondary.

- Pool BCM, where the steam generator primary and secondary levels overlapped.

System refill was generally prolonged. HPI leak cooling kept the core-region fluid cool, but the primary often approached mass and energy equilibrium. Actuation of the hot leg high-point vent hastened refill in several tests.

The composite tests indicated the usefulness of appropriate operator actions, as well as the ability of the model to provide operator experience. OTIS obtained a wealth of code-challenging data.

## REFERENCES


1. H. R. Carter, "Integral System Test Program," B&W Operating Experience Seminar, 1983.

2. Y. Taitel, D. Bornea, and A. E. Dukler, "Modelling Flow Pattern Transitions for Steady Upward Gas-Liquid Flow in Vertical Tubes," AIChE 26, 3, May 1980.

3. G. B. Wallis, "Flooding Velocities for Air and Water in Vertical Tubes," UKAEA Report AAEW-R123, 1961.

# RESEARCH RELATED TO REACTOR VESSEL HEAD VENT EXEMPTION: CORE COOLING BY NATURAL CIRCULATION AND FEED/BLEED IN THE PRESENCE OF NON-CONDENSABLES

Sponsored by the Florida Power Corporation and the Sacramento Municipal Utility District and performed by the Babcock and Wilcox Company at Alliance, Ohio, April-May, 1984.

Edwin H. Davidson, Florida Power Corporation.
Robert L. Black, Babcock and Wilcox Company.

## Summary of Tests 1 and 2 - Edwin H. Davidson, Florida Power Corporation

Two tests, fully financed by Florida Power Corporation (FPC) and the Sacramento Municipal Utilities District (SMUD), were conducted by Babcock and Wilcox (B&W) at the Once Through Integral System (OTIS) facility during April and May of this year. The utilities' interests in these tests were stimulated by suggestions of the NRC (Dr. Brian Sheron, in particular) and appeared to be relevant to FPC's and SMUD's interest in obtaining a permanent exemption from installation of a head vent. Both utilities are currently operating under a temporary exemption. The Crystal River Unit 3 (CR-3) is operated by FPC and the Rancho Seco unit is operated by SMUD. Both Nuclear Steam Supply Systems were manufactured by Babcock and Wilcox.

The only modification made in OTIS for these tests was an adjustment to the size of the hot leg high point vent to provide appropriate orifice scaling considered applicable to the CR-3 and Rancho Seco systems. Arrangements for the use of OTIS were made through the B&W Reactor Owners Group Analysis Committee.

The title of this presentation is shown in Slide 1.

**Research Related to Reactor Vessel Head Vent Exemption: Core Cooling by Natural Circulation and Feed/Bleed in the Presence of Non-condensables**

**E.H. Davidson - Florida Power Corporation**
**R.L. Black - Babcock & Wilcox**

SLIDE 1

As indicated, the research performed was in support of an interest by FPC and SMUD in obtaining a permanent exemption from the installation of a reactor vessel head vent. The purpose of the NRC requirement for a head vent was to permit controlled release of non-condensable gasses (including hydrogen) from the reactor vessel head following a postulated inadequate core cooling accident similar to that experienced at Three Mile Island Unit 2 in 1979.

The research sponsored by FPC and SMUD was conducted by B&W in the OTIS facility which has been described previously in this session (a summary description is also attached to this paper). The only slide needed here is the general arrangement of OTIS, shown in Slide 2.

**OTIS General Arrangement**

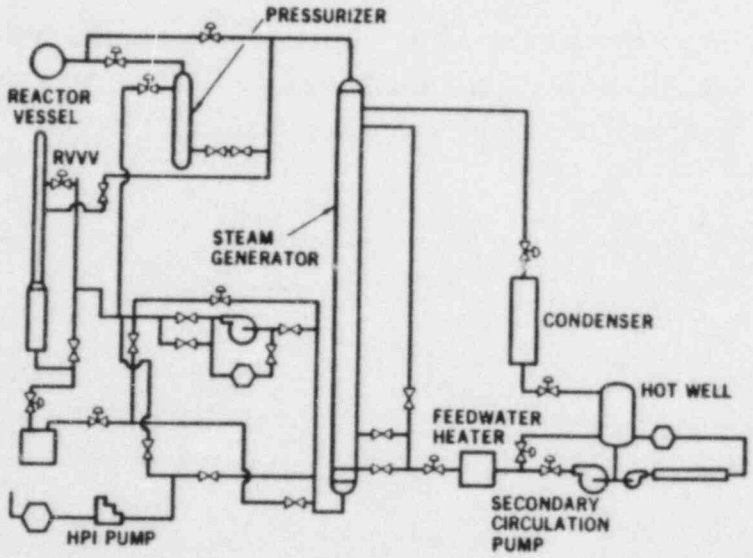


SLIDE 2

Note that the high point in the OTIS arrangement is at the bend of the hot leg and that a vent is provided at this location. The bend is called the hot leg U-bend (HLUB). The vent is called the hot leg high point vent (HLHPV). Also recall that, in OTIS, the single hot leg and steam generator represent the two hot legs and steam generators of a B&W reactor cooling system. Note also that OTIS provided a mockup of the reactor vessel, reactor vessel head volume, reactor core decay heat, pressurizer, pressurizer vents, high pressure injection cooling, and other features. This facility arrangement permitted demonstrations of recovery from an inadequate core cooling scenario in which non-condensable gasses have evolved (from damaged fuel and from the zircaloy/water chemical reaction which generated quantities of hydrogen) sufficient to saturate the coolant and to displace water in the reactor vessel head down to the level of the hot legs.

The principal interest in Test 1 was to show that, during depressurization and cooling of the reactor primary system, the non-condensable gasses which evolve from the gas-saturated coolant and which expand from the reactor vessel head will enter the hot leg and can be vented through the HLHPV without interrupting core cooling by natural circulation. The purpose of Test 1 is shown in Slide 3.

## Purpose of OTIS Test I

**Demonstrate that with a bubble of non-condensable gas in the head and the hotleg vents open the core can be cooled down using natural circulation**

SLIDE 3

Note that the hot leg high point vents remained open during Test 1 to permit continuous evolution of non-condensables which moved to the hot leg U-bends.

The initial conditions for Test 1 are summarized in Slide 4.

## Initial Conditions
## OTIS Test I

- **Inadequate core cooling**
  - **Saturate system with non-condensable gas**
  - **Inject non-condensable gas into RV head**
  - **Simulate decay heat at constant 1% power**
- **RCS pressure boundary intact**
- **Emergency feedwater available to steam generators**
- **High pressure injection available**
- **Reactor coolant pumps unavailable**

SLIDE 4

Note that the first asterisk indicates the gas saturated coolant, the filling of the reactor vessel head with non-condensable gasses and the decay heat level (constant). The second asterisk indicates that the pressure boundary is again intact (e.g., if the initiating event was a loss of pressure and coolant inventory through a valve, that valve has been closed). Remaining asterisks show that emergency feedwater and high pressure injection are assumed available, but reactor coolant pumps are not.

Slide 5 shows the procedure used in Test 1.

## Procedure Used in
## OTIS Test I

1. **Establish natural circulation cooling of core**
2. **Interrupt natural circulation by injecting non-condensable at Hotleg High Point Vent (HLHPV)**
3. **Open HLHPV, regain natural circulation, and keep HLHPV open during test**
4. **Depressurize and cool system to 284 psig and 280°F using natural circulation with a 50 to 100°F/hr cooldown rate and appropriate subcooling margin**

SLIDE 5

Note that in Item 2, the interruption of natural circulation cooling of the core was an initial condition and was initiated by displacing water in the hot leg U-bend when a non-condensable (nitrogen) gas was added. The purpose of Item 3 was to show that releasing the gas by opening the hot leg high point vent would restore natural circulation. Keeping the vent open during the test provided a release path for non-condensables evolved from the coolant or by expansion from the reactor vessel head into the hot legs. The fourth item provided consistency with current natural circulation cooldown procedures at CR-3.

Slide 6 shows a Pressure-Temperature plot of the principal points of interest in Test 1. At time 0 minutes (Point 1), natural circulation has been interrupted. At time 5 minutes (Point 3), natural circulation has been restored. At time 73 minutes (Point 4), the operator re-entered the operating band and cooldown continued. (This slide will be shown again for more detailed discussion by Bob Black.)

**Test - 1**

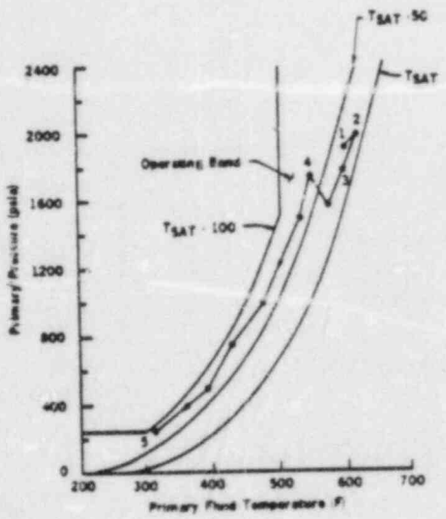


SLIDE 6

Slide 7 shows the purpose of the second test in OTIS.

## Purpose of OTIS Test II

**Demonstrate that if natural circulation cooling is interrupted by non-condensables, the core can be cooled by the HPI/PORV (Feed and Bleed) technique**

SLIDE 7

Note that the intent was to show that an alternate method is available for cooling the core, even if natural circulation cooling is interrupted.

The initial conditions for Test 2 are shown in Slide 8.

## Initial Conditions OTIS Test II

**(Same as Test I)**

- **Inadequate core cooling**
  - **— Saturate system with non-condensable gas**
  - **— Inject non-condensable gas into RV head**
  - **— Simulate decay heat at constant 1% power**
- **RCS pressure boundary intact**
- **Emergency feedwater available to steam generators**
- **High pressure injection available**
- **Reactor coolant pumps unavailable**

SLIDE 8

Note that these conditions are the same as shown in Slide 4 for Test 1.

The procedure intended for Test 2 is shown in Slide 9.

## Procedure Intended for OTIS Test II

1. **Establish natural circulation cooling of core**
2. **Interrupt natural circulation by injecting non-condensables at HLHPV**
3. **Open HLHPV to restore natural circulation cooldown of core**
4. **Close HLHPV, continue cooldown and depressurization until non-condensables interrupt natural circulation**
5. **Transfer cooldown of core from natural circulation to feed/bleed cooling using HPI/PORV**
6. **Depressurize and cool system to 284 psig and 280°F**

SLIDE 9

The difference in procedure for Test 2 as compared to the procedure for Test 1 begins in Item 4 when the HLHPV is closed rather than remaining open. The intention was to let natural circulation be interrupted and to demonstrate that cooldown of the core could be transferred to feed/bleed cooling using HPI/PORV for the remainder of the cooldown.

Slide 10 shows the Pressure-Temperature plot for Test 2. Note that after the HLHPV was closed, natural circulation cooling was lost and the transition to feed/bleed cooling was initiated and continued to Point 5 at which time a quasi-equilibrium occurred. More will be said about this point by Bob Black. In order to continue system cooldown, the decision was made to make a transition back to natural circulation cooling, long after the primary and secondary cooling systems had been decoupled. The transition was successful and cooldown continued to Point 7. (This slide will also be discussed later by Bob Black.)

## Test - 2

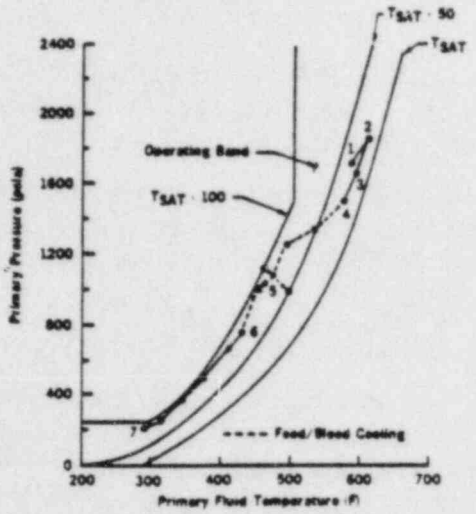


SLIDE 10

Slides 11, 12, and 13 show, respectively, the Results of OTIS Test 1, Results of OTIS Test 2, and the Summary and Conclusions of Testing.

## Results of OTIS I

1. **Natural circulation cooling of core is not interrupted with HLHPV continuously open during cooldown and depressurization**
2. **Cooldown rates of 50°F/hr to 100°F/hr were easily controlled**
3. **Adequate subcooling margin (50-100°F) was easily maintained throughout system cooldown**
4. **The non-condensable gas bubble in the head had no effect on the ability to cooldown**

SLIDE 11

## Results of OTIS Test II

1. Natural circulation was interrupted after closing HLHPV
2. Cooldown of core was transferred from natural circulation to feed/bleed cooling by adding HPI and opening PORV
3. The feed/bleed heat removal method reached an equilibrium condition before complete cooldown could be obtained
4. To continue cooldown, HLHPV was also opened to increase flow through core
5. Prior to reaching new feed/bleed and decay heat power equilibrium, a transition was made from feed/bleed cooling to natural circulation cooling
6. Cooldown continued to 284 psig, 280°F

SLIDE 12

## III. Summary and Conclusions of Testing

If the low probability event of inadequate core cooling occurred and the coolant were saturated with non-condensables with a bubble in the RV head:

- Two mechanisms are available for core cooling
  - — Natural circulation
  - — HPI/PORV (feed/bleed)

  The two mechanisms are complementary and interchangeable in sequence
- Non-condensables which remain in the RV head do not affect core cooling
- Non-condensable gases in the reactor coolant can be vented through the reactor coolant system HPV's and do not affect core cooldown
- Natural circulation cooling can be maintained with HLHPV's always open
- If intermittent operation of the HLHPV's were desired to minimize release of $H_2$ to the containment, natural circulation could be restored if interupted

SLIDE 13

The next portion of the presentation will be made by Bob Black.

Operator Actions and Facility Response - Robert L. Black

This portion of the presentation is intended to review the parameters available to the operator, to discuss the pressure-temperature curves shown earlier in more detail (from an operator's point of view), and to indicate the lessons learned (from a procedural standpoint) in Tests 1 and 2.

Before describing the tests in detail, several points must be discussed. Throughout the duration of both tests, the data made available to the operator was restricted to those parameters that would be available in an actual Control Room. These parameters are shown in Slide 14:

## OTIS Parameters Used by Operator

**Hot leg temperature**

**Cold leg temperature**

**Incore temperature**

**Primary pressure**

**Secondary pressure**

**Steam generator level**

**HPI flow**

SLIDE 14

Throughout the test discussions, reference is made to "indications of regaining natural circulation." To do this, the operator must check several indications. The cold leg temperature should be just about equal to the saturation temperature in the steam generator. The hot leg and incore thermocouple temperatures will increase as necessary to develop the driving head required for flow. The temperature difference between the hot leg and cold leg temperatures should be between 50°F and 60°F. As natural circulation is lost, as was the case in Test 2, this temperature difference reached >90°F indicating natural circulation was lost.

Slide 15 again shows the Pressure-Temperature trace for Test 1.

**Test - 1**

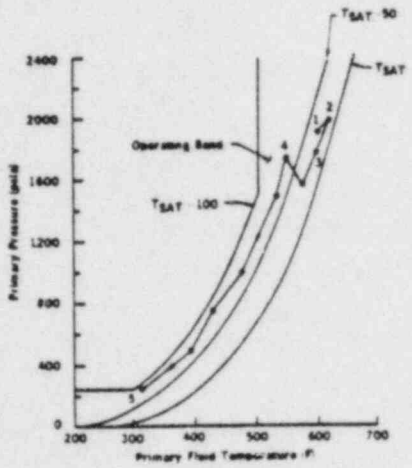


SLIDE 15

Simulating the recovery from a transient resulting in inadequate core cooling, the operator is given control of the facility with no flow in the RCS, due to the gas bubble in the hot leg U-bend, no heat being removed by the steam generator and no HPI flow through the core (i.e., no core cooling). In order to regain natural circulation and re-establish core cooling, the operator opens the HLHPV and initiates Auxiliary Feedwater (AFW) spraying high in the OTSG attempting to remove the gas blocking the HLUB and creating a low pressure area on the primary side of the OTSG and raising the heat sink's thermal center to establish conditions for natural circulation. In less than five minutes, the operator has indications that the actions taken have regained natural circulation and, with the HLHPV open, a normal, natural circulation cooldown is initiated by lowering steam pressure. To maintain the system pressure-temperature relationship between 50°F and 100°F subcooled, the operator periodically depressurizes by spraying into the pressurizer using the Auxiliary Spray System. This cooldown-depressurization continues until conditions are met for starting the Decay Heat Removal (DHR) System when the test is terminated.

Slide 16 again shows the Pressure-Temperature trace for Test 2.

**Test - 2**

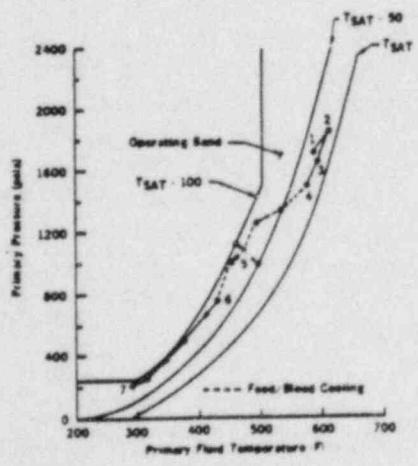


SLIDE 16

This test is initialized at the same point as Test 1 simulating the same conditions. The initial operator actions were identical: open the HLHPV and initiate Auxiliary Feedwater flow high in the OTSG. Once subcooled natural circulation is regained, the HLHPV is shut. As the system continues to cool down and depressurize, gasses come out of solution and begin to accumulate in the HLUB. The only indication to the operator that this is occurring is the slow increase of differential temperature between the incore temperature and the cold leg temperature above the desired 40°F to 50°F. As more and more gasses come out of solution, the incore-to-cold leg differential temperature increases to above 90°F. At this point, the operator determines that natural circulation is lost and proceeds to an alternate method of core cooling by initiating full HPI and opening the PORV, commonly referred to as feed and bleed cooling.

Feed/bleed cooling continued for several hours until a quasi-equilibrium was reached. The quasi-equilibrium is shown as Point 5 on Slide 16. At this point, as HPI flow was increased, system temperature decreased and pressure remained relatively constant. As HPI flow was decreased, system temperature increased and pressure again remained relatively constant. The reason postulated in the Control Room for this equilibrium occurring was that core power was atypically held at a 1% scaled power and equilibrium had been reached between the energy being put into the system by core power and HPI and the energy being removed from the system by the PORV and to ambient. Another reason to be discussed later was given after the data was analyzed. However, regardless of the reason for the occurrence of the quasi-equilibrium, the decision made by the operator was correct: in order to continue cooling the system to meet conditions for DHR System operation, the HLHPV was opened to provide another path for energy removal.

The opening of the HLHPV had two effects on the system. First, the system again began to cool down as more energy was being relieved out the vent. Second, with the HLHPV open, all the gas that had come out of solution and from the RV head region and had blocked natural circulation was slowly being bled off and the system began to refill. Once the system was refilled, the decision was made to attempt to regain natural circulation.

To regain natural circulation, the hottest portions of the system should be low in the loop and the coldest part of the system should be high. When the decision was made to regain natural circulation, just the opposite was true. The hottest part of the system was in the HLUB and the coldest portion was in the cold leg where the Reactor Coolant Pump would have been located. Therefore, two attempts to regain natural circulation were made attempting to re-establish the proper temperature profiles. To make the transition from feed/bleed cooling to natural circulation cooling, the following steps occurred.

1. The HPI flow was stopped.

2. The PORV was shut.

3. AFW was initiated high in the OTSG.

4. Steam was bled from the OTSG.

After the first two attempts, the temperature profile had almost realigned itself for natural circulation and on the third attempt, natural circulation was regained.

With a normal, natural circulation cooldown in progress and the HLHPV again opened, the system was cooled down and conditions were established to operate the decay heat removal system.

## EFFECTS ON EMERGENCY OPERATING PROCEDURES FROM TESTS 1 AND 2

The results from these tests indicate that the guidance provided in the B&W-developed Abnormal Transient Operating Guidelines for cooling down with a gas laden Reactor Coolant System was accurate. In addition, the results from Test 2 indicate that if an operator error were to occur and the HLHPV's were shut, the transition to feed/bleed cooling and back to a normal, natural circulation cooldown is achievable.

## DISCUSSION OF QUASI-EQUILIBRIUM

During Test 2, an equilibrium was reached in the system that did not allow any further cooling. The Control Room conversation indicated that the energy into the system had reached a balance with the energy being removed and, therefore, no further cooling would occur unless something changed. After reviewing the Test 2 data, a different interpretation for this equilibrium was hypothesized.

With no flow through the saturated hot leg, the hot leg eventually became the hottest portion of the system. As the system cooled and depressurized, a point was eventually reached where system pressure was being maintained by the conditions in the saturated hot leg, and system pressure could not decrease below this value. (In effect, the voided hot leg U-bend was acting as a system pressurizer.) With system pressure being maintained constant and the operator attempting to maintain system conditions between 50°F and 100°F subcooled, HPI flow was increased to decrease system temperature until the 100°F subcooled margin line was reached and then HPI was decreased to increase system temperature until the 50°F subcooled margin line was reached. At no time during this equilibrium was core cooling interrupted or was the core in danger of being uncovered.

In an actual plant, this process should continue while system pressure decreases as the hot leg cools by heat losses to ambient temperature. However, because the OTIS facility hot leg loop was guard heated, the losses to ambient were minimized and the depressurization was very slow.

For either explanation, opening the HLHPV resulted in the regaining of system cooldown and was the appropriate operator action.

The last slide indicates the lessons learned from OTIS Tests 1 and 2 which are believed to be applicable to the operators at CR-3 and Rancho Seco, assuming the continued absence of a reactor vessel head vent.

# Operator's Lessons Learned

- Post ICC; open and leave open HLHPV
- Limit depressurization rate to limit gas evolution rate
- $T_{core}$ to $T_{cold}$ $\Delta T$ gives accurate indication of natural circulation status
- Transition between long-term feed/bleed cooling and natural circulation cooling is achievable

SLIDE 17

## APPENDIX

## OTIS SYSTEM DESCRIPTION

OTIS is an experimental test facility at B&W's Alliance Research Center, designed to evaluate the thermal/hydraulic conditions in the reactor coolant system and steam generator of a raised-loop B&W reactor, during the natural circulation phases of a Small-Break-Loss of Coolant Accident (SBLOCA). The test facility is a scaled 1x1 (one hot leg, one cold leg) electrically heated loop simulating the important features of the plant. The facility is used to perform separate effect and integral system tests at simulated scaled power levels of 1 to 5%.

The loop consists of one 19-tube Once-Through Steam Generator (OTSG), a simulated reactor, a pressurizer, a single hot leg, and a single cold leg. Reactor decay heat following a scram is simulated by electrical heaters in the reactor vessel. No pump is included in the basic system, but a multipurpose pump in an isolatable cold leg bypass line may be used to provide forced primary flow. The test loop is full raised-loop plant elevation, approximately 95 feet high, and is shortened in the horizontal plane (to approximately 6 feet) to maintain approximate volumetric scaling.

Other primary loop components include a reactor vessel vent valve (RVVV), pressurizer power-operated relief valve (PORV) or safeties, and hot leg and RV high point vents. Auxiliary systems are available for scaled high pressure injection (HPI), controlled primary leaks in both the two-phase and single-phase regions, a secondary forced circulation system for providing auxiliary feedwater (AFW) to the OTSG, steam piping and pressure control, a cleanup system for the secondary loop, gas addition, and gas sampling.

### Scaling

The configuration of the test loop is dictated by scaling considerations. The four scaling criteria used to configure OTIS, in order of priority, are:

- Elevations
- Post-SBLOCA Flow Phenomena
- Volumes
- Irrecoverable Pressure Loss Characteristics

OTIS power and volume scaling originates with the size of the model OTSG. The model OTSG contains nineteen (19) full-length and plant-typical tubes, which represent the 16013 tubes in each of the two steam generators used in the 205 FA plants. Therefore, the dominant power and volume scaling in the loop is:

$$\text{Scaling Factor} = \frac{19}{2 \times 16013} = \frac{1}{1686}$$

The distance between secondary faces of the lower and upper tubesheets in the 19-tube OTSG is full length. Auxiliary feedwater nozzles are located in the model steam generator at two elevations. The tubesheet thicknesses in the model OTSG are not plant-typical, and the model inlet and outlet plenums are reducers. Therefore, the hot leg-to-steam generator inlet and steam generator-to-cold leg lengths are atypical. Piping runs beyond the steam generator and plenums are used to retain plant-typical elevations.

The hot leg inside diameter is scaled to preserve Froude number, and thus the ratio of inertial to buoyant forces. This criterion is considered to preserve two-phase flow regimes and reflooding phenomenon according to certain correlations. Scaling with Froude number results in a hot leg diameter twice that indicated by ideal volumetric scaling. Although this adds approximately 20% to the ideal system (total loop) volume, this choice of hot leg inside diameter is considered most likely to avoid the whole-pipe slugging behavior observed in other scaled SBLOCA test facilities.

The spillover elevation of the plant hot leg U-bend is retained in OTIS by matching the elevations of the bottom (inside) of the plant and model hot leg U-bend pipes. The radius of the U-bend obtains exact volumetric scaling.

The pressurizer in OTIS is volume and elevation scaled. The elevation of the bottom of the pressurizer is plant typical, as is the spillunder elevation of the pressurizer surge line. The centerline elevation of the hot leg-to-pressurizer surge connection matches that of the plant.

An electrically heated reactor vessel provides heat input to the primary fluid to simulate reactor decay heat levels up to 5% scaled power. Based on a plant power rating of 3600 mwt, 1% of scaled full power in OTIS is 21.4 kw. The model core heat input capacity is 180 kw. OTIS primary flow scaling obtains 1% of scaled full flow - 0.259 lbm/s; on the secondary side, 1% of scaled full secondary flow = 0.0265 lbm/s.

The annular downcomer of the plant reactor vessel is simulated by a single external downcomer in OTIS. The spillunder elevation in the horizontal run at the bottom of the model downcomer corresponds to the elevation of the uppermost flow hole in the plant lower plenum cylinder. The OTIS reactor vessel consists of three regions: a lower plenum, a heated section, and an upper and top plenum. The center of the heated length of the core vessel corresponds to the center of the active fuel length in the plant core. The core region of the model reactor vessel contains excess volume due to construction constraints; therefore, to maintain the total reactor vessel scaled volume, the reactor vessel is shorter than plant-typical. Non-flow lengths were sacrificed to maintain reactor vessel scaled volume.

Cold primary fluid enters the downcomer from the cold leg, and heated primary fluid leaves the upper plenum to enter the hot leg. The center of the cold leg to downcomer connection in OTIS corresponds to the cold leg-to-reactor vessel nozzle centerline in the plant. Similarly, the center of the hot leg-to-upper plenum connection in OTIS corresponds to the reactor vessel-to-hot leg nozzle centerline in the plant.

The model cold leg does not contain an in-loop pump, since OTIS is designed to simulate the natural circulation phases of a SBLOCA. A flange is provided in the cold leg piping upstream of the reactor coolant pump spillover point to admit a flow restrictor which simulates the irrecoverable pressure loss characteristic of a stalled reactor coolant pump rotor.

The model cold leg originates at the lower plenum of the 19-tube OTIS and extends downward to match the spillunder elevation of the plant cold leg. The highest point in the cold leg (the spillover into the sloping cold leg discharge line) matches the reactor coolant pump spillover elevation in the plant. Because horizontal distances are shortened in OTIS, the slope of the cold leg discharge line is atypically large.

OTIS atypicalities are summarized as follows:

- OTIS is predominantly a one-dimensional, vertical system, due to the shortened horizontal distances and small cross sections of the various components such as steam generator and reactor vessel.

- Because of the small size of the piping used in the model, the ratio of loop piping wall surface to fluid volume is approximately 20 times that of the plant. Therefore, the fluid and wall-surface temperatures are much more closely coupled than those of a plant.

- In high-pressure models, the ratio of metal volume to fluid volume increases as the model piping is made smaller. The ratio of model metal volume to fluid volume in OTIS is approximately twice that of the plant.

The pipe surface to fluid volume ratio atypicality of scaled facilities results in higher heat losses in the scaled facilities than in the plants. This atypicality can be minimized by using both guard heaters and passive insulation on the model piping. Guard heating is used for the OTIS hot leg, pressurizer, surgeline, and RV upper head.

The OTIS secondary system provides the steam generator secondary inventory, and those fluid boundary conditions which impact SBLOCA phenomena. These include steam generator level control, auxiliary feedwater, and steam pressure control valves.

The OTIS instrumentation includes pressure and differential-pressure measurements; thermocouple (TC) and resistance temperature detector (RTD) measurements of fluid, metal, and insulation temperatures; level and phase indications by optical-ports and conductivity probes as well as by differential pressures; and pitot tubes and flowmeters for measurements of flowrates in the loop. In addition to these measurements, loop boundary conditions are metered: HPI, HPV (hot leg and RV), (controlled) leak, PORV, and secondary steam and feed flow are measures; non-condensable gas (NCG) injections are controlled and metered; NCG discharges with the two-phase primary effluent streams are measured; and the aggregate primary effluent are cooled and collected for integrated metering. OTIS instrumentation consists of approximately 250 channels of data which are processed by a high-speed data acquisition system. The data acquisition rate can be either event-actuated or adjusted by the loop operator to acquire and store a full set of data as often as every 5 seconds.

## LIST OF REFERENCES


1. Babcock & Wilcox Report 12-1152307-00, "OTIS Hot Leg High Point Vent Test #240100" for Florida Power Corporation and Sacramento Municipal Utility District, July, 1984.

2. Babcock & Wilcox Report 12-1152308-00, "OTIS Hot Leg High Point Vent Test #2040200" for Florida Power Corporation and Sacramento Municipal Utility District, July, 1984.

3. Babcock & Wilcox Report RDD:84:4091-24-01:01, "Once Through Integral System Test Program, OTIS Loop Functional Specification", issued for review 9/13/84.

# TRAC-PF1/MOD1 SUPPORT CALCULATIONS FOR THE MIST/OTIS PROGRAM*

by

Robert K. Fujita and Thad D. Knight
Safety Code Development Group
Energy Division
Los Alamos National Laboratory
Los Alamos, New Mexico 87545

We are using the Transient Reactor Analysis Code (TRAC), specifically version TRAC-PF1/MOD1, to perform analyses in support of the MultiLoop Integral-System Test (MIST) and the Once-Through Integral-System (OTIS) experiment program. The MIST/OTIS experiment program is funded jointly by the Nuclear Regulatory Commission (NRC), Babcock and Wilcox (B&W), the B&W Owners Group, and the Electric Power Research Institute (EPRI) to address remaining regulatory issues for the B&W plant design.

We have analyzed Geradrohr Dampferzeuger Anlage (GERDA) Test 1605AA to benchmark the TRAC-PF1/MOD1 code against phenomena expected to occur in a raised-loop B&W plant during a small-break loss-of-coolant accident (SBLOCA). These results show that the code can calculate both single- and two-phase natural circulation, flow interruption, boiler-condenser-mode (BCM) heat transfer, and primary-system refill in a B&W-type geometry with low-elevation auxiliary feedwater.

The GERDA facility was modified to create the OTIS facility. We made pretest predictions for OTIS Tests 220100 and 220402. Test 220100 is the nominal case for the OTIS test series and simulates a 10-cm$^2$ break in the pump-suction piping. The OTIS test facility was modeled completely with TRAC one-dimensional components because all OTIS components have very large length-to-diameter ratios, and therefore, do not need multidimensional representation. The OTIS model consists of 31 TRAC components that have been subdivided into 200 computational cells. A component schematic of the test facility is shown in Fig. 1. The steam-generator model has a single-flow channel to simulate the flow of primary fluid through the 19 tubes of the steam generator. The auxiliary feedwater (AFW) is injected through a minimum wetting nozzle near the top of the steam-generator secondary. This steam-generator model assumes that all 19 tubes will be wetted by the AFW during periods of AFW injection.

The TRAC pretest calculations were performed in a manner similar to the actual planned test procedures. A steady-state calculation was completed to establish the desired steady-state conditions during natural-circulation mode.

---

*This work was funded by the US NRC Office of Nuclear Regulatory Research, Division of Accident Evaluation.

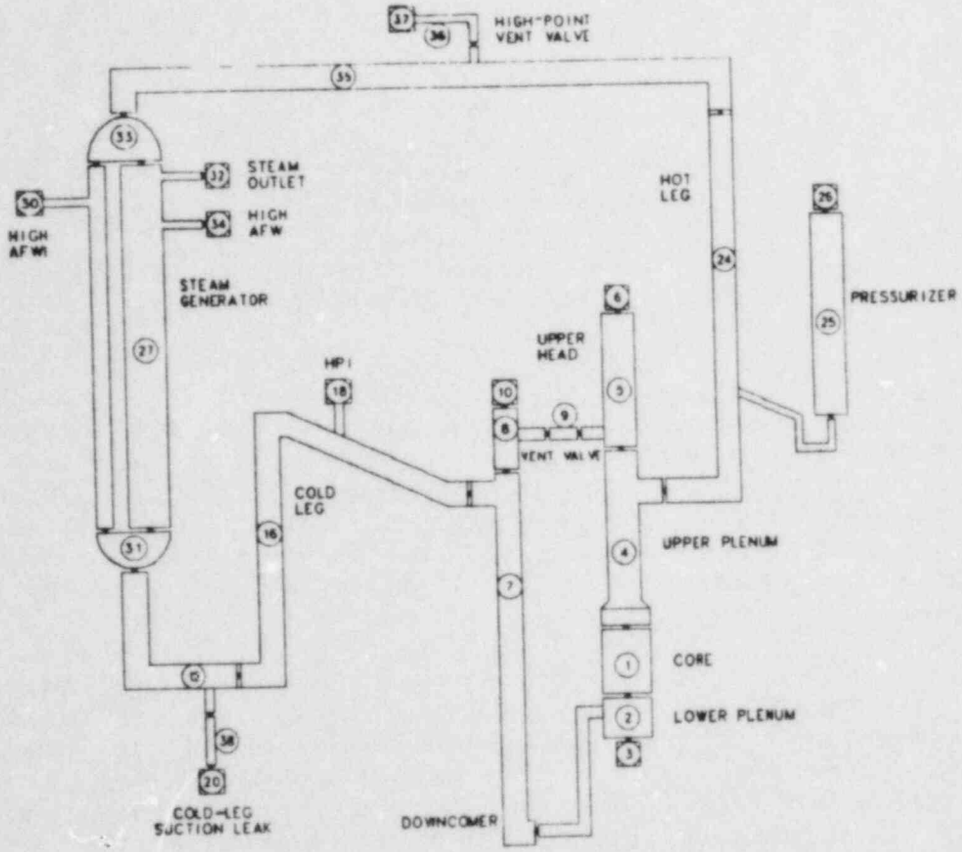


Fig. 1.
Component schematic for the OTIS test facility.

The steady-state test conditions are given in Table I. The transient calculation was initiated from the final steady-state conditions and proceeded in a systematic fashion as summarized in Table II. The significant features of Test 220100 are listed in Table III. The transient was run for 25,200 s (7 h) to complete the refilling of the primary system with the high-pressure-injection (HPI) system. The sequence of predicted events for this test are given in Table IV.

The calculated upper-plenum and steam-generator-secondary pressures are compared in Fig. 2. This figure shows the primary-and secondary-pressure responses caused by some of the events given in Table IV. On the primary side, the pressure oscillations from 1000 s to 2500 s result from condensation induced by the interaction of HPI fluid in the cold leg and steam flowing through the reactor-vessel vent valve from the upper plenum. The sharp drop in the secondary-side pressure was caused by the continuous AFW flow during the steam-generator filling that condensed a significant amount of steam on the secondary side.

TABLE I

STEADY-STATE TEST CONDITIONS FOR OTIS SINGLE-VARIABLE TESTS

| Parameter | Calculated Results | |
|---|---|---|
| System pressure | 1.517 MPa | (2200 psia) |
| Steam-generator-secondary pressure | 8.15 MPa | (1182 psia) |
| Hot-leg fluid temperature | 594.1 K | (609.7° F) |
| AFW temperature | 572.7 K | (100.0° F) |
| HPI fluid temperature | 294.2 K | (70.0° F) |
| Flow rate | 0.95 kg/s | (2.09 lbm/s) |
| Core power | 117.7 kW | |
| Steam-generator-secondary liquid level | 1.39 m | (4.56 ft) |
| Pressurizer liquid level | 3.05 m | (10.0 ft) |

TABLE II

SUMMARY OF THE TRAC CALCULATIONAL PROCEDURES

- Initiate transient by opening cold-leg-suction leak valve
- Perform the following operations when the pressurizer liquid level decreases to 0.61 m (2 ft) relative to the bottom of the pressurizer
  - Trip HPI system at cold-leg discharge
  - Initiate core-power decay
  - Begin filling the steam-generator secondary at a rate of 0.91 m/min (3 ft/min) to the prespecified level
  - Maintain constant steam-generator-secondary pressure at initial steady-state pressure
- When the steam-generator-secondary level reaches the prespecified level perform the following
  - Start steam-generator-secondary pressure control to reflect secondary-cooling rate of 28 K/h (50° F/h)
  - Maintain steam-generator-secondary level as per test specifications (band control and/or constant)
- Terminate test when hot-leg U-bend is refilled

TABLE III

MAIN FEATURES OF OTIS TEST 220100

- Nominal-case test
- Natural-circulation initial conditions
- Steam-generator AFW injected at upper injection port
  - AFW characteristics are "OTIS nominal"
- Initial core power 3.66% of scaled full power
  - Additional 0.5% for system heat losses
- Scaled 10-$cm^2$ cold-leg-suction leak
  - Leak is maintained throughout test
- HPI at cold-leg discharge
  - Tennessee Valley Authority high-head, full-capacity flow characteristics
- Steam-generator-secondary level increased from 1.52 m (5 ft) to 11.58 m (38 ft) at 0.91 m/min (3 ft/min)
- Steam-generator-secondary pressure controlled to simulate 28 K/h ($50^{\circ}$F/h) cooldown
- Reactor-vessel vent valve in automatic-control mode with open/close set points of 1724-Pa (0.250-psid) and 862-Pa (0.125-psid) pressure differentials
- Hot-leg high-point vent used only to decrease test termination time 5 h into the transient (orifice is scaled 3 $cm^2$)

TABLE IV

SEQUENCE OF PREDICTED EVENTS FOR OTIS TEST 220100

| Event | Time (min) |
|---|---|
| Cold-leg-suction leak initiated | 0.0 |
| Core-power decay and HPI started (also steam-generator secondary started to fill from 5 ft to 38 ft) | 1.8 |
| Pressurizer emptied (first time) | 2.4 |
| Steam-generator-secondary level reached 38 ft; cooldown of steam-generator secondary began at 28°K/h | 14.2 |
| Primary-loop natural circulation terminated | 16.7 |
| Primary-system pressure oscillated | 7.0-42.0 |
| Core region saturated | 33.5 |
| Emergency core coolant reached cold-leg leak region | 34.1 |
| Steam-generator BCM started | 71.8 |
| Minimum core liquid level reached | 85.8 |
| Refilling of hot leg began | 89.7 |
| HPI and leak flows crossed | 98.3 |
| Steam-generator BCM terminated | 100.1 |
| Refilling of pressurizer began | 260.1 |
| Steam-generator primary refilled | 272.2 |
| Steam-generator-secondary cooldown terminated | 291.7 |
| Hot-leg high-point vent opened | 300.1 |
| Pressurizer emptied (second time) | 301.8 |
| Core region refilled | 367.9 |
| Hot leg refilled | 403.3 |
| Calculation terminated | 420.0 |

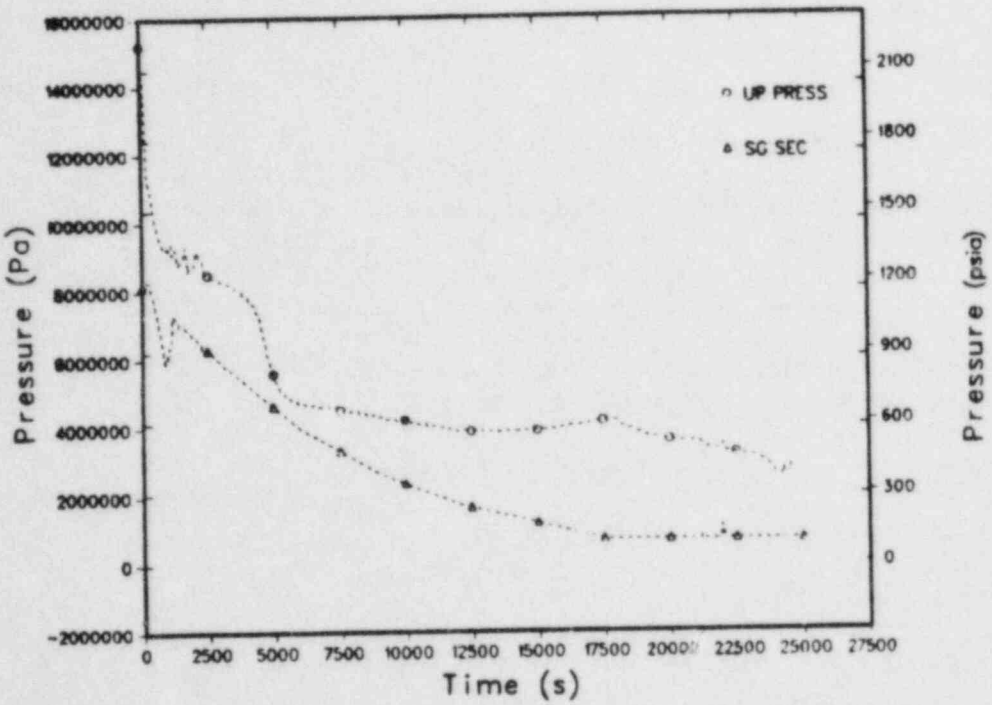


Fig. 2.
Calculated primary and secondary pressures for OTIS Test 220100.

The sudden decrease in primary pressure beginning at 4300 s corresponds to the initiation of the steam-generator BCM heat transfer. The high rate of energy removal from the primary to the secondary side of the steam generator caused by the BCM lasted for 1700 s and resulted in a primary-pressure decrease of 3.40 MPa (493.1 psia). At the end of the BCM, the primary pressure was reduced to within 0.57 MPa (82.9 psia) of the secondary pressure. During the next 12,000 s, the primary pressure remained fairly constant until the hot-leg high-point vent valve was opened at 18,000 s. Also at this time, the secondary-side cooldown was terminated and the pressure remained constant for the duration of the transient. The primary pressure began to decrease gradually after the high-point vent valve was opened until the hot-leg U-bend was filled completely at 24,200 s, at which time the primary system was refilled and the pressure increased rapidly.

The occurrence of BCM is evident in Fig. 3, which shows the calculated steam-generator primary and secondary collapsed-liquid-level histories. The initial intersection of the primary and secondary levels at 4300 s signifies the start of BCM and the separation of levels at 6000 s is the end of BCM. The steam-generator primary side began to refill at 5000 s because the rapidly decreasing primary pressure caused an increase in HPI flow and a decrease in leak flow, resulting in a net increase of system mass. The spikes in the primary-side liquid level that occurred after the end of BCM (6000 s to 12,000 s) are the result of steam condensation in the upper tube region during periods of AFW flow. The steam-generator primary side was refilled at 16,330 s.

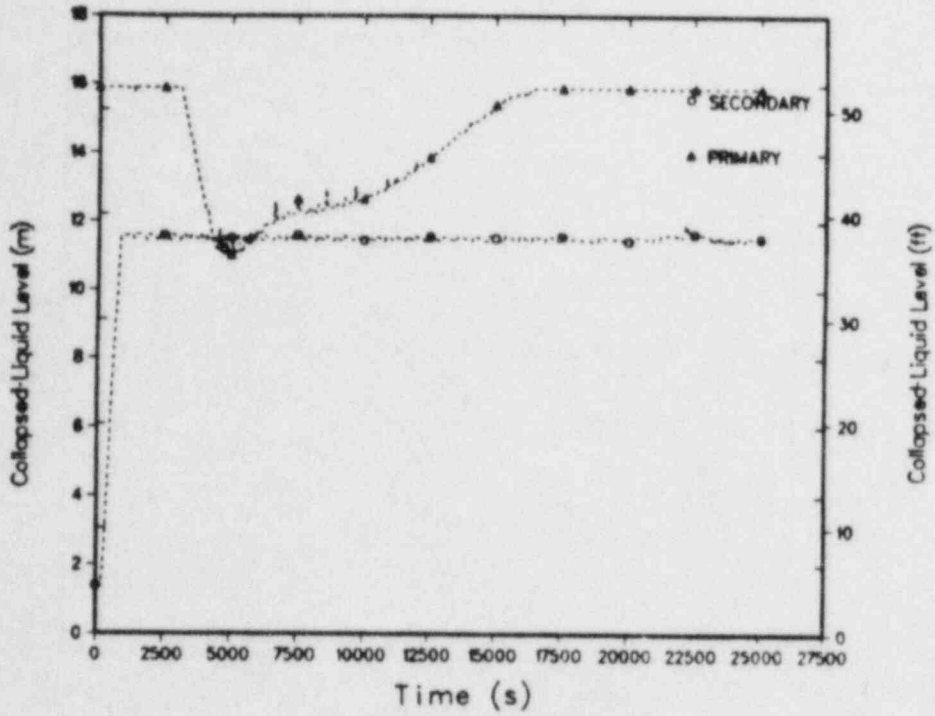


Fig. 3.
Calculated steam-generator collapsed-liquid levels for OTIS Test 220100.

The collapsed-liquid-level histories of the hot-leg upflow and downflow sides are shown in Fig. 4. The elevations shown at time zero represent the liquid level at the top of the hot-leg U-bend. Natural circulation was interrupted at 1000 s. The hot-leg level reached its minimum value at 4000 s and began to refill steadily until the hot-leg high-point vent was opened. Once the high-point vent was opened, the hot-leg levels increased rapidly. The sudden decrease in levels at 21,000 s was due to the collapsing of all voids in the core and upper-vessel regions as the liquid there subcooled. The collapsing of the voids resulted in a significant hot-leg liquid flow into the reactor vessel. This liquid was vaporized in the core region causing the hot-leg levels to increase once again. This cycle was repeated another time at 22,000 s and thereafter, the hot-leg refilling resumed and was completed at 24,200 s.

The steam-generator characteristics experiment, Test 220402, was used to characterize the effects of the steam-generator-secondary level and level control on post-SBLOCA transients. This test starts from the same initial conditions as used for the nominal case, Test 220100. The basic difference between Tests 220100 and 220402 is the control of the secondary-side steam-generator liquid level. The core power decay, HPI, leak size and location, and steam-generator-secondary pressure control are also the same as those for Test 220100. Upon test initiation, the secondary level is increased from 1.52 m (5 ft) to 3.20 m (10.5 ft) at full AFW capacity. The secondary level is maintained at 3.05 ± 0.115 m (10 ± 0.5 ft) using band control for the

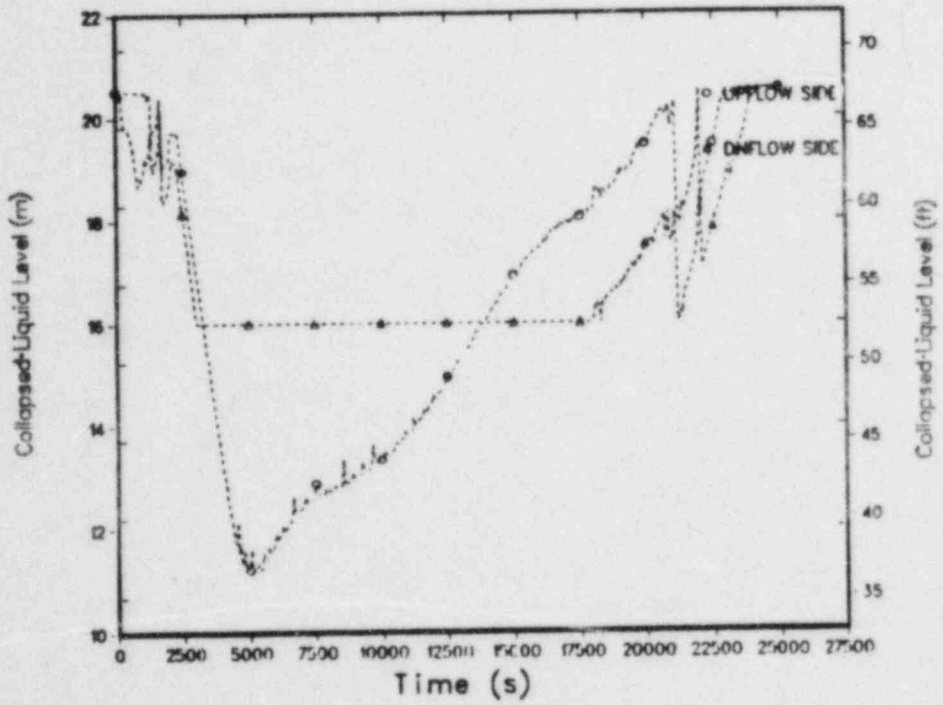


Fig. 4.
Calculated hot-leg collapsed-liquid levels for OTIS Test 220100.

next 15 min. After this 15 min period, a constant level control of 3.05 m (10 ft) is maintained for the duration of the test.

The TRAC calculation for Test 220402 was run for 201 min. This test is expected to require a considerable period of time to fill the primary system completely. Therefore, this prediction was ended after assurance that the hot leg was refilling continuously. The sequence of predicted events for this test is given in Table V.

The maximum secondary level allowed during this test is 3.20 m (10.5 ft) and the minimum primary level predicted was 6.9 m (22.6 ft), see Fig. 5. Consequently, the BCM was not calculated during this transient and the primary and secondary pressures, shown in Fig. 6, never became closer than 1.7 MPa (243 psia). The lack of good primary-to-secondary energy transfer was responsible for delaying certain events relative to those predicted for Test 220100.

The sharp spikes beginning at 5000 s in the steam-generator-primary liquid level (Fig. 5) result from the condensation of steam in the upper-tube region during periods of AFW injection. The primary pressure shown in Fig. 6 also shows the effects of the AFW injection into the upper steam-generator-secondary region. The calculated AFW injection ranged from 7 to 12 s and occurred at intervals of 300 to 500 s. The reduction in primary pressure caused by high AFW injection was significant for this test even without BCM being activated. The steam-generator refilling began at 8900 s and progressed at a rate of

TABLE V

SEQUENCE OF PREDICTED EVENTS FOR OTIS TEST 220402

| Event | Time (min) |
|---|---|
| Cold-leg-suction leak initiated | 0.0 |
| Core-power decay and HPI tripped on (also the steam-generator secondary filled from 1.52 m (5 ft) to 3.20 m (10.5 ft) | 1.9 |
| Pressurizer emptied | 2.4 |
| Steam-generator-secondary level reached 3.05 ± 0.15 m (10.0 ± 0.5 ft) (cooldown of steam-generator-secondary started at 28 K/h (50°F/h) | 5.8 |
| Steam-generator secondary-level band control terminated and constant level control began at 3.05 m (10 ft) | 20.8 |
| Natural-circulation mode terminated | 24.1 |
| Core region saturated | 41.4 |
| Liquid subcooling at cold-leg-suction leak caused by HPI injection increased significantly | 41.7 |
| Downcomer region saturated | 44.2 |
| Refilling of hot leg began | 148.0 |
| Calculation terminated | 201.2 |

0.024 m/min (0.08 ft/min). The upflow- and downflow-side collapsed-liquid levels in the hot leg are shown in Fig. 7. Again, the levels shown at time zero correspond to a liquid full condition. The upflow-side level shows the same characteristics as the steam-generator primary-side level discussed above.

After the completion of the actual tests, it was observed that the depressurization of the primary system differed considerably from the TRAC predictions. The experiment pressures in the primary system depressurized slower than the predicted pressures during the portion of the transient where the AFW was at full flow to fill the steam-generator secondary to the prescribed level. The OTIS steam-generator single-channel model described earlier assumed that the AFW wetted all 19 tubes, whereas in the facility, the AFW injected through a minimum wetting nozzle is assumed to wet only 3 tubes.

Because the MIST facility will use the OTIS steam generator, a new steam-generator model, shown in Fig. 8, with two parallel flow channels was developed to account for the wetted and unwetted tubes. One flow channel represents flow through three tubes and represents the AFW-wetted channel; the

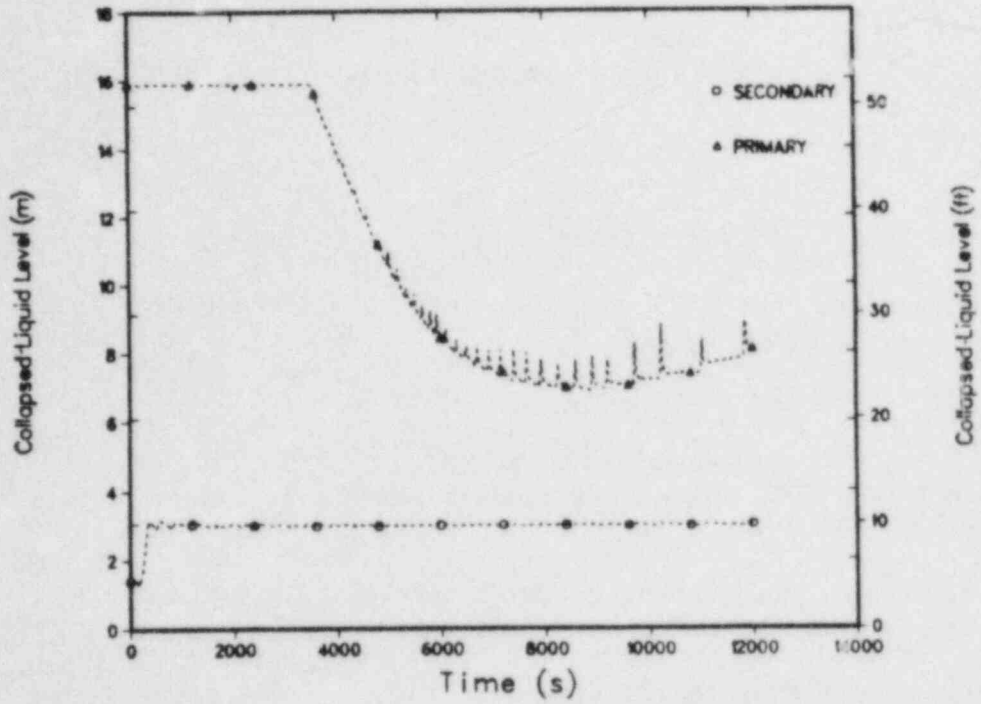


Fig. 5.
Calculated steam-generator collapsed-liquid levels for OTIS Test 220402.

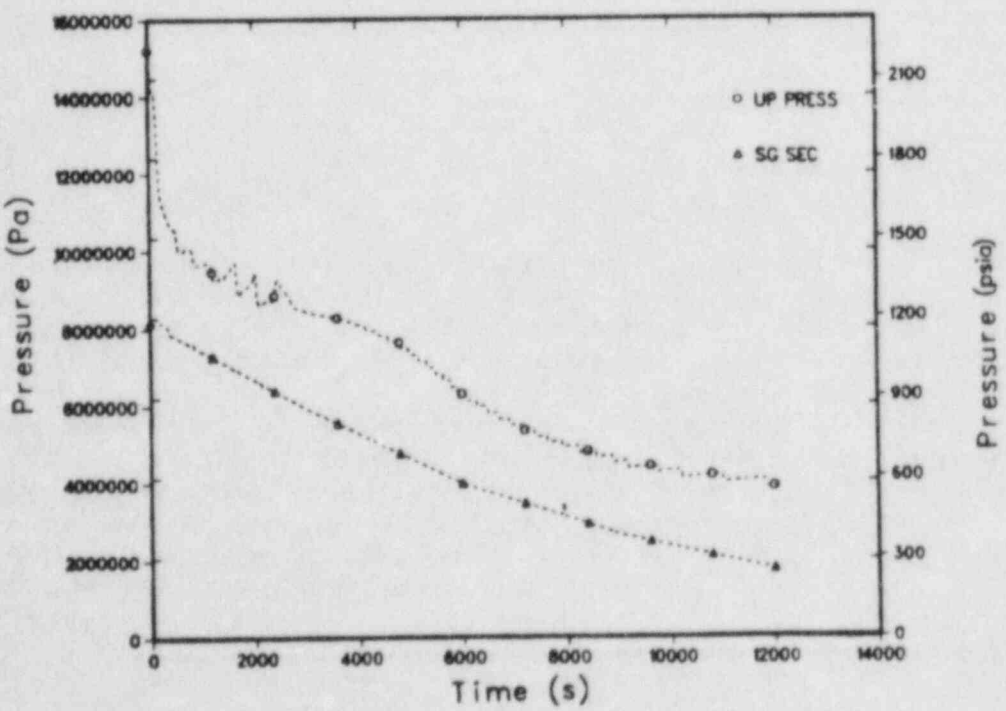


Fig. 6.
Calculated primary and secondary pressures for OTIS Test 220402.

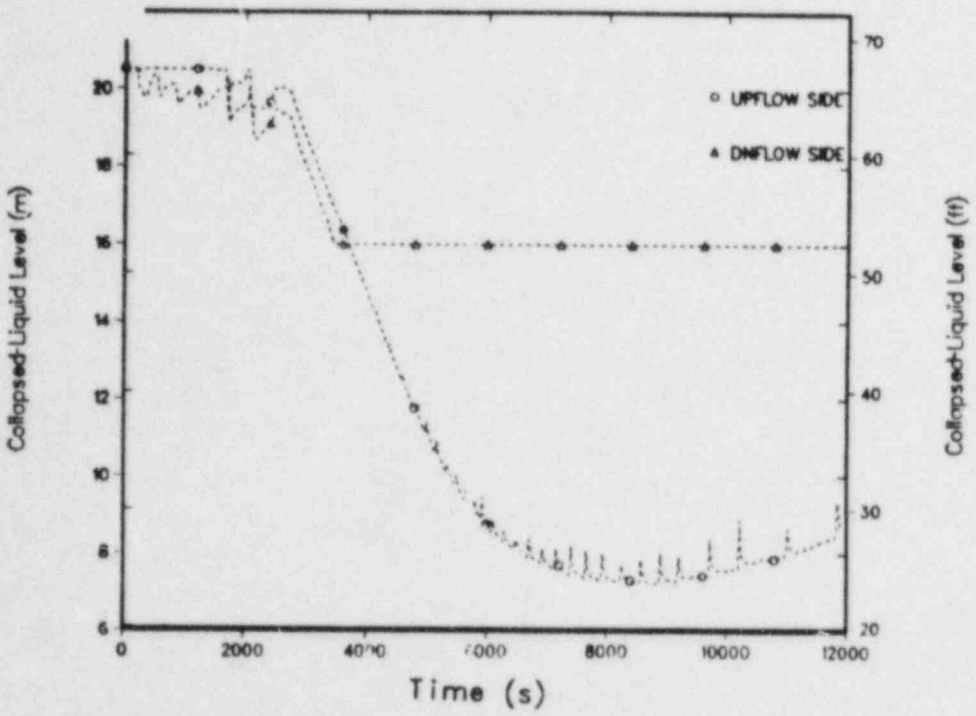


Fig. 7.
Calculated hot-leg collapsed-liquid levels for OTIS Test 220402.

other channel represents the unwetted tube region. The new steam-generator model was benchmarked with experiment data taken from GERDA Test 20245, which was a steady-state experiment that utilized high AFW injected through the minimum wetting nozzle.

A separate-effects calculation involving only the GERDA steam generator was performed to benchmark the new steam-generator model. The initial and boundary conditions for GERDA Test 20245 were held constant during the test. The results of the calculation are shown in Fig. 9. This figure shows the primary-side liquid temperature vs steam-generator-tube elevation for the wetted and unwetted tubes.

The experiment data show a multidimensional effect in that a portion of the AFW flowed across the tube bundle and cooled the primary liquid in the tubes not directly wetted by the AFW. The curves described by "One AFW" represent the predicted temperatures for a calculation where 100% of the AFW was injected into the wetted tube flow channel. Because our steam-generator model does not have any cross-flow junctions (the addition of cross-flow connections did not improve the comparison and slowed the calculation), the cooling of the unwetted region by the AFW was not correctly modeled as the predicted unwetted primary-side liquid temperatures were much higher than the data for most of the tube length. To compensate for the lack of secondary-side AFW cross flow, an additional fill component was utilized to apportion a fraction of AFW into the "unwetted" tube region.

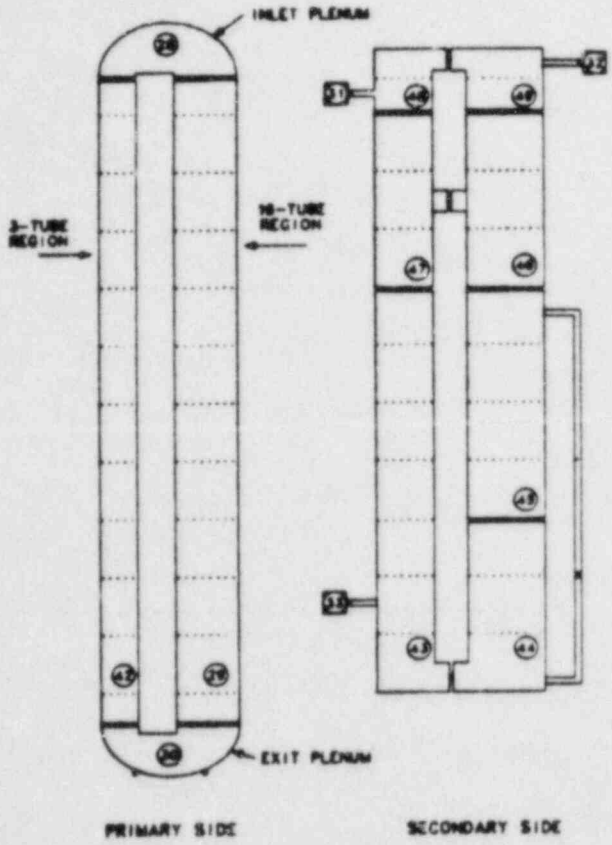


Fig. 8.
MIST intact-loop steam-generator noding.

The curves denoted "Two AFW" in Fig. 9 are the results of a calculation with the AFW flow directed into each region of the secondary. An AFW flow split of 70%/30% with respect to the wetted and unwetted tube region, respectively, gave the best comparison of primary-side liquid temperatures for this particular GERDA test.

The steam-generator model was benchmarked further with posttest calculations of the two OTIS tests that were previously described as our pretest calculations. The steam-generator model benchmarked with the GERDA Test 20245 data was incorporated into the OTIS input model. Initially, using the 70%/30% AFW flow split, the predicted early depressurization of the primary system for Test 220100 was better than the pretest results but still not good enough to make reasonable comparisons with the experiment data. A second calculation was performed with 100% of the AFW injected into the three-tube (wetted) region only. The results of the second posttest calculation for OTIS Test 220100 with the parallel-channel steam-generator model are shown in Figs. 10 and 11 along with the experiment data and pretest predictions. The primary-system pressures (Fig. 10) are now in very good agreement with each other. Similarly, the

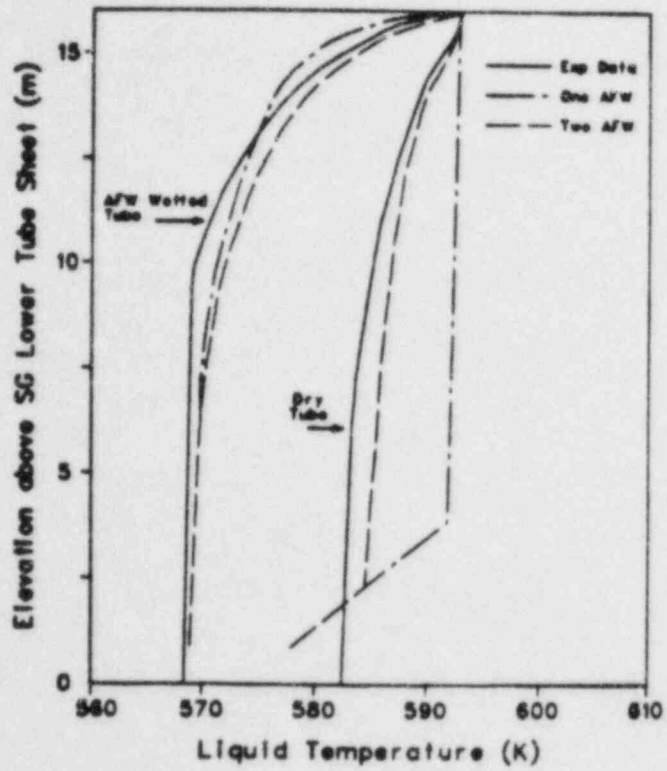


Fig. 9.
Comparison of steam-generator primary-fluid temperatures for GERDA high-AFW Test 20245.

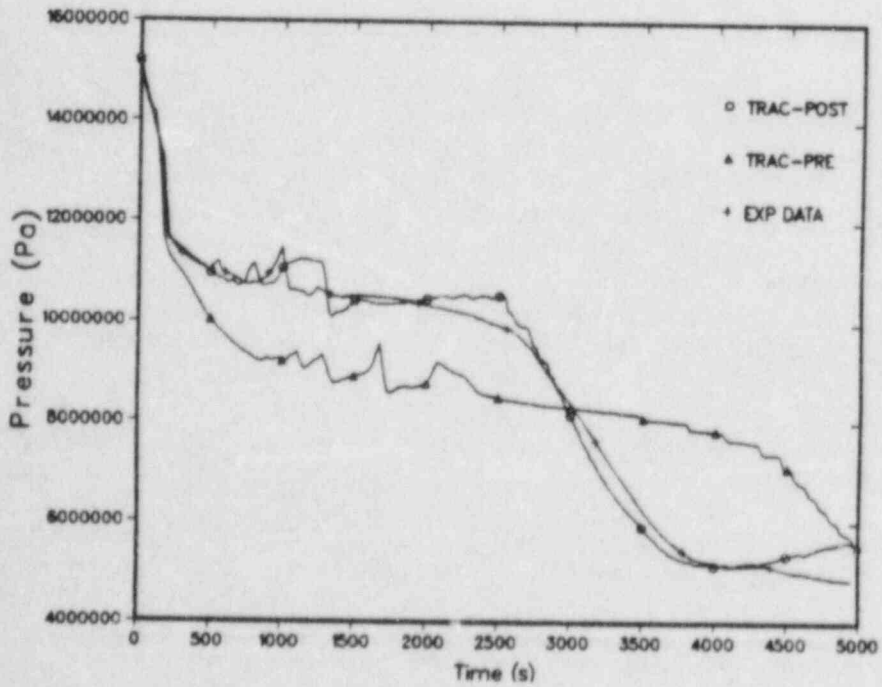


Fig. 10.
Comparison of upper-plenum pressures for OTIS Test 220100.

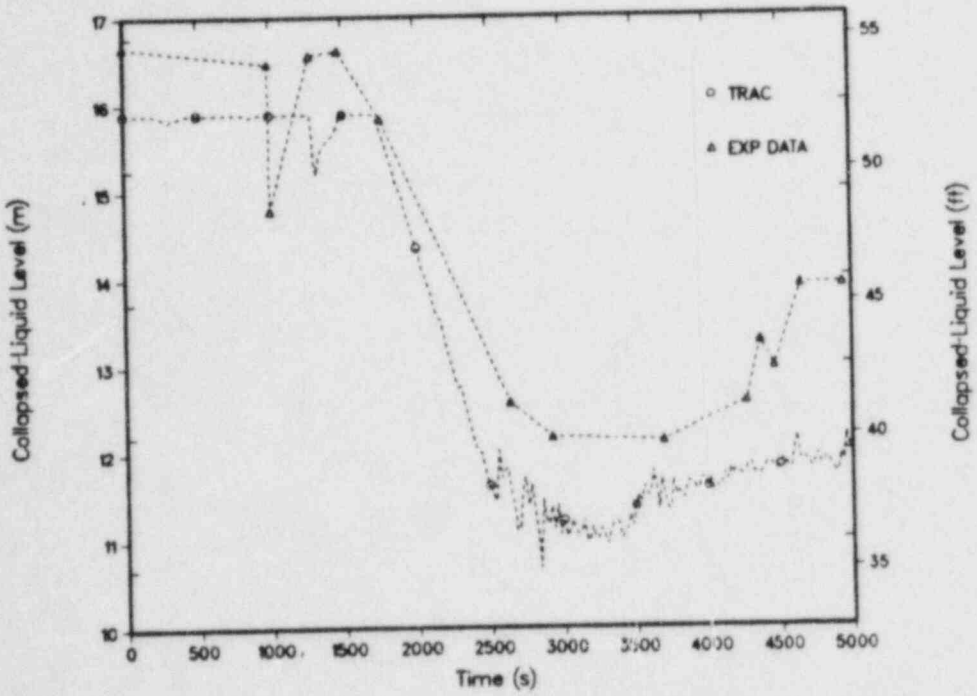


Fig. 11.
Comparison of steam-generator primary-liquid levels for OTIS Test 220100.

comparison is also good for the steam-generator primary-side collapsed-liquid level.

The results of the posttest calculation for OTIS Test 220402 are presented in Figs. 12-14. The BCM heat-transfer phenomena associated with the AFW instead of the secondary liquid pool were predicted correctly by TRAC with the same steam-generator model used for the second posttest calculation of Test 220100. During the actual test, the secondary-side liquid-level controller did not function properly and the secondary level deviated somewhat from the desired level of 3.05 m. The measured liquid level (Fig. 12) was used as a boundary condition for the posttest calculation whereas the AFW flow was allowed to increase or decrease (Fig. 13) to give the correct liquid level. The primary-system pressure comparison in Fig. 14 shows the effect of differences in steam-generator behavior for the two steam-generator models used in the pretest and posttest calculations.

The injection of 100% of the AFW flow into the three-tube region of the parallel-channel steam-generator model gave the best results with respect to the OTIS posttest predictions of Tests 220100 and 220402. We decided to use the same modeling of the steam generators for the MIST facility analyses because MIST will use the OTIS steam generator and another steam generator constructed with the same design criteria. Also, the MIST tests are expected to show behavior similar to that observed in the OTIS tests.

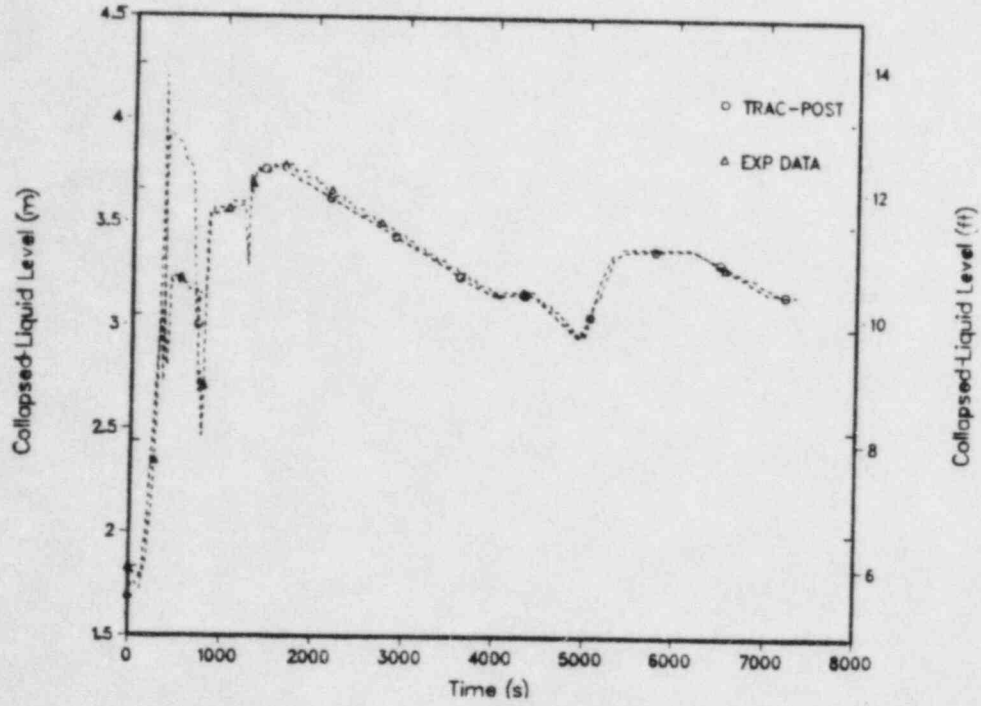


Fig. 12.
Comparison of steam-generator secondary-liquid levels for OTIS Test 220402.

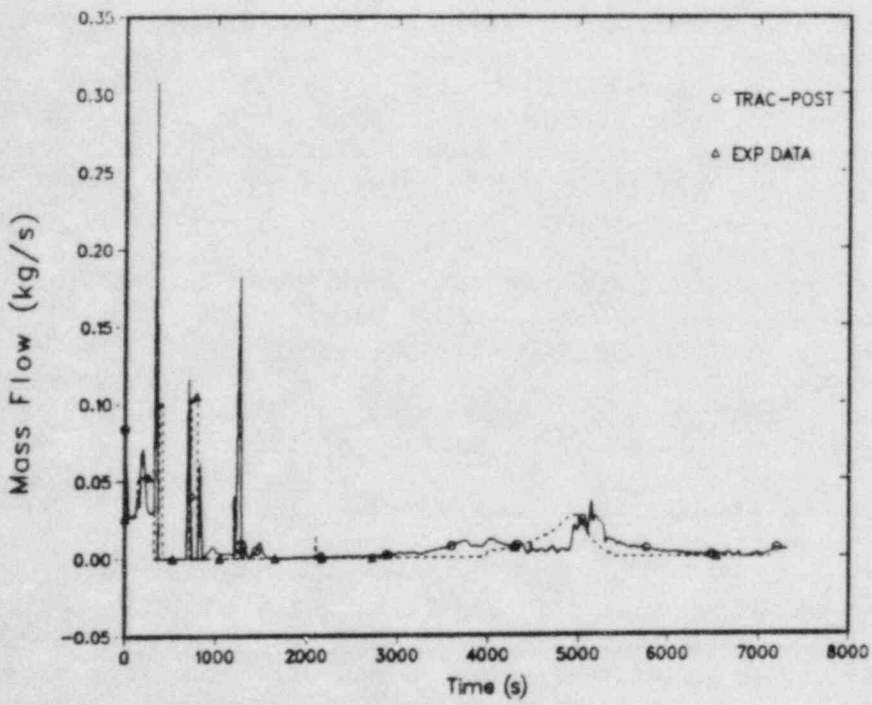


Fig. 13.
Comparison of steam-generator AFW flows for OTIS Test 220402.

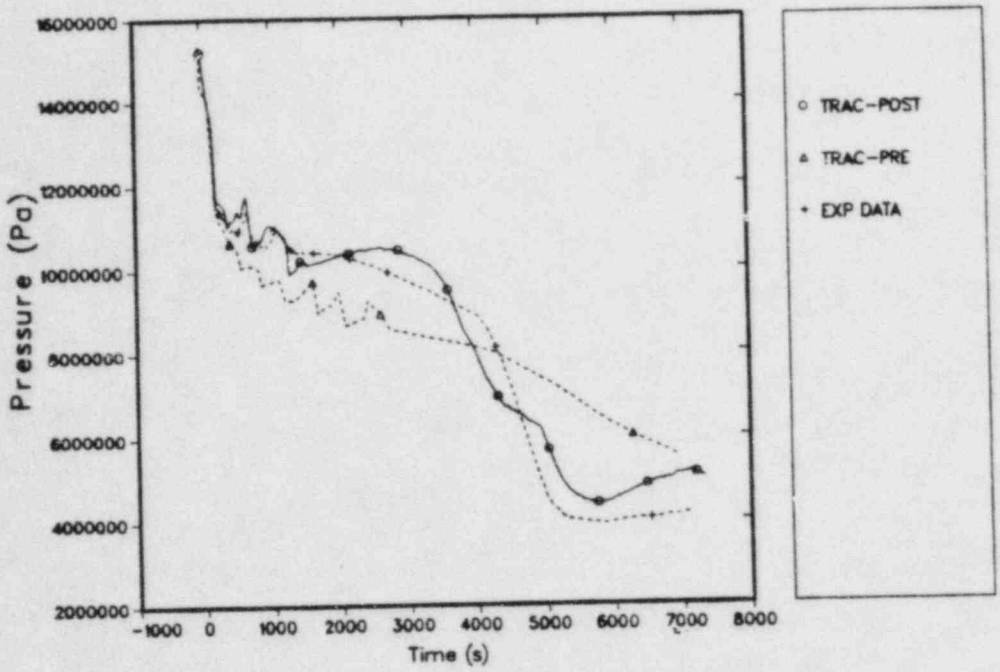


Fig. 14.
Comparison of upper-plenum pressures for OTIS Test 220402.

We performed a pretest prediction of the MIST nominal experiment that simulates a lowered-loop B&W plant design. The MIST facility was modeled with 51 TRAC one-dimensional components divided into 257 hydrodynamic cells. A component schematic of the facility model is shown in Fig. 15. The MIST nominal experiment, designated Test 300000, will simulate a scaled 10-cm$^2$ pump-discharge-break transient. The initial conditions for this test are given in Table VI.

The steady-state and transient calculational procedures are very similar to the OTIS calculations with the exception of boundary-condition variations. The steady-state was run for 1000 s and the transient for 3800 s. A sequence of predicted events for the transient calculation are listed in Table VII. All of the phenomena observed in the OTIS test, such as single- and two-phase natural circulation, flow interruption, BCM heat transfer, and primary-system refill, also were predicted to occur in the MIST nominal experiment. This calculation also predicted loop asymmetries that obviously could not be detected in the single-loop OTIS test facility.

The upper-plenum pressure history is shown in Fig. 16. Most of the predicted events for this test, listed in Table VII, correspond to changes in the primary pressure. The upper regions of the primary system became saturated at 50 s, and by 200 s, the flow in Loop A was interrupted. Loop B flow was interrupted by 267 s, and the initial emptying of the pressurizer followed thereafter. Interruption of primary-loop flow resulted in the repressurization

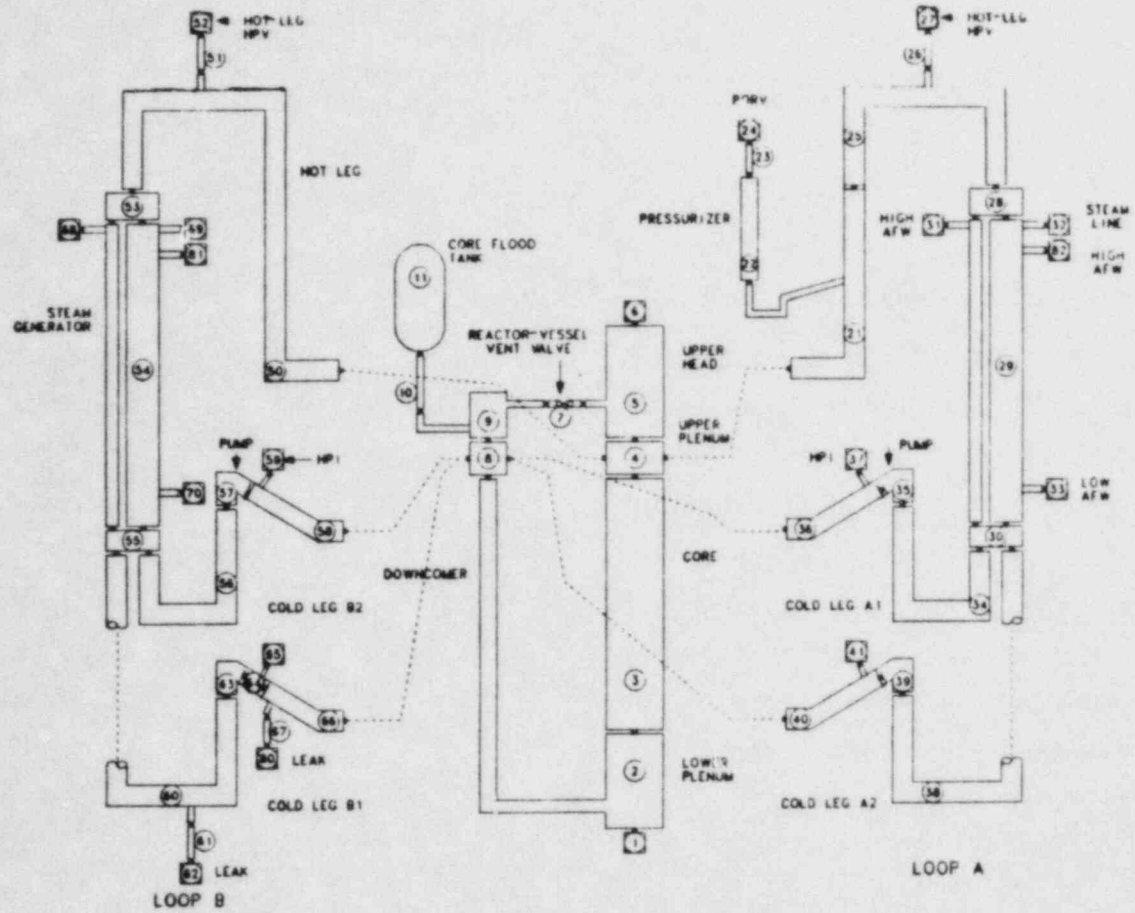


Fig. 15.
Component schematic for MIST facility.

TABLE VI

STEADY-STATE TEST CONDITIONS FOR MIST TEST 300000

| Parameter | Calculated Results | |
|---|---|---|
| System pressure | 11.72 MPa | (1700 psia) |
| Steam-generator-secondary pressure | 6.96 MPa | (1010 psia) |
| Hot-leg fluid temperature | 590.2 K | (602.7°F) |
| Cold-leg fluid temperature | 560.9 K | (550.°F) |
| AFW temperature | 310.9 K | (100.0°F) |
| HPI fluid temperature | 294.2 K | (70.0°F) |
| Loop mass flow | 0.34 kg/s | (0.75 lbm/s) |
| Core power | 115.7 kW | |
| Steam-generator-secondary liquid level | 1.5 m | (5.05 ft) |
| Pressurizer liquid level | 0.77 m | (2.53 ft) |

TABLE VII

SEQUENCE OF PREDICTED EVENTS FOR MIST TEST 300000

| Event | Time (s) |
|---|---|
| Cold-leg leak initiated | 0.0 |
| Pressurizer level decreased to 0.305 m (core power decay, HPI, and refilling of steam-generator secondary initiated) | 78.4 |
| Natural circulation in Loop A interrupted | 200.0 |
| Natural circulation in Loop B interrupted | 267.0 |
| Pressurizer emptied (first time) | 280.0 |
| Steam-generator secondary filled to 9.63 m | 437.7 |
| BCM commenced in intact-loop steam generator | 2000.0 |
| BCM commenced in broken-loop steam generator | 2073.0 |
| Pressurizer emptied (second time) | 2167.0 |
| Primary-system refill began | 3800.0 |
| Calculation terminated | 3830.0 |

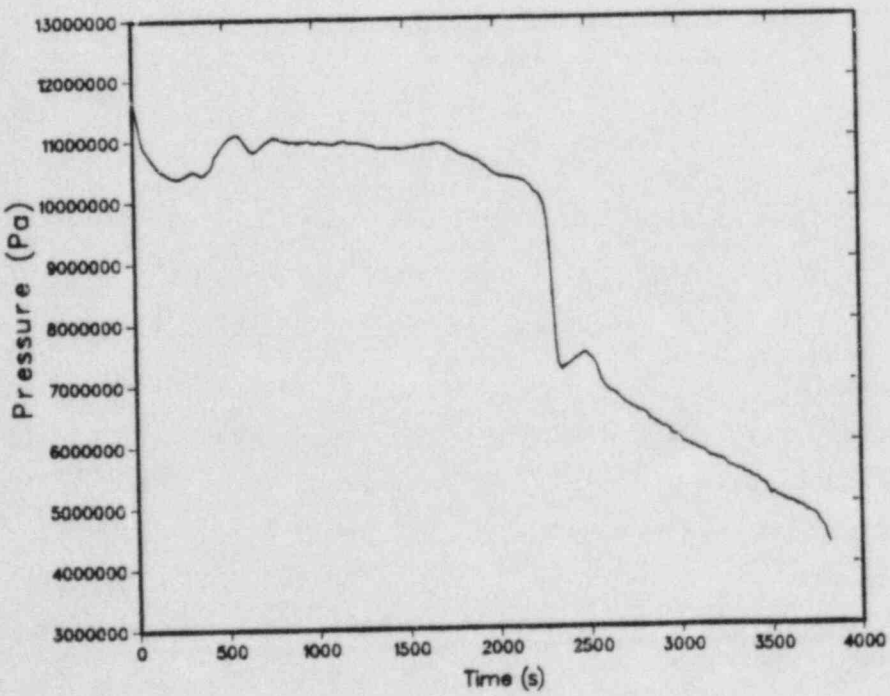


Fig. 16.
Calculated upper-plenum pressure for MIST 300000.

of the system. The primary pressure remained fairly constant from 400 s to 1700 s.

The leak flow increased substantially at 1700 s because the highly subcooled liquid from the HPI reached the leak location. This increased leak flow resulted in a decreased primary pressure and the redraining of the pressurizer. The BCM was begun by 2073 s in both steam generators and, when the pressurizer finally drained completely, the primary pressure decreased very rapidly and then abruptly increased at 2360 s. This abrupt change in pressure behavior was due to the leak fluid becoming saturated and, thus, less energy was being removed from the primary system. Also, the lower primary pressure caused an increase in the HPI flow. Hence, the lower leak flow and higher HPI flow caused the primary pressure to rise slightly.

Increased voiding of the core region also occurred after 2360 s and resulted in level increases in the hot legs and steam generators (Figs. 17-19). The primary-side collapsed-liquid levels in both steam generators tended to level out slightly above the secondary-side levels. The oscillations in the primary levels (Figs. 18 and 19) are due to the cycling of the AFW that is being used to maintain a constant level on the secondary side. The cycling of the AFW also is responsible for the continued decrease in primary pressure at a rate greater than that before the pool BCM period at 2250 s. This AFW BCM heat transfer continued until 3800 s at which time the HPI flow became greater than the leak flow and caused the primary system to begin refilling.

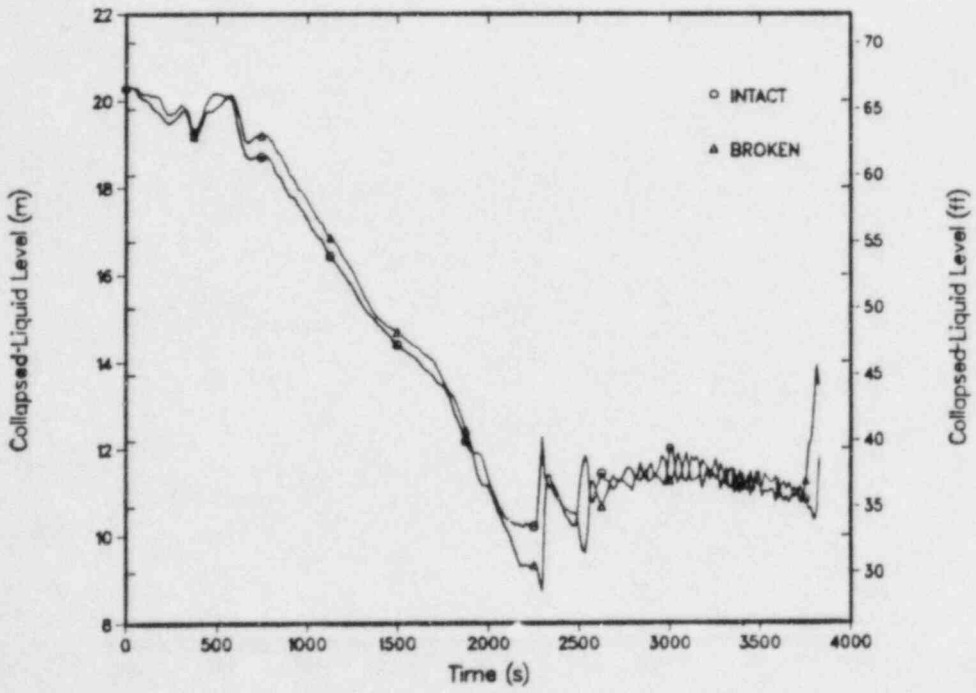


Fig. 17.
Calculated hot-leg collapsed-liquid levels for MIST 300000.

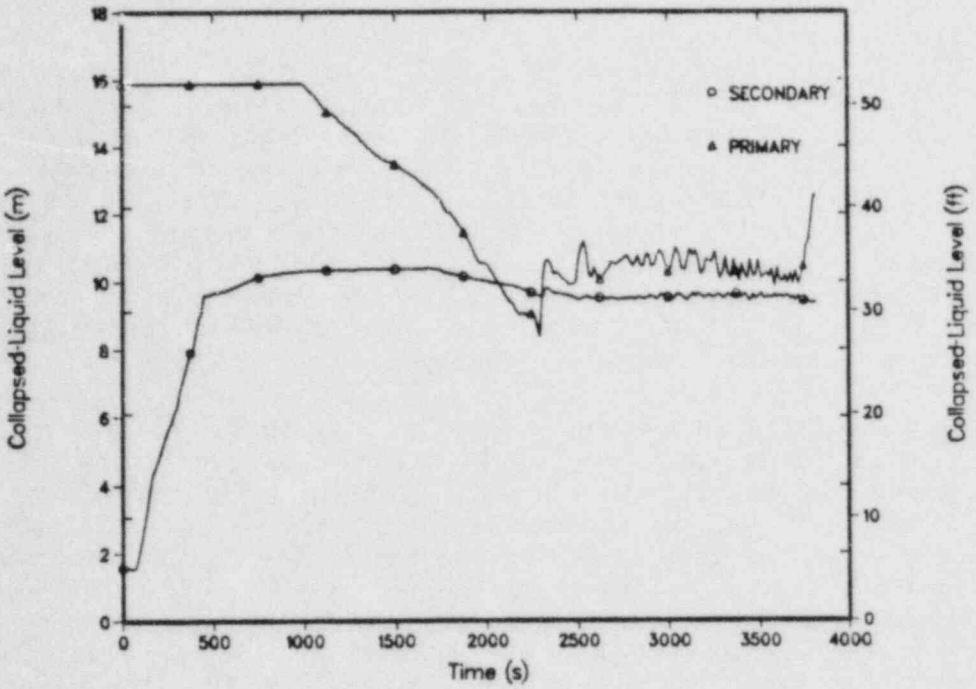


Fig. 18.
Calculated intact-loop steam-generator liquid levels for MIST 300000.

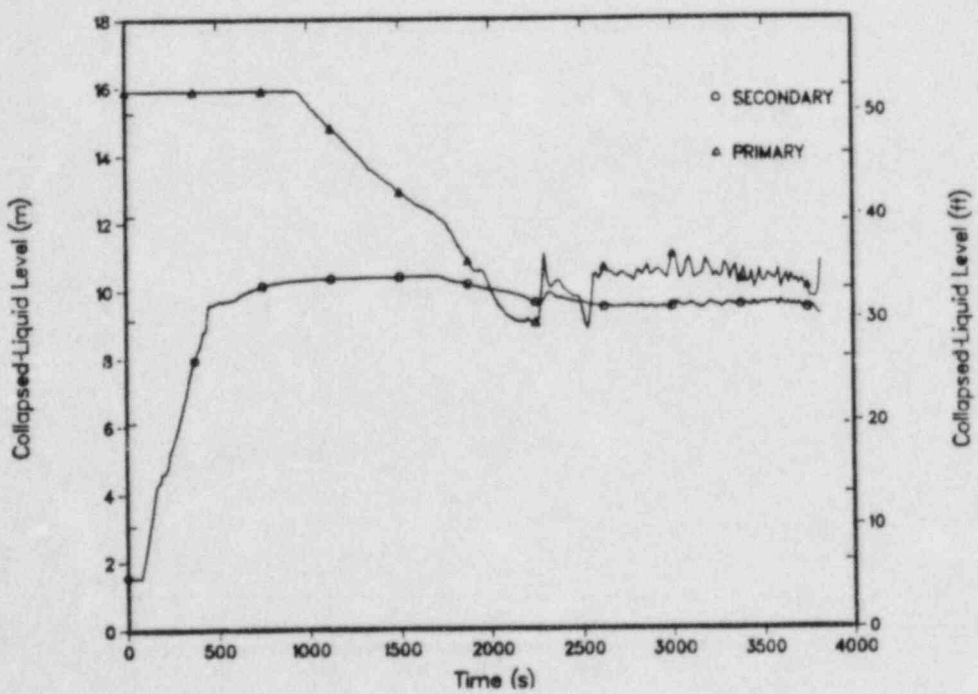


Fig. 19.
Calculated broken-loop steam-generator liquid levels for MIST 300000.

All of the GERDA and OTIS calculations performed for the support of the MIST/OTIS experiment program have shown that TRAC can predict with reasonable accuracy the actual phenomena observed in the GERDA/OTIS tests and that are expected to occur in the MIST tests. The results of the analysis to date have supported the validity of the facility design within the one-dimensional modeling assumption. We have used the analysis results to support the addition of densitometers in the hot and cold legs and to confirm the need for most of the other instrumentation.

# THE UNIVERSITY OF MARYLAND 2X4 B&W SIMULATION LOOP

by

F. J. Munno, Y.Y. Hsu, M. DiMarzo, G. A. Pertmer

D. W. Sallet, M. Popp, M. Massoud, W. Lin

The University of Maryland
College Park, Md. 20742

## INTRODUCTION

The UMCP 2X4 B&W Simulation Loop is a scaled model of the B&W lowered loop reactor system. The Loop, built of stainless steel, operates at 300 psia. The purpose of the Loop is to investigate natural circulation and small break LOCA phenomena in the system. The analyses of results from the experimental program will provide information to the overall IST program. Additionally, the data will complement the code assessment data base on the B&W systems.

This paper presents an overview of the UMCP Loop project. Scaling and design of the facility is discussed and the final design of the system is described. The facility contains a significant amount of instrumentation, and the instrumentation systems are outlined. Finally, the planned test matrix for both the natural circulation and the small break LOCA experiments is presented.

## LOOP SCALING AND DESIGN

This section presents an overview of the scaling and design of the UMCP 2X4 Loop. A full detailed report of the steady state and transient scaling, as well as the single phase and two phase criteria used, will be presented in a future paper.

When developing the rationale used in the scaling of the system, it was recognized that it is not possible to two phase scale all parameters and components for all experimental tests planned. Therefore, the approach was to perform a single phase scaling, along with a parallel effort investigating two phase parameters. In this way, the final loop scaled design brackets all important two phase scaling parameters for the anticipated test matrix.

The UMCP 2X4 Loop scaling is derived from first principles for both the steady state and transient cases. This section provides a brief overview of the scaling methodology and presents the final scaling parameters.

For a simplified loop (Figure 1), the energy equation written between a and b is written as:

$$\frac{P_a}{\gamma_a} + \frac{V_a^2}{2g} + z_a = \frac{P_b}{\gamma_b} + \frac{V_b^2}{2g} + z_b + h_{losses} \qquad (1)$$

where $h_{losses}$ are the total losses due to friction (wall friction, bends, entrance and exit, etc.)

$$h_{losses} = f\frac{L}{D}\frac{V^2}{2g} + k\frac{V^2}{2g} \qquad (2)$$

The continuity equation:

$$\rho_a V_a A_a = \rho_b V_b A_b = \rho VA = \rho Q \qquad (3)$$

allows Equation 1 to be written

$$\frac{P_a}{\gamma_a} - \frac{P_b}{\gamma_b} = (z_b - z_a) + h_{losses} \qquad (4)$$

Similar equations can be written between b and c and c and a, completing the loop.

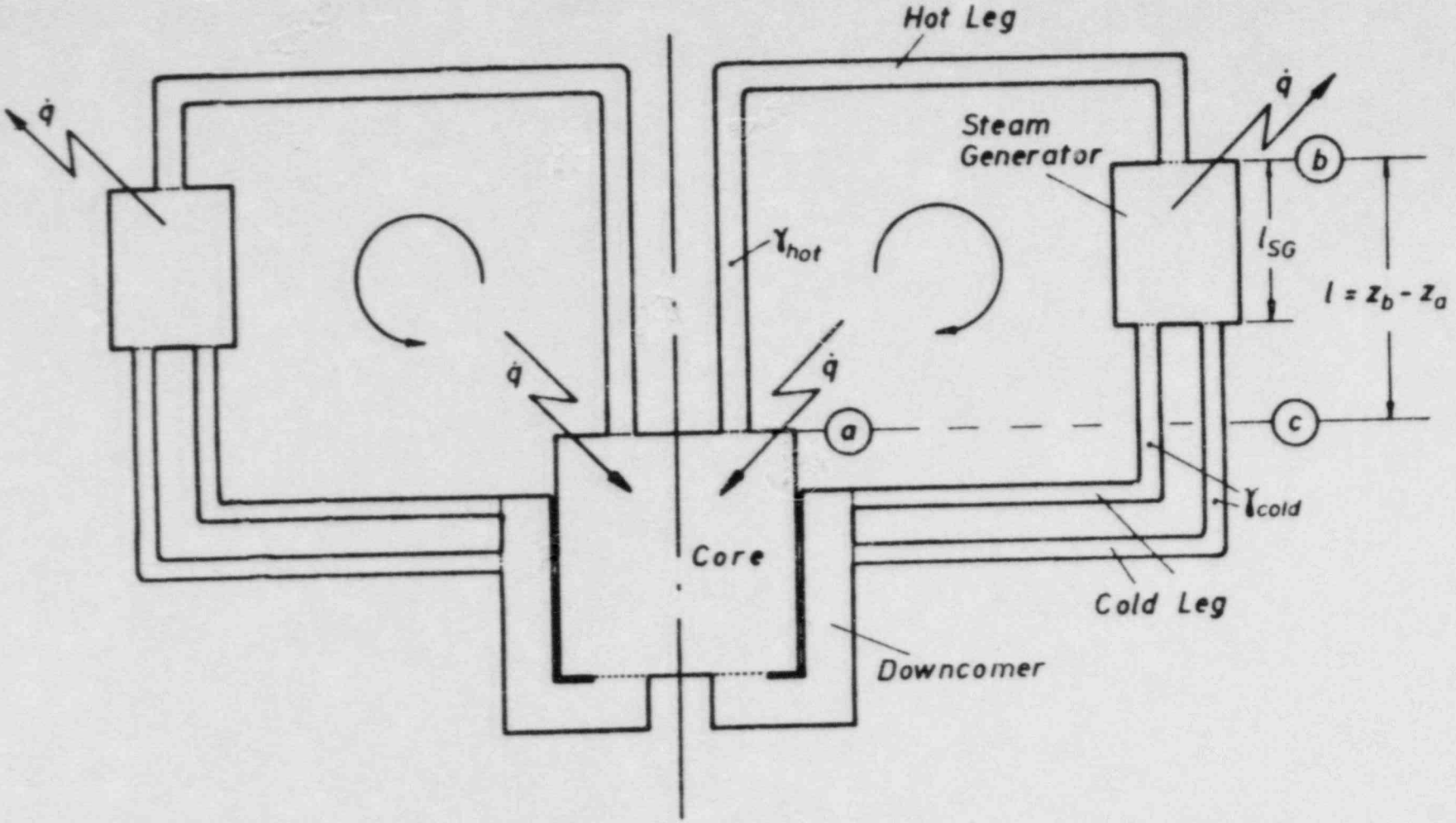


Figure 1 : Simplified Schematic of Model Loop

Assuming that heat is added at a and removed at b, then the energy equations around the loop can be summed:

$$(z_b - z_a)\ (\gamma_{cold} - \gamma_{hot}) = \gamma_{hot} h_{Lab} + \gamma_{cold}(h_{Lbc} + h_{Lca}) \quad (5)$$

Defining:

$$\ell = z_b - z_a \quad (6)$$

and an average $\gamma$ :

$$\gamma_{hot} h_{Lab} + \gamma_{cold}(h_{Lbc} + h_{Lca}) = \gamma h_L \quad (7)$$

then:

$$\left( \frac{\gamma_{cold} - \gamma_{hot}}{\gamma} \right) \ell = f \frac{L}{D} \frac{V^2}{2g} + k \frac{V^2}{2g} \quad (8)$$

The left hand side of this equation represents the driving force, and the right hand side represents the loss terms.

This equation is the key equation for steady state loop behavior. There are two important points that should be emphasized. First, the equation is derived from conservation of mass and energy. Second, the parameter "$\ell$" is the vertical distance between effective heat addition and removal locations and should not be confused with the flow path length.

Using the volumetric expansion coefficient $\beta$:

$$\beta = \frac{1}{v} \left( \frac{\partial v}{\partial T} \right)_p \quad (9)$$

defining a loss flux term K* in terms of the flow losses in each component, and using the steady flow energy equation:

$$q = \rho Q c \Delta T \quad (10)$$

results in the final form of Equation 1:

$$Q = \left( \frac{2g\beta\ell q}{\rho\, cK^*} \right)^{1/3} \quad (11)$$

The quantities in this equation are:

$Q \equiv$ volume flow rate through one loop. One loop includes one Hot Leg and two Cold Legs. The total volume flow through the entire vessel or the entire Downcomer is 2 Q

$g \equiv$ gravitational acceleration

$\beta \equiv$ volumetric expansion coefficient

$\ell \equiv$ loop-characteristic length (effective thermal height)

$q \equiv$ one-half of the total heat is input rate to the fluid at the core; q is the heat subtracted by one steam generator.

$\rho \equiv$ density of fluid

$c \equiv$ specific heat

$K^* \equiv$ loss flux term

The transient loop response analysis is somewhat more complex and will be presented in detail in a future paper. With suitable simplifications, analytical solutions to the transient problem can be found. The value of this analysis lies not in its use to accurately predict transient loop response, but rather in its use to understand the importance of various physical phenomena and parameters and its use in scaling.

In summary, the transient problem analyzes two different physical phenomena. These are the time-dependent heat transfer into and out of the water in the loop, and the fluid flow transient in the loop when a slug of hot water starts to rise in the Hot Leg and has to overcome the inertia of the water in the loop and the increasing flow losses.

Equation 11 is used to determine the sizes of the various components in the loop. It is desireable to make $\ell$ as large as possible, since flow losses can always be introduced, by adding orifice plates, for example. The basic rationale behind size choice was that the loop components should be large enough to enable meaningful thermal hydraulic investigations of two phase flow in the hot legs and through the vent valves.

The hot leg diameter is 3.5", with a length of 15 feet. The water volume ($\approx 1\ ft^3$) compares to a volume of 489.5 $ft^3$ in the prototype. The volume scaling of the hot leg is, therefore, 1/489.5, or, rounding, 1/500.

The derivation of the loop steady state and transient responses showed the importance of the individual components in the loop. The volume scale of each component and, therefore, the overall volume scale, is 1/500.

Once the volume is scaled, the power is scaled by solving for q in Equation 11. For similarity,

$$\frac{\dot{q}_{prototype}}{\dot{q}_{model}} = \left( \frac{Q_p}{Q_m} \right)^3 \frac{\left( \frac{\rho c}{2g\beta} \right)_p}{\left( \frac{\rho c}{2g\beta} \right)_m} \left( \frac{K_p^*}{K_m^*} \right) \frac{\ell_m}{\ell_p} \qquad (12)$$

The second term in brackets on the right hand side depends on system pressure and temperature. For model conditions at 300 psi, and the prototype at 600 psi:

$$\frac{\dot{q}_p}{\dot{q}_m} = 3455 \qquad (13)$$

At a prototype pressure of 2100 psi, the ratio is 1209.

This ratio determines the Full Power Scaling. For a prototype power of 2800 MWt and loop power 200 kW

$$FPS = \left( \frac{200(10^3)}{2800(10^6)} \right) \frac{\dot{q}_p}{\dot{q}_m} \qquad (14)$$

$$= 24.7\% \quad (600 \text{ psi})$$
$$= 8.6\% \quad (2100 \text{ psi})$$

Using the ANS decay curve, the FPS values fall within approximately 1-5 seconds after prototype shutdown

What these values show is that the loop power is sufficient to begin simulation relatively soon after shutdown. The strong time dependency of the decay heat during the first few minutes after shutdown indicates that natural circulation phenomena during this time are highly non-steady. Also, the inertial effects of the pumps as they coast down will be significant, and are likely to dominate the behavior of the fluid in the prototype during this initial phase of the natural circulation.

## LOOP FINAL DESIGN

This section describes the final design of the loop structural components. Additionally, the loop instrumentation is discussed. Figure 2 shows elevation and plan views of the overall loop assembly, and is drawn to scale.

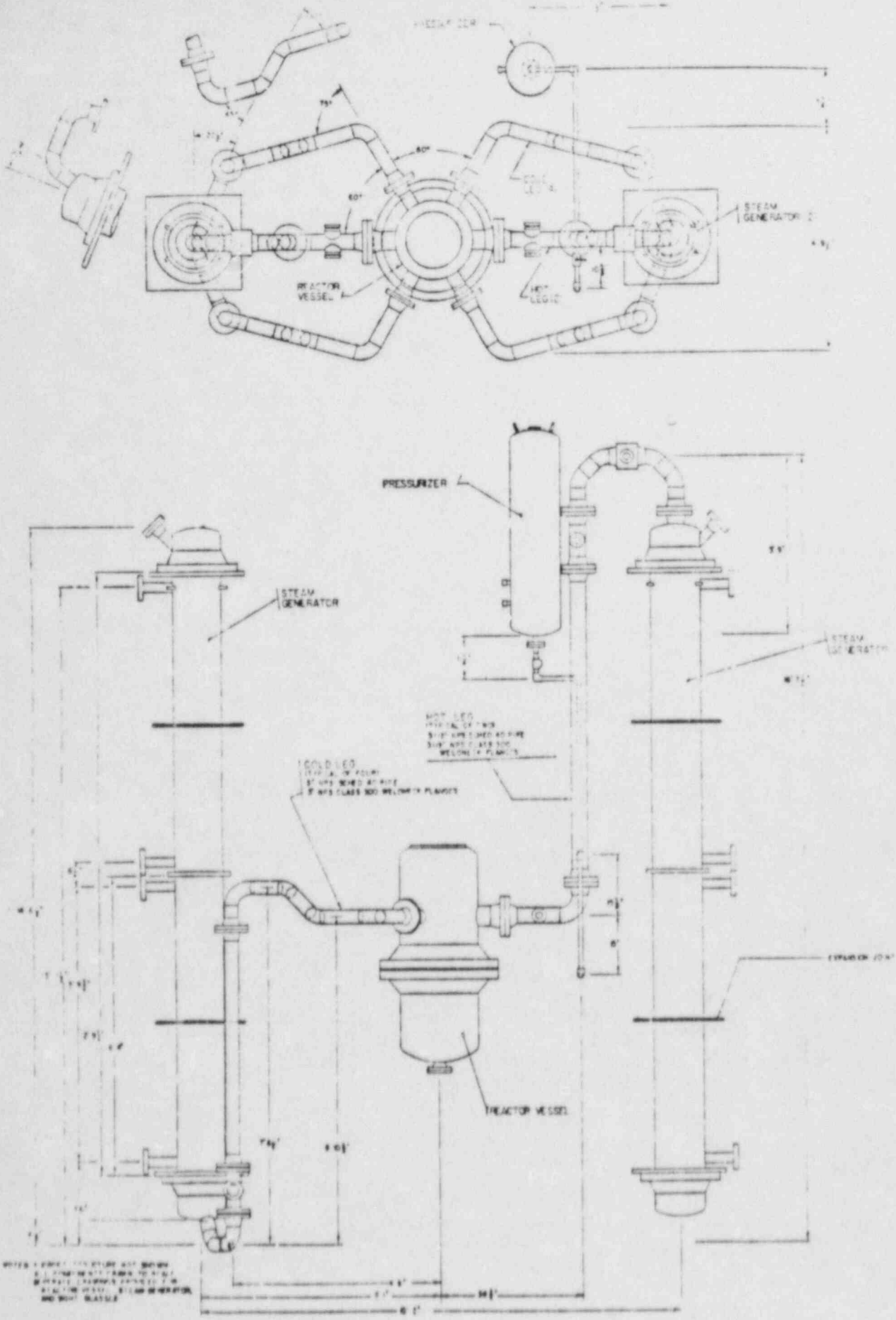


Figure 2 : Overall Loop Assembly

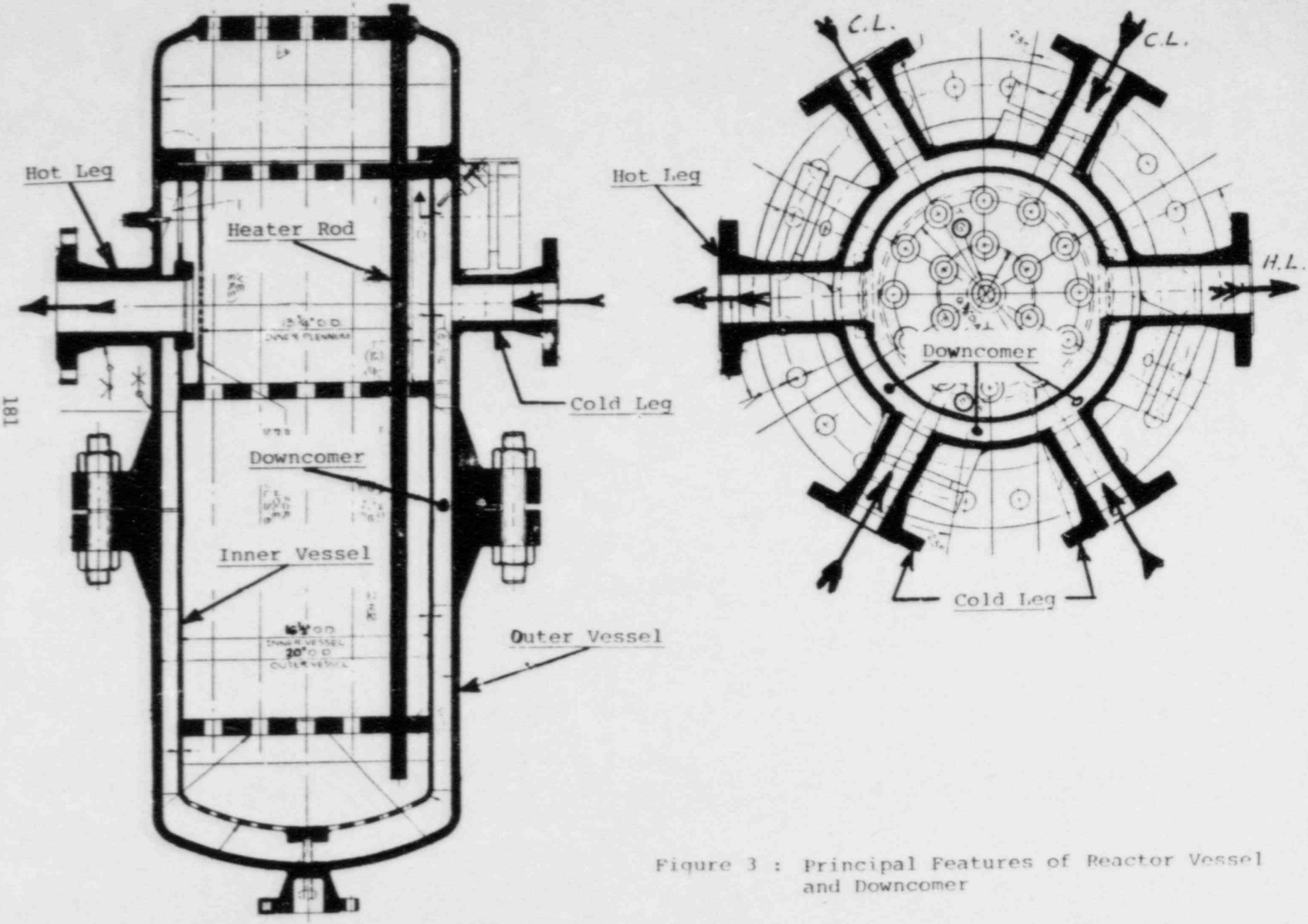


Figure 3 : Principal Features of Reactor Vessel and Downcomer

Loop Components

The reactor vessel is shown in Figure 3. The vessel is 20 inches in diameter and 50.25 inches in height. The annular downcomer, between the inner core barrel and the outer vessel, is 1.25 inches. The core barrel can be skirted to decrease downcomer size; an increase in size requires replacement of the core barrel. The vessel has 19 top head penetrations for heater rods and instrumentation, and four view ports which allow visual observation of the vent valves.

The core barrel has eight vent (flapper) valves. Penetrations are provided through the vessel which allow selected valves to be held at any open position or fully closed, if desired, by set screws. The valves open due to a differential pressure, and the onset of the opening and the dynamic characteristics of vent valve action can be altered using machined weights on the flapper.

Sixteen heater rods extend through the top head (one is a spare). The heated length is the bottom 24 inches of each rod. The total maximum heat input is 202.5 kW. Five banks of three heaters each can be controlled by the loop DAS, either individually or jointly.

The hot legs are 3.5" (ID) stainless steel piping and weld neck flanges. Each hot leg contains three view ports: one in the horizontal section near the vessel outlet, one in the vertical section, and one in the "candy-cane" U-bend. The view ports are designed to minimize any dead water region or flow disturbance.

The cold legs are 3.0" (ID) stainless steel piping and weld neck flanges. Each cold leg contains a view port in the vertical section. Penetrations are provided for HPI injection and connection to the water treatment system.

Flow losses in the loop can be increased by inserting screens or orifice plates at selected locations. Recesses are machined into one flange at each flange location to allow insertion of the flow loss device.

The two steam generators each contain 28 stainless steel tubes, 12.8' in length, 1.18" ID, 1.25" OD. The outer shell is 12" (OD) stainless steel. The middle tube sheet divides the secondary side into two sections. This feature permits a great deal of flexibility in the positioning of the thermal center. The shell side also has four nozzles near the top for auxiliary feedwater spray.

The stainless steel pressurizer is 52" long and 12" in diameter. Connection to the hot leg uses a 3/4" stainless steel pipe. Two electric heaters (2.5 kW each) are inserted near the bottom, and spray and relief valve penetrations are at the top.

## Loop Instrumentation

The basic instrumentation guideline is to provide a large number of penetrations in the system. This allows the insertion of pressure and temperature measuring instruments at many locations around the loop.

The main data acquisition system is a Hewlett-Packard 3054A Automatic DAS. The 3054A is a computer based system which measures and analyzes data from the loop instruments and also provides control signals to the loop components as required.

A second DAS utilizes an Apple IIe computer interfaced to an Analogic ANDS 4400. At present, plans are to use this DAS for any specialized applications required.

Local temperature measurements are made using sheathed thermocouple assemblies. In addition, four element thermocouple rakes are used to measure temperature profiles along the centerline diameter of the pipe at selected locations. The steam generator (primary) has, at present, one five element rake, extending from the top, in one tube. Plans are to add more instrumentation, vertical and/or horizontal thermocouple rakes, in more tubes.

Pressure measurements are made around the entire loop using electronic dp cells. Also, four cells will be positioned radially around the vessel and will monitor downcomer pressure. These dp's are used to measure circumferential fluctuations as a result of asymmetric vent valve opening.

The technique to perform flow measurement is still being investigated. An LDA system will be used, making use of the view ports for laser beam access to the flow. Additional consideration is being given to hot wire/hot film, tracer techniques, and so forth.

Table 1 shows location of the temperature and pressure measurement points on the loop.

## TEST MATRIX

The planned test matrix consists of both natural circulation and small break LOCA experiments. The entire test matrix is designed to span a wide range of conditions in the system.

The natural circulation tests include the following:

Single phase circulation - the objectives are determination of flow conditions as a function of primary system power and pressure and secondary side cooling rate

Two-phase circulation - the objectives are similar to the single phase tests, but an additional variable is the primary side void fraction

Table 1

# INSTRUMENTATION LOCATION

## THERMOCOUPLES

| | |
|---|---|
| COLD LEG (EACH) | 9 - SG OUTLET TO VESSEL INLET |
| HOT LEG (EACH) | 4 - VESSEL OUTLET TO SG INLET |
| VESSEL | 3 THROUGH TOP HEAD TO INSIDE OF CORE BARREL |
| | 4 RADIALLY AT TWO ELEVATIONS |
| RAKES | 4 ELEMENT AT EACH U-BEND |
| | 4 ELEMENT IN TWO COLD LEGS |

STEAM GENERATOR PRIMARY (EACH)

5 ELEMENT RAKE (6' LONG, FROM TOP) IN ONE TUBE

PLANNED: 5-10 ELEMENT RAKE, EXTENDING ENTIRE LENGTH

ADDITIONAL RAKES (HORIZONTAL AND/OR VERTICAL)

STEAM GENERATOR SECONDARY (EACH)

INLETS AND OUTLETS

## DIFFERENTIAL PRESSURE CELLS

CAPABLE OF MEASURING PRESSURE AT EACH T/C LOCATION

PRESENT: $\Delta P$ AROUND ENTIRE LOOP

| | |
|---|---|
| HOT LEG (EACH) | 4 BETWEEN VESSEL OUTLET AND SG INLET |
| SG (EACH) | 1 BETWEEN INLET AND OUTLET |
| COLD LEG (1 OF 4) | 2 BETWEEN SG OUTLET AND VESSEL INLET |
| VESSEL | 1 BETWEEN VESSEL INLET AND OUTLET |
| | 4 RADIAL FOR RVVV OPENING |

Flow blockage/resumption - these tests will determine system conditions necessary to stop flow and methods of restarting

Upper head bubble - these tests will investigate mechanisms to remove a bubble from the vessel upper head

Asymmetric flow between loops - the mechanisms that cause asymmetric flow will be studied, due to void distribution, secondary side cooling, vent valve effects, and so forth

The small break LOCA tests include the following:

Effect of break size and location - these tests will study the effects on coolant inventory distribution, ECC response, and so forth. Break flow will be collected and measured. Each instrument penetration is a possible break location

Steam generator tube rupture - breaks into both the liquid and vapor region in the steam generator will be studied

Vent valve opening - these tests will investigate conditions that lead to valve opening, due to such events as flow stoppage, break size/location, and ECC. Consequences include simultaneous vs. sequential opening, multi-loop circulation imbalance, and so forth

ECC system - the effect of ECC injection on loop response will be studied

Pressurizer draining - these tests will investigate the effects of pressurizer draining on the coolant inventory in the hot leg

It should be noted that this is the planned test matrix at present. Should, in the future, additional tests be required or planned tests be changed, the test matrix can be appropriately adjusted.

## CONCLUSIONS

The UMCP 2X4 B&W Simulation Loop is designed to be a flexible system that allows for many different investigations into the overall thermal hydraulic behavior of the B&W system. Configurations, such as view port location and instrumentation placement, can be changed, if desired, to support an experimental series.

The test matrix will be initiated in late 1984. The results from the planned experiments will provide a better understanding of a number of phenomena that occur in the B&W 2X4 system.

# Two-Phase Flow Behavior Observed in a Transparent Inverted U-Bend Pipe

W.K. Lin & Y.Y. Hsu

Department of Chemical & Nuclear Engineering

University of Maryland, College Park, MD 20742

## A. Introduction:

One special feature of the B&W power plant is the "Candy-Cane" shaped hot leg. Since there is an inverted U-bend at the top, it is easy for the accumulation of vapor/gas in the high point to form a void. The void could be formed so big as to break the continuous flow of liquid. If such a situation is encountered during long term cooling by natural circulation, the void pocket may break the syphon and thus interrupt the flow. Thus it is important to know how does the void pocket grow, i.e., how does vapor phase separate from the liquid phase as the two-phase mixture approaches the $\cap$ -bend. In the existing codes the phase separation is based upon bubble-rising model or drift-flux model (1,2,3) correlations obtained from vertical pipe data. The validity of such correlations for the case of curved-channel is questionable.

The objective of this study is to determine the effect of curvature on the drift-flux correlation, on bubble distribution, on bubble trajectory, and on bubble shape. All these parameters will affect the phasic separation through either rising velocity or void-distribution profile.

This paper will include the experimental set-up and procedure; report the data obtained from photographic study and void fraction measurements; (4,5) and discuss

the possible ramification of the observation to the phase separation model for the bubbly flow in a curved channel.

B. Experimentation

The experimental investigation consisted of the determination of the velocity component of an air bubble rising in an upward flowing stream of water between the 'bend' section, the void fraction of an air bubble rising between the vertical section under essential isothermal conditions. A loop containing a 'U' bend and vertical plastic test section of 3 inch diameter was constructed for this purpose.

The water loop, Fig. 1, is an open loop operating under atmospheric conditions containing a raised 500 gal water tank which provided a high-static head for the pump. A constant speed A.C. motor of 3500 r.p.m. was employed to drive a centrifugal pump (rated capacity 500 gpm), in order to obtain the desired flow range with a minimum of fluctuations. Water flow to the test unit was controlled by means of two ball valves. The first 5/8 inch ball valve was connected to the outlet of the pump to the bypass to the drain. The second 5/4 inch ball valve was connected in the discharge line from the pump. 3/4 inch piping was employed throughout the system for connecting lines. The average bulk water velocity in the test section extending from 4.847 cm/sec (3.5 gpm) to approximately 21 cm/sec (15 gpm).

The water from the control valving system was passed through a horizontal run of 3/2 inch diameter, where a rotometer was installed. The bulk flow rate of the system was determined from the metering float The water then

passes through a reducer to connect a 5/8 inch pipe and into the inverted 'U' bend pipe.

The air passed through a rotometer ranging from o to 80 $ft^3/min$. A Bourdon Pressure Gauge was employed behind the rotometer to monitor the pressure, the air then flowed through a ¼ I.D. inch 66-p tubing and injected upward to the plastic pipe as shown in Fig. 1.

Since the air can be separated from water in a vertical channel due to the static pressure head difference one may obtain the liquid hold up data from the height of collapsed liquid columns in each of the two Dp-tubes Fig. 1, in the test section A and B, the dimensions of the two Dp-tubes are given:

| Dp - tubes | Section A | Section B |
|---|---|---|
| Internal diameter of the tubes | ¼ inch | ¼ inch |
| Length for the tubes | 18 inch | 13.5 inch |
| Distance from the bottom of the pipe to the center of the tubes | 52.5 inch | 68.1 inch |

C. Test Results

There are two parts of the tests, the photographic study and the drift-flux study. For the photographic (6,7) study, a high-speeed cinemagraphic record was obtained. The images were analyzed on the UMCP movie analyser and data was fed into the UMCP computer. From these analyses, information was deduced in the following categories:

(1) Bubble size distribution

(2) Bubble trajectory

(3) Bubble velocity

(4) Bubble aspect ratio (major oxiz/minor oxiz)

For the drift-flux study, the superficial velocities $J_G$ and $J_{L'}$ as well as average void fraction in the stations (1 ft. long section each) were recorded.

From such information, the drift-flux correlation can be obtained for each station.

The ranges test conditions for these tests are:

1. Room temperature

2. For the measurements of bubble velocity and size distribution

Bulk Water Velocity: 4.84 to 9.7 cm/sec

System Reynolds number: 3200 to 6400

3. For the measurements of void fraction by Dp-method.

Bulk Water Velocity: 1.8 to 21 cm/sec

System Reynolds number: 1200 to 14000

Gas Void Fraction: 0.2 to 0.8

In the following section, the test results will be presented.

1. Bubble Size Distribution

In general, the larger bubble tends to migrate toward the out-side curvature, while the smaller bubbles accumulate in the inside curvature. (Fig. 2)

The relative velocity, $U_{b,r}$, of a bubble rising, in a mixture stream with stream velocity, j, is shown in Fig. 3. The component of velocity that is perpendicular to the centerline is $U_{b,r} \sin\theta$. If we assume $U_{b,r}$ is a positive

function of bubble radius, then the larger bubbles are given with a larger normal velocity which causes those bubbles to move further toward the outside curvature.

2. Bubble trajectory

Some bubbles images in the movie were tracked frame-by frame to yield bubble trajectories. Some typical trajectories are shown in Fig. 4. It is obvious that larger bubbles tend to go straight, while the smaller bubbles tend to follow the secondary flow to circulate.

Apparently, the straight trajectories of large bubbles are caused by two reasons: the large bubbles rise faster; and they also migrate more toward the outer curvature due to a larger normal velocity vector. The smaller bubbles tend to have less rising velocity and thus get caught by the flow stream. Besides since they stay more in the inside curvature, where there is more secondary flow, their trajectories are more circulatory.

3. Bubble velocity

The bubble velocities with respect of the fixed frame are shown in Fig. 5. Unfortunately, since this bubble rising velocity is the vector combination of the stream velocity and the drift velocity, Fig. 5 does not yield any information about drift velocity, which should be a function of bubble size and possibly other factors. One needs information about local stream velocity before one can deduce the drift velocity. Such tests will have to be carried out with local measurement, and we are planning to do so in the future.

4. Bubble aspect ratio

The aspect ratio is defined as $\frac{d \text{ major axis}}{d \text{ minor axis}}$

The aspect ratios are plotted as a function of bubble size in Fig. 6. Also shown in Fig. 6 are the aspect ratios expected from idealized bubbles: the small Stokian bubbles and the large cap bubbles (8). As one may notice from Fig. 6, when bubbles are small, the aspect ratio trend is qualitatively in accord with the Stokian bubbles; while for large bubbles, there is a range of bubble size in which the experimental aspect ratios are close to that of the ideal cap bubble. But these are two anomallies. One is in a narrow range of bubble size the aspect ratio vary widely, from one to five. The second anomally is the break of aspect ratio into three segments in the cap bubble region.

The wide variation of aspect ratio could be attributed to four possible causes:

(1) twist and turns of the turbulent eddies

(2) wake effect of leading bubble

(3) shedding of a rising bubble in spiral fashion

(4) secondary flow in the curved channel.

We plan to identify the cause by process of elimination. Cause (4) can be checked by using a straight pipe, cause (1) can be checked by running tests in different Reynolds numbers and flow of different turbulence scale, cause (2) can be checked by comparing behavior of leading bubbles with that of trailing bubble, cause (3) can be checked

by varying surface tension. It is felt that cap bubble behavior probably is more associated with cause (3) while small bubbles are more associated with cause (1), (2), and (4).

The aspect ratio of a bubble reflects the oscillation and wobbling of a bubble, which in turn would influence the flow field around the bubble, and finally, influence the bubble rising velocity. A thorough study of bubble aspect ratio may shed light on the wide variation of bubble velocity.

5. Drift-flux correlation

The drift-flux formulation is a very useful invention in that it relates the microscopic flow parameters such as spatially averaged void fraction and superficial velocities with the microscopic information such as velocity and void fraction profile and the drift velocity (Fig. 7).

In the present study, the void fraction was measured at two stations and the resulting drift-flux relationship is shown in Fig. 8. Note that as the flow approaches the curved section of the pipe, both the drift-flux slope and the intersect change. The slope $C_o$ is a function of both the void profile and velocity profile. For a fully developed flow in a straight pipe both profiles can be represented by the power law with exponential index of 5 or 6. The resulting $C_o$ is about 1.2 for the curved channel, the void is skewed to the outside curvature and the velocity profile is skewed lower or even reversed near the inside curvature. The resulting $C_o$ is thus lowered, since the drift velocity represented by the intercept

is one value in the idealized flow, while in the case of the curved channel, the bubbles are segregated into two sizes in two regions, then some average value weighted by various bubble populations must be used.

The abcve experimental information on drift-flux model indicates that the straight pipe correlation can not be applied to a curved channel. Furthermore, qualitatively, we should expect Co to decrease and "drift-velocity intercept" to increase as we approach the curved section. More data and analysis are needed if a prior expansion for drift-flux model can be developed for a curved channel.

## D. CONCLUSION:

In this preliminary study, experimental data are obtained which indicate:

(1) Large bubbles tend to migrate toward the outside curvature and move more straightly while smaller bubbles tend to stay in the inner curvature and follow the flow stream.

(2) The existence of secondary flow can strongly influence bubble trajectory and void distribution.

(3) Bubble aspect ratios vary widely with bubble size and may be a parameter to be studied to determine bubble velocity versus flow.

(4) The drift-flux correlation for curved channel is different from that of straight tube due to phase segregation and secondary flow.

Acknowledgement:

This study was carried out under the sponsorship of US NRC. The Cinemographic films were recorded and analyzed using the facility of the University of Maryland Department of Physical Education with the assistance of Mr. W. R. Chen, who has been very helpful.

REFERENCES


1. Y.Y. Hsu and Robert W. Graham, "Transport Processes in Boiling and Two-Phase Systems", Hemisphere Publishing Corporation. (McGraw-Hill), N.Y. 1976 - Ch. 5.
2. Zuber, N. and Findlay, J.A., J. of Heat Transfer, Trans. ASME, 453 (1865).
3. N. Zuber and J.A. Findlay, "The Effects of Non Uniform Flow and Concentration Distributions and the Effect of the Local Relative Velocity on the Average Volumetric Concentration in Two-Phase Flow", GEAP-4542, General Electric Co., 1964.
4. Lockhart, R.W. and Martinelli, R.C., "Proposed Correlation of Data for Isothermal Two-Phase Two-Component Flow in Pipes", Chem. Engr. Progress, 45, 3P (1949).
5. Toks Oshinowo and M.E. Chalres., "Vertical Two-Phase Flow: Part II - Holdup and Pressure Drop", The Canadian Journal of Chemical Engr. 438, Vo. 52, Aug. 1974.
6. Hewitt, G. F., Dehaye, J. M., Hsu, Y.Y. and Lieberman, A., "Measurement Techniques", Tn Hanolbook of Multiphase Systems (Hetsroni, G. ed.), Hemisphere Publ. (McGraw Hill), N.Y. 1982, ch. 10.
7. J. G. Collier and G. F. Hewitt, "Experimental Techniques in Two-Phase Flow", British Chemical Engineering, p. 1526, Dec. 1966, Vol. 11, No. 12.
8. Rosenberg, B., "The Drag and Shape of Air Bubbles Moving in Liquids", David Taylor Model Basin Report No. 727 (1950).

# NOMENCLATURE

A: area of pipe

Co: distribution Coefficient

d: diameter

$J_G$: $(Q_G/A)$: superficial velocity of gas

$J_L$: $(Q_L/A)$: superficial velocity of liquid

Jmix: mixture mean superficial velocity

$Q_G$ : gas volumetric vlowrate

$Q_L$ : liquid volumetric flowrate

$V_b$ : absolute upward velocity of bubble

$V_{df}$ : drift velocity of bubble

$U_{b,r}$ : bubble relative velocity

$U_G$ : bubble mean superificial velocity

Req: equivalent radius of bubble

$\alpha$ : void fraction of gas

Subscripts:

b: bubble

df: drift

eq: equivalent

G: gas phase

L: liquid phase

mix: mixture

r : relative

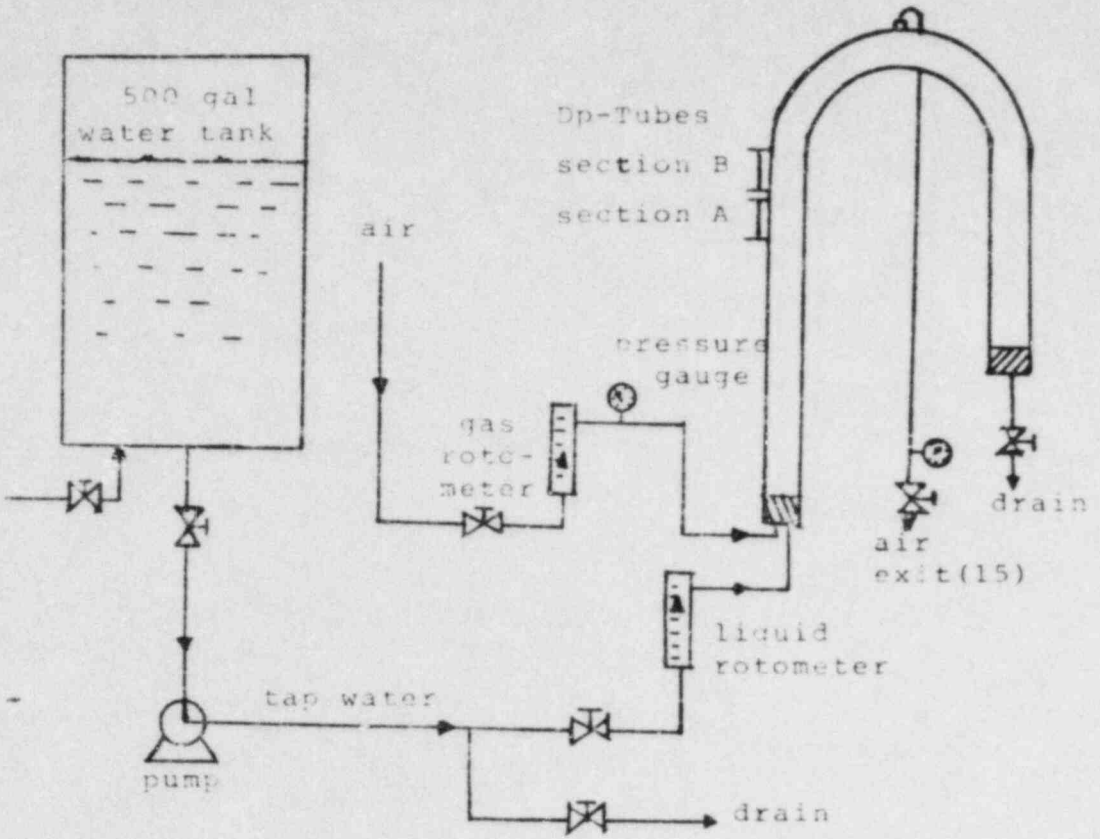


Fig 1. Schematic diagram of experimental equipment

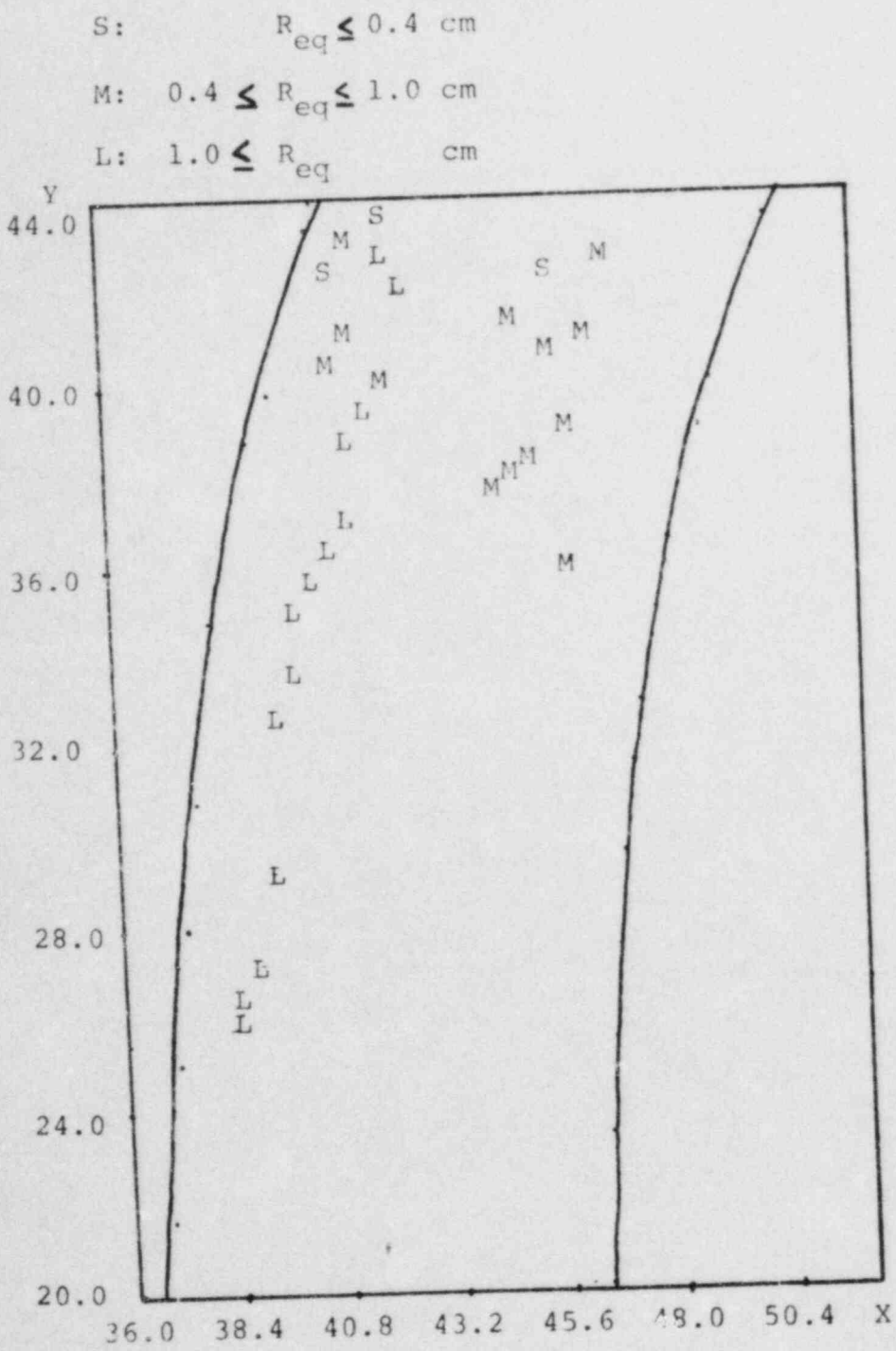


Fig 2. SIZES DISTRIBUTION OF THE BUBBLES IN THE BEND OF THE PIPE

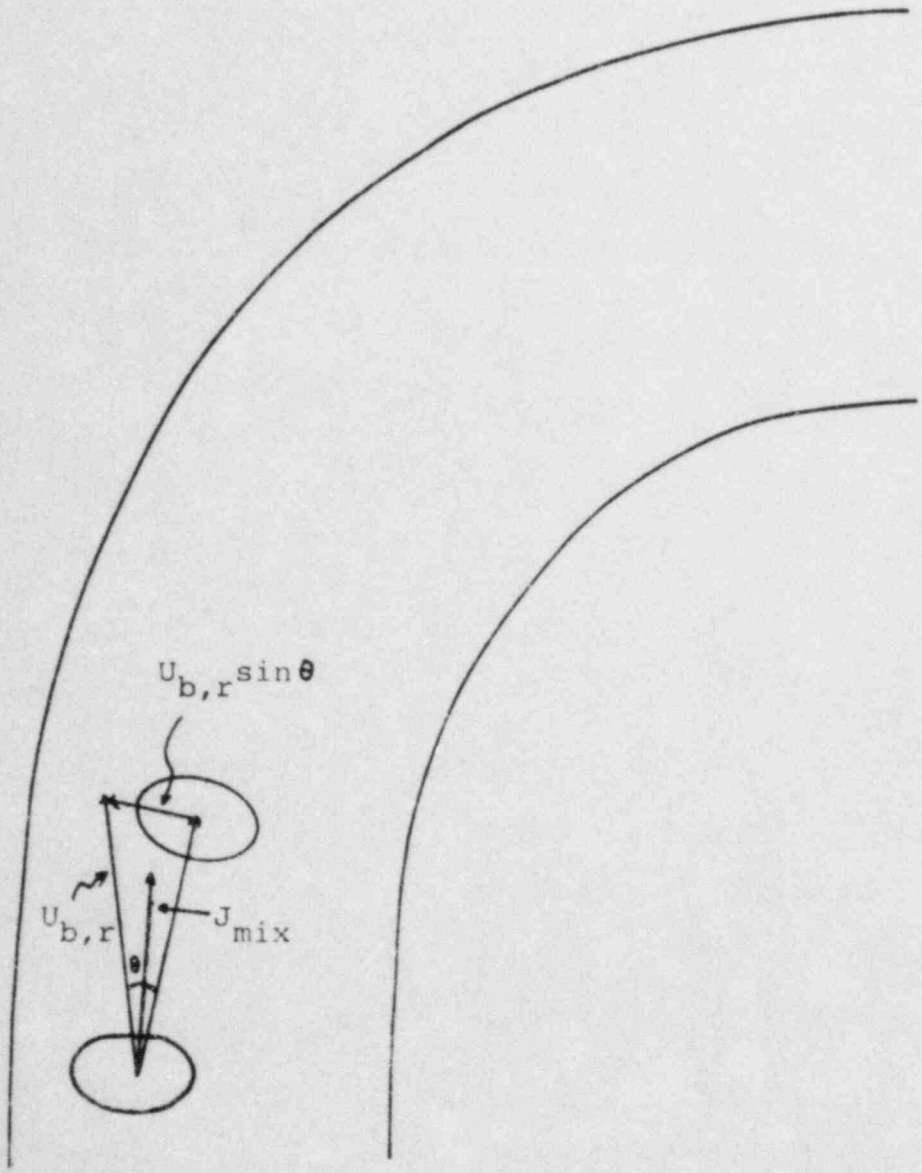


Fig 3. BUBBLE RELATIVE VELOCITY COMPONENT

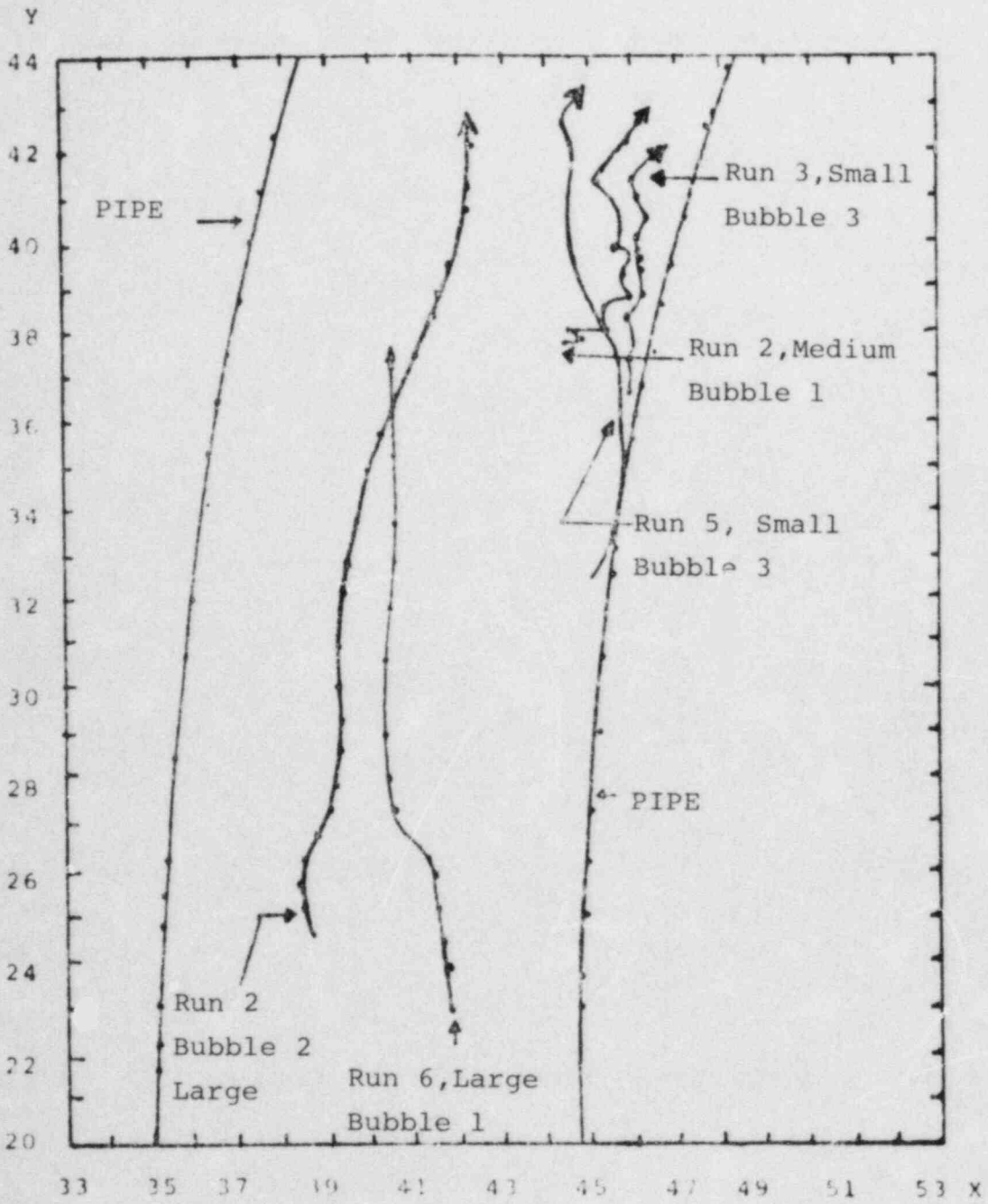


Fig 4. BUBBLE TRAJECTORY

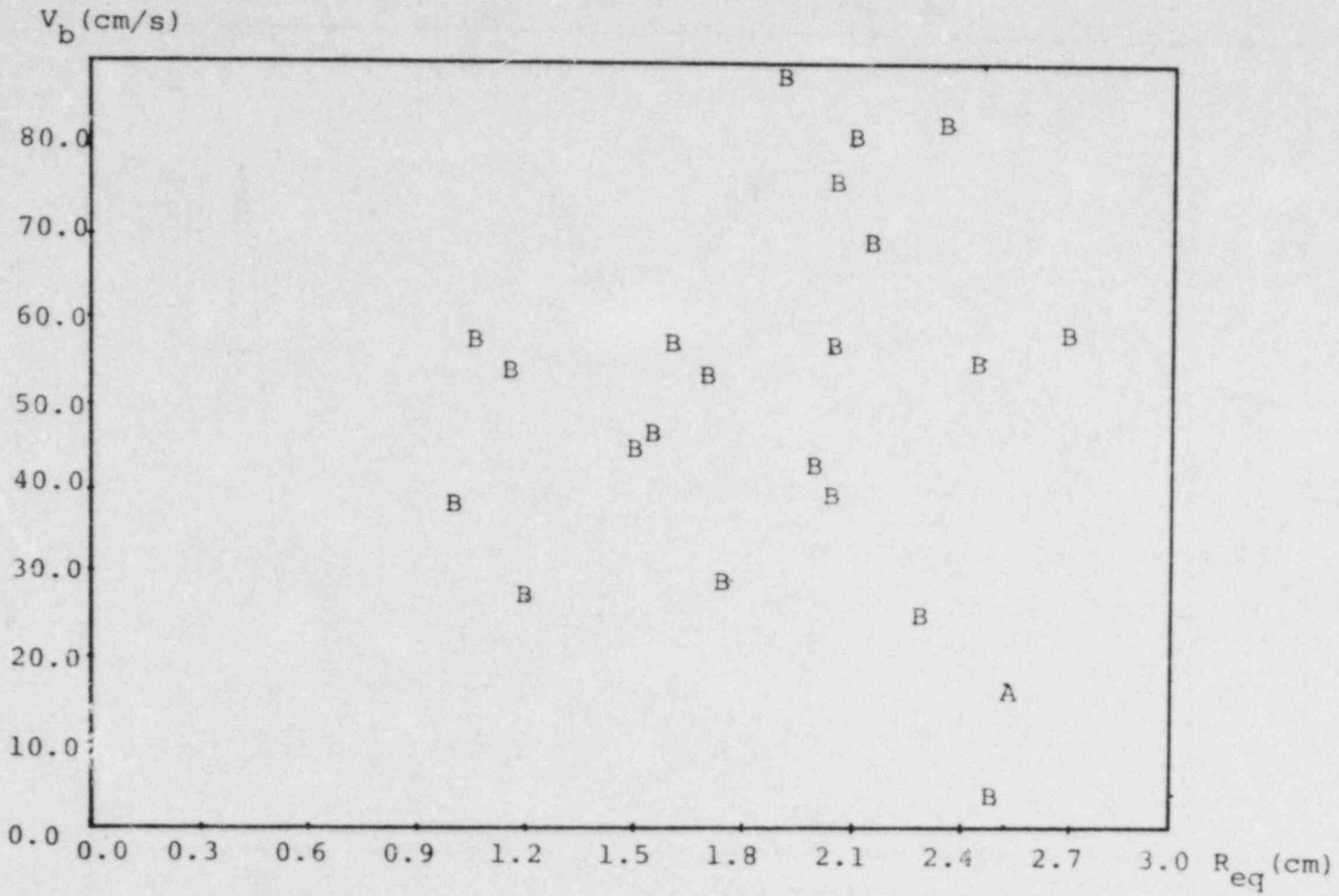


Fig 5. BUBBLE ABSOLUTE VELOCITY-EQUIVALENT RADIUS
3 inch diameter pipe
Run 3, bubble 1
water average velocity: 9.69 cm/s

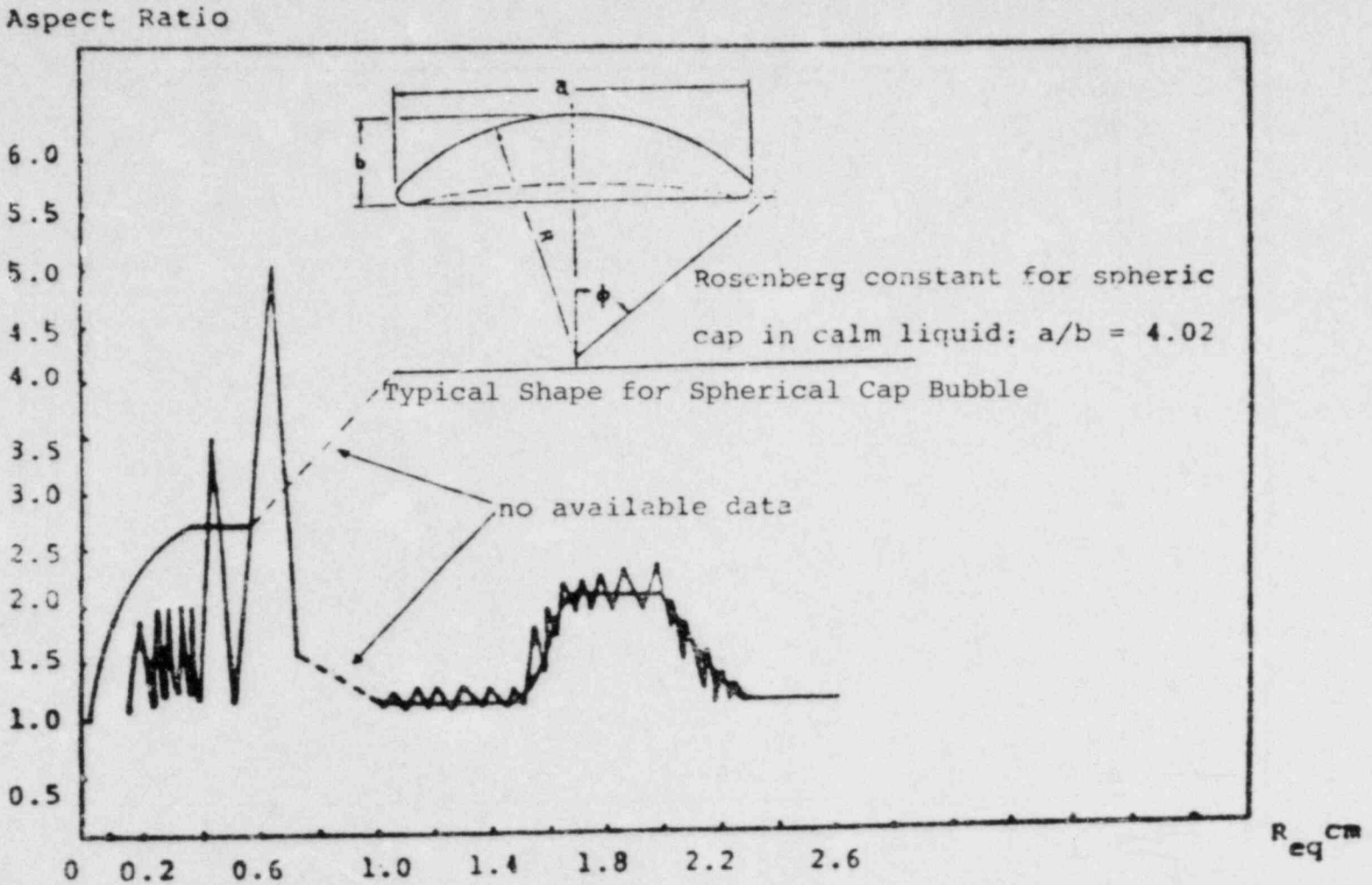


Fig 6. BUBBLE ASPECT RATIO-EQUIVALENT RADIUS FOR ALL TESTS

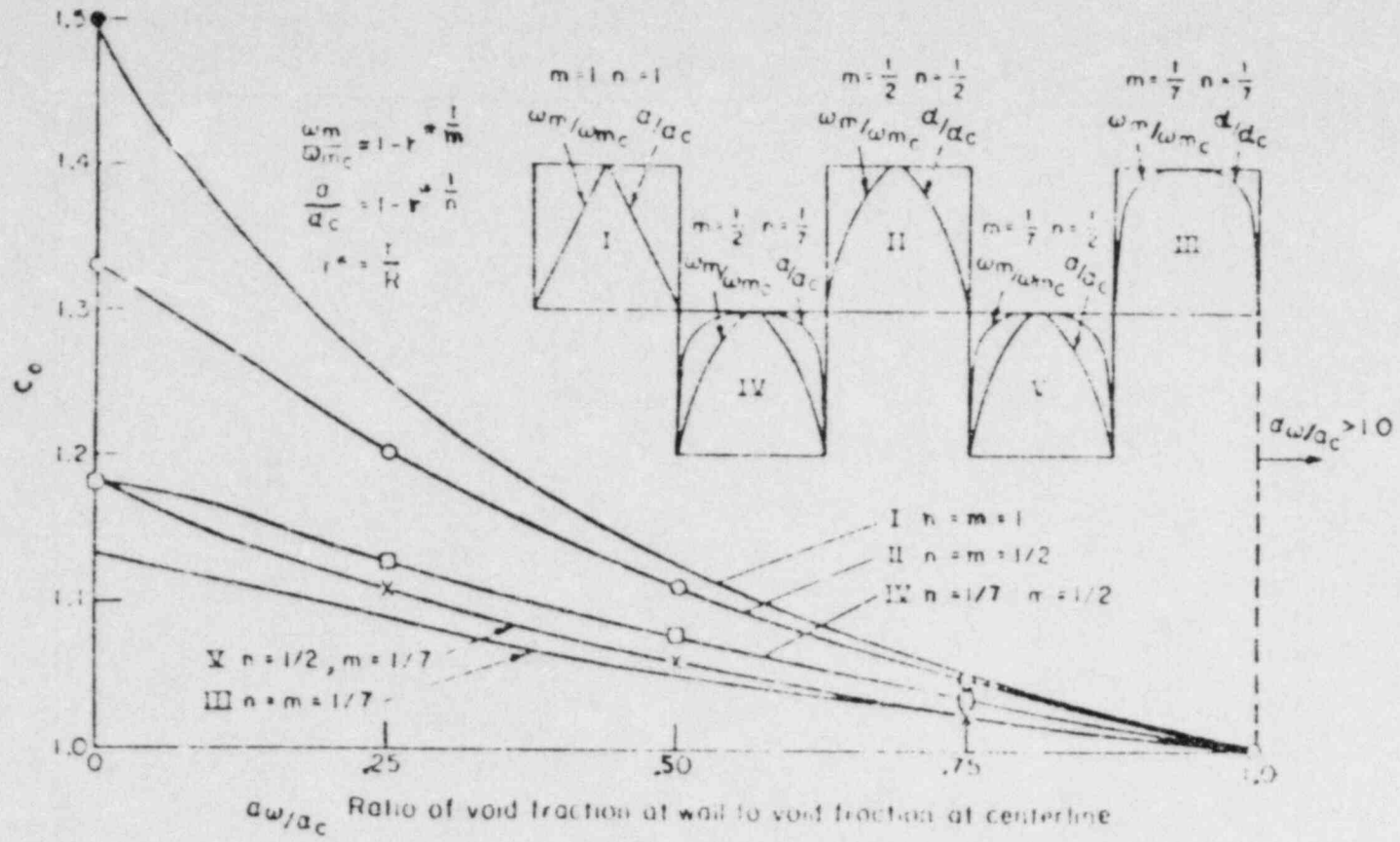


FIG. 7. Variation of the parameter $c_o$ with void and velocity profiles (Zuber and Findlay[4]).

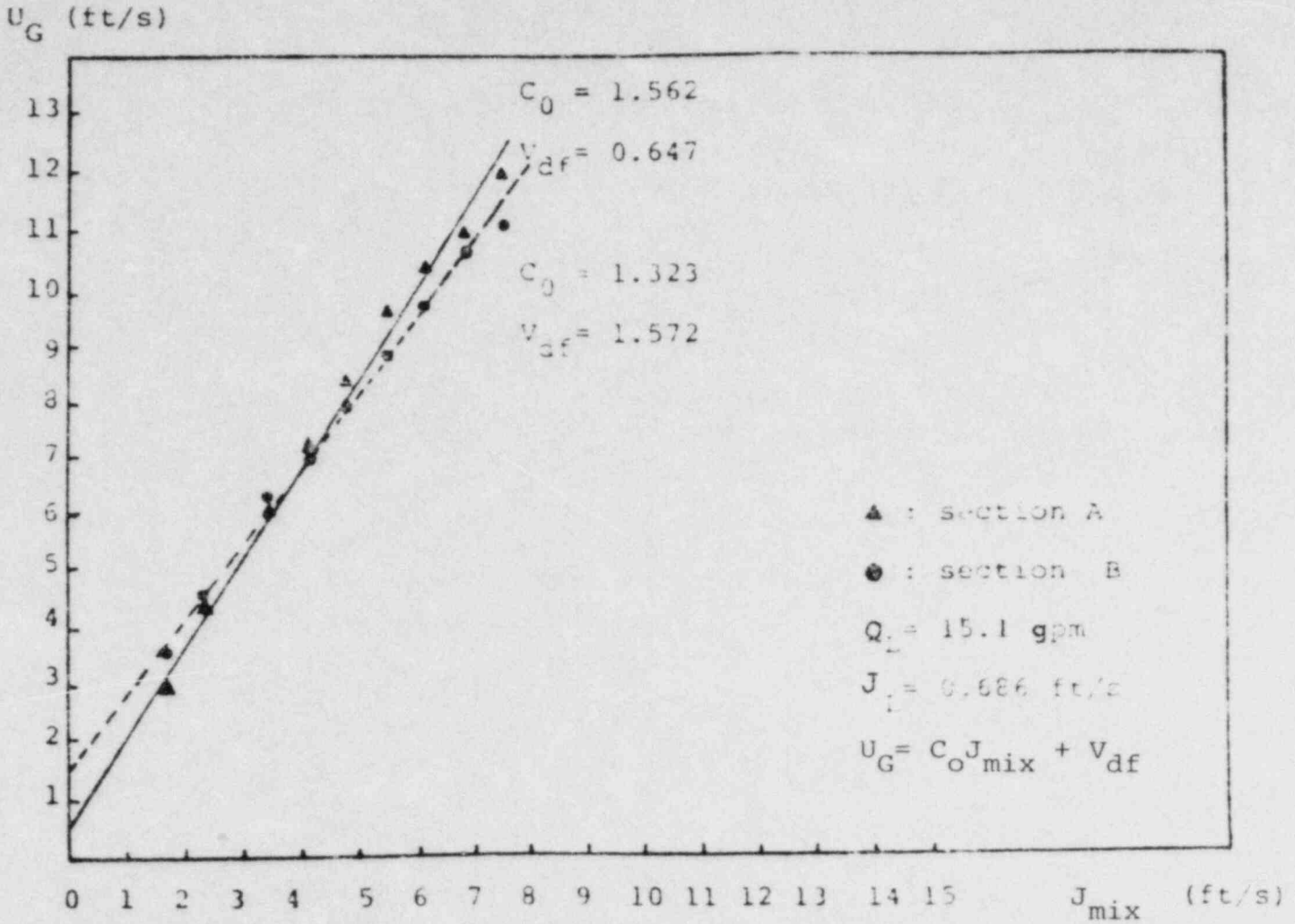


Fig 8. CORRELATION OF HOLDUP IN UPWARD SLUG FLOW

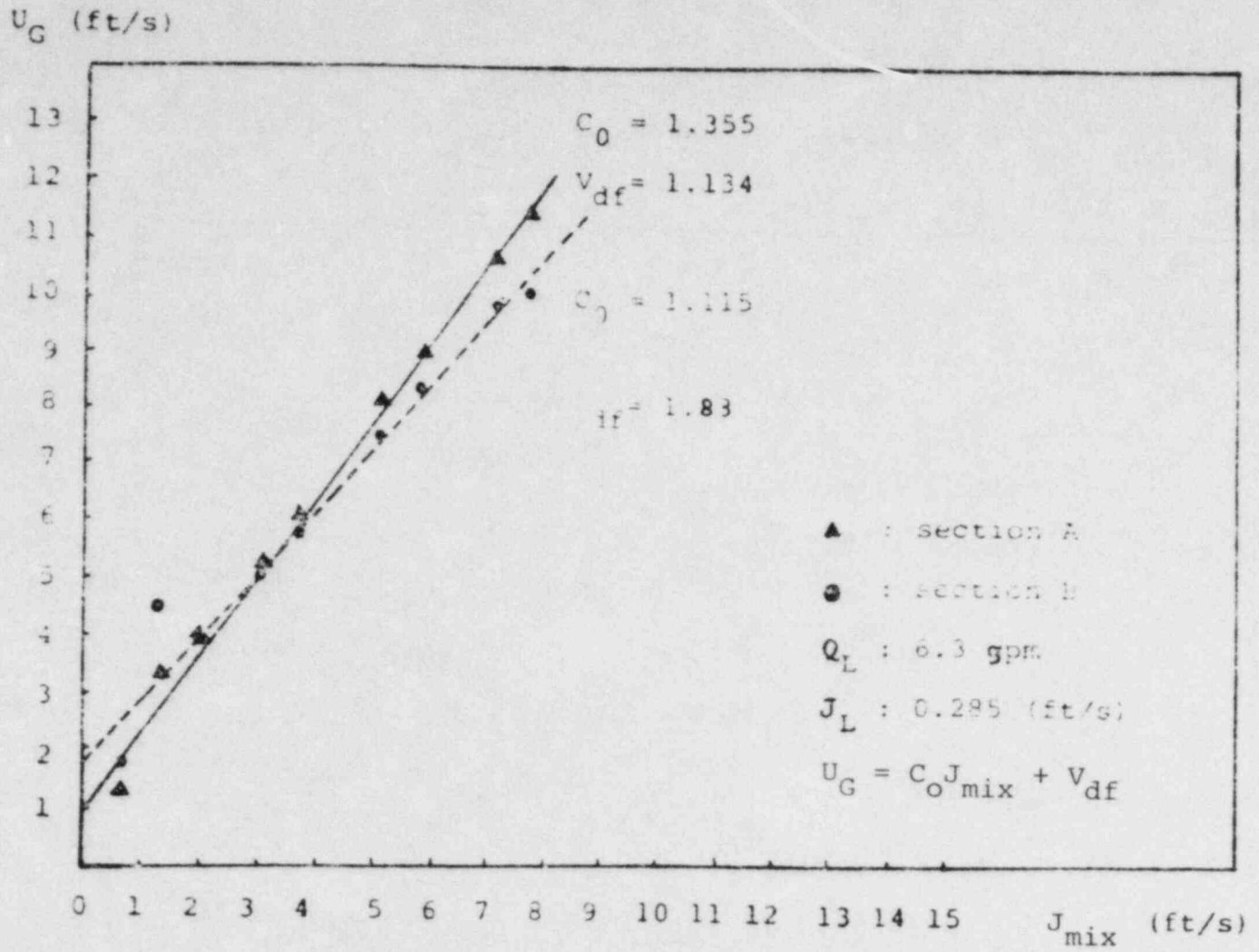


Fig 8. CORRELATION OF HOLDUP IN UPWARD SLUG FLOW

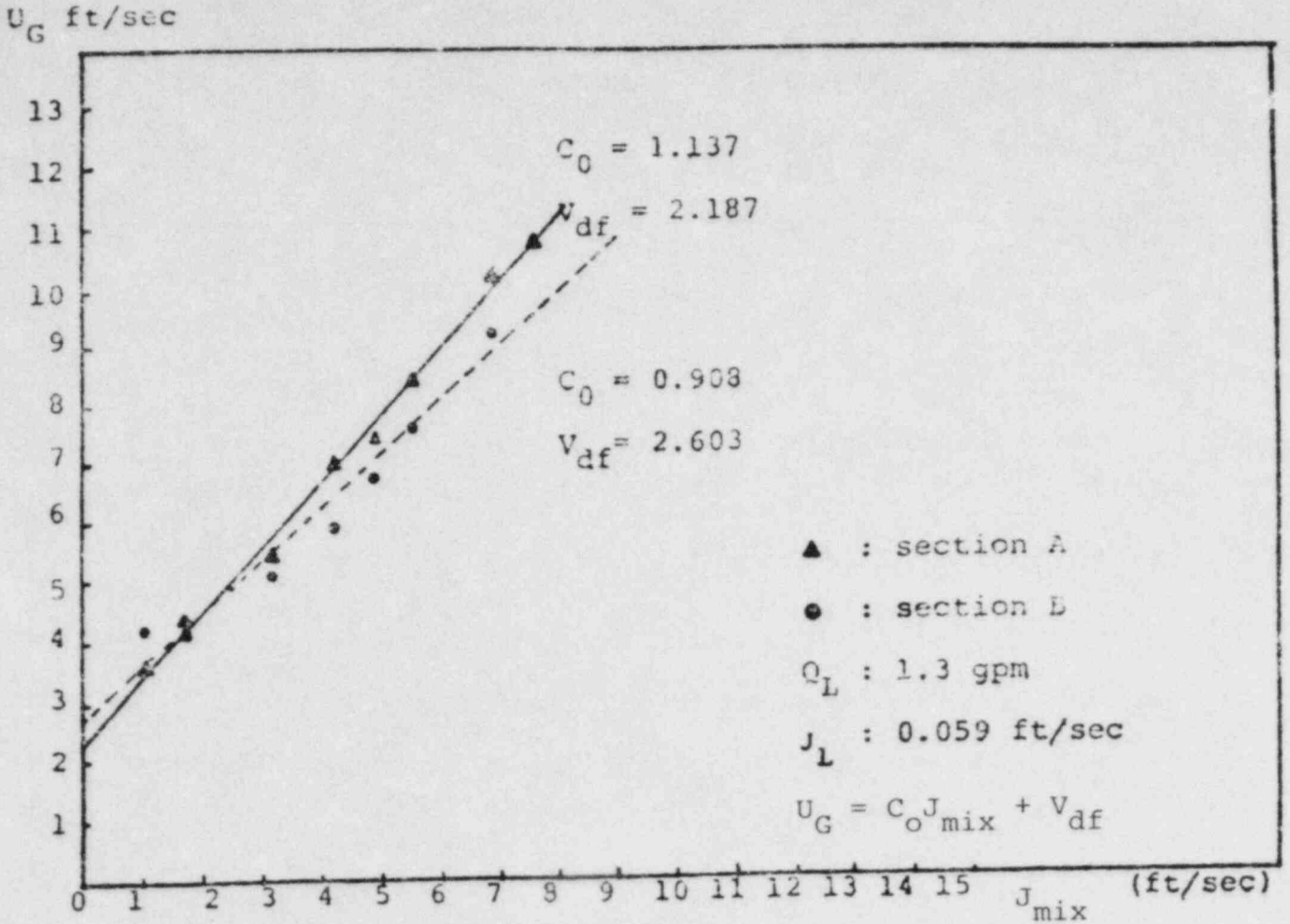


Fig 8. CORRELATION OF HOLDUP IN UPWARD SLUG FLOW

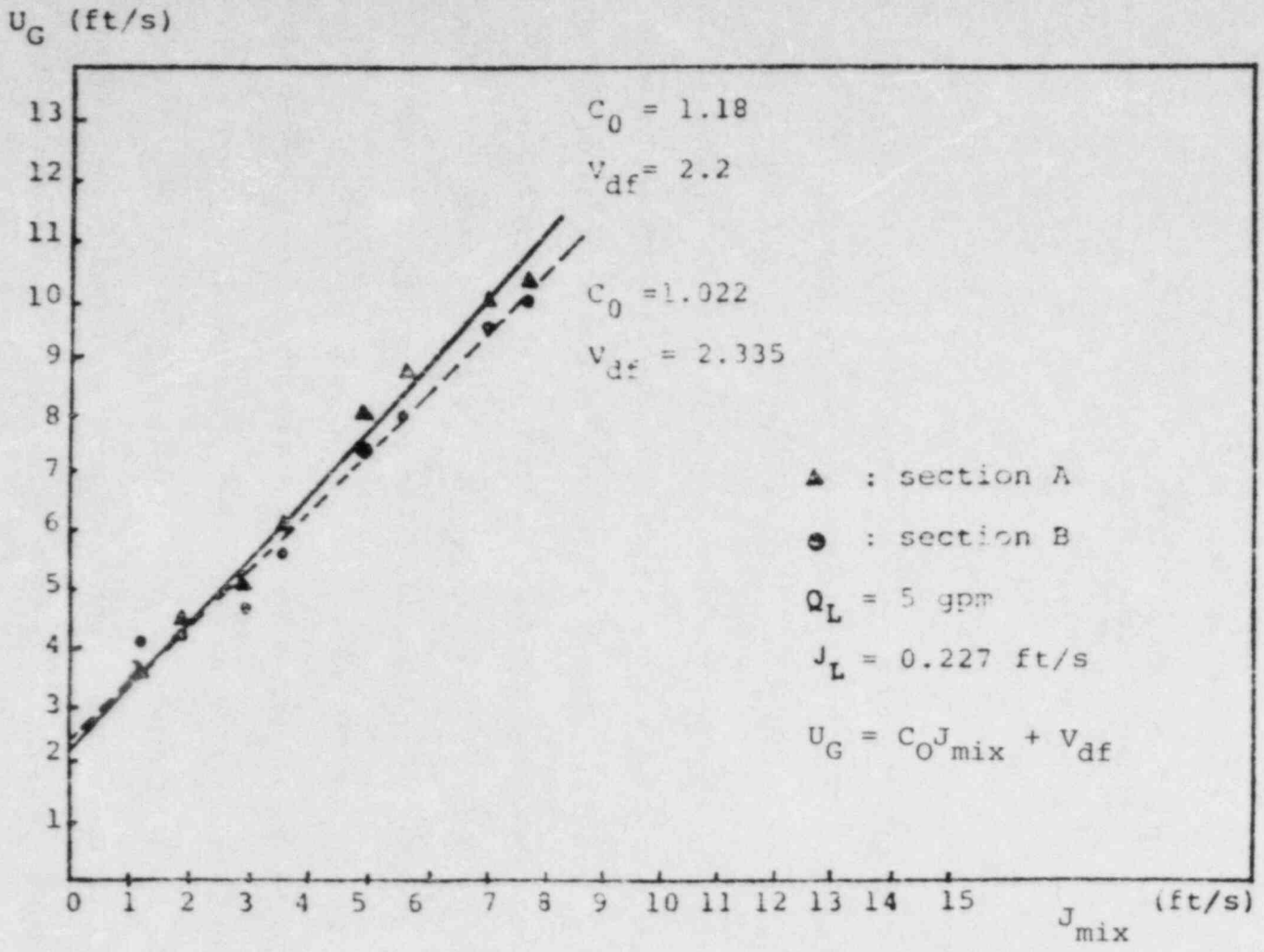


Fig 8. CORRELATION OF HOLDUP IN UPWARD SLUG FLOW

# Phenomenological Modeling of Two-phase Flow for LWRs
## I. Experimental Study of Hydrodynamics of Inverted Annular Flow
## II. Simulation Study of Hot Leg U-bend Two-phase Flow

by

M. Ishii, G. De Jarlais, and S. B. Kim

Reactor Analysis and Safety Division
Argonne National Laboratory
9700 South Cass Avenue
Argonne, Illinois 60439

## I. INTRODUCTION

The objective of this NRC sponsored research program is to develop rigorous two-phase flow models and correlations which are the foundation of reliable and accurate LWR safety analyses. The current effort is on the establishment of the two-fluid model, development of scaling criteria, derivation of interfacial transfer terms and prediction of hydrodynamic transients based on phenomenological modeling. This task will provide overall modeling of the basic equations and two-phase correlations to be used in large-scale LWR safety codes such as TRAC and RELAP, as well as the scaling criteria for the safety experiments. With the present highly advanced capability in numerical analyses, the essential limitations of these codes are imposed by not-well-understood two-phase thermal-hydraulics under various accident conditions. Therefore, rigorous two-phase flow models and properly scaled correlations which are developed under the program will significantly improve the reliability and accuracy of the advanced codes and safety analyses. The modeling efforts cover two-phase equations, interfacial shear, interfacial energy transfer, interfacial area, entrainment, droplet size, flow regime transitions, effects of reactor geometry on two-phase thermal-hydraulics and scaling of two-phase phenomena.

In FY 1984 three specific tasks which are all related to not-well-understood two-phase phenomena of importance to LWR accidents have been identified under the program. These three tasks are:

1) inverted annular flow experiments and modeling,

2) hot leg U-bend two-phase flow simulation study,

3) development and evaluation of two-phase flow scaling criteria.

Some of the important results obtained under Tasks (1) and (2) are reported in this paper.

## II. INVERTED ANNULAR FLOW STUDY

Inverted flow is important in the areas of LWR accident analysis and other confined film boiling applications. And yet, while many analytical and experimental studies of heat transfer in this regime have been performed, there is very little understanding of the basic hydrodynamics of inverted annular flow. As a result, many film boiling applications are amenable to only limited analysis at present. One example of this can be seen in large-scale LWR safety codes such as TRAC and RELAP, which are essentially constrained by the not-well-understood two-phase thermo-hydraulics under various accident conditions, including those resulting in inverted flow in the post CHF region.

Inverted annular flow can be visualized as a liquid jet-like core surrounded by a vapor annulus, see Fig. 1. The shape of the liquid/vapor interface, the stability of the liquid jet core, and the disintegration/entrainment of this liquid core must be understood, and predictive methods established, in order to clarify the modeling of this regime and the development of interfacial transfer correlations.

For confined flow conditions the boiling curve beyond the dryout point may differ greatly from the classical boiling curve due to two-phase flow hydrodynamics. Flow regimes before and after CHF become important in

determining heat transfer (along with mass and momentum transfer). Pre-CHF flow regimes may be predicted by using the criteria developed by Ishii and Mishima [1] and Mishima and Ishii [2], while flow regimes immediately beyond the dryout point may be viewed as the inverse forms of pre-CHF regimes (see Figs. 2 and 3).

Thus the criteria for the initial flow regimes beyond the dryout point or rewetting front can be given in the following form [1,2].

(I) Initially Inverted Annular to Initially Inverted Slug of Churn Flow

The flow regime transition criterion is given by

$$\alpha > 0.3 \tag{1}$$

for a two-fluid model formulation. For a drift flux formulation the same criterion may be expressed in terms of volumetric fluxes as

$$j_F < \left(\frac{3.33}{C_o} - 1\right) j_G - \frac{0.76}{C_o}\left(\frac{\sigma g \Delta\rho}{\rho_F^2}\right)^{1/4} \tag{2}$$

where the distribution parameter $C_o$ [3], is given by

$$C_o = 1.2 - 0.2\sqrt{\rho_G/\rho_F} \tag{3}$$

(II) Initially Inverted Slug or Churn to Initially Dispersed Droplet Flow

The transition criterion is given by

$$j_G > \sqrt{\frac{\Delta\rho g D}{\rho_G}}\,(\alpha - 0.11) \quad \text{and} \quad \alpha > \alpha_m \tag{4}$$

or

Table I. Initial Flow Regime

| Pre-CHF Flow Regime | | Post CHF Flow Regime |
|---|---|---|
| Subcooled Liquid<br>Bubbly | ⟶ | Inverted Annular Film Boiling |
| Slug<br>Churn Turbulent | ⟶ | Inverted Slug or Churn |
| Annular<br>Annular Mist | ⟶ | Dispersed Droplet |

$$j_G > \left(\frac{\sigma g \Delta p}{\rho_G^2}\right)^{1/4} N_{\mu F}^{-0.2} \tag{5}$$

where the viscosity number is given by

$$N_{\mu F} = \mu_F \Big/ \left(\rho_F \sigma \sqrt{\frac{\sigma}{g\Delta\rho}}\right)^{1/2} \tag{6}$$

Here $\alpha_m$ is the void fraction at the slug to churn turbulent flow transition and it is given by

$$\alpha_m = 1 - 0.813\left\{\frac{(C_o - 1)\, j + 0.35\sqrt{\Delta\rho g D/\rho_F}}{j + 0.75\sqrt{\frac{\Delta\rho g D}{\rho_F}}\left(\frac{\Delta\rho g D^3}{\rho_F \nu_F^2}\right)^{1/18}}\right\}^{0.75} \tag{7}$$

The first criterion corresponds to the transition due to flooding of a liquid film along a large churn flow bubble, whereas the second criterion corresponds to the droplet entrainment induced transition.

It should be noted that the flow regime transitions within the post dryout region are quite different from the standard two-phase flow regime

transitions. Consequently, the criteria for initial flow regime given by Eqs. (1) to (4) cannot be used for subsequent flow regime transitions beyond the CHF points.

For high quality, confined flow (annular flow) prior to CHF, post CHF flow is characterized by film dryout, with a transition to dispersed droplet flow. Heat transfer at the wall will be strongly influenced by droplet/wall and droplet/vapor interactions. At moderate quality, confined flow conditions, slug, or churn turbulent flow will occur prior to CHF. Just beyond CHF, the flow regime will be inverted slug, with large liquid slugs in a vapor continuum. Transition or stable film boiling may develop, with the size and motion of the liquid slugs affecting transfer rates. Well downstream of the CHF point. break-up of the liquid slugs by the vapor stream will result in dispersed droplet flow. Finally, at low quality, confined flow conditions, pre-CHF flow will be in the bubbly or subcooled liquid regime. Beyond CHF, transition boiling and stable film boiling will result in a transition to inverted annular flow. The liquid core surrounded by a gas annulus is hydrodynamically unstable, and transfer rates across the vapor film may vary greatly with core surface wave motion. After the break-up of the liquid core, inverted slug, inverted churn, or dispersed droplet flow will occur, leading to the dispersed droplet regime. The above is summarized in Table II.

From the above discussion, it can be seen that post dryout heat transfer cannot be properly assessed without knowledge of the hydrodynamics of the various two-phase flow regimes possible in confined boiling heat transfer. A review [4] of post-CHF heat transfer studies reveals that knowledge of the relevant thermo-hydraulics is still quite limited. Prior to 1950, the only significant work in the area was the 1756 treatise by Leidenfrost, who observed the film boiling of small droplets on heated surfaces. Following early

Table II. Post-CHF Flow Regime Transition

| Pre-CHF | CHF | Post CHF |
|---|---|---|
| Bubbly | | Inverted Annular → Inverted Slug → Dispersed Droplet |
| Slug or Churn Turbulent | | Inverted Slug → Dispersed Droplet |
| Annular Annular Mist | | Dispersed Droplet → Steam |

studies such as those by Bromley et al. [5] and by Hsu and Westwater [6]), a great deal of post CHF work was done (Kalinin et al. [7], Groeneveld and Gardiner [8], Groeneveld [9], Collier [10], Mayinger and Langner [11], Clements and Colver [12], Hsu [13], and Bressler [14]) but understanding of the basic hydrodynamics, especially those of inverted annular and slug flow, has not progressed greatly. In typical film boiling experiments, control and measurement of the flow parameters necessary for such an understanding are difficult, if not impossible, to achieve. Confined geometries and the minimum temperatures required for film boiling often prevent even simple flow visualization.

There have been, however, a few inverted annular flow studies in which limited hydrodynamic information was obtained as discussed in the previous section. In the analytical study by Jensen [15], break-up lengths of the inverted annular flow liquid core were calculated, along with surface wavelengths. In the transient film boiling experiment of Kurilenko et al. [16] and the steady state film boiling experiment of Ottosen [17], flow regime observations and void fraction measurements were made. In the FLECHT SEASET

series of tests, such as those reported in Lee et al. [18], dispersed droplet sizes and velocities were measured at distances well beyond the CHF point. Recently, Ishii and De Jarlais [19-23] performed adiabatic inverted annular flow experiments with controlled inlet conditions, and obtained data on jet instability, jet break-up, droplet entrainment, and droplet generation. Based on these data preliminary correlations for jet break-up length, wave length, entrainment, and droplet size have been developed [19-23] It must be noted that this adiabatic simulation of inverted annular flow, while producing a great deal of useful information, does have certain limitations. These limitations are

1) wetting of the wall by impinging liquid,
2) downward flow direction,
3) secondary break-up not visible,
4) turbulent jet (high liquid flow) only,
5) no effect of phase change.

In view of the several shortcomings of the adiabatic experiments [19-23], a new experimental apparatus, see Figs. 4 and 5, has been constructed in which film boiling heat transfer can be established in a transparent test section. The schematics of the test section is shown in Fig. 4. This test section consists of two coaxial quartz tubes. The annular gap between these two tubes is filled with a hot, clear fluid (such as syltherm 800) so as to maintain film boiling temperatures and heat transfer rates at the inner quartz tube wall. Temperatures of up to 250°C and heat transfer of up to 4.5 KW can be established in this quartz annulus. Inverted annular flow film boiling can be established by introducing saturated or subcooled test fluids such as R-113 into the inner quartz tube directly. In addition, simplified inverted annular flow geometry of liquid core and gas annulus can be simulated, by introducing

test liquids into the test section core through thin-walled tubular nozzles coaxially centered within the inner quartz tubing, while vapor or gas is introduced into the annular gap between the liquid nozzle and the inner quartz tube.

A number of experiments involving the heated, transparent test section has been carried out. One of the important focuses is to investigate the applicability of the results obtained from the previous adiabatic simulation study. The test liquid is subcooled Freon 113, with superficial velocities of 0.12 to 1.1 m/s, and the gas annuli is nitrogen, helium, and Freon vapor (to give a range of gas densities of 0.16-5.2 $kg/m^3$) with superficial velocities ranging near zero to 40, 100, and 20 m/s, respectively. The inner quartz tube is 1.36 cm ID, and various liquid nozzle diameters are used to establish initial void fractions from 0.16 to near 1.0. The heated test section length is 100 cm and flow is upward. The data from the above experiments are used to test the validity of the inverted flow model and droplet size correlations developed under the present study.

Photographic observation of the hydrodynamic behavior within the test section can be accomplished with both still photography and high speed motion pictures. Still photographs are taken with a 35 mm camera. Lighting comes from a 3 μs strobe light. This short exposure time allows small (~0.2 mm) droplets traveling at high speeds (above 10 m/s) to be observed. The strobe light is bounced off a white background, to provide backlighting of the test section, and the strobe/background unit can traverse the length of the test section. The still camera is mounted in front of the Lucite view port, on a mount which is tied to the motion of the strobe/background. Motion pictures are taken on a variable speed (100-10,000 fps) Photec IV camera, using VNX 430 film and four 450 W flood lights. The flood lights are directed onto the same background used for still photography, to again backlight the test section.

Typical photographs of various inverted flows observed in the above test apparatus are shown in Figs. 6, 7, and 8. Liquid Freon 113 is injected into the test section through a nozzle which appears black in the photographs. The interfacial waves appear on the liquid jet core almost immediately after the exit of the nozzle. For upward flow cases, there is a tendency for a liquid jet to expand to fill the flow area due to the gravity deceleration, whereas in the downward flow cases, the liquid jet tends to become thinner due to the gravity acceleration. This jet expansion effect is much more pronounced in low liquid flow cases than in high flow cases because of the differences in the initial kinetic energy.

In these heated wall experiments, a liquid jet seems to disintegrate into small droplets in somewhat more complicated and violent manners than in the adiabatic experiments. However, the dominant overall mechanisms are quite similar. The roll wave entrainment and jet instability are the two predominant mechanisms of the jet disintegration.

One of the most important characteristics of the heated wall experiments of the inverted annular flow is the existence of the agitated section beyond the roll wave section. Typically, this agitated section is 10 to 30 cm long. In most cases this agitated section propagates downstream in a quasi-periodic pattern. It appears as if liquid slugs are generated at the agitated section and transported downstream. The agitated section is most notable at moderate to low liquid flow rates. At very high liquid flow rate the significance of this agitated section seems to diminish.

The photographic observation indicates that the interfacial geometry of this agitated section is very rough and complicated. This implies that the interfacial area concentration is very high, and, therefore, the interfacial momentum and energy transfers are also relatively high in this section. The

liquid in the agitated section seems to be moving as densely packed, small droplets, or as a hollow, cylindrical liquid sheet with a very wavy surface. The high speed movies clearly show that the liquid associated with this region moves much faster upward than the liquid mass in the jet core section. This agitated section and the jet core section often coexist above the roll-wave section. Quite different velocities and motions of these two sections suggest that the liquid in the agitated section is not directly connected to the liquid core jet. It appears that the cloud of droplets or sheet of very wavy liquid surrounds the core liquid jet but moves independently. The higher upward velocity of the agitated section can be explained by the higher interfacial area concentration in relation to the liquid jet section.

At moderate to low liquid flow rates, the liquid jet core expands rapidly. At the same time, large amplitude surface waves appear on the liquid-gas interface. These surface waves quickly develop into roll-waves. When this happens, the interface becomes very rough and agitated. It is considered that a large number of small droplets are generated at this point. Furthermore, the crest of the roll-waves are pulled out of the original jet core and may form a thin liquid sheet surrounding the jet. These droplets and liquid sheets form the above mentioned agitated section. Very often this agitated section is not stable and chugging like behaviors can be observed. The agitated section quasi-periodically ejects a cloud of droplets and liquid sheets upward with a much higher velocity than the liquid in the core.

At very low liquid flow rates, a coherent core liquid jet cannot be observed above the agitated section. The original jet is disintegrated to multiple liquid ligaments having few cm length and 1 to 2 mm diameter. Further downstream these ligaments disintegrate into relatively large droplets with the maximum droplet diameter of 1 to 2 mm. The agitated section induced

chugging behaviors are much more pronounced at these very low liquid flow rates. The agitated section seems to produce droplets of much smaller sizes than those from the ligaments. The majority of droplets from the agitated section seem to be in the order of 200 μm or smaller in diameter. These droplet sizes are consistent with the results of the adiabatic experiments [19-23].

At moderately low liquid flow rates, the remnant of the original core liquid jet is visible. However, the diameter of the jet is considerably reduced due to roll wave entrainment. As the liquid flow rate is decreased, the jet tends to split into two or more branches and eventually into multiple ligaments mentioned above. The behavior of the liquid jet above the agitated section is quite similar to the adiabatic experimental cases. Thus it disintegrates into ligaments due to the jet instabilities.

At relatively high liquid flow rates, the effect of the agitated section is very small. The behavior of the core liquid jet is basically the same as that in the adiabatic experiments. The jet becomes initially unstable in the sinuous mode of the classical jet instabilities.

The above observations of the jet break-up in the inverted annular flow is summarized in Table III. In an actual film boiling situation, the liquid jet expansion section does not exist. It is expected that the surface wave phenomena immediately occur. However, the subsequent events described in Table III are expected in the same order. As discussed in detail above, there are very strong similarities between the adiabatic and heated wall experiments in terms of the hydrodynamics of the inverted annular flow. In both cases, the surface wave phenomena, classical jet instability, and roll-wave entrainment dominate the process of the liquid jet break-up into droplets. Furthermore, the droplet sizes in the dispersed droplet regime seem quite similar in

Table III. Jet Break-up in Heated Wall Experiments

| Low Liquid Flow | Moderate Flow | | High Flow |
|---|---|---|---|
| Inverted Annular Flow<br>Liquid Core Jet<br>Gas Annulus Jet | | | |
| | Liquid Jet Expansion | | Surface Wave |
| | Surface Wave → Roll Wave<br>Entrainment | | |
| | Agitated Section<br>Small Droplets<br>Rough Liquid Sheet | | |
| | Chugging Like Droplet Propagation | | |
| | Multiple Jet | Single Jet | |
| | Jet Break-up | | Sinuous Jet Break-up<br>Entrainment |
| | Multiple Liquid Ligaments & Drops | | Liquid Slugs<br>Small Drops |
| Large Drops (~1 mm) | | | |
| Small Drops (≲200 μm) | | | |

both experiments. This also indicates that the basic hydrodynamic phenomena involved in the jet disintegration process should be very closely related. Although final correlations and models for the jet disintegration based on the heated experiments are not available yet, the correlations based on adiabatic data should be quite useful for analyzing the hydrodynamics of inverted annular flow. However, it should be noted that there are certain phenomena, such as the existence of the agitated section, which require further research. The agitated section and the droplet propagation phenomenon are particularly important in terms of heat transfer because of the large interfacial area associated with them. It is most probable that they play a key roll in

precursory cooling of a hot wall downstream of the dryout point. Furthermore, the existence of these small droplets is very important in determining the thermal nonequilibrium between the vapor and liquid.

## III. SIMULATION STUDY OF HOT LEG U-BEND TWO-PHASE FLOW

In view of the inherent difficulties associated with full-scale testing, scale models of prototype systems have been extensively used to predict the behavior of nuclear reactor systems during normal and abnormal operations, as well as under accident conditions. The severity of the accident that occurred at the Three Mile Island Unit-2 plant has increased interest in this area. New scaling criteria for a two-phase system has been developed based on a rigorous perturbation method by Ishii et al. [24,25]. This new approach has been used to evaluate the design parameters of the new 2 x 4 simulation loop under the MIST program [25]. In view of certain scaling difficulties and distortions of the large scale simulation facility, a supporting experimental study to investigate the hot leg U-bend two-phase behavior and associated scaling problem has been initiated in FY 1984.

A simulation loop for studying the hot leg U-bend flow interruption and hot leg two-phase flow regime has been constructed based on the scaling criteria developed by Ishii et al. [24,25]. The overall loop schematic is shown in Fig. 9. This two-phase flow loop is designed such that it can be operated either in a natural circulation mode or in a forced circulation mode using nitrogen gas and water. The 5 cm ID riser simulates the vertical section of the hot leg. At the end of a riser section there is an inverted U-bend and the flow is turned downward into a gas-liquid separator which simulates the once-through steam generator. At present, the loop is 5 m in height and the test section is made of Corning Pyrex glass tubes with a U-bend radius of 9 cm. However, smaller or larger diameter test sections can easily be fitted to the loop.

Attached to the bottom of the riser is a stainless steel plenum which holds a multiple nozzle gas injector. The nozzles are made of hypodermic tubing molded into a epoxy plate. These stainless steel tubes, having a nominal 0.015 cm ID and a nominal 0.03 cm ID, are arranged in different patterns to achieve various injection modes. The number of nozzles per plate is varied from 49 to 621. Some plates are constructed to achieve a volumetric injection of the gas to the water flow. This is achieved by arranging the tubes so that their ends are symmetrically spaced at nine different heights over a 10 cm axial length. The gas is injected vertically into the riser through these nozzles. The gas flow rate and pressure are measured between the plenum and 0.5 $m^3$ gas accumulator. The gas ($N_2$) is supplied in high pressure cylinders, and reduced in pressure through the manifold regulator filling the accumulator. The accumulator dumps out variations in pressure and temperature as the gas is delivered from the regulator. The differential pressure is measured at five locations as indicated in Fig. 9. At low liquid flow (< 2 m/sec) these pressure transducers give very accurate measurement of void fractions. The liquid flow is measured by a paddle wheel type flow meter which has very small $\Delta p$. The two-phase flow section is all transparent, such that flow visualization, high speed still photography (3 μsec), and high speed cinematography (100-10,000 fps) are possible. The test section consists of various length Corning Pyrex glass tubes with pressure taps between them. It is designed such that various local instrumentations for two-phase flow measurements can be easily accommodated if they become necessary.

The loop design is based on the scaling criteria developed in the present study [24,25]. However, enough flexibility is built into the design such that certain scaling distortions can be studied by changing some components. One of the important aspects is that the height of the separator, as well as the

liquid level within the separator, can be changed in order to study systematically the effect of the thermal center of the steam generator.

There are several important differences between the present loop and the prototype. These are listed below:

| Item | Present Loop | Prototype |
|---|---|---|
| Loop | Single Loop | 2 x 4 Loop |
| Core | No Simulation | Core and Steam Dome |
| Hot Leg | No Horizontal Section | Horizontal Section |
| Vapor Source and Sink | Gas Injection<br>Gas Ejection | Boiling<br>Condensation |

Preliminary tests have been performed under bubbly and slug flow conditions with a natural circulation mode, i.e., with the pump turned off. At the bottom of the hot leg, bubbly flow was generated by injecting nitrogen gas through multiple nozzles. This gas injection simulated the boiling process in the prototype. The difference in the hydrostatic head in the riser (hot leg) section and downcomer section induced a natural circulation along the loop. The initial flow regime was always bubbly flow by the design of the nozzles and gas flow rates.

At low gas flow rates, the entire hot leg was in the bubbly flow. A phase separation ocurred at the top of the inverted U-bend. A slightly inclined separated flow led the water to fall along the inner side of the U-bend wall. A small number of bubbles are still entrained in the water at this stage; however, most of the gas was separated from the water and formed a continuous space from the top of the U-bend to the separator.

As the gas flow rates increased, formations of cup bubbles and slug bubbles could be observed. It appears that the transition to slug flow is gradual and depends on axial locations. This indicates the significant entrance effect on the flow regimes. The natural circulation flow interruption seemed to occur in two different modes, namely, quasi-periodic and semi-permanent modes. Appearances of large slug bubbles led to the quasi-periodic flow interruption. However, it appears that the natural circulation can be reestablished if there is sufficient hydrostatic head in the downcomer. It was found that one of the most important parameters determining the flow interruption is the water level in the separator. When the water level was sufficiently low, the semi-permanent flow interruption occurred. Then the two-phase level in the hot leg could not reach the U-bend section. This indicates that accurate knowledge of the void fraction in the hot leg is very important for the prediction of the flow interruption.

It was also observed that under certain conditions quite periodic flow oscillations occurred. The period was in the order of 20 to 30 sec. At present, the nature of this flow instability is not clear. The void and pressure oscillations appeared similar to those of the density wave instability.

ACKNOWLEDGMENTS

This work was performed under the auspices of the U.S. Nuclear Regulatory Commission. The authors would like to thank Mr. M. Young and Dr. N. Zuber for valuable discussions on the subject.

NOMENCLATURE

| | |
|---|---|
| $C_o$ | Distribution parameter |
| $d$ | Droplet diameter |
| $d_{max}$ | Maximum droplet diameter |
| $D$ | Hydraulic diameter |
| $D_J$ | Free jet, or core jet, diameter |
| $g$ | Gravity acceleration |
| $j$ | Total volumetric flux ($= j_F + j_G$) |
| $j_F$ | Liquid volumetric flux |
| $j_G$ | Gas volumetric flux (superficial velocity) |
| $L_B$ | Jet break-up length |
| $N_{\mu F}$ | Liquid viscosity number |
| $Re_{G,rel}$ | Gas Reynolds number ($= \rho_G v_{rel} D_H/\mu_G$) |
| $Re_J$ | Liquid jet Reynolds number ($= \rho_J v_J D_J/\mu_J$) |
| $v_J$ | Liquid jet velocity |
| $v_{rel}$ | Relative velocity ($= \lvert v_G - v_J \rvert$) |
| $We_{G,rel}$ | Gas Weber number ($= \rho_G v_{rel}^2 D_J/\sigma$) |
| $We_J$ | Liquid jet Weber number ($= \rho_J v_J^2 D_J/\sigma$) |
| $We_{J,rel}$ | Liquid jet Weber number ($= \rho_J v_{rel}^2 D_J/\sigma$) |

Greek Symbols

| | |
|---|---|
| $\alpha$ | Void fraction |
| $\Delta\rho$ | Density difference |
| $\lambda$ | Wavelength of maximum growth rate |
| $\mu_F$ | Liquid viscosity |
| $\mu_G$ | Gas viscosity |
| $\rho_F$ | Liquid density |
| $\rho_G$ | Gas density |
| $\sigma$ | Surface tension |

REFERENCES


1. Ishii, M. and Mishima, K., "Study of Two-fluid Model and Interfacial Area," NUREG/CR-1873, ANL-80-111 (1980).

2. Mishima, K. and Ishii, M., "Flow Regime Transition Criteria Consistent with Two-fluid Model for Vertical Two-phase Flow," NUREG/CR-3338, ANL-83-42 (1983).

3. Ishii, M., "One dimensional Drift Flux Model and Constitutive Equations for Relative Motion between Phases in Various Two-phase Flow Regimes," ANL-77-47 (1977).

4. Ishii, M. and De Jarlais, G., "Hydrodynamics of Post CHF Region," Intl. Workshop on Fundamental Aspects of Post-dryout Heat Trans., Salt Lake City, April 2-4, 1984.

5. Bromley, L. A., LeRoy, N. R., and Robbers, J. A., "Heat Transfer in Forced Convection Film Boiling," Ind. Eng. Chem., 45, 2639 (1953).

6. Hsu, Y. Y. and Westwater, J. W., "Approximate Theory for Film Boiling on Vertical Surface," Chem. Eng. Progr., Sump. Ser. 56(30), 15-24 (1960).

7. Kalinin, E. K., Berlin, I. I., and Kostyuk, V. V., "Film Boiling Heat Transfer," Advance in Heat Transfer 11, 51-197 (1975).

8. Groeneveld, D. C. and Gardiner S. R. M., "Post CHF Heat Transfer under Forced Convective Conditions," Proc. Sym. on the Thermal and Hydraulic Aspects of Nuclear Reactor Safety, ASME 1, 43-73, New York (1977).

9. Groeneveld, D. C., "Post Dryout Heat Transfer: Physical Mechanics and a Survey of Prediction Methods," Nucl. Eng. & Design 32, 283-294 (1975).

10. Collier, J. G., "Post-dryout Heat Transfer -- A Review of the Current Position," Two-phase Flows and Heat Transfer II, 769-813, Proc. NATO Advanced Study Institute, Instanbul, Turkey (1977).

11. Mayinger, F. and Langner, H., "Post-dryout Heat Transfer," Proc. 6th Intl. Heat Trans. Conf. 6, 181-198, Toronto, Canada (1978).

12. Clements, L. D. and Colver, C. P., "Natural Convection Film Boiling Heat Transfer," Ind. Eng. Chem. 62, No. 9, 26-46 (1970).

13. Hsu, Y. Y., "A Review of Film Boiling at Cryogenic Temperatures," Advances in Cryogenic Eng. 17, 361-381 (1972).

14. Bressler, R. G., "A Review of Physical Models and Heat Transfer Correlations for Free-convection Film Boiling," Advance in Cryogenic Eng. 17, 382-406 (1972).

15. Jensen, R. T., "Inception of Liquid Entrainment during Emergency Cooling of Pressurized Water Reactors," Ph.D. Thesis, Utah State University (1972).

16. Kurilenko, A. A., Dymenko, S. R., and Kochelaev, Yu. S., "Phase Slip and Heat Transfer to the Liquid in Film Boiling of a Cryogenic Liquid in Piston Flow," J. Eng. Phys. 39, 961 (1980).

17. Ottosen, P., "An Experimental and Theoretical Investigation of Inverse Annular Film Flow and Dispersed Droplet Flow, Important under LOCA Conditions, Riso National Laboratory Report No. R-424, Denmark (1980).

18. Lee, N., Wong, S., Yeh, H. C., and Hochreiter, L. F., "PWR FLECHT SEASET Unblocked Bundle, Forced and Gravity Reflood Task Data Evaluation and Analysis Report, NUREG/CR-2256 (1981).

19. Ishii, M. and De Jarlais, G., "Phenomenological Modeling of Two-phase Flow in Water Reactors at ANL (Inverted Annular Flow Modeling)," 10th Water Reactor Safety Research Information Meeting, Gaithersburg, Maryland, Oct. 12-15, 1982.

20. Ishii, M. and De Jarlais, G., "Inverted Annular Two-phase Flow Experiments and Modeling," Trans. 11th Water Reactor Safety Research Information Meeting, Gaithersburg, Maryland (1983).

21. De Jarlais, G., "An Experimental Study of Inverted Annular Flow Hydrodynamics Utilizing an Adiabatic Simulation," NUREG/CR-3339, ANL-83-44 (1983).

22. De Jarlais, G. and Ishii, M., "Hydrodynamic Stability of Inverted Annular Flow in an Adiabatic Simulation," Interfacial Transport Phenomena HTD 23, ASME Proc., 75-83 (1983).

23. De Jarlais, G. and Ishii, M., "Hydrodynamics of Adiabatic Inverted Annular Flow - An Experimental Study," 3rd Multiphase Flow and Heat Trans. Sym., Miami Beach, Florida, April 18-20, 1983.

24. Ishii, M. and Kataoka, I., "Similarity Analysis and Scaling Criteria for LWR's under Single-phase and Two-phase Natural Circulation, NUREG/CR-3267, ANL-83-32 (1983).

25. Kocamustafaogullari, G. and Ishii, M., "Scaling Criteria for Two-phase Flow Natural and Forced Convection Loop and Their Application to Conceptual 2 x 4 Simulation Loop Design, NUREG/CR-3420, ANL-83-61 (1983).

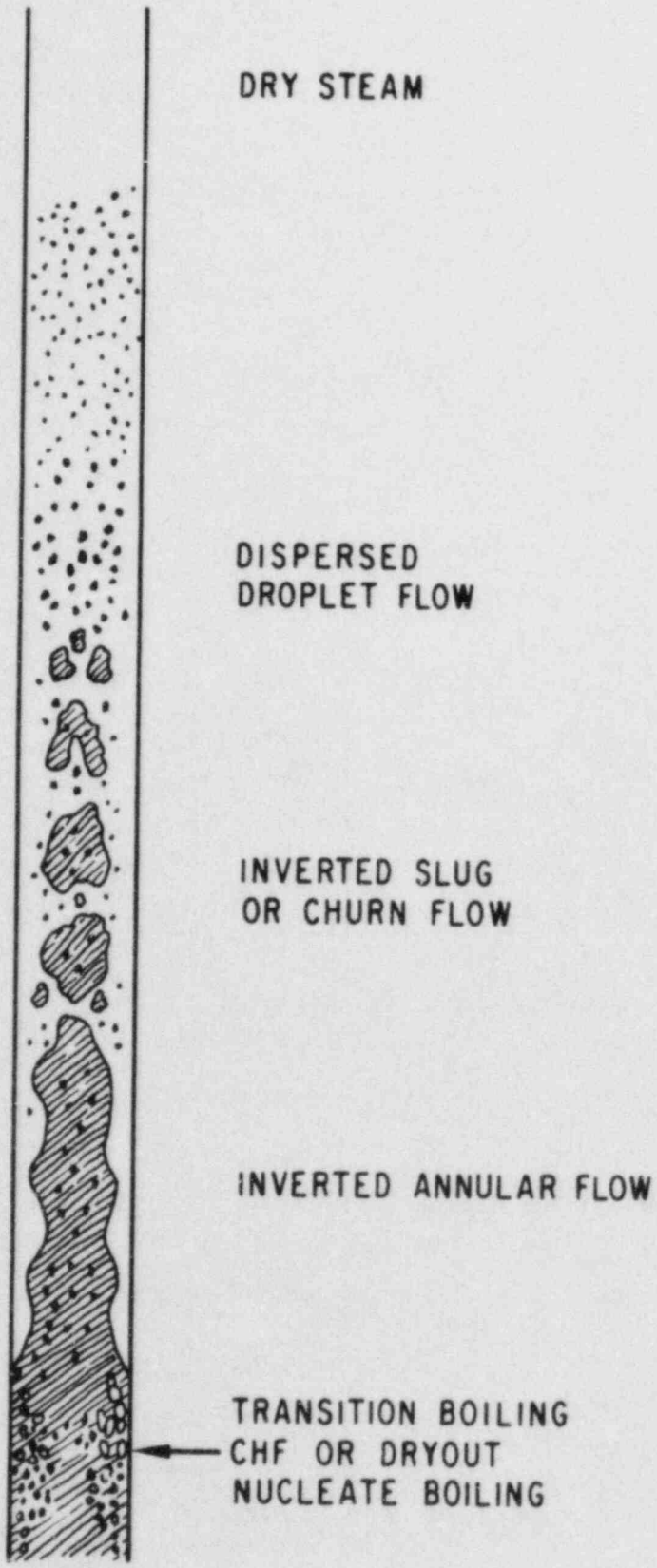


Fig. 1. Possible Flow Regimes in Post Dryout Region

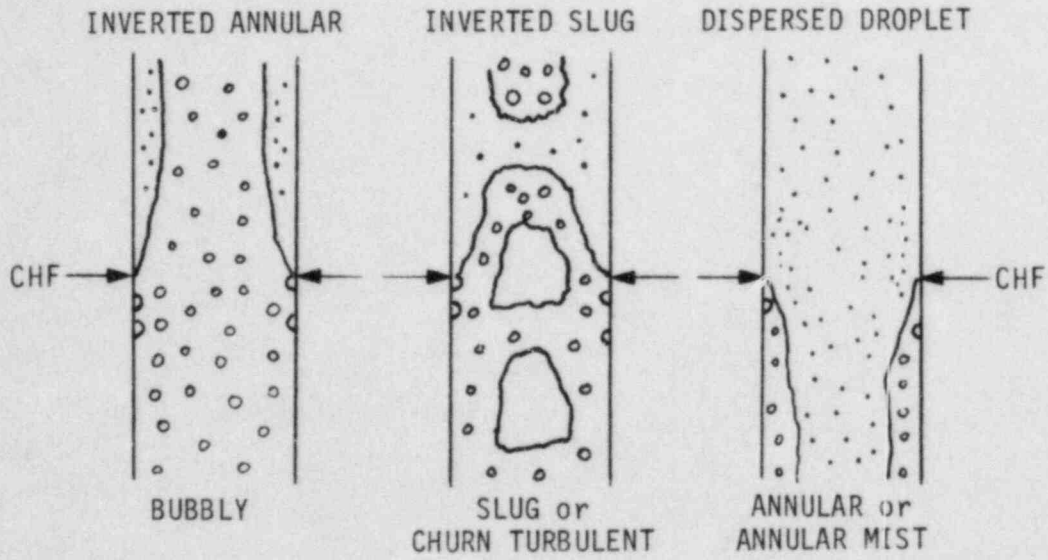


Fig. 2. Flow Regime Transitions at Dryout Point or Rewetting Front

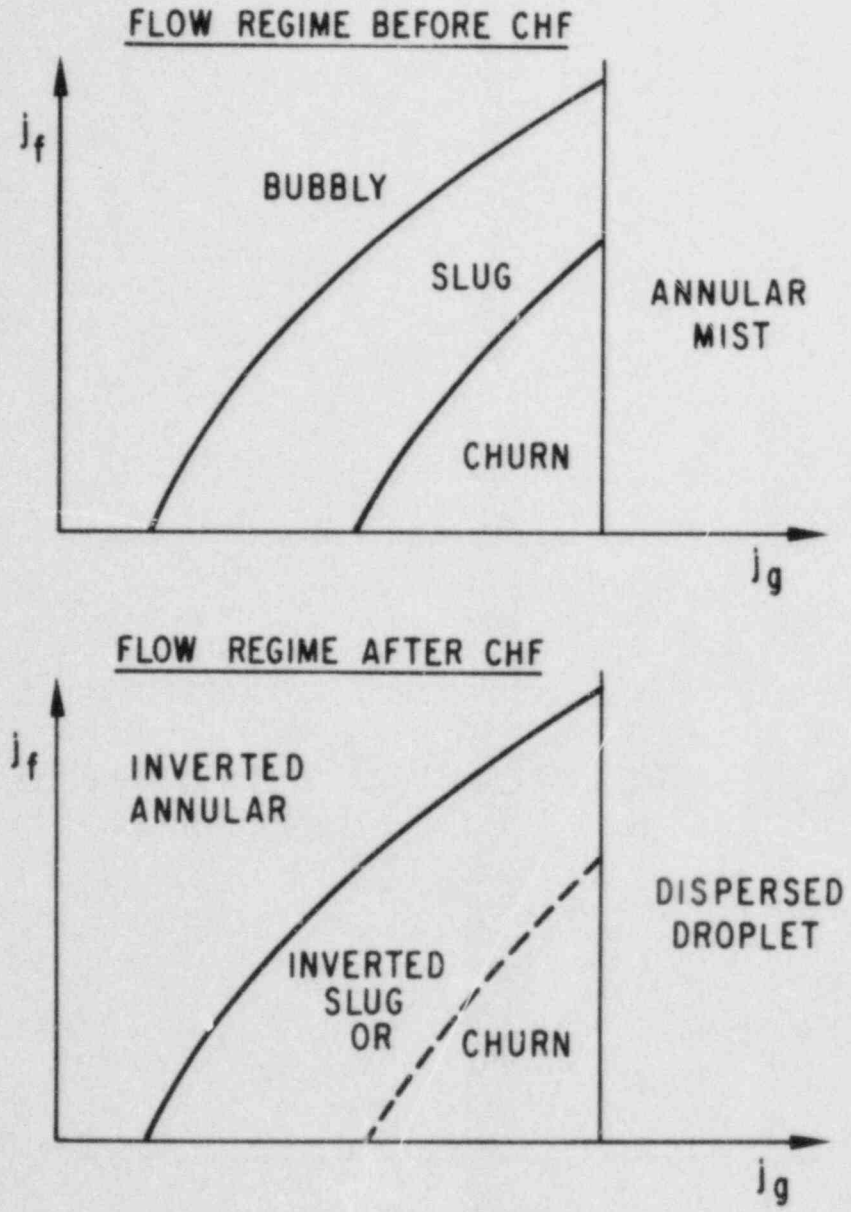


Fig. 3. Criteria for Initial Flow Regime at Dryout Point or Rewetting Front

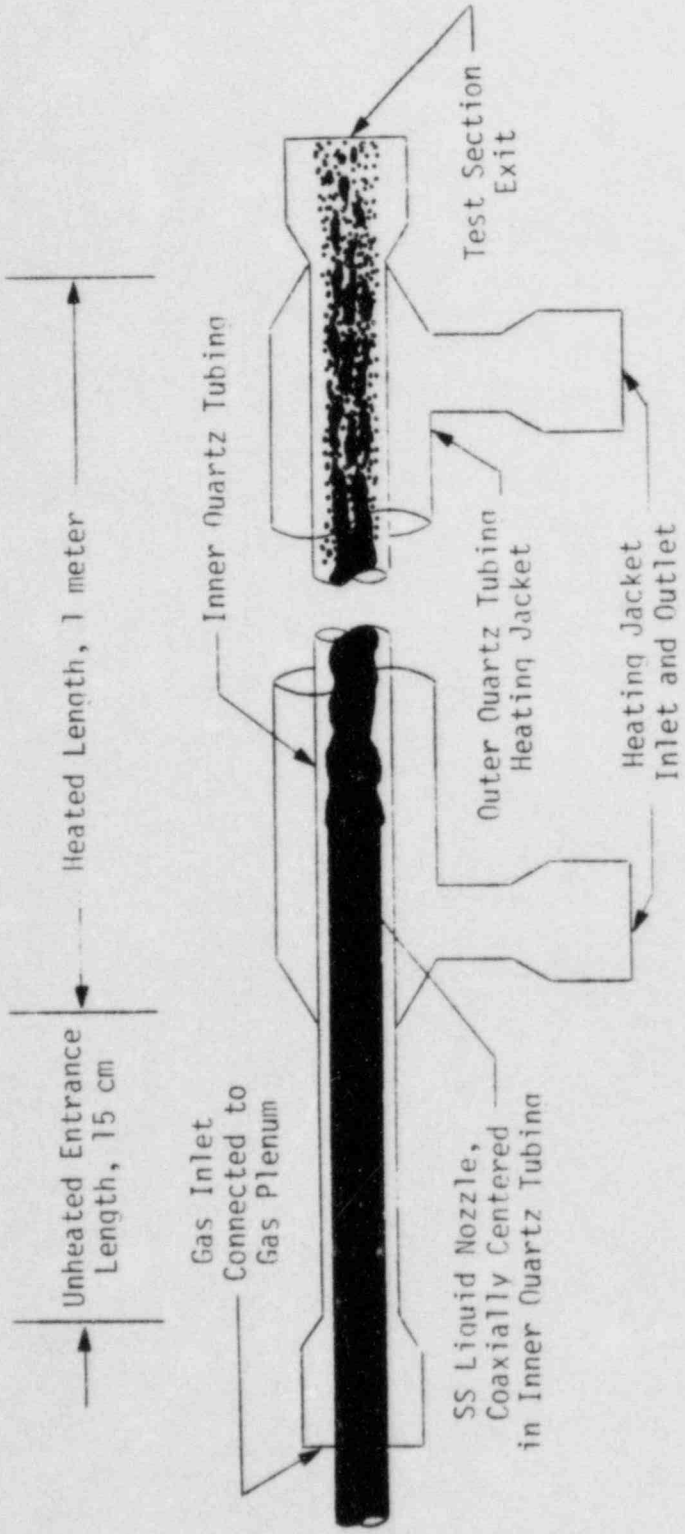


Fig. 4. Schematics of Test Section for Inverted Annular Flow Experiments

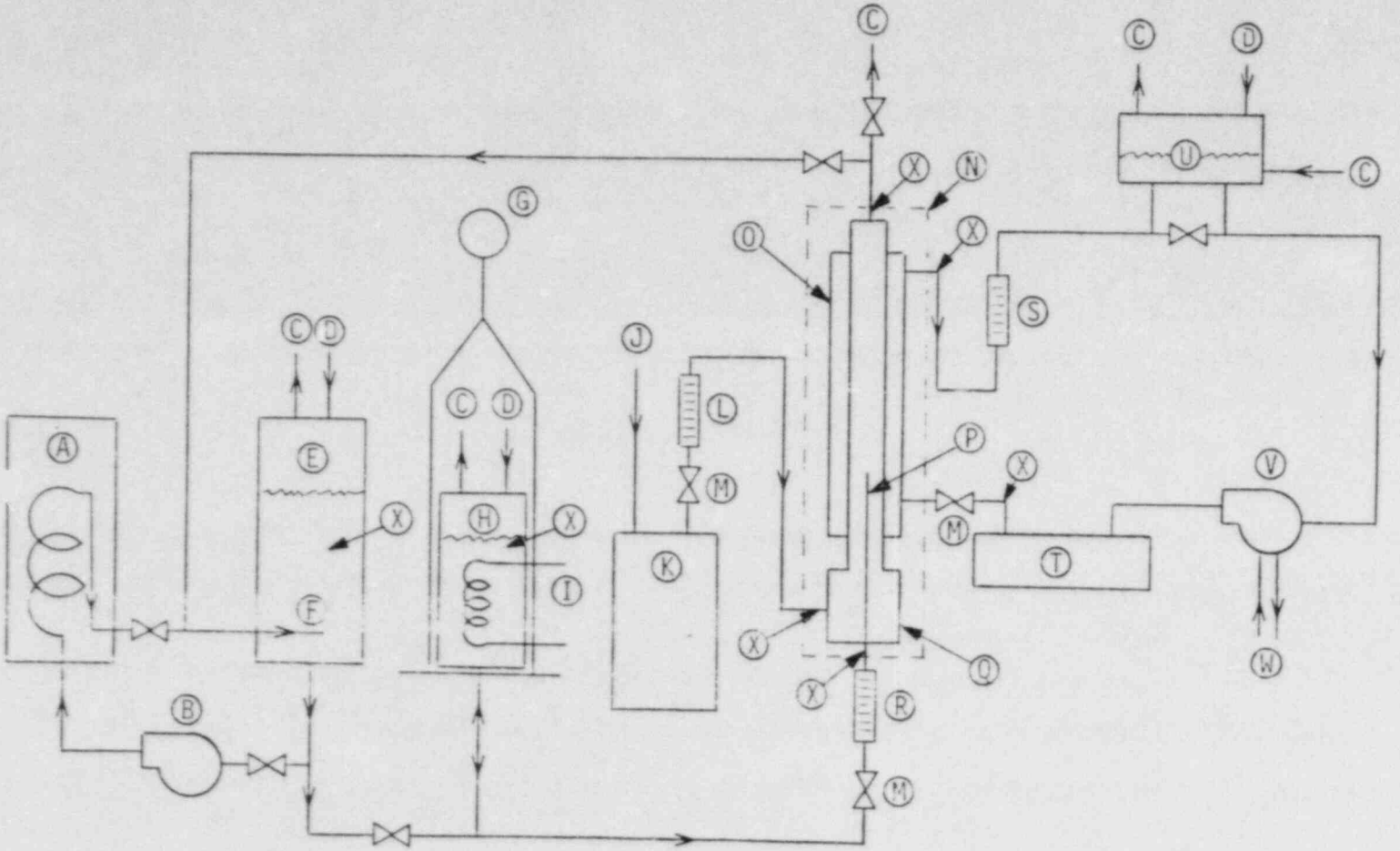

A Cold Sink Heat Exchanger
B Freon Pump
C Vent Lines
D $N_2$, He Blanket/Purge
E Freon Dump Tank
F Bubbly Mixing Nozzle
G Load Cell, $N_2$ Flowrate
H Freon, $N_2$ Delivery Tank
I De-gassing Heater
J Gas Supply, Pressure Regulator
K Gas Accumulator
L Gas Flowmeter
M Throttling Valves
N Test Section
O Heating Jacket
P Liquid Nozzle
Q Gas Plenum
R Freon Flowmeter
S Heating Fluid Flowmeter
T Circulation Heater
U Expasion Tank
V Heating Fluid Pump
W Pump Seal Cooling
X Thermocouple

Fig. 5. Schematics of Inverted Annular Flow Experiment Loop

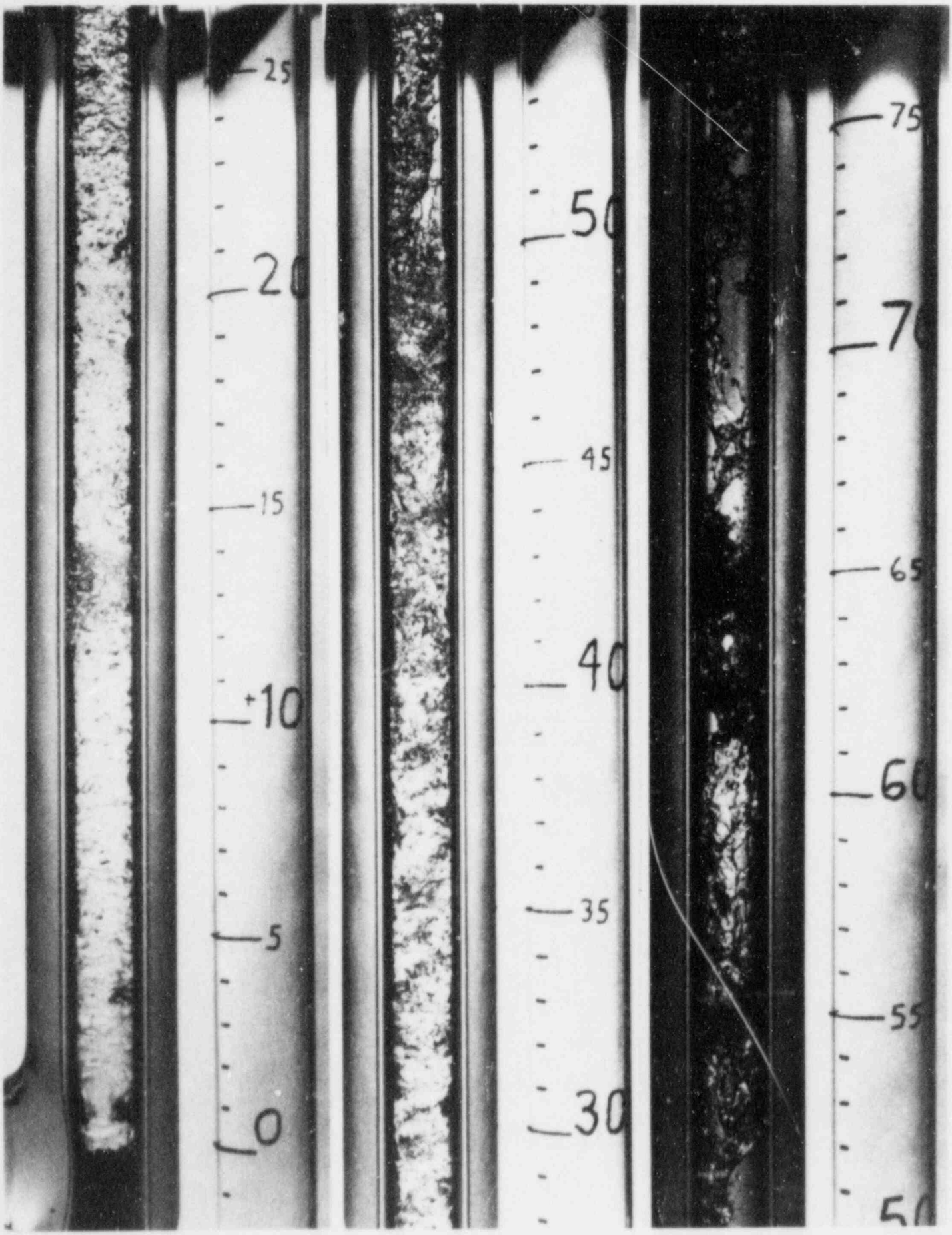


Fig. 6. Photograph of Inverted Annular Flow with Inlet Conditions of $v_J$ = 16 cm/s, $v_G$ = 1.9 cm/s, $D_J$ = 1.08 cm, $\alpha$ = 0.37 and Freon-113 Temperature = 27°C

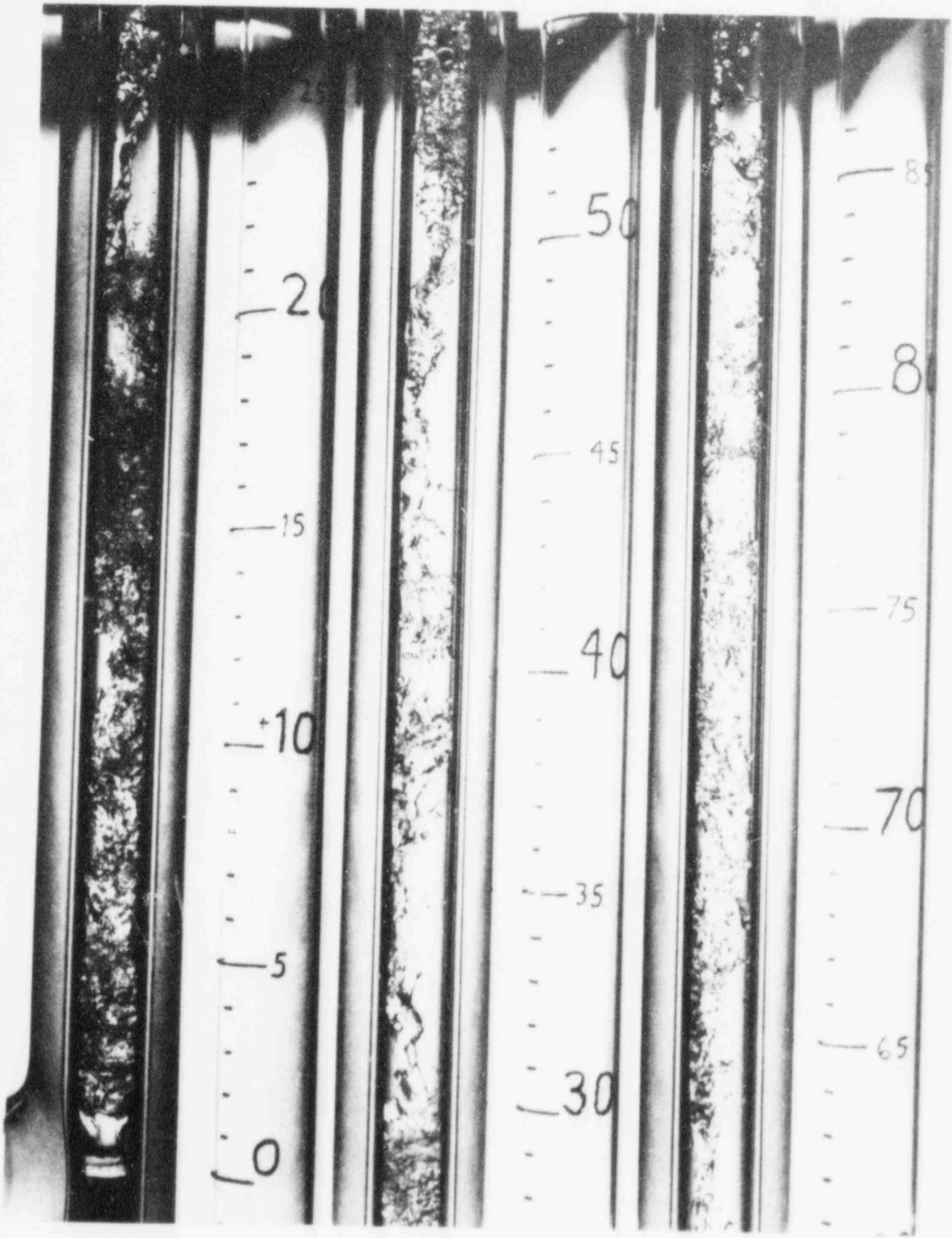


Fig. 7. Photograph of Inverted Annular Flow with Inlet Conditions of $v_J$ = 16 cm/s, $v_G$ = 68 cm/s, $D_J$ = 1.08 cm, $\alpha$ = 0.37 and Freon-113 Temperature = 27°C

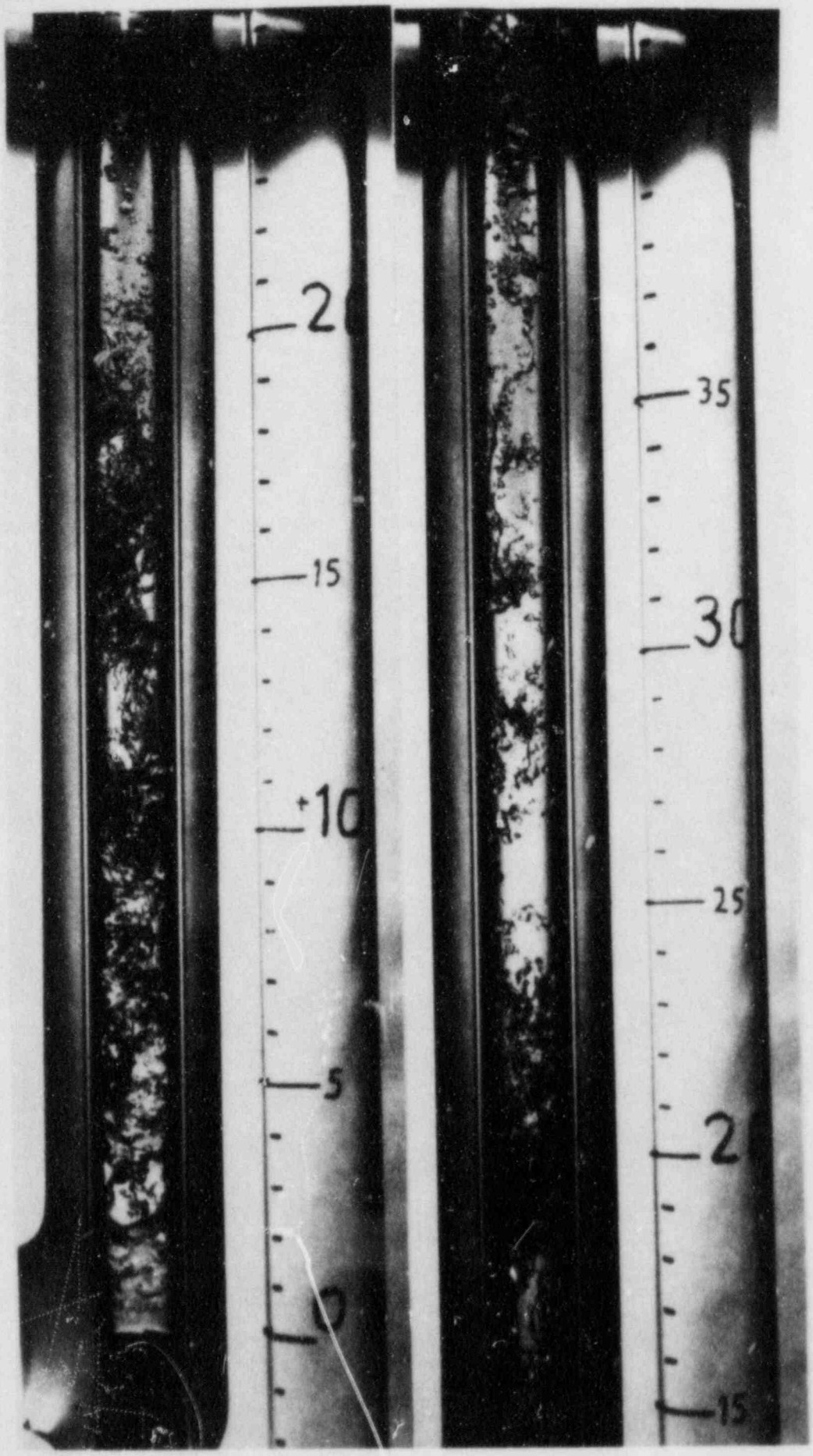


Fig. 8. Photograph of Inverted Annular Flow with Inlet Conditions of $v_j$ = 3.2 cm/s, $v_G$ = 4.6 cm/s, $D_j$ = 1.08 cm, $\alpha$ = 0.37 and Freon-113 Temperature = 37°C

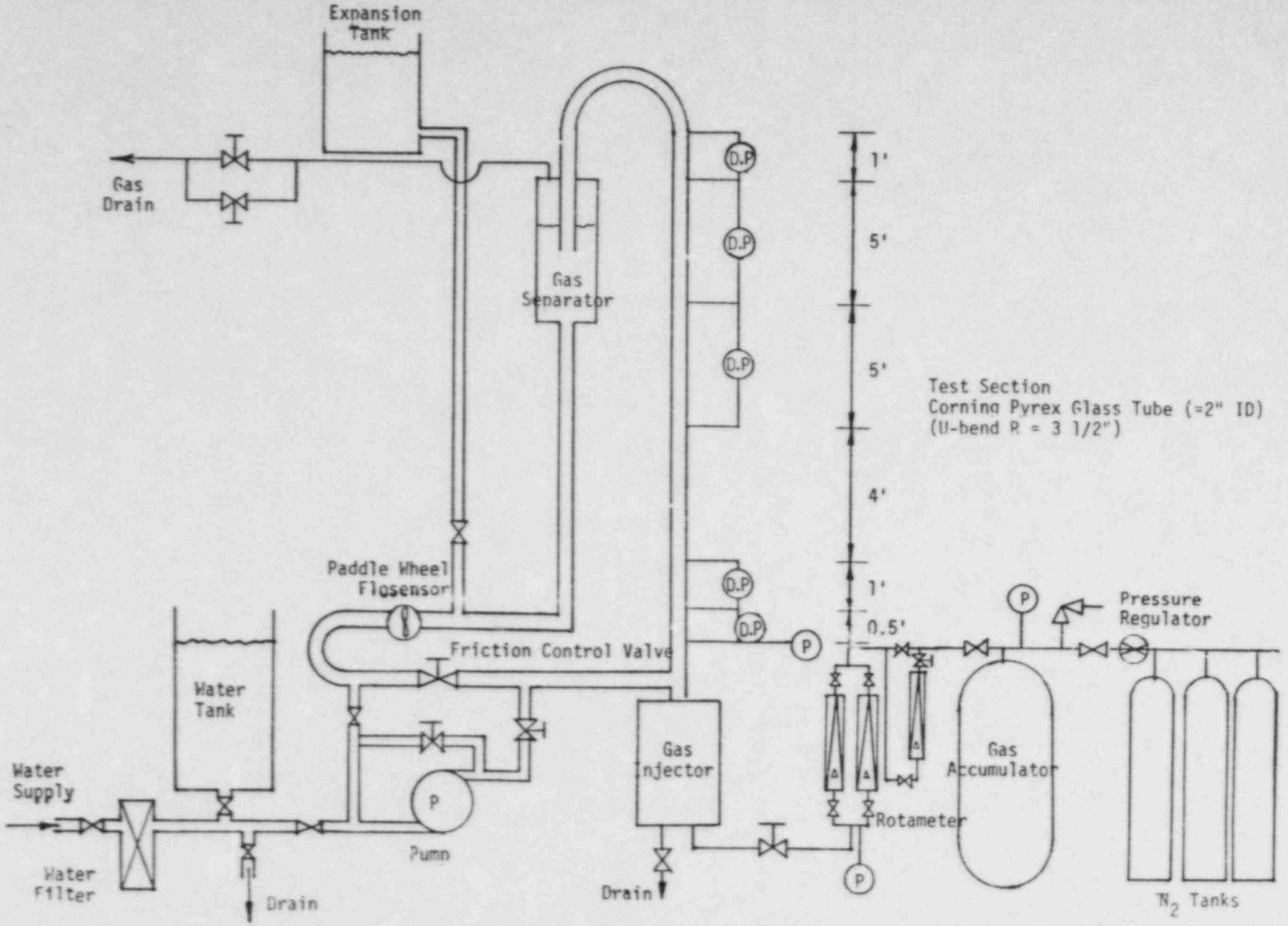


Fig. 9. Overall Loop Schematics of Hot Leg U-bend Simulation Experiment

# Steam Generator Carryover and Fallback

Lih-Yih Liao
Alex Parlos
Research Assistants, NE
and
Peter Griffith
Professor of ME
MIT

## Abstract

Preliminary results from a small, simulated steam generator for the carryover and fallback from a steam generator secondary during a main steam live or feed line break are presented. The drift flux model constants which best calculate the carry over or fall back are presented. A direct measurement for carryover using a weigh tank that quenches and traps the blowoff fluid is described.

INTRODUCTION

A steam line or feed line break and the resulting depressurization and increased heat transfer on the steam generator secondary side may lead to pressurized thermal shock. As a part of the effort mounted to resolve this issue, a research program has been set up in M.I.T. The objective of this program is to model and measure the carryover, fall back and heat transfer on the secondary side of a steam generator so that realistic estimates of the steam generator thermal-hydraulic behavior can be made and appropriate strategies for handling the transients identified. Carryover is also significant when a steam generator tube ruptures and high water on the secondary side causes liquid to be released out the relief valve.

To help study the processes on the secondary more easily, the secondary side of steam generator is decoupled from the primary side in these experiments. In other words, the behavior of the steam generator secondary side is studied without confusing heat transfer and fluid mechanics on the primary. The only heat transfer is due to the heat capacity of the metal. A best estimate computer code is being developed to help understand what is happening. It is expected that these experimental results will provide useful information for understanding a variety of transients and, in combination with the results from the analysis will lead to useful for making recommendations for modeling the thermal-hydraulic behavior of steam generators. Because of the similarity of the processes occuring in this experiment with these occuring in other transients, this study

will also contribute to understanding in the following areas: (1) radiation transportation in the steam line break and steam generator tube rupture accident (2) the impact of the break flow on the containment and in containment components and (3) BWR blowdown.

In this paper we shall describe the experiments, present a sample of the results for the fallback, the variation of the water level and the break flow. We shall close with a review of our plans for the remainder of the program.

Experiment

The steam generator simulator, shown in Figure 1, is only an approximate model of a PWR steam generator. Its overall dimensions are 10 ft. high by 4 in. diameter. It consists of the following elements:

* Outer Shell
* Downcomer
* Tube Bundle (to be added)
* Separators (to be added)
* Blowdown section and Supression Pool
* Suppression pool

The goal of this first phase of experiments is to establish a data base of liquid carryover as a function of break size for the range of conditions expected in a steam line break. Variations due to changes in the initial pressure, the initial inventory, and the steam generator internals will all be

examined.

A load cell mounted on a counterbalanced supression tank is used to measure the liquid carryover directly. It allows continuous and accurate (after the starting transient has died out) recording of this quantity as a function of time. The system pressure and temperature is also recorded as the transient proceeds.

The procedure used in these tests is to fill up the vessel with approximately 11 gallons of water and heat up the system. During the heat up, the vessel is vented for about 10 min. so that any air trapped in the water or in the space above the water can escape. Then the system is sealed and brought up to pressure (Max. 1050 psi). After the system pressure is stabilized at the desired value, the electric heaters are turned-off, the recording is started and the blowdown is initiated. The scanning interval was set at 10 msec., due to the very fast nature of the transient. This, however, can be adjusted for slower transients.

To investigate the effects of a downcomer, different tests were performed with the downcomer valve open or closed with an initial temperature difference of 20°F between the main vessel and downcomer. Each of these tests was performed for the five different simulated break sizes of 1/2", 3/8", 1/4", 1/8" and 1/16". For this vessel, this range of break sizes simulates the range of steam velocities at the pool surface that are of interest in steam line and feed line breaks.

In the near future, we shall use surpression pool temperature measurements to determine the amount (and rate) of

energy removed from the blowdown vessel as a function of time. Both the blowdown quality and the blowdown mass flow rates will then be measured directly.

Analysis

A fast calculating computer code using almost no iteration has been developed for the thermal hydraulic analysis in the steam generator secondary side. Prediction of the pressure, the blowdown mass and energy, the mixture water level, the void fraction distribution, the local superficial vapor and liquid velocities and the local heat transfer from walls of steam generator have been made. In all these analysis, emphasis has been put on developing an understanding of the thermal hydraulic phenomena and physical models as well as trying to make accurate predictions.

In our model, only two conservation equations are used, namely the mixture mass equation and the mixture energy equation. The momentum equation is left out because we believe that detailed pressure distribution in a large vessel is not important during the blowdown process. Fauske's two phase, critical flow model serves as the boundary condition at the top of the vessel for the calculation of the flow rate throughout the vessel. The transient two phase flow is assumed to be in equilibrium but not homogeneous. The difference between liquid phase velocity and vapor phase velocity is taken into account by the drift flux model. The constants in the drift flux model are flow regime dependent. The mixture water level is tracked by Wulff's model

and by the model used in the TRAC code. Flow regime transition criteria, water level reappearance criteria and a metal heat conduction model are also included in the code. For geometrical modeling, the test section is divided into several control volumes. The unknown mass and energy in each control volume is solved by use of a finite difference method.

When this model is applied to the mixture water level calculation (for an empty vessel), we find that the water level response is very sensitive to the drift flux model constants, therefore, an investigation into the drift flux constant has been made. The comparison of various mean drift velocities, $V_{gj}$, as function of void fraction at pressure of 300 psi, for example, are shown in Fig. 2. The legend for all the curves, except curve 5 are listed in Table 1.

Table 1. Legend for Curves in Figure 2

| Curve Number | Description |
|---|---|
| 2 | Wallis' model for bubbly flow |
| 3, 6, 7 | Ishii's (1) model for churn-turbulent flow, annular flow and liquid dispersed flow respectively |
| 4 | Zuber's model for churn-turbulent flow |
| 8 | Reformulation of Wilson's (2) bubble rise velocity |
| 9 | For slug flow regime |

Curve 5 originates from Zuber's report. He points out that mean

drift velocity may be strong function of pressure and proposes a form of mean drift velocity, $V_{gj}$:

$$V_{gj} = K \left( \frac{\sigma g \, \Delta \rho}{\rho_g^2} \right)^{0.25} \qquad (1)$$

Following this approach, Debertodano (3) proposes K = 0.33 and this becomes curve 5. From the results in Fig. 2, it is observed:

1. The mean drift velocity is flow regime dependent.
2. The discrepancies between available models are large.

Various mean drift velocities in Fig. 2 accompanied by the void and flow distribution parameter $C_o$ given by Ishii's (1) model has been used to calculate water level response for GE blowdown test no. 5801-15 (4). Reasonably good agreement between the prediction and the experimental data has been obtained by using the mean drift velocity proposed by Debertodano. Because the pressure range of GE blowdown test is the same as that of steam line break, it is recommended to use the mean drift velocity proposed by Debertodano as a first trial estimation when there is no other available information. These recommendations may have to be altered when some internals are put into the vessel.

By applying the above mentioned drift flux model constants, a typical mixture water level response in our test section can be calculated and is presented in Fig. 3. Initially, there is a

distinct water level in the vessel. When the transient begins, the mixture water level rises quickly due to flashing. Wulff's (5) model is used to track water level response in this period. As the mixture level rises further, it may reach the top of the vessel and the two phase mixture level disappears. This condition will be maintained until the phase separation becomes apparent, due to gravity, and then mixture level reappears. After the mixture level reappears, the water level tracking model in TRAC code is used to calculate the mixture water level. In a real steam generator, the process may be somewhat different. There is no distinct water level when it is operating at design conditions in steady state but the processes for later periods in the transient are similar.

During blowdown, liquid droplets will be entrained in the space above the mixture level. We are also interested in knowing whether this entrainment is important for modeling the system transient response for a MSLB or FLB transients. Specifically, we are interested in the effect of entrainment above the pool on the total amount of water carried out and on water level propagation during blowdown. It is noted that entrainment from a sharp water-vapor interface in a large diameter tube is similar to pool entrainment. According to Ishii (6), there are three different regions in terms of entrainment above a bubbling pool, i.e., the near surface, the momentum controlled and the deposition controlled regions. By applying Ishii's model to our test section with typical blowdown vapor velocities, it is found that beyond a certain height above the mixture level, (that being

in the deposition controlled region), the entrainment is essentially negligible. Therefore, there is little or no carryover due to entrainment when there is a large distance between the mixture level and the break. It is also clear that there is no entrainment as such when the mixture level disappears. Therefore, it is only the period when the mixture level is close to the break but not high enough to reach it where pool entrainment has any effect on the break flow rate. The fact that this period is short results in almost identical values for the total amount of liquid carried out for the cases when there is no entrainment in the calculation and when there is entrainment. This is shown in Fig. 4. The effect of entrainment on the water level response is very small because the large liquid to vapor density rates makes the entrained liquid volumtric flow rate negligible at the mixture level.

Fig. 5 shows the comparison between the calculated total amount of outgoing fluid and the experimental data. It should be noted that the analytical result which includes the effect of heat addition from the wall yields good results while a large discrepancy exists between the adiabatic analytical result and the experimental data. It is concluded that the effect of heat transfer is quite important to the blowdown process in the steam generator secondary side. Although this conclusion is drawn from our experiment, we expect the heat transfer effect in a real steam generator will be more rather than to be less important for much more heat transfer area is provided by the huge number of tubes.

## Conclusions

This program has provided some insight into the thermal hydraulic phenomena occurring in the steam generator secondary side during blowdown. It has been found that the mixture water level may disappear during blowdown and reappear some time later. The heat transfer from vessel wall can be very important to the blowdown process. Various drift flux models has been studied and a large discrepancy has been found for currently available drift flux model constants. These discrepancies have a large effect on the water level prediction. The pool entrainment phenomena, on the contrary, has only a small effect on both total amount of outgoing fluid and the transient water level response. Finally, it should be pointed out that although our model is very simple, it does reproduced the experimental results quite well.

## Plans

The next task in the experiments involves using a temperature measurement in the supression tank to determine energy flows out the break and using pressure difference measurements in the bundle to determine void. The dryout front propagation measurement will also be measured. These measurements will be performed after the installation of the internals (simulated steam generator tubes). The existing range of break sizes will be used to complete a test matrix. In parallel with the experimental work, model development will be continued. After the installation of internals, the geometry becomes much more complex. The flow area may expand or contract

following the flow path. The tube support plate may serve as a barrier for downflowing liquid and very likely flooding will occur in the gap between the tube support plate and the simulated tubes. Consequently, multiple water levels may appear during the latter part of blowdown. This is a problem to be solved in future model developement. We also realize that the dryout front is different from the mixture level. The relationship between these two parameters and the importance of this difference is yet to be established.

The behavior of the separators on the top of PWR steam generators is unknown during a steam line break or combined steam line break plus tube rupture. When a steam line break occurs, the changes from normal operating conditions can cause the flow direction in the separator drain line to reverse so that liquid will have no place to go but up and out the main steam line. For a tube rupture plus steam line break accident, where almost all the radiation released is in the form of iodine, the separation efficiency over the entire range of operation can be an important factor in determining the amount of iodine released. How the separator will perform under those circumstances is not clear at this time.

The goal of the separator program is to develop a method of predicting how the separator will perform under these off-design conditions and to provide modeling instructions that can be adapted to any PWR separator. For this reason, we will start by building a generic separator and then map the separator performance showing the region where the drain is flowing up, and

where it is flowing down. Then, the performance of the separator for each region on the map will be related to the fluid properties and separator geometry. At all times, the effort will be on developing a simple, physically based generic steam separator model that can be incorporated into a system code such as TRAC or RELAP-5.

Reference


1. M. Ishii, "One Dimensional Drift Flux Model and Constitute Equations for Relative Motion Between Phases in Various Two-Phase Flow Regimes", ANL-77-47, October, 1977.

2. J.F. Wilson, R.J. Grenda, J.F. Patterson, "Steam Volume Fraction in a Bubbling Two-Phase Mixture", Trans. ANS 5 Ser. 25, 151 (1962).

3. M.A.L. de Bertodano, "Fast Computational Methods for Two Phase Flow Situations in Pressurized Water Reactors", Nuclear Engineering Thesis, Jan. 1983.

4. J.A. Findlay, "BWR Refill-Reflood Program Task 4.8 - Model Qualification Task Plan", NUREG/CR-1899, August 1981.

5. M.S. Plesset, "Transient Two-Phase Flow", Proceedings of the Third CSNI Specialist Meeting, Hemisphere Publishing Corporation, 1983.

6. M. Ishii, "Mechanistic Modeling and Correlations for Pool Entrainment Phenomenon" NUREG/CR-3304, April, 1983.

Figure 1 General View of Experimental Apparatus

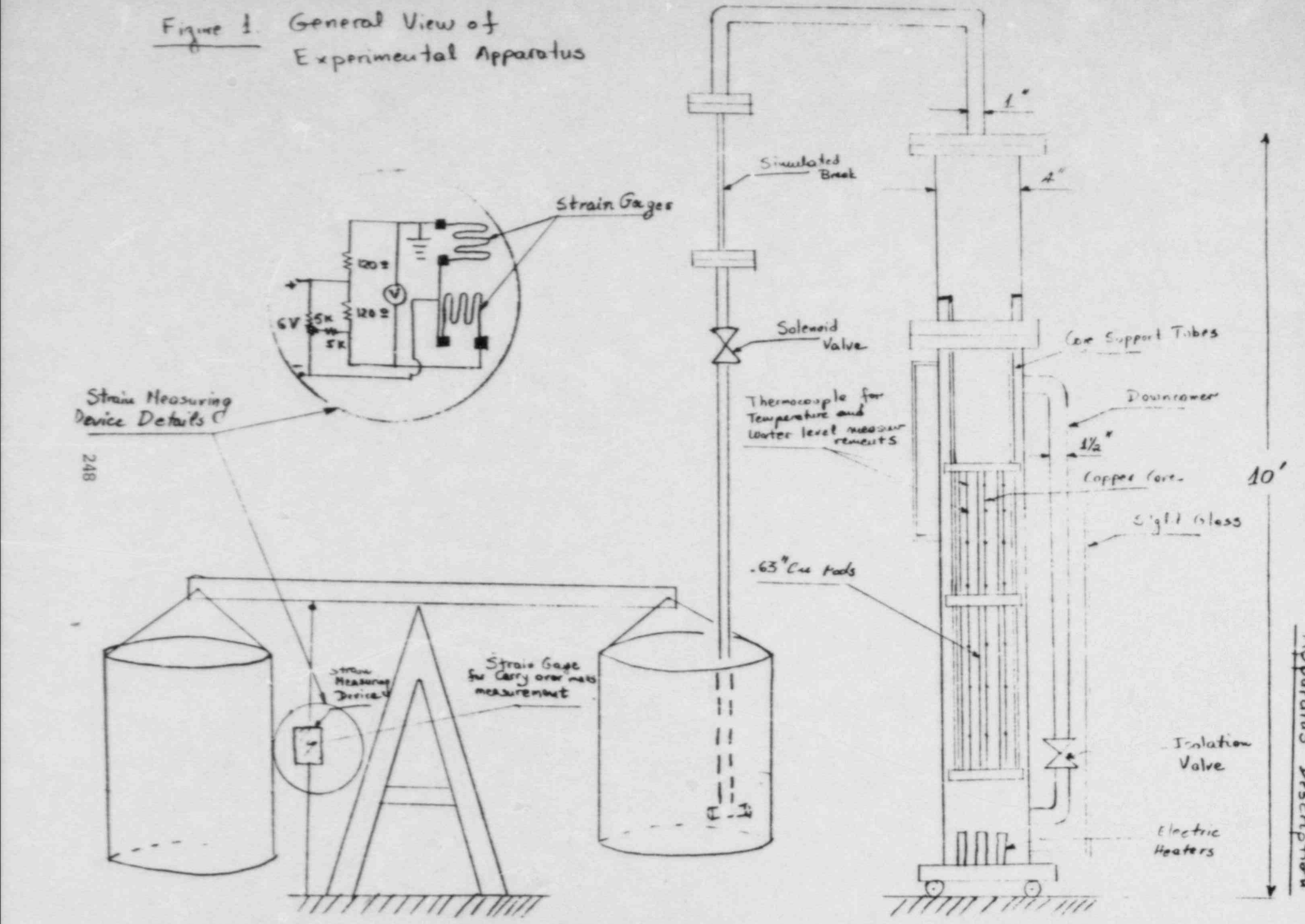

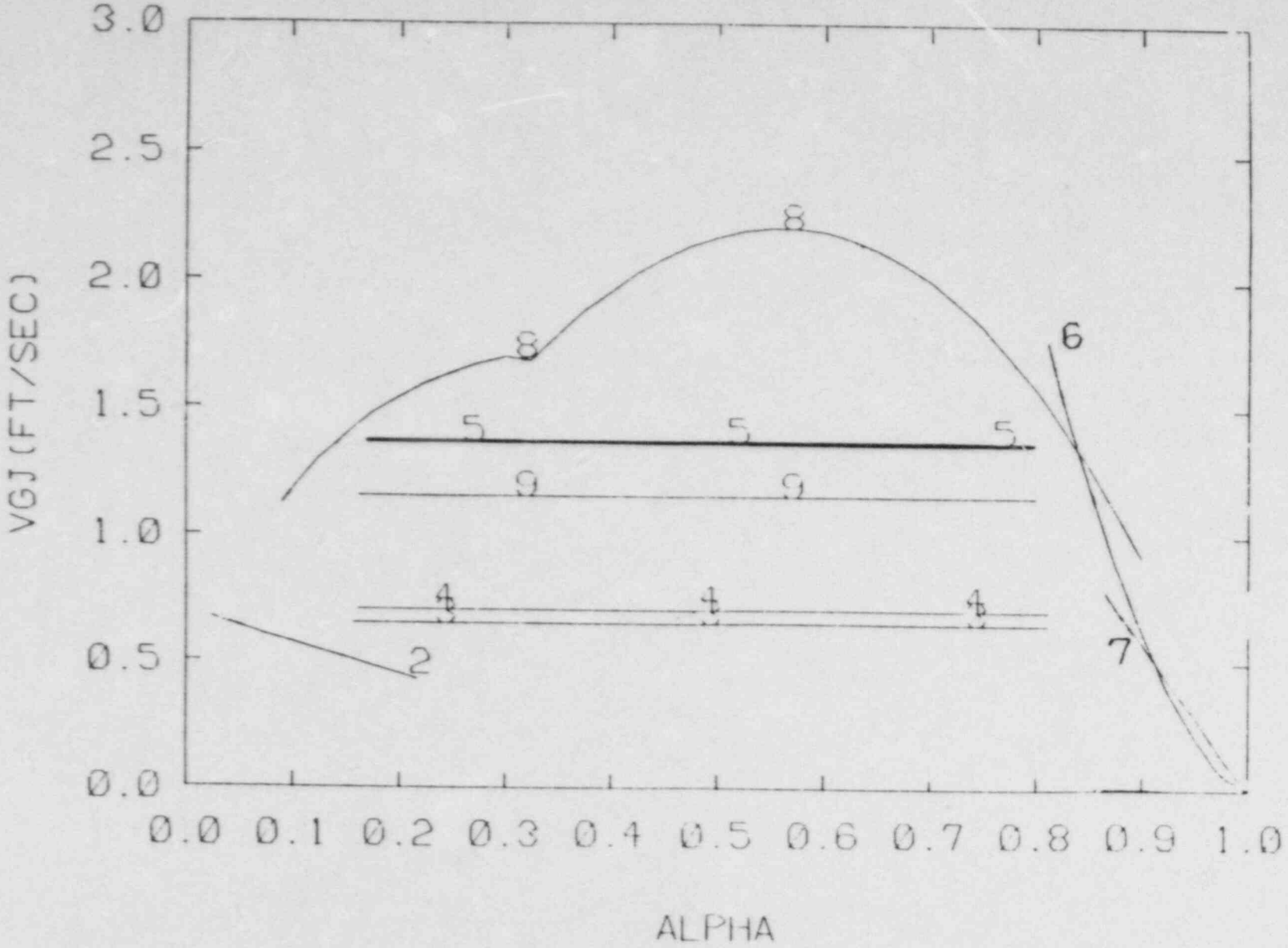


FIGURE 2. COMPARISON OF $V_{gj}$, p=300psi

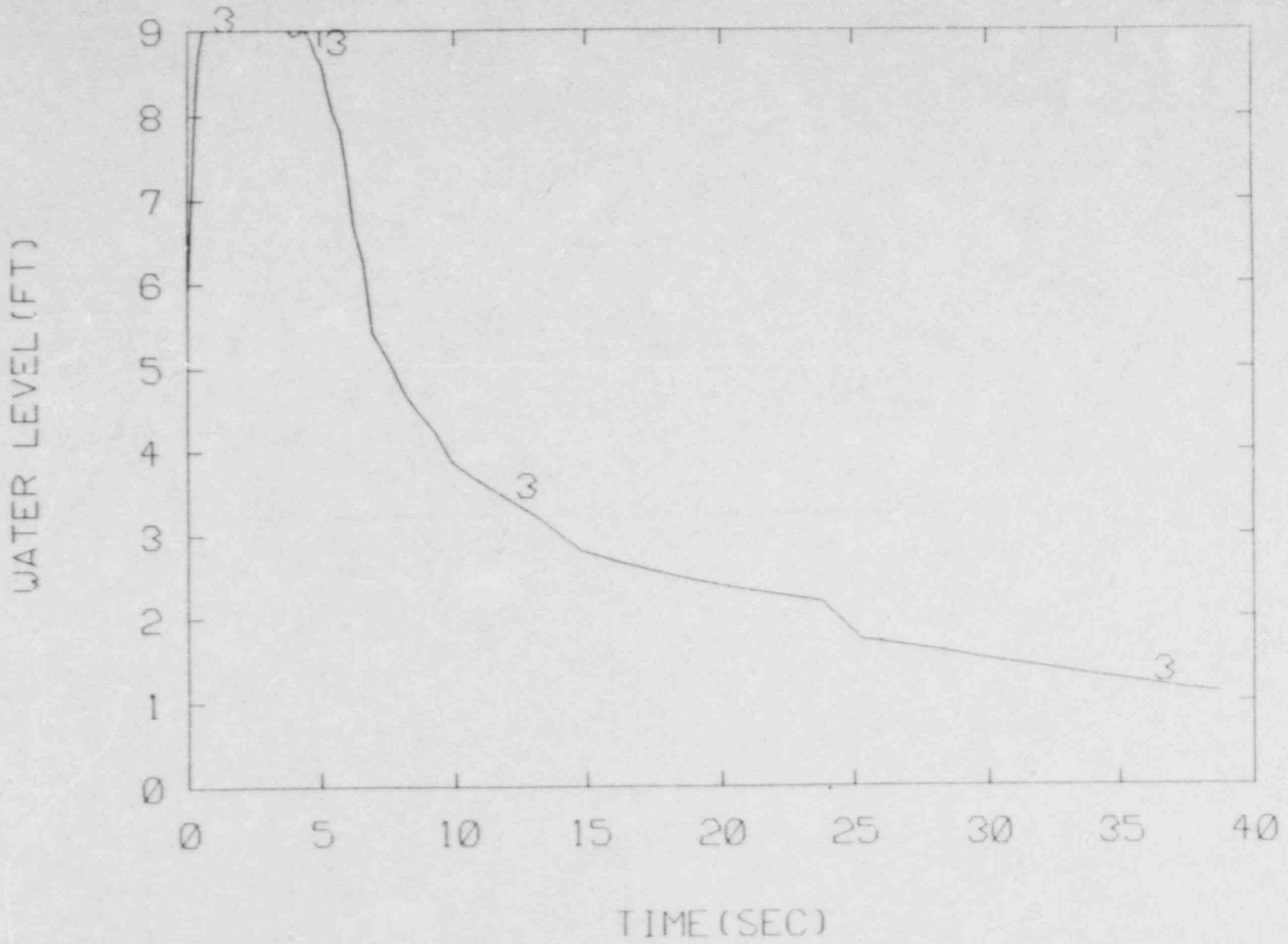


Figure 3. Water level response for 3/8" break, initial pressure = 1055psi.

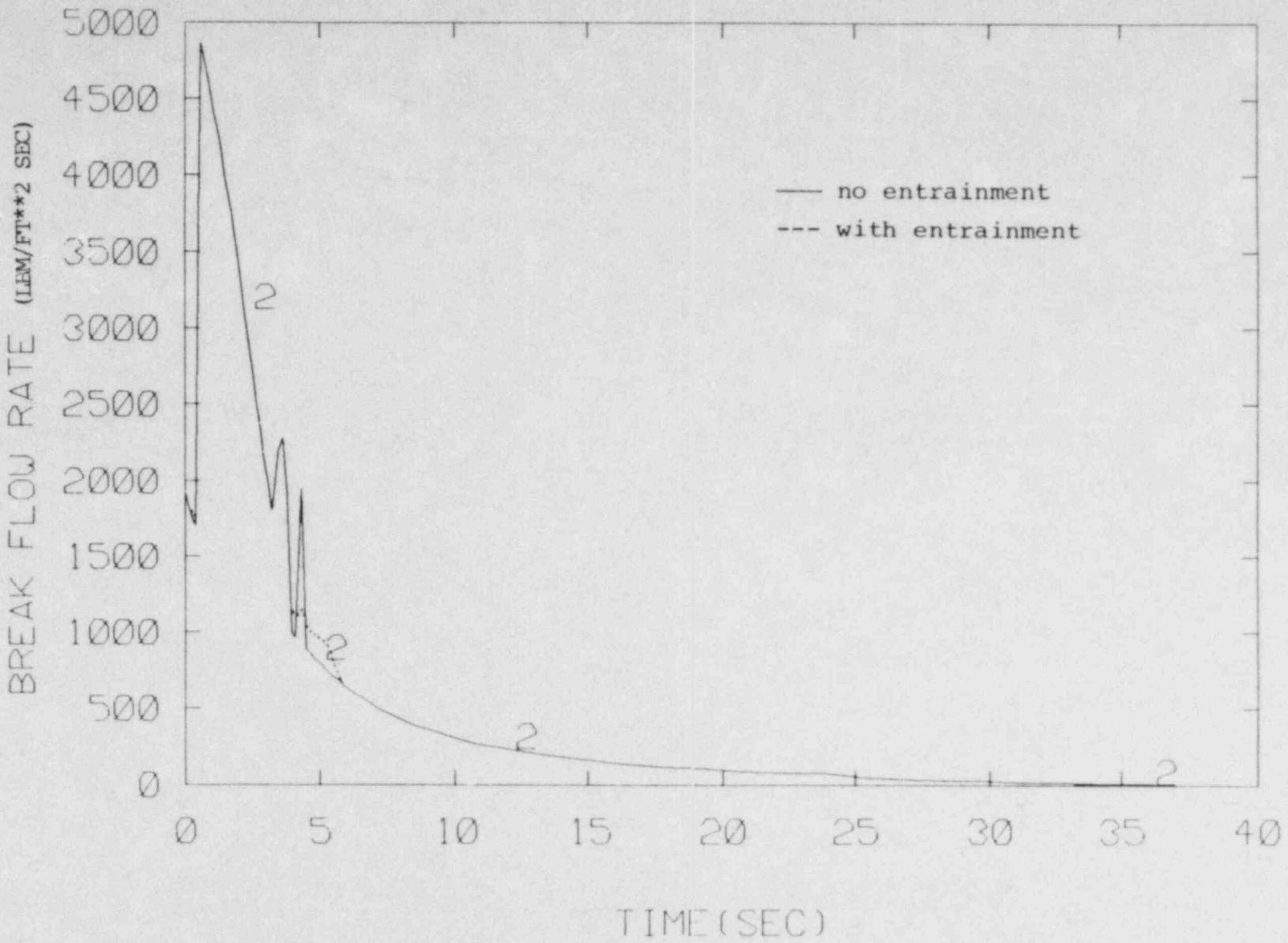


Figure 4. Break flow rate for 3/8" break, initial pressure = 1055psi.

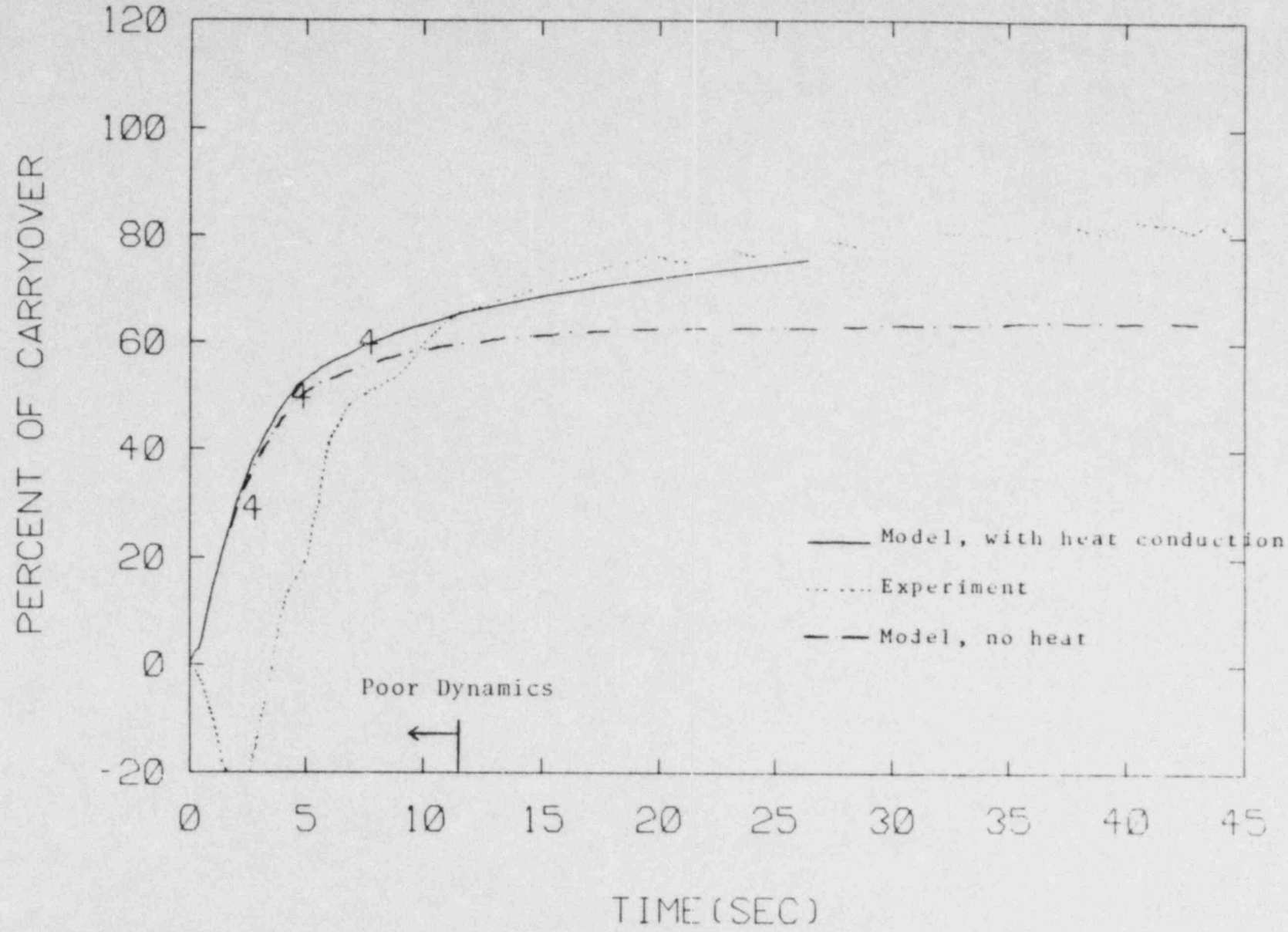


Figure 5. Comparison between the predicted and measured carryover for 3/8" break empty vessel test with initial pressure 1055psi.

# PWR PRESSURIZER MODELING

Peter Griffith
Professor of
Mechanical Engineering
MIT

## ABSTRACT

A non-equilibrium model for a PWR pressurizer is proposed. Heat and mass transfers occuring during various transients are examined and the most significant retained. A variety of transients are calculated and compared to data taken on a small low pressure pressurizer. Good comparisons between the data and the analysis are obtained.

The following conclusions can be drawn. The only significant heat transfer to the pool occurs during an insurge into an empty tank. Wall heat transfer is significant only during insurge transients when condensation occurs. Vapor is saturated virtually all the time. Liquid superheat is negligible. Heat transfer is practically instantaneous on spray. The pool is generally stratified.

INTRODUCTION - During several reactor transients such as small break LOCA's or overcooling transients, the commonly used equilibrium pressurizer models are not good enough to predict the behavior of the system in detail. They do not allow one to examine various accident handling alternatives in a realistic way. The equilibrium pressurizer models really give limiting answers which are unable to predict some of the trends found in the data. This paper reports the results of two years of work on pressurizer modeling performed at MIT and reported in detail in references [1], [2], [3] and [4]. Reference [1] particularly, contains all the details that one needs to develop a pressurizer model of one's own including a number of completely documented runs to which one can compare an analytical model. References [2], [3] and [4] are studies of various heat and mass transfer processes occuring in pressurizers which are also reported in references [5], [6] and [7] in brief form.

THE PRESSURIZER MODEL - The heart of the pressurizer model is the heat and mass balance which is performed on the bubble in the pressurizer. In order to calculate the course of a transient it is necessary to evaluate these heat and mass transfers. The control volumes which are used to do this one given in Figure (1) in which heat transfers are shown as dotted lines and mass transfers (condensation or evaporation) are shown as solid lines.

These assumptions are as follows:

1. All of each region is modeled as having a single value for each of the state variables describing it. That is

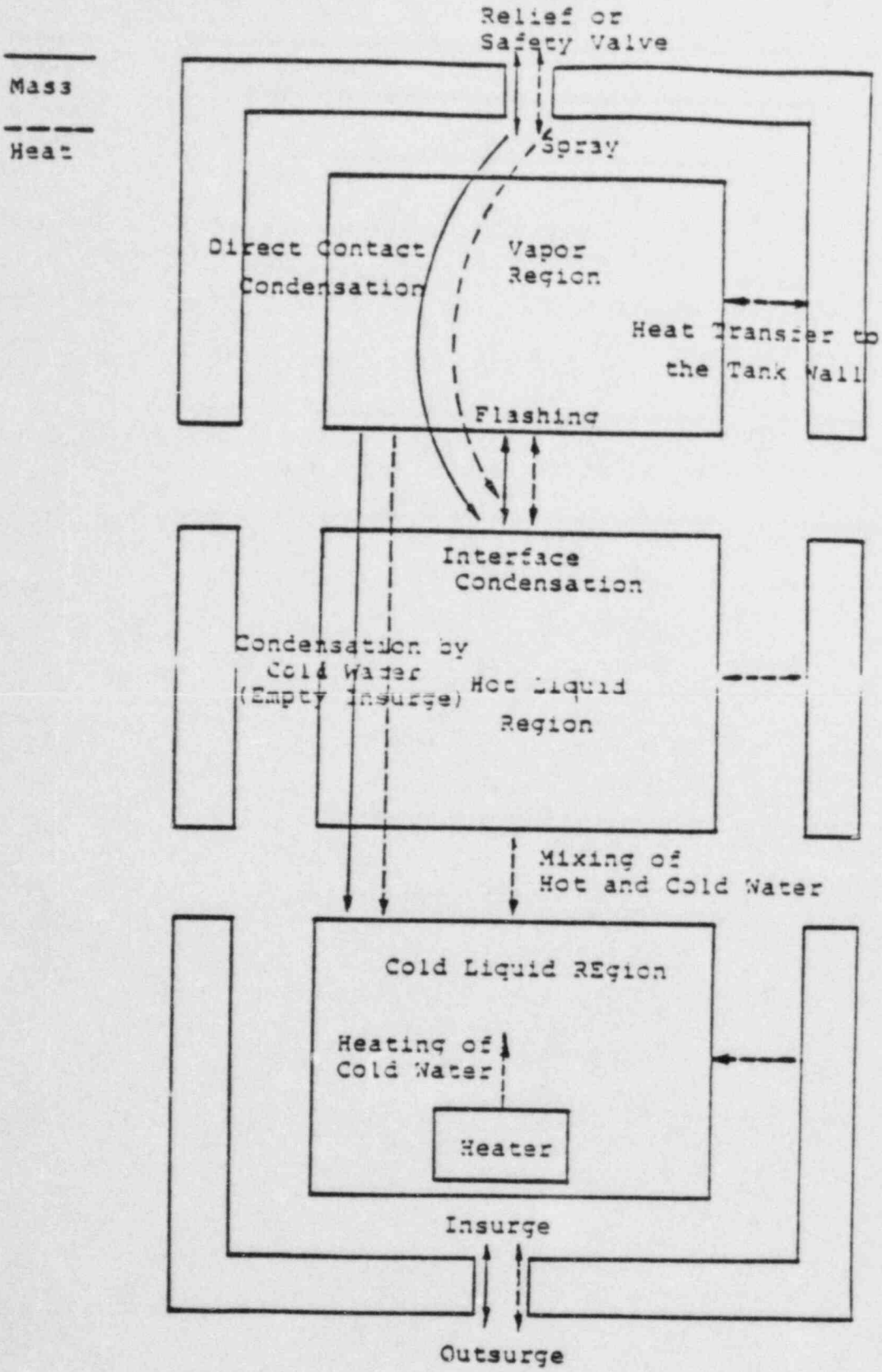


Figure 1. Control volumes constituting the pressurizer model. Heat and Mass transfers are evaluated from Table 1. Reference [1]

temperature and pressure. The variable for a wall slab is temperature.

2. The state of the vapor phase is always saturated (3).

3. All the condensate on the wall and rainout is assumed to be deposited on the top of the hot liquid immediately.

4. The condensing interface is saturated.

5. All the spray is assumed to be saturated as soon as it enters pressurizer (4), (5).

6. When the steam is expanding in an outsurge transient, the state of steam is always saturated (not subcooled).

The equations into which these assumptions are incorporated are as follows:

Mass Conservation Equation for an Open System.

$$\frac{d}{dt}\int_{c.v} \rho \, dV + \int_{c.s} \rho \, \vec{V}_r \cdot \vec{n} \, dS = 0 \tag{1}$$

Energy Equation

(Deformable Control Volume for an Open System)

$$Q - W = \frac{d}{dt}\int_{c.v} \rho \, e \, dV + \int_{c.s} \rho \, h \, \vec{V}_r \cdot \vec{n} \, dS + \int_{c.s} p \, \vec{V}_b \cdot \vec{n} \, dS \tag{2}$$

Equation of State.

$$h = e + p\,v \tag{3a}$$

$$V = M\,v = \text{Const.} \tag{3b}$$

$$v = v(p,H) \tag{3c}$$

The heat transfer on the right hand side of equation (2) is evaluated by means of the heat transfer matrix shown in Table 1.

The structure of the solution is as follows. The initial pressure, temperature, and mass of the bubble is known. The vapor is assumed to be saturated, the bubble internal energy is known. As a result of the various heat transfers some vapor is condensed or evaporated and, in general, the volume changes as a results of an insurge or outsurge. Because of these changes a new internal energy and bubble mass can be calculated. The bubble mass, internal energy and volume is sufficient to fix the pressure in the bubble and thus the pressure in the pressurizer.

The details of the actual calculation procedure chosen depend on the nature of the steam properties which are available to the user. For the results reported in reference [1], equations (1) and (2) were expanded into difference form and the saturation properties curve fix for convenient machine calculation.

EXPERIMENTS - The experiments were performed in a model stainless steel pressurizer, described in detail in references [1] and [4] and briefly in [5], [6] and [7]. The vessel was 45 inches high and 8 inches inside diameter. The walls were .5 inches thick. A schematic of the test apparatus is shown in Figure 2. Provision was made to admit steam, and hot or cold water into the vessel and record the pressure and various temperatures. The primary comparison between theory and experiment used the pressure-time trace.

TABLE 1

Summary of heat transfer calculation recommendations:

1) Heat transfer to the wall.

   a) If the wall below the liquid level and if $T_{wall}$ is less than $T_{saturation}$, then heat transfer occurs by natural convection.

   b) If the wall is below the liquid level and if $T_{wall}$ is greater than $T_{saturation}$ then the heat transfer coefficient is essentially infinite and wall conduction governs.

   c) If the wall is above the liquid level and if $T_{wall}$ is less than $T_{saturation}$ then film condensation occurs.

   d) If the wall is above the liquid level and if $T_{wall}$ is above the saturation temperature heat transfer occurs by natural convection to the vapor.

2) Interface heat transfer - Use Figure 5

3) Spray - heat transfer is instantaneous

4) Flashing in the bulk - Occurs with 1°F superheat

5) Heater should be modeled as a first order system with a time constant of about 1 minute.

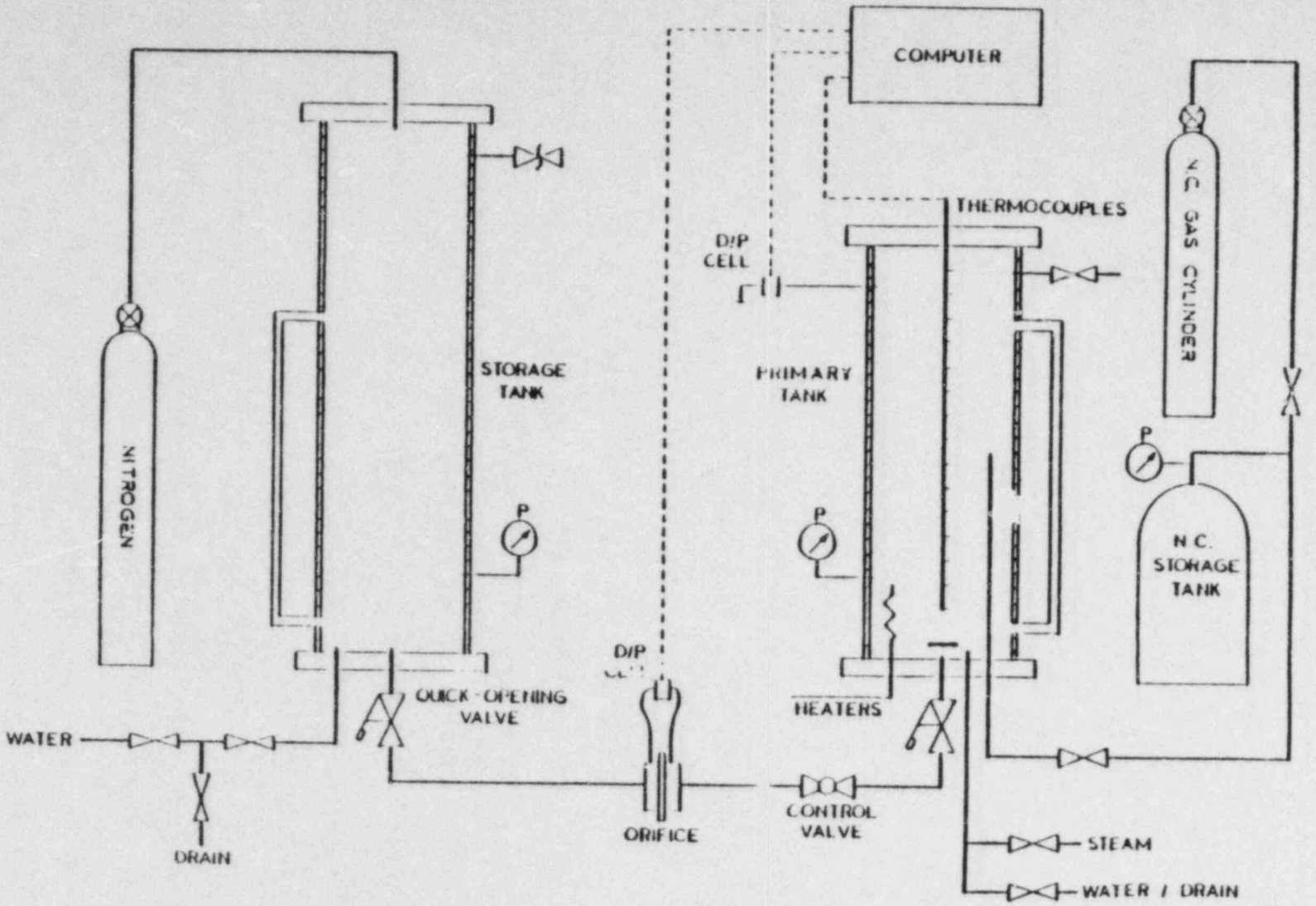


Figure 2. Apparatus in which transidnts were run. References [1 thru 7].

A variety of experiments were run including insurges and outsurges. References [1] and [4] report a variety of runs completely including temperature-time for various locations on the wall and in the pool and vapor space. These runs are useful for testing any pressurizer model that an analyst might construct.

The pressure-time plot for one of the more complex transients is shown on Figure 3 along with the calculation for the insurge portion of the transient. This transient was as follows. The system was brought to a uniform temperature by the heaters in the bottom. That temperature was the saturation temperature for 113 psia. The tank was then vented and the pressure dropped to about 85 psia. The wall remained close to the saturation temperature for 113 psia. After the pool settled down, an insurge of cold liquid occurred compressing the bubble and the pressure increased. Wall condensation did not occur, however, until the pressure got up close to the original saturation pressure and the walls were subcooled with respect to the steam. Then condensation occurred and the rate of pressure rise decreases. After the insurge ceases, the pressure drops slightly while the wall comes to a uniform temperature which is equal to the saturation temperature of the steam. Initial conditions, insurge flow rates and a variety of temperature traces for this run are presented in reference [1].

Pool heat transfer is negligible for this run. The hot water stayed practically unmixed on the top of the cold liquid that surged in. Wall heat transfer was negligible until condensation

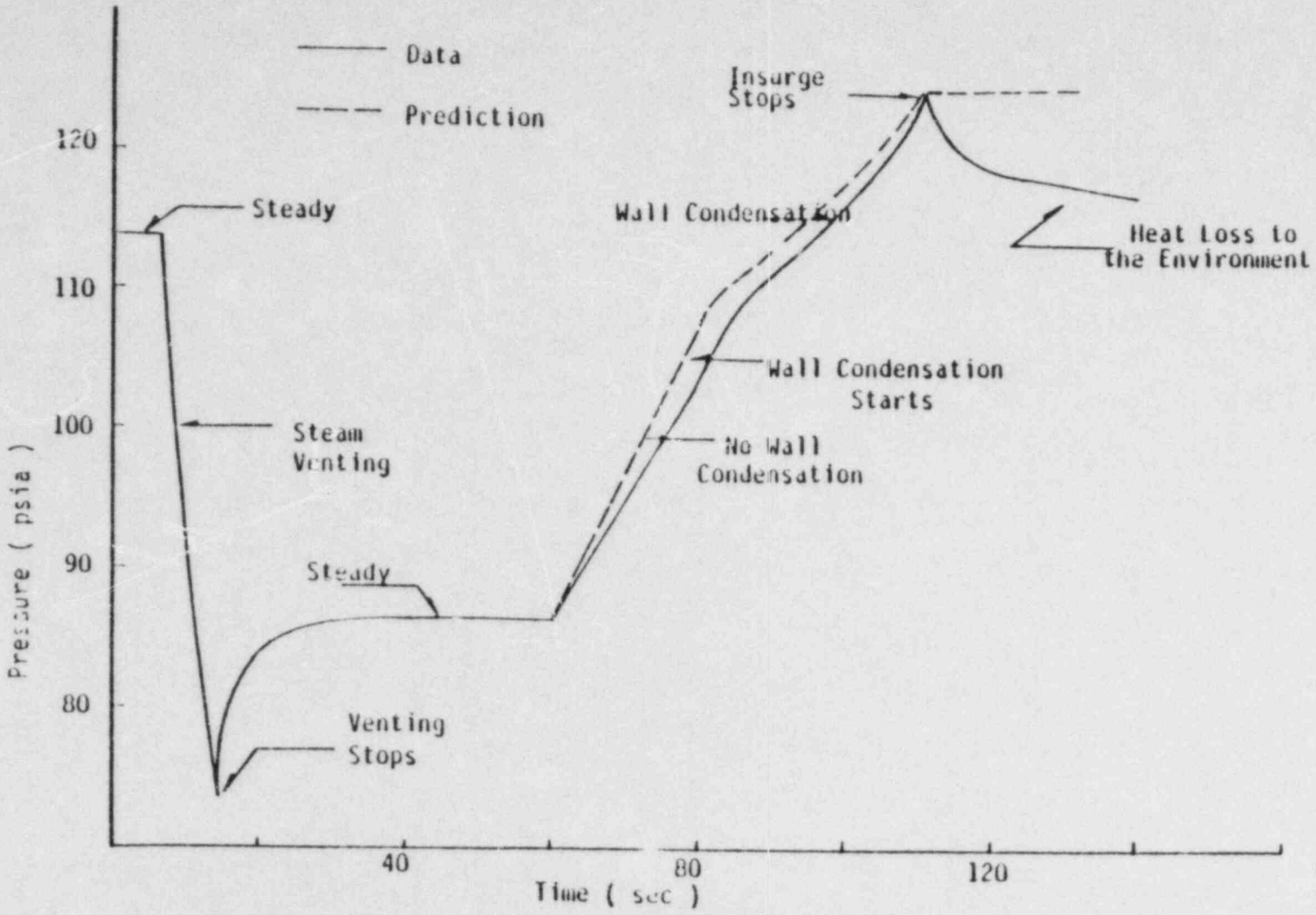


Figure 3. Pressure time as measured fora a transient in which the sequence of events is venting, soaking, insurge and soaking. Reference [1].

could occur at which point the rate of pressure increase decreased. All other heat transfers were negligible.

In a full sized pressurizer at operating pressure the effects of heat transfer are less dramatic, primarily because the heat capacity of the vapor is much more. Figure 4 shows the effect of various heat transfers for an insurge run performed at Connecticut Yankee. Spray heat transfer is excellent and wall heat transfer is barely perceptable. All other heat transfers are negligible.

Because the subcooling of the insurge water can be significant, pool heat transfer is a major concern. Reference [3] reports the heat transfer on a pool for various inlet distributor geometries. If these measurements are used to calculate pool heat transfer , except for an empty tank insurge, the pool heat transfer is entirely negligible. The heat from the heaters is usually the only significant heat input. Figure 5 from Reference 3 is a composite plot of the heat transfer coefficients for a variety of distributor geometries.

For empty tank insurges it was found that the presence of a non-condensible gas could have a major effect on the pool heat transfer. The greatest effect was evident for a non-condensible gas with a molecular weight greater than steam such as $N_2$. Figure 6, Reference shows the pressure time traces for insurges where several different non-condensible gases (originally 10% by weight) present. Light gases like $H_2$ which is always present have a negligible effect. Heavy gases like $N_2$ pool up on the cold insurge water and practically stop pool heat transfer. They also impede the wall heat transfer.

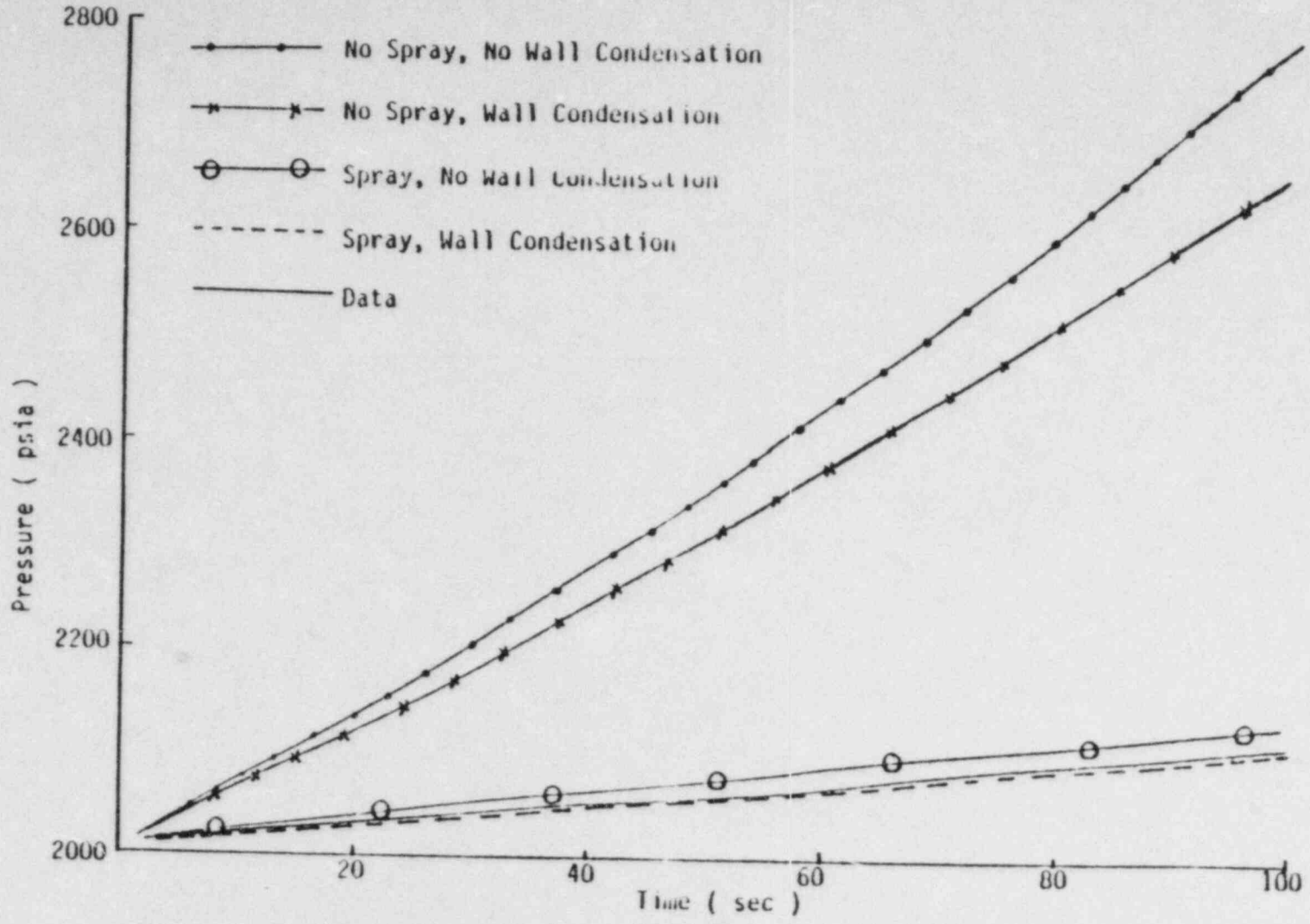


Figure 4. Pressure time for an insurge into a full size pressurizer showing the relative importance of the various fluxes. Reference [1].

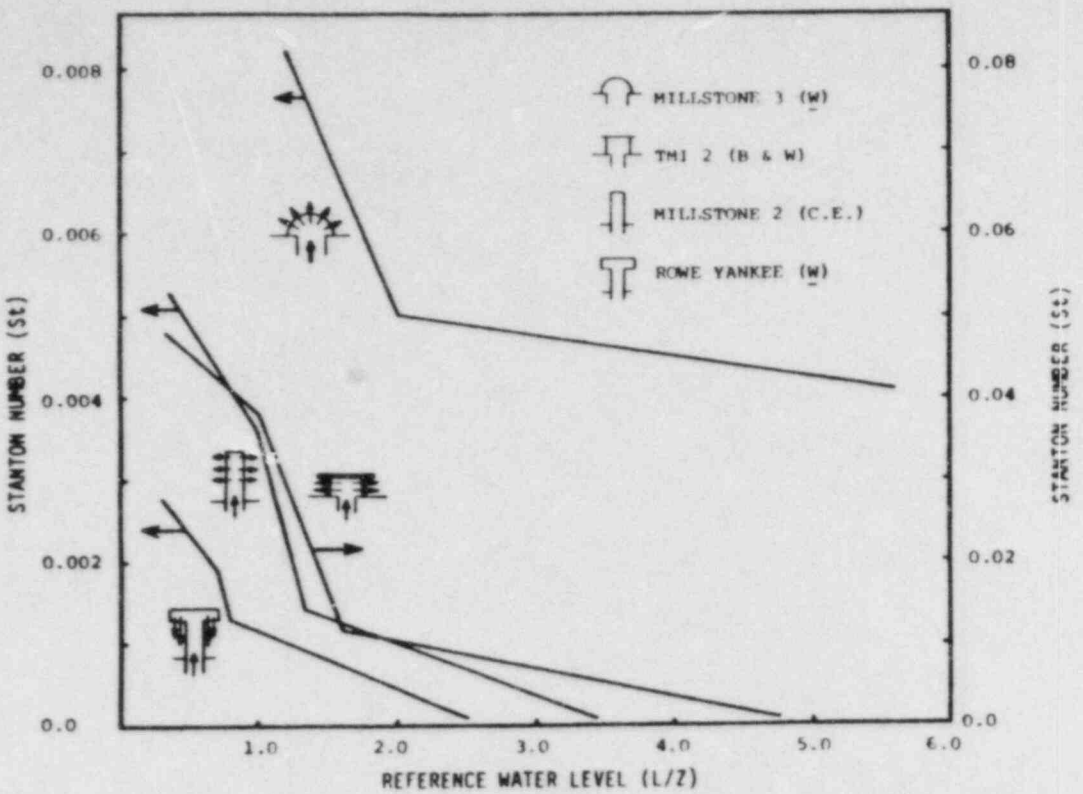


Figure 5. Pool heat transfer for various sparger geometries as a function of pool depth. Reference [3].

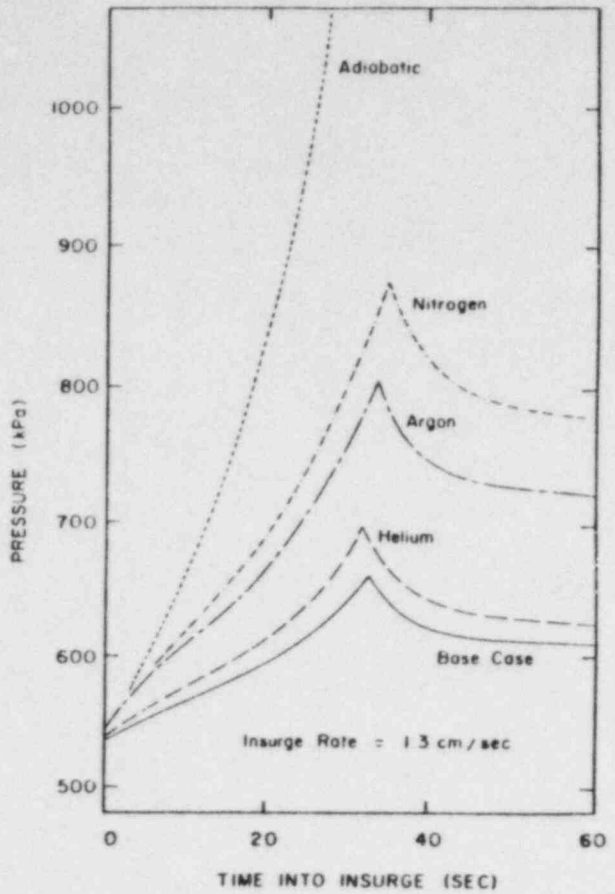


Figure 6. Pressure time for an insurge transient with various non-condensible gases present at 10% by weight to start.

CONCLUSIONS -

1. For an insurge, heat transfer to the pool in a pressurizer in which a pool is already present, is negligible. The pool stratifies and negligible condensation occurs.

2. Wall heat transfer during an insurge transient does have perceptable effect.

3. Heat transfer on the spray is practically instantaneous.

4. Outsurges occur with the pool generally in equlibrium with the steam. Flashing and wall heat transfer occurs with very small temperature differences. The pool and steam are at the same temperature.

5. Non-condensible gases are only significant in empty tank insurges in which are heavy gases (MW > 18) are present. They practically stop pool heat transfer.

6. The vapor is always virtually saturated.

7. The heat transfer matix of Table 1 can be used to estimate all heat transfers.

## REFERENCES


1. Kim, Sang-Nyung, "An Experimental and Analytical Model of a PWR Pressurizer during Transients". Ph.D. Thesis in Nuclear Engineering, MIT, February, 1984.

2. Leonard, M.T., "The Effect of a Non-Condensible Gas on Pressurizer Insurge Transients", MS Thesis in Nuclear Engineering, MIT, December, 1983.

3. Kang, S. W., "Pool Heat Transfer in a Simulated PWR Pressurizer", MS Thesis in Mechanical Engineering, MIT, December, 1983.

4. Seide, Hamid Reza, "Insurge Pressure Response and Heat Transfer for a PWR Pressurizer", MS Thesis in Mechanical Engineering, MIT, December, 1982.

5. Leonard, M., Peter Griffith, "The Effects of Non-Condensible Gas on Pressurizer Insurge Transients", ANS Transactions Vol. 46, pp. 844-845, 1984.

6. Kang, Shin-won, Peter Griffith, "Pool Heat Transfer in a Simulated PWR Pressurizer", ANS Transactions Vol. 49, pp. 845-846, 1984.

7. Saedi, H.R., Peter Griffith, "The Pressure Response of a PWR Pressurizer During an Insurge Transients", ANS Transactions, Vol. 44, pp. 606-607, 1983.

# CRITICAL FLOW THROUGH PIPE CRACKS AND FOR SMALL BREAKS WITH STRATIFIED UPSTREAM REGION

V. E. Schrock, S. T. Revankar
R. Mannheimer, S. Y. Lee and C-H Wang

Department of Nuclear Engineering
University of California
Berkeley, California 94720

## Summary

A knowledge of two-phase critical flow rate is essential for the prediction of effluent rates from an accidental break in a nuclear reactor. The discharge flow rate, resulting from a loss of coolant accident (LOCA) represents a loss of inventory in the cooling system. This coolant loss controls the heat transfer in the core and the depressurization rate of the coolant system. Phenomena of a large break (e.g., a sheared pipe which contains a flowing fluid) are well defined, though the flow rates from the large breaks may be difficult to predict accurately. On the other hand phenomena of a small break (characterized by a large main channel flow diameter to break flow diameter ratio) tend to be more ill-defined. The accident at Three Mile Island (TMI) has brought the attention of researchers on many aspects of the small break LOCA. The need for small break LOCA flow regime studies lies in the need to predict the spectrum of reactor behavior in small break accidents, where break size and locations are variable. Recent studies on large scale small break LOCA experiments LOFT L3-5 [1,2] have revealed that the critical flow rate models incorporated in the computer codes, such as TRAC and RELAP-5, do not adequately predict the loss of coolant or pressure measured. Thus the inability to accurately model the small break LOCA demands a need for investigation of small break simple integral experiments where the break has well-defined size and location.

When a small break LOCA occurs in a pipe, the geometry of the system at the break as well as the flow pattern in the vicinity of the break is of great concern. Because of slow depressurization rates which would accompany a small break LOCA, the steam and water can separate and lead to a stratified two-phase flow in the horizontal sections of the system. Under these conditions the position of the break relative to the steam-water interface governs the flow pattern which in turn greatly affects the amount of coolant leaving the system through the break. The various two-phase phenomena which may occur in horizontal pipes during a small break LOCA have been discussed by Zuber [3]. When a small break or fracture occurs below the liquid level in a horizontal pipe which is carrying a two-phase stratified flow, a vortex accompanied by vapor pull-through may establish itself at the entrance to the break. The quality entering the break depends on the liquid-vapor interface above the break. With the break located above the horizontal interface, liquid can be entrained due to vapor acceleration (Bernoulli effect). For the break at the level of vapor-liquid interface, the flow pattern at the break may take the combined features of top and bottom break flow. Reimann and Khan [4] have recently studied a low pressure critical flow using air and water discharging from stratified regions in 20 cm horizontal pipe through bottom oriented small pipes of diameters 6mm, 12mm and 20 mm. An experimental program is in progress at Berkeley [5] to obtain data on steam-water systems, with a 10.2 cm horizontal pipe discharging through pipes of diameters 3.9mm, 6.3mm and 10.2mm with various orientations (down, up, side). The Idaho National Engineering Laboratory [6] is carrying experiments with stratified flow in a 28.4 cm ID horizontal pipe

at 6.2 MPa discharging through a 16mm break line for various orientations with steam-water systems.

The experimental set-up used in the present study, as shown in Figure (1), mainly consists of a water reservoir to supply steam and water flow, a horizontal pipe with break tube and a recirculation loop to achieve flow of the stratified fluid past the break. Experiments were carried out with saturated steam-water and air-cold water system at stagnation pressure ranging from 0.37 MPa to 1.07 MPa for bottom oriented break. The gas and liquid mass flow rates through the break tube and hence quality entering the break tube were measured for different liquid interface levels in the horizontal pipe. The flow patterns observed near the break entrance for bottom oriented 3.9mm ID break tube showed that the gas pull-through occurred with vortex and vortex-free depending on the liquid interface level. In Figure (2) the gas-inception data of steam-water and air-water systems are shown. The data for incipient gas pull-through in steam-water flow do not agree with the relation of the form

$$Fr \left(\frac{\rho_\ell}{\rho_\ell - \rho_g}\right)^{0.5} = B \left(\frac{h_b}{d}\right)^C$$

Where Fr is Froude number, $\rho_\ell$, $\rho_g$ are the liquid and gas densities, $h_b$ is the interface height at which the beginning of first bubble or continuous gas pull-through occurs, d is the diameter of break tube, and B and C are constants. In Figures(3) and (4) the break liquid and gas mass flux are presented for two different stagnation pressures as a function of non-dimensional interface level, h/D, where D is the pipe diameter and h is the liquid interface level. In Figure (5) the quality is shown as function of h/D. With the increase in pipe stagnation pressure higher value of break

entrance quality was observed, in general, although this observation did not hold true for smaller value of quality ($x<5x10^{-3}$). The non-dimensionalized total mass flux $G_T/G_b$ (where $G_T$ is the total two-phase mass flux and $G_b$ is the liquid single phase mass flux in the break) is presented as function of $h/h_b$ in Figure (6). The data fall into separate curves each for particular stagnation pressure. From the figure it is observed that the total mass flux is larger with the higher stagnation pressure for the same liquid interface level. From pressure profiles measured, choking of the two-phase flow in the break was observed to occur near the break entrance. Further experiments for top and side orientations of the break tube are in progress.

An analytical model has been proposed to calculate the leak rates through intergranular stress corrosion cracks (IGSCC) in pipes and to reproduce the measured data of Battelle Columbus Laboratory (BCL) [7]. Previous models [7,8] extended the Henry's model [9] to account for friction and flow area change in the crack channel. The present model is 1D model that assumes homogeneous equilibrium flow with the flashing point of the liquid determined at the point in the crack channel where a saturation pressure condition is reached. The inlet region of the crack is assumed frictionless. The pressure drops due to phase change and area change and the friction pressure drop are accounted in the present model. The governing equations were reduced into finite difference forms and the pressure and quality at each grid point on the crack channel were determined with assumed mass flow rate. With iteration procedure the mass flow rate for choking near the exit point was determined. The calculated results from the present model for some test numbers of the BCL experiments are shown in Table 1 along with previous measured and calculated data. The present predictions compare fairly well with the measured data.

References


1. Doa, L. T. C. and Carpenter, J. M., "Experiment Data Report for LOFT Nuclear Small-Break Experiment L-35/L3-5A," NUREG/CR-1695, EGG-2060, November 1980.

2. Condie, K. G., "LOFT LOCE L3-5/L3-5A Result and Analysis," paper presented at the LOFT Review Group Meeting, Idaho Falls, Idaho, November 6, 1980.

3. Zuber, N., "Problems in Modeling of Small Break LOCA" NUREG-0724, October 1981.

4. Reimann, J. and Khan, M., "Flow Through a Small Break at the Bottom of a Large Pipe with Stratified Flow," presented at the 2nd International Topical Meeting on Nuclear Reactor Thermal Hydraulics, Santa Barbara, CA, January 11-14, 1983.

5. Schrock, V. E. et al., "Critical Flow Through a Small Break on a Large Pipe With Stratified Flow," Report UCB-NE-4053, October 1984.

6. Anderson, J. L., private communication.

7. Collier, R. P. et al., "Two-Phase Flow Through Intergranular Stress Corrosion Cracks and Resulting Acoustic Emission" Final Report NP-3540-LD, RP T118-2, April 1984.

8. Abdollahian, D. and Chexal, B., "Calculation of Leak Rates Through Cracks in Pipes and Tubes" EPRI Report NP 3395, Dec. 1983.

9. Henry, R. E., "Two-Phase Critical Discharge of Initially Saturated or Subcooled Liquid", Nucl. Sci. and Eng. Vol. 41, p. 336, 1970.


TABLE I

| Test No. | Stagnation Conditions | | *Measured Discharge Rate, $\dot{m}$[kg/sec] | BCL Predictions | | EPRI Predictions, $\dot{m}$[kg/sec] | Present Predictions | | |
|---|---|---|---|---|---|---|---|---|---|
| | $P_o$[MPa] | $T_o$[$^oC$] | | $\dot{m}$[kg/sec] | Revised $\dot{m}$[kg/sec] | | $\dot{m}$[kg/sec] | Exit Quality | $P_{exit}$ [MPa] |
| 1 | 7.316 | 272.8 | $1.02\times10^{-3}$ | $3.07\times10^{-3}$ | $7.67\times10^{-4}$ | $3.00\times10^{-3}$ | $2.60\times10^{-3}$ | 0.1316 | 2.382 |
| 4 | 9.412 | 260.6 | $1.10\times10^{-3}$ | $6.92\times10^{-3}$ | $1.25\times10^{-3}$ | $6.77\times10^{-3}$ | $3.52\times10^{-3}$ | 0.0427 | 3.582 |
| 6 | 9.322 | 267.8 | $1.10\times10^{-3}$ | $5.54\times10^{-3}$ | $1.12\times10^{-3}$ | $5.27\times10^{-3}$ | $3.40\times10^{-3}$ | 0.0931 | 2.929 |
| 7 | 9.301 | 284.4 | $5.49\times10^{-5}$ | $7.98\times10^{-5}$ | $6.58\times10^{-5}$ | $8.07\times10^{-5}$ | $1.63\times10^{-4}$ | 0.1487 | 2.723 |
| 12 | 5.868 | 260.0 | $1.09\times10^{-4}$ | $4.41\times10^{-5}$ | —** | $4.43\times10^{-5}$ | $1.54\times10^{-4}$ | 0.1624 | 1.236 |

Note. * Battelle Columbus Lab's Phase-II Experimental Data for Intergranular Stress Corrosion Crack.

** not available.

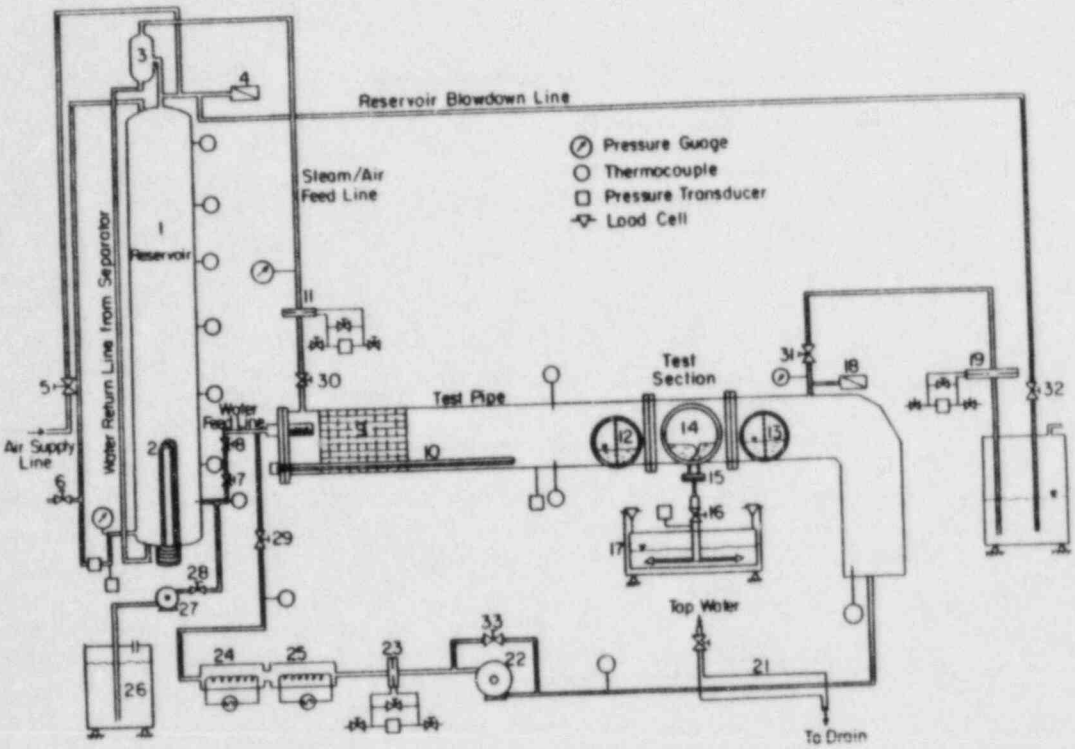


Figure 1. Experiment System Schematic

Key to Figure 1

| Component Number | Description |
|---|---|
| 1 | Pressure Vessel Steam Water Reservoir |
| 2 | Pressure Vessel Immersion Heaters |
| 3 | Steam Separator |
| 4 | Reservoir Pressure Relief Valve |
| 5 | Air/Nitrogen Supply Shut-Off Valve |
| 6 | Vessel Vent Line Valve |
| 7 | Water Feed Regulating Valve |
| 8 | Water Feed Shut-Off Valve |
| 9 | Honeycombed Test Pipe Flow Homogenizer |
| 10 | Test Pipe Immersion Heater |
| 11 | Gas Entry Orifice Meter |
| 12 | Upstream View Window for Liquid Level Indicator |
| 13 | Downstream View Window for Liquid Level Indicator |
| 14 | Test Section Flow Entry View Window |
| 15 | Break Discharge Section |
| 16 | Break Discharge Gate Valve |
| 17 | Weigh Tank |
| 18 | Test Pipe Pressure Relief Valve |
| 19 | Gas Exit Orifice Meter |
| 20 | Quench Tank |
| 21 | Double Pipe Heat Exchanger |
| 22 | Water Recirculation Pump |
| 23 | Water Recirculation Orifice Meter |
| 24 | Water Recirculation Preheater |
| 25 | Water Recirculation Reheater |
| 26 | Distilled Water Storage Tank |
| 27 | Reservoir Fill Pump |
| 28 | Reservoir Fill Line Regulating Valve |
| 29 | Recirculation Rate Regulating Valve |
| 30 | Gas Entry Regulating Valve |
| 31 | Gas Exit Regulating Valve |
| 32 | Reservoir Blowdown Regulating Valve |
| 33 | Pump Bypass Line Regulating Valve |
| 34 | Heat Exchanger Cold Water Feed Regulating Valve |

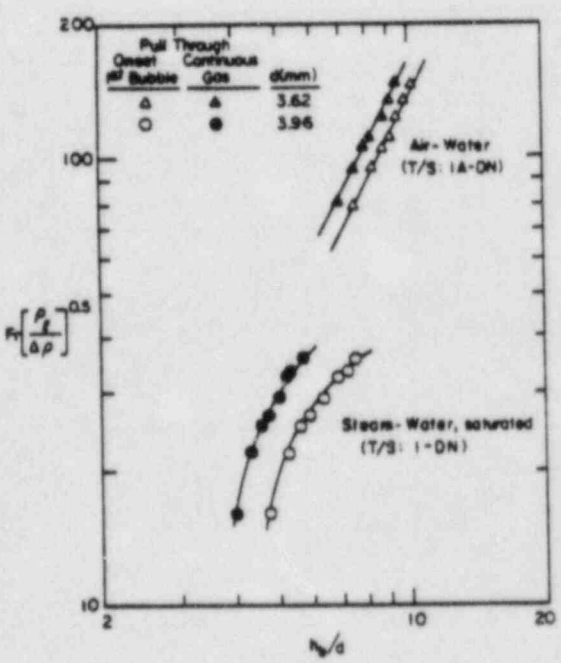


Figure 2. Data of onset of gas pull-through

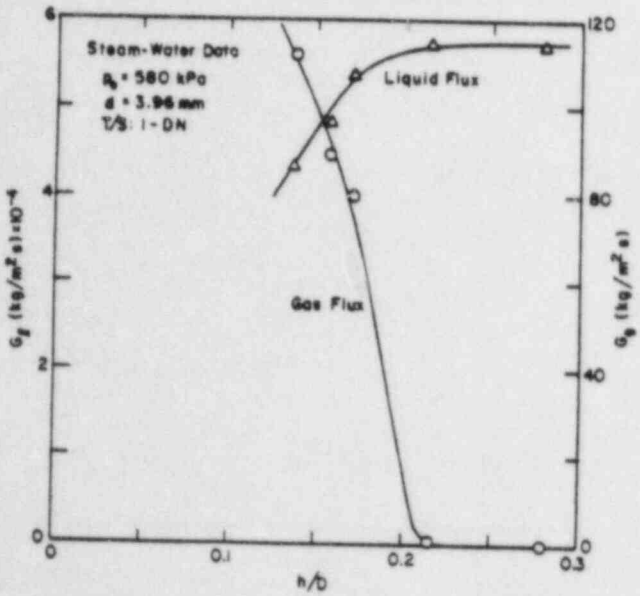


Figure 3. Break liquid and gas mass flux $P_0$ = 580 kPa, air-water data.

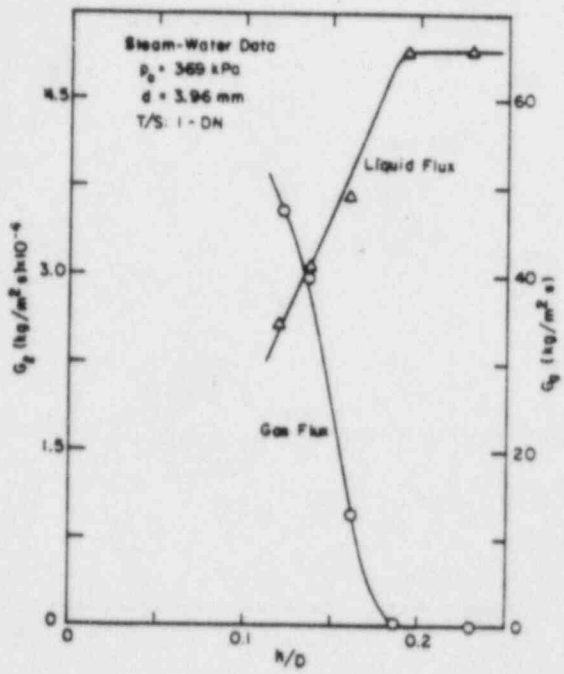


Figure 4. Break liquid and gas mass flux at $P_0$ = 369 kPa, steam-water data.

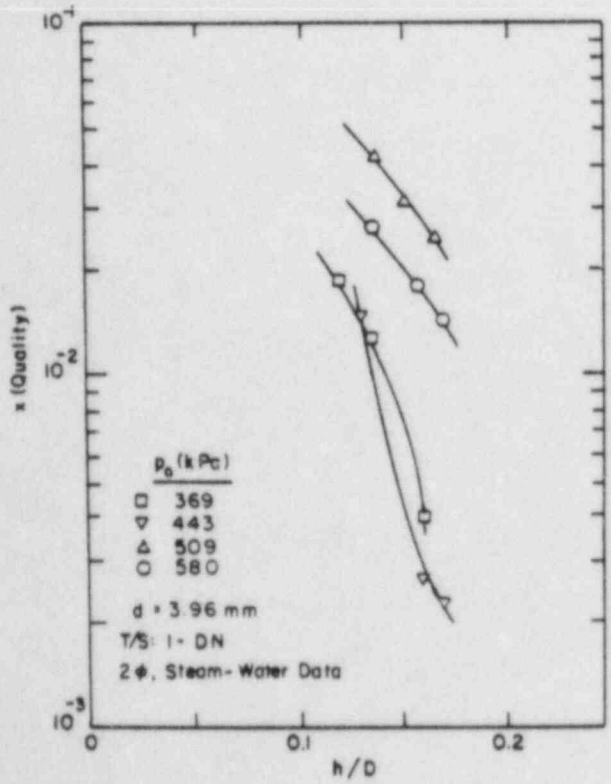


Figure 5. Break entrance quality as function of h/D

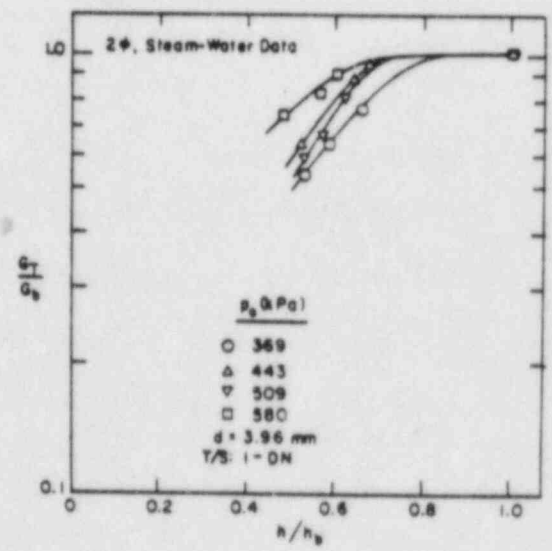


Figure 6. Non-dimensional break total mass flux

# Identification of Inadequate Core Cooling Utilizing Existing Ex-Core Neutron Detectors

A. J. Baratta
M. L. Gundy
E. W. Okyere
W. A. Jester
T. J. Gillen

The Pennsylvania State University

As a result of the TMI accident, utilities are required to provide a means of reactor vessel level indication and to instruct operating personnel on the various control room indications available to them which would aid in mitigating core damage. Based on work at the Loss of Fluid Test Facility (LOFT) at the Idaho National Engineering Laboratory, the authors have found that deviations in the nuclear instrumentation readings from normal values provide a reliable indicator of abnormal thermal hydraulic condition in the reactor pressure vessel. This work is an outgrowth of efforts funded by NRC to investigate a non-invasive liquid level and density gauge based on ex-core fast neutron detectors.

Data obtained from the TMI-2 source range monitor during the accident showed annomolous structure (see fig. 1).[1] Various groups including EPRI, Argonne National Laboratory, and the authors have analyzed the observed structure.[1,2,3] Based on their analysis and estimates of the hydraulic conditions in the vessel, they concluded that the observed structure was due to a variation in the neutron flux seen by the detector. The variation in flux was caused by the various hydraulic conditions experienced during the accident.

For example, the analysis of the deviation from the normal shutdown curve during the period from 20 minutes to approximately 100 minutes has been attributed to the build-up of voids in the downcomer and core region.

Lack of detailed hydraulic data, however, precludes quantitative analysis of the data. Void formation, however, is consistent with the fact that the pressure in the primary system had reached saturation by that time, and with the fact that reactor coolant flow rate had decreased to a value consistent with pumping a two-phase mixture.

In connection with ongoing work at LOFT, the authors have obtained LOFT source, intermediate, and power range neutron monitor data from several small- and large-break loss of coolant accidents.

The LOFT facility is ideal for this type of study since it is a fully operational PWR. The LOFT experimental system consists of a reactor system, primary coolant system, blowdown suppression system (used during LOCA experiments), emergency core cooling system, and secondary cooling system.[4] With the exception of the blowdown suppression system, the major systems are representative of typical PWR subsystems. The coolant volumes and flow areas at LOFT were scaled using the ratio of LOFT power (50 MWt) to a commercial 3000 MWt PWR. Furthermore, the systems are heavily instrumented to provide continuous monitoring of the nuclear, thermal, and hydraulic conditions during LOCA's.

The LOFT nuclear instrumentation consists of three types of instrumentation similar to that found in a commercial PWR. The instrumentation includes uncompensated ion chambers for power range measurement, compensated ion chambers for intermediate range measurement, and boron triflouride neutron detectors for source range measurement. As in a commercial PWR, range overlap between these instruments is provided.

Data was obtained from the installed nuclear instrumentation for several LOFT LOCA experiments. Included in these experiments are data from L2-5 and LP-02-6, both large-break LOCA's, and SB-3, a small-break LOCA. In addi-

tion, clad thermocouple data as well as conductivity probe data was also obtained. The thermocouple data gives fuel cladding temperature during the accident and shows when regions of the core became dry. The conductivity probe data provides estimates of water level in various regions of the vessel during the LOCA experiments. Figure 2 shows data obtained from a fuel cladding thermocouple during the L2-5 experiment and Figure 3 shows a so-called "bubble plot" from the L2-5 experiment. The bubble plot gives estimates of void fraction in the vessel at various elevations and is obtained from the conductivity probe data.

Experiment L2-5

The L2-5 experiment, conducted on June 16, 1982, simulated a large-break, double-ended rupture of an inlet pipe in a PWR. This experiment differed from previous large break LOCA's in that an atypically fast coast-down of the primary coolant pumps was simulated. Within the first second, primary system depressurization occurred and the core departed from saturation. A series of refloods occurred with the core becoming fully quenched by 65 seconds.[5]

During this time, the nuclear instrumentation both power and intermediate range departed from the normal shutdown curve. Figure 4 shows the response of one of the intermediate range detectors during the first 1000 seconds. Note the peak centered on approximately 30 seconds.

Subsequent to core reflood and quench, an attempt was made to control reactor pressure vessel level below the nozzles. During this phase at approximately 190 seconds, a second core uncovery occurred as evidenced by thermocouple data. Again, the nuclear instrumentation responded by deviating from the normal shutdown. Although HPIS and LPIS flow was initiated at

274 seconds and 347 seconds respectively, the core remained at least partially uncovered until approximately 430 seconds. A third partial uncovery occurred at approximately 500 seconds.

In each case, the nuclear instrumentation responded by first increasing from the normal shutdown value and then leveling off. The response finally returned to normal after core reflood and quench occurred.

The response of the nuclear instrumentation is due to a loss of shielding combined with a loss of neutron moderation. The loss of shielding initially dominates as coolant is lost from the core and neutron leakage increases. Eventually this loss of coolant produces a loss of moderation, causing a drop in the neutron source strength. As a result, the nuclear instrumentation response levels off at a value above the normal shutdown value. It returns to the normal value once the core is reflooded. To confirm the source of behavior of the detector output, the LOFT core was modeled using a quasi-static adiabatic method, the DOT 4.3 neutron transport code, and a point reactor kinetic code.[6] The hydraulic conditions obtained from the conductivity and thermocouple data was input to the code to describe fuel temperature and water density in the core. The resulting intermediate range detector response was calculated from this analysis. The results are shown in Figure 5. Excellent agreement with the observed response was obtained, thus confirming the source of the behavior of the detector output.

Experiment LP-02-6

Experiment LP-02-6 occurred on October 3, 1983. This experiment was a design-basis accident involving a double-ended offset shear of an inlet pipe coincident with loss of offsite power.[7] Within 0.1 seconds, satura-

tion conditions were reached in the reactor vessel. Primary coolant pumps were tripped and allowed to coast down, simulating loss of offsite power. Cladding temperatures deviated from saturation at about 0.5 seconds. At about 5.2 seconds, a rewet of the core occurred, which lasted until about 9.1 seconds. At about 15 seconds, fuel cladding temperatures again departed from saturation. Final core quench was completed at about 56 seconds.

Figure 6 shows the response of one of the LOFT power range detectors during the accident. Again, during the initial heat-up one notes an increase in the output of the detector. This increase is terminated when the rewet occurs at about 5 seconds. A second departure occurs at about 15 seconds with a return to normal values at about 50 seconds, nearly coincident with final core quench.

The response of the power range detector shows that, at least during the initial stages of a large-break LOCA, it too provides an indication of inadequate core cooling. The response of this detector is similar to that of the intermediate range detector observed during the L2-5 experiment. Analysis of this response during LP-02-6 showed that the detector was responding in the same manner as the intermediate range detectors during the L2-5 experiment.

Experiment SB-3

Experiment LP-SB-3 was conducted on March 5, 1984. The experiment simulated a small cold leg break LOCA.[8] The primary system depressurized, reaching saturation condition at about 100 seconds. Primary coolant pumps were kept operating, resulting in a homogenization of the steam-liquid flow through the reactor core. The primary coolant pumps were tripped at 1600 seconds. Core heat-up and uncovery began at 3800 seconds, with the break

being isolated at 4750 seconds. Steam generator feed and bleed occurred at 5415 seconds, with LPIS injection occurring at 6785 seconds.

This experiment simulates to a very high degree the TMI-2 accident scenario. As a result, the response of the nuclear instrumentation should be similar. Figure 7 shows the source range detector response during the SB-3 LOCA experiment. After initially following the normal shutdown curve, the detector response deviates at around 1000 seconds, leveling off and then increasing. During this time period, the primary coolant pumps were pumping a homogenous steam-water mixture through the core. Coincident with the trip of the primary coolant pumps at 1600 seconds, a sudden drop occurs in the detector response. This drop is most likely due to separation of the steam-water mixture with the water settling into the core. The detector output then follows nearly a normal shutdown curve until about 3600 seconds, when the core began to heat up. A rise occurs in the detector output until the core is about half emptied, at around 4200-4300 seconds. At this point, the output levels off until steam generator feed and bleed occurs at 5415 seconds. A peak results, followed by another peak coincident with accumulator injection at 5558 seconds. There is a return to near the normal shutdown curve at around 5800 secods. The initiation of LPIS injection at 6785 seconds produces a drop in the signal at about that time.

The observed response demonstrates the sensitivity of the source range detector to voiding condition in the reactor core. The initial rise prior to pump trip is produced by a decrease in shielding as the void fraction in the core region increases. The rise in detector output as the core boils off and heats up is due to a similar effect. The leveling off of the response is most likely due to a loss of moderation and resulting decrease in $k_{eff}$. The two peaks are probably due to the core filling in part with low

quality fluid producing an increased $k_{eff}$. The drop results from an increase in shielding as the core refills.

## Conclusion

In each of the experiments described here, the output of the neutron detectors increases as the core uncovers. A leveling off results when the loss of shielding due to the loss of coolant is offset by the loss of moderation, a resulting decrease in source strength. A return to near normal output does not occur until the core is nearly refilled and normal conditions exist in the core. The detectors thus provide a sensitive indication of inadequate core cooling during both small and large break LOCA's

## Acknowledgements

The authors would like to thank Yi Chen and A. Hon (both NRC) for their support in this work. In addition, the authors wish to thank D. Taylor, B. Goodrich, and D. Croucher (all EGG, Idaho) for their assistance in obtaining the LOFT data. This work was funded in part by a grant from the USNRC, Grant No. NRC-G-04-81-024. This asistance is gratefully acknowledged.

## References


1. H. Warren, et. al., "Interpretataion of TMI-2 Instrument Data," Nuclear Safety Analysis Center NSAC-28 (May 1982).

2. D. J. Malloy and Y. I. Chang, "Neutronic Analysis of the Three Mile Island Unit 2 Ex-Core Detector Response," Argonne National Laboratory ANL-81-75 (October 1981).

3. A. J. Baratta, et. al., "Feasibility Study on the Development of a Non-Invasive Liquid Level Gauge for Nuclear Power Reactors," US NRC NUREG/CR-3290 (May 1983).

4 C. L. Nalezny, "Summary of Nuclear Regulatory Commission's LOFT Program Experiments," NTIS NUREG/CR-3214 (July 1983).

5. J. P. Adams, "Quick-Look Report on LOFT Nuclear Experiment L2-5," EG&G Idaho, Inc., EGG-LOFT-5921 (June 1982).

6. M. L. Gundy, "Application of the Adiabatic Spatially Dependent Reactor Kinetics Method to Voided Pressurized Water Reactor," Ph.D. Thesis, Pennsylvania State University (August 1984) unpublished.

7. J. P. Adams, et. al., "Quick-Look Report on OECD LOFT Experiment LP-02-6," EG&G Idaho, Inc., OECD LOFT-T-3404 (October 1983).

8. M. Tanaka, "Quick-Look Report on OECD LOFT Experiment LP-SB-3," EG&G Idaho, Inc., OECD-LOFT-T-3604 (March 1984).

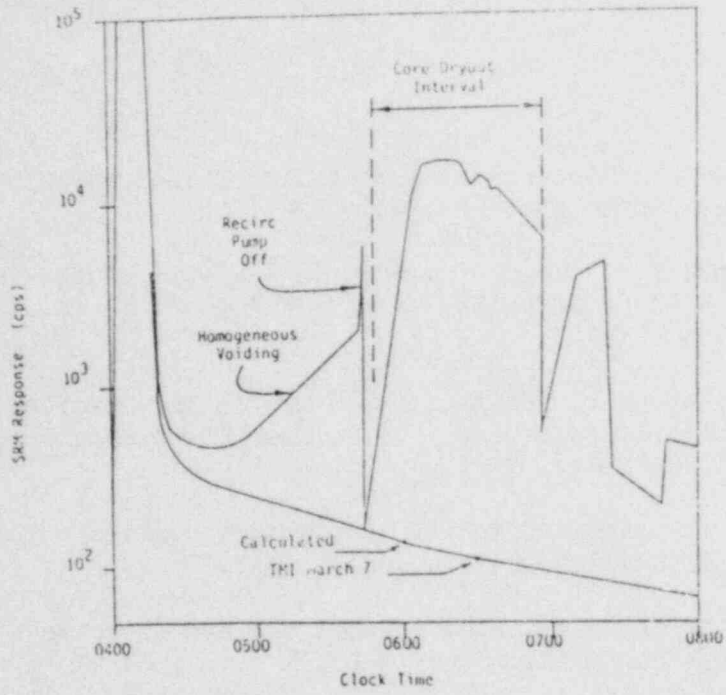


Figure 1. Observed, "Normal," and Calculated SRM Response following Reactor Shutdown

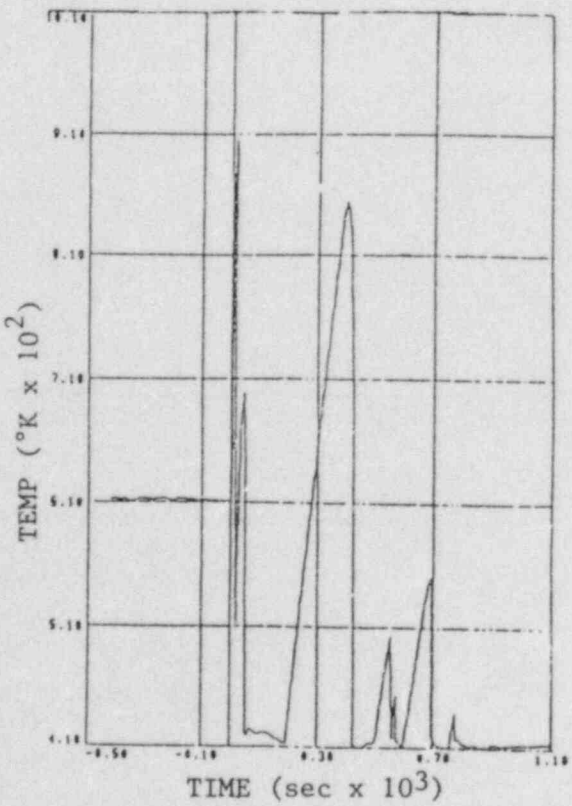


Figure 2. Clad thermocouple response
LOFT L2-5 LOCA Experiment

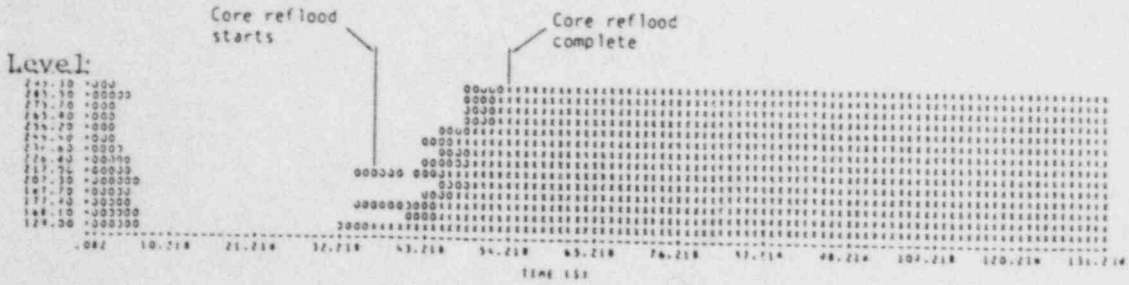


Figure 3. Liquid level in the central fuel assembly for Experiment L2-5 as determinied from conductivity probe data.

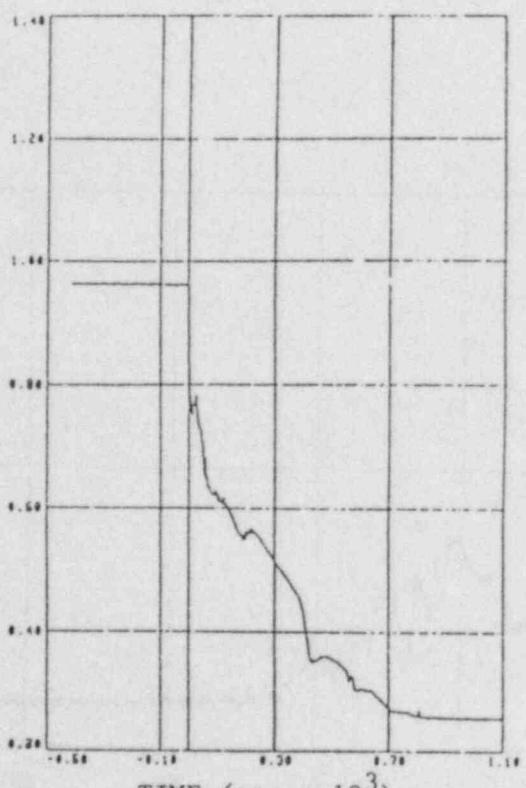


Figure 4. Normalized intermediate range detector response LOFT L2-5 LOCA Experiment

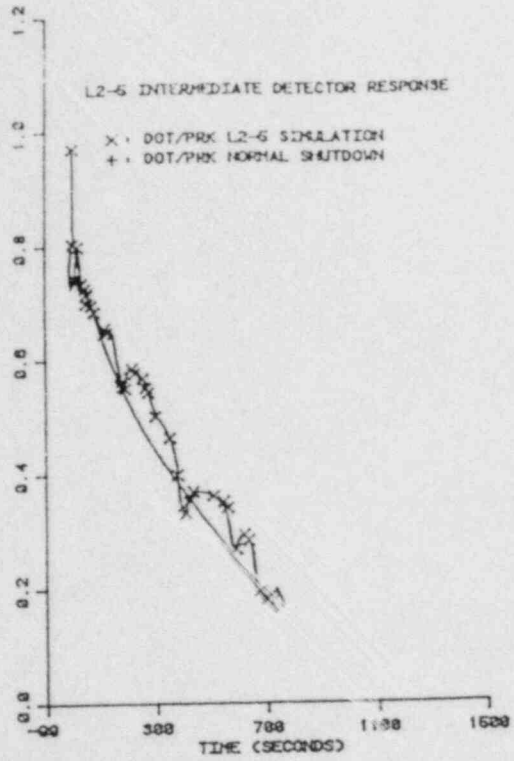


Figure 5. DOT/PRK Simulation of the LOFT L2-5 LOCA Experiment for the installed intermediate detector normalized response

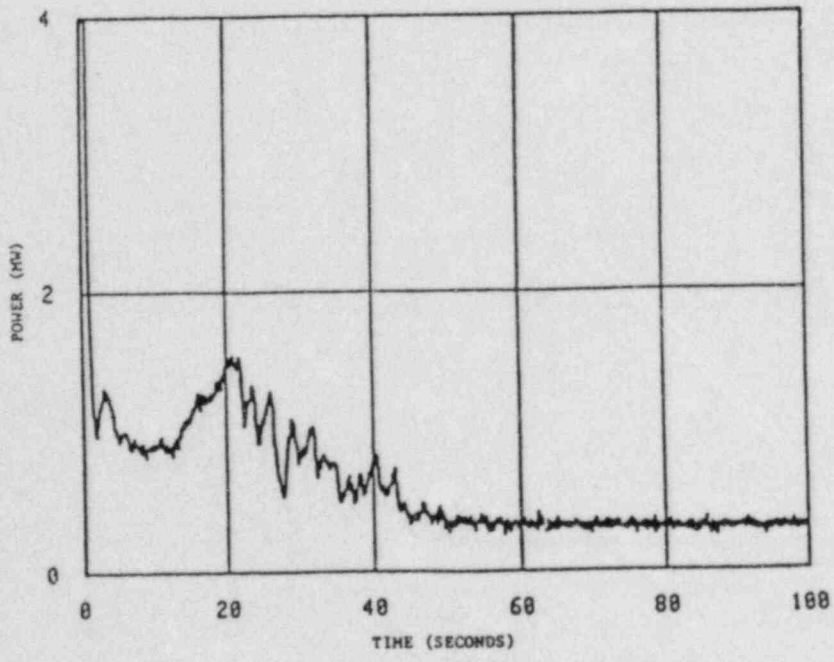


Figure 6. Output of LOFT Power Range Detector LP-02-6 LOCA Experiment

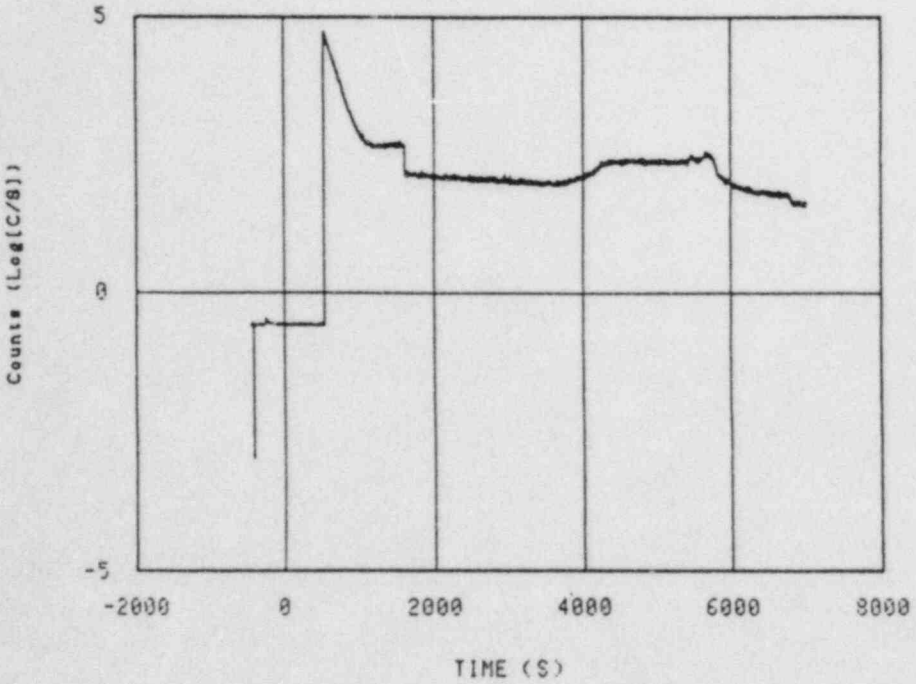


Figure 7. Source range detector output
LOFT LP-SB-3 LOCA Experiment.

# A STUDY OF MIST COOLING ENHANCEMENT FROM GRID SPACERS IN LOCA REFLOOD OF A PWR COMBINED GROSS HEAT TRANSFER AND LOCAL TEMPERATURE AND LDA DROPLET SIZING ANALYSIS

S. L. Lee

Department of Mechanical Engineering
State University of New York at Stony Brook
Stony Brook, New York 11794, USA

and

P. Ihle

Kernforschungszentrum Karlsruhe
Institut für Reaktorbauelemente
Postfach 3640, 7500 Karlsruhe
Federal Republic of Germany

## Summary

Results of two different experimental programs are presented including a short review of grid spacer effects on local reflood heat transfer.

Transient tests performed under various forced feed reflood conditions using a full length bundle of 5x5 rods of PWR dimensions show transient heat transfer enhancement downstream of grid spacers during mist cooling mainly. Rewetting behavior and temperature transients of grid spacers are discussed.

Steady state steam cooling as well as two-phase flow cooling tests under controlled condition of droplet injection using a short 2x2 rod bundle provide information about local droplet sizing and steam temperature upstream and downstream of a grid spacer.

The combined analysis of the results of both experimental programs shows quality and importance of the individual cooling mechanisms.

Turbulence enhancement downstream of a grid spacer exerts the most significant effect. Increased amount of small droplets in the flow improves cooling moderately and lowers steam superheat significantly. Quenching of a grid spacer is initiated at the trailing edge of it. Premature quenching of the rod claddings downstream of a grid characterizes most of the cases. Grid quenching scarcely influences cladding temperatures.

## 1. Introduction

The prediction of the peak cladding temperatures of nuclear fuel rods during the core reflooding transient of a loss of coolant accident (LOCA) in a pressurized water reactor (PWR) is of great importance [1]. The number of ruptured fuel rods, the cladding deformations and their influence on coolability must be predicted as well. Prediction uncertainties are covered by conservative assumptions. However, the knowlegde of the individual safety margins is of interest. Besides the uncertainty e.g. about the real water mass flux reflooding a core there is further uncertainty e.g. about the peak cladding temperatures for a mass flux known precisely. One of the reasons for the latter uncertainty is the grid spacer effect on local cooling conditions. Its influence on the local peak cladding temperatures as well as on the development of the axial cladding temperature profiles is not yet taken into account in prediction codes. Experimental results make evident the decrease of the cladding temperatures downstream of grid spacers as well as the interaction between thermal-hydraulics and fuel clad ballooning [2, 3]. Computer code modeling is under way for the description of the thermal-hydraulic phenomena at grid spacers. However, more detailed information is needed about the most effective cooling mechanisms.

The aim of this study is to separate out from experimental results - obtained with two different test facilities - dominant grid spacer effects and to describe the physical mechanisms as extented as possible by a combined analysis.

## 2. Grid Spacer Effects on Two-Phase Flow Cooling, Status

The effects of grid spacers on local cladding temperatures have been observed in several reflood tests investigating emergency core cooling in simulation fuel rod bundles. The main results are touched in a short and necessarily incomplete review:

In a full length 5x5 rod bundle of PWR dimensions the midplane grid spacer (one of seven) had been removed. Comparison of the local heat transfer conditions with and without grid spacer at bundle midplane made evident that the grid spacer lowers the cladding temperatures downstream of it significantly. These findings obtained from FEBA tests [2, 4] were confirmed qualitatively by results e.g. of FLECHT/SEASET tests [5], of THETIS tests [6], as well as of ERSEC tests. The latter tests included different grid spacer geometries with and without mixing vanes [7]. However, the integral effect of increased flow turbulence and droplet break up as well as evaporation obtained from full length bundle tests needed to be analyzed more distinctly. Computer code modeling calls for further analysis and more detailed experimental results.

During the reflood transient a number of different physical mechanisms is active at a grid spacer having different importance depending on reflood parameters and time as well. The flow conditions are characterized by the sequence of superheated steam at initiation which entrains an increasing amount of water, at first small droplets, later on larger water particles, until the flow channels are filled with water containing steam bubbles. The temperature rise up to the peak cladding temperatures, and occasional ballooning with burst of the claddings continued during reflooding, occur during the highly dispersed - mist - flow regime. This is especially true for the

cases of low water injection rates. Under these flow conditions prediction of the cooling effects is not satisfactory yet even for flow in undisturbed coolant channels. Comparison of selected experimental data with analytical results post-calculated by a typical analysis code, not accounting for grid spacer effects, showed overprediction of the cladding temperatures for the mist flow regime inspite of the use of artificially adjusted values of the empirical code input parameters [8]. A mean droplet diameter assumed or calculated for given boundary conditions seems not to be sufficient. This is presumably true for modeling grid spacer effects as well.

Therefore, the droplet behavior at grid spacers has been investigated in further experiments suitable for measurement techniques not applicable in the full length bundle tests mentioned above. Smaller and/or shorter rod bundles allowed Laser-Doppler Anemometry (LDA), high speed movie or still photography technique for analysis of droplet dynamics in air and steam flow under controlled dispersed flow conditions.

In a short 2x2 rod bundle direct measurement of droplet dynamics across a grid spacer has been realized under steady state controlled dispersed flow conditions. Droplet velocity and size distribution have been measured simultaneously in the center subchannel of the unheated 2x2 rod bundle by a special LDA technique [9, 10]. In a series of tests the influence of a PWR grid spacer at room temperature on the droplet size population and velocity distributions in the mist flow downstream has been investigated [11, 12, 13]. Droplets of a mean diameter of 1.3 mm have been injected ahead of the grid spacer. The increases in the population of small droplets in the order of 0.2 mm diameter measured downstream are mostly due to the reentrainment of droplets from the trailing edge of the wet grid spacer. Since, early in the mist flow transient the grid spacers have been found to be hot and dry it has been suggested to perform similar experiments in a heated rod bundle [14]. The investigations have been continued using identical LDA technique and an electrically heated 2x2 rod bundle. Controlled supply of large water droplets upstream of the grid spacer into the flow of superheated steam has created a significant amount of small droplets at the dry grid spacer as well and corresponding enhancement of cooling downstream. Furthermore, the tests have shown that the dry hot grid spacer creates more small droplets than the wet quenched grid spacer under the same water droplet flux [15, 16, 17].

Droplet breakup and entrainment at both wet and dry PWR spacer grids have been investigated in a short 44 rod bundle using still photography as well as high speed movie photography. It is suggested that for nonwetted grids the drop size will depend on fragmentation at initial impact: Close to the quench front at the rods unquenched grids will have little influence on drop size (low steam velocity), but far above the quench front in the bundle where steam and droplet velocities are higher unwetted grids are likely to introduce a population of smaller drops into the flow [18].

Droplet size distributions upstream and downstream of a grid spacer simulated by wires of 0,72 mm diameter have been obtained using the 44 rod bundle and the photography techniques mentioned. The results obtained from droplets injected into the steam flow in the bundle subchannels have shown a significant decrease of the mean droplet size across the wire grid and increased number of droplets [19].

The high speed movie photography applied for measuring technique detects droplets of equivalent diameters down to about 0.1 mm. The LDA technique [15] detects droplets of equivalent diameters down to less than 0.01 mm. The overall diameter reduction across the different grid spacers (wire grid in the 44 rod bundle; PWR grid in the 2x2 rod bundle) was about the same: Upstream 1.3 mm (SMD = 1.58 mm, Sauter mean diameter), downstream 0.25 mm (SMD = 1.13 mm) for the 2x2 rod bundle. However, the droplet cooling enhancement is expected to be important as well for the relatively large number of very small droplets smaller than 0.1 mm [20, 21, 22].

It is concluded from THETIS data that for the two-phase flow the grid spacer enhancement is very much larger if the grid is wet, presumably due to the additional effect of steam desuperheating besides the turbulence enhancement. Steam desuperheating was not measured downstream of the dry grid spacer placed immediately downstream of the extented 90 % blockage in the 49 rod bundle [6]. This is in seeming contradiction to e.g. data measured in the REBEKA6 49 rod bundle clad ballooning experiment indicating somewhat larger steam desuperheating for the dry grid spacer [23]. From an analysis of the transient full length bundle experiments, it is difficult to distinguish whether the change from dry to wet grid spacer leads to steam desuperheating for the same droplet flux or the change of the fluid conditions (steam velocity, droplet flux) leads to increased grid spacer effects and increased desuperheating of the steam and, consequently, then to rewetting of the grid spacer. The design of the individual grid spacers influences the magnitude of these effects as well.

## 3. Grid Spacer Effects on Reflood Heat Transfer in a Full Length 5x5 Rod Bundle, Gross Measurements

### 3.1 Experiments

Forced feed reflood tests have been performed for constant system pressures of 2 bar and 4 bar and flooding velocities of 3.8 cm/s and 5.8 cm/s (i.e. the water flow velocity in the cold bundle). A 120 % ANS-Standard reflood decay heat transient has been simulated by electrical heating of the rods of German PWR dimensions.

The square array of 5x5 rods of 10.75 mm outer diameter, 14.3 mm pitch and 3.9 m heated length is placed in a square housing. Original PWR grid spacers without mixing vanes are installed at the bundle midplane and other levels at 545 mm intervals throughout the rod assembly. The cosine power profile of the rods is approximated by seven steps of different specific rod power, the peak to average ratio of which amounts to 1.19.

The test facility, the test procedure, the measurement techniques as well as the outer dimensions and the power distribution of the bundle are the same as for the FEBA tests [2]. However, the fuel rod simulators of REBEKA design [3] used for the experiments presented consist of electrically heated rods of 6 mm outer diameter placed in the center of annular $Al_2O_3$ pellets simulating $UO_2$ pellets. As for a nuclear fuel rod, the pellets are encapsulated in a Zircaloy cladding tube of 10.75 mm outer diameter and 0.73 mm thickness. The space between the pellets and the Zircaloy cladding is filled with helium of low pressure to prevent the claddings from ballooning during the tests performed in the SEFLEX program [24]. The test facility, grid spacer locations and instrumentation as well as rod power distribution are shown schematically

in Figs. 1 and 2. The results of the tests concerning the grid spacer effects are described in the following.

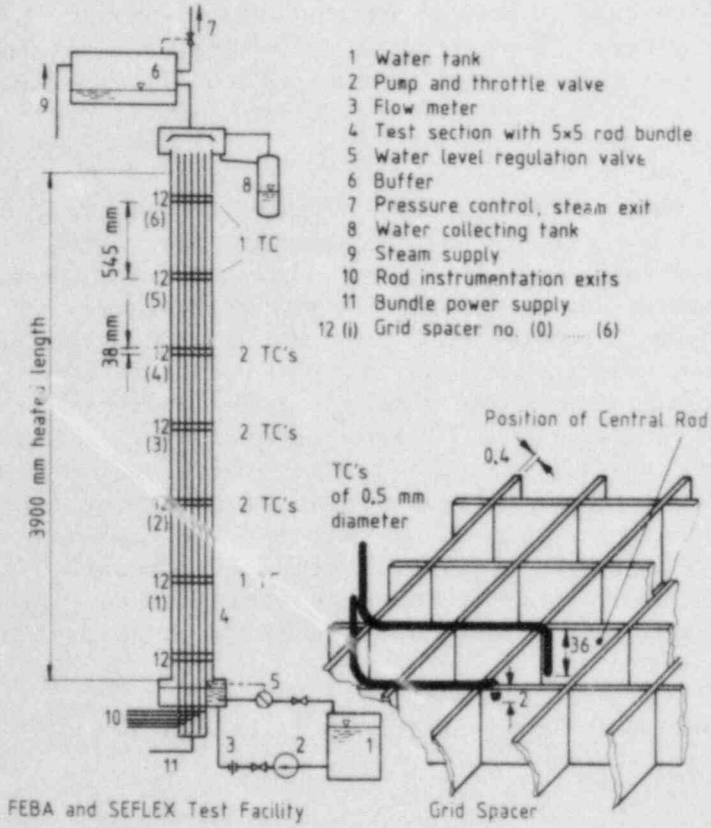


Fig. 1 5x5 rod bundle test facility and grid spacer TC locations in SEFLEX tests

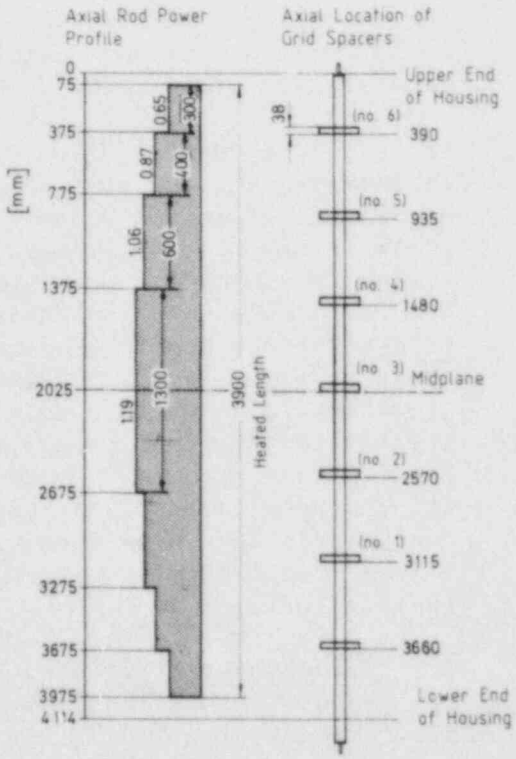


Fig. 2 Power profile of the rods of REBEKA design and grid spacer locations in the 5x5 rod SEFLEX bundle

## 3.2 Results from the 5x5 Rod Bundle Tests Concerning Grid Spacer Effects

From the sample of tests performed under different reflood conditions data measured at the 5x5 rod bundle midplane are selected for description of grid spacer effects from gross measurements. Figure 3 shows cladding and grid spacer temperatures for the set of tests performed with system pressures of 2 and 4 bar and with flooding velocities of 3.8 and 5.8 cm/s. The temperatures of the grid spacer are measured near the leading edge and near the trailing edge of it, respectively (see Fig. 1). The cladding temperatures are obtained from thermocouples embedded in the cladding of the center rod of the 5x5 rod bundle at the elevation of the leading edge, and 12 mm downstream of the trailing edge of the grid spacer, respectively. At initiation of reflood the temperatures of the cladding as well as of the grid spacers are close to 800 C diverging from each other rapidly within the first 10 seconds of the re-

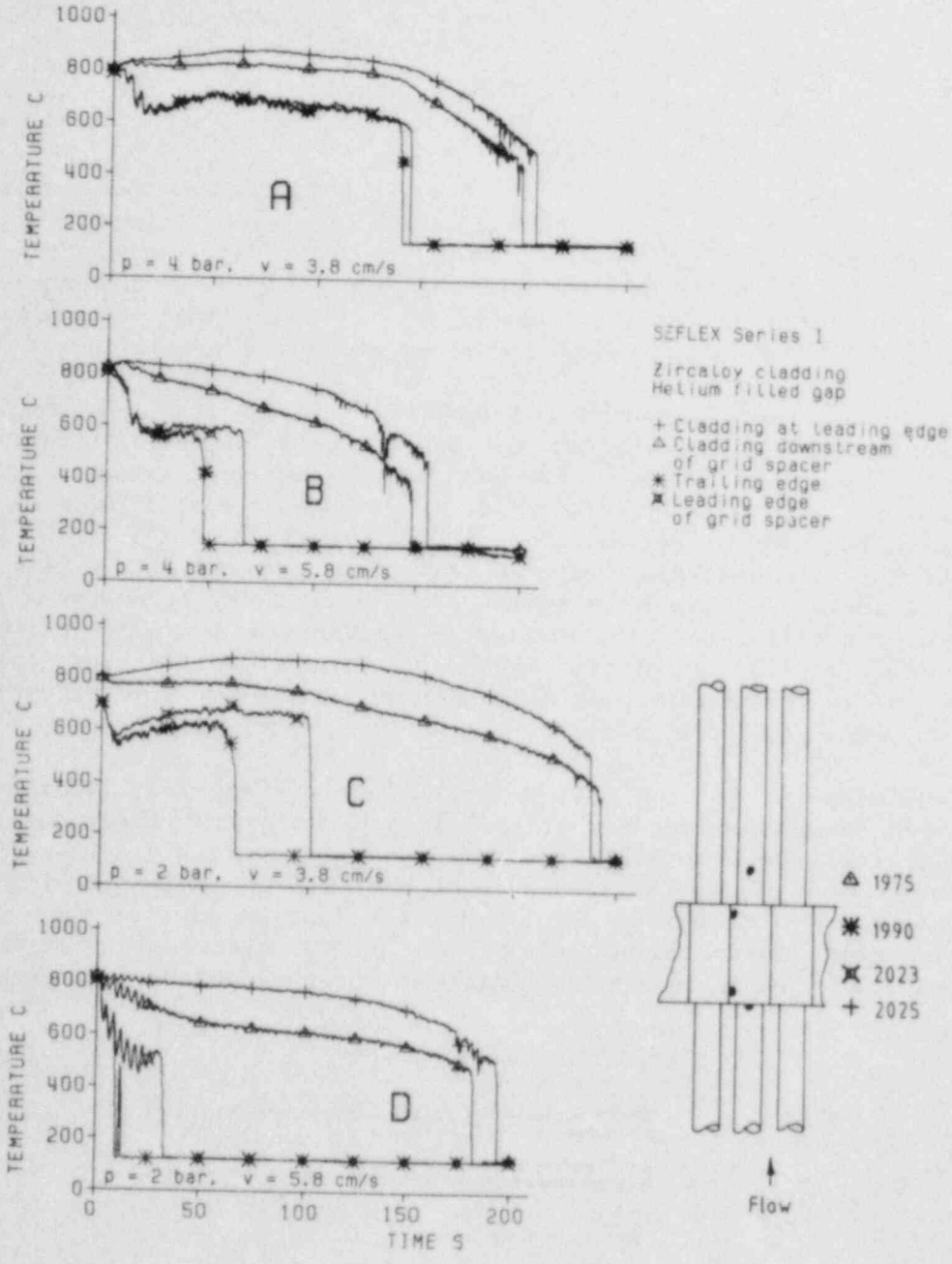


Fig. 3 Cladding and grid spacer temperatures at the leading edge and downstream of the midplane grid in the 5x5 rod bundle for various reflood conditions.

flood transient. The cladding temperatures downstream of the grid spacer then are lower than those upstream of it. The temperature differences amount to 50 K or 150 K depending on the reflood conditions. After the initial drop the temperatures of the grid spacer are being stabilized quasi for a certain time span at about 200 K below the cladding temperature measured near the leading edge of the grid. The level of this temperature transient results from the radiation heat transfer from the rods to the grid, and from the dispersed flow cooling of the grid by superheated steam and water droplets being at saturation temperature. Quenching of the grid spacers occurs at different times and the ratio grid quench time to cladding quench time is different

depending on the reflood conditions. The reasons for this behavior will be explained in Section 5.

It is important to mention that quenching is initiated at the trailing edge of a grid spacer for all cases investigated. The counter current quench front at the grids needs a time span of 3 up to 36 seconds to travel from the trailing edge down to the leading edge for the total of grid spacers instrumented and of tests performed. There is no indication from the measurements that droplet impact on the leading edge promotes grid spacer quenching.

For most of the cases premature rod quenching is initiated downstream of the grid spacers as well. For the bundle midplane this is shown in Fig. 3, detail (A), (B) and (D). This leads to the conclusion that heat transfer enhancement is significant in the early portion of the transient mist flow regime. During that period the grid spacer is hot and dry. The slope of the cladding temperature transient downstream compared with that upstream of the grid spacer is scarcely changed when the grid spacer changes from dry to wet condition. Therefore, the individual droplet breakup mechanisms at a dry grid or the droplet deposition at a wet grid including reentrainment at the trailing edge seem to lead to comparable results concerning the gross heat transfer enhancement downstream of the grids.

Heat transfer analysis from data measured confirms previous findings [4] that cooling enhancement downstream of grid spacers shows a maximum for the early portion of the transient mist flow regime. The heat flux at the rod surface 12 mm downstream of the trailing edge of the grid spacer is about 20 % higher than that at the rod surface neighboring the leading edge of the grid spacer. The enhancement disappears towards the end of the mist cooling period as shown in Fig. 4. There is a second maximum for the cooling enhancement at the

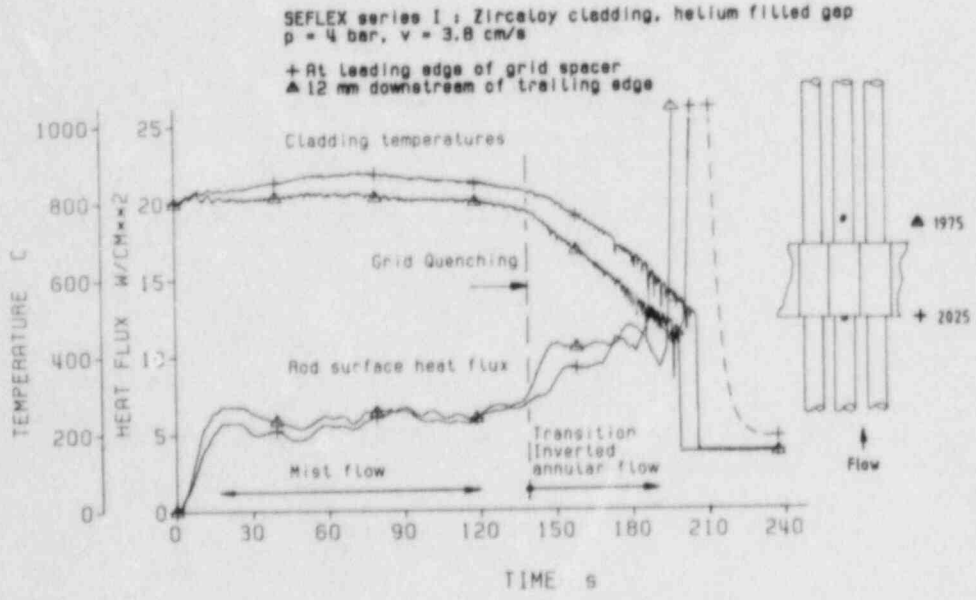


Fig. 4 Cladding temperatures and surface heat flux at leading edge and 12 mm downstream of the midplane grid spacer (5x5 rods)

onset of transition film boiling characterized by increased water content in the two-phase flow. The increase of the water content has presumably led to grid spacer rewetting coincidently in the case shown in Fig. 4. This coincidence is not observed in this test for the remaining grid spacers at different elevations in the bundle or for other tests performed with different reflood conditions. The cooling enhancement from the grid during the transition film boiling regime is of the same order of magnitude as that during the mist flow regime. However, concerning clad ballooning local cooling enhancement is more important during the mist flow regime.

The axial extension of the grid spacer effect on the local cooling enhancement depends on the reflood conditions. The results are consistent with previous findings [4]. Surface heat flux and cladding temperatures upstream and further downstream of the midplane grid spacer are shown in Fig. 5 complemen-

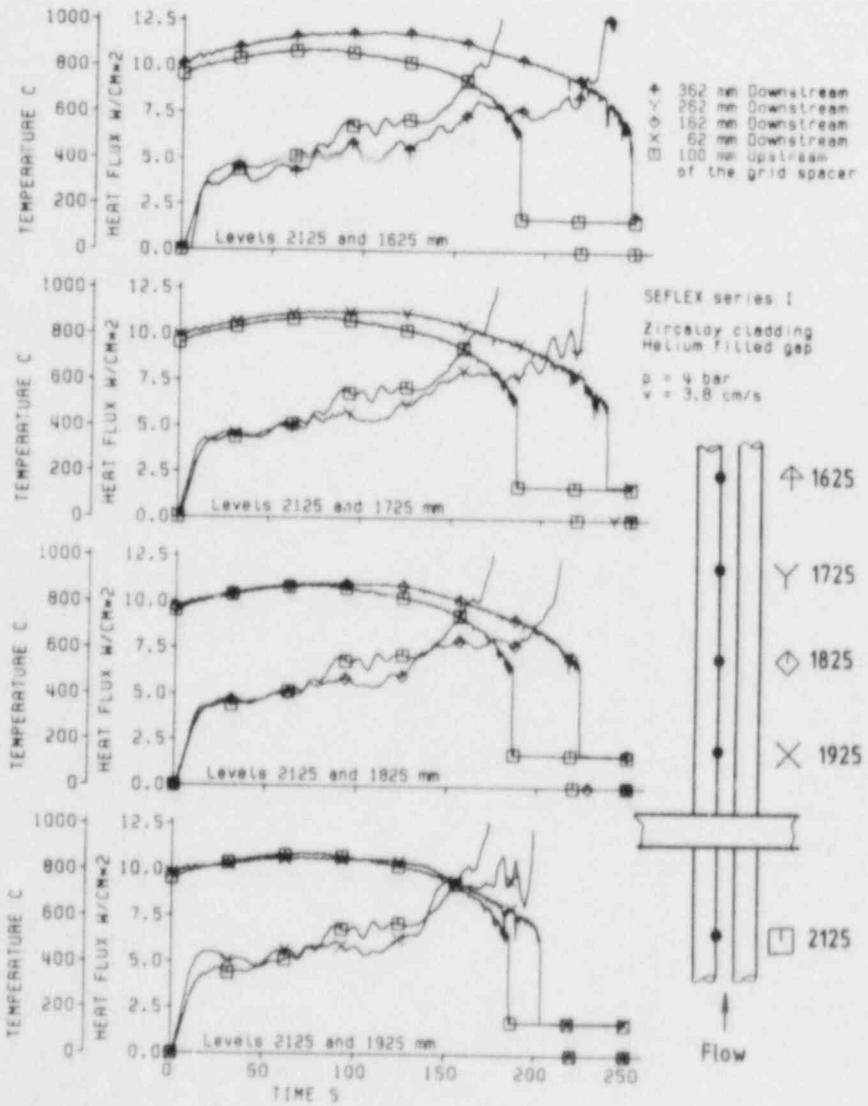


Fig. 5 Surface heat flux and cladding temperatures up- and downstream of the midplane grid spacer

ting the data of the test plotted in Figs. 3(A) and 4. 62 mm downstream of the trailing edge the grid spacer cooling enhancement only remains for the early portion of the mist flow regime compared with the cooling conditions 100 mm upstream of the grid (compare levels 2125 and 1925 mm). 162 mm as well as 262 mm downstream the cooling conditions still are approximately the same as 100 mm upstream of the grid during the early portion of the mist flow regime inspite of the increased distance from the quench front. 362 mm downstream there is no more grid spacer effect under the reflood conditions mentioned.

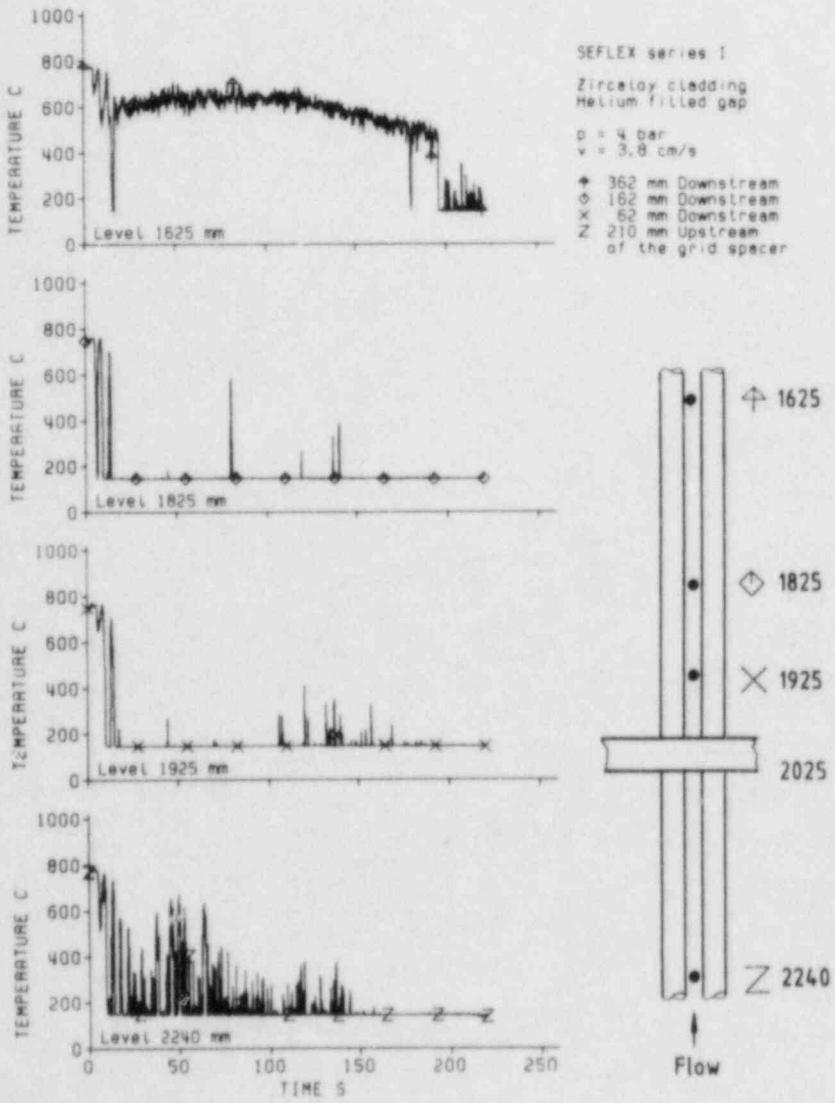


Fig. 6 Fluid TC signals up- and downstream of the grid spacer at the bundle midplane (5x5 rods)

Investigation of the fluid flow conditions leading to the cooling enhancement quantified calls for information about the droplet size and velocity distribution as well as about the local steam temperature and flow turbulence. The contribution from the 5x5 rod bundle gross measurements about the steam temperature signals are obtained from thermocouples (TC) of 0.25 mm outer sheath diameter protruding into a bundle subchannel.

Figure 6 shows fluid TC signals measured upstream and downstream of the 5x5 rod bundle midplane complementing the data plotted in Figs. 3 (A), 4 and 5. The fluid temperature signal measured 215 mm upstream of the leading edge of the grid spacer indicates significant steam superheat. However, liquid droplets impinging upon the TC tip lead to repeated quenching of the probe preventing the measurement of the real steam temperature (see level 2240 mm). Far downstream of the grid steam superheat is clearly indicated lasting for the whole mist flow transient (see level 1625 mm). Quenching of the grid spacer at t = 140 s does not affect the steam temperature measured 362 mm downstream of the trailing edge of the grid. At the levels 1925 and 1825 mm (i.e. 62 and 162 mm downstream of the trailing edge of the grid) is less information about the steam temperature presumably due to increased droplet impinging upon the individual probe tips by the increased number but smaller size of droplets in that portion of the rod bundle.

## 4. Grid Spacer Effects Under Controlled Flow Conditions on Local Droplet Sizing and Steam Temperature in a Short 2x2 Rod Bundle

### 4.1 Experiments

Steady state steam cooling as well as two-phase flow cooling tests under controlled condition of droplet injection in a short 2x2 rod bundle have been performed. The square bundle housing with 7.94 mm thick walls and an inside dimension of 36x36 mm is heated electrically by strip heaters wrapped around the outside and covered with ceramic fiber insulation in order to avoid radial heat loss. The 1.60 m-long bundle of 2x2 rods is heated uniformly over a length of 1.10 m by heating coils embedded in MgO inside the rods. The heated length corresponds to an axial section between three grid spacer elevations of a PWR fuel rod bundle. At bundle midplane a PWR grid spacer without mixing vanes is placed spacing the rods of 10.75 mm outer diameter for a pitch of 14.3 mm (i.e. the same geometry as for the full length 5x5 rod bundle described in section 3).

A controlled mass flux of superheated steam flows from the lower to the upper end of the 2x2 rod bundle. A thin water nozzle is placed 37 mm upstream of the leading edge of the midplane grid spacer to feed the water droplets into the center of the central bundle subchannel under controlled conditions. The rod surface temperatures are measured at various elevations by thermocouples embedded in the NiCr claddings of 1 mm thickness. For measuring the temperatures of the water and the steam coolant phases at various locations within the bundle an unshielded thermocouple sheathed by an Inconel tube of 0.25 mm outer diameter can be moved along the bundle subchannels. The experimental facility is shown in Fig. 7 schematically.

Two pairs of quartz glass windows at elevations respectively just upstream and downstream of the test grid spacer are provided for *in situ* Laser-Doppler anemometry (LDA) measurement of droplet dynamics across the spacer in the center subchannel. The two optical measurement schemes, one for large drop-

lets [9] and one for small droplets [10] are alternately applied with an essentially identical optical arrangement, a sketch of which is shown in Fig. 8.

## 4.2 Review of the Results from the 2x2 Rod Bundle Steady State Cooling Tests

A sample of the results published in e.g. [15] is reviewed for the combined analysis presented in section 5.

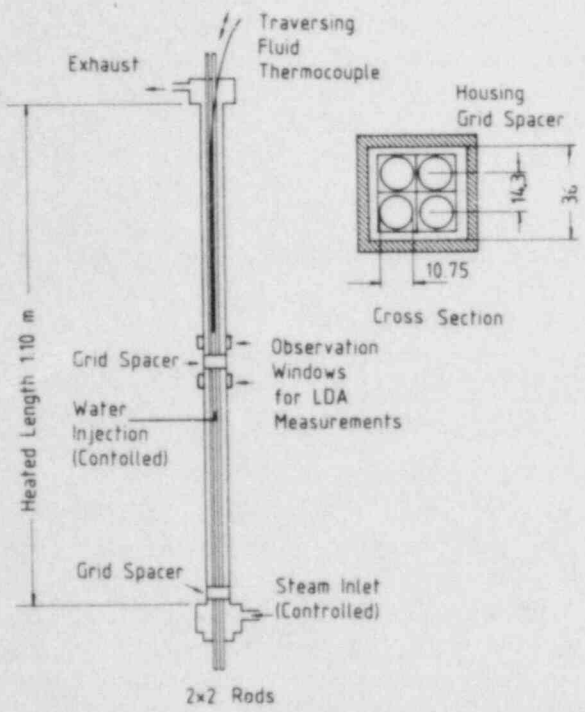


Fig. 7 2x2 rod bundle test facility, grid spacer and LDA measurement locations

The axial profiles of cladding and fluid temperatures in the 2x2 rod bundle are obtained under quasi steady state flow and power conditions. For a given steam mass flux without water injection the steady increase of the cladding and the fluid temperatures from bottom to top of the bundle is interrupted across the mid-plane grid spacer and downstream of it. Increased turbulence leading to local cooling enhancement lowers the cladding temperatures and rises the temperature of single phase steam flow (The effect of heat loss at the observation windows without thermal insulation on the cladding temperatures is included). Water injection into the steam flow lowers both, the local cladding temperatures and the steam temperature. Quantitative examples are shown in Fig. 9. The grid spacer heated by radiation from the rods is quenching at a given water injection rate independently from the steam mass flux within the range indicated in Fig. 10. Table 1 shows a sample of droplet size distribution measured with LDA upstream and downstream of the grid spacer for given flow conditions.

Table 1 Sample of LDA droplet size distribution measurement under steady state flow conditions in the 2x2 rod bundle [15]

| Steam Mass Flux (kg/h) | Water Inj. Rate ($cm^3$/min) | Size Meas. Scheme | Meas. Position | Sauter Mean Diameter (mm) | Data Rate (No./s) | Mean Droplet Velocity (m/s) |
|---|---|---|---|---|---|---|
| | | Large | Upstream | 1.566 | 4.17 | 11.14 |
| 24.3 | 10.5 | Small | Upstream | 0.179 | 3.99 | 13.21 |
| (LOW) | (Dry Grid | Large | Downstream | 1.307 | 3.16 | 11.30 |
| | Spacer) | Small | Downstream | 0.177 | 90.7 | 11.01 |
| | | Large | Upstream | 1.657 | 22.4 | 11.37 |
| 24.3 | 32.0 | Small | Upstream | 0.175 | 57.4 | 11.23 |
| (LOW) | (Wet Grid | Large | Downstream | 1.558 | 83.0 | 9.65 |
| | Spacer) | Small | Downstream | 0.177 | 630.0 | 10.40 |

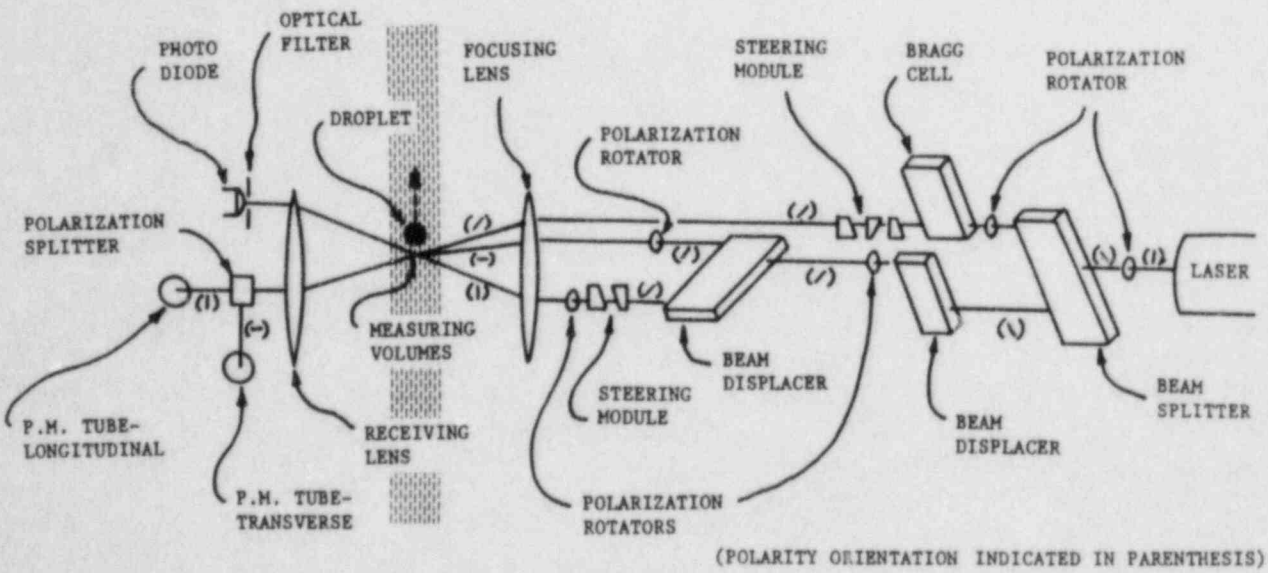


Fig. 8 Optical scheme for in situ Laser-Doppler anemometry measurement of droplet dynamics in a subchannel of the heated 2x2 rod bundle.

## 5. Combined Gross Heat Transfer and Local Temperature and Droplet Sizing Analysis of Grid Spacer Effects

The transient cooling enhancement downstream of grid spacers during the mist flow regime of the reflood phase has been quantified for various reflood conditions. These results obtained from the full length 5x5 rod bundle tests are being analyzed using the results of the local measurements of cladding and fluid temperatures as well as of droplet dynamics from the short 2x2 rod bundle tests. In order to determine the physical background of the cooling enhancement downstream of a grid spacer the integral effect is being divided into

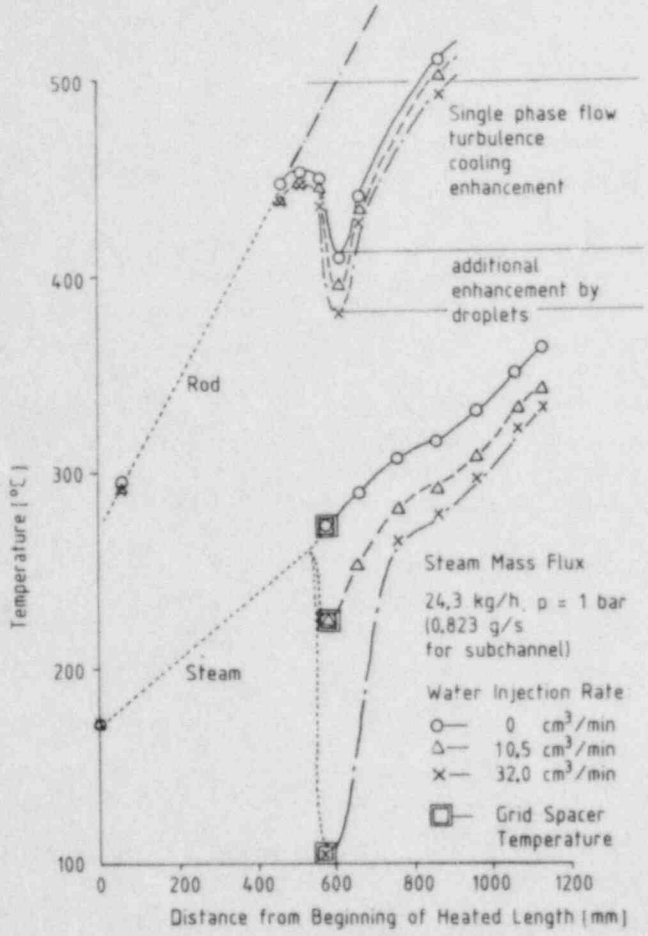


Fig. 9 Axial rod cladding and fluid temperature profiles from steady state 2x2 rod bundle tests

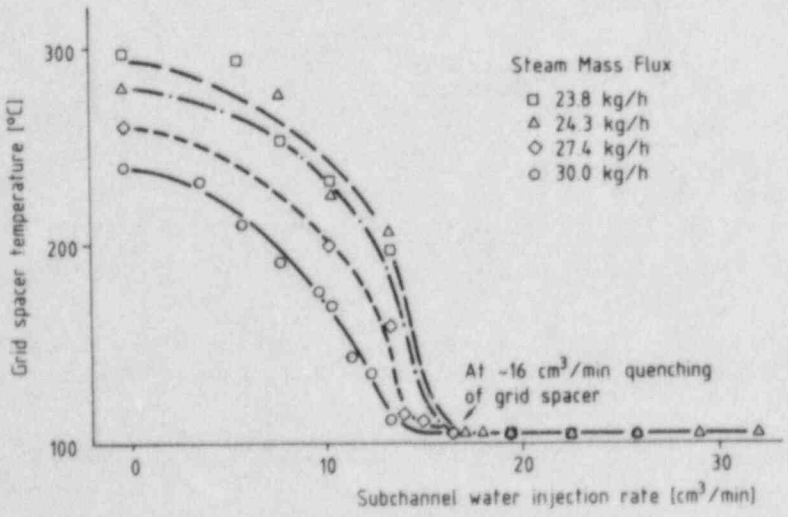


Fig. 10 Quenching of grid spacer depending on water injection and steam mass flux (2x2 rod bundle)

- turbulence enhancement in single phase steam flow and
- droplet effects in superheated steam.

## 5.1 Turbulence Enhancement Effect on Cooling Downstream of a Grid Spacer

It is evident from the results shown in Fig. 9 that turbulence enhancement in single phase superheated steam lowers the cladding temperatures downstream of the grid significantly. Due to the locally increased heat removal the temperature of the dry steam increases somewhat faster downstream of the grid than it would increase corresponding to the steady temperature profile along the bundle axis. This effect can be quantified for various velocities and pressures of superheated single phase steam adapting well established computer code models. Therefore, emphasis is placed on analyzing the additional cooling enhancement by water droplets carried with superheated steam.

## 5.2 Droplet Effects on Cooling Enhancement Downstream of a Grid Spacer

It is evident again from the results shown in Fig. 9 that additional cooling enhancement by droplets has to be taken into account depending on the water content of the two-phase flow. The data base available is not sufficient yet for quantification of the droplet effects for various pressures and flow conditions representative for PWR reflood. However, an approach is made to determine

- the water content in a subchannel leading to rewetting of grids in a full length bundle calculating the droplet generation rate above the bundle quench front, and

- the droplet enhancement of cooling downstream of a dry and a wet grid spacer, respectively.

### 5.2.1 Correlation of Grid Spacer Quenching for the 5x5 Rod Bundle Reflood Conditions

Due to the content of water droplets in the mist flow, the grid spacer quenches far ahead of the arrival of the rod bundle quench front. The conditions for rewetting the grid heated by radiation from the rods and cooled mainly by the water entrained with the superheated steam essentially depend on
- the rod power at the grid spacer ($P_G$),
- the rod power at the rod bundle quench front ($P_Q$),
- the system pressure (p), and
- the flooding velocity (v)

for a given bundle geometry and distribution of transient rod power. The last three parameters influence the flow conditions downstream of the rod bundle quench front mainly. The conditions for the full length 5x5 rod bundle have been evaluated for the two system pressures of 2 and 4 bar and the two flooding velocities of 3.8 and 5.8 cm/s respectively. The results are listed in Table 2 for example.

Table 2 Grid spacer quench conditions evaluated from 5x5 rod bundle reflood tests

| System Pressure p, bar | Flooding Velocity, $V_f$, cm/s | Grid Spacer Number | Grid Spacer Location $L_G$, mm | Grid Spacer Quench Time, s | Rod Power at Grid Spacer, $P_G$, kW/m | Quench Front Location $L_Q$, mm | Rod Power at Quench Front, $P_Q$, kW/m |
|---|---|---|---|---|---|---|---|
| 4 | 3.8 | 1 | 3115 | 20.6 | 2.00 | 3550 | 1.38 |
| | | 2 | 2570 | 75.0 | 1.91 | 3038 | 1.82 |
| | | 3 | 2025 | 138.8 | 1.77 | 2500 | 1.70 |
| | | 4 | 1480 | 195.6 | 1.54 | 2075 | 1.62 |
| | | 5 | 935 | 246.3 | 1.41 | 1663 | 1.52 |
| | | 6 | 390 | 122.5 | 1.13 | 2638 | 1.68 |

The data from the whole set of tests and from 5 grid spacers located in the central portion of the bundle (compare Fig. 1) have been correlated empirically including the parameters mentioned as follows:

$$P_Q = 1.20\ p^{0.136} P_G^{0.833} / v^{0.2} \qquad (1)$$

where $P_Q$ = Rod power at quench front at quench time for grid spacer, kW/m
$P_G$ = Rod power at grid spacer at quench time for grid spacer, kW/m
p = System pressure, bar
v = flooding velocity in the cold bundle, cm/s

$P_Q$ and $P_G$ are depending on axial location in the bundle as well as on reflood time.

From the 2x2 rod bundle tests the water injection rate leading to grid rewetting is known (compare Fig. 10). The results are obtained by droplet injection such that all the water droplets are intercepted by the grid spacer. In the reflood mist flow situation the droplets are distributed across the subchannel flow area and therefore not all droplets are intercepted by the grid spacer. Using the effective capture thickness of a grid spacer [11, 12, 13] and a typical mean droplet diameter of 1.2 mm [3], an extrapolation has been made from the droplet volume flux injected in the 2x2 rod bundle to the local droplet volume flux in the 5x5 rod bundle for the cases of rewetting of the individual grid spacers. The instanteneous local rod power at the grids has to be taken into account as the heat source parameter for the grids. From differential pressure measurements evaluated concerning the axial distribution of the water content in full length bundles it has been found that there is only small axial decrease of droplet volume flux in the mist flow regime [2]. Therefore, downstream of the inverted annular flow, i.e. shortly downstream of the bundle quench front, the droplet content remains roughly the same up to the grid spacers quenching far downstream of the bundle quench front. It can be assumed that the droplet volume flux at a quenching grid spacer ($Q_{1G}$) is not essentially lower than that closely above the rod bundle quench front ($Q_1 \approx Q_{1G} = f(P_G)$). Under these conditions, including the conversion of the droplet volume flux in the 2x2 rod bundle into that in the 5x5 rod bundle as well as the correlation (1), the droplet generation rate,

closely above the quench front and the droplet volume flux, respectively, have been correlated:

$$Q_l = f\ (P_Q,\ v,\ p) \qquad (2)$$

where $Q_l$ = Water droplet volume flux in a subchannel for mist flow condition leading to grid spacer quenching

Table 3 gives an example of $P_Q$ and bundle quench front location for one test and the resulting droplet volume flux. Replacing $P_Q$ by the axial location of the bundle quench front for the various reflood conditions of the set of tests of the 5x5 rod bundle a correlation is obtained following the function

$$Q_l = f(x_Q,\ v,\ p) \qquad (3)$$

where $x_Q$ = location of the quench front measured from the bottom end of the heated zone of the full length 5x5 rod bundle depending on time, $x_Q = 3975 - L_Q$ (see Table 3).

A plot of the correlation $Q_l$ versus reflood time for the set of four different reflood conditions makes evident that the droplet volume flux is low for high pressure and low flooding velocity as shown in Fig. 11. In this plot grid spacer quench times are indicated for the set f tests. The comparison of the grid spacer quench times in the individual tests with the corresponding droplet volume flux explains the relatively late grid spacer quenching for the case of p = 4 bar and v = 3.8 cm/s. Under these conditions the lowest droplet volume flux arises during the mist flow regime. Under the conditions indicated for the remaining tests the droplet volume flux is increasing faster, and it is reaching higher levels, respectively, during the same period. Thus, the grid spacers are quenching earlier for lower pressure and/or for increased flooding velocity.

It has to be mentioned that the correlations (2) and (3) only are valid for the mist flow condition which is terminated at transition to inverted annular flow.

Table 3 Subchannel droplet volume flux calculated from combined test data for the reflood conditions in the full length 5x5 rod bundle

| Test Data | | | | | Calculation |
|---|---|---|---|---|---|
| System Pressure, p, bar | Flooding Velocity, $V_f$, cm/s | Grid Spacer Number | Quench Front Location $L_Q$, mm | Rod Power at Quench Front | Droplet Volume Flux, $Q_l$ $cm^3/s$ |
| 4 | 3.8 | 1 | 3550 | 1.38 | 1.060 |
| | | 2 | 3038 | 1.82 | 1.289 |
| | | 3 | 2500 | 1.70 | 1.226 |
| | | 4 | 2075 | 1.62 | 1.184 |
| | | 5 | 1663 | 1.52 | 1.132 |
| | | 6 | 2638 | 1.68 | 1.215 |

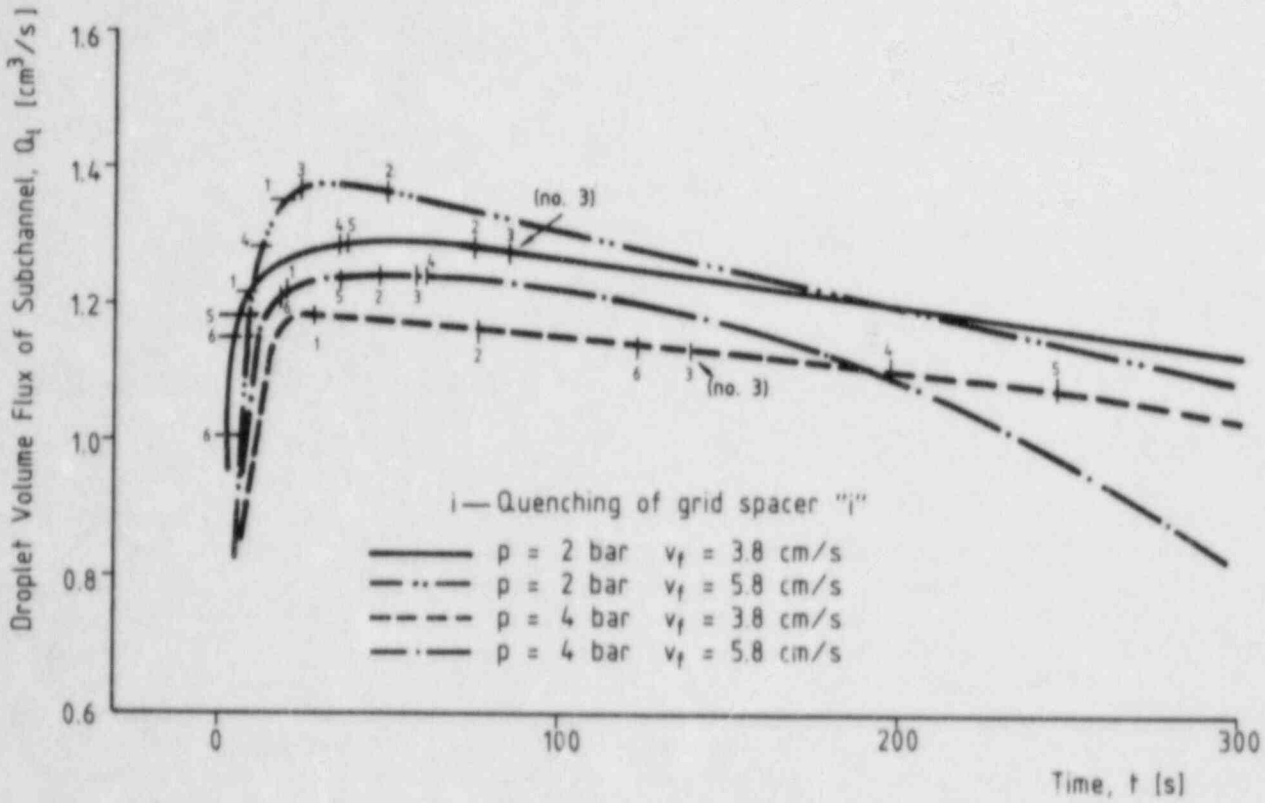


Fig. 11 Transient droplet volume flux during mist flow correlated from 2x2 rod and 5x5 rod bundle test data, grid quenching indicated.

5.2.2 Separation of Droplet Effects on Cooling Enhancement for Dry and for Wet Grid Spacer Condition

The transient cooling conditions during reflood tests make difficult the distinction whether the change of the grid spacer condition from dry to wet or the change of the arriving fluid influence the grid spacer effect. From the steady state 2x2 rod bundle tests the following information is obtained: For the case of the wet grid spacer and the high water injection rate the cooling enhancement downstream is higher than for the case of the dry grid spacer and the low water injection rate. It is not possible to run a steady state experiment using the same injection rate for dry and wet grid spacer as well.

Therefore, from the transient 5x5 rod bundle tests boundary conditions are selected characterized by rather stable mist flow conditions for the time span in which a grid spacer is quenching. Furthermore, the bundle section upstream and downstream of the grid spacer selected has to be instrumented sufficiently. For the midplane grid spacer the desired flow conditions are not given during the test performed with p = 4 bar and v = 3.8 cm/s because of the change of the fluid conditions at quenching of the grid as shown in Fig. 4. The test performed with p = 2 bar and v = 3.8 cm/s provides more stable flow conditions during the period in which the midplane grid is quenching. Figure 12 shows cladding temperatures and surface heat flux at leading edge and 12 mm downstream of the midplane grid spacer versus time. Quenching of the grid is initiated at the trailing edge at t = 65 s and terminated at the leading edge at t = 101 s. At t = 65 s the heat transfer is increasing downstream as well as upstream by about the same amount as indicated by the

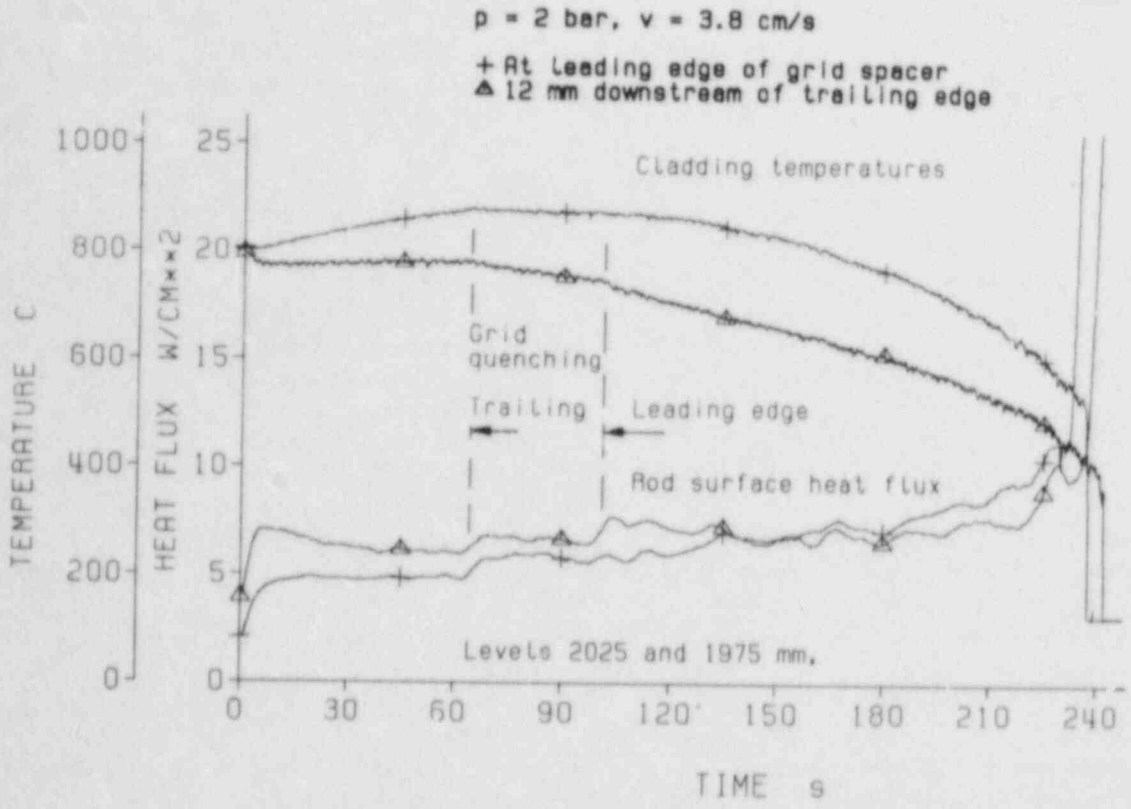


Fig. 12 Cladding temperatures and surface heat flux at leading edge and 12 mm downstream of the midplane grid spacer (5x5 rods)

heat flux transients. This is presumably due to the change of the conditions of the fluid arriving at the grid spacer elevation. At t = 101 s the surface heat flux is increasing downstream of the grid spacer only.

Analyzing this effect, the same problem arises as mentioned above for the steady state 2x2 rod bundle tests: The grid spacer effect may be increased at t = 101 s due to different droplet effects induced by the wet grid as well as due to increased droplet volume flux. However, this situation does not last for a long time. The rod surface heat flux increases then at the leading edge and decreases at the trailing edge after the peak at t = 101 s.

Comparing the magnitude of the grid spacer effect during the early portion of the mist flow regime with that evaluated for the period of grid rewetting it becomes evident that the grid spacer effect is more important during the early portion of reflood. There is a minor effect on the cooling enhancement later on time whether the grid spacer is dry or wet.

## 6. Conclusions

The results of transient tests performed under various reflood conditions using a full length 5x5 rod bundle with seven grid spacers provide informations about the grid spacer temperatures and the local effects on gross heat transfer.

The results of quasi steady state short 2x2 rod bundle cooling tests using controlled dispersed flow conditions show local droplet dynamics at grid spacers and their thermal effects.

The study of mist cooling enhancement from grid spacers under LOCA reflood conditions of a PWR combining the results of both the experimental programs leads to the following conclusions:

- The grid spacer effect is important during the early portion of the mist flow regime.
- The cooling enhancement takes place downstream of the grid spacer mainly.
- There is a minor effect on the rod cooling enhancement along the height of the grid spacer.
- There is again a minor effect on the cooling downstream later on time when the grid spacer is changing from dry to wet condition. Droplet breakup mechanisms at the grid itself do not seem to be important.
- Quenching of a grid spacer is initiated at the trailing edge of it.
- There is premature quenching of the rod claddings downstream of the grid spacers for most of the cases.
- Turbulence enhancement in single phase flow leads to cooling enhancement downstream of the grid spacer significantly.
- Droplet suspension in the region of enhanced turbulence increases local cooling moderately, and, lowers steam superheat significantly.
- Local steam desuperheating, and hence, increased steam mass flux seem to be more important for the cooling conditions further downstream.
- The influence of a grid spacer on droplet size and population downstream of it is being assessed, and, needs further investigations.
- The droplet dynamics and evaporation in the region of turbulent flow downstream of a grid spacer seem to remain the most important problems calling for continued experimental as well as analytical investigations.

## 7. References


1. "ECCS Evaluation Models", Appendix K, Part 50 - Licensing of Production and Utilization Facilities, Federal Register, 39, No. 3, p. 1003, 1974.

2. Ihle, P. and Rust, K., "FEBA-Flooding Experiments with Blocked Arrays, Evaluation Report", Report No. KfK 3657, Kernforschungszentrum Karlsruhe, March 1984.

3. Erbacher, F.J., "Interaction Between Fuel Clad Ballooning and Thermal Hydraulics in a LOCA" Proc. of the Fifth Internat. Meet. on Thermal Nuclear Reactor Safety, Karlsruhe, FRG, Sept. 9-13, 1984 (to be published)

4. Ihle, P., Rust, K., "Einfluß der Stababstandshalter auf den Wärmeübergang in der Flutphase eines DWR-Kühlmittelverluststörfalles", Report No. KfK 3178, Kernforschungszentrum Karlsruhe, June 1981.

5. Lee, N., Wong, S., Yeh, H.C. and Hochreiter, L.E., "PWR FLECHT SEASET Unblocked Bundle, Forced and Gravity Reflood Task Data Evaluation and Analysis Report", NRC/EPRI/Westinghouse Report No. 10, NUREG/CR-2256, EPRI NP-2013, WCAP-9891, November 1981.

6. Pearson, K.G. and Cooper, L.A., "Reflood Heat Transfer in Severely Blocked Fuel Assemblies", International Workshop on Fundamental Aspects of Post-Dryout Heat Transfer, Salt Lake City, Utah, April 1-4, 1984.

7. Clement, P.; Deruaz, R.; Veteau, J.M., "Reflooding of a PWR Bundle, Effect of Inlet Flow Rate Oscillations and Spacer Grids", NUREG/CP-0027 Vol. 3, Feb. 1983, pp. 1763-1770.

8. Rust, K., Ihle, P. and Lee, S.L., "Comparison of FEBA Test Data with RELAP4/MOD6 Postcalculations", Thermal-Hydraulics of Nuclear Reactors (M. Merilo, ed.), American Nuclear Society, LaGrange Park, Ill., pp. 731-737, 1983.

9. Lee, S.L. and Srinivasan, J., "A LDA Technique for In Situ Simultaneous Velocity and Size Measurement of Large Spherical Particles in a Two-Phase Suspension Flow," Int. J. of Multiphase Flow, Vol. 8, pp. 47-57, 1982.

10. Lee, S.L. and Srinivasan, J., "An Laser-Doppler Velocimetry Technique for In-Situ Local Measurement of Dilute Two-Phase Suspension Flows," Eng. Appl. of Laser-Velocimetry, (H.W. Coleman, ed.), ASME, New York, pp. 117-125, 1982.

11. Lee, S.L., Rob, K. and Cho, S.K., "LDA Measurement of Mist Flow Across Grid Spacer Plate Important in Loss of Coolant Accident Reflood of Pressurized Water Reactor," Proc. Int. Symp. on Appl. of Laser-Doppler Anemometry to Fluid Mech., Lisbon, pp. 5.3.1 to 5.9.1 to 5.9.7, 1982.

12. Lee, S.L., Cho, S.K., Rob, K., Sheen, H.J. and Aghili, M., "An LDA In-Situ Study of Droplet Hydrodynamics Across Grid Spacers in PWR-LOCA Reflood," Proc. Tenth-Water Reactor Safety Information Mt., Gaithersburg, Md., NUREG/CP-0041, Vol. 1, pp. 253-274, 1982.

13. Lee, S.L., Cho, S.K., Rob, K. and Sheen, H.J., "Reentrainment of Droplet from Grid Spacer in Mist Flow Portion of LOCA Reflood of PWR," Proc. Joint NRC/ANS Mt. on Basic Thermal Hydraulic Mechanisms in LWR Analysis, Bethesda, Md., pp. 477-485, 1982.

14. Chiou, J., Hochreiter, L.E., Utton, D.B. and Young, M.Y., "Spacer Grid Heat Transfer Effects During Reflood", Proc. Joint NRC/ANS Meeting on Basic Thermal Hydraulic Mechanisms in LWR Analysis, Bethesda, Md., pp. 445-475, 1982.

15. Lee, S.L., Sheen, H.J., Cho, S.K., Issapour, I. and Hua, S.Q., "Measurement of Grid Spacer's Enhanced Droplet Cooling under Reflood Condition in a PWR by LDA", Proc. Eleventh Water Reactor Safety Information Mt., Gaithersburg, Md., NUREG/CP-0048, Vol. 1, pp. 233-250, 1984.

16. Lee, S.L., Sheen, H.J., Cho, S.K. and Issapour, I., "Laser-Doppler Anemometry Measurement of Droplet Dynamics in Mist Cooling of Rod Subchannel of a Pressurized Water Reactor", Proc. Int. Symp. on Two-Phase Annular and Dispersed Flows, Pisa, Italy, June 24-29, 1984, pp. D5-1 to D5-3.

17. Lee, S.L., Sheen, H.J., Cho, S.K. and Issapour, I., "LDA Measurement of Water Droplet-Vapor Mist Flow Across a Heated Grid Spacer Important in Reflood Cooling of Pressurized Water Reactor in Loss of Coolant Accident", Proc. Second Int. Symp. on Application of Laser Anemometry to Fluid Mechanics, Lisbon, July 2-4, 1984, pp. 16-3-1 to 16-3-6.

18. Adams, J.E. and Clare, A.J., "Droplet Breakup and Entrainment at P.W.R. Spacer Grids", International Workshop on Fundamental Aspects of Post-Dryout Heat Transfer, Salt Lake City, Utah, April 1-4, 1984.

19. Clare, A.J. and Fairbairn, S.A., "Droplet Dynamics and Heat Transfer in Dispersed Two-Phase Flow", International Workshop on Fundamental Aspects of Post-Dryout Heat Transfer, Salt Lake City, Utah, April 1-4, 1984.

20. Ihle, P., Rust, K. and Lee, S.L., "Experimental Investigation of Reflood Heat Transfer in the Wake of Spacer Grids," Proc. Joint NRC/ANS Mt. on Basic Thermal Hydraulic Mechanisms in LWR Analysis, Bethesda, Md., pp. 417-443, 1982.

21. Ihle, P., Rust, K. and Lee, S.L., "Mist Core Cooling During the Reflood Phase of PWR-LOCA," Proc. Int. Mt. on Thermal Nuclear Reactor Safety, Chicago, Ill, pp. 1801-1809, 1982,.

22. Lee, S.L., Ihle, P. and Rust, K., "On the Importance of Grid Spacer Induced Mist Cooling on the Suppression of Core Peak Cladding Temperature During Reflood of PWR", Proc. ASME-JSME-Thermal Eng. Joint Conf., 1983, Honolulu, Hawaii, Vol. 3, pp. 381-385, 1983.

23. Wiehr, K., Erbacher, F., Harten, U., Just, W. and Schäffner, P., "Untersuchungen zur Wechselwirkung zwischen aufblähenden Zircaloy-Hüllen und Einsetzen der Kernnotkühlung (REBEKA-Programm)", in: Projekt Nukleare Sicherheit, Annual report 1983, Report No. KfK 3450, Kernforschungszentrum Karlsruhe, June 1984, pp. 4200-42 to 4200-97

24. Ihle, P., Rust, K. and Schneider, H., "Fuel Rod Simulator Effects in Flooding Experiments (SEFLEX-Program)", in Projekt Nukleare Sicherheit, Annual Report 1983, Report No. KfK 3450, Kernforschungszentrum Karlsruhe, pp. 4200-93 to 4200-111, June 1984.

# TRANSIENT CRITICAL HEAT FLUX MODELING

By

F.S. Gunnerson, K.O.Pasamehmetoglu and E.R. Hosler

College of Engineering
University of Central Florida
Orlando, Florida 32816

## ABSTRACT

The relative merits of various steady-state critical heat flux (CHF) correlations in predicting transient CHF behavior has been assessed. Primary emphasis was given to the large break loss-of-coolant accident (LBLOCA) since the hypothetical LOCA in a pressurized water reactor (PWR) would result in the most rapid and severe thermal-hydraulic transient. Most available experimental data likewise focus in this area. In addition, transient CHF behavior for the small break loss-of-coolant accident (SBLOCA), the loss-of-flow accident (LOFA) and the reactivity initiated accident (RIA) scenarios have also been qualitatively assessed from first principles.

Results suggest that a combination of the steady-state Biasi and Griffith-Zuber correlations may be used for a 'first estimate' of the LBLOCA and SBLOCA transient CHF behaviors.

An analytical model for transient CHF prediction is presented and is used to assess the limitations of steady-state correlations in modeling transient CHF behavior.

NOMENCLATURE:

| | |
|---|---|
| CHFR | Critical Heat Flux Ratio = $q_c/q$ |
| D | Diameter, hydraulic or equivalent (m) |
| $E_v$ | Liquid layer evaporation rate (kg/sec) |
| G | Mass velocity ($kg/m^2$-sec) |
| L | Heated axial length (m) |
| P | Pressure (Pa) |
| $P_{cr}$ | Critical pressure (Pa) |
| q | Local heat flux ($W/m^2$) |
| $q_c$ | Critical heat flux ($W/m^2$) |
| $T_c$ | Coolant temperature (K) |
| t | Time into transient (sec) |
| $t_{0.5}$ | Time required for 50% reduction (sec) |
| x | Quality |
| $W_f$ | Liquid supply rate to microlayer (kg/sec) |
| $\delta_f$ | Microlayer thickness (m) |
| $\phi$ | Transient contribution to CHF = ($W/m^2$) |
| $\tau$ | Exponential period (sec) |

Subscripts:

| | |
|---|---|
| o | initial value |
| ss | steady state |
| TR | transient |
| P | pressure |
| G | flow |
| x | quality |
| q | power |

# I. INTRODUCTION

A major limitation on the thermal design of a light water reactor (LWR) is the necessity to maintain an adequate safety margin between the critical heat flux (CHF) and the local heat flux. The safety margin is generally quantified by the ratio of the CHF to the local heat flux, and is commonly termed as the departure from nucleate boiling ratio (DNBR) or the critical heat flux ratio (CHFR). Since the CHFR is a measure of the safety margin to CHF, a value less than unity implies that the CHF has been exceeded. Extended operation at local power levels in excess of the CHF can lead to high temperature oxidation and embrittlement of the zircaloy cladding thus jeopardizing the fuel rod's integrity.

Transient critical heat flux phenomena continue to elude all attempts of complete analytical modeling, and consequently, predictive techniques continue to rely on emipirical correlations. Since most transients consist of simultaneous pressure, flow, and power transients, it is difficult to unravel the individual and combined effects of these parameters on the CHF.

Over the years, many experiments have been conducted to investigate transient behavior within an environment indicative of a commercial LWR. Most experiments were designed for thermal-hydraulic code development and verification or for assessing fuel rod behavior. Often, the CHF behavior was of secondary importance, and the experimental components were not specifically instrumented to detail the CHF behavior. Additionally, the resultant experimental data bases may not be directly applicable to LWR transients. Much of the available data are based on single-rod or small bundle geometries, with electric heater lengths considerably shorter than commercial LWR nuclear rods. The influence of certain parameters, such a grid spacers, cladding thermocouples, and heating mode (electric vs. nuclear) are often neglected. Therefore a large uncertainty may be expected when applying the experimental CHF results from a variety of tests to a specific LWR transient.

Steady-state CHF correlations are likewise subject to considerable uncertainty. Most correlations, even when applied within the suggested parametric range of its data base have CHF uncertainities on the order of $\pm$ 10 to 30 percent. Even larger errors could be expected when the steady-state correlations are called upon for predicting transient behavior. Therefore, it is suggested that if steady-state CHF correlations are to be used for modeling transient CHF behavior, the predictions should be considered as 'best-estimate' only and under certain conditions are subject to considerable error.

An overview of transient CHF modeling with steady-state correlations is presented within Section II of this report. A correlation package, developed from steady-state CHF correlations, is proposed for a 'first estimate' of transient CHF during the large and small break loss-of-coolant accident scenarios. Considerable uncertainty, however, may result if the correlation package is applied to other transient conditions.

Analytical aspects of the transient CHF are presented in Section III. An appropriate mathematical model, based on first principles, is generated and is used to assess the applicability and limitations of the steady-state CHF correlations in predicting transient CHF behavior. Conceptual transient CHF curves are presented and are used to illustrate the conditions when the steady-state correlations will predict early, late or exact transient CHF behavior.

Section IV summarizes the results of this study.

## II. TRANSIENT CHF MODELING WITH STEADY-STATE CORRELATIONS

To compare the relative merits of various steady-state CHF correlations, CHFR's and DNBR's from the correlations have been compared with experimental transient data. The one-dimensional computer program CODA, developed by Leung and Gallivan [1], was used to perform the calculations for each correlation. The coolant-dynamic analysis (CODA) computer program is a one-dimensional, thermal-hydraulic program based on the homogeneous flow assumption. It requires coolant flowrate, coolant temperature, pressure and heat flux for input parameters. A detailed description of the program can be found in Reference 2. The steady-state correlations that have been assessed in this and previous studies [2], [3] include: Biasi, Local Barnett, Bowring, CISE, B&W-2, Westinghouse-3, Griffith-Zuber, Modified-Zuber, GE, Condie, Hsu-Becker, BWC, LOFT, CE-1, Savannah River, and Katto correlations. These correlations were selected since they are internationally recognized within the nuclear communitites. Many additional correlations are available and may warrant future assessments.

The transient CHF data used for this comparison study and in previous studies [2,3] include blowdown transients. Additional domestic and foreign transient data are available, but due to time limitations, were not included in this study. The blowdown data stems from hot leg and cold leg blowdown tests conducted in the Semiscale (Mod-1,3), THTF, PBF, Columbia University and ANL-Freon facilities. Details of the experimental data are not reported here but can be found within reference [2].

The experimental CHF data and predicted results are presented in the form of the time-to-CHF at various axial locations for each CHF correlation. Figure 1 illustrates a comparison of various steady-state CHF correlations in predicting transient CHF behavior for a single blowdown test. Comparative figures of this type have been previously reported [2], [3] for most available transient CHF data and, due to space limitations, cannot be presented in this report. Table I summarizes the blowdown CHF results of Leung [2] and Lo [3] and this study. A large circle indicates good predictions; a small circle acceptable, and a darkened circle implies poor results.

Caution must be exercised, however, in interpreting the results given in Table I. For more precise conclusions figures similar to Figure 1 for individual tests must be examined. For example the good prediction obtained by most of the correlations

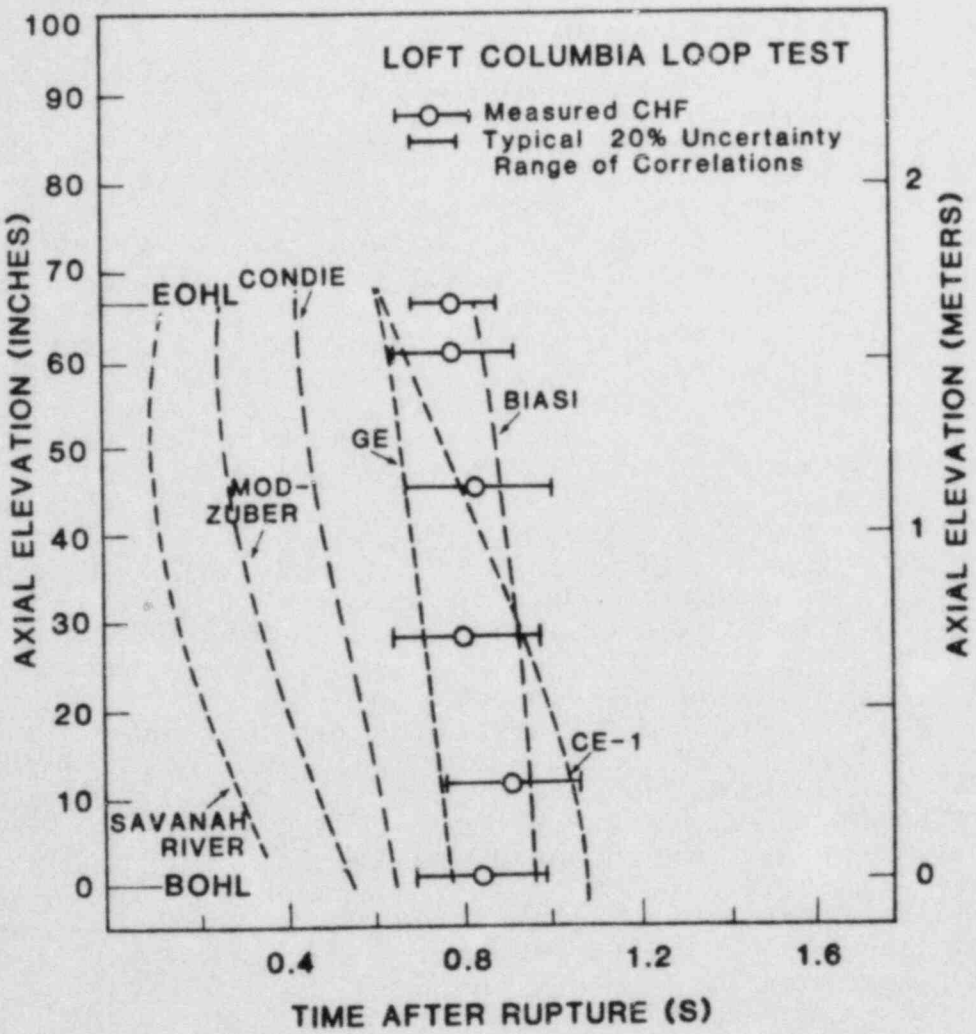


Figure 1 Critical Heat Flux Predictions Via Steady-State Correlations for the LOFT Columbia Loop Test (Simulated Blowdown, Uniform Power Profile, Electric Heat, Two 25-Rod Bundles, 52.5kW/m, Blowdown From 15.2 MPa).

TABLE I Summary of Blowdown Heat Transfer Results

| Tests and Specifications | Bowring | Biasi | CISE | Griffith-Zuber | GE | Condie Mod-7 | B&W-2 | Hsu-Beckner | x-1.0 | W-3 | Savannah River | CE-1 | Local Barnett | LOFT | BWC | Modified Zuber |
|---|---|---|---|---|---|---|---|---|---|---|---|---|---|---|---|---|
| CE/EPRI Rod-Bundle BHT-25 | ○ | ○ | ○ | ○ | ○ | ○ | ○ | ○ | ○ | ○ | ● | ○ | ○ | ○ | ● | ○ |
| LOFT Columbia Loop | ○ | ○ | ○ | ● | ○ | ▲ | ○ | ● | ○ | ● | ● | ○ | ○ | ● | ● | ● |
| PBF LOC-11C | ● | ● | ● | ○ | ○ | ○ | ● | ● | ● | ● | ● | ● | ● | ● | ● | ▲ |
| THIF Bundle #1 | | | | | | | | | | | | | | | | |
| Test 105 | ▲ | ○ | ○ | ▲ | ○ | ▲ | ▲ | ● | ○ | ● | ● | ▲ | ○ | ○ | ● | ● |
| Test 104 | ○ | ○ | ○ | ▲ | ○ | ▲ | ▲ | ● | ○ | ▲ | ● | ▲ | ○ | ▲ | ▲ | ▲ |
| Test 178 | ○ | ○ | ○ | ▲ | ▲ | ▲ | ▲ | ▲ | ○ | ● | ● | ● | ▲ | ● | ● | ▲ |
| Test 181 | ▲ | ○ | ○ | ▲ | ▲ | ▲ | ● | ▲ | ○ | ● | ● | ● | ● | ● | ● | ● |
| Test 177 | ● | ○ | ○ | ○ | ○ | ▲ | ● | ▲ | ○ | ● | ● | ● | ● | ● | ● | ▲ |
| Semiscale Mod-1 | | | | | | | | | | | | | | | | |
| S-02-1 | ● | ● | ● | ○ | ● | ● | ● | ▲ | ● | ● | ● | ● | ● | ● | ● | ● |
| S-02-9 | ○ | ○ | ○ | ● | ▲ | ▲ | ○ | ● | ● | ● | ● | ○ | ○ | ● | ● | ● |
| S-29-2 | ○ | ▲ | ○ | ● | ▲ | ▲ | ▲ | ● | ● | ● | ● | ○ | ○ | ● | ● | ● |
| S-28-1 | ○● | ○▲ | ○▲ | ●○ | ○○ | ▲● | ○▲ | ▲● | ●● | ●● | ●● | ○● | ○▲ | ●● | ●● | ●○ |
| (Early and delay CHF) | | | | | | | | | | | | | | | | |
| S-06-6 | ● | ● | ● | ▲ | ● | ○ | ● | ▲ | ● | ● | ● | ● | ● | ● | ● | ● |
| Semiscale Mod-3 | | | | | | | | | | | | | | | | |
| S-07-3 | ○ | ○ | ○ | ● | ○ | ▲ | ○ | ● | ▲ | ● | ● | ○ | ● | ● | ● | ● |
| S-07-9 | ○ | ○ | ○ | ▲ | ▲ | ▲ | ▲ | ▲ | ▲ | ● | ● | ● | ● | ● | ● | ▲ |

NOTATION: ○ GOOD PREDICTION ▲ ACCEPTABLE (USUSALLY EARLY $t_{CHF}$ PREDICTED) ● UNACCEPTABLE (MANY CASES NO CHF PREDICTION)

in CE/EPRI rod-bundle BHT-25 test was due to the fact that no CHF was observed during the test and the correlations did not indeed predict any CHF, although they resulted in different values for CHFR. In some other tests, the correlations classified as providing good prediction were, in general, unable to predict the CHF in a few locations or predicted CHF at certain elevations where no CHF was experimentally observed. Similarly, the CHF which occurred after rewet could not be predicted by any of the correlations.

The correlations of Katto [4 through 6], which are not included in Table I, provided very poor predictions in all the blowdown tests. This is thought to be due to the characteristics inherent to the development of these correlations. They were derived for a uniform heat flux distribution and for subcooled or saturated inlet conditions. These two restrictions are directly reflected in the computational form of the Katto correlations. However, for blowdown experiments, especially the cold-leg break tests which result in flow reversal situations where a fictious inlet needs to be defined in the middle of the flow channel, the inlet conditions were resulting in high quality ($x>0.1$) two phase flow.

The salient results of this and the previous studies indicate the following with respect to blowdown transient CHF modeling via steady-state correlations:

(i) The Biasi [7] and CISE [8] correlations, in general, provided the best predictions for most hot-leg and cold-leg LBLOCA conditions where significant coolant flow continued. Both of these correlations, however, could not model low flow CHF.

(ii) For conditions of low flow the Griffith-Zuber [9] correlation predicted best.

It is therefore suggested that a simple combination of the Biasi and Griffith-Zuber correlations may be used for a best 'first-estimate' of LBLOCA transient CHF. A more elaborate steady-state correlation package may be possible to enhance the predictive accuracy, but within the uncertainity of the correlations themselves and the uncertainity of the experimental data, such endeavors may be only academic.

Figure 2 quantitatively illustrates three-dimensonal CHF surfaces in CHF-quality-mass flux space. These surfaces are generated from the suggested combination of the Biasi and Griffith-Zuber steady-state CHF correlations, and illustrate the CHF behavior at two different pressures of interest.

## III. THEORETICAL ASPECTS OF THE TRANSIENT CRITICAL HEAT FLUX

A steady-state CHF correlation may be written in the following general form:

$$q_{c,ss} = q_{c,ss}\,[P,G,x,\ L/D] \qquad 1)$$

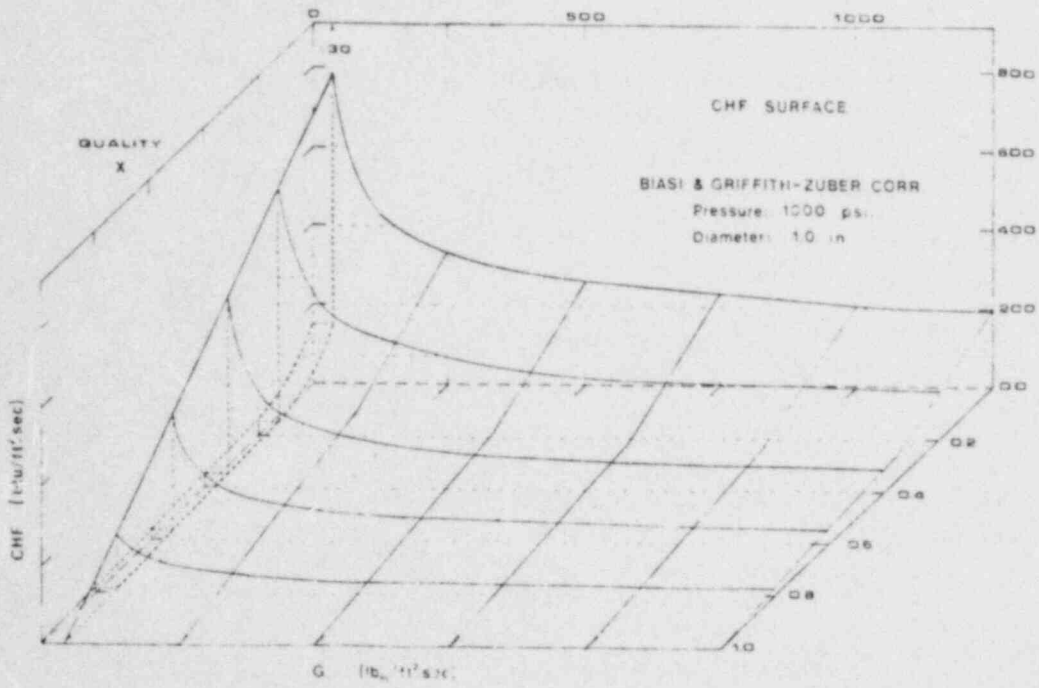


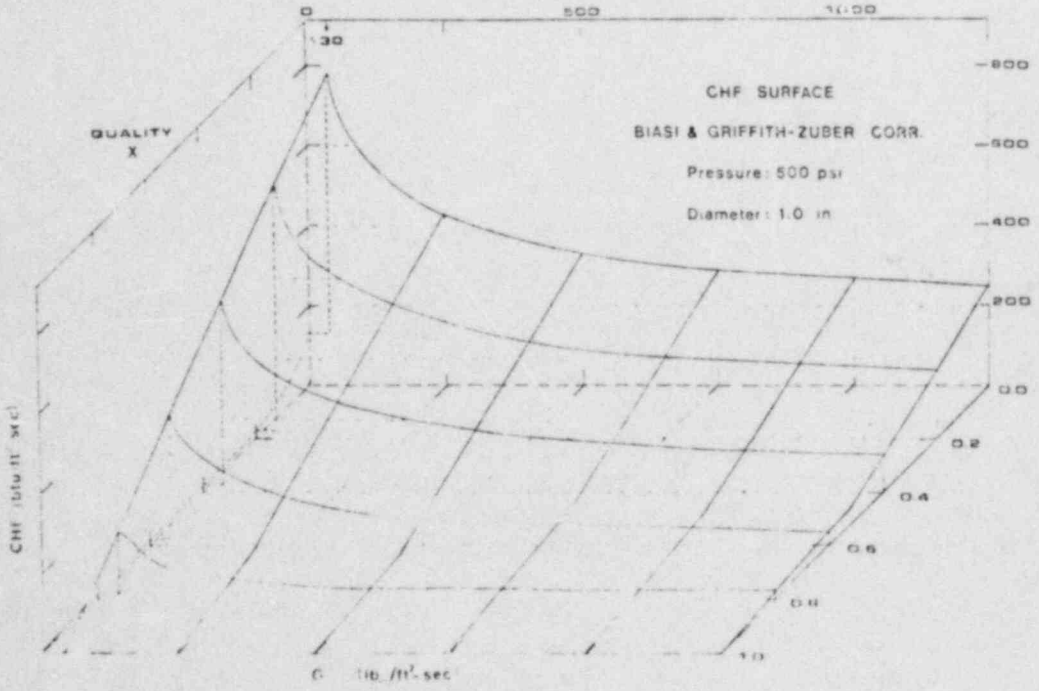


Figure 2 Critical Heat Flux Surface for Pressures of 1000 and 500 psi, Generated From Biasi and Griffith-Zuber Steady-State Correlations. (Biasi Correlation is Extrapolated to Zero Quality From 0.05 at 500 psi and From 0.1 at 1000 psi)

For a given facility L/D is constant and the correlation may be rewritten in terms of the major CHF parameters:

$$q_{c,ss} = q_{c,ss}\,[P,G,x] \tag{2}$$

For transient CHF, time is also a major parameter, thus

$$q_{c,TR} = q_{c,TR}\,[t,P(t),G(t),x(t)] \tag{3}$$

Assuming that no major discontinuities exist in the CHF behavior and that for a given set of thermal-hydraulic conditions the value of the CHF is unique, a continuous CHF curve for a given transient may be obtained with respect to the time. The total derivative of the critical heat flux with respect to time becomes:

$$(dq_c/dt) = (\partial q_c/\partial t) + (\partial q_c/\partial P)\,(dP/dt) + (\partial q_c/\partial G)\,(dG/dt) + (\partial q_c/\partial x)\,(dx/dt) \tag{4}$$

If $(\partial q_c/\partial t) \simeq 0$, then quasi-steady state conditions are satisfied and the transient CHF is approximately equal to the steady state CHF, or:

$$q_{c,TR} \simeq q_{c,ss}\,[P(t),\ G(t),\ x(t)] \tag{5}$$

Integrating Equation 4 with respect to time, yields:

$$q_{c,TR}\,(t) = \int_0^t (\partial q_c/\partial t)\,dt + q_{c,ss}\,[P(t),\ G(t),\ x(t)] \tag{6}$$

where time zero corresponds to the onset of the transient. Denoting the integral as $\phi$, where

$$\phi = \int_0^t (\partial q_c/\partial t)\,dt \tag{7}$$

the problem of applying steady state correlations to transient conditions reduces to identifying the function $\phi$. In general, $\phi$ is a function of the rate of changes and the instantaneous values of the transient variables given by and may be represented by:

$$\phi = \phi[t,\ G_o,\ P_o,\ x_o,\ q_{,o},\ (dP/dt),\ (dG/dt),\ (dx/dt),\ (dq/dt)] \tag{8}$$

The function $\phi$ has to satisfy the following condition:

$$\phi = 0 \text{ if } (dP/dt) = (d|G|/dt) = (dx/dt) = (dq/dt) = 0 \tag{9}$$

Obviously under steady state conditions there is no difference between steady state and transient CHF. A simple mathematical function which satisfies the above conditions and which superimposes the effects of the individual transients on $\phi$ is assumed; and is formulated by

$$\phi = C_1(dP/dt)\ |(dP/dt)|^a + C_2(d|G|/dt)\ |(dG/dt)|^b + C_3(dx/dt)\ |(dx/dt)|^c + C_4(dq_L/dt)\ |(dq_L/dt)|^d \quad (10)$$

where $C_1$, $C_2$, $C_3$, $C_4$, a, b, c, d are constants or functions of $P_o$, $G_o$, $x_o$, $q_o$, P(t), G(t), x(t) and q(t).

Therefore, for a given set of conditions, the function $\phi$ may be examined in four parts, each reflecting the effect of the individual transient variable or:

$$\phi = \phi_P + \phi_G + \phi_x + \phi_q$$

where

$$\phi_P = C_1\ (dP/dt)\ |(dP/dt)|^a$$

$$\phi_G = C_2\ (d|G|/dt)\ |(dG/dt)|^b \quad (11)$$

$$\phi_x = C_3\ (dx/dt)\ |(dx/dt)|^c$$

$$\phi_q = C_4\ (dq/dt)\ |(dq/dt)|^d$$

Unfortunatly, the state of the art in the theory of CHF, in conjunction with available experimental transient CHF data, does not permit the functions $C_1$, $C_2$, $C_3$, $C_4$ and a, b, c, d to be readily quantified. The qualitative nature of the functions, however, can be described for most transients of interest and this is done within the sections that follow.

## 1. Parametric Effects

### 1.1 Effect of Rapid Depressurization

Sakurai et al. [10] studied the effect of rapid depressurization on transient CHF for the case of pool boiling. Transient boiling phenomena caused by rapid depressurization on a test heater which was initially in non-boiling state in a pool of water was investigated. The tests incorporated a horizontal platinum wire 1.2mm in diameter and 71.6mm in length which was placed in a pool of subcooled water. The electric heat generation rate was held constant throughout each experiment. The change in system pressure was adjusted such that it followed an exponential decay given by:

$$P = P_o \exp(-t/\tau) \quad (12)$$

Pressure transient experiments were performed for the initial pressures of 0.59, 1.08, 1.9 MPa and for the water temperature of 353 and 373 K. The pressure reduction period, $\tau$, was varied from 3 ms to 60 ms. It was observed that transient CHF values were lower than the steady state CHF corresponding to

the instantaneous pressure. The values were less for shorter reduction periods and for lower initial heat fluxes. For very long periods the transient CHF approached the value of the steady state CHF.

For short reduction periods the heater surface temperature drops rapidly as the boiling initiates. The initial steady-state thermal boundary layer in the coolant may not vary as rapidly as the reduction in the surface temperature, therefore the change in the temperature at some position away from the surface is delayed. Likewise, as the saturation temperature decreases due to a pressure reduction, a thicker layer of superheated liquid than that of steady-state nucleate boiling will result. These factors may account for the lower CHF values during rapid depressurizations.

Figures 3, 4, illustrate the results of Sakurai, et al. [10]. They show the effects of initial system pressure, initial heat flux, depressurization rate and the coolant temperature on the transient heat flux. Such data may be useful for evaluating the functions $C_1$ and $\phi_p$ given in Equation (11). These figures are useful for obtaining a first estimate of $\phi_p$ values for zero mass velocity conditions. Since the transient CHF value is always lower than the steady-state value during rapid depres-, surization, $C_1$ must be a positive valued function. It can be seen from Figure 4 that the magnitude of $\phi_p$ may be as high as approximately (2/3) of the steady-state CHF.

The effect of depressurization on the transient CHF during forced convection has likewise been investigated by Westinghouse Electric Corporation in their separate effects test program [11] [12]. In their J-loop test facility, they obtained depressur-

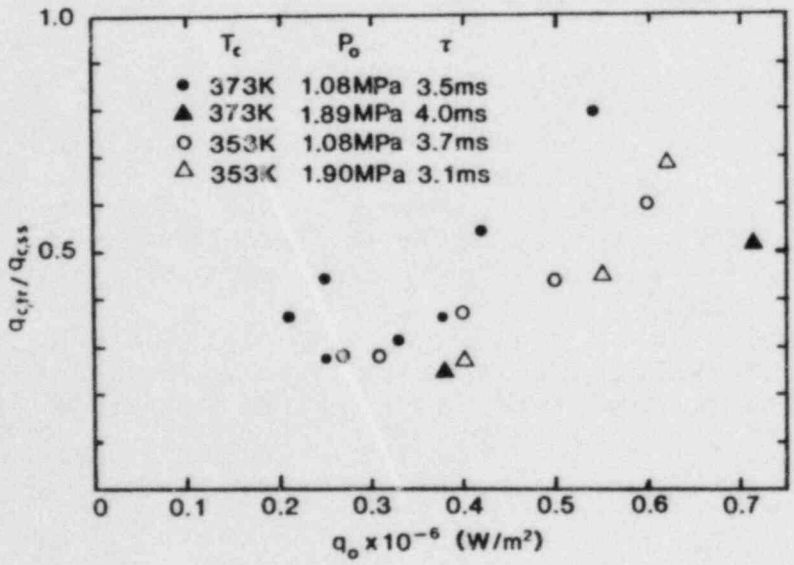


Figure 3 Ratio of the Transient Maximum Heat Flux to the Corresponding Steady-State Critical Heat Flux [10].

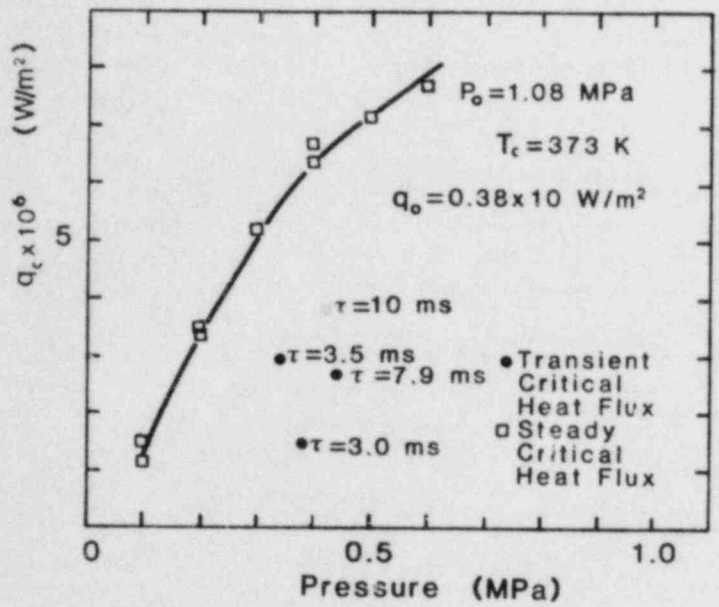


Figure 4 Effect of Pressure Reduction Periods on Transient Maximum Heat Flux [10].

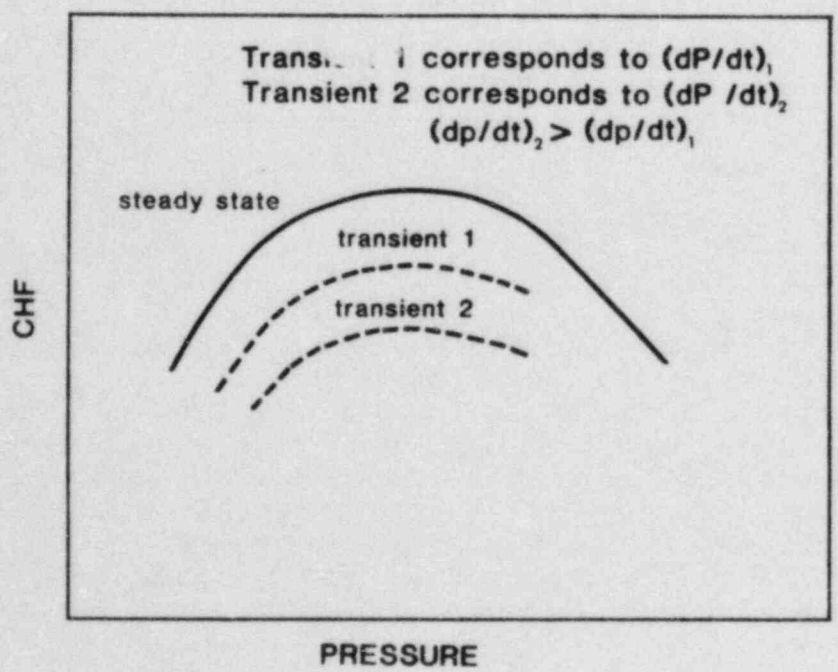


Figure 5 Conceptual Transient CHF Versus Pressure Curve.

ization test data where the mass flux was held constant. Although test conditions at the time of CHF were within the range of the Biasi correlation, this correlation did not predict any CHF. Such results also indicate that the transient CHF is lower than its corresponding steady state value during depressurization. The general functional form of $\phi_P$ cannot be determined from these limited results but specific values of $\phi_P$ may be estimated for the parametric range covered in these tests.

A qualitative transient CHF versus pressure curve is conceptually illustrated in Figure 5.

## 1.2 The Effect of Mass Flow Rate Transients

Cumo et al. [13] experimentally investigated mass velocity reduction effects on the transient CHF. They obtained experimental data with constant pressure and uniform heat flux in a freon loop simulating an exponential flow decay of the form:

$$G(t) = G_0 \exp(-t/\tau) \tag{13}$$

At the beginning of a flow transient, the coolant was either subcooled or very low in quality. At the onset of the CHF the quality spanned the range from 0.2 to 0.6, typical of annular flow dryout. Based on their experimental data they developed the following transient CHF correlation:

$$q_{C,TR} = q_{c,ss}\,[G(t)] + C.F. \tag{14}$$

where the correction factor C.F. is given as:

$$C.F. = 0 \quad \text{if} \quad \frac{t_{0.5}\, q_{c,TR}\, (P_{cr}/P)^{2.2}}{q_{c,ss}\,(G_o)} > 24 \text{ sec.} \tag{15}$$

$$C.F. = \{q_{c,ss}\,(G_0) - q_{c,ss}\,[G(t)]\} \exp(-gt)$$

$$\text{where: } g = 0.82\,(t_{0.5})^{0.15}\,(P_{cr}/P)^{1/2}$$

In this correlation the additional term C.F. corresponds to $\phi_G$ in the general transient CHF relation (Equation 11). Since the range of quality and corresponding flow regimes were not specifically reported, extrapolation to higher and lower qualities may be erronuous. Their results, however, may provide a first estimate of $\phi_G$, and some qualitative information about $C_2$.

The correction factor C.F. given in Equation (14) is positive for low quality, since it is known that in low quality regions steady state CHF increases with increasing mass velocities.
Therefore, at low qualities:

$$q_{c,ss}\,(G_0) > q_{c,ss}\,[G(t)] \text{ since } G_0 > G(t). \tag{16}$$

On the other hand, at higher qualities, an opposite trend is

observed as the steady state CHF increases with a decrease in mass velocity. Therefore, at higher qualities:

$$q_{c,ss}\ (G_o) < q_{c,ss}\ [G(t)] \text{ since } G_o > G(t). \qquad (17)$$

As a result, it may be concluded that for qualities less than the turnaround point on CHF versus G curve ( $\sim$10%) $C_2$ is a negative valued function and for qualities greater than the turnaround point $C_2$ is a positive valued function. This suggests a general functional form in terms of the quality contribution to the function $C_2$. In general $C_2$ may assume the following form:

$$C_2 = f(G_o, P_o, q_o, G)(x-x^*)/g(x_o,x) \qquad (18)$$

where $x^*$ is the turnaround quality for a given pressure.

For high quality, annular type of dryout, Walley et al. [14] applied their analytical model to the Moxon and Edward's tests [15] with favorable results, although the empirical CHF correlations predicted earlier CHF than measured, which again shows the positive contribution of the $\phi_G$ term to steady state CHF. This trend may also be justified by analysing the analytical solution for annular flow dryout by Levy [16]. The details of this analysis are not included here but Levy's results show that:

- The CHF is strongly dependent on the deposition rate and the mass transfer coefficient for high steam qualities and low heat fluxes.
- The mass transfer coefficient decreases with increasing mass velocity.

These results used in accordance with the following assumptions show the positive trend of $\phi_G$ mentioned above.

- Among all the other terms, the liquid concentration away from the liquid film has the slowest response time to mass velocity transients.
- The critical quality under transient conditions is greater or equal to the critical quality under steady state conditions.

For low quality conditions, the onset of the CHF is strongly dependent on the complete evaporation of the liquid microlayer underneath the bubbly boundary layer. This in turn is highly dependent on the liquid supply rate [17] which depends on the radial velocity fluctuations and the turbulent eddies [17,18]. It may be shown that for high mass velocity reduction rates, the transient CHF is higher than the steady state CHF. This assumes the following:

- For high reduction rates the initiation and growth of the bubbly boundary layer may be delayed since it takes time for a bubble to grow and depart from a nucleation site
- Once the bubbly boundary layer is formed, lower mass velocity provides more opportunity for the bubbles to

spread into the core thereby preventing bubble crowding The change in liquid supply rate (to the microlayer) may be slower than the change in mass velocity due to the response time of radial fluctuations and turbulent eddies at the edge of the bubbly boundary layer

Therefore, it follows that for low quality conditions a fast reduction in mass velocity gives rise to a higher transient CHF which means a negative valued $C_2$ function. This however is mainly of theoretical interest since for nuclear reactor accident situations dealing with rapid flow reduction transients, the CHF is usually detected at high quality conditions.

Based on this discussion, a conceptual CHF versus mass velocity curve may be drawn as shown in Figure 6.

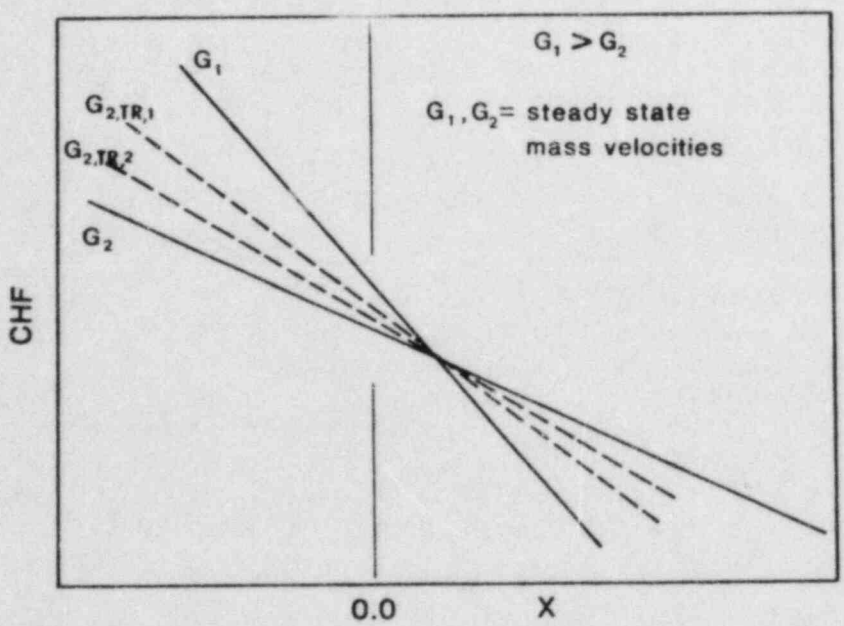


$G_{2,TR,1}$ The mass velocity is decreased to $G_2$ with a reduction rate $(dG/dt)_1$

$G_{2,TR,2}$ The mass velocity is decreased to $G_2$ with a reduction rate $(dG/dt)_2$ where $(dG/dt)_1 > (dG/dt)_2$

Figure 6 Conceptual Transient CHF Versus G Curve.

In the Westinghouse J-Loop test series, some flow transient test were also run. For these tests, the Biasi correlation (W-3 correlation in the low quality test 318) seemed to do the better job in predicting the CHF even for high flow reduction rates. In most of these tests, however, the quality at the onset of the CHF is around where the critical heat flux remains essentially constant with a change in mass velocity. There is, of course, the possibility that even the highest rate of change in these tests were still slow in terms of a considerable effect on the steady state critical heat flux value.

## 1.3 The Effect of Rapid Changes in Quality

The transient nature of quality is due to the combined effects of the rate of change in pressure, mass velocity and the local heat flux with respect to time. Thus, separate effect can be neglected as:

$$\phi_x \ll \phi_i \quad i = P, G, q$$

or $$C_3 \simeq 0 \tag{19}$$

## 1.4 The Effect of Rapid Changes in Local Heat Flux

Serizawa [17] theoretically predicted the maximum heat flux during power transients. His study addressed low quality conditions where the critical heat flux is related to the complete evaporation of the liquid microlayer underneath the bubbly boundary layer. He started with the basic physical observation that the consumption of the liquid layer is compensated by the continuous supply of liquid from the surrounding medium, which mathematically may be formulated as:

$$\Delta E_v = E_v - W_f \tag{20}$$

where $E_v$ is the rate of liquid layer evaporation and $W_f$ is the rate of liquid supply. The liquid supply rate $W_f$ was assumed not to exceed a certain critical value determined by the thermo-hydrodynamic conditions around the heater. When the heat flux reaches the steady state CHF level, $\Delta E_v = 0$. During an RIA power transient heat flux increases with time. By the time the microlayer completely dries out, the heat flux reaches a value higher than the steady state CHF, which is the transient CHF. This behavior is illustrated in Figure 7.

This simple physical model implies that $C_4$ has to be a positive valued function. The value of $\phi_q$ may be evaluated in terms of the microlayer thickness $\delta$, and the liquid supply rate $W_f$ both of which are strongly dependent on mass velocity, pressure, quality and local heat flux.

Although this approach is only valid for low quality DNB, an analogous model may be developed for high quality annular flow

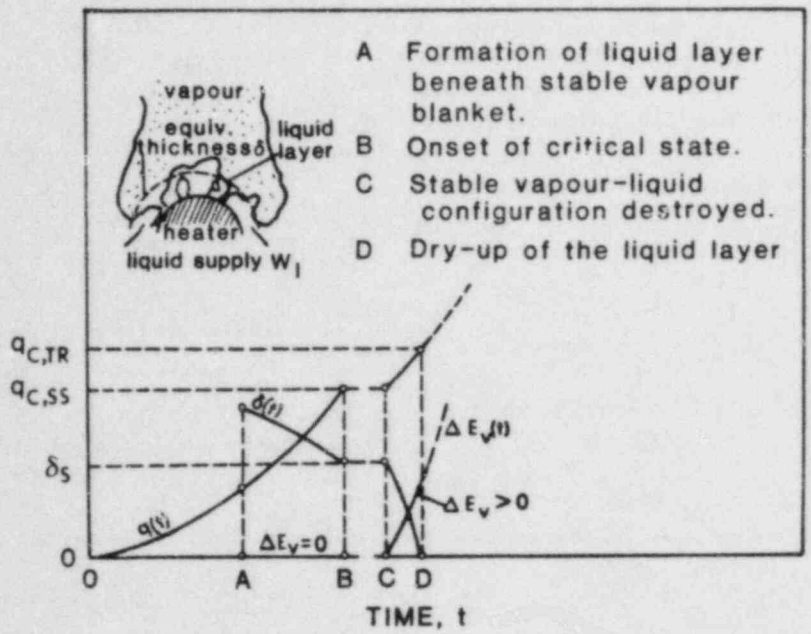


Figure 7 Physical Model for Transient CHF in Power Transients [17].

dryout in terms of liquid film thickness, deposition and entrainment rates.

Hence it is likely that for both low quality and high quality conditions, $C_4$ must be a positive valued function.

## 2. Conceptual Comparison of Transient and Steady-State CHF

Figure 8 illustrates the parametric behavior for a conceptual experiment and is used to show the separate effect influence of mass velocity and pressure on the transient CHF. The qualitative thermal-hydraulic parameters illustrated include the time dependent quality, pressure, absolute mass velocity, local heat flux, steady-state CHF and the transient CHF. The steady-state CHF curve corresponds to that predicted by a steady-state CHF correlation, such as the Biasi correlation, at the instantaneous local fluid conditions. The qualitative transient CHF curve is conceptual in nature and is used only for comparison with the steady-state CHF.

During the initial phase of the conceptual transient experiment, from time zero to 'A' (Figure 8), pressure is held constant and flow is decreased. Since the flow reduction occurs at low quality, it has a positive effect on the CHF (as discussed

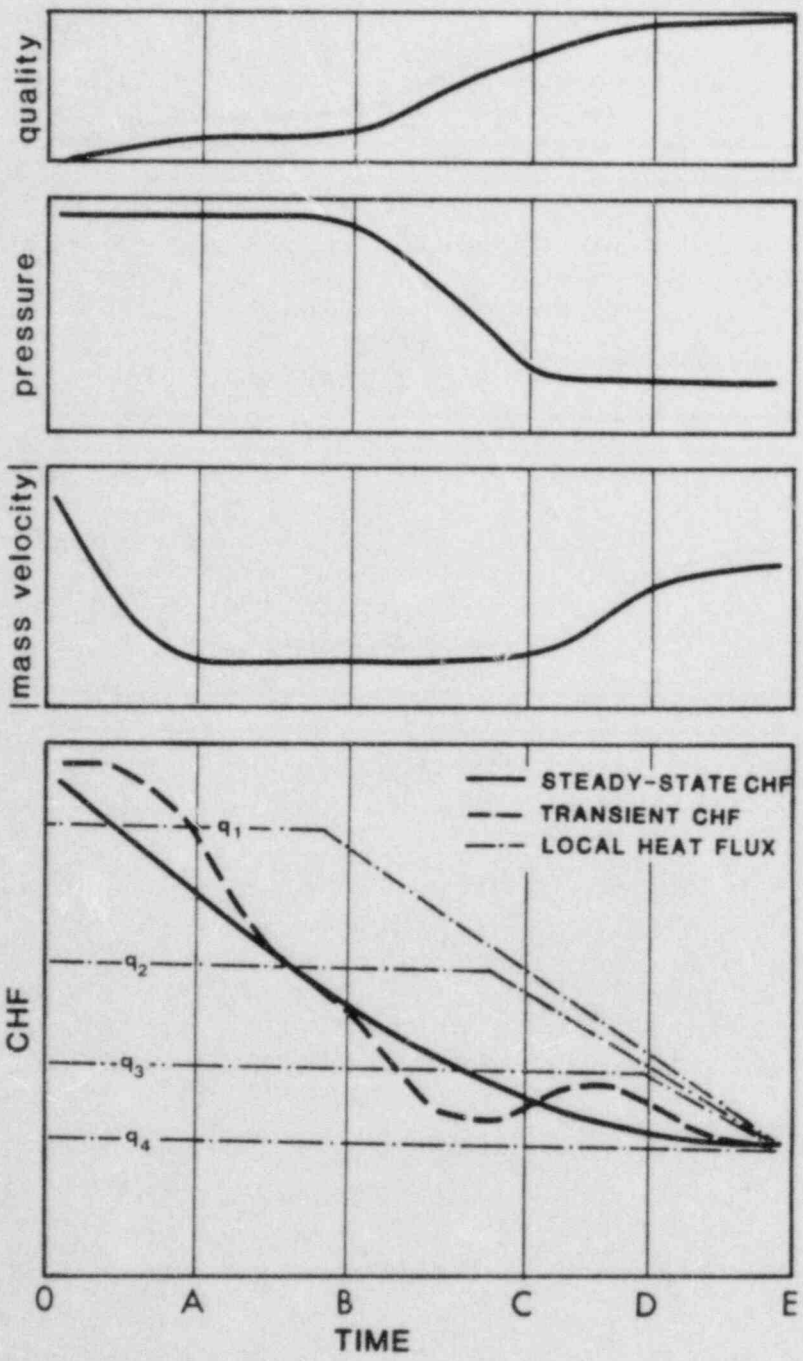


Figure 8 Conceptual Transient CHF Curve.

in Section 1.2) and the transient CHF curve lies above the steady-state one. For the time period 'A' to 'B', both the flow rate and the pressure are held constant and the steady-state and transient CHF curves coincide. For the period B to C, the flow rate remains constant and pressure is rapidly reduced, the net effect producing transient CHF values that are lower than the corresponding steady-state CHF values. From 'C' to 'D', there is a rapid increase in flow at a corresponding constant pressure. For the high quality conditions shown, the transient CHF will be greater than the corresponding steady-state. Finally, from 'D' to 'E', where all parameters illustrated change slowly, the transient and steady-state CHF behaviors will again coincide.

The differences between the transient and steady-state CHF values illustrated in Figure 8 are expected to be greater for the more rapid separate effect transients. The magnitude of the differences, however, have yet to be quantified and additional investigation in this area continues.

Figure 8 also illustrates the importance of the local heat flux in predicting the CHF via steady-state correlations during a particular transient. If the local heat flux follows the path $q_1$, the CHF will be overpredicted, whereas if it follows $q_3$, the CHF will be underpredicted. For the same experiment, the conclusion that "the steady-state correlations model perfectly the transient behavior" will be erronuously reached if the local heat flux followed the path of either $q_2$ or $q_4$.

Another important effect of the local heat flux is in its contribution to critical heat flux ratio. Dividing both sides Equation 6 by q(t), the following equation is obtained, in terms of the critical heat flux ratios:

$$CHFR_{TR} = \phi/q(t) + CHFR_{ss} \qquad (21)$$

Since the magnitude of depends mostly on the hydrodynamic parameters (especially for flow and/or pressure transients) the instantaneous hydrodynamic parameters and the rate of change of these parameters will fix the magnitude of $\phi$. If the operating conditions supply a high local heat flux at that instance, the contribution of $\phi/q$ ratio will be very small and could lie within the error band of the steady-state correlation or within the error dictated by the thermocouple response time. Conversely, under certain conditions if the same magnitude of $\phi$ is obtained, this time with a lower local heat flux, the contribution of the ratio could be considerable. Therefore when the prediction capability of the steady-state correlations is discussed for practical purposes Equation 21 explains more about the difference between the steady-state and the transient critical heat flux predictions than Equation 6.

## 2.1 Coincidence Hypothesis

So far the prediction capability of steady-state correlations was attributed to the transients being very slow and

allowing enough response time to the system to adjust itself to changing conditions at time to CHF. This is indicated by Equation 6. If (dP/dt), (d|G|/dt), (dx/dt), (dq/dt) are small the contribution of the term will be negligible. Equation 11 also suggests other possibilities for transient CHF and the steady-state CHF being almost the same.

Under certain combined transients, even though the individual transients may not be slow, the net effect on the term may be very small due to the competing contributions of the individual transient terms $\phi_P$, $\phi_G$, $\phi_x$, $\phi_q$ as summarized in Table II.

TABLE II

Summary of Individual Transient Terms

| | $C_1$ | $\varphi_P$ | |
|---|---|---|---|
| $dP/dt < 0$ | $> 0$ | $< 0$ | |
| | $C_2$ | $\varphi_G$ | |
| $dG/dt < 0$ | $< 0$ | $> 0$ | Low Quality |
| $dG/dt > 0$ | $> 0$ | $> 0$ | High Quality |
| | $C_3$ | $\varphi_x$ | |
| $dx/dt$ | $\simeq 0$ | $\simeq 0$ | |
| | $C_4$ | $\varphi_q$ | |
| $dq/dt > 0$ | $> 0$ | $> 0$ | |

This situation is illustrated in Figure 9, where again a combination of mass velocity and pressure transient are shown. At low quality region, between time B and C, the pressure and the mass velocity are both reduced very rapidly. The transient obviously may not be considered slow but due to the positive and negative contributions of $\phi_G$ and $\phi_P$ respectively the transient

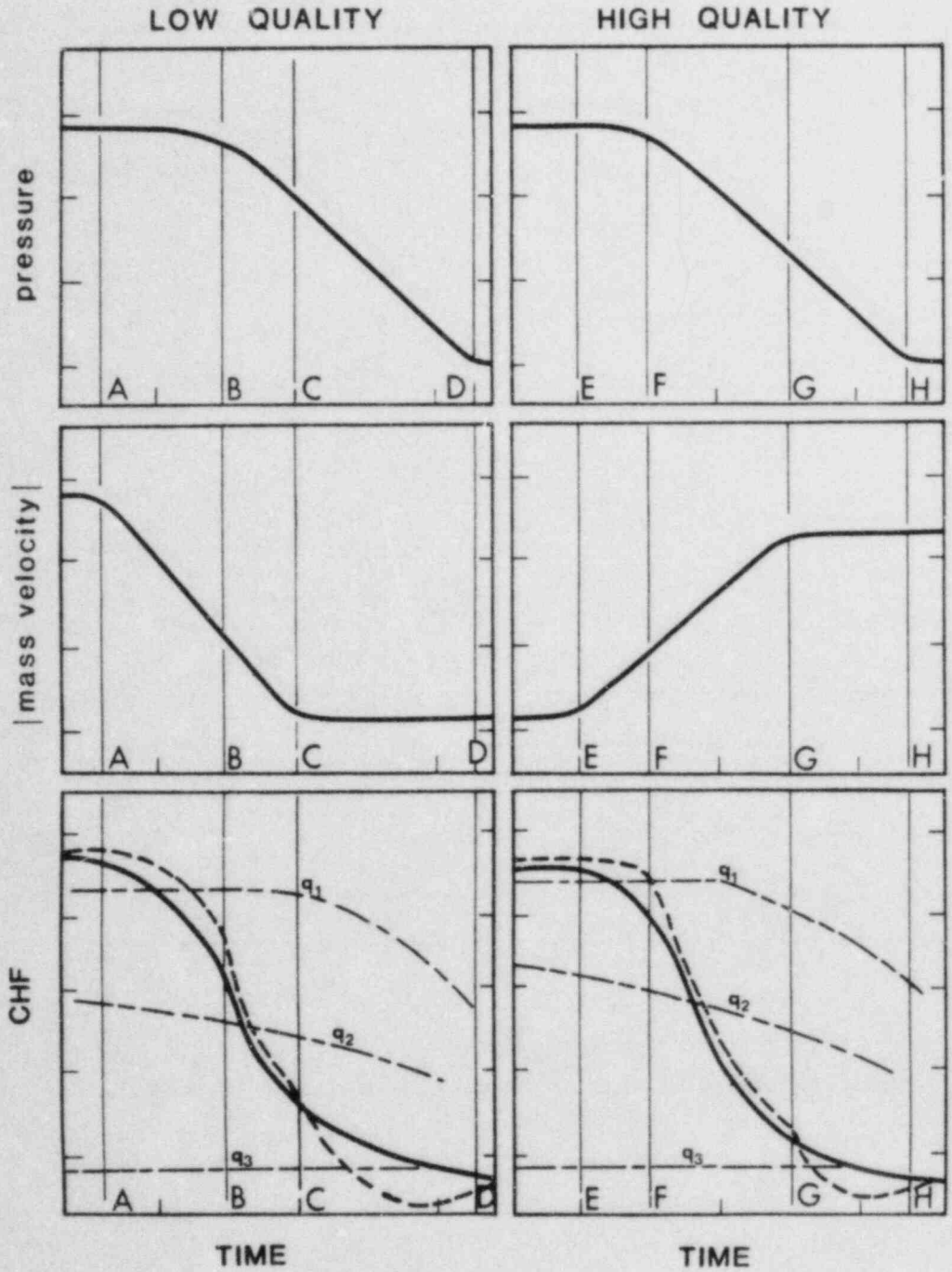


Figure 9 Illustration of "Coincidence Hypothesis".

CHF curve may be very close to the steady-state one. This situation may be anticipated to occur in the beginning of a LBLOCA.

At high quality conditions, within the time period F to G, both pressure and mass velocity are reduced very rapidly. And again due to opposite contributions the transient CHF curve may remain within the close vicinity of the steady-state curve. This situation is also typical of LBLOCA's after flow reversal.

The following observations suggested that this coincidence behavior may play an important role in predicting the transient CHF, in combination to the path followed by the local heat flux discussed in the previous section:

(i) In the THTF LBLOCA tests studied by Leung [2], the critical heat flux usually occurs under the conditions described under the high quality section of Figure 9 and a number of steady-state correlations (namely Biasi and CISE correlations) give good prediction.

(ii) In the combined effect test run by Westinghouse Electric Corporation [11] [12] in the J-loop facility, the Biasi correlation,which did a poor job in separate effect tests, gave an excellent prediction at certain locations. The initial conditions and fluid properties at initial CHF of this test are given in Reference [12].

## IV. CONCLUSIONS AND FINAL REMARKS

This study has addressed the applicability of steady-state CHF correlations in predicting transient CHF behavior. The relative merits of many widely used CHF correlations in predicting transient behavior were assessed by comparison with experimental data and from theoretical considerations.

Results suggest that steady-state CHF correlations may be used to estimate transient CHF behavior only under certain conditions. For most transients of interest, including the LBLOCA, SBLOCA and LOFA, a combination of the Biasi and Griffith-Zuber correlations is recommended for a best 'first estimate' of the transient CHF behavior. These correlations are presently incorporated in many large computer programs used in safety assessment studies. Table III summarizes the applicability of the steady-state correlations for predicting certain transient CHF behaviors.

In general, 'separate effect' CHF transients which are characterized by a single, rapidly changing parameter are poorly modeled by the steady-state correlations. Usually, the more rapid the transient, the poorer the prediction. Depending upon the quality and power conditions at the onset of CHF, steady-state correlations may predict late or early CHF behaviors with CHFR's significantly different than unity.

Section IV of this report discussed the type of CHF behaviors expected for various transients.

The steady-state CHF correlations which model blowdown-type

TABLE III

Applicability of Steady-State Correlations For
Predicting Transient CHF Behavior

| Type of Transient | Expected CHF Prediction From Steady-State Correlations | Predicted CHFR | Predicted Time-to-CHF | Comments |
|---|---|---|---|---|
| 1. Rapid flow reduction at constant pressure (LOFA) | Good (quality 5-15%) | ∿1 | Good | . For very low quality, transient CHF will be greater than predicted (Sec. 1.2) |
| | Poor (low quality) | <1 | Early | |
| 2. Rapid depressurization with changing flow (LBLOCA) | Good | ∿1 | Good | . Low power (SCRAM)<br>. For conditions with flow reversal, competing flow and pressure behaviors cancel, see coincidence hypothesis (Sec. 2.1)<br>. If power is not low, predictive errors may occur |
| 3. Slow depressurization with slowly changing flow (SBLOCA) | Good | ∿1 | Good | . Governing physical phenomena have sufficient time to approach steady-state |
| 4. Rapid depressurization at constant flow | Poor | >1 | Late | . Transient CHF will be lower than predicted (Sec. 1.1) |
| 5. Rapid reactivity or power increase (RIA) | Poor | <1 | Early | . Transient CHF will be greater than predicted (Sec. 1.4) |

transients well may do so partly because the competing pressure-flow contributions to the CHF cancel. Section 2.1 of this report discusses this phenomenon from a 'coincidence hypothesis' perspective.

## V. REFERENCES


1. Leung, J.C., "Transient Critical Heat Flux and Blowdown Heat Transfer Studies", ANL-80-53, May 1980.

2. Leung, J.C., "Transient Critical Heat Flux and Blowdown Heat Transfer Studies", Ph.D. Dissertation, North Western University, June 1980.

3. Lo, R.K., "Private Communications".

4. Katto, Y., "A Generalized Correlation of Critical Heat Flux for the Forced Convection Boiling in Vertical Uniformly Heated Round Tubes," Int. J. Heat Mass Tr., Vol. 21, 1978, pp. 1527-1542.

5. Katto, Y., "A Generalized Correlation of Critical Heat Flux for the Forced Convection Boiling in Vertical Uniformly Heated Round Tubes, A Supplementary Report, Int. J. Heat Mass Tr., Vol. 22, 1979, pp. 783-794.

6. Katto, Y., "CHF of Forced Convection Boiling in Uniformly Heated Vertical Tubes (Correlation of CHF in HP Regime and Determination of CHF Regime Map)," Int. J. Heat Mass Tr., Vol. 23, 1980, pp. 1573-1580.

7. Biasi, L. et al. "Studies on Burnout, Part 3. A New Correlation for Round Ducts and Uniform Heating and Its Comparison with World Data", Energia Nucleare, 14, September (1967).

8. Bertoletti, S. et al. "Heat Transfer Crisis with Steam-Water Mixtures", Energia Nucleare, 12, 121 (1965).

9. Griffith, J.F. Pearson and Lepkowski, R.J. "Critical Heat Flux During a Loss of Coolant Accident", Nuclear Safety, 18, (3), 298 (1977).

10. Sakurai, A. et al., "Transient Boiling Caused by Rapid Depressurization from Initial Non-boiling State", in Multiphase Transport (Edited by N. Veziroglu) V:2, Hemisphere 1980.

11. Westinghouse Electric Corp., "Full-Scale Controlled Transient Heat Transfer Tests-Data Report", EPRI-NP-1810 Vol. 1, April 1981.

12. Westinghouse Electric Corp., "Full-Scle Controlled Heat Transfer Data Analysis Report", EPRI-NP-2547, August 1982.

13. Cumo, M. et al, "Transient Critical Heat Flux in Loss of Flow Accidents (LOFA)", Int. J. Multiphase Flow, 4, 1978, pp: 497-509.

14. Walley, P.B., et al., "Prediction of Annular Flow Parameters for Transients and for Complex Geometries", European Two-Phase Flow Group Meeting, Haifa, Israel, 1975.

15. Moxon, D. and Edwards, P.A., "Dryout During Flow and Power Transients", AEEW-R 553, 1967.

16. Levy, S., "Prediction of Critical Heat Flux for Annular Flow in Vertical Pipes", EPRI-NP-1619, November 1980.

17. Serizawa, A., "Theoretical Prediction of Maximum Heat Flux Power Transients", Int. Jr. Heat Mass Transfer, 26, 1983, pp: 921-932.

18. Weisman, J. and Pei, B.S., "Prediction of Critical Heat Flux in Flow Boiling at Low Qualities", Int. J. Heat Mass Tr., 26, 1983, pp: 1463-1477.

# UK STUDIES OF POST-DRYOUT HEAT TRANSFER

BY

G.F. HEWITT, G. COSTIGAN AND D.H. LEE
UNITED KINGDOM ATOMIC ENERGY AUTHORITY

## ABSTRACT

This paper describes experimental and analytical work aimed at improving fundamental understanding of post-dryout heat transfer. The application of various advanced modelling techniques to dispersed flow heat transfer data obtained earlier in the UKAEA is reviewed. Then, more recent work on post-dryout heat transfer in the low void fraction (low quality) region is described and recent comparisons between the data and the TRAC-PF1 code are reviewed. A basic version of the code predicts rewetting under conditions which are well established as being in the post-dryout region and modifications to the code are described to rectify this. Plans are described for extending these experiments to a wider range of pressure and mass flux. In the final section of the paper, recent experimental work is described in which the two phase flow patterns associated with post-dryout heat transfer in the reflooding situation have been investigated using neutron radiography. The flow patterns at low reflood rates are somewhat different to those which had been previously assumed.

## 1. INTRODUCTION

A central issue in reactor safety calculations is that of the prediction of the temperature which the fuel elements will reach if and when they become dry during the unlikely event of a LOCA. There is considerable interest, therefore, in post-dryout heat transfer and the models used for this region in the codes are often important in assessing the consequences of postulated accidents. This paper describes work carried out in the UK (and specifically at the Harwell and Winfrith Laboratories of the UKAEA) relating to the post-dryout region.

Here, we shall define "dryout" as the point at which there is an inordinate decrease in heat transfer coefficient with increase of wall temperature or an inordinate increase in wall temperature with an increase in wall heat flux. Thus, in the "post-dryout" region, the wall temperature is usually greater than that immediately preceding dryout and usually indicates the presence of a dry or only - intermittently wetted wall.

The objectives of the Harwell and Winfrith work in this area are as follows:

(1) To develop and investigate models for post-dryout heat transfer for ultimate use in LOCA codes.

(2) To gain an understanding of flow and heat transfer phenomena in the post dryout region so as to understand modelling limitations.

It is often assumed that post-dryout heat transfer can be calculated in terms of a "boiling surface", which may be specified for any given mass flux (G), pressure (p) and system geometry. The boiling surface relates the surface temperature in the channel to the local quality and local heat flux; a typical boiling surface is illustrated in figure 1, which is taken from the book of Collier (1981). In the LOCA codes, the boiling surface is represented in a somewhat stylised form as is illustrated by the example (for the TRAC-PD2 code) shown in figure 2. As will be seen, this curve may be seen as representing (for the given mass flux, pressure and geometry) a cross section through a boiling surface of the form shown in figure 1. It should be noted that the actual shape of the boiling surface will vary with pressure and mass flux, reflecting the changes in flow regime and heat transfer regime with these parameters.

A major limitation of the use of the boiling surface approach is that the surface itself may actually be affected by "history" effects. Thus, for example, the extent to which the vapour is superheated at a given quality will depend on the previous flow history. Thus, conditions for a given local quality may vary depending on the upstream heat flux profile. In reviewing the current status of models for the post-dryout region, one may make the following observations:

(1) The physics of the two phase flow and heat transfer in the post-dryout region is highly complex and currently beyond detailed modelling, and certainly beyond the level of modelling normally considered feasible in LOCA codes.

(2) Empirical or (at best) semi-empirical models must be used which are based on limited data and do not normally cover the full range of interest in reactor calculations.

(3) The limitation of storage and running time in many LOCA codes forbids the inclusion of detailed history effects which are known to be important and which can be represented to some extent by more complex codes.

The work described in this paper is aimed at investigating the importance of these deficiencies and, hopefully, of producing better and more suitable models.

Work on post-dryout heat transfer within the UKAEA can be broadly classified as follows:

(1) **Steady-state studies.** The work in this area can be classified under two main headings:

(a) High quality dispersed flow. Here, experiments on post-dryout heat transfer in single vertical Nimonic tubes was started in the 1960s and Harwell reports describing this work are those of Bennett et al. (1967) (uniform heat flux) and Keeys et al. (1971) (cosine axial flux distribution). In this earlier work, modelling methods were developed which quite successfully predicted the temperature profile provided the dropsize was specified. In later modelling studies (Whalley et al., 1982) methods were developed for the prediction of dropsize and velocity spectra at the dry-out point and in the present paper, further applications of this later method and comparisons with TRAC code predictions are described.

(b) Low void fraction heat transfer. Here, the so-called "hot patch" technique is used in which there is a high heat flux zone near the inlet and outlet to prevent ingress of rewetting fronts into the tube. This allows the conditions within the tube itself to be controlled and unequivocal data obtained on post-dryout heat transfer coefficients over a wide range of mass flux and quality. Results obtained from this technique are described by Costigan (1984) and further presentation and analysis of this data (including analysis by the TRAC-PF1 code) is given in this paper. This work has so far been at low pressure (typically less than 5 bar); it is now planned to carry out tests over a wide range of pressures and mass fluxes in the high pressure loop facilities at the UKAEA Winfrith Laboratories and these plans are reviewed in the present paper.

(2) **Slow transients.** Valuable data on post-dryout heat transfer can be obtained using test sections whose walls are very thick and where pre-stored heat is released from the walls, the rewetting front progressing very slowly along the test section. Sophisticated test sections in which the wall consisted of a series of cylindrical copper blocks have been developed at Harwell and work of this type is described by Newbold et al. (1976) and Costigan (1983). No further review of this work is included in the present paper.

(3) **Rapid transients (reflood).** A wide range of single-tube reflood experiments have been carried out within the UKAEA and are described, for instance, by Denham (1981) and Costigan

(1984). In the latter work, visualisation of the reflood process was achieved using neutron radiography. In the present paper, further studies using this technique are described and the implications in modelling of the post-dryout region are discussed.

## 2. DISPERSED FLOW HEAT TRANSFER

As was stated in the introduction, work has continued at Harwell on analysis of the dispersed flow post-dryout heat transfer data reported by Bennett et al. (1967) and Keeys et al. (1971). The modelling codes used have included the following:

(1) **POST.** This code is a development of the model described originally by Bennett et al. (1967). Wall-to-vapour and vapour-to-droplet heat transfer is calculated with the local parameters being established by integration along the channel starting at the dryout point. Here, it is necessary to input the location of the dryout and also to specify a drop diameter at the dryout location.

(2) **HANA-POST.** This code is essentially identical to POST for the post-dryout region, but uses the annular flow modelling code HANA (whose basis is described, for instance, by Whalley et al., 1974) to give the dryout point. The HANA code integrates the evaporation, droplet entrainment and deposition processes along the channel to determine the point at which the film flow becomes zero and dryout occurs.

(3) **PRG2.** This operates in a similar way to HANA-POST but attempts to predict the dropsize and drop velocity spectra at the dryout point. This is done by dividing the pre-dryout annular flow region into a series of zones, from each of which droplets are created at a size determined from an empirical correlation of annular flow drop size derived in parallel studies at Harwell. The drops for each zone are accelerated by the vapour phase and, of course, some of them are redeposited within the pre-dryout region itself. However, the number density and velocity of drops from a particular zone arriving from the dryout point can be calculated and, and in the post-dryout region, the subsequent behaviour of this group of drops can be evaluated together with the behaviour of all other groups of drops. Thus, the need for an arbitrary specification of drop size at the dryout point (implicit in the POST code) is avoided. Further details of the methods used in PRG2 are given by Whalley et al. (1982).

(4) **TRAC-PF1.** This code is used in its standard (MOD-0) mode.

Comparisons of the performance of the model are shown in figure 3-5. In figure 3, the comparisons are for a uniform heat flux case (Bennett et al. 1967) and it will be seen that the POST code gives the best predictions. This is perhaps not surprising since the dryout point and initial drop size are specified (a drop size of 300 microns was assumed). The HANA-POST code also predicts the correct trend though the dryout point is predicted slightly upstream of the experimental value. The PRG2 code indicates a lower wall temperature, reflecting the fact that this code predicts a smaller mean drop size and greater slip between the drops and

the vapour at the dryout point than that assumed in the POST code. Although the TRAC-PF1 code predicts the correct trends of wall temperature in the post-dryout region, its prediction of the dryout point is well upstream of the experimental value as shown. However, it should be noted that this represents only a small change in the dryout flux.

Figures 4 and 5 show comparisons between the various codes and the data obtained by Keeys et al. (1971) for a cosine axial heat flux profile. The two sets of curves are for a constant mass flux (720 $kg/m^2s$) but with two different heat flux levels. At the lower heat flux level, the HANA-POST and PRG2 codes give an excellent prediction of the dryout position with PRG2 giving the best prediction of the post-dryout temperature distribution. For the higher heat flux (figure 5) the HANA-POST and PRG2 codes predict dryout slightly downstream of the experimental position. The POST code gives a good prediction of wall temperature distribution though there are indications that the PRG2 code is underpredicting the temperature in this case also, presumably for similar reasons to that adduced for the uniform heat flux case (figure 3).

For the non-uniform flux distribution, the TRAC-PF1 code gives rather poor predictions though the code is clearly capable of predicting the correct trends (in contrast to some other less sophisticated models). The main problem is that of prediction of the dryout point. TRAC-PF1 uses a "local conditions" correlation (Biasi) and previous experience (Keeys et al., 1971) indicates that such correlations predict the location of dryout well upstream of that which actually occurs. A saving grace here is that the prediction of maximum wall temperature is clearly conservative! This is not the case with some of the more empirically-based models when applied to cosine heat flux distribution.

It would seem, therefore, that improvements are needed in the TRAC-PF1 code relating to the prediction of the dryout location and work towards this is proceeding in the UKAEA.

## 3. STEADY-STATE POST-DRYOUT HEAT TRANSFER EXPERIMENTS USING THE "HOT PATCH" TECHNIQUE

In order to obtain steady-state post-dryout data for the low quality, low void fraction region, a test section of the form illustrated in figure 2 was employed. The test section in which the measurements were made consisted of an 8 mm bore Nimonic 90 tube which had an outside diameter of 9.5 mm and a length of 900 mm. The tube was heated by passing a high current through it from an AC power supply (0-30 volts, 0-2500 amps). This tube was connected, (at top and bottom) to specially designed cylindical sections in which a high heat flux was induced, initiating film boiling and maintaining the test tube in a post-dryout condition. These cylindrical blocks consisted mainly of copper with a brazed-on clad of stainless steel on the inner bore.

The experimental procedure was as follows: the desired pressure, the flow rate and inlet water temperature were set by circulating water through a by-pass before beginning a test run, the copper blocks and the tube were heated to 550°C with no cooling applied. The water flow was then diverted from the by-pass into the test section and the power to the tube was increased to prevent the tube from quenching. Once steady-state conditions had been established, the wall temperature profiles were measured and are exemplified by those shown in figure 7. There, typical results are shown

for the effect of mass flux for both upwards and downwards flow. As will be seen, there is a considerable influence of flow direction and of mass flux on the wall temperature (i.e. on the heat transfer coefficient). Also shown on figure 7 are comparisons between experimental and predicted heat transfer coefficients, the predicted values being estimated from an equation of the Bromley (1950) type, in the form derived by Andersen (1977) for vertical surfaces:

$$\alpha = 0.5 \left[ \frac{\lambda^3_v \, \rho_v \, (\rho_L - \rho_v) \, \Delta h_{LV}}{\eta_v \, (T_w - T_{SAT}) z} \right]^{1/4} \qquad (1)$$

where $\lambda_v$, $\rho_v$ and $\eta_v$ are the thermal conductivity, density and viscosity of the vapour, $\rho_L$ the density of the liquid, $\Delta h_{LV}$ the latent heat of evaporation, $T_w$ the wall temperature, $T_{SAT}$ the saturation temperature and z the distance from the quench front. The wall temperature was calculated from:

$$T_w = \left( \frac{\dot{q} - \dot{q}_r}{\alpha} \right) + T_{SAT} \qquad (2)$$

where $\dot{q}$ is the heat flux and $\dot{q}_r$ the radiation flux to the liquid calculated from the expression:

$$\dot{q}_r = \frac{\sigma_R}{\frac{1}{\varepsilon_w} + \frac{1}{\varepsilon_L} - 1} \left( T_w^4 - T_s^4 \right) \qquad (3)$$

where $\sigma_R$ is the Stephan-Boltzman constant and $\varepsilon_w$ and $\varepsilon_L$ are the emissivities of the wall and the liquid phase (taken as 0.3 and 1.0 respectively).

As will be seen, the above equations underpredict the heat transfer coefficient except at the highest mass fluxes in upwards flow. The discrepancy in downwards flow is particularly serious. These descrepancies were the main reason for pursuing better visualisation of the actual flow patterns associated with the post-dryout region which are described in section 4 below.

It is interesting to compare the results from the low-pressure hot patch experiments with the behaviour predicted using the TRAC-PF1 code. In its standard form, the code always predicted that the test section would rewet following liquid ingress. Typical results for the associated transient are illustrated in figure 8. As will be seen, the predictions indicate that the test section would be rewetted from the bottom upwards, rewetting of the whole section being completed in around 35-40 seconds. This rewetting is, of course, contrary to the experimental results where the test section reached an asymptotic post-dryout condition. This has led to the search for a better package of heat transfer relationships for post-dryout heat transfer in the TRAC-PF1 code. In the basic code, the following relationships are used for calculating the heat transfer coefficients from the wall to the vapour and from the wall to the liquid respectively:

$$\alpha_{wv} = \max \left[ \alpha_{Br} \, , \, \alpha_{NC} \, , \, \alpha_{DR} \right] \qquad (4)$$

$$\alpha_{wL} = \alpha_{rad} + \alpha_{FR} \qquad (5)$$

where $\alpha_{Br}$ is the heat transfer coefficient calculated from the Bromley equation, $\alpha_{NC}$ is the natural convection heat transfer coefficient, $\alpha_{DR}$ is the heat transfer coefficient calculated from the Dougal-Rohsenow correlation, $\alpha_{rad}$ is the radiation heat transfer coefficient and $\alpha_{FR}$ is the heat transfer coefficient calculated from the correlation of Forslund and Rohsenow which estimates the drop-to-wall heat transfer coefficient. The code has been modified to change the coefficients as follows:

$$a_{wv} = \max [\alpha_{NC} , \alpha_{DR}] \quad (6)$$

$$\alpha_{wL} = \alpha_{rad} + (1-\varepsilon_g)(1-E)\ \alpha_{BR} + \alpha'_{FR} \quad (7)$$

where $\varepsilon_g$ is the void fraction and E the fraction of the liquid phase entrained as droplets. The Forslund-Rohsenow coefficient ($\alpha'_{FR}$) is assumed to be zero for $\varepsilon_g > 0.5$. A more detailed discussion of these changes is given by Afifi (1984).

With the above changes introduced, the predictions for the same case as that shown in figure 8 take the form shown in figure 9. Now, rewetting does not occur and an asymptotic temperature profile is reached.

Figure 10 shows comparisons of predicted asymptotic temperatures as a function of distance along the test section for two of the test conditions for upwards flow. The predictions from the modified version of TRAC-PF1 are generally below the experimental values with the agreement being closer at the lower mass flux. Also shown on figure 10 are results calculated using TRAC-PF1 with the drop-wall (Forslund-Rohsenow) term omitted as suggested by O'Mahoney (1984). Although removal of this term completely does obviate the rewetting predicted by the standard version, the temperatures are much lower than the experimental values as illustrated.

It is noteworthy that the above changes in the post-dryout heat transfer package have also led to improvements in the prediction of reflood (Afifi, 1984).

A considerable extension of the "hot patch" experiments is planned for execution in the high pressure facilities at AEE Winfrith. Here, experiments will be carried out at pressures up to 70 bar using a test section which has powers up to 100 kW and using a once-through loop. The range of conditions planned for these experiments is illustrated in figure 11. The test section has been constructed and operation is expected to commence shortly. Comparison of these results with various prediction methods is expected also to reveal further shortcomings in these methods and there will be a parallel development of improved modelling techniques.

## 4. VISUALISATION OF REFLOODING USING DYNAMIC NEUTRON RADIOGRAPHY

As was revealed in the discussion above, considerable discrepancies may occur between existing models and experimental data in post-dryout heat transfer, and in particular in the low quality, low void fraction region. In an attempt to improve physical insight of the actual processes occurring in this region, the UKAEA Harwell team has been applying neutron radiography techniques to the study of reflood in a vertical tube.

In the visualisation experiments, a 12.2 mm outside diameter, 9.25 mm bore, 600 mm long stainless steel tube was used. This was preheated to

600°C and water introduced at the bottom at a fixed rate to reflood and rewet the tube. The tube was mounted in the neutron beam area of the Harwell Dido reactor with the arrangements shown in figure 12. In the first studies (Costigan and Wade, 1984) a video camera was used to record the images but, in more recent work, a cine camera has been used.

The tube was instrumented with 1 mm diameter sheathed Ni Cr-Ni Al thermocouples brazed into 1 mm deep holes in the tube walls at 2 cm from the tube inlet and then at every 8 cm subsequently. The traces recorded on the thermocouples are illustrated in figure 13 and these can be analysed to produce boiling curves of the form illustrated in figure 14.

In upwards flow (the case considered here - some discussion of down-flow is given by Costigan and Wade, 1984), the flow pattern observed was very dependent on the quench rate as illustrated in figure 15. Nucleate boiling extended about 4 mm axially along the tube wall and formed a distinct "neck" on the thin central column of liquid which flowed passed the quench front.

Ahead of the quench front, a central liquid filament was in violent motion and rarely reached an axial length of more than 10 cm before it broke down. Occassionally, the vapour formed in the "neck" at the base of the liquid core would separate the core completely from the quench front. The progression of the quench front up the tube wall was, however, quite uniform.

The liquid core either broke down to droplets (varicose instability) or ligaments (sinuous instability) which were then levitated by the vapour. The chaotic flow pattern which was formed higher in the tube was characterised by large diameter (approximately 6 mm) elongated drops preceded and followed by satellite drops of one or two millimetres diameter. The larger drops travelled quite slowly and often fell back down the tube. They become larger by collisions with other drops, before they were propelled forward again by the vapour generated below them. Near the exit end of the tube, there was a larger population of smaller droplets but their velocities were still quite low.

A turbulent falling film was observed to quench the upper most 10 cm of the tube. The film appeared to absorb the larger droplets rising in the tube and thus progressed downwards until it met the rising quench front. At the higher quench rates, water flowed passed the quenched front to form a flow pattern more akin to the conventional model of inverted annular flow. A much greater concentration of droplets above the liquid, was evident at the higher reflooding rates. These droplets appeared to have considerably higher velocities than in the low flooding rate case. The incidence of stagnant or falling droplets was much lower and, near the exit of the tube, more smaller diameter higher velocity droplets were observed.

It is clear from these visualisation experiments that the flow at and above the quench front is actually quite complex and it is perhaps not surprising that existing models fail to give accurate predictions.

## 5. CONCLUSIONS

Based on the UKAEA post-dryout heat transfer work summarised in this paper, one may conclude that:

(1) Though the TRAC-PF1 code gives inferior predictions to those obtained from more advanced codes in the dispersed flow, post-dryout region, it does produce the correct trends and its predictions could probably be improved quite considerably if a better estimate of the dryout point was achieved.

(2) Predictions of the Harwell low-pressure, low-quality "hot patch" experiments by the standard version of TRAC-PF1 indicated that the tube would rewet, contrary to the experimental observations. The predictions could be improved by introducing modifications to the heat transfer package these modifications also improving the code in its predictions of reflood.

(3) Neutron radiography studies of the flow regimes in reflood indicate that these regimes may be very different to those normally assumed. A particularly noteworthy feature is the "necking" of the core liquid column in the region of the quench front.

Overall, one may state that the post-dryout region is highly complex and not yet fully understood. The current programme of UKAEA studies is aimed at producing a broader data base for the region and, of course, improved modelling.

REFERENCES

AFIFI, J. (1984). Evaluation of some large best-estimate computer codes for the prediction of loss of coolant accidents in light water reactors. Ph.D. Thesis, University of London.

ANDERSEN, J.G.M. (1977). Low flow film boiling heat transfer on vertical surfaces. Part 1: Theoretical model. A.I.Ch.E. Symp. Series v.73, no. 164, pp. 2-6.

BENNETT, A.W., HEWITT, G.F. et al. (1967). Heat transfer to steam-water mixtures flowing in uniformly heated tubes in which the critical heat flux has been exceeded. AERE-R5373.

BROMLEY, L.A. (1950). Heat transfer in stable film boiling. Chem. Eng. Progress, v.46, p. 221.

COLLIER, J.G. (1981). Convective boiling and condensation, second edition. McGraw Hill.

COSTIGAN, G. (1983). The quenching of thick-walled nickel test sections. 2nd Int. Topical Meeting on Nuclear Reactor Thermal Hydraulics Sta. Barbara, Ca.

COSTIGAN, G., HOLMES, A.W., RALPH, J.C. (1984). Steady state post-dryout heat transfer in a vertical tube with low inlet quality. 1st U.K. National Heat Transfer Conference, Leeds.

COSTIGAN, G., WADE, C.D. (1984). Visualisation of the reflooding of a vertical tube by dynamic neutron radiography. International Workshop on Post-Dryout Heat Transfer, Salt Lake City, Utah.

DENHAM, M.K. (1981). Heat transfer near the quench front in single tube reflooding experiments. AEEW-R1436.

KEEYS, R.F.K., RALPH, J.C., ROBERTS, D.N. (1971). Post burnout heat transfer in high pressure steam water mixtures in a tube with cosine heat flux distribution. AERE-R6411.

NEWBOLD, F.J., RALPH, J.C., WARD, J.A. (1976). Post-dryout heat transfer under low flow and low quality conditions. AERE-R8390.

O'MAHONEY, R. (1984). Experience of calculating separate effects reflooding tests using TRAC-PD2 MOD-1 and TRAC-PF1 MOD-0. CSNI Workshop on User Experience with RELAP5 MOD-1 TRAC-PD2 and TRAC-PF1, Vienna May, 1984.

WHALLEY, P.B., HUTCHINSON, P., HEWITT, G.F. (1974). The calculation of critical heat flux in forced convection boiling. Paper B6.11, 5th Int. Heat Transfer Conference, Tokyo.

WHALLEY, P.B., AZZOPARDI, B.J., HEWITT, G.F., OWEN, R.G. (1982). A physical model for two phase flows with thermodynamic and hydrodynamic non-equilibrium. Paper CS29, 7th Int. Heat Transfer Conference, Munich.

---

ACKNOWLEDGEMENT

The authors wish to acknowledge the assistance provided by Jalal Afifi and Alistair Govan in carrying out the calculations using the TRAC-PF1 and post-dryout modelling codes respectively.

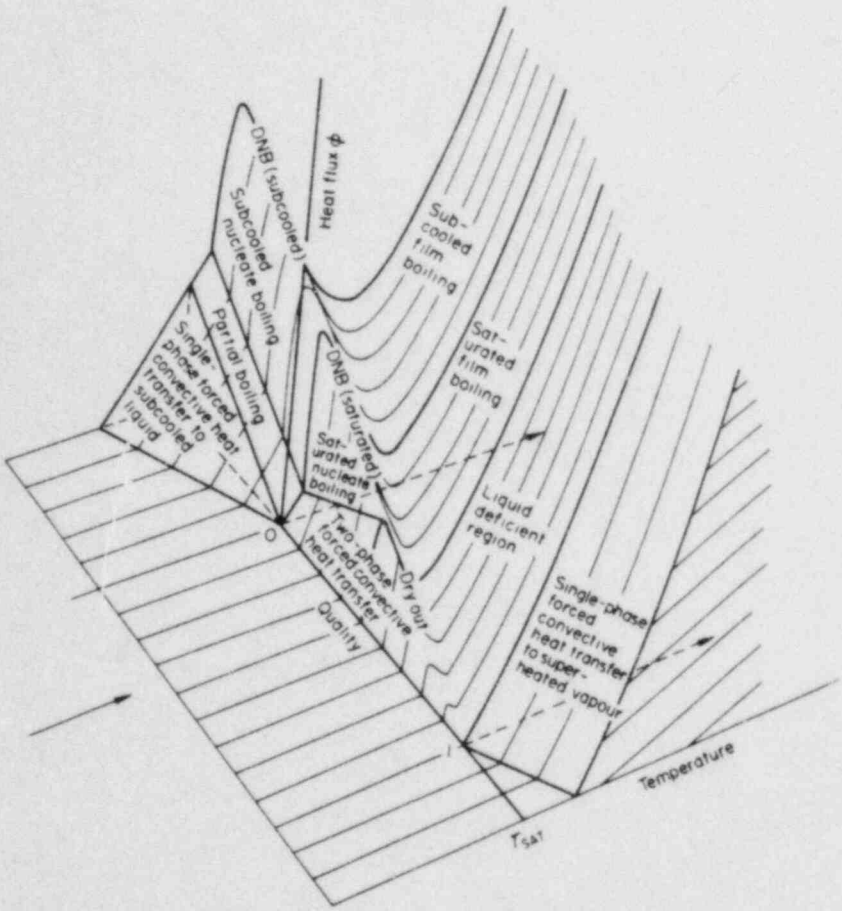


FIGURE 1: 'Boiling Surface' (heat flux and wall temperature as a function of quality and flow regime). From Collier (1981)

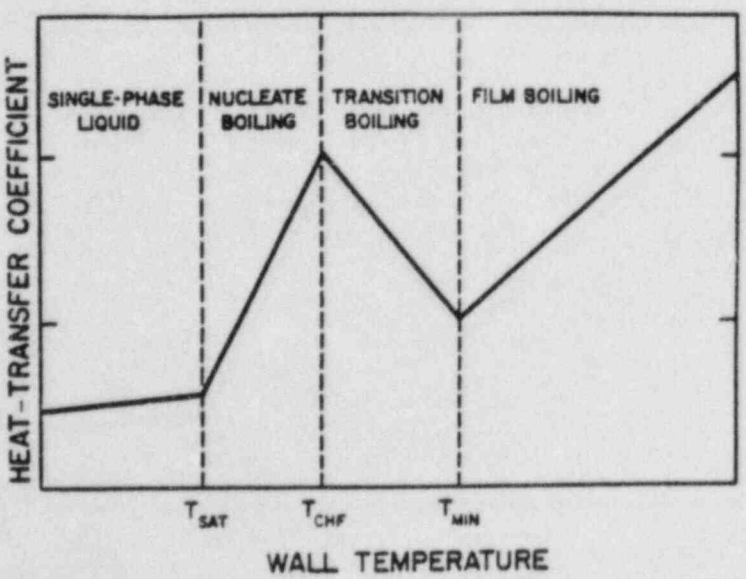


FIGURE 2: Stylised boiling curve used in TRAC-PD2 computer code.

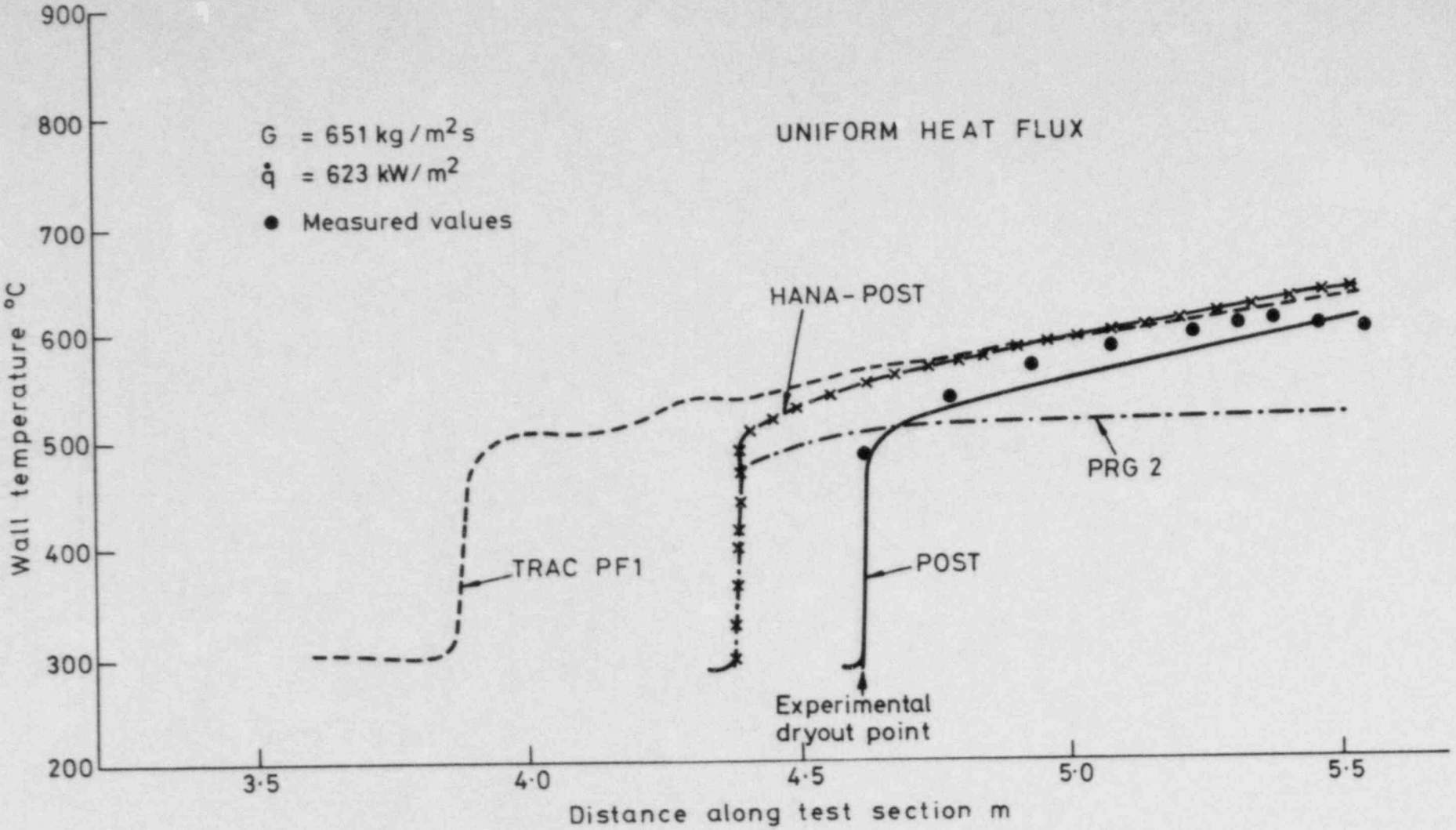


FIG. 3. COMPARISON OF UNIFORM-FLUX POST-DRYOUT DATA OF BENNETT ET AL (1967) WITH MODELLING CODES.

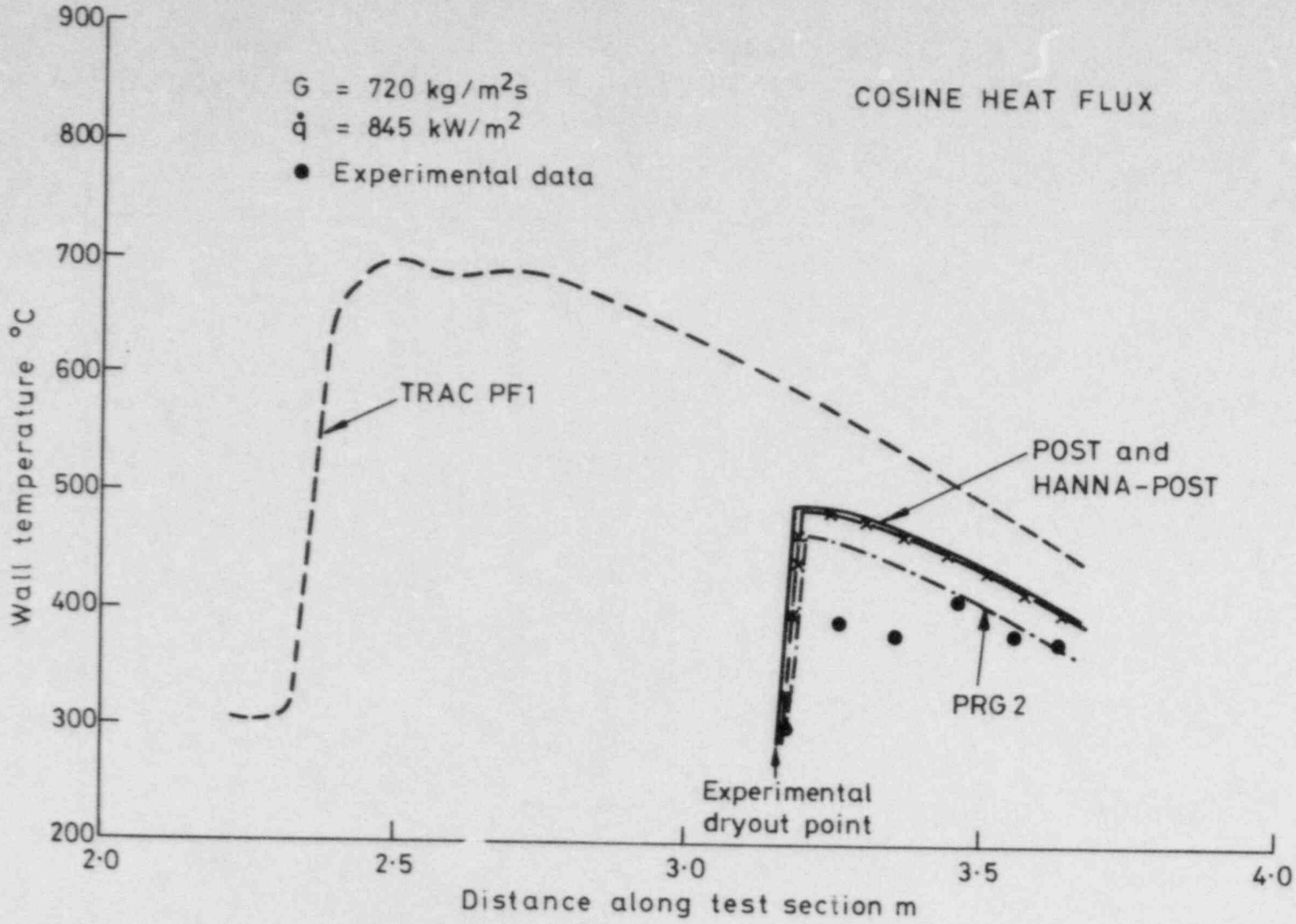


FIG.4. COMPARISON OF COSINE HEAT FLUX POST-DRYOUT DATA OF KEEYS ET AL (1971) WITH MODELLING CODES.

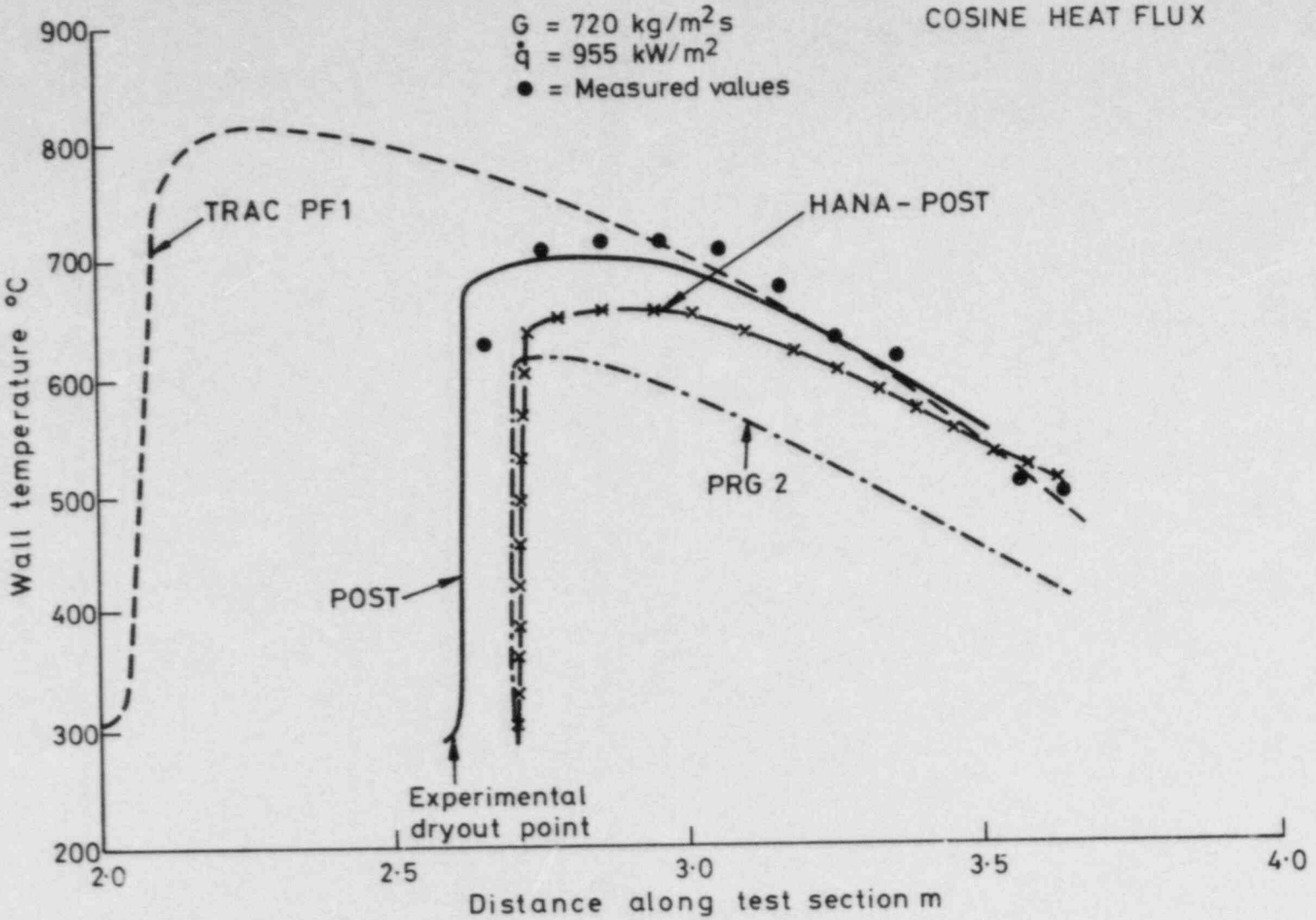


FIG. 5. COMPARISON OF COSINE HEAT FLUX POST-DRYOUT DATA OF KEEYS ET AL. (1971) WITH MODELLING CODES.

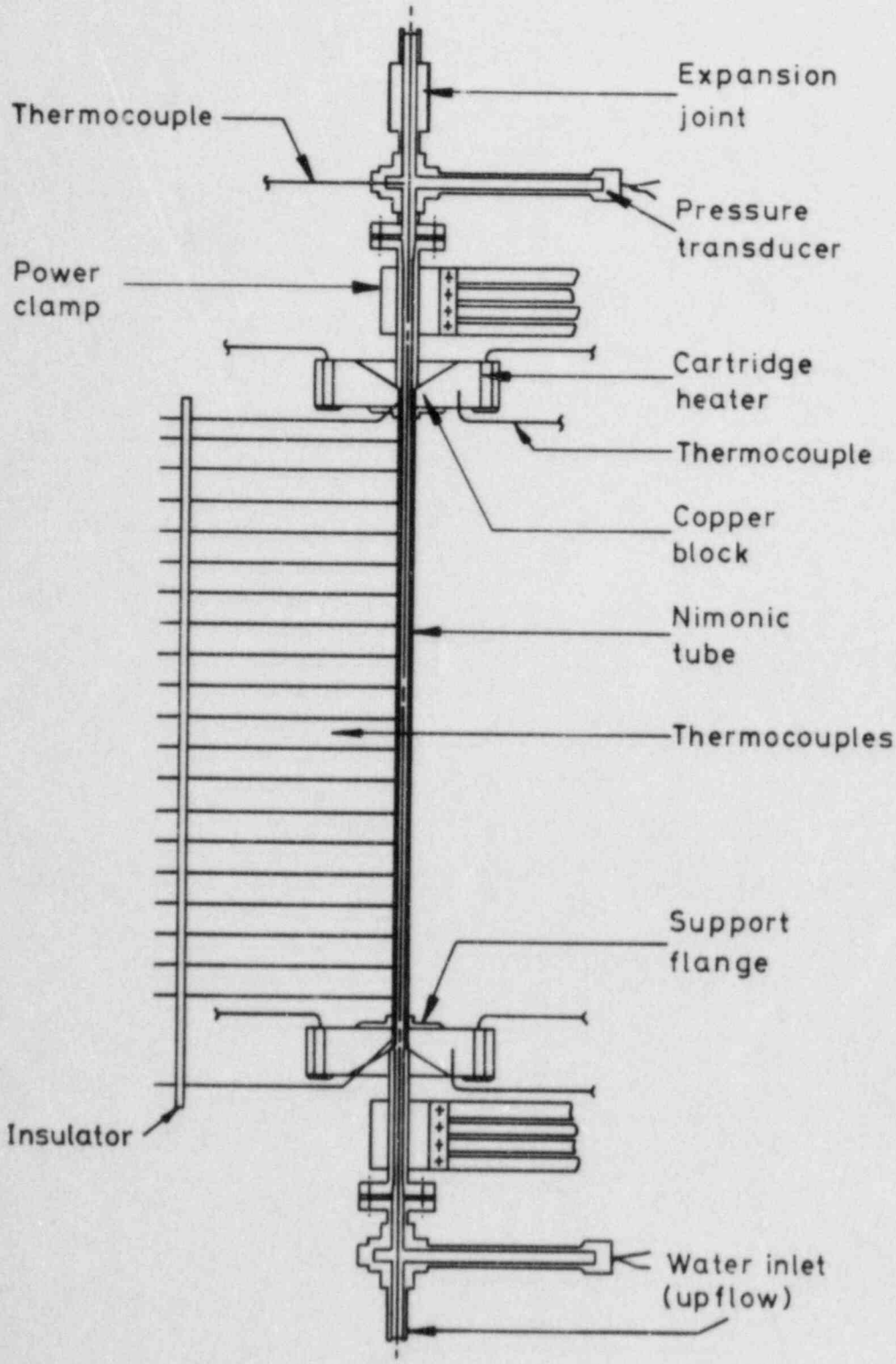


FIG. 6. TEST SECTION USED IN THE HARWELL LOW-PRESSURE 'HOT PATCH' TEST.

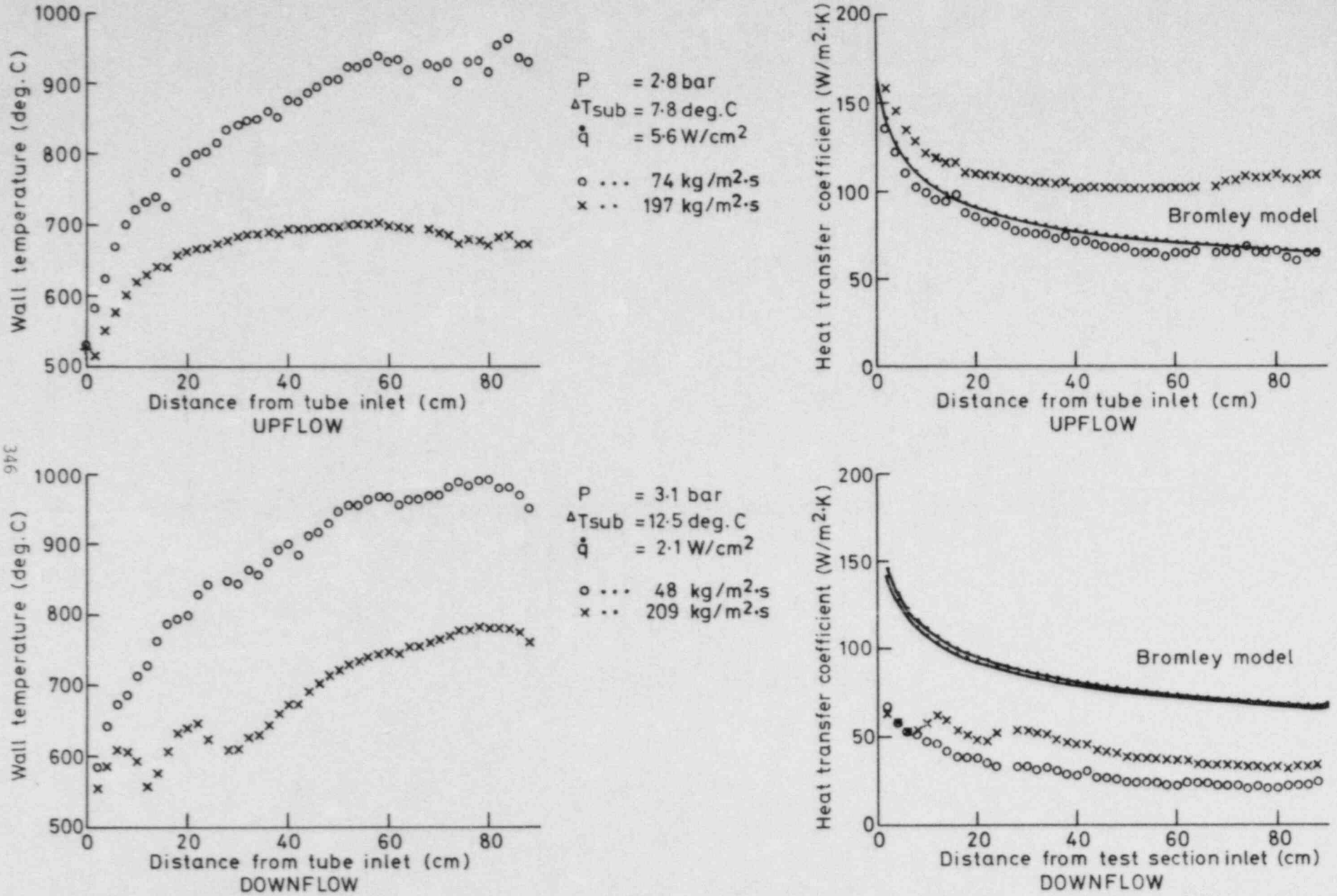


FIG.7. TYPICAL PLOTS OF WALL TEMPERATURE AND HEAT TRANSFER COEFFICIENT OBTAINED IN THE HARWELL HOT-PATCH TESTS FOR UP-FLOW AND DOWN-FLOW RESPECTIVELY.

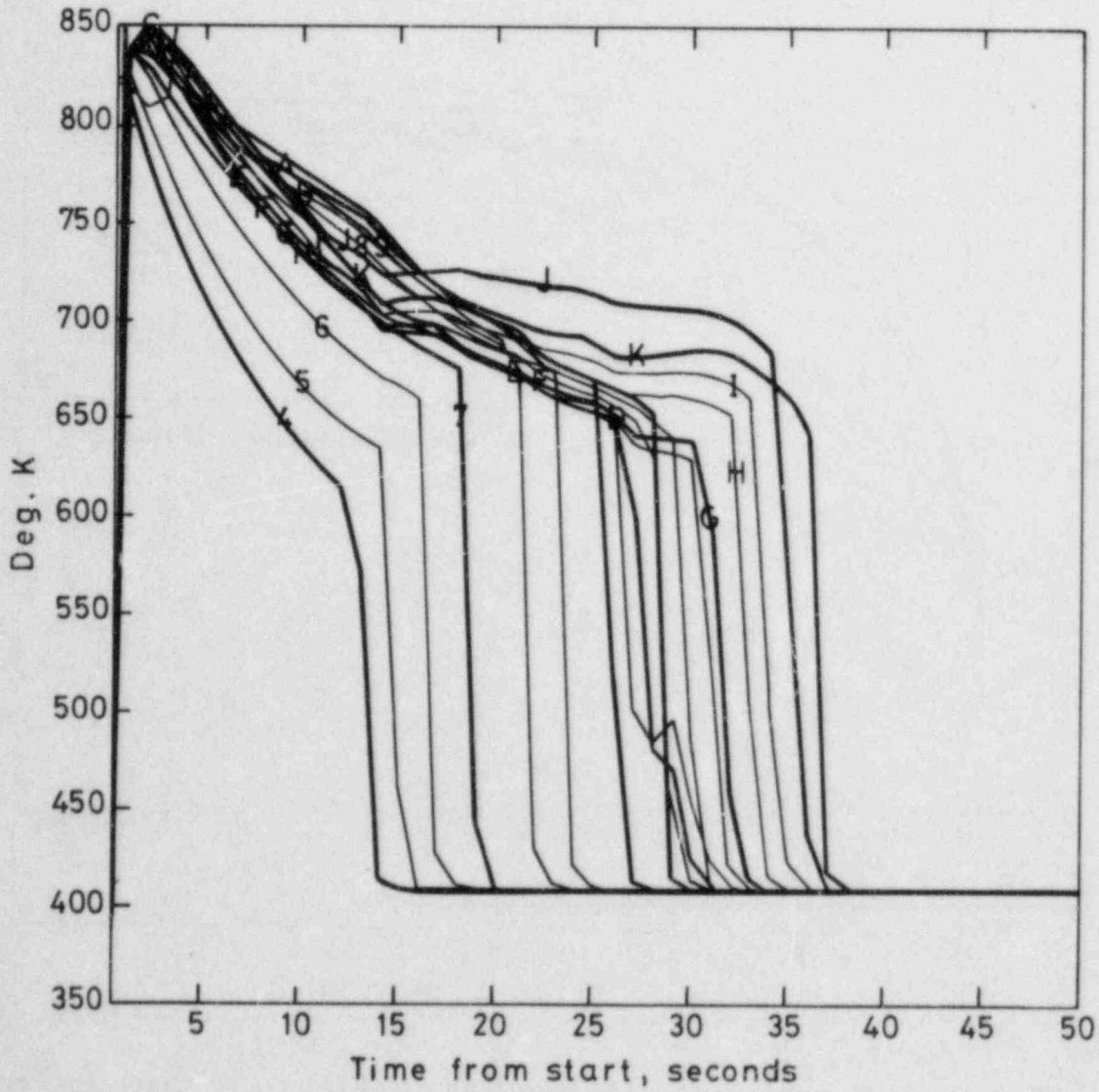


FIG. 8. TYPICAL PREDICTIONS OF HARWELL HOT-PATCH EXPERIMENT USING STANDARD VERSION OF TRAC-PF1 CODE.

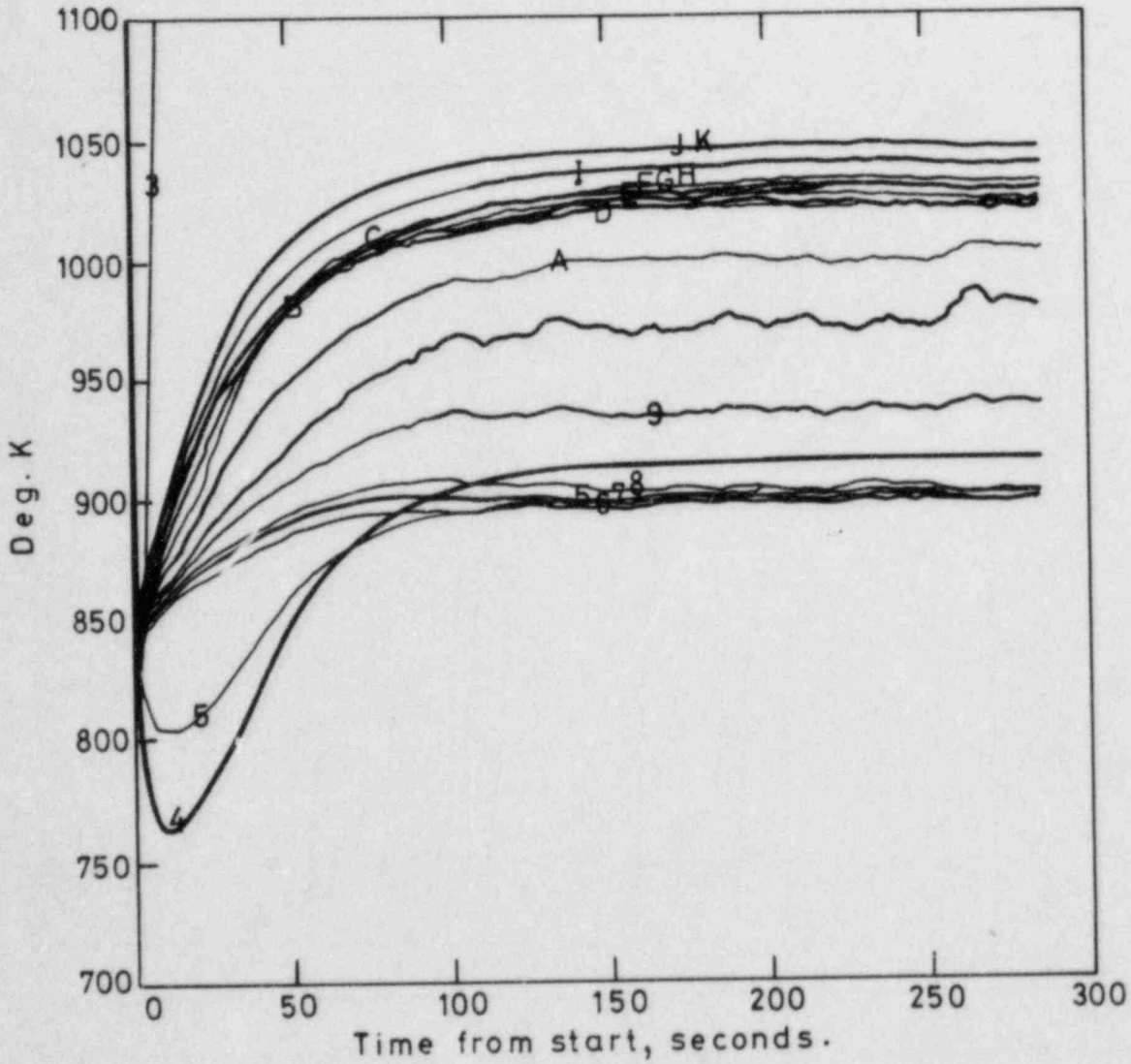


FIG.9. PREDITIONS OF TYPICAL HARWELL HOT-PATCH EXPERIMENTAL DATA USING MODIFIED VERSION OF TRAC-PF1 CODE.

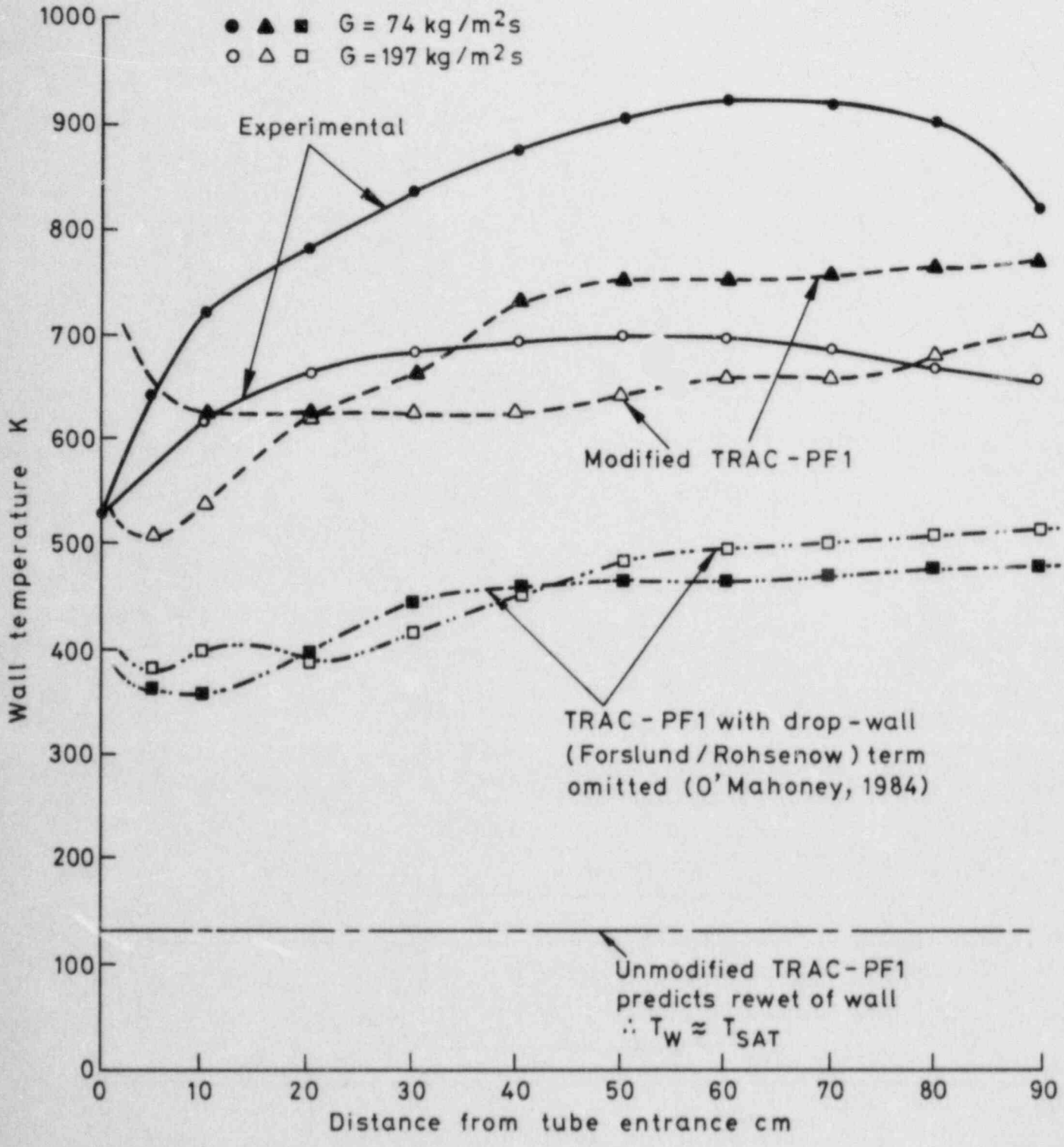


FIG.10. COMPARISON OF PREDICTED AND EXPERIMENTAL ASYMPTOTIC TEMPERATURE DISTRIBUTIONS FOR THE HARWELL 'HOT-PATCH' EXPERIMENTS WITH UPWARDS FLOW.

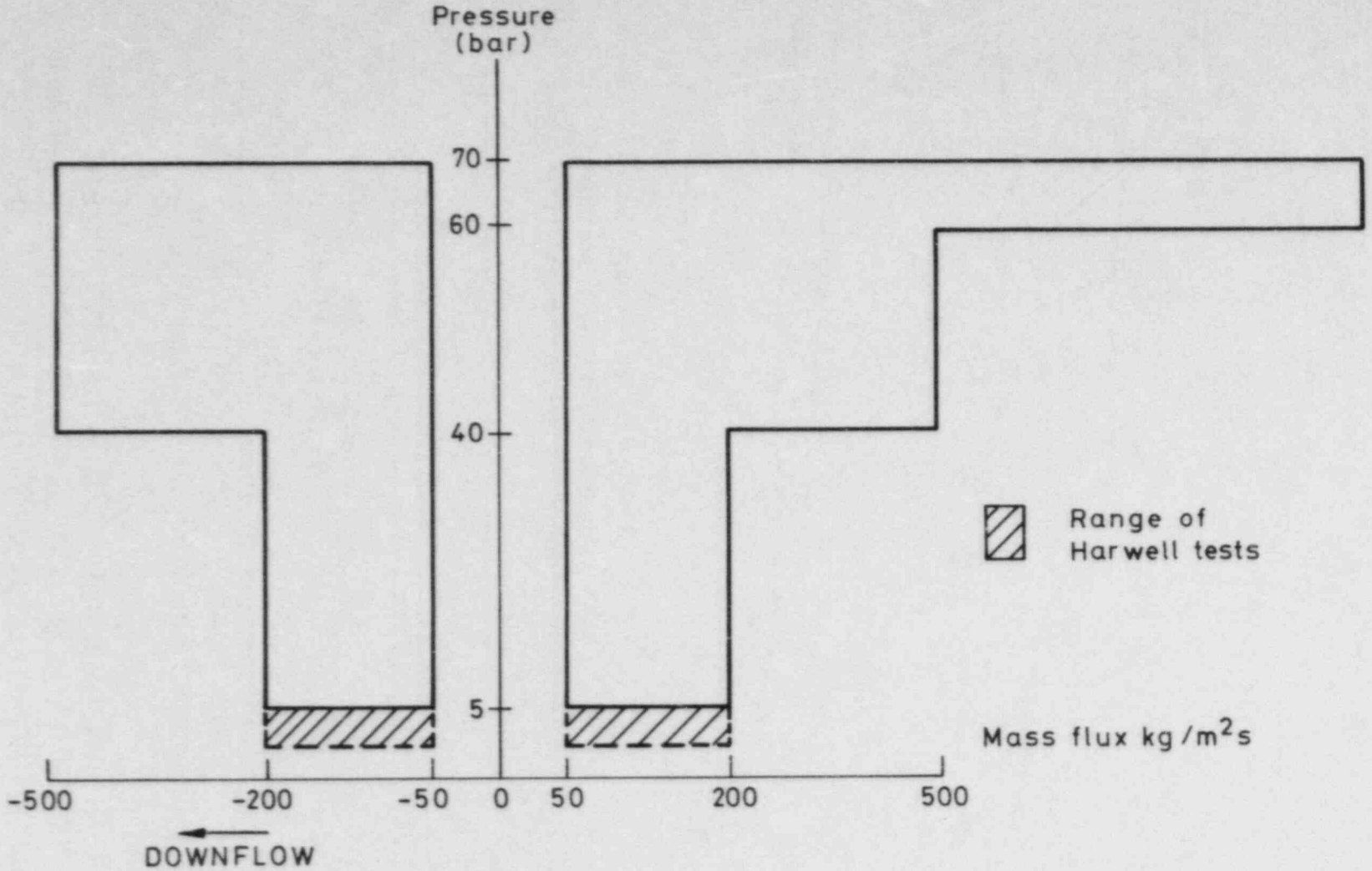


FIG.11. RANGE OF CONDITIONS TO BE COVERED IN THE AEE WINFRITH HIGH-PRESSURE HOT-PATCH TESTS.

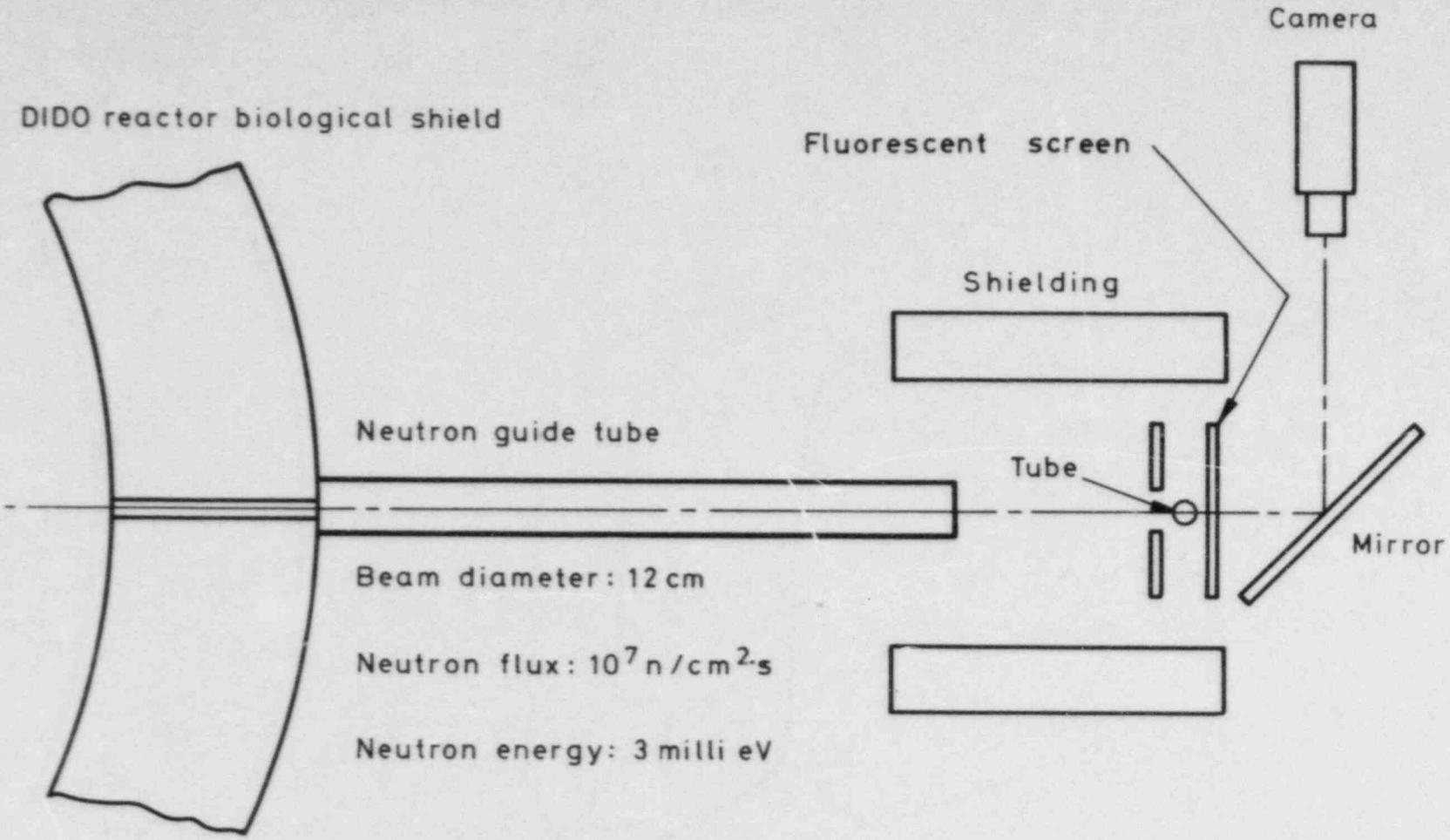


FIG. 12. NEUTRON RADIOGRAPHY ARRANGEMENT.

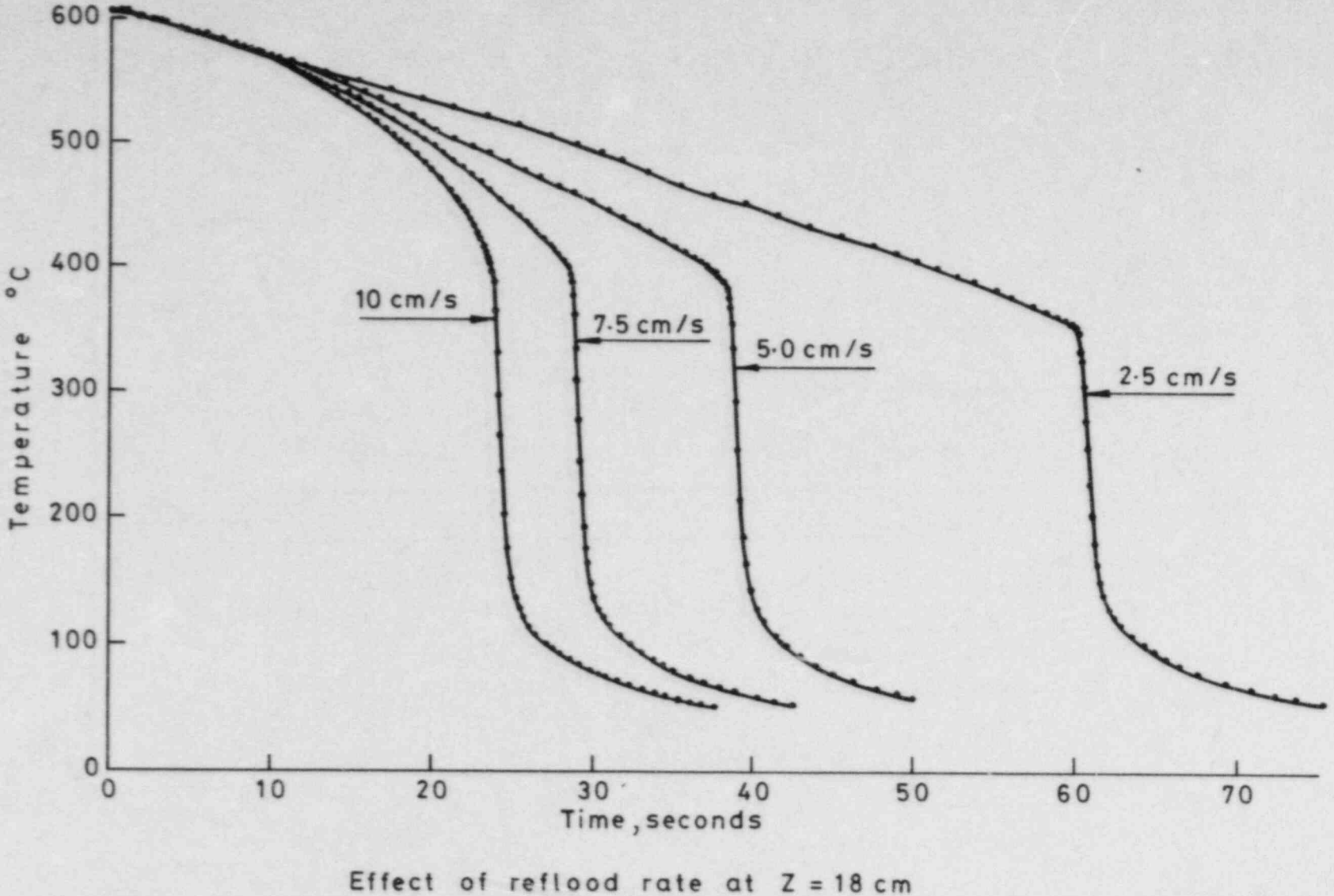


FIG.13. WALL TEMPERATURE / TIME HISTORIES AT A FIXED POSITION, AND AS A FUNCTION OF REFLOOD RATE, FOR THE NEUTRON RADIOGRAPHY REFLOOD VISUALISATION TESTS.

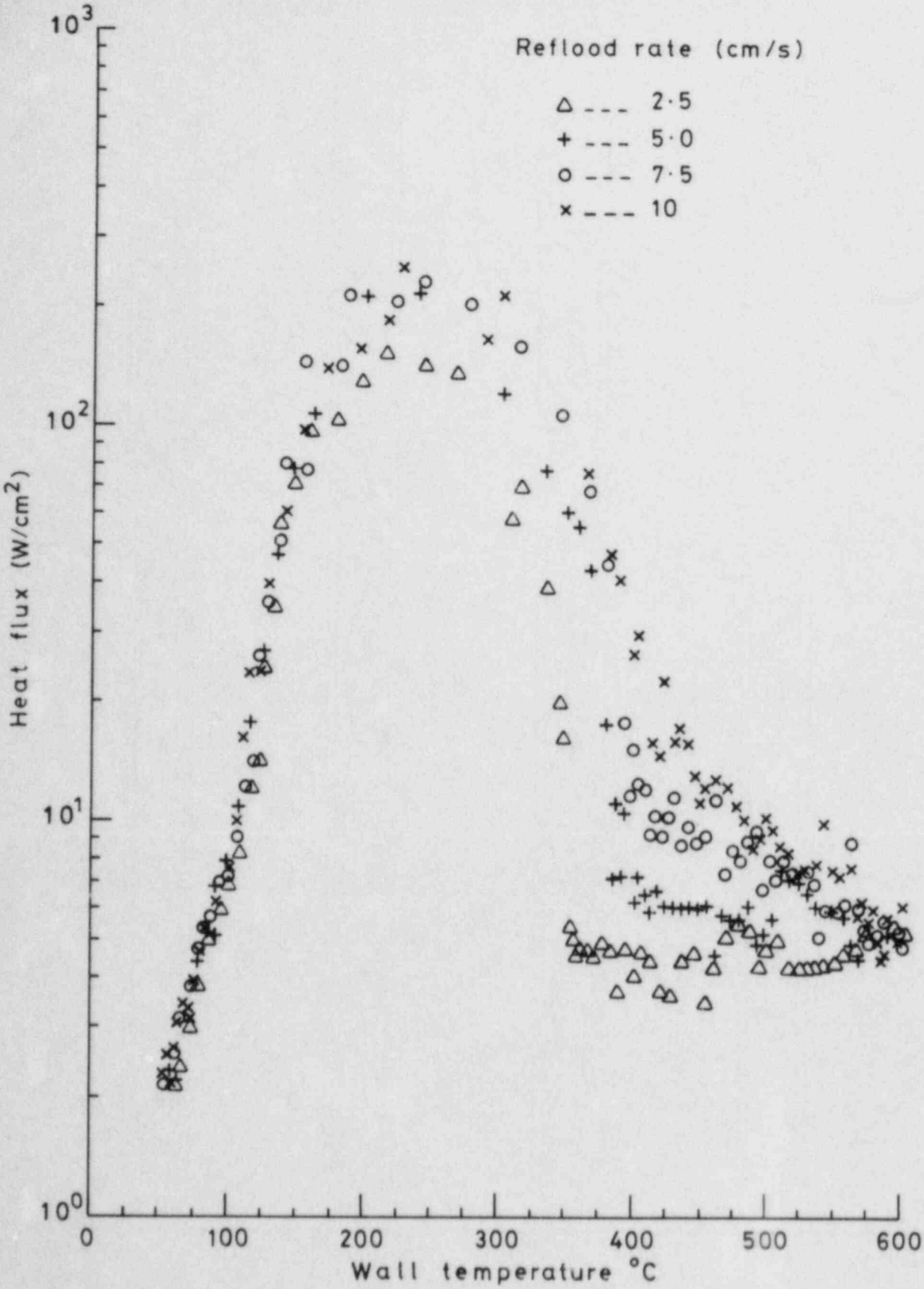


FIG.14. BOILING CURVES CALCULATED FROM THE WALL TEMPERATURE HISTORIES FOR THE NEUTRON RADIOGRAPHY REFLOOD TESTS.

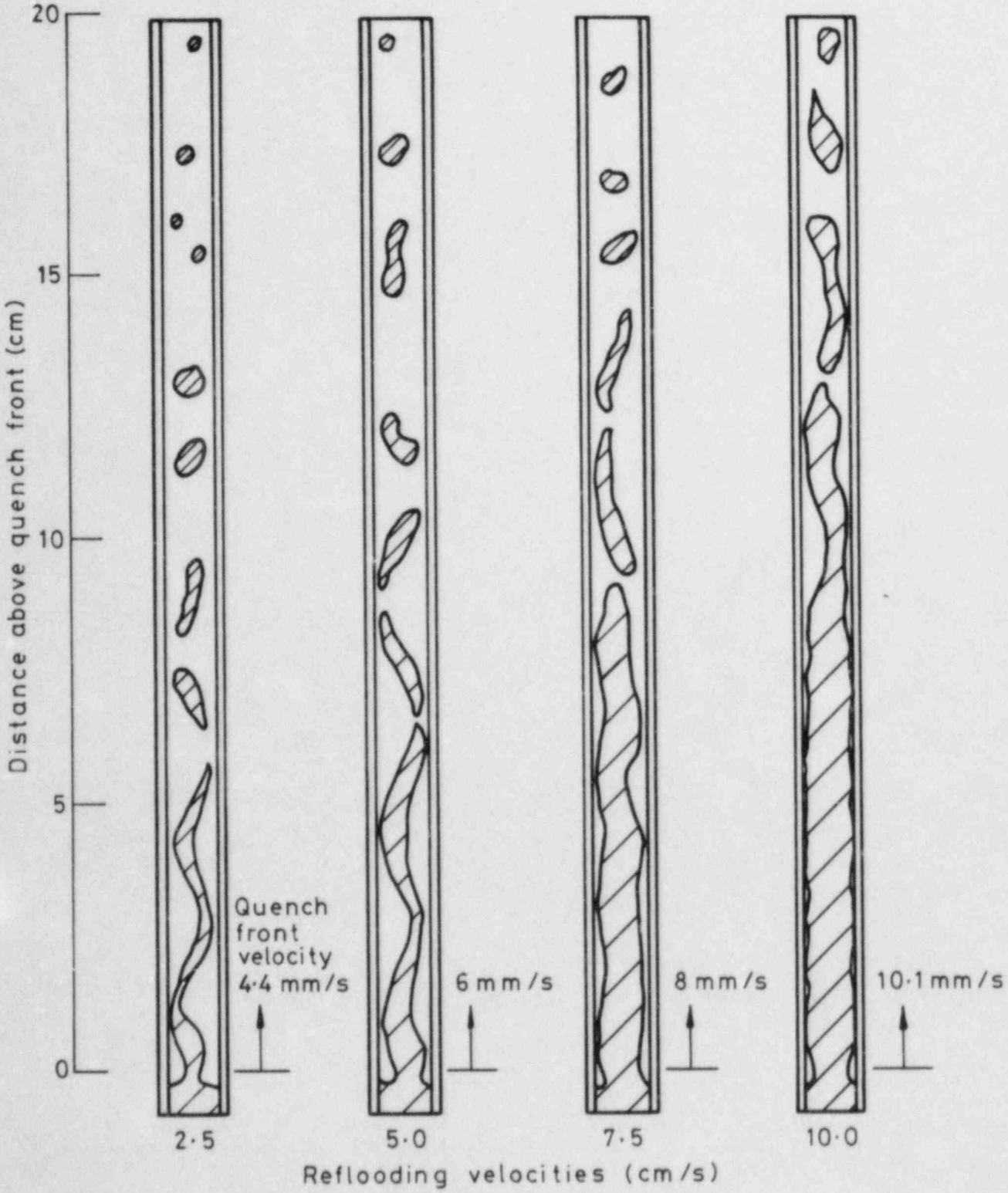


FIG.15. FLOW PATTERNS ABOVE THE QUENCH FRONT OBSERVED BY NEUTRON RADIOGRAPHY.

# Post-CHF Heat Transfer and Rewetting in Heated Tubes

D. Hein and W. Köhler

Kraftwerk Union AG, Erlangen

## Abstract

A range of tests, carried out on inside cooled tubes, was performed to advance the knowledge of basic thermohydraulic phenomena. Using the results it is possible to verify multi-dimensional computer codes with respect to their correct modelling of separate effects.

The investigations deal with

- heat transfer in post-CHF-region under steady state conditions
- effect of pressure and enthalpy transients on heat transfer
- rewetting through flooding of hot surfaces and
- effect of wetting state on pressure loss.

The experiments were aimed at development of fossil fired steam generators and at advancing emergency core cooling analysis of light water reactors. The results were evaluated and by using models incorporating the appropriate physical effects calculations were made possible.

## Introduction

If a flowing two-phase mixture does not wet a heated surface it generally means that relatively low heat transfer coefficients are to be expected. It follows that in these regions high wall temperatures exist which calls for careful design and material selection.

Internally cooled tubes are well suited for a large number of different thermal hydraulic investigations. The local flow parameters can be determined in a relatively simple way by means of mass, momentum and energy balances. For this reason this kind of experiments are employed to verify heat transfer and pressure loss computer models developed for two and three dimensional flow.

A large amount of data covering a host of thermal hydraulic problems was obtained at KWU from experiments involving internally cooled tubes. Within a program concerned with design improvement of fossil fired steam generators - in this special case BENSON steam generators - heat transfer in the evaporator tubes was investigated for both steady state and transients. Two phase flow pressure loss and especially the influence of the degree of surface wetting on pressure loss were included in the analysis. Experimental program covering LWR emergency core cooling systems investigated rewetting mechanisms in internally cooled tubes. Apart from heat transfer the hydraulic behaviour was also determined from measurement of momentum, pressure loss and water carry over.
Experiments for fossil fired steam generators were carried out up to supercritical pressure while rewetting was investigated at ambient pressure or slightly above it. Specific heating power and mass flow differed according to the two problems under investigation.

In the following it is shown how the appropriate physical effects are extricated through systematic experiments, over a large parameter field, in heated tubes and then used in computer modelling.

## Heat Transfer at High Pressure under Steady State Conditions

Heat transfer tests devised to facilitate the design of fossil fired steam generators were carried out in the BENSON test facility, shown in Fig. 1.

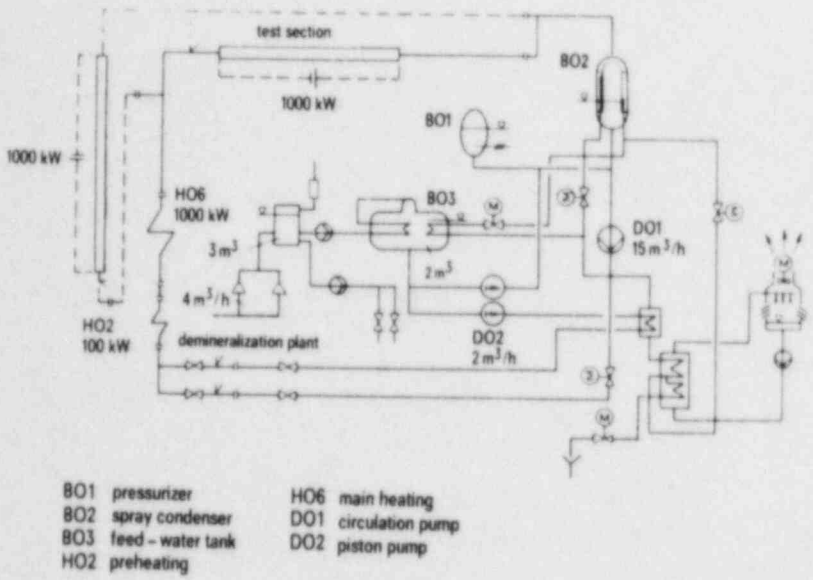


Fig. 1: BENSON-Test Rig

The experimental plant essentially consists of a high pressure loop, 1000 kW DC power supply unit, cooling tower and a water treatment plant. The rig is suitable for conducting tests with water, steam or two-phase mixture, its capability extends to supercritical pressures up to 330 bar. A detailed description of the test facility is given in /1/.

The investigation of heat transfer in the post-dryout region was carried out using internally cooled 6 m long tubes. In order to achieve high flow stability the rig was operated in once-through mode.

Fig. 2 shows an instrumented test section. By soldering 45 thermocouples along the entire legth of the tube the temperature and hence the heat transfer could be determined.

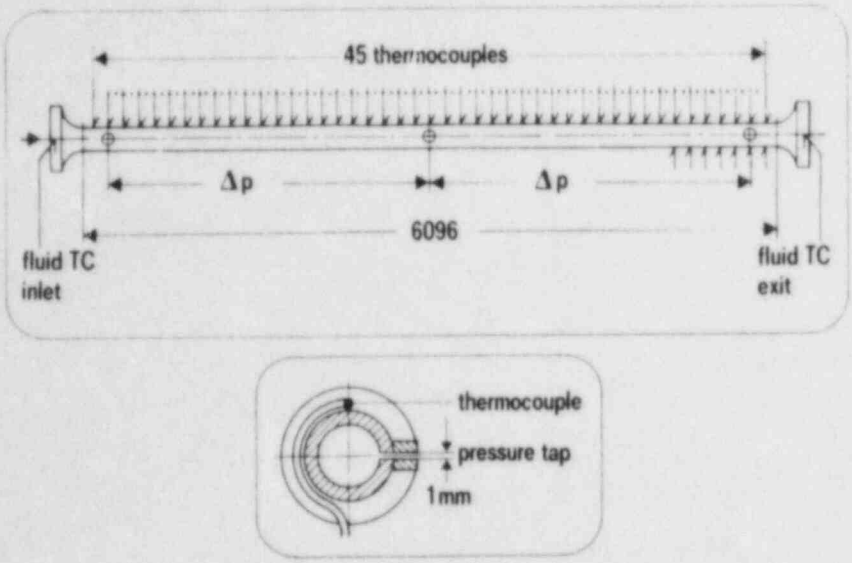


Fig. 2: Instrumentation of Test Section

The test matrix in post-dryout experiments comprised altogether 500 tests which covered the following parameters:

| | | | |
|---|---|---|---|
| Pipe diameter: | | 12.5, 14.0, 24.3 | mm |
| Pressure | : | 50 - 250 | bar |
| Mass flux | : | 300 - 2500 | $kg/m^2$-s |
| Heat flux | : | up to 600 | $kW/m^2$ |

Based on the above experiments and results from the literature a heat transfer model was developed which covered the post-CHF-region up to the critical pressure. The model takes into account representative thermal non-equilibrium between the steam and water phases. The degree of steam superheat is determined from energy balance, Fig. 3. The remaining unknown quantities are heat transfer coefficient $\alpha$ between the water droplets and steam as well as the surface area F of the evaporating droplets.

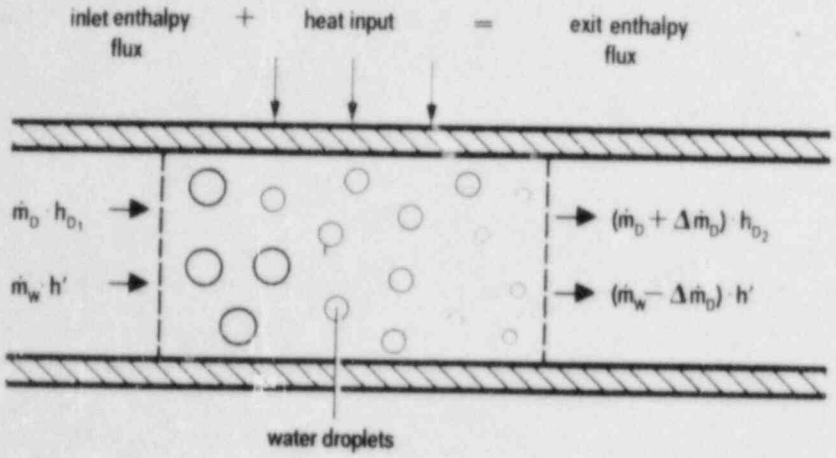


Fig. 3: Determination of Thermal Non-Equilibrium from Energy Balance

In order to avoid taking into account the droplet size spectrum and phase slip for all possible parameter combinations only the product($\alpha \cdot F$)was investigated in detail. It turned out that the above product is approximately constant and thus independent of the steam mass fraction. The value of ( $\alpha \cdot F$) was determined experimentally as a function of mass flux and Laplace-constant. Using the calculated steam superheat and a conventional single-phase heat transfer equation it is possible to calculate the surface temperature. A good agreement exists between experiments and results computed by the above model in the region 50 bar up to critical pressure, Fig. 4.

Fig. 5 depicts in a three dimensional view the calculated heat transfer coefficient as a function of the enthalpy of the fluid and pressure. In the region of fully developed nucleate boiling the heat transfer coefficient was calculated according to JENS and LOTTES /3/, in single-phase flow GNIELINSKI's correlation /4/ was used. The location of the boiling crisis which forms the boundary between the wetted and unwetted part of an evaporator tube was calculated according to KON'KOV /5/. A detailed description of the applied computer modell appears in /6/.

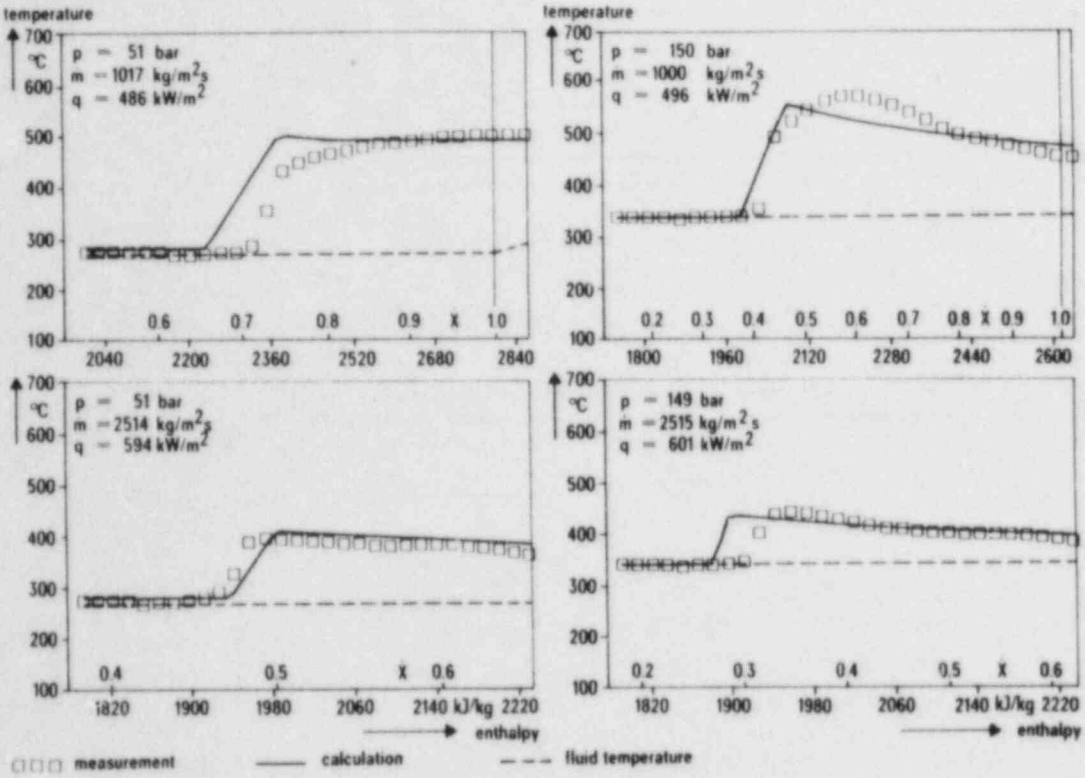


Fig. 4: Calculated and Measured Wall Temperature Distribution (d = 12,5 mm)

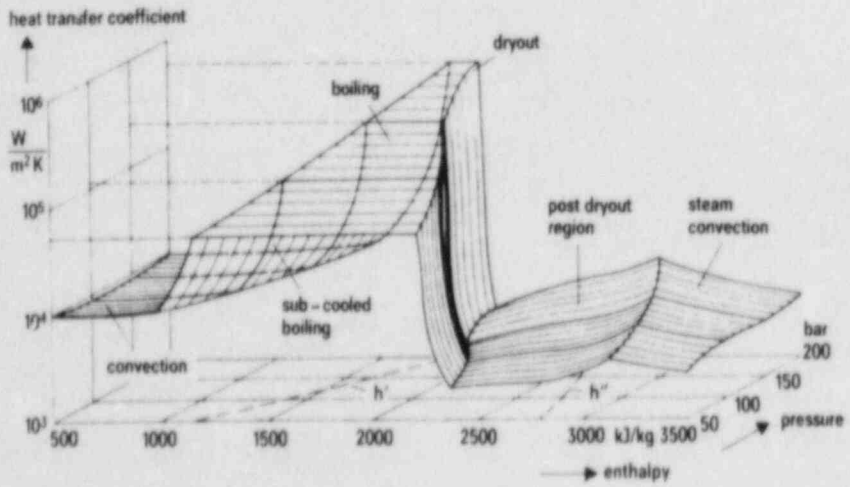


Fig. 5: 3-Dimensional Representation of Heat Transfer for Forced Flow Conditions in Tubes

## Pressure and Enthalpy Transients at High Pressures

In internally cooled tubes in post-CHF region and at high pressures it is possible to observe temporarily higher wall temperatures than the ones known to exists under steady state heat transfer conditions. This effect is attributed to pressure and enthalpy transients and was observed when the location of the boiling crisis moved towards the pipe exit (as a result of changed parameters determining the new state) which was up till then unwetted. To analyse this phenomenon experiments were carried out in which pressure reduction from super- to subcritical state initiated rewetting or alternatively by reducing the inlet flow enthalpy the boiling crisis location was moved further downstream.

The transient phenomena were also investigated in the above mentioned BENSON test facility. The transients were simulated in the following manner:

1. Reduction of System Pressure
   By spraying cold water into the pressurizer the system pressure was reduced by 5 to 20 bar per minute. The remaining system parameters e.g. pump mass flow and heating power were not changed.

2. Reduction of Enthalpy at Test Tube Inlet
   By reducing the pre-heating power the enthalpy at test pipe inlet was lowered by 200 to 400 kJ/kg.
   Pump mass flow, system pressure and test tube heating were kept constant.

Both transient phenomena as described above led in most cases to considerable deterioration of heat transfer in the post-CHF region. The deterioration observed over long time periods was worst when the pressure and enthalpy reduction took place near the critical pressure.

A typical tube wall temperature history following a pressure reduction from super- to subcritical state is shown in Fig.6. In the initial state at 247 bar, i. e. at supercritical pressure, the temperature along the entire pipe lies between 380 and 400°C. After 165 s temperature profile is established which, at the location where the value of fluid enthalpy $h = 1750$ kJ/kg is reached, formes a steep gradient, indicating

the boiling crisis. In the course of the experiment the boiling crisis location moves downstream whereby the maximum temperature decreases again and after 600 s steady state with maximum temperature of 430°C is reached.

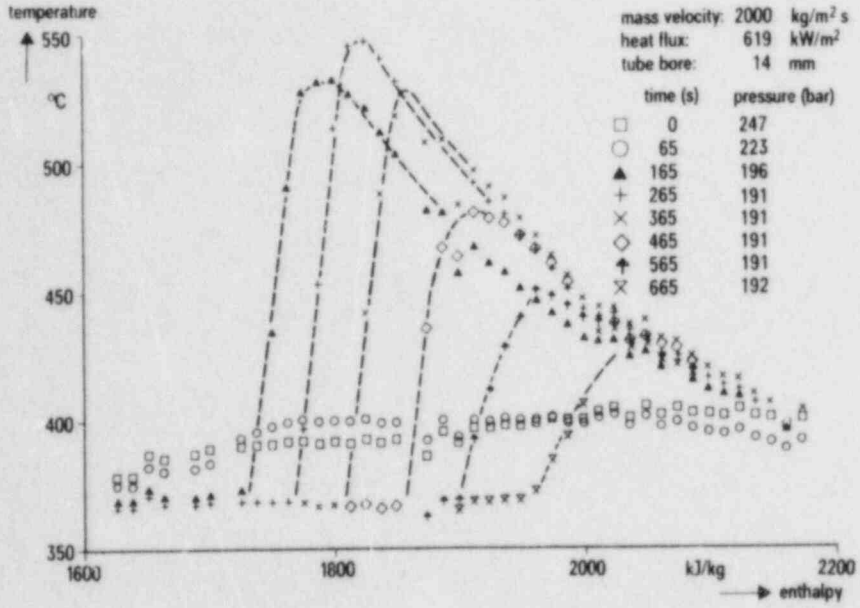


Fig. 6: Wall Temperature Distribution due to Pressure Transients

A detailed analysis of this test using a computer program capable of simulating dynamic phenomena in a steam generator /7/ shows that near the critical pressure the rewetting front adjusts only sluggishly to the changing conditions in the evaporator tube. As a result test tube sections were observed with small or even negative steam generation (based on energy balance) in the unwetted region. This means that film boiling can take place and two-phase flow velocities at the boiling crisis location are considerably reduced, as compared to steady state, resulting in reduced cooling effect and increased temperature.

A similar temperature excursion is caused by enthalpy reduction at the test tube inlet. Also in this case, by comparing the enthalpies at the boiling crisis location, the considerable increase in wall temperature can be attributed to delayed (relative to steady state) surface wetting.

What is the reason for the delay in surface wetting in the high pressure region?
Applying the YAMANOUCHI model /7/, well known from reactor emergency core cooling investigations, to transient phenomena in an evaporator tube one finds that the quench front progression depends strongly on the difference between the wetting temperature and the saturation temperature. Measurements of wetting temperature under forced convection conditions show that in the vicinity of the critical point a strong reduction of the above mentioned temperature difference takes place e. g. the wetting temperature in subcritical region already approaches the fluid saturation temperature, Fig. 7. Consequently in the high-pressure region the quench front progression is delayed producing the above mentioned effects on heat transfer in post-CHF region.

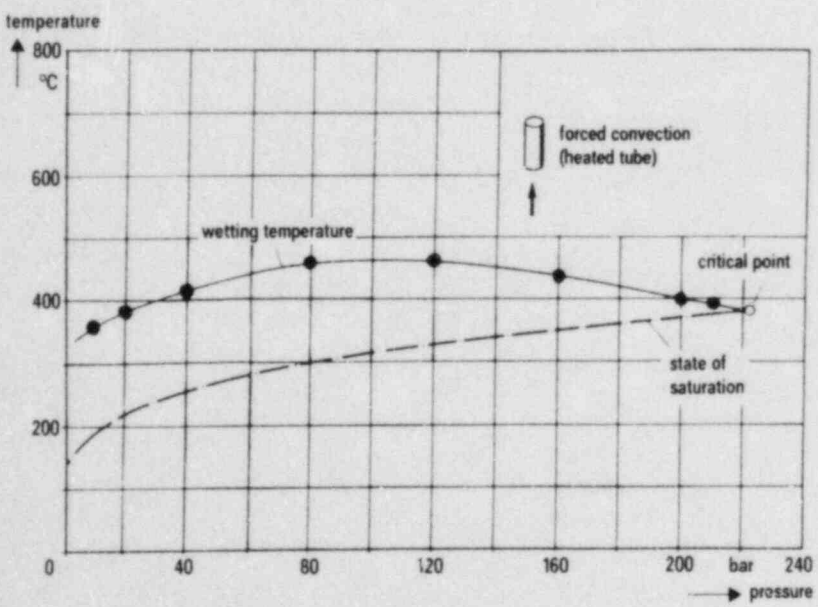


Fig. 7: Dependence of Wetting Temperature on Pressure for Flooding Conditions (from Ref. 8)

Based on experimental results and the YAMANOUCHI model a semi-empirical equation was developed which describes the quench front progression as a result of pressure and enthalpy changes. Fig. 8 shows a comparison between the calculated and measured quench front progression.

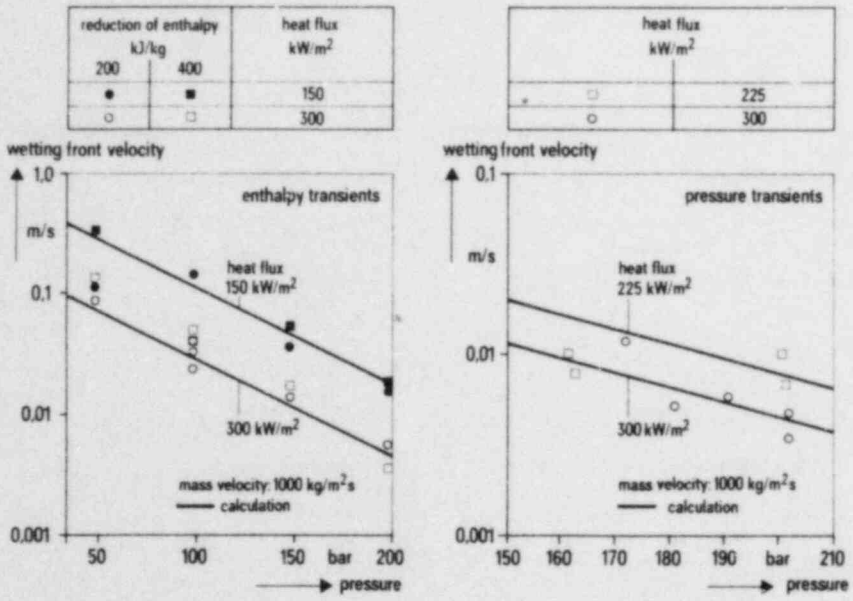


Fig. 8: Wetting Front Progression in Enthalpy and Pressure Transients (from Ref. 9)

## Rewetting Through Flooding

Rewetting of heated tubes under forced-flooding conditions was investigated using internally cooled pipes. Tests were started by employing direct electrical heating to set up the initial tube temperature and wall heat flux in the 3 m long test tube. This was followed by bottom flooding at a specified flooding rate.

The tests covered the following parameter range:

| | |
|---|---|
| tube internal diameter | 11.8 and 16.8 mm |
| pressure | 1.5 and 4.5 bar |
| flooding rate | 20 to 100 mm/s |
| steady state heat flux | 20 to 60 kW/m² |
| inlet subcooling | 3 to 120 K |

The reflooding along the tube could be tracked by monitoring the wall temperature, Fig. 9. A sharp temperature decrease is recorded when the pipe wall rewets in the immediate vicinity of the thermocouple in question. By using this information from all the wall thermocouples along the pipe the quench front movement is determined, Fig. 9.

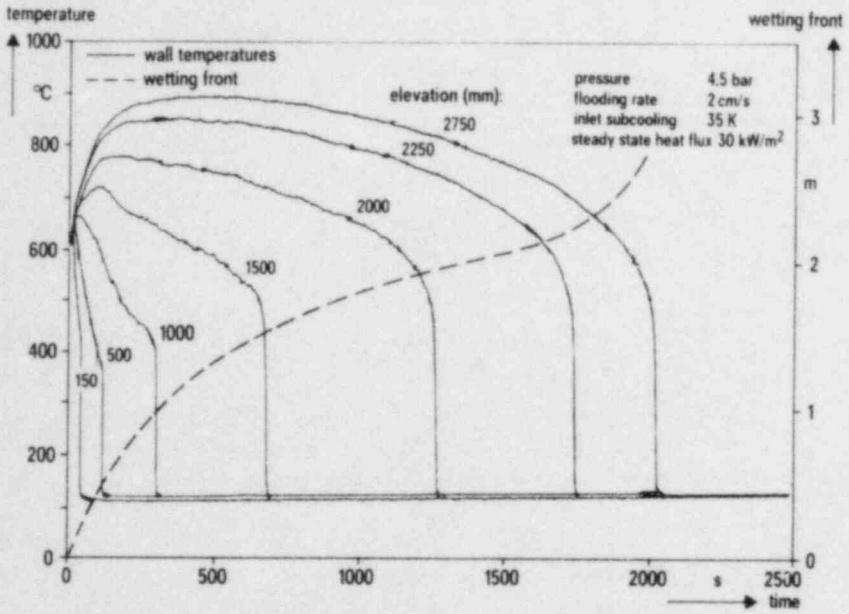


Fig. 9: Wall Temperatures and Wetting Front Progression during Flooding

In order to describe the reflooding process precisely it is necessary to know not only the heat transfer but also the hydraulics. Only then it is possible to check whether computer code assumptions were made on correct physical basis. If, in addition, there is information available on thermal non-equilibrium between the steam and water phase i. e. on the temperature of the steam then it is possible to make a realistic assessment of the heat transfer.
Fig. 10 shows quantities describing the hydraulics and determination of thermal non-equilibrium.

In particular the following quantities are determined:

- steam temperature $\vartheta_D$ at channel exit
- steam mass flow rate $\dot{m}_D$ at channel exit
- water carry over $\dot{m}_W$
- water inventory in test tube
- droplet size
- droplet velocity
- momentum flux i of the flow

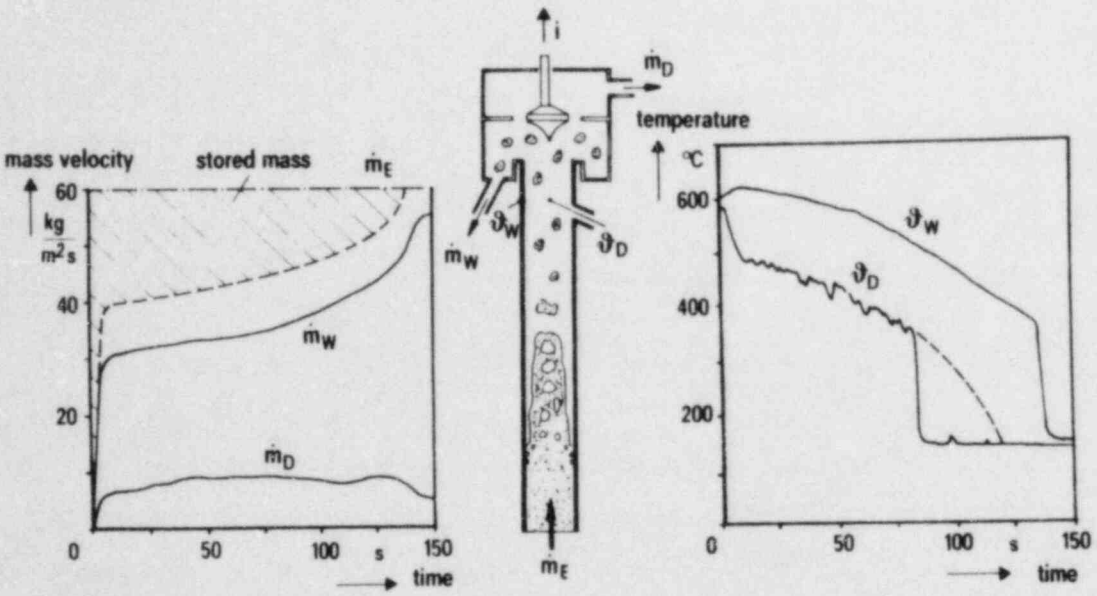


Fig. 10: Flooding Hydraulics

By measuring the exit steam mass flow rate, water carry over as well as the injected water flow rate it is possible to form mass balance for the whole tube as shown in Fig. 10. Droplet size and velocity are determined at the pipe exit using photographic techniques.
The degree of steam superheat is measured by means of a thermocouple located in the tube centre. Typical values of wall and steam temperatures measured at the same elevation are shown in the right half of Fig. 10

The momentum flux of the flow is determined by measuring the force necessary to deflect the flow by 90°. From this information it is possible to evaluate the slip ratio, depicted in Fig. 11 as a function of steam mass fraction. With increasing steam mass fraction the slip approaches 1 i. e. steam and water have the same velocity.

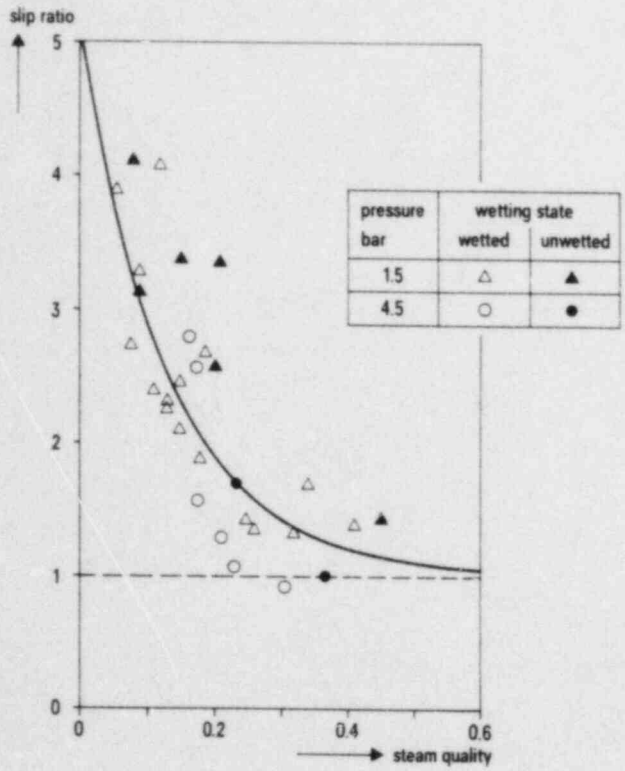


Fig. 11: Slip as a Function of Steam Quality

Based on experimental investigations and models as described in /10/ a computer code HYDROFLUT was developed which describes with good accuracy the flooding phenomena in internally cooled tubes. This code was, among others, verified through precalculations of the OECD-CSNI LOCA Standard Problem No. 7 /11/.

## Frictional Pressure Loss for Wetted and Unwetted Heating Surfaces

In experiments investigating heat transfer in evaporator tubes and rewetting the pressure drop were also measured.
From these measurements the frictional pressure loss was calculated by eliminating the acceleration and gravitational components. It became apparent that the state of the heating surface (wetted/unwetted) has a strong influence on the frictional pressure loss which is considerably higher in the wetted than in the unwetted region. This phenomenon was observed both at high pressure and mass flux (parameter for fossil fired steam generators) and at low pressure and mass flux (parameters for rewetting experiments).
Fig. 12 shows typical changes in two-phase flow multipliers as determined for wetted and unwetted regions of an evaporator tube. To facilitate interpretation the boiling crisis position was located between two tube sections in which their respective pressure drops were measured. It can be seen that the wetted region exhibits considerably higher pressure loss.

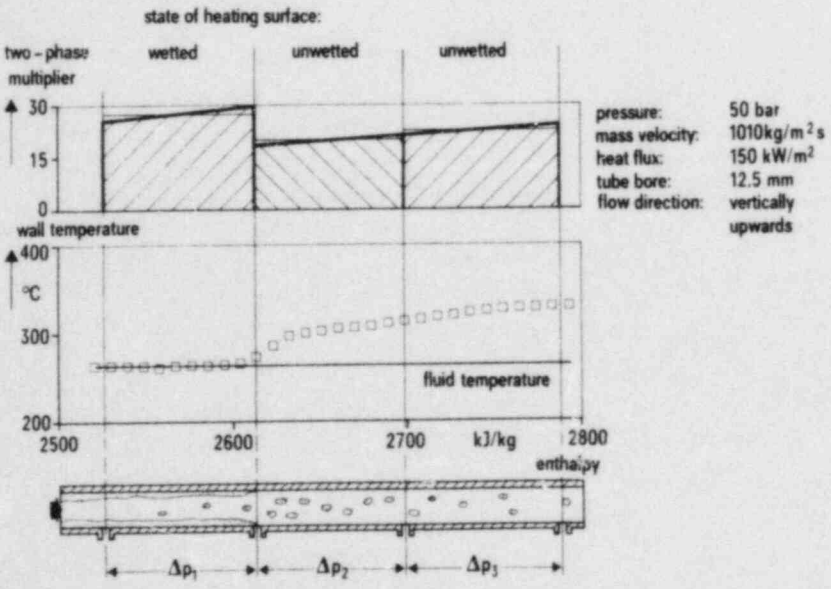


Fig. 12: Two-Phase Multiplier in the Wetted and Unwetted Zones of Heated Tube Flow

Calculated pressure loss in the post-CHF region showed good agreement with experimental results when the BEATTIE model /12/ was used. In wetted region the frictional pressure loss is influenced by a number of factors which do not appear in an exact form in commonly used equations. In the parameter range applicable to fossil fired steam generators the FRIEDEL equation /13/ is sufficiently accurate for frictional pressure loss calculations.

Fig. 13 shows a typical comparison between calculated and measured two phase flow multipliers in wetted and unwetted regions. In the same figure it can also be seen that the frictional pressure loss of non-heated flow is higher than that of heated flow in an unwetted region.

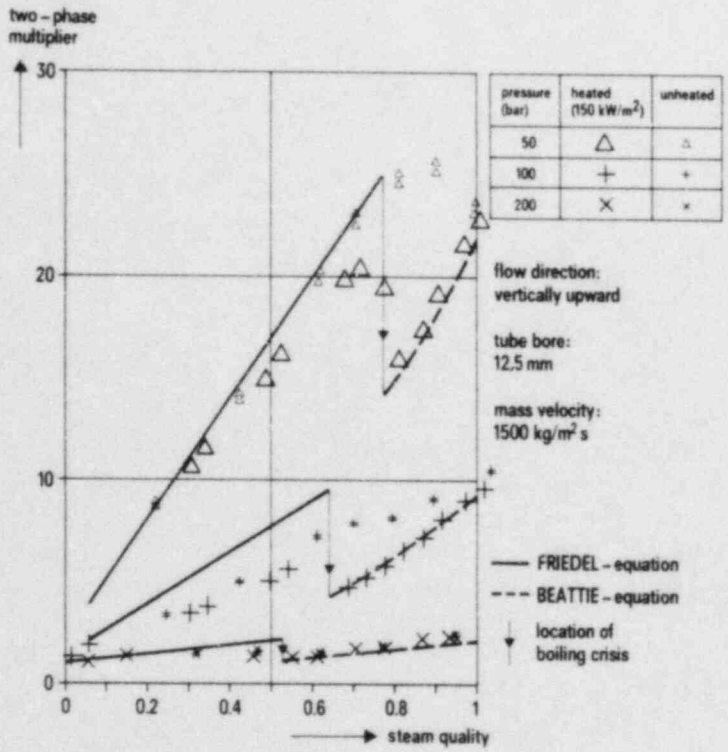


Fig. 13: Influence of Heating on the Two-Phase Pressure Drop

## Conclusions

The experiments on heat transfer and pressure loss described in this paper cover, to the various programs' aims, a large parameter range. Nevertheless, the examined phenomena have the same physical basis. The thermal non-equilibrium between the two phases influences the steam mass fraction as well as the heat transfer in the post-CHF region. Also the condition of a heating surface e. g. wetted or unwetted can be shown to influence the frictional pressure loss as was borne out in experiments concerned with fossil fired steam generators as well as in those carried out within nuclear reactor safety programs.

Computer models developed and verified using simple geometrical configurations and known initial and boundary conditions constitute valuable elements for multidimensional computer codes simulating far more complex phenomena.

## References


/1/ Hein, D., Keil, H. und Köhler, W.
The BENSON Test Rig
VGB-Kraftwerkstechnik
57th Annual Series, No. 6, June 1977

/2/ Herkenrath, H., Mörk-Mörkenstein, P. et al.
Wärmeübergang an Wasser bei erzwungener Strömung
im Druckbereich von 140 bis 250 bar
EUR 3658 d - EURATOM Ispra (1967)

/3/ Jens, W.H., Lottes. P.A.
Analysis of heat transfer, burnout, pressure drop
and density data for high pressure water
USAEC Report ANL-4627 (1951)

/4/ Gnielinski, V.
Neue Gleichungen für den Wärme- und Stoffübergang
in turbulent durchströmten Rohren und Kanälen
Forsch. Ing.-Wes. 41, Nr. 1 (1975)

/5/ Kon'Kov, A.S.
Experimental Study of the Conditions under which Heat Exchange Deteriorates when a Steam-Water Mixture Flows in Heated Tubes
Teploenergetika, Vol.13 (1965) Nr. 12, S. 77

/6/ Hein, D. and Köhler, W.
A Simple - To - Use Post Dryout Heat Transfer Model Accounting for Thermal Non-Equilibrium
Int. Workshop on Fundamental Aspects of Post-Dryout Heat Transfer, April 2 - 4, 1984
Salt Lake City, USA

/7/ Yamanouchi, A.
Effect of Core Spray Cooling in Transient State after Loss of Coolant Accident
J. Nucl. Sci. Technol. 5 (1968) 547 - 558

/8/ Hein, D., Kefer, V. and Liebert, H.
Maximum Wetting Temperatures Up to Critical Pressure
Int. Workshop on Fundamental Aspects of Post-Dryout Heat Transfer, April 2 - 4, 1984,
Salt Lake City, USA

/9/ Köhler, W.
Einfluß des Benetzungszustandes der Heizfläche auf Wärmeübergang und Druckverlust in einem Verdampferrohr
Dissertation, TU-München, 1984

/10/ Hein, D.
Modellvorstellungen zum Wiederbenetzen durch Fluten
Dissertation, Universität Hannover, 1980

/11/ Deruaz, R. and Tellier, N.
Comparison Report on OECD-CSNI Loca Standard Problem No. 7, DSN - C.E.A.-France, CSNI-Report No. 55
June 1979

/12/ Beattie, D.R.H.
A Note on the Calculation of Two-Phase Pressure Losses, Nucl. Engng. and Design 25, pp 395 - 402 (1973)

/13/ Mayinger, F.
Strömung und Wärmeübergang in Gas-Flüssigkeits-Gemischen
Wien (1982) S 54.

# High Pressure Steam/Water Two-Phase Flow in Large Diameter Horizontal Pipes

K. Tasaka, M. Kawaji, Y. Anoda, Y. Koizumi

Japan Atomic Energy Research Institute

## INTRODUCTION

As part of the ROSA-VI program to investigate small break Loss-of-Coolant Accidents (LOCA) and transients for PWRs, an experimental program has been initiated in August, 1983 to study the two-phase flow behavior in a large horizontal pipe. The two-phase flow behavior in a hot leg of a reactor is of particular concern because of its effect on the decay heat removal from the reactor core.

Although horizontal two-phase flow has been studied in the past by many investigators, most of these studies have been conducted with low-pressure, air/water systems in small diameter pipes. Experimental data on high-pressure, steam/water two-phase flow in large diameter pipes have not been reported previously. Thus, the present experiments are intended to provide detailed data on the structure of two-phase flow such as phase and velocity distributions in a large horizontal pipe, in addition to macroscopic behavior including flow pattern transitions at pressures up to 12 MPa.

Among the two-phase flow models available, the two-fluid model is considered to be the most suitable for predicting the thermal hydraulics of a small break LOCA, because relatively low flow rates are expected to occur in

pipes and components leading to phase separation and a large slip between the phases. The data from the present experiments would be useful in developing or validating flow transition correlations and various constitutive relations needed in two-fluid models.

## TEST FACILITY AND INSTRUMENTATION

The experimental facility used is the Two-Phase Flow Test Facility (TPTF) recently constructed at Japan Atomic Energy Research Institute's Tokai Establishment (Nakamura et al(1983)). This facility has been designed to perform various steam/water two-phase flow and heat transfer experiments at steady state for pressures up to 12.8 MPa.

The flow loop used in the present series of experiments is shown in Figure 1 and consists of an electrically heated boiler, separate pumps for steam and water lines, a mixer and a 10 m long, 180mm I.D. horizontal test section. The demineralized water is heated in the boiler to saturation conditions at a desired system pressure. Saturated steam is pumped from the top of the boiler through an orifice meter into the mixer located at the entrance of the test section. Similarly, saturated liquid is drawn from the bottom of the boiler and pumped through an orifice meter into the mixer.

The mixer is tee-shaped as schematically shown in Figure 2. Steam is introduced horizontally and liquid from the bottom of the tee. Two different types of inlet mixers have been used so far. A homogeneous mixer contains a bundle of tubes and steam is forced out into liquid through numerous holes drilled along the side of each tube. Thus, a nearly homogeneous mixture of liquid and vapor is obtained that enters the test section. The second type

contains a flat plate that separates steam and water, and supplies to the test section a separated two-phase flow.

The test section consists of five sections of Sch. 120, 180mm I.D. stainless steel piping, each 2 m long and joined by Gray Locks. The overall length is 10.0m and the length-to-diameter ratio is 56. The volumetric flow rates of vapor and liquid entering the test section can be changed independently by adjusting the control valves and changing the pump speed. The maximum mass flow rate varies with pressure but ranges slightly above 1000 $kg/m^2s$. In terms of superficial velocities, the liquid and vapor flow rates are 1.9 m/s and 7.6 m/s respectively. The water level in the boiler can be maintained either above or below the exit of the test section.

The test section is equipped with various two-phase flow instruments as shown in Figure 2. In order to obtain detailed information about the flow, several instruments are designed to traverse across the pipe cross section. To measure the density (or void) distribution, gamma densitometers are traversed across the pipe in both horizontal and vertical directions (Figure 3).

To measure momentum flux, a water-purged Pitot tube is employed. As shown in Figure 4, the Pitot tube is attached to a driving mechanism which moves the probe vertically along the centerline of the pipe. The water-purge is necessary to prevent voiding of pressure sensing lines and the purge rate is fixed at 30 ml/min. Due to purging, the response of the Pitot tube is reduced in comparison with a non-purged reference Pitot tube. Therefore, the Pitot coefficient was determined for single-phase water and steam flow by separately conducting single-phase calibration tests.

In addition to the gamma densitometers, a set of five conductivity probes forming a vertically oriented rake (Figure 5) is used to determine the phase

distribution. A drag screen is installed to determine its measurement characterictics under two-phase flow conditions.

The instrument signals are sent to a data logger, sampled and recorded on a magnetic tape at a rate of 5 Hz for 800 seconds in each run. The conductivity probes are separately sampled at 100 Hz for 40 seconds. The data collected were processed by an off-line computer.

## TEST CONDITIONS AND PROCEDURE

The parameters that are varied in the present series of experiments include the system pressure and the corresponding saturation temperature, inlet mass flux and flow quality as listed in Table 1. In order to determine the conditions for transition among the separated, intermittent and annular flow patterns, mass flux and inlet quality are varied as widely as possible within the maximum operating limits of the present system as shown in Figure 6. Also shown in Figure 6 are the flow pattern transition conditions calculated from correlations proposed by Choe et al(1978) and Weisman et al(1979) and expressed in terms of mass flux and quality. Most of the existing correlations are based on low pressure, small diameter pipe data, however, Weisman et al (1979) used the air/water two-phase flow data of Simpson et al(1977) obtained in pipes with larger diameters (21.5 cm and 12.7 cm) at low pressure, in addition to the data from smaller diameter pipes in developing their correlation.

## EXPERIMENTAL RESULTS AND DISCUSSION

Altogether, 90 two-phase flow runs have been performed in the present

series of experiments. In this section, representative distributions of mass and momentum flux measured with traversing gamma densitometers and a Pitot tube will be discussed and a methodology used in flow pattern identification from the data will be outlined.

## Void and Momentum Flux Distribution

The chordal-average void fraction profiles obtained at 7.5 MPa are shown in Figure 7. This run represents a high mass flux (1000 $kg/m^2s$) with low quality (0.2) case. A symmetrical void fraction profile for the center beam and inclined profiles for the other two beams suggest a separated or wavy flow pattern as evident from comparison with those calculated for an idealized stratified flow with an equivalent liquid holdup. For the separated flow, the void fraction profile can be used to construct a collapsed liquid level profile in the pipe as shown in Figure 8. The collapsed liquid level in the pipe has been observed to be relatively flat in all separated flow situations.

The momentum flux distribution along the centerline of the pipe obtained in the run discussed above is shown in Figure 9 together with the void distribution measured with a vertically traversing gamma densitometer, and a velocity profile calculated from those data. The momentum flux increases steadily from the bottom of the pipe upward. After reaching a peak, it rapidly drops and remains at a lower value in the upper part of the pipe. The peak in momentum flux is observed to occur near the collapsed liquid level shown earlier.

It is clear from the void and momentum distribution data shown, that the bottom part of the pipe is occupied by the liquid and the upper part by the vapor phase. Smoothness of the momentum flux in the vapor phase region rules out

the existence of liquid slugs hitting the Pitot tube. This observation is also supported by the conductivity probe signals. The variation of void fraction near the interface is seen to be rather gradual due probably to the presence of interfacial waves. The Pitot tube calibration was checked by calculating the total flow rate based on the momentum flux and void distribution data for stratified flow. The calculated flow rates are compared with the inlet flow rates as shown in Figure 10.

## Interfacial Shear

For a two-fluid model, calculation of interfacial shear is important in accurate prediction of flow behavior. Based on a momentum balance method outlined by Agrawal et al(1973) and recently used by Johnston (1984) for the analysis of cocurrent and countercurrent stratified flows, the interfacial shear was calculated from the data and compared with the wall-vapor and wall-liquid shear stresses in Figures 11 and 12 respectively. The interfacial shear is greater than the wall-vapor shear roughly by a factor of three, and less than the wall-liquid shear by a factor of 0.8. The interfacial shear is also observed to decrease with liquid holdup and increase with mass flux as shown in Figure 13. For stratified and wavy flows, the preliminary analysis indicates that the interfacial shear increases with the waviness of the interface estimated from the available vertical void distribution data.

## Flow Patterns

The flow patterns determined from the data obtained with a homogeneous

inlet mixer are shown in Figure 14. Within the test conditions shown in Table 1, only the separated flow pattern was found to occur. With a separated flow mixer, however, slug flow has been detected at a pressure of 3 MPa and mass flux of about 500 $kg/m^2s$. Slug flow was determined by a combination of gamma densitometer, Pitot tube and conductivity probe signals as shown in Figure 15. In any case, separated flow pattern has been observed over a much wider range of test conditions, in comparison with Choe et al and Weisman et al's transition correlations. The void fraction profiles measured near the inlet of the test section also indicate that despite being well mixed at the inlet, the phases tend to separate in a short distance from the inlet and readily form a separated flow pattern.

## CONCLUDING REMARKS

High pressure, steam/water two-phase flow in a large horizontal pipe is experimentally investigated with an emphasis on detailed measurement of flow structure. The data obtained indicate occurrence of the separated flow pattern (stratified or wavy) over a wider range of mass flux and quality in comparison with the existing flow pattern transition correlations. Future plans include a similar series of experiments with a 87 mm I.D. pipe.

## REFERENCES

Nakamura, H., Tanaka, H., Tasaka, K., Koizumi, Y., and Murata, H., "System Description for ROSA-VI Two-Phase Flow Test Facility (TPTF)," JAERI-M-83-042, March, 1983.

Choe, W.G., Weinberg, L., and Weisman, J., "Observation and Correlation of Flow Pattern Transitions in Horizontal Cocurrent Gas-Liquid Flow," in Two-Phase

Transport and Reactor Safety (Edited by Vesiroglu, T.N., and Kakac, S.), Hemisphere Publishing Co., Washington, 1978.

Agrawal S.S., Gregory, G.A., and Govier, G.W., "An Analysis of Horizontal Stratified Two Phase Flow in Pipes," Canadian Journal of Chemical Engineering, Vol. 51, June 1973, pp.280-286.

Johnston, A.J., "An Investigation into the Interfacial Shear Stress Contribution in Two-Phase Stratified Flow," International Journal of Multiphase Flow, Vol. 10, No.3, 1984, pp.371-383.

Weisman, J., Duncan, D., Gibson, J., and Crawford, T., "Effects of Fluid Properties and Pipe Diameter on Two-Phase Flow Patterns in Horizontal Lines," International Journal of Multiphase Flow, Vol. 5, 1979, pp.437-462.

Simpson, H.C., Rooney, D.H., Gratton, E., and Al-Samarral, F , "Two-Phase Flow in Large Diameter Horizontal Lines," Paper H6, European Two-Phase Flow Group Meeting, Grenoble, 1977.

TABLE 1

Test Conditions

| | |
|---|---|
| Pressure (Temperature) | 3.0 MPa (233.9°C)<br>7.5 MPa (290.6°C)<br>12.0 MPa (324.7°C) |
| Flow Rate | 10~1000 $kg/m^2s$ |
| Quality | 0~1.0 |
| Test Section | I.D. 180 mm, Length 10 m |

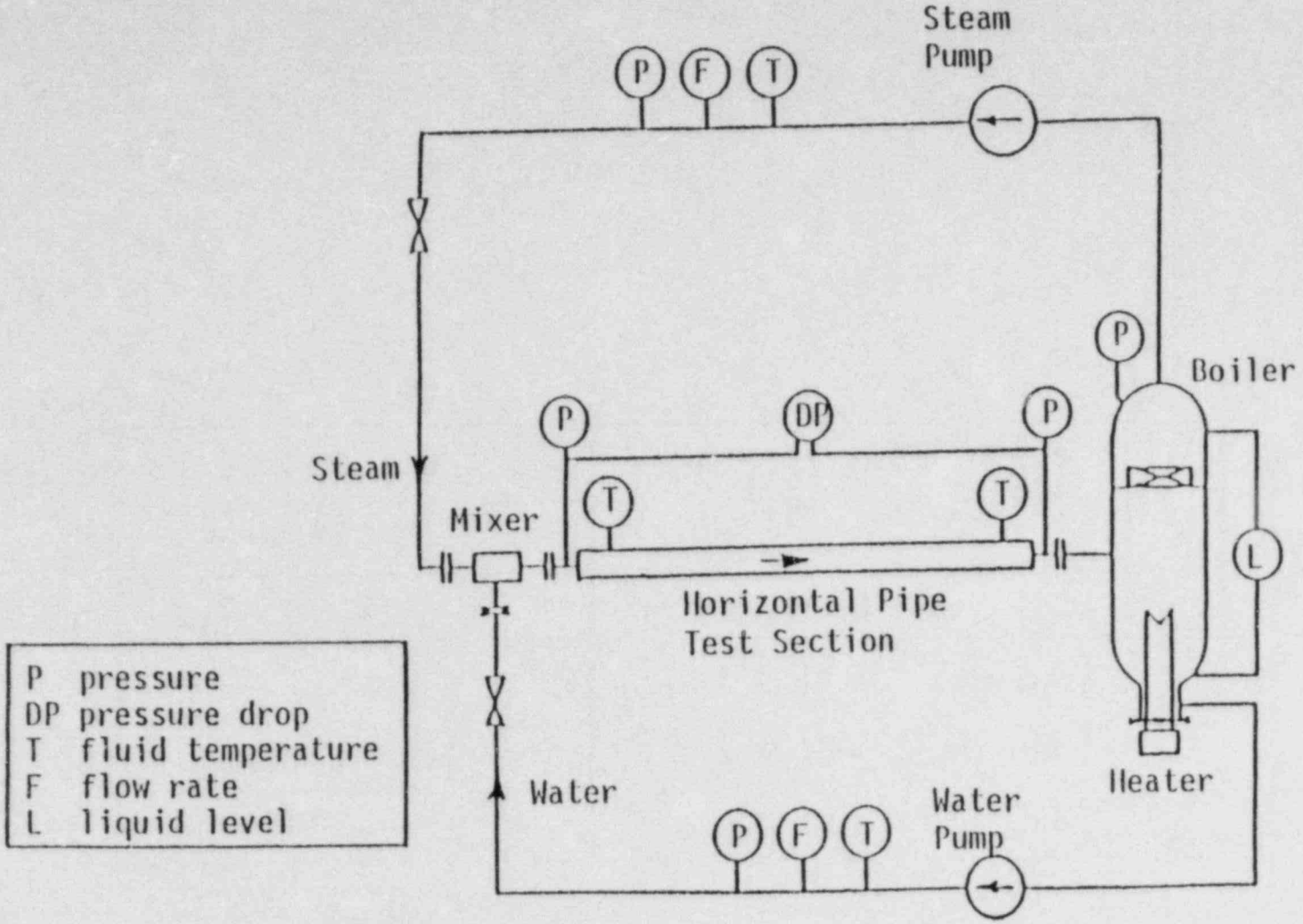


FIG. 1 Test Facility (TPTF Horizontal Pipe Test Section)

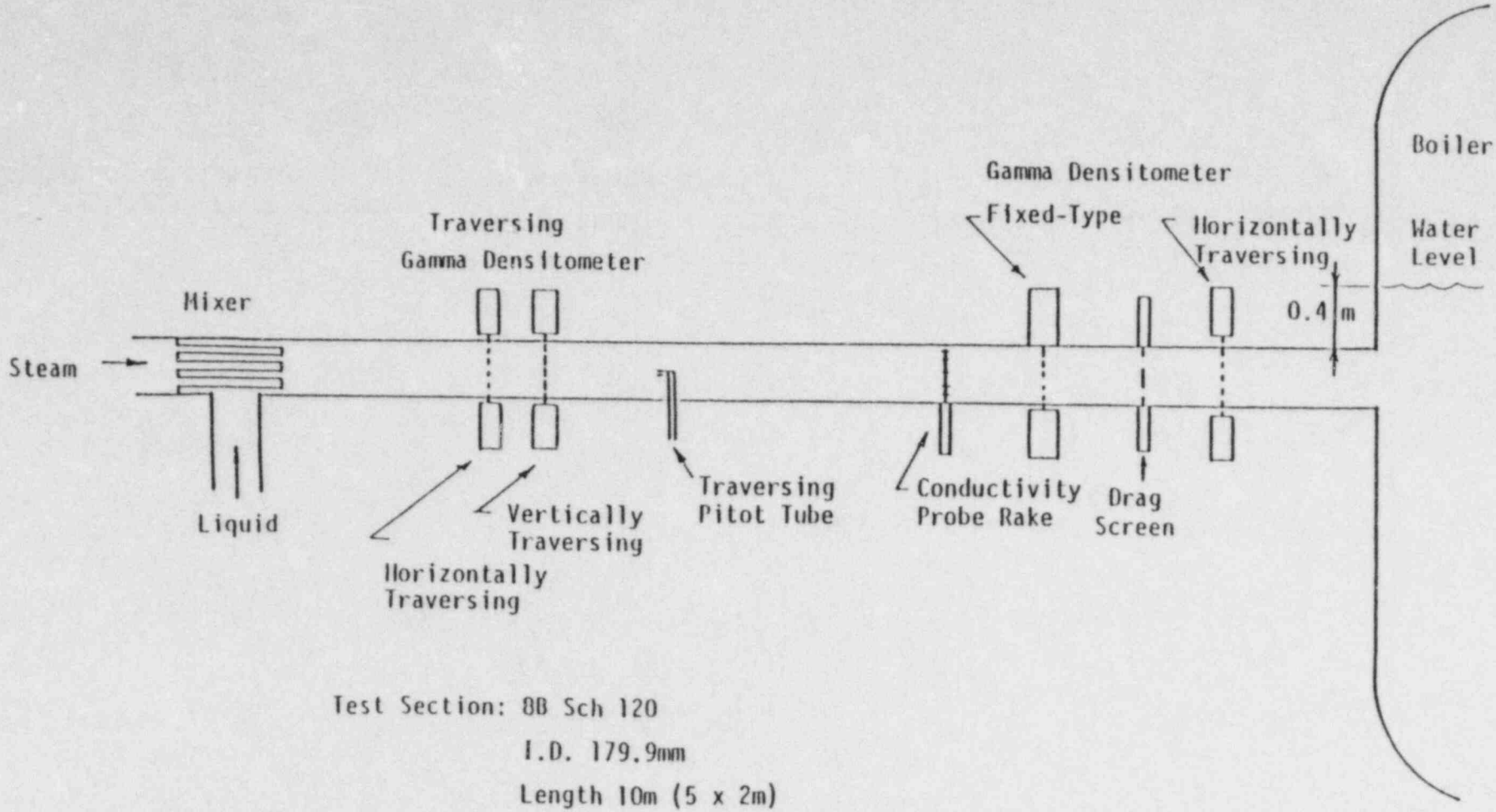


FIG.2 Arrangement of Two-Phase Flow Instruments

FIG. 3 Types of Gamma Densitometer

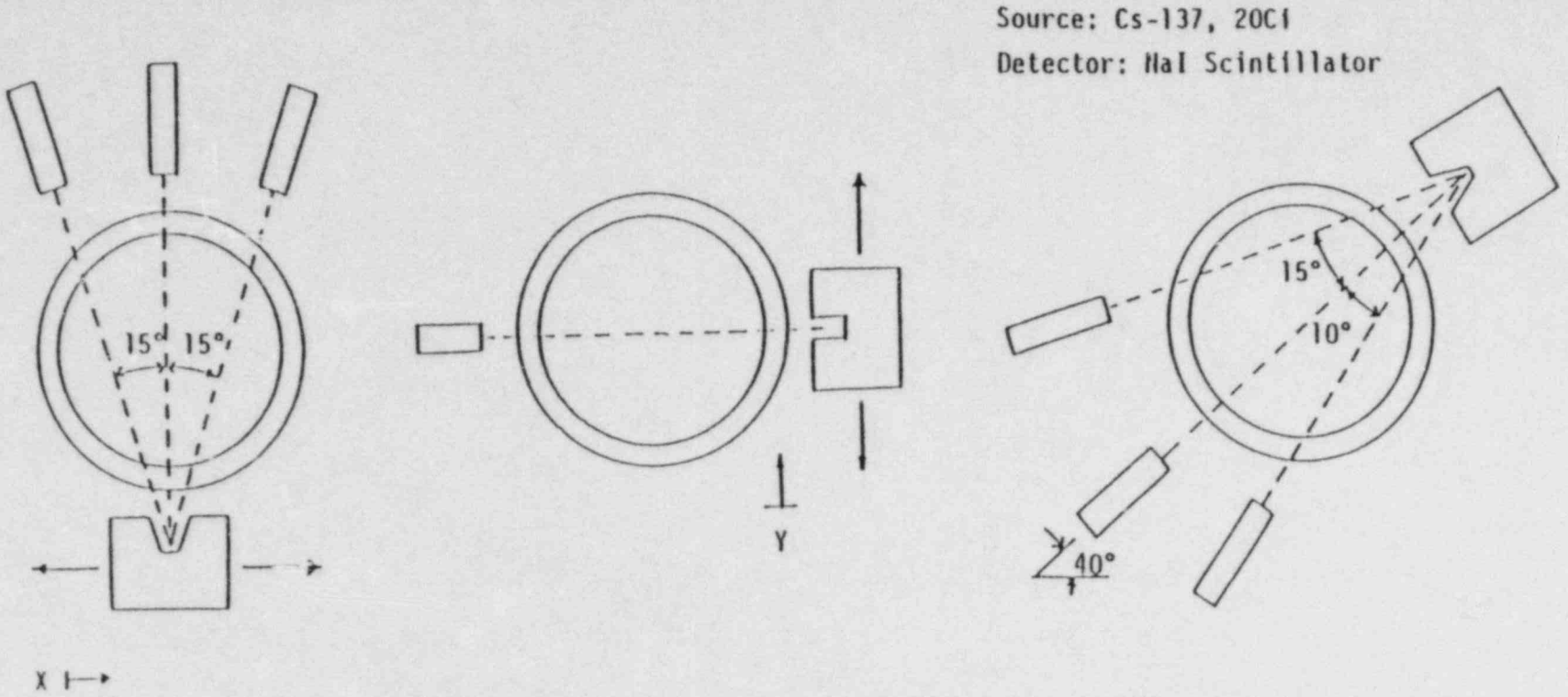


Horizontally Traversing
Gamma Densitometer

Vertically Traversing
Gamma Densitometer

Fixed-Type
Gamma Densitometer

FIG. 4 Vertically Traversing Purged Pitot Tube

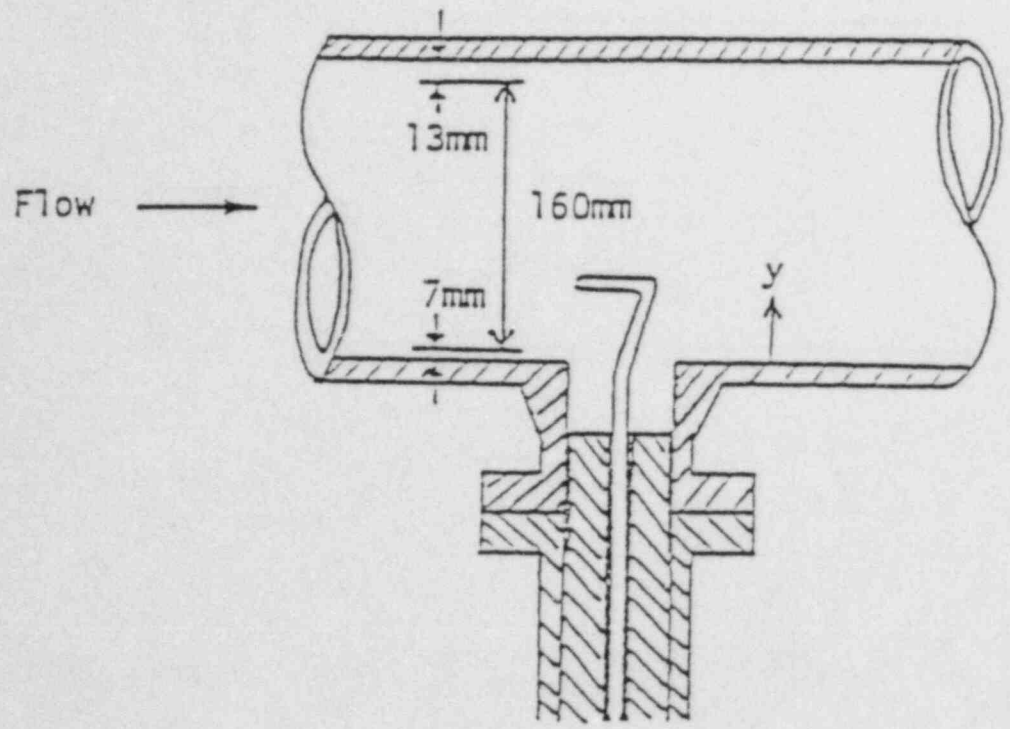


DP cell x 2
Traversing Mechanism
Purge Water Supply System

FIG. 5 Conductivity Probe Rake

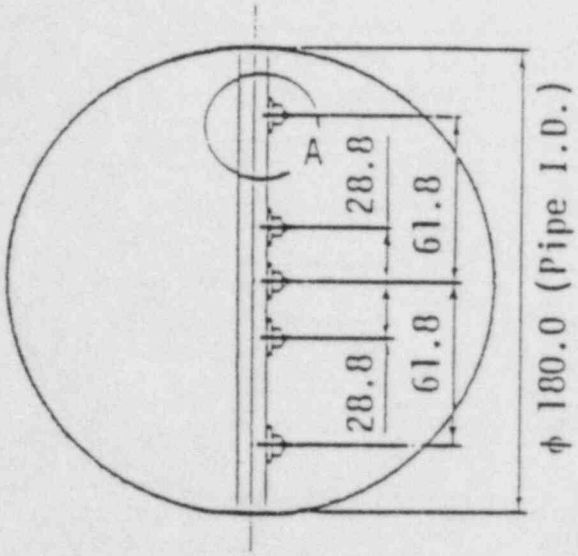


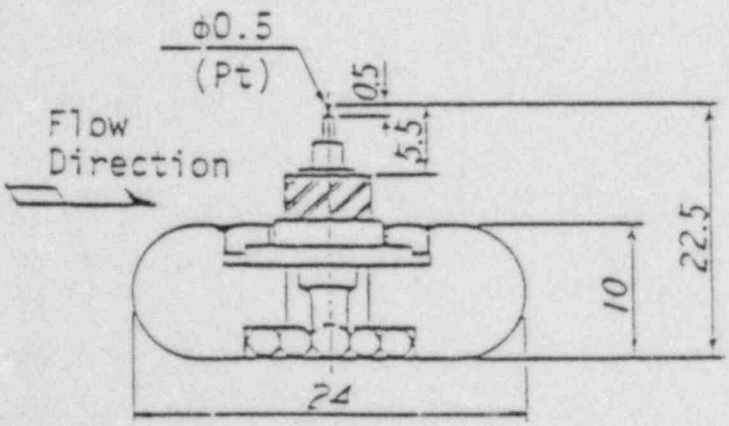


Section " A "

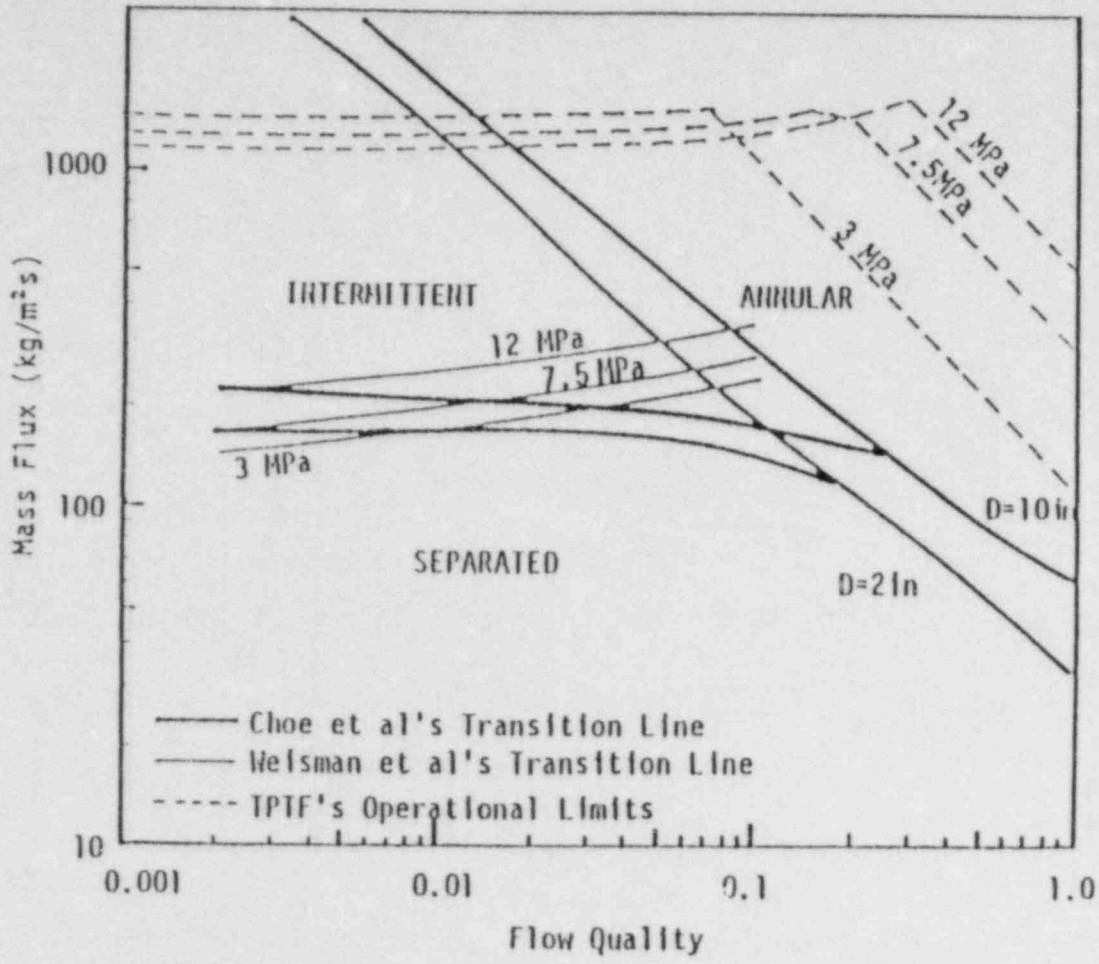


FIG. 6 Comparison of TPTF's Experimental Conditions with Flow Pattern Maps by Choe et al(1976) and Weisman et al(1979)

Horizontally Traversing Gamma Densitometer Data

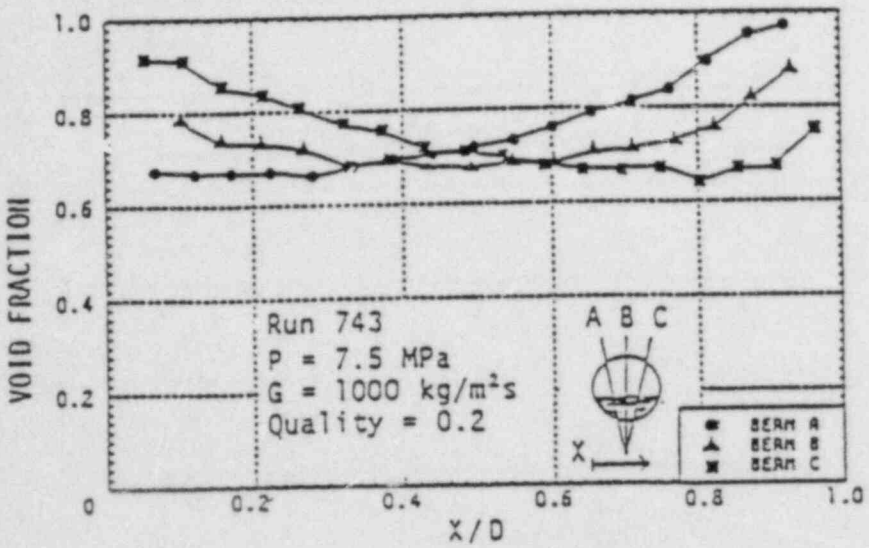


Void Fraction Profile for Idealized Stratified Flow

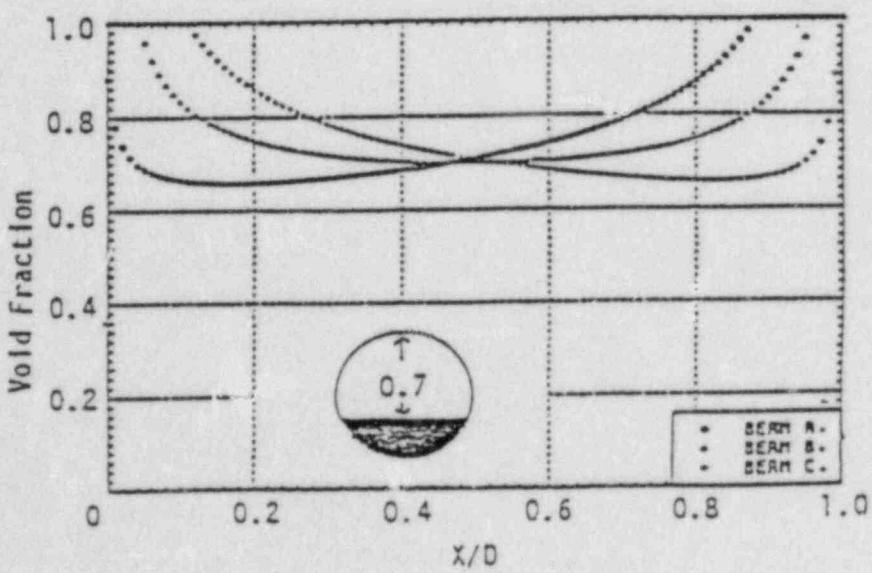


FIG. 7

FIG. 8 Calculated Liquid Level

Run 743
P = 7.5 MPa
G = 1000 kg/m$^2$s
Quality = 0.2

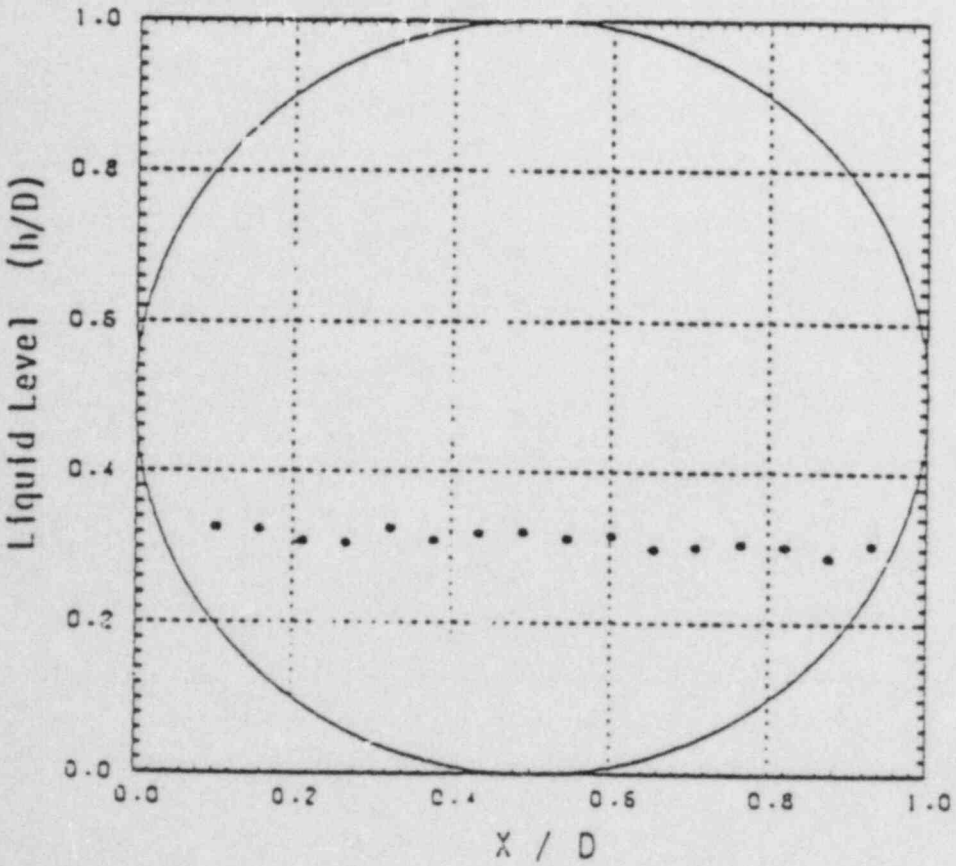

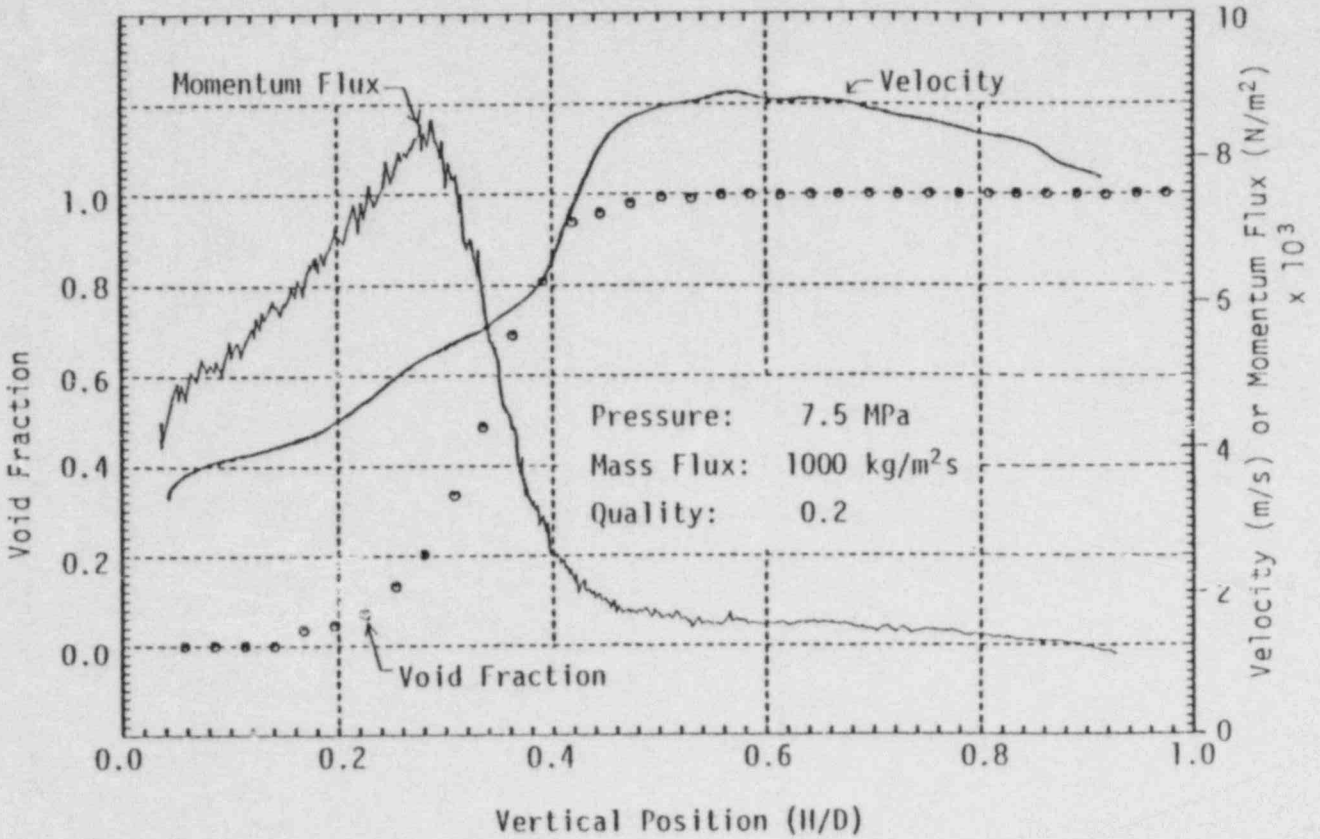


FIG. 9 Vertical Momentum Flux and Void Distributions in Separated Flow

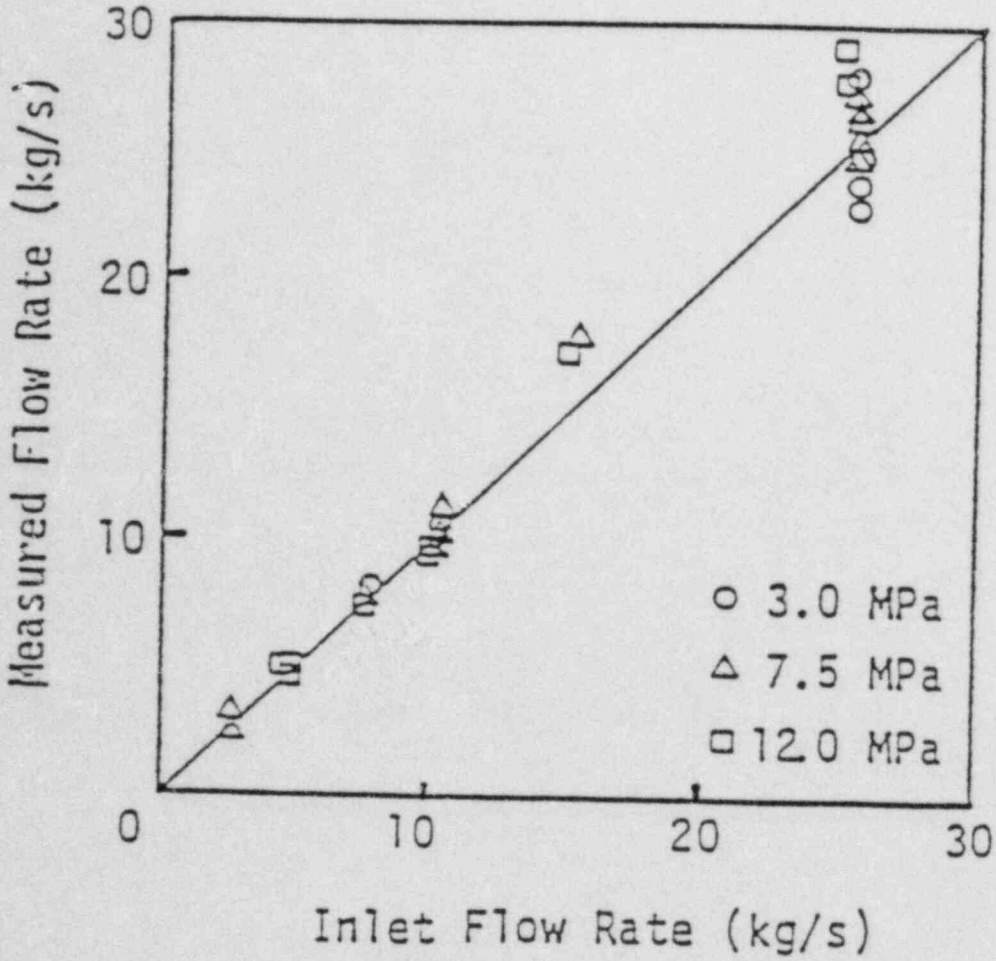


FIG. 10 Comparison of Measured and Inlet Flow Rate

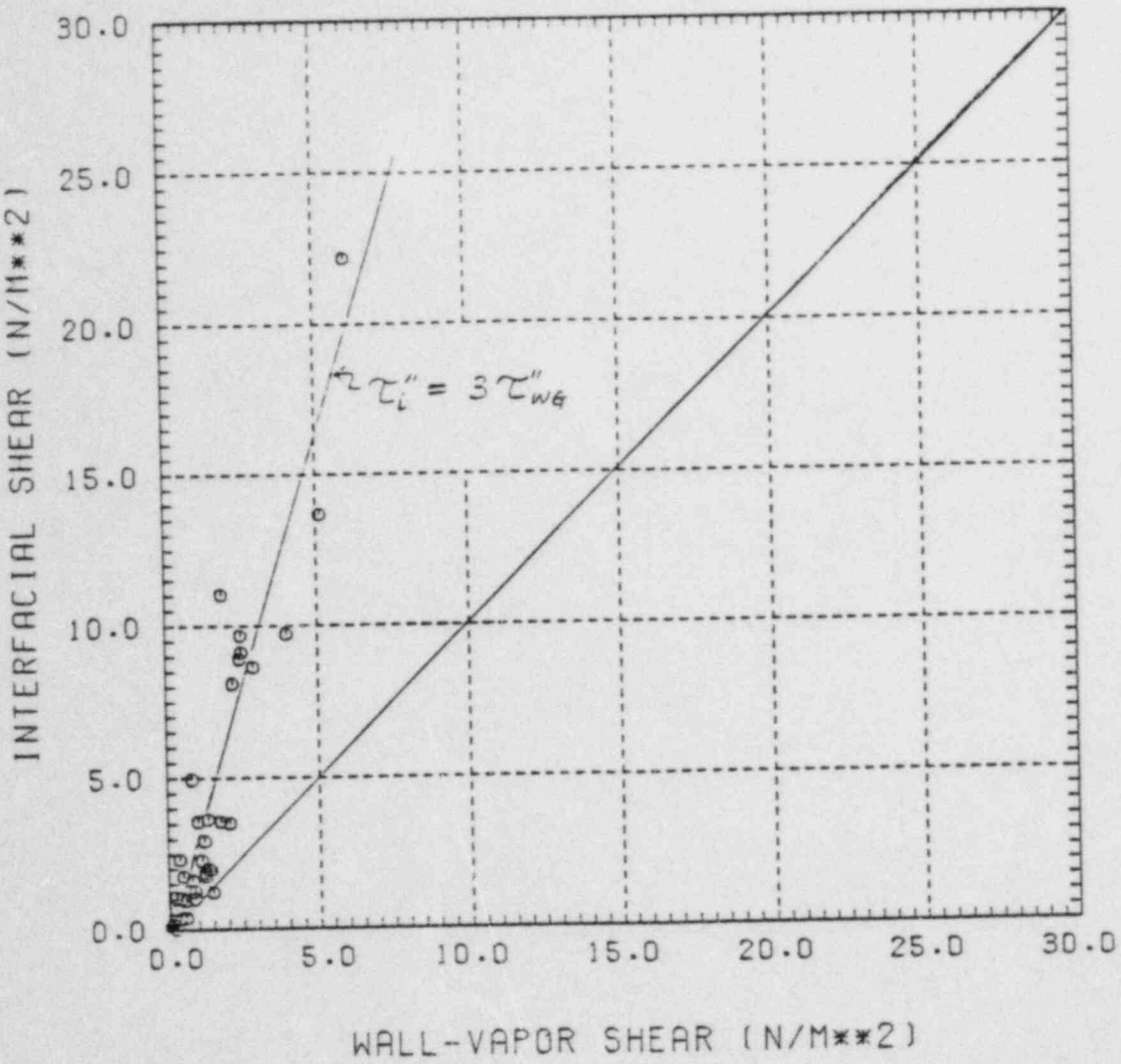


COMPARISON OF INTERFACIAL SHEAR WITH WALL-VAPOR SHEAR STRESSES

FIG. 11

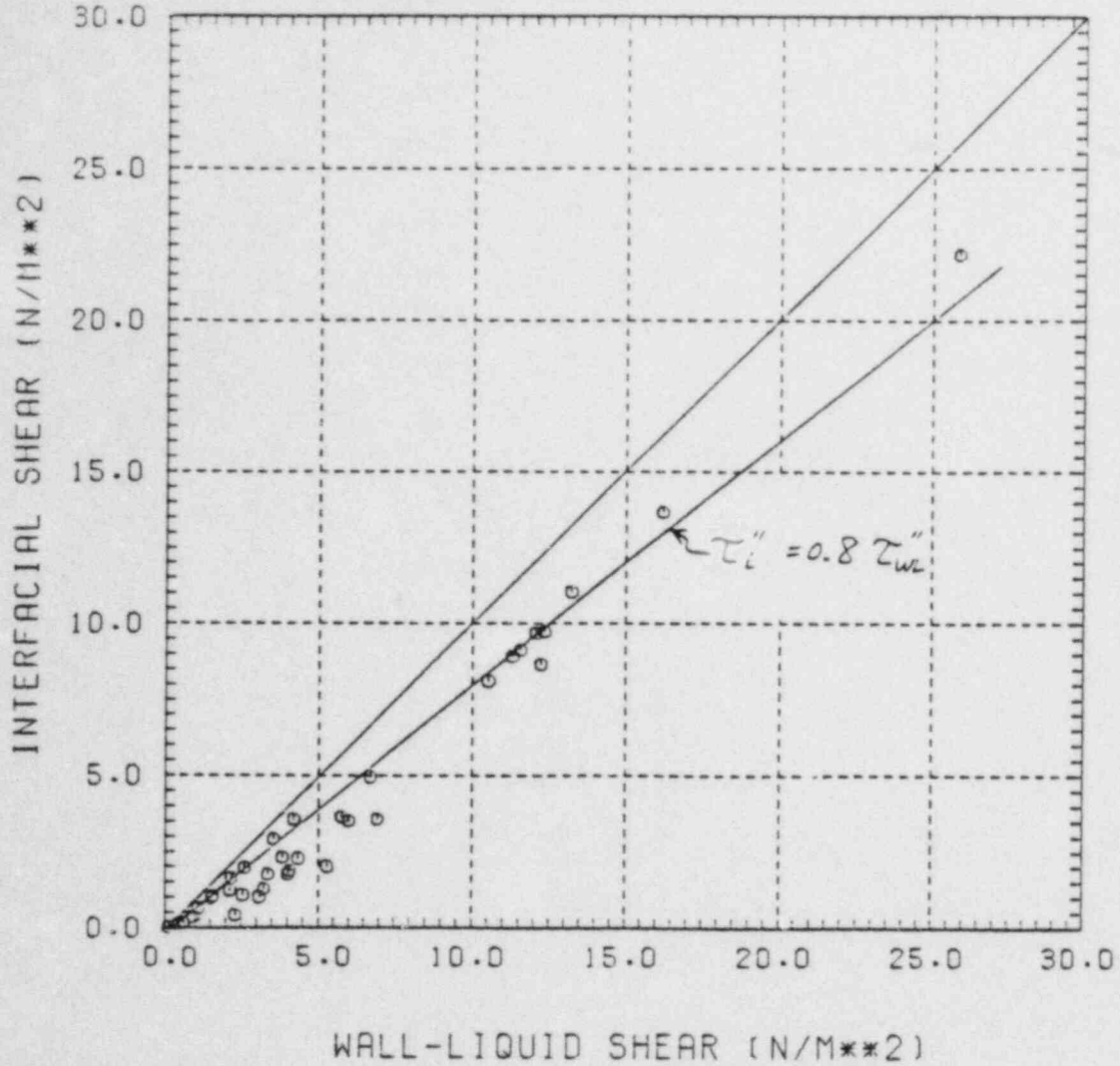


COMPARISON OF INTERFACIAL SHEAR WITH WALL-LIQUID SHEAR STRESSES

FIG. 12

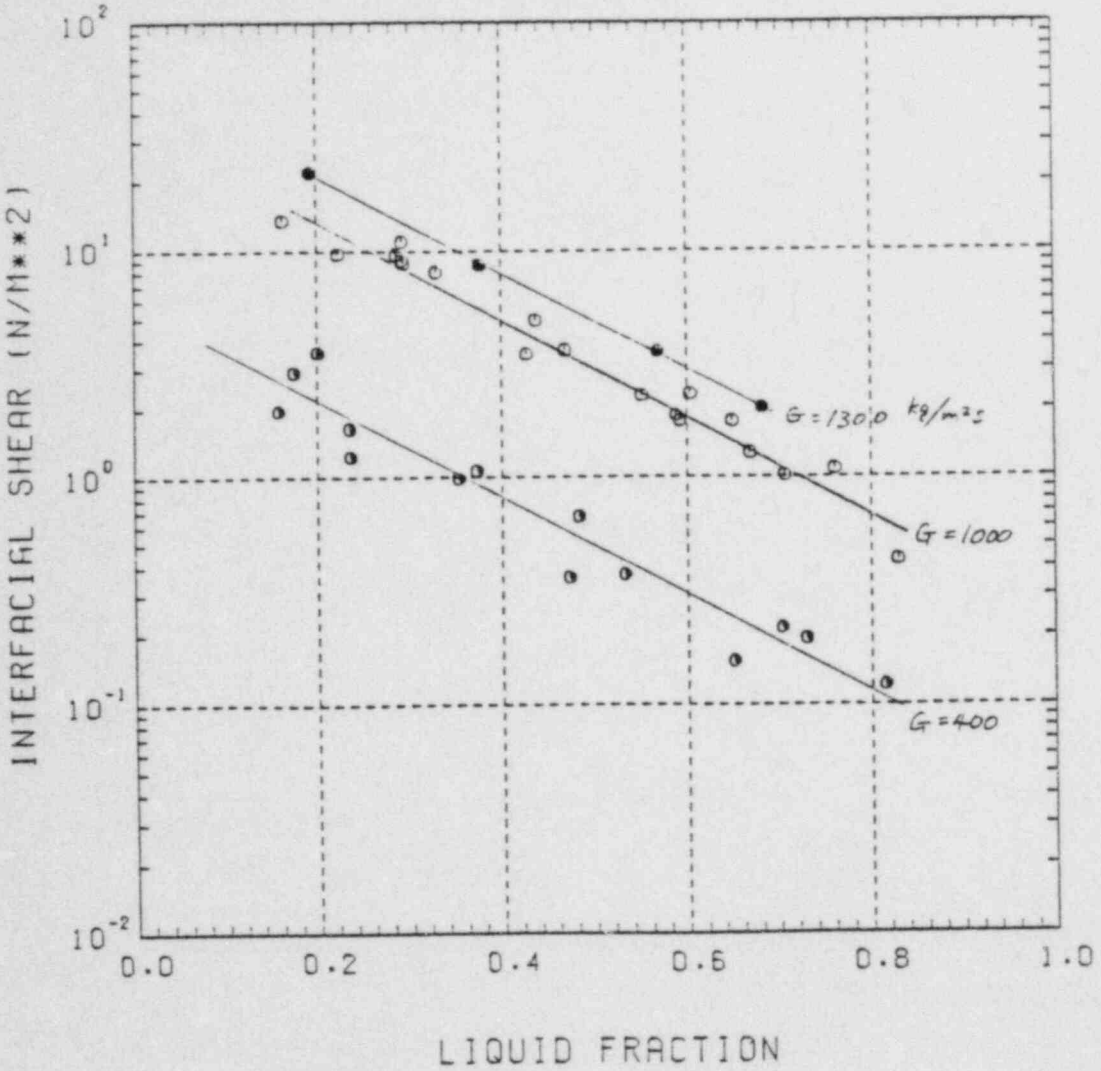


COMPARISON OF INTERFACIAL SHEAR WITH LIQUID FRACTION

FIG. 13

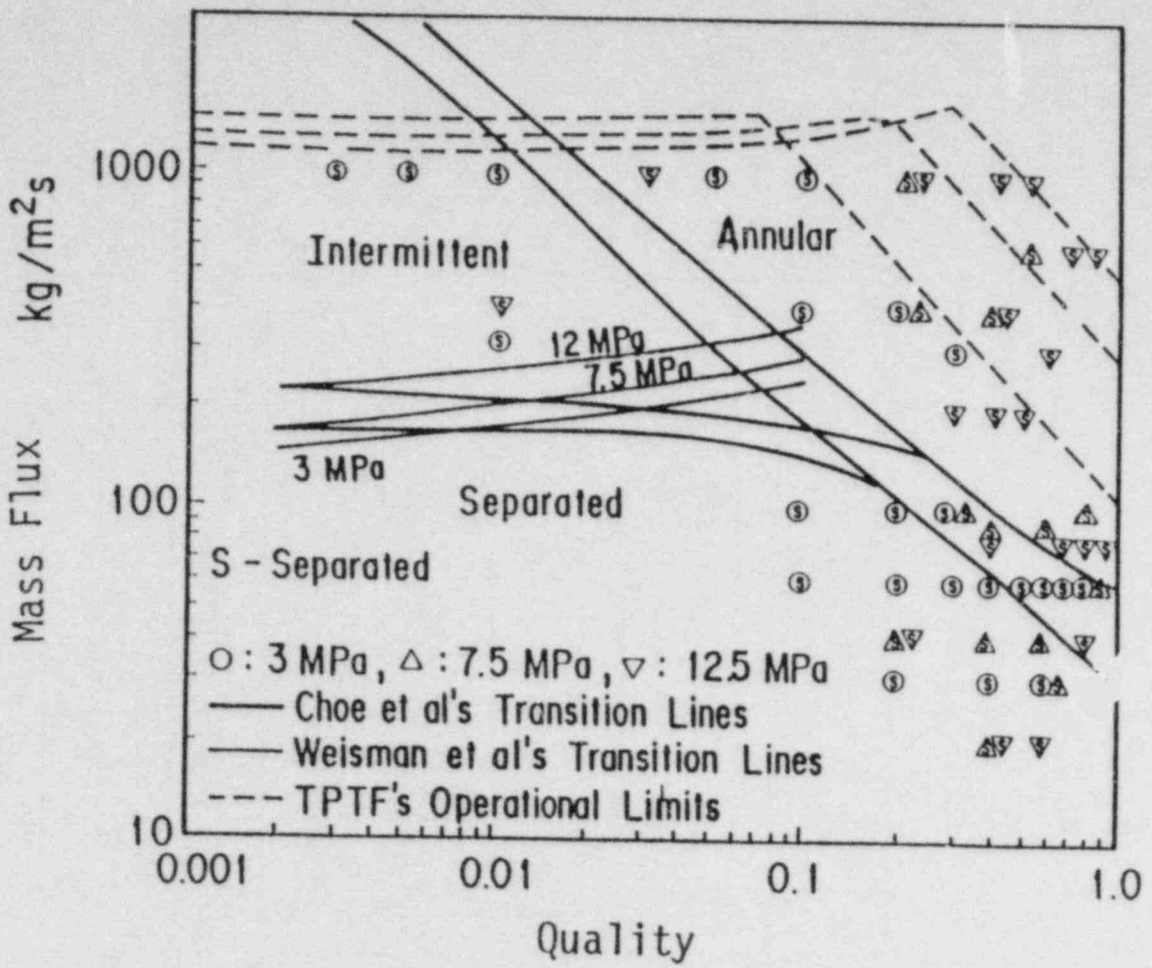


FIG. 14 Flow patterns observed for a large diameter pipe using a homogeneous type mixer.

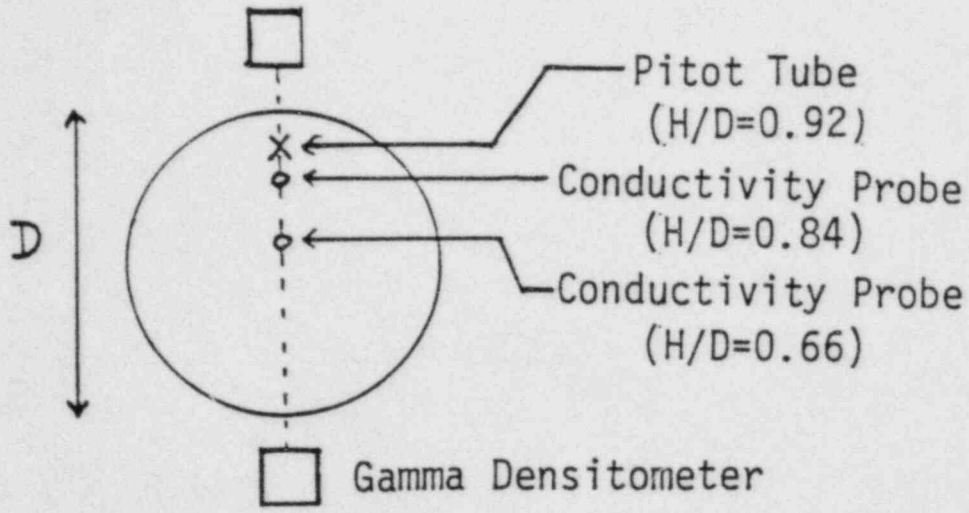


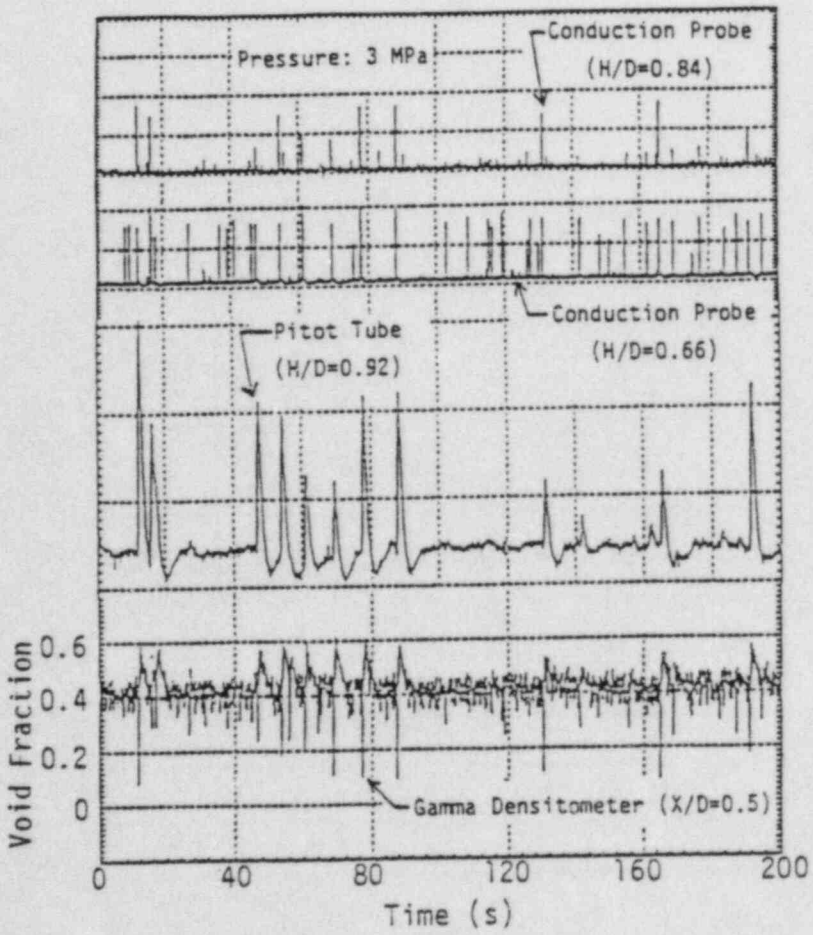


FIG. 15 Detection of Slug Flow

# LARGE BREAK ANALYSIS OF A BWR/6-218 USING TRAC-BD1/MOD1 A BEST ESTIMATE CODE COUPLED WITH EVALUATION MODEL TYPE BOUNDARY CONDITIONS

P. D. Wheatley
EG&G Idaho, Inc.
Idaho National Engineering Laboratory

## ABSTRACT

An analysis of a boiling water reactor (BWR)/6 was conducted at Idaho National Engineering Laboratory (INEL). The analysis used the Transient Reactor Analysis Code (TRAC) BWR version (TRAC-BD1/MOD1) to calculate a design basis, large break loss-of-coolant accident with evaluation model type boundary conditions. This analysis is a part of a Nuclear Regulatory Commission (NRC) study of plant safety margin. Results of the analysis are presented showing a large margin between the calculated peak cladding temperature and the Appendix K limits.

## INTRODUCTION

The Nuclear Regulatory Commission (NRC) has carried out an extensive research program over the past 10 to 15 years to insure the safety of plants and gain a better understanding of phenomena occurring during accident or off-normal conditions. Results of this research have been incorporated in several "best estimate" type computer codes for calculation of transients. The results of the research , however, have not been included in the evaluation model calculations required by the licensing arm of the NRC. To gain an understanding of the safety margin of a reactor during a design basis, large break loss-of-coolant accident, comparisons of a best estimate calculation using evaluation model type boundary conditions and a pure evaluation model calculation can be performed. This paper discusses the calculation performed using a best estimate code, TRAC-BD1/MOD1 (Reference 1), with evaluation model boundary conditions.

## FACILITY DESCRIPTION

A BWR/6-218 reference plant nuclear steam supply system (NSSS) was assumed for this analysis. The BWR/6-218 facility consists of a pressure vessel with two external recirculation loops, as shown in Figure 1. Each recirculation loop provides drive flow for 10 jet pumps located in the downcomer region of the vessel. The vessel also accommodates penetrations for feedwater, emergency core cooling (ECC) water, and steamlines located at appropriate elevations.

The vessel internals include; the downcomer, jet pumps, lower plenum, core, upper plenum, steam separators, steam dryers, and a steam dome. The downcomer is the region from the jet pump support plate to just below the

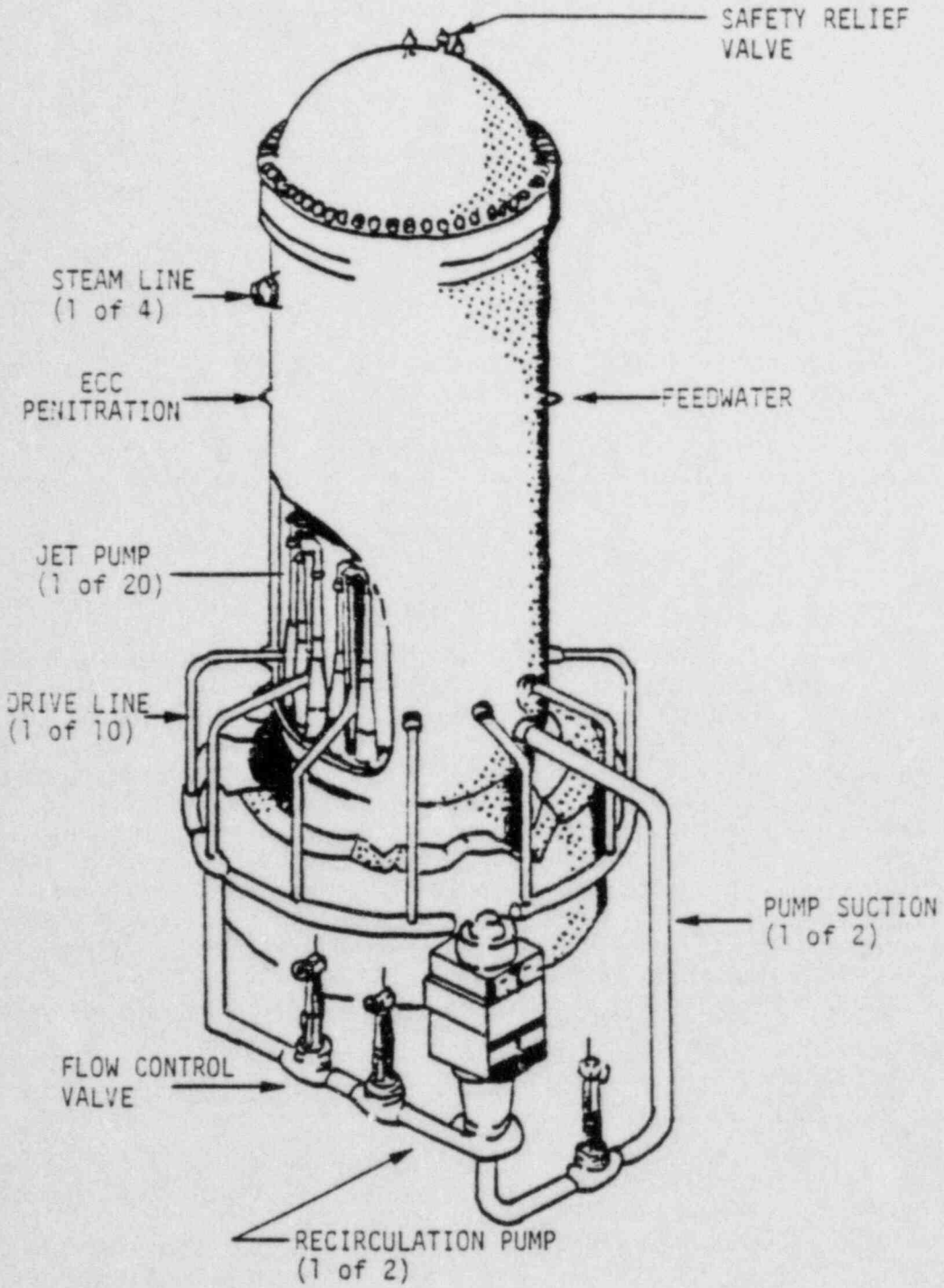


Figure 1. BWR/6-218 vessel and recirculation loops.

steamline exits and between the core shroud and vessel wall. Feedwater is supplied to the upper downcomer as is the liquid from the steam separators. The downcomer also provides liquid for jet pump suction. The 20 jet pumps supply the core with cooling water. The pumps receive one third of their flow from the driveline and induce two-thirds of the total flow from the downcomer. The lower plenum allows mixing of the jet pump flow and houses the control rod guide tubes.

The core consists of 624 fuel bundles. Each bundle contains two water rods and 62 fuel rods in an 8x8 matrix surrounded by a zircaloy channel box, as shown in Figure 2. The core is rated at 2894 MW of thermal power. Water circulated through the core is boiled and exits the core with an approximate quality of 0.15. The two-phase mixture passes through the upper plenum to the steam separators where the liquid is extracted and returned to the downcomer. The steam passes through the steam dryer which removes any remaining liquid before exiting the vessel via one of the four main steamlines to the turbines.

## CODE AND MODEL DESCRIPTION

TRAC-BD1/MOD1 is an advanced best estimate computer code for analysis of BWR loss-of-coolant accidents and other transients. The latest version of TRAC was used for this analysis, Version 21. Version 21 is essentially TRAC-BD1/MOD1 prior to formal release. TRAC-BD1/MOD1 allows consistent and unified analysis capability for all areas of a large or small break loss-of-coolant accident, beginning with the blowdown phase, through heatup, reflood with quenching and finally, the refill phase of the accident.

Unique features of the code include: (a) a full nonhomogeneous, nonequilibrium two-fluid thermo-hydraulic model of two-phase flow in all portions of the BWR system, with a three-dimensional thermal-hydraulic treatment of the vessel; (b) detailed modeling of a BWR fuel bundle, including a thermal radiation heat transfer model for radiative heat transfer between multiple fuel rod groups, liquid and vapor phases, and the fuel channel wall with quench front tracking on all fuel rod surfaces and the inside and outside of the fuel channel wall for both bottom flooding and falling film quench fronts; (c) detailed models of BWR hardware such as jet pumps and separator-dryers; and (d) a countercurrent flow limiting model for BWR-like geometries. Other features of the code include a nonhomogeneous, thermal equilibrium critical flow model, and flow regime dependent constitutive relations for the interchange of mass, energy, and momentum between the fluid phases and between the phases and the structure.

A TRAC-BD1/MOD1 input model of the BWR/6 was assembled specifically for design basis accidents. The VESSEL component was used to model the lower plenum, bypass, downcomer, upper plenum, standpipes, separators, dryer, and the steam dome. Figure 3 shows the nodalization of the vessel. Levels one through three form the lower plenum. Levels four and five are the bypass region, with six and seven making up the upper plenum. The separator/dryers were modeled in levels eight and nine. Level ten formed the steam dome.

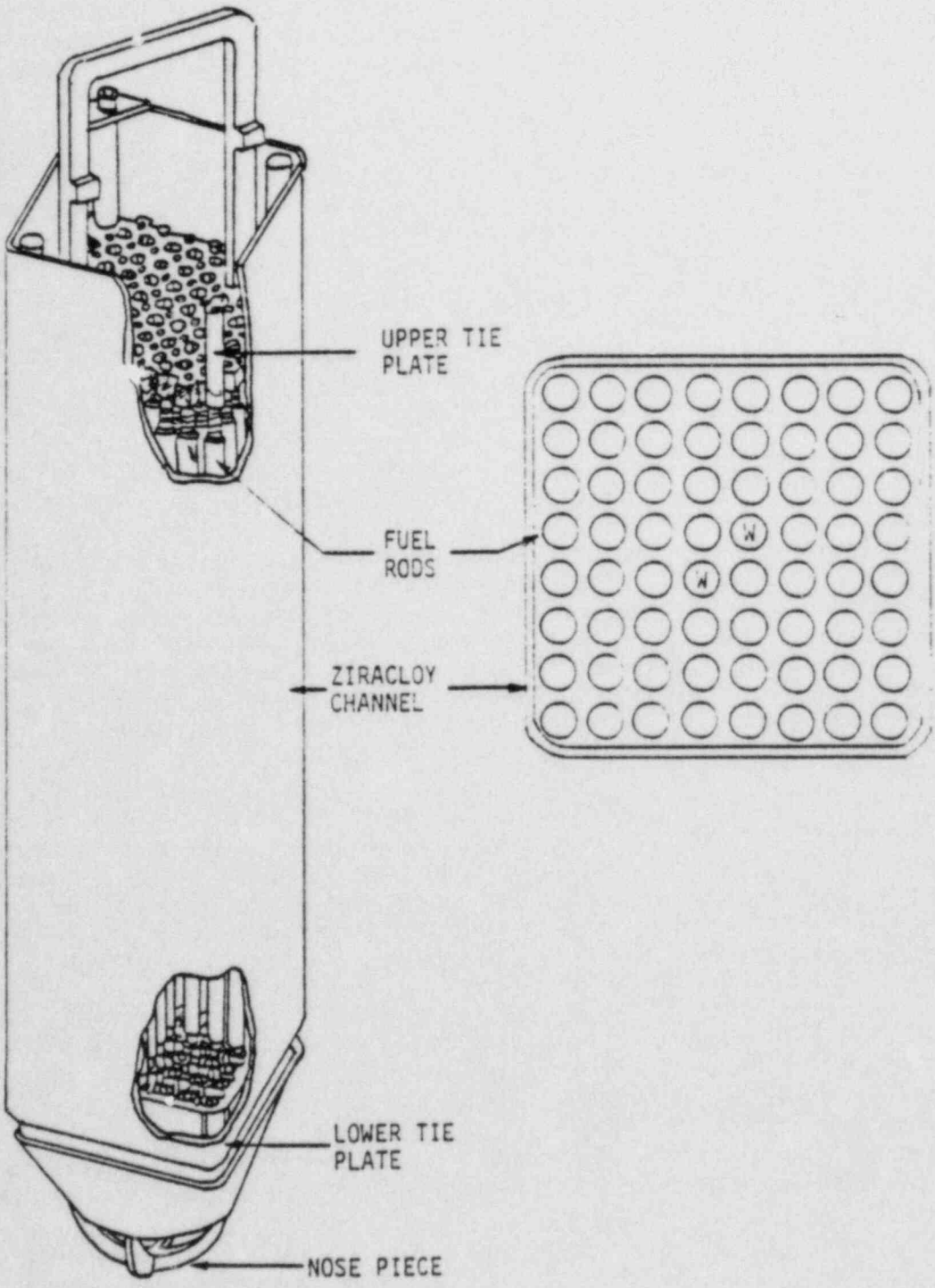


Figure 2. BWR 8x8 fuel bundle.

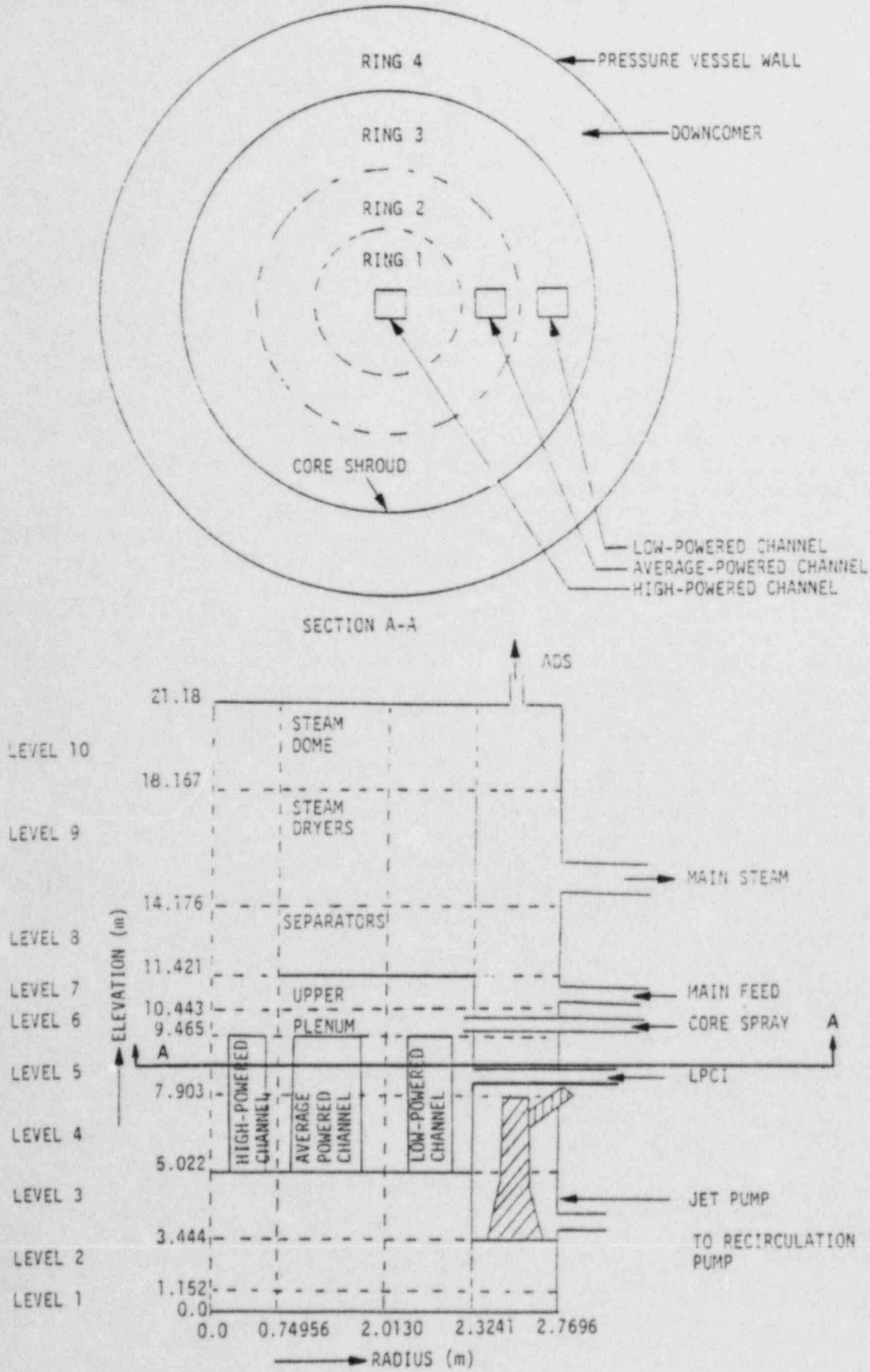


Figure 3. BWR/6-218 vessel nodalization.

Four radial rings were modeled to accommodate the three channels and the downcomer. Ring one, levels four and five, contained the high power CHAN component and the bypass region around the high power bundles in a BWR. Ring two modeled the average power CHAN and the corresponding bypass region. Ring three was the low power CHAN with the low power bypass region. Ring four modeled the downcomer region. The metal mass heat slabs inside the vessel were divided into three groups; double side heat slabs on the radial boundaries (vessel walls, core shroud, etc), lumped heat slabs (thin walled components), and walls of the one-dimensional components contained within the vessel (guide tubes, jet pumps).

The CHAN component was used to model the the 624 fuel bundles in a BWR/6-218. The CHAN in ring one simulated 76 high power bundles with side entry orifices (SEO); the CHAN in the second ring simulated 472 average power bundles with SEOs; and the third ring simulated 44 low power bundles with bottom entry orifices and 32 low power bundles with peripheral SEOs. The CHAN components were nodalized with eleven axial cells. The average and low power CHANs contained one rod group with the high power CHAN containing four rod groups. The high power CHAN also used a fine rod mesh during reflood. The additional rod groups and the fine mesh were used in the high power channel because of the expected high temperatures.

Each recirculation loop in the BWR was modeled. The feedwater, HPCS, LPCS, and LPCI systems were modeled using a PIPE and a FILL component for each system. The FILLs were input as velocity versus pressure tables to simulate the pressure response of the ECC systems.

The BWR/6-218 model was run in the steady state mode to establish the initial operating conditions. Once the model had been balanced and a steady state reached, the deck was restarted for the transient calculations. Table 1 lists the TRAC calculated initial conditions and the target values. The target values were determined by review of a current final safety analysis report and BWR/6 standard plant data (Reference 2). The TRAC calculated values were all within a few percent of the target values. Those values were deemed acceptable as further efforts would not affect the transient results.

At the start of the transient, the feedwater flow and recirculation pumps were tripped. The feedwater was ramped off during the first second of the transient. The pump coastdown was calculated by the code. The core power was scrammed at 0.0 s. The decay core power was calculated by the code. No multiplier was used on the decay power in contrast to evaluation model calculations that use a multiplier of 1.2. The current TRAC decay heat model is based on the ANS 1979 standard (Reference 3).

The MSIV closure and the ADS trip were initiated when the water level in the downcomer reached Level 1 (6.172 m above the jet pump support plate). There was a 105 s delay in the ADS activation, whereas the MSIV ramped closed during the four seconds after the trip, The pressure control valve was assumed to function until the MSIV was fully closed.

TABLE 1. INITIAL AND BOUNDARY CONDITIONS

| Condition | Target | TRAC |
|---|---|---|
| 102% Core power (MW) | 2951 | 2951[a] |
| Core inlet flow (kg/s) | 10,640 | 10,392 |
| Core leakage flow (%) | 8-10 | 7 |
| Core inlet temperature (K) | 553.0 | 556.7 |
| Steam dome pressure (MPa) | 7.205 | 7.223 |
| Peak linear heat generation rate (W/m) | 43,963 | 44,076[a] |
| Core average gap conductance ($W/m^2K$) | 3405 | 3405[a] |
| Core power profile | chopped cosine | chopped cosine |
| ECC temperature (K) | 323 | 323 |

a. Evaluation model boundary conditions.

HPCS was activated on assumed drywell high pressure at time 0.0 s with a 27 s delay for diesel startup and valve opening times. The low pressure systems were activated on low water level. However, they did not actually begin injection until the vessel pressure was below the pump shutoff head (1.5 MPa for LPCI and 1.85 MPa for LPCS), later in the transient. All ECC flows were governed by input velocities versus pressure FILL tables derived from BWR/6 standard plant data. Both the HPCS and LPCS were assumed fully operational but one LPCI diesel was assumed failed, resulting in only one operational LPCI pump.

## RESULTS

Rod cladding temperatures in the low and average power bundles remained relatively cool during the entire transient. Figure 4 shows the cladding temperatures of the low power CHAN with Figure 5 showing the cladding temperatures in the average power CHAN. The temperatures in these CHANs remained below 620 K throughout the transient,the steady state operating temperature is about 580 K. The average and low power CHANs represented approximately 88% of the core.

The remaining 12% of the core, the high power bundles, experienced a more significant heat-up during the transient. Figure 6 shows the cladding temperatures at the bundle mid-plane and above. It is noted that there are two separate heat-ups, one early during blowdown with a quench and then a long term heat-up during the refill/reflood portion of the transient. The early heat-up and phenomena will be discussed and then the refill/reflood heat-up will be addressed.

The early heat-up was a result of the relatively high core power and the rapid core flow coastdown. Figure 7 shows a rapid increase in the void fraction in the upper parts of the high power bundles. Figure 8 illustrates the heat-up during the flow coastdown. A maximum cladding temperature of 855 K (at the 2.56 m elevation) was reached at 19 s. This was the peak cladding temperature reached during the transient. Lower plenum flashing, level swell and the resulting core flow halted the cladding temperature increase and quenched the cladding at 25 s.

Cladding temperatures once again increased as the fluid from lower plenum flashing was converted to steam producing a highly voided mixture (i.e. approaching 1.0) in the hot bundles. The majority of the hot bundle, from the 0.993 m elevation to the 3.81 m elevation, started to heat up from about 27 s to 45 s as the fluid was converted to vapor and the two-phase level decreased in the bundle. A peak temperature during the refill/reflood of 838 K was reached at 170 s at the 2.0 m elevation, Figure 6. This was 17 K below the blowdown peak of 855 K. Refill/reflood of the bundles by the ECC system provided sufficient fluid and increased heat transfer to halt the cladding heat-up and began a reduction in the cladding temperatures. The calculation was terminated prior to complete quenching of the hot bundles. However, the temperature had been reduced by about 100 K, from the peak value, and quenching was occurring in the upper elevations. It was estimated that the core would have been completely quenched by 400 s.

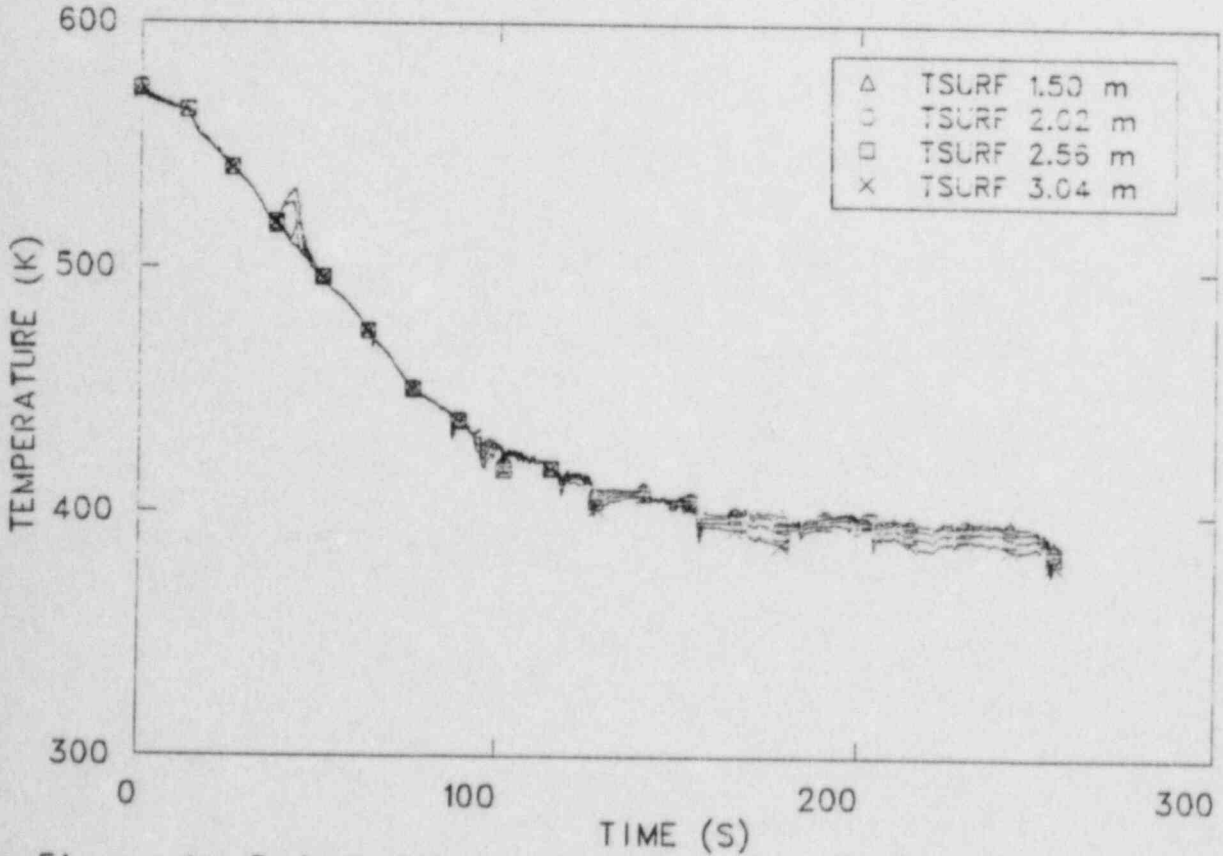


Figure 4. Rod cladding temperature low power CHAN.

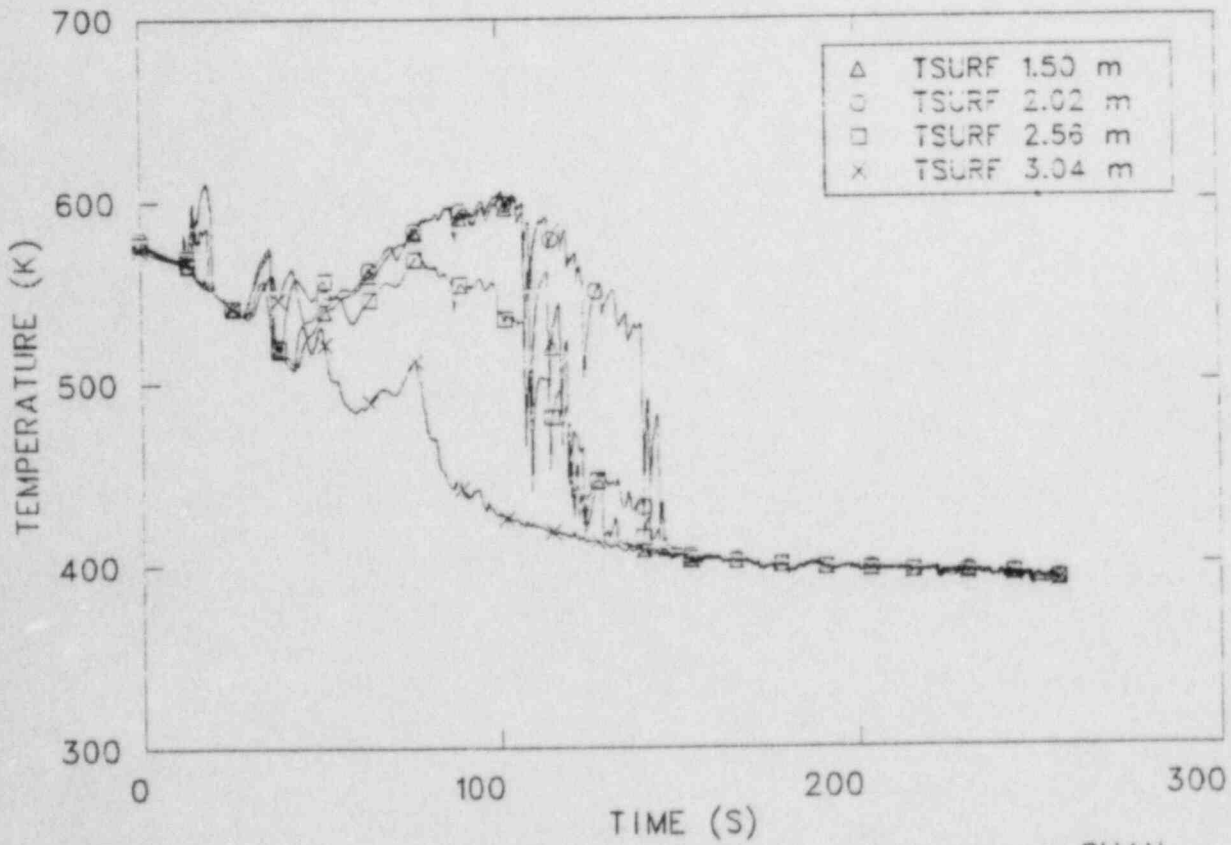


Figure 5. Rod cladding temperatures average power CHAN.

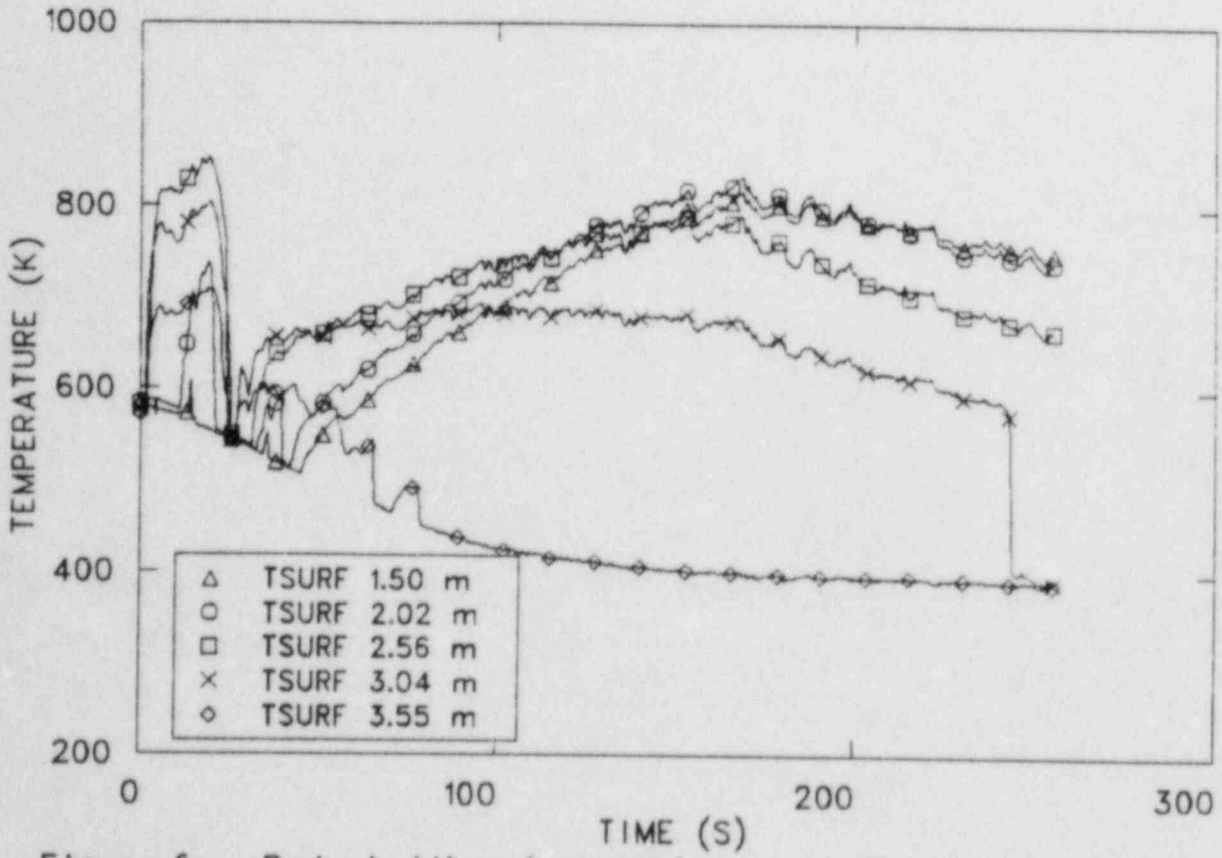


Figure 6. Rod cladding temperatures mid-plane and above, high power bundles.

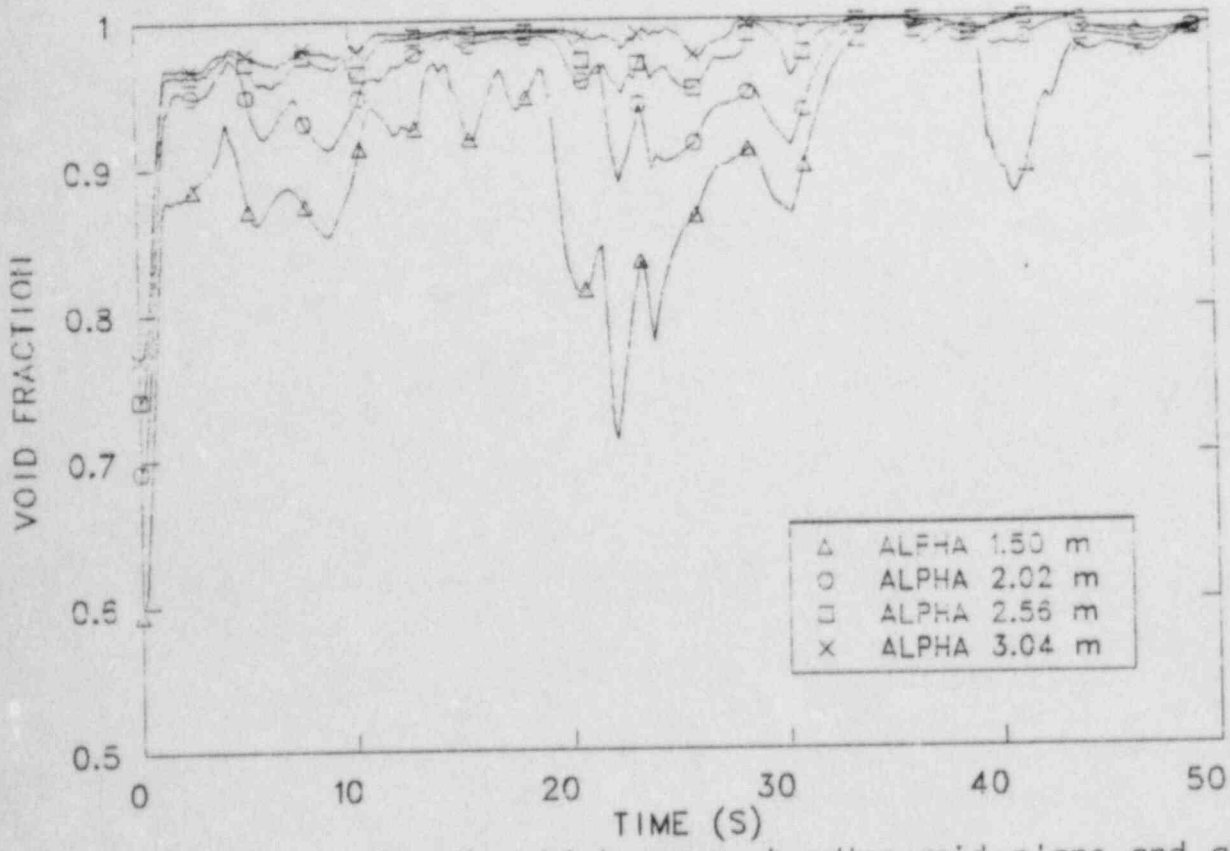


Figure 7. Void fraction high power bundles mid-plane and above.

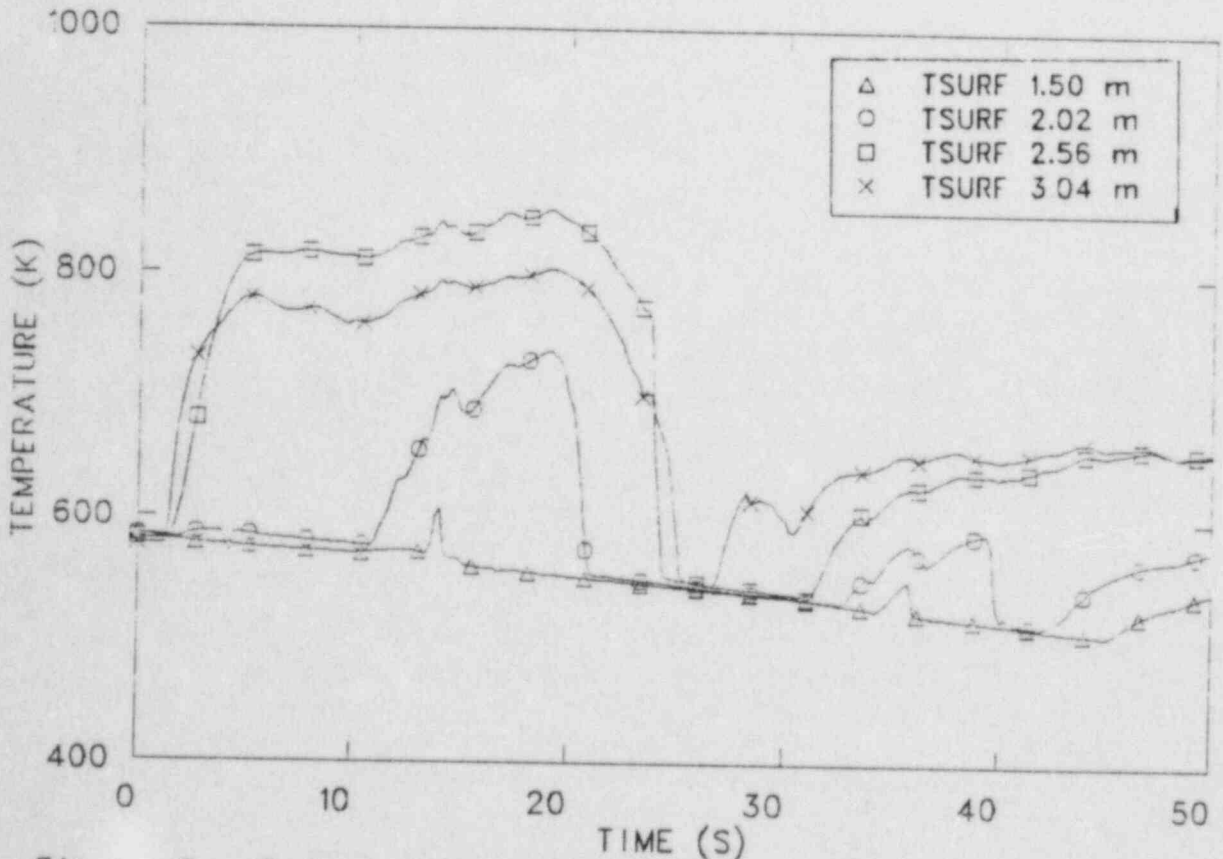


Figure 8. Rod cladding temperatures mid-plane and above, high power bundle (0-50 sec).

As discussed above, the peak cladding temperature occurs early during the blowdown portion of the transient. The difference between the blowdown peak cladding temperature and the maximum temperature during refill/reflood was only 17 K. The difference is thought to be within the uncertainty of the analysis and thus this study does not preclude the actual peak temperature in a BWR occurring either in the blowdown or the refill/reflood portion of the transient. Evaluation model calculations indicate the peak cladding temperature during refill/reflood is due to several factors: 20% higher decay power, mandated reduced heat transfer during parts of the transient, and other imposed limitations during the transient.

Confidence in the documented calculation was sustained by limited comparisons with experimental data and other best estimate calculations with best estimate boundary conditions. or events and their timing are shown in Table 2. This timing was compared the event timing in a BWR/6 calculation with best estimate bou conditions (Reference 4) and was found to be in good agreement. A comparis was also made between the event timing in this study and the Full Integral Simulation Test (FIST) Test 6DBA1B (Reference 5) and was also found to be in good agreement. The peak cladding temperatures in both references were lower and quenching occurred earlier due to best estimate conditions versus the evaluation model type conditions used in this analysis.

Analysis of the thermal-hydraulic behavior of the core indicated the flow patterns were similar to those observed during the Steam Sector Test Facility (SSTF) (Reference 6) testing. The low power bundles filled with liquid from the low pressure ECC and drained into the lower plenum via co-current down flow as shown in Figure 9. The average power channels were counter-current flow limited (CCFL) during the transient, Figure 10. The high power bundles oscillated between CCFL and a co-current upflow until the average power channels began refilling, as shown in Figure 11. Refill of the average bundles limited the amount of steam which escaped the lower plenum via the average power bundles. Therefore the high power bundles assumed a co-current upflow for the remainder of the transient. Thus the core behavior was similar to that observed in SSTF.

The analysis indicated that even with two of the LPCI pumps disabled during the transient, sufficient core cooling was maintained. Figure 12 shows the integrated breakflow compared with the integrated ECC flow. Even with the rapid loss of system inventory early in the transient the ECC systems were able to replace this loss. The ECC systems would have replaced all the inventory lost by about 410 s.

## CONCLUSIONS

Conclusions resulting from this analysis are summarized below.

This analysis showed that even with evaluation model type boundary conditions there was a large margin between the peak cladding temperature of 855 K and the licensing of 1477 K.

TABLE 2. KEY EVENT TIMING

| Event | EM Time (s) | BE Time (s) | FIST Time (s) |
|---|---|---|---|
| Scram, pump trip, feedwater trip | 0.0 | 0.0 | 0.0 |
| MSIV trip | 7.5 | 7.2 | -- |
| Jet pump suction uncovery | 8.5 | 9.4 | 5.0 |
| MSIV fully closed | 11.5 | 11.2 | -- |
| Recirculation pump suction uncovery | 12.5 | 12.2 | 8.5 |
| Lower plenum flashing | 18.0 | 17.0 | 11.5 |
| HPCS initiation | 27.0 | 27.0 | 27.0 |
| LPCS initiation | 59.5 | 57.0 | 64.0 |
| LPCI initiation | 64.0 | 62.0 | 75.0 |
| Peak clad temperature (ave. bundle) | 105.0 | 100.0 | 110.0 |
| (hot bundle) | 19.0 | 95.0 | |
| Final quench (ave. bundle) | 145.0 | 116.0 | 125.0 |
| (hot bundle) | <450.0[a] | 131.0 | -- |

a. Estimated limit, calculation terminated before final quench.

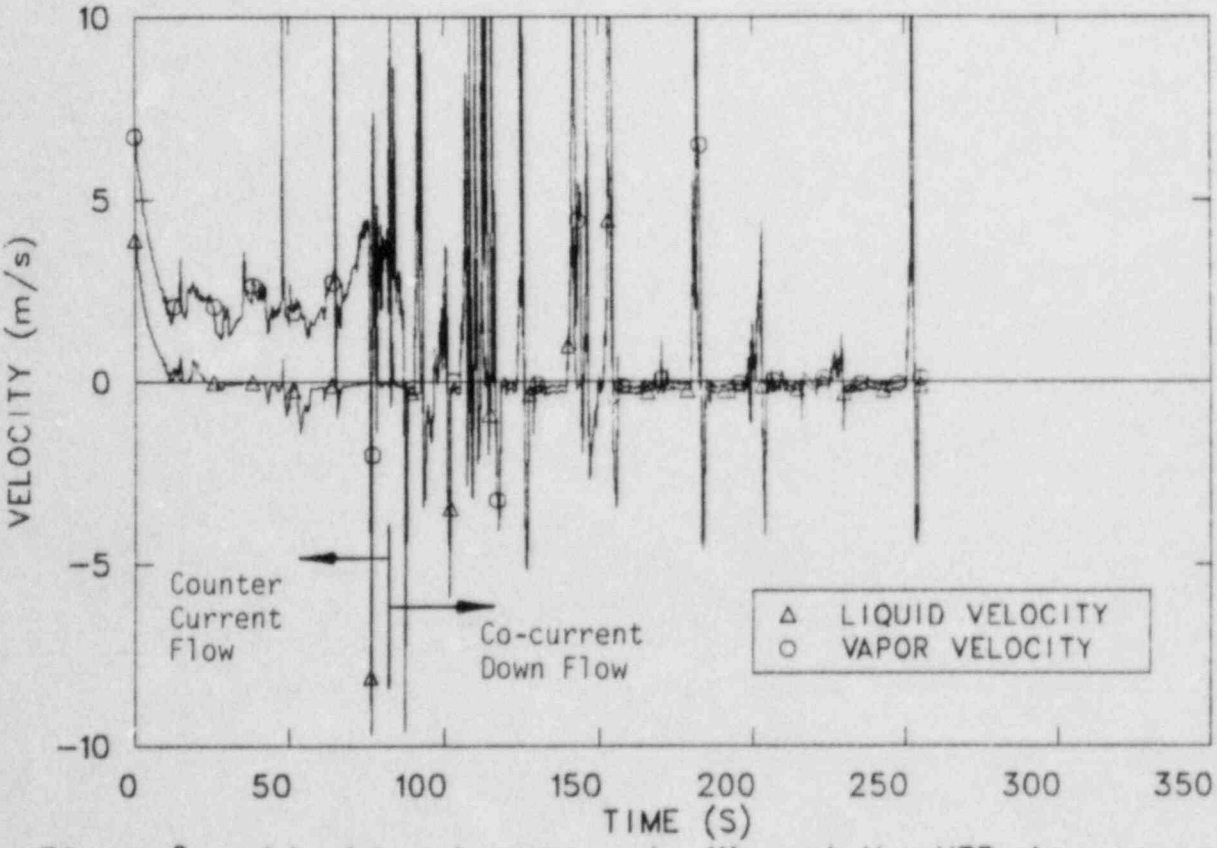


Figure 9. Liquid and vapor velocities at the UTP, low power CHAN.

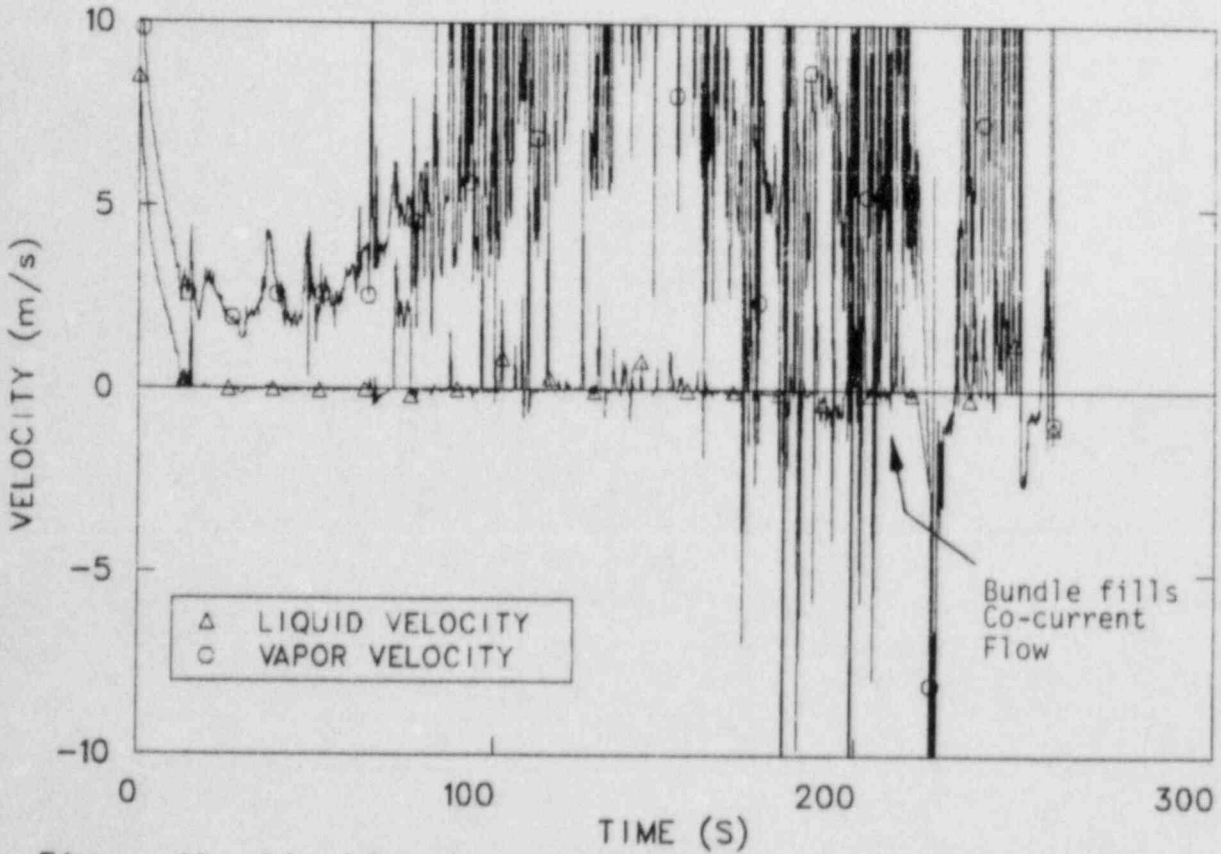


Figure 10. Liquid and vapor velocities at the UTP, average power CHAN.

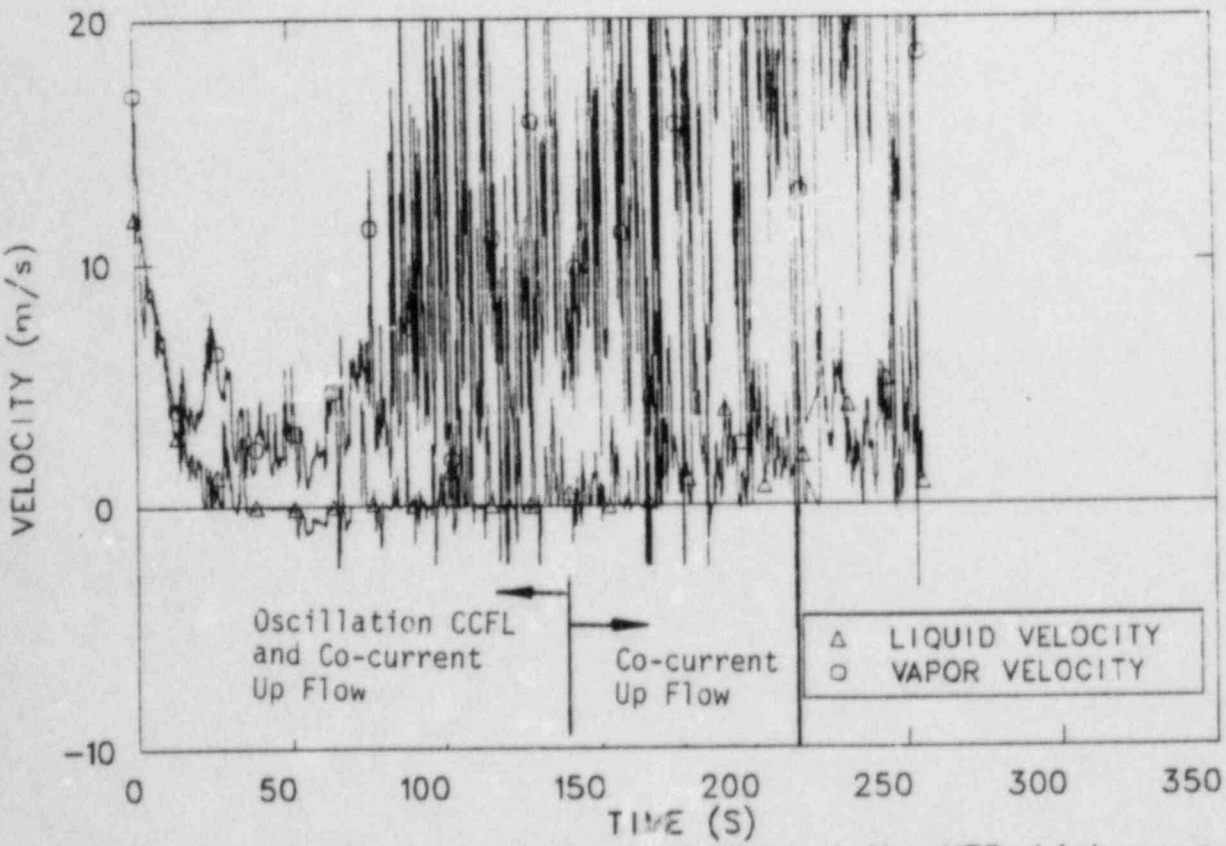


Figure 11. Liquid and vapor velocities at the UTP, high power CHAN.

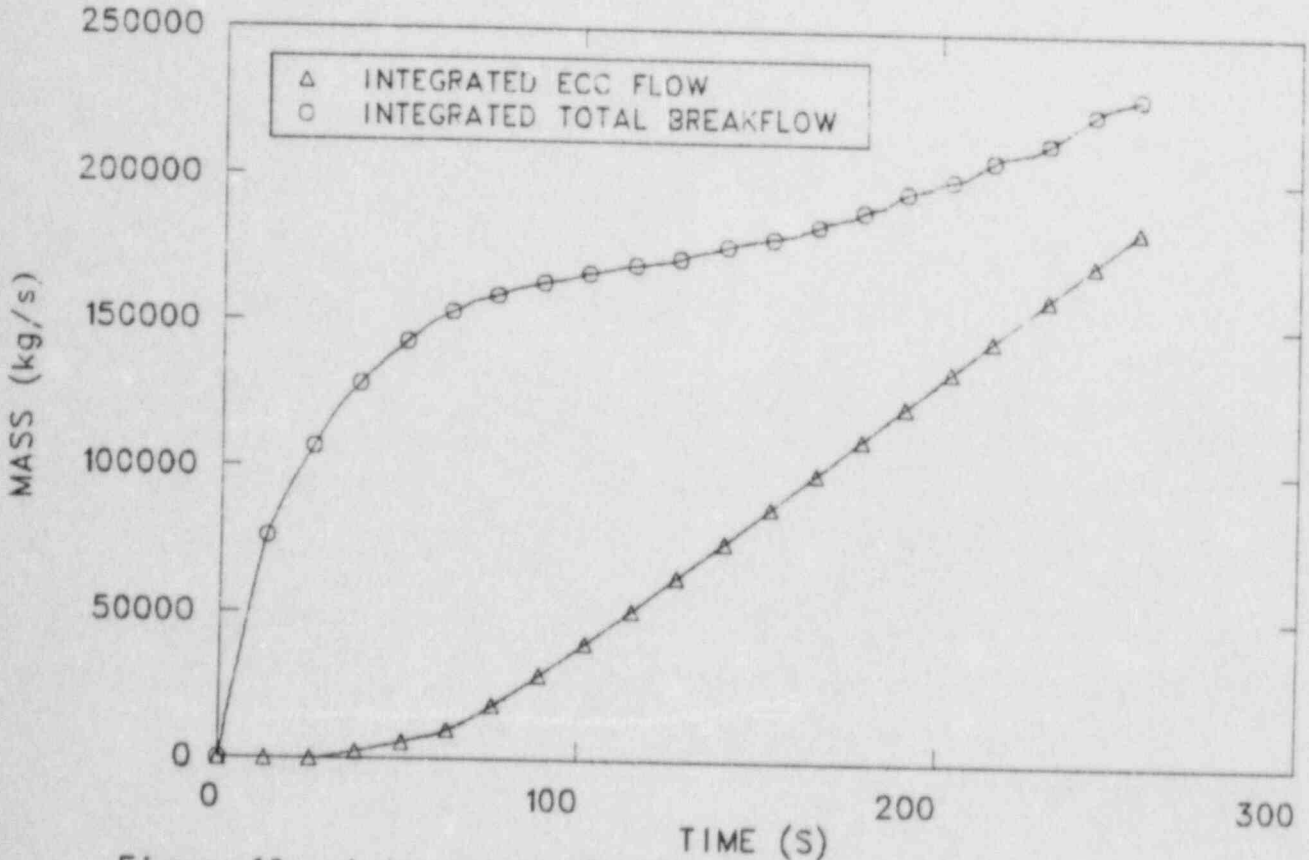


Figure 12. Integrated ECC flow versus integrated breakflow.

The peak cladding temperature in this analysis occurs during the blowdown portion of the transient. Pure evaluation model calculations show the peak occurring during the refill/reflood portion of the transient.

Analysis of the calculation indicated that the system behavior was much like experimental data and best estimate calculations employing best estimate boundary conditions. Limited comparisons were made with FIST, SSTF, and a best estimate calculation with best estimate boundary conditions.

The ECC systems were able to supply sufficient coolant during the transient. Two LPCI pumps were assumed failed yet the cladding temperatures were well below Appendix K limits and the vessel inventory would have been replaced by about 410 s.

## REFERENCES


1. J. W. Spore et al., TRAC-BD1: An Advanced Best Estimate Computer Program for Boiling Water Reactor Loss-of-Coolant Accident Analysis, NUREG-CR-2178, EGG-2109, October 1981.

2. T. R. Charlton, ltr to P. E. Litteneker, TRC-104-83, Initial and Boundary Conditions for the TRAC BWR/6 Best Estimate Calculation, October 18, 1983.

3. ANS Standards Committee Working Group, "ANS-5.1: Decay Heat Power in Light Water Reactors," ANS, ANSI/ANS-5.1-1979, LaGrange Park, Illinois, August 1979.

4. P. D. Wheatley, Scaling Analysis of the FIST Facility Using TRAC-BD1, EGG-NTAP-6073, October 1982.

5. W. S. Hwang et al., BWR Full Integral Simulation Test (FIST) Phase I Test Results, General Electric Company, GEAP-30496, November 1983.

6. D. G. Schumacher, BWR Refill-Reflood Program Task 4.4-CCFL/Refill System Effects Tests Experimental Task Plan, General Electric Company, GEAP-24893, April 1981.

# DETERMINATION OF APPENDIX K CONSERVATISMS FOR WESTINGHOUSE PWR USING TRAC-PD2/MOD1*

U. S. Rohatgi, C. Yuelys-Miksis and P. Saha

Department of Nuclear Energy
Brookhaven National Laboratory
Upton, New York 11973, U.S.A.

## ABSTRACT

A 200% cold leg break accident in a Westinghouse four-loop RESAR-3S plant has been analyzed using the best-estimate code TRAC-PD2/MOD1. Three TRAC calculations, one with the best-estimate or realistic initial and boundary conditions and scenarios, and the other two with the licensing conditions one with and the other without locked rotor resistance, have been performed. These calculations produced the peak cladding temperatures of 800°K, 1072°K, and 1153°K, respectively. Comparison of these results with the Westinghouse licensing calculations performed in accordance with the Appendix K rule, shows an overall safety margin of 664°K, of which 353°K is due to the conservative initial and boundary conditions and scenario. The remaining 311°K is due to conservative physical models. The locked rotor resistance contributed about 81°K in PCT.

## INTRODUCTION

This study was undertaken to estimate the conservatism due to the licensing or evaluation models for various thermohydraulic processes and fuel behavior, boundary and initial conditions, and transient scenarios. These were prescribed by the U. S. Nuclear Regulatory Commission in Appendix K of 10CFR50 for the prediction of peak clad temperatures in large and small break LOCA and were based on the understanding of two-phase thermohydraulics and fuel behavior in the early seventies. Significant progress has been made in the knowledge of two phase flow and fuel behavior since then and the current best-estimate models are quite different from those described in Appendix K. The TRAC-PD2/MOD1[1] code was selected for this study as it was the most assessed best-estimate large break LOCA code available at this time. This code was applied to a Westinghouse RESAR-3S four-loop plant for the analysis of a 200% cold leg break.

The first task in this study was to determine the sensitivity of the peak clad temperature to the nodalization and fuel models. This was accomplished by performing various best-estimate calculations, one of which was selected as the benchmark BNL best-estimate calculation. Westinghouse supplied a licensing calculation for RESAR-3S plants taking into account all of the evaluation models, boundary and initial conditions, and scenarios prescribed in Appendix K. The Reactor Coolant Pumps (RCPs) were tripped in the Westinghouse calculations, while they were kept running in the best-estimate calculation. These two calculations provided the lower, i.e., best-estimate, and the upper, i.e., Appendix K, limits for the peak clad temperature and clad temperature histories during the accident.

*This work was performed under the auspices of the U.S. Nuclear Regulatory Commission.

Besides these two bounding calculations, two intermediate calculations were also performed at BNL with the TRAC-PD2/MOD1 code (best-estimate models), but using the evaluation or licensing type initial and boundary conditions and transient scenario similar to the Westinghouse licensing calculation. In subsequent sections, BNL calculations will be described in detail.

## NODALIZATION

A RESAR-3S plant was modeled with TRAC-PD2/MOD1 with 556 one-dimensional nodes in four loops and a three-dimensional VESSEL with 224 cells as shown in Figure 1. The inner 8 cells from the top of Level 3 to the top of Level 8 represented the core. Each of these cells contained an average rod and an additional hot rod. The average rods had the same axial power peaking but different radial peaking. The models for each loop contained a cold leg, a reactor coolant pump (RCP), a steam generator (SG), a hot leg, and a TEE component connected to safety injection FILLS and an accumulator component. The pressurizer was connected to Loop 2. At the time of LBLOCA, the cold leg of Loop 4 was replaced by two pipe sections with BREAK models. TRAC-PD2/MOD1 uses a numerical or self choking model which requires fine nodalizations near the breaks. The containment pressure was supplied as a boundary condition at the BREAK components. This nodalization was arrived at after several calculations and represents the minimum amount of detail needed without sacrificing accuracy.

## BEST-ESTIMATE (BE) CALCULATION

The first calculation performed with TRAC-PD2/MOD1 was with the most probable boundary and operating conditions as shown in Table 1. The safety system performed as designed. The AC power was available throughout the transient.

Figure 2 shows the system pressure as predicted by the code. Initially the system pressure rapidly decreased to saturation pressure due to subcooled blowdown; thereafter, the rate of pressure change slowed down due to choking at the breaks. At approximately 2.5 seconds, the rate of pressure change decreased again as the vapor generation in the core increased due to flow oscillation at the core inlet as shown in Figure 3. Initially the flow also reversed at the core inlet due to the breaks, but as the break flow decreased below the net cold leg flows, the flow into the core was re-established, enhancing the vapor generation in the core. At approximately 20 seconds the system pressure was close to the containment pressure, indicating the end of the blowdown phase.

Figure 4 shows the clad surface temperatures at four axial locations for the hot rod. There are two temperature peaks in the blowdown phase. The first peak of 800°K at 2.5 seconds represents the peak clad temperature for the transient. This peak occurred when the initial clad heat up due to flow stagnation was quenched when the flow at the core inlet was restored as shown in Figure 3. The second clad heat up was quenched when the flow reversed at the core outlet as shown in Figure 5 generating the second peak. All of the axial locations were quenched by 45 seconds. Figure 6 shows the liquid fraction in the core, which increased rapidly during the reflood phase (time > 39 seconds). At the time of quenching the liquid fraction was around 35%.

The sequence of these and other events during the transient have been summarized in Table 2. The accumulators started the water injection at 10.5 seconds while the safety injections started at 2.5 to 7.6 seconds due to the built-in delay of 1.5 to 6.5 seconds in their initiation. The lower plenum was full (95%) at 39 seconds indicating the end of refill and the beginning of the reflood phase.

## EVALUATION MODEL (EM) TYPE CALCULATION

The EM type BNL calculations with TRAC-PD2/MOD1 were performed using the licensing type boundary and operating conditions and scenarios as shown in Table 1. The single failure criterion as prescribed in Appendix K was satisfied by eliminating one of the two safety injection trains. Furthermore, the loss of AC power was also assumed which resulted in tripping the RCPs. Initially the core power was 102% of the licensed power, while the decay power was 120% of the ANS 1971 Standard. These calculations consisted of best-estimate models, but evaluation model type (licensing) boundary and operating conditions. Therefore, they are called the Evaluation Model (EM) type calculation.

The nodalization in these calculations were the same as in the previous best-estimate calculation. However, there were some changes in the placement of the rods and their radial peakings. Appendix K requires at least two channel analysis, one of which should be the hot channel and the hot rod should be placed there. This requirement was satisfied by designating one of the inner quadrants as the hot channel as shown in Figure 7. The average rod in this quadrant had the highest radial peaking (1.38). The hot rods in the other inner quadrants had the same power density. This arrangement brought the conditions in this calculation closer to the Westinghouse licensing calculation[2-3].

Figures 8 and 9 show the rod surface temperatures at four axial locations for the hot rods in the hot channel and an adjacent channel for the first EM type calculation. The peak clad temperatures for both rods occurred in the reflood phase and the highest clad temperature of 1072°K occurred for the hot channel rod at 55 seconds. The peaks in the blowdown phase was relatively smaller and were governed by the core inlet and outlet flows as were explained earlier for the BE calculation. All the rods were either quenched or close to quenching by 270 seconds. The long duration between the timings of PCT and quenching was due to smaller safety injection and accumulator flows, and because together they were of the same order of magnitude as the break flows. The hot channel did affect the clad temperature history as can be seen from Figures 8 and 9. The difference between the PCT of the hot channel and the other channels in the blowdown phase was of the order of 50°K, and in the reflood phase it varied from 20°K to 100°K.

The timings of the sequence of events for this calculation are summarized in Table 2. The safety injections came on quite late due to the assumption of 25 seconds delay in starting the diesel generators. The lower plenum was full by 48.5 seconds and the reflood phase began. The core liquid fraction as shown in Figure 6 was increasing at the termination of the calculation indicating that the core was in the process of complete quenching.

The second EM type calculation was performed to account for the effect of locked rotor resistance. Appendix K states that locked rotor resistance should be considered in the reflood phase if it results in higher PCT. This calculation was started at 48.5 seconds, with the RCP speed set to zero. The vapor flow rate through the broken hot leg decreased due to additional pump resistance. This also slowed down the liquid penetration in the downcomer and the core and diminished the core cooling. The fuel clad started to heat up faster than in the previous EM calculation as shown in Figure 10. The peak clad temperature of 1153°K occurred at 100 seconds into the transient. Both of the EM type calculations were qualitatively similar. The calculation was terminated when the clad started to cool down.

## DISCUSSION

The best-estimate (BE) calculation was performed with the best-estimate code (TRAC-PD2/MOD1) and with all the safety systems working as designed. The evaluation model (EM) type calculations were performed with licensing type boundary and operating conditions and scenario but with the best-estimate code. Besides these calculations, results of a fourth calculation performed by Westinghouse[3] with licensing or evaluation model type boundary and operating conditions and physical models were also available. The clad temperatures for these calculations have been compared in Figure 10.

A comparison between the Westinghouse and the BNL BE calculations indicates that the licensing or Appendix K requirements contribute to a conservatism of 664°K in the PCT prediction. A comparison of the EM type calculation (EM/BNL/locked rotor) with these two bounding calculations indicates that the licensing type operating and boundary conditions and scenarios are responsible for 353°K conservatism in PCT while the Appendix K required physical models contribute about 311°K to the conservatism of PCT estimation. The peak clad temperature in the best-estimate calculation occurred very early in the transient, and was not affected by the ECC system. On the other hand, the ECC system did affect the other calculations. A comparison of the two EM type BNL calculations indicates that the PCT is affected by locked rotor resistance and the sensitivity is of the order of 81°K.

## CONCLUSIONS

This study indicates that there is a large safety margin in the licensing or Appendix K requirements. The contribution to this safety margin due to the required physical models such as subtraction of safety injection fluid collected during the blowdown phase from coolant inventory and restriction on return of nucleate boiling or transition regime in the core before the reflood phase, etc. are of the same order of magnitude as due to the boundary conditions operating conditions, and scenario. Furthermore, it has been shown that a hot channel analysis is conservative, and if licensing type calculations are to be performed with TRAC, then one of the quadrants should represent a hot channel. The Appendix K guideline of setting the pump to locked rotor conditions also contribute significantly to the conservatism in PCT.

## ACKNOWLEDGEMENT

The authors gratefully acknowledge the valuable assistance and advice provided by Dr. Fuat Odar of USNRC, D. R. Hochreiter and Mr. R. Kemper of Westinghouse Electric Co., and Dr. K. Williams of LANL in performing this study. The typing of Ms. A. Fort is genuinely appreciated.

## REFERENCES

1. Liles, D. R. et. al., "TRAC-PD2, An Advanced Best Estimate Computer Program for Pressurized Water Reactor Loss-of-Coolant Accident Analysis," USNRC Report, NUREG/CR-2054, 1981.

2. Kemper, R., Westinghouse Electric Company, Private Communication.

3. Fujita, R. K, et. al., "Comparison Between a Most-Probable and a Licensing Calculation of a 200% LOCA in a Four Loop 17 x 17 Westinghouse PWR," National Heat Transfer Conference, Niagara Falls, NY, August 5-8, 1983.

Table 1. Comparison of BE and EM Conditions and Scenario

| Appendix K/10CFR50 | BE/TRAC-PD2 | EM/TRAC-PD2 |
|---|---|---|
| **Operating Conditions** | | |
| 1) Core Power, 1.02 of licensed power. | Licensed power. | 1.02 Licensed Power |
| 2) Fuel and clad properties as functions of temperature and other applicable time dependent variables. | Considered | Considered |
| 3) Peaking factor should be realistic. | Most probable values during fuel cycle. | Beginning of fuel cycle. |
| 4) Decay power, 120% of 1971 ANS. | 100% of 1979 ANS. | 120% of 1971 ANS. |
| **Boundary Conditions** | | |
| 1) Containment pressure should be conservative and should account for all pressure reducing devices. | Realistic containment pressure history considered. | Most conservative pressure history considered. |
| 2) Single failure criterion for ECC system requires that at least one equipment with worst effect should be considered. | Not considered. | Disabling one diesel generator results in loss of one HPI pump (Safety injection) and one LPI pump (residual heat removal). This reduces the amount of net injection to all the loops. |
| **Scenario** | | |
| 1) RCP pump tripped and locked rotor considered after reflood. | Pump on. | Pump coasting down with or without locked rotor. |
| 2) Delay in restarting the safety injection pumps after the safety injection signal is activated. | 1.5 sec for LPI pumps. 6.5 sec for HPI pumps. | 25 sec for all pumps. |

Table 2. Comparison of Sequence of Events for BE and EM Calculations

| | EVENTS | TIME (s) | | |
|---|---|---|---|---|
| | | BE/BNL | EM/BNL/1 | EM/BNL/2 |
| 1. | Break | 0.0 | 0.0 | 0.0 |
| 2. | Safety Injection Signal Generated | 1.1 | 5.1 | 5.1 |
| 3. | Broken Loop Accumulator Injection | 2.2 | N/A | N/A |
| 4. | Intact Loop Accumulator Injection | 10.5 | 11.3 | 11.3 |
| 5. | Pressurizer Empties (Water Level < 0.005 m) | 16 | 17.5 | 17.5 |
| 6. | Safety Injection (Charging, Residual Heat Removal, High Head Safety Injection) | 2.6 to 7.6 | 30.1 | 30.1 |
| 7. | Lower Plenum Refilled (Liquid Fraction 0.95) and Beginning of Reflood | 39 | 48.5 | 48.5 |
| 8. | Peak Clad Temperature | 2.5 | 65 | 100 |
| 9. | Accumulator Empty* | Did Not | 86.5 | 87.5 |
| 10. | Cooling of Hot Spots Begins | 44 | 244 | |

*This is subjective and based on loop 1 accumulator reaching collapsed liquid level of 0.3 m and liquid inventory of 700 kg.

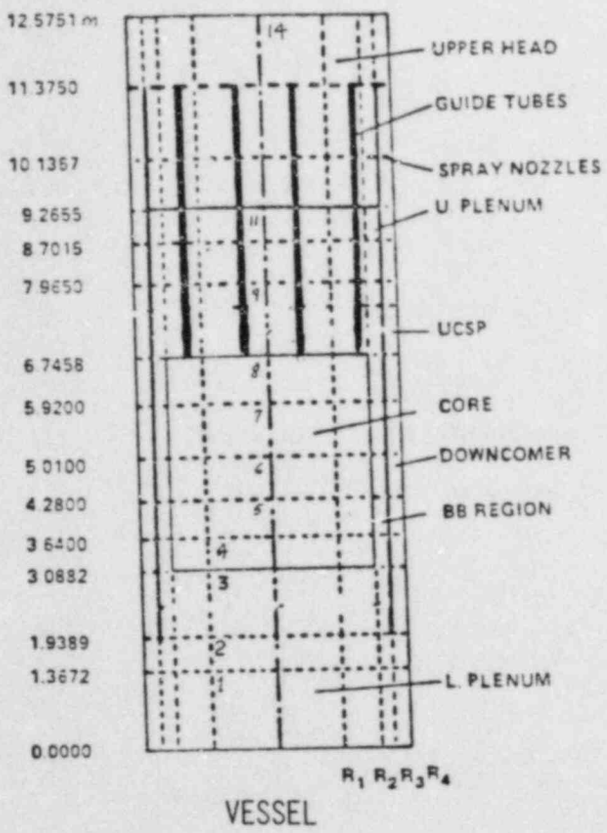


Figure 1 Nodalization in the VESSEL Component.

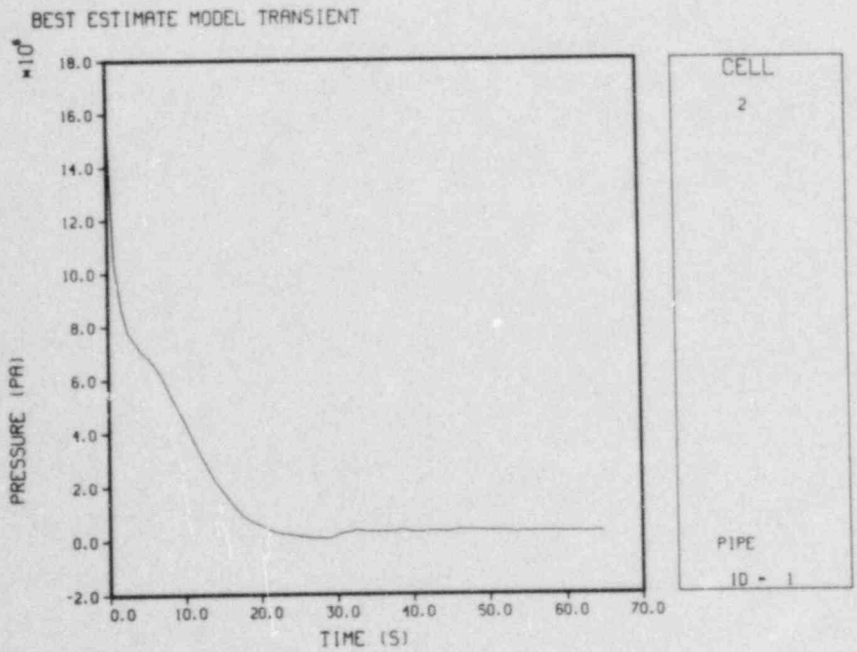


Figure 2 System Pressure in the Best-Estimate Calculation.

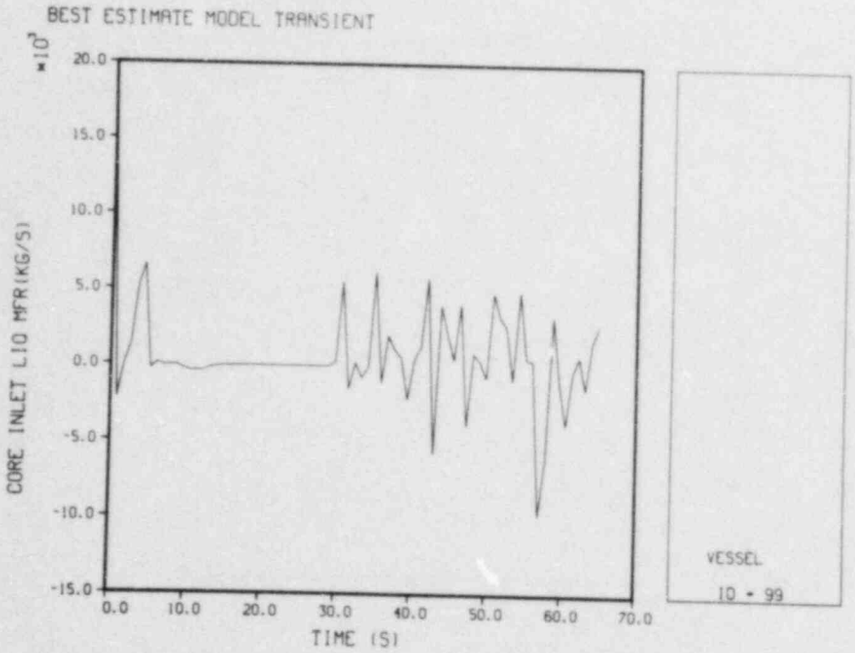


Figure 3 Core Inlet Liquid Mass Flow Rate for Best-Estimate Calculation.

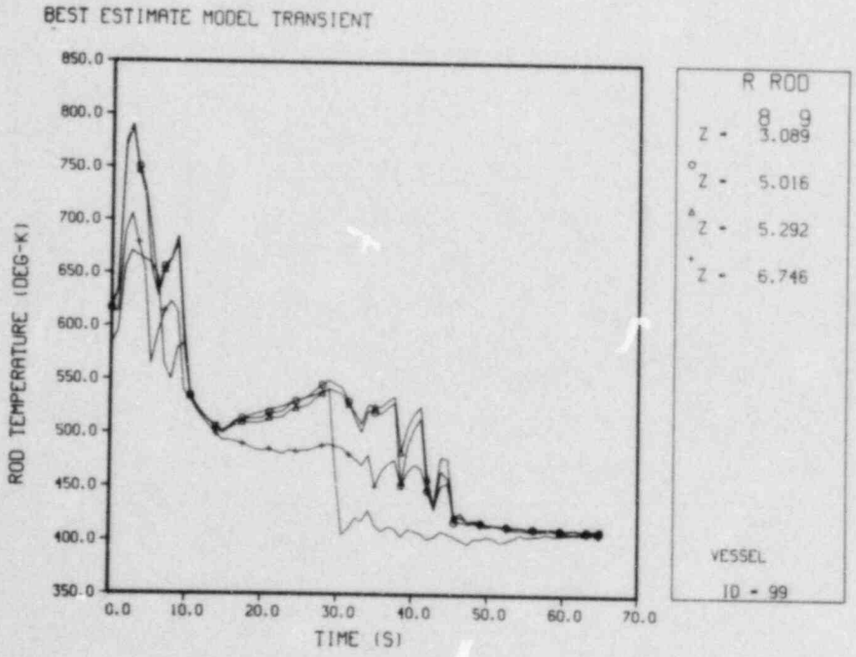


Figure 4 Clad Surface Temperatures for Hot Rods in BE Calculation.

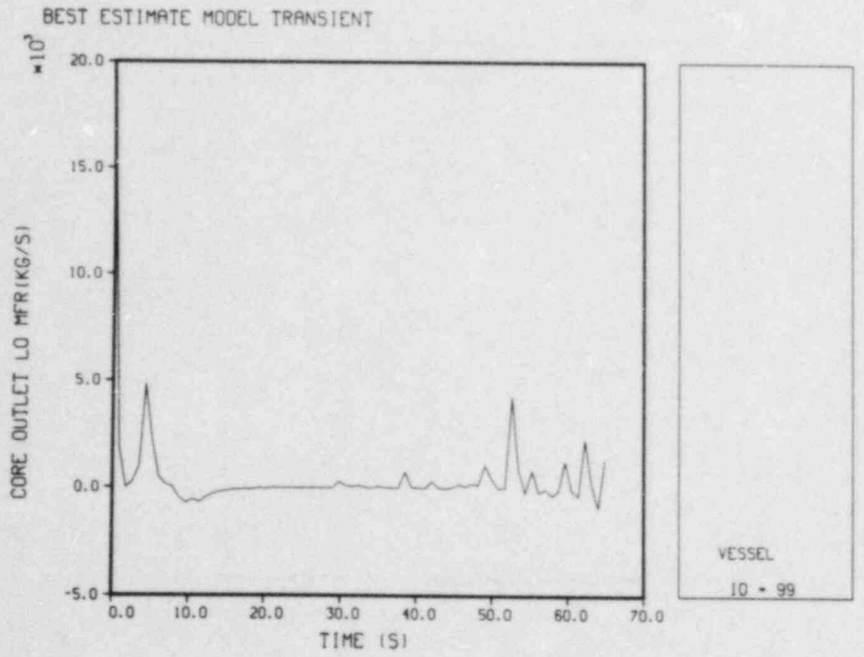


Figure 5 Core Outlet Mass Flow Rate for Best-Estimate Calculation.

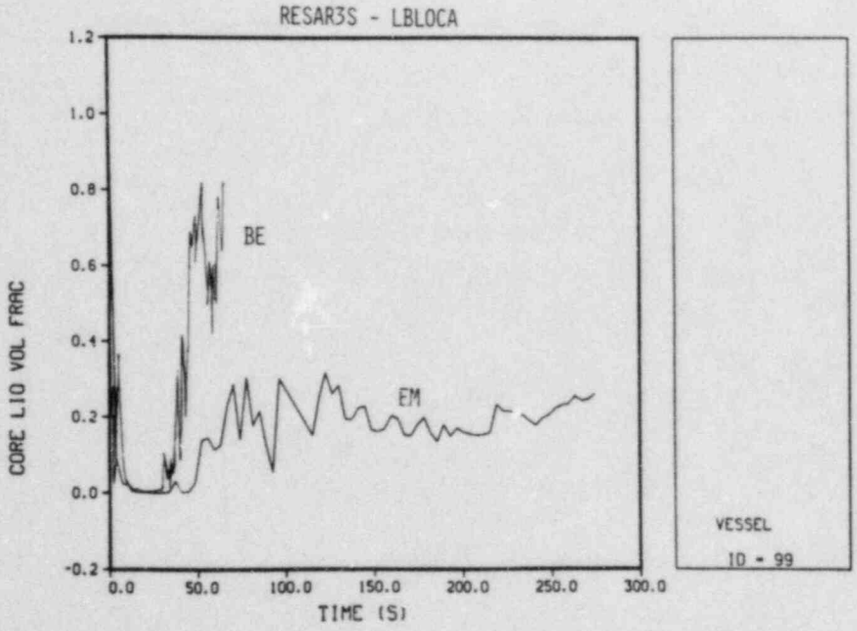


Figure 6 Comparison of Core Liquid Volume Fractions in BE and First EM Type BNL Calculations.

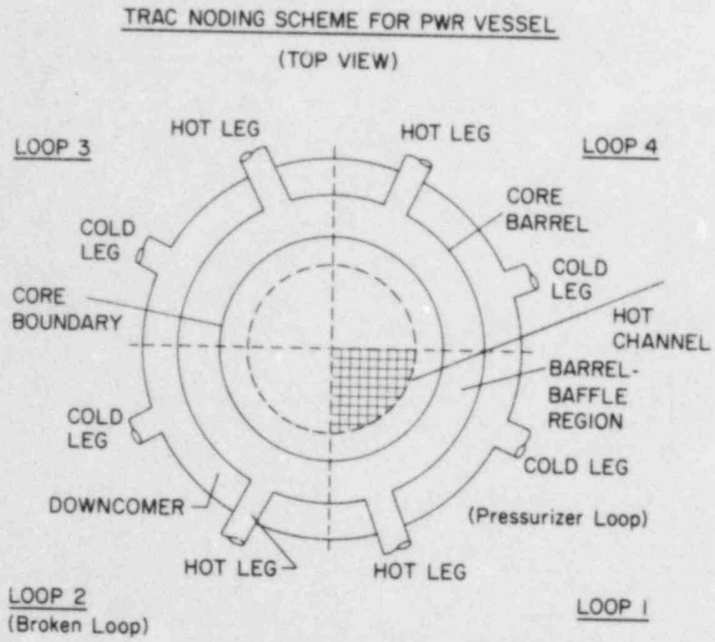


Figure 7 Vessel Cross Section for EM Calculation

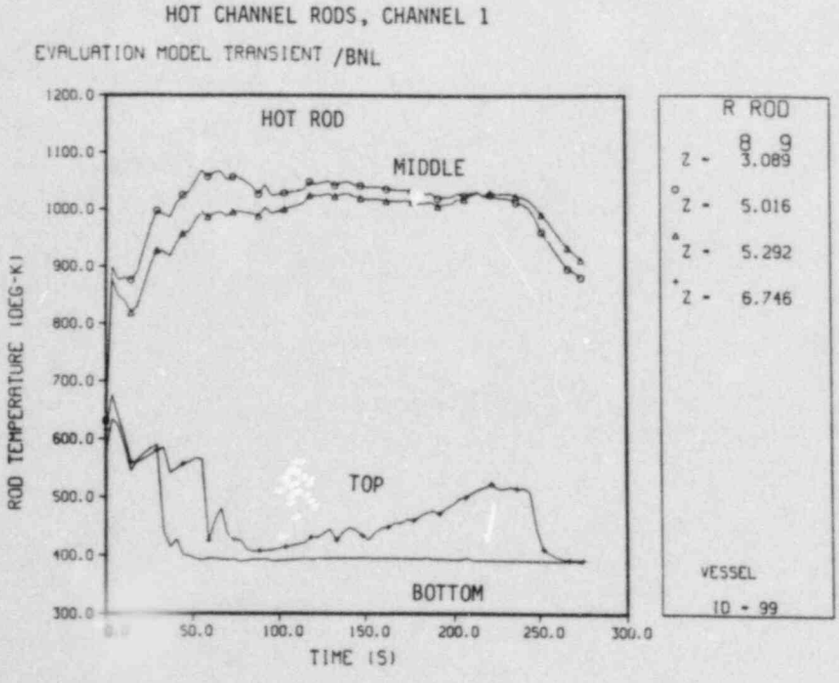


Figure 8 Clad Surface Temperatures for Hot Rod in Hot Channel For First EM Calculation.

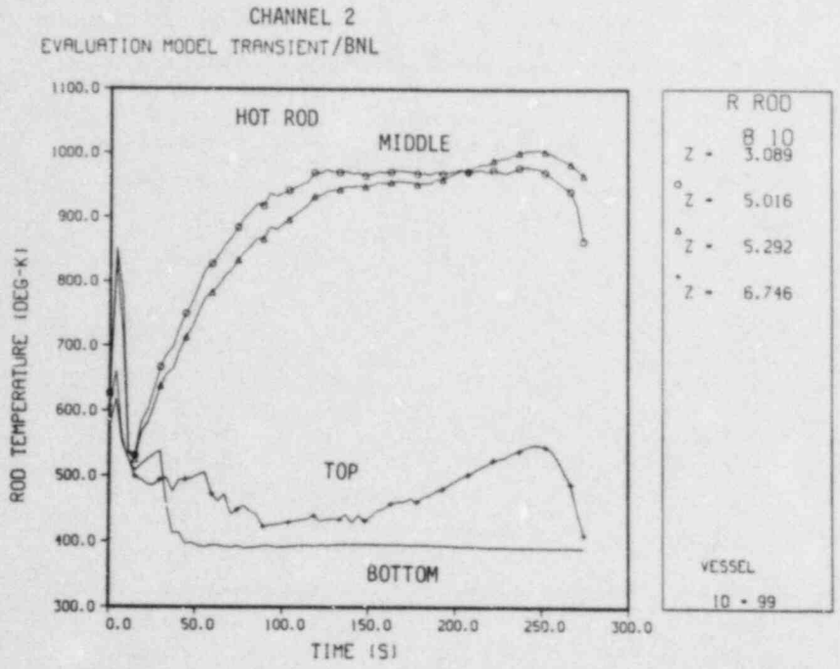


Figure 9 Clad Surface Temperatures for Hot Rod in Other Channel in First EM Calculation.

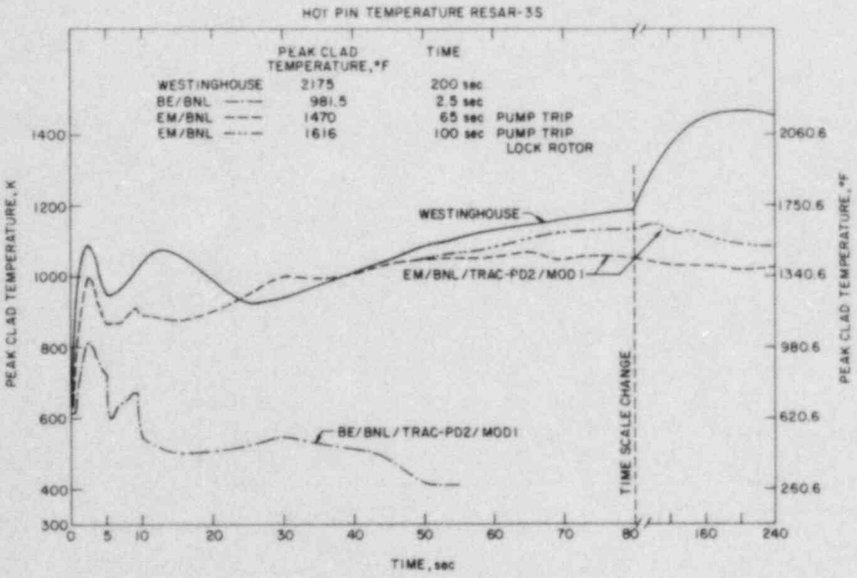


Figure 10 Comparison of Clad Temperature for Hot Rods for Westinghouse and BNL Calculations.

NRC FORM 335 (7.77)

U.S. NUCLEAR REGULATORY COMMISSION

**BIBLIOGRAPHIC DATA SHEET**

1. REPORT NUMBER *(Assigned by DDC)*
NUREG/CP-0058, Volume 1

4. TITLE AND SUBTITLE *(Add Volume No., if appropriate)*
Proceedings of the Twelfth Water Reactor Safety Research Information Meeting

2. *(Leave blank)*

3. RECIPIENT'S ACCESSION NO.

7. AUTHOR(S)
Compiled by: Stanley A. Szawlewicz, Consultant

5. DATE REPORT COMPLETED
MONTH: December YEAR: 1984

9. PERFORMING ORGANIZATION NAME AND MAILING ADDRESS *(Include Zip Code)*
Office of Nuclear Regulatory Research
U. S. Nuclear Regulatory Commission
Washington, DC 20555

DATE REPORT ISSUED
MONTH: January YEAR: 1985

6. *(Leave blank)*

8. *(Leave blank)*

12. SPONSORING ORGANIZATION NAME AND MAILING ADDRESS *(Include Zip Code)*
Same as Item 9.

10. PROJECT/TASK/WORK UNIT NO.

11. CONTRACT NO.

13. TYPE OF REPORT
Collection of Conference Papers

PERIOD COVERED *(Inclusive dates)*
October 22-26, 1984

15. SUPPLEMENTARY NOTES

14. *(Leave blank)*

16. ABSTRACT *(200 words or less)*

The papers published in this six volume report were presented at the Twelfth Water Reactor Safety Research Information Meeting held at the National Bureau of Standards, Gaithersburg, Maryland during the week of October 22-26, 1984. The papers describe progress and results of programs in nuclear safety research conducted in this country and abroad. Foreign participation in the meeting included twenty-six different papers presented by researchers from seven European countries, Japan, and Canada.

17. KEY WORDS AND DOCUMENT ANALYSIS

17a. DESCRIPTORS

reactor safety
separate effects
thermal hydraulics
integral systems

17b. IDENTIFIERS/OPEN-ENDED TERMS

18. AVAILABILITY STATEMENT
Unlimited

19. SECURITY CLASS *(This report)*
Unclassified

21. NO. OF PAGES
434

20. SECURITY CLASS *(This page)*
Unclassified

22. PRICE
$

NRC FORM 335 (7.77)

UNITED STATES
NUCLEAR REGULATORY COMMISSION
WASHINGTON, D.C. 20555